Arthritis & Rheumatology

An Official Journal of the American College of Rheumatology
www.arthritisrheum.org and wileyonlinelibrary.com

Cover design: Todd Machen

♾ This journal is printed on acid-free paper.

Arthritis & Rheumatology
An Official Journal of the American College of Rheumatology
www.arthritisrheum.org and wileyonlinelibrary.com

VOLUME 69 JULY 2017 NO. 7

Cover image: The figure on the cover (from Ambra et al., page 1366) shows hyaline cartilage from juvenile donors that was morselized into ~1-mm cubes for use in a procedure called particulated juvenile allograft cartilage. Use of this technique to repair articular cartilage defects has shown promising results at short-term follow-up.

In this Issue

Highlights from this issue of *A&R* | By Lara C. Pullen, PhD

Learning Collaborative Helps to Achieve Treat-to-Target Goals for RA

Treatment programs for rheumatoid arthritis (RA) do not always follow the recommended treat-to-target (TTT) approach. In this issue, Solomon et al (p. 1374) describe their evaluation of a group-based multisite improvement learning collaborative and its effect on adherence to TTT. The Treat-to-Target in RA: Collaboration to Improve Adoption and Adherence (TRACTION) trial was a pragmatic, cluster-randomized controlled trial. The study encompassed 5 sites with 23 rheumatology providers and 320 patients who were randomized to intervention and 6 sites with 23 rheumatology providers, and 321 patients who were randomized to the waitlist control. The intervention incorporated rapid-cycle improvement methods, and the effects were documented by trained staff who measured efficacy of the learning collaborative with a composite TTT implementation score, defined as the percentage of 4 required items recorded in the visit notes for each patient at 2 time points. This measure was the primary outcome. The investigators noted that it was a process measure and does not necessarily reflect clinical outcomes.

p. 1374

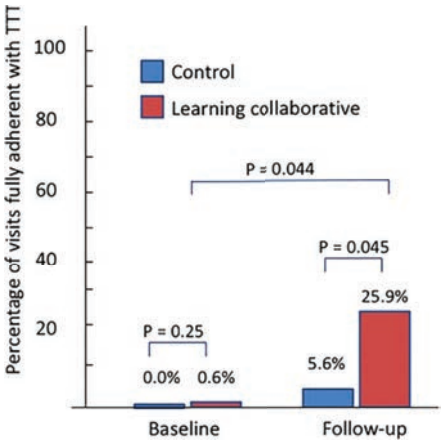

Figure 1. Percentage of visits at baseline and follow-up that were in full adherence to the treat-to-target (TTT) protocol, the secondary outcome of the Treat-to-Target in RA: Collaboration to Improve Adoption and Adherence (TRACTION) trial.

At baseline, both groups had a mean TTT implementation score of 11%. After the 9-month intervention, the mean TTT implementation score was 57% in the intervention group and 25% in the control group, indicating that the learning collaborative was able to substantially improve adherence to TTT. Moreover, the investigators did not observe excessive use of resources or an excessive number of adverse events in the intervention arm. The researchers write that the implementation of TTT was far lower than desired and cite previous studies suggesting that this might be because of patient preference or because rheumatologists prefer not to adjust medications for symptoms that might be associated with irreversible joint damage. Nevertheless, the research supports the use of an educational collaborative to improve quality, not just in RA but in other medical conditions as well.

Insights Into Pediatric AAV Outcomes

In this issue, Morishita et al (p. 1470) describe data from the largest study to date assessing disease outcomes in pediatric patients with antineutrophil cytoplasmic antibody (ANCA)–associated vasculitis (AAV). Their multicenter international study is important because, unlike adult AAV, very little is known about pediatric outcomes in this group of diseases. The investigators focused their analysis on the early disease course and documented 12-month outcomes.

p. 1470

Children eligible for this inception cohort study were those who had been entered into the Pediatric Vasculitis Initiative study and had been diagnosed before their eighteenth birthday as having granulomatosis with polyangiitis (Wegener's) (GPA), microscopic polyangiitis, eosinophilic granulomatosis with polyangiitis (Churg-Strauss), or ANCA-positive pauci-immune glomerulonephritis. The median age of the children at diagnosis was 13.8 years, and the majority of them had GPA. The primary outcome measure was achievement of disease remission at 12 months, as demonstrated by a Pediatric Vasculitis Activity Score (PVAS) of 0 in a patient taking a corticosteroid dosage of <0.2 mg/kg/day. Inactive disease was defined as a PVAS of 0 with any corticosteroid dosage. The researchers found that only 42% of patients achieved remission. This is lower than the 90% remission rate that has previously been reported in the literature.

The majority of patients did, however, respond to treatment, even if they did not achieve inactive disease. This was evidenced by the fact that 92% of patients experienced 50% improvement in the PVAS score from the time of diagnosis to postinduction. Approximately one-fourth of the patients experienced minor relapses after inactive disease had been achieved postinduction.

As a secondary outcome, the investigators documented damage to organs at 12 months using the Pediatric Vasculitis Damage Index (PVDI) score (0 = no damage and 1 = 1 damage item present; total of 64 potential damage items). Unfortunately, the majority of patients experienced damage to various organ systems early in the course of disease. Specifically, the median PVDI score at 12 months was 1, and 63% of patients had ≥1 PVDI damage item present at 12 months.

Understanding the Relationship Between Obesity and Osteoarthritis

Obese individuals are known to be at increased risk of osteoarthritis (OA). In this issue, Harasymowicz et al (p. 1396) found that infrapatellar fat pad (IPFP) and synovium tissue depots not only differed significantly between obese and lean patients, but the differences were associated with the patients' body mass index. Adipocytes from the IPFP of obese patients were also significantly larger than those from the IPFP of lean patients. In addition, the synovium of obese patients displayed marked fibrosis, increased macrophage infiltration, and higher levels of Toll-like receptor 4 (TLR-4) than did the synovium of lean patients.

p. 1396

When the investigators examined the adipose-related markers peroxisome proliferator–activated receptor γ (PPARγ) and adiponectin, they found that PPARγ was expressed at lower levels in the IPFP and synovium of obese patients compared to lean patients. The IPFP and synovial tissue of obese patients also had increased numbers of CD45+ hematopoietic cells, CD45+CD14+ total macrophages, and CD14+CD206+ M2-type macrophages.

These results suggest that the IPFP and synovium may contain 2 different white adipose tissue depots. The findings also support the theory that patients with class II and class III obesity may have inflammation-induced OA. The authors call for further investigation to determine whether these findings indicate a potentially reversible, or at least suppressible, cause of OA in obese patients.

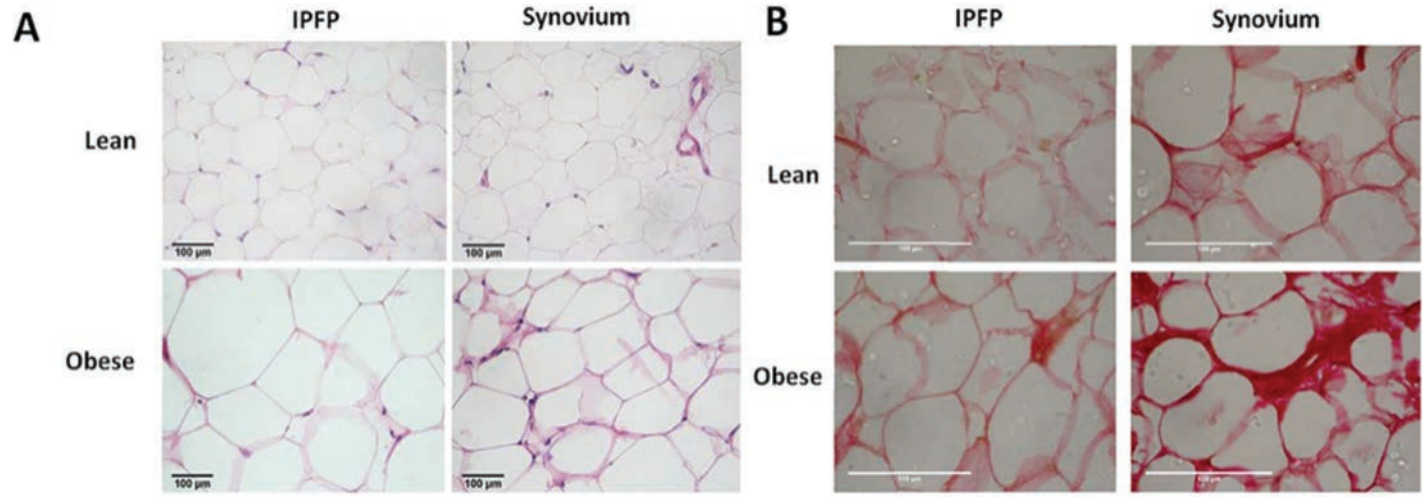

Figure 1. **A** and **B**, Representative hematoxylin and eosin staining (**A**) and picrosirius red S staining (**B**) of adipose tissue depots in the infrapatellar fat pad (IPFP) and synovium from lean and obese patients with end-stage knee osteoarthritis (OA) (n = 10 samples per group).

Insight Into the Reactivity of Anti–Carbamylated Protein Antibodies

Investigators have noted an association of the risk and severity of rheumatoid arthritis (RA) with anti–carbamylated protein (anti-CarP) antibodies, which are frequently directed against fibrinogen. The physiology behind the anti-CarP antibody reactivity has thus far remained murky, making it difficult to fully analyze the immunopathogenic association. In this issue, Jones et al (p. 1381) report on their mapping of anti-CarP antibody epitope reactivity in the sera of patients with RA.

p. 1381

The investigators found that anti-CarP antibodies appear to preferentially target the specific regions of the human fibrinogen β-chain that contain homocitrullines. The researchers began by evaluating serum from an RA patient for specific reactivity with carbamylated, but not citrullinated, fibrinogen β-chain. They then used liquid chromatography mass spectrometry to identify carbamylation of 9 of 34 lysines in the human fibrinogen β-chain.

When they mapped immunoreactivity using tryptic peptide fragments, they found several candidate carbamylated epitopes in fibrinogen. In particular, serum from a patient with RA had anti-CarP antibodies with strong reactivity to a homocitrulline at position 83 of the β-chain of fibrinogen. Additional reactivity to peptides containing homocitrullines at positions 52, 264, 351, 367, and 374 was seen. The researchers note that, while some anti-CarP antibodies exhibit homocitrulline polyreactivity, most react with the posttranslational modification in the specific peptides found in the fibrinogen β-chain. The authors hypothesize that the fact that humoral immunoreactivity appears to be relatively restricted in some patients suggests it may be possible to determine a specific relationship between humoral immunoreactivity and disease phenotype.

Clinical Connections

REDD1 Deficiency Impairs Autophagy and Mitochondrial Biogenesis in Articular Cartilage and Increases the Severity of Experimental Osteoarthritis

Alvarez-Garcia et al, *Arthritis Rheumatol* 2017;69:1418–1428.

CORRESPONDENCE
Martin K. Lotz, MD: mlotz@scripps.edu

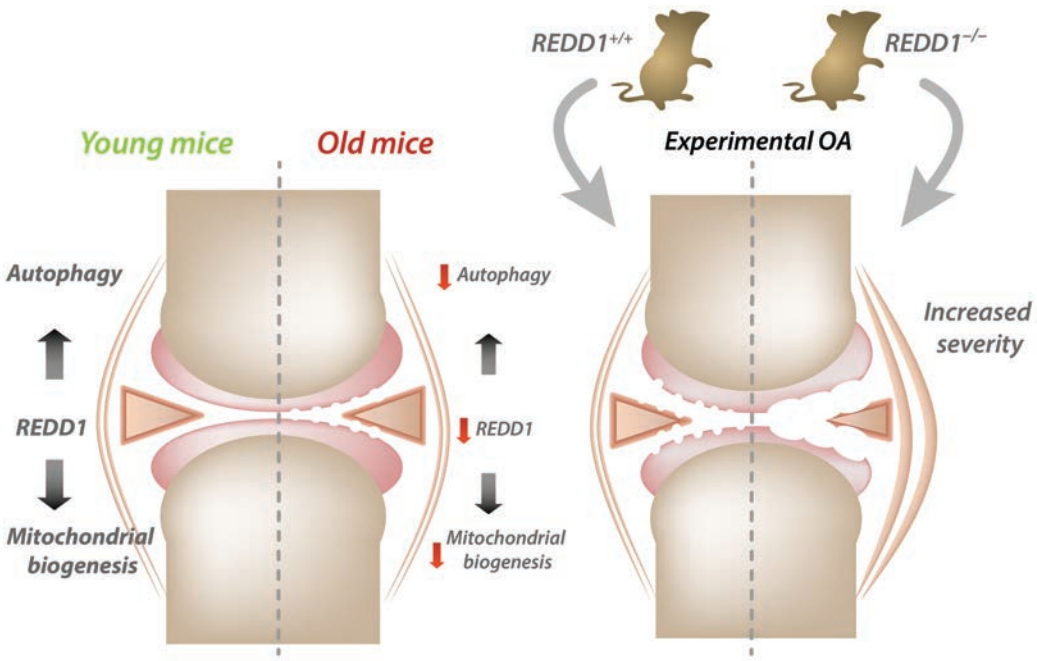

KEY POINTS

- Aged and OA cartilage in humans and mice have reduced expression of REDD1, a key regulator of cell metabolism and stress responses.
- Reduced REDD1 is associated with deficient autophagy and mitochondrial biogenesis in articular chondrocytes.
- Genetic deletion of REDD1 increases the severity of experimental OA in mice.

SUMMARY

During aging, articular chondrocytes undergo changes in homeostatic processes that compromise their function and may contribute to cartilage degradation and osteoarthritis (OA). The regulated in development and DNA damage response 1 (REDD1) protein regulates cell metabolism and coordinates cellular stress responses. Previous studies showed that REDD1 expression is reduced in aged and OA articular cartilage and is a positive regulator of autophagy. Alvarez-Garcia et al examined the role of REDD1 in OA development and identified novel REDD1 functions in articular chondrocytes. Using a mouse model with genetic deletion of REDD1 (REDD1$^{-/-}$), they showed that the severity of OA in the destabilized medial meniscus model was increased compared with wild-type (REDD1$^{+/+}$) mice and that REDD1 deficiency was associated with decreased expression of markers of autophagy and mitochondrial biogenesis in articular cartilage. They further demonstrated that REDD1 is necessary for maintaining normal levels of mitochondrial biogenesis. Maintaining normal levels of REDD1 in articular cartilage during aging may be a promising novel therapeutic strategy for preventing OA.

Chemogenetic Inhibition of Pain Neurons in a Mouse Model of Osteoarthritis

Miller et al, *Arthritis Rheumatol* 2017;69:1429–1439.

CORRESPONDENCE
Anne-Marie Malfait, MD, PhD: anne-marie_malfait@rush.edu

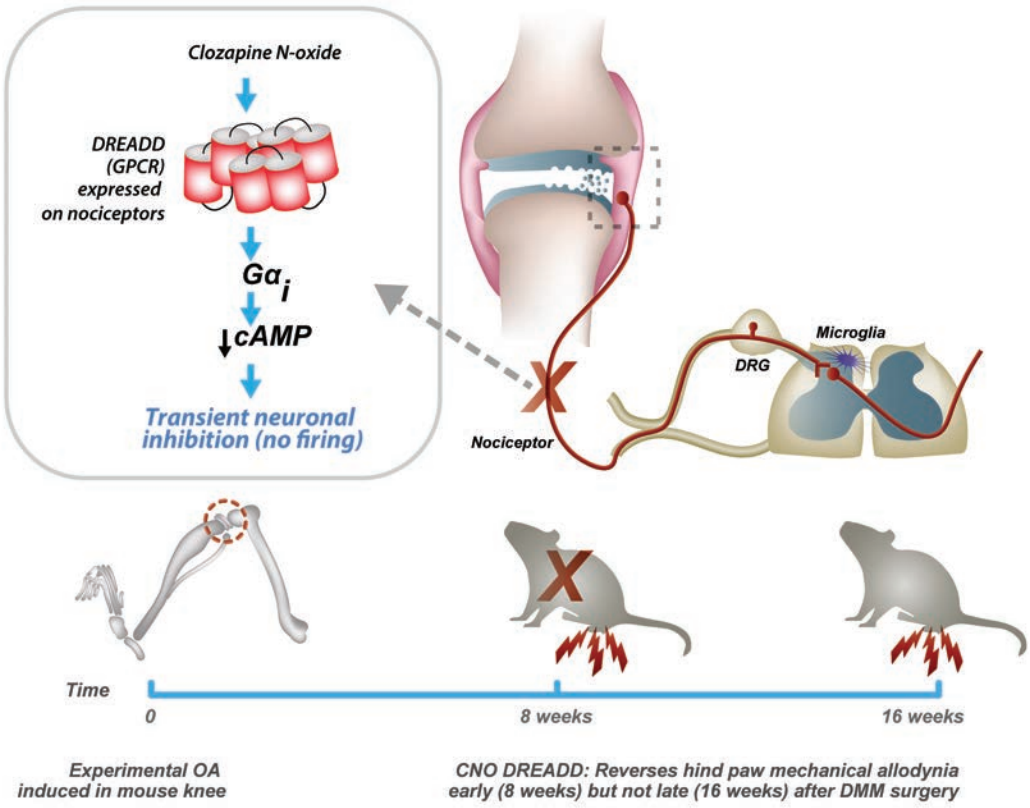

KEY POINTS

- Novel DREADD receptors (synthetic GPCRs) were used to inhibit the activity of pain-sensing neurons (nociceptors) in the knee joint in a mouse model of OA.
- Inhibition of nociceptors expressing $Na_V1.8$ reduced mechanical pain in early, but not later, stages of experimental OA, although morphine blocked pain at all phases of the disease.
- Opioids developed to selectively activate peripheral rather than central opioid receptors may not be effective in treating OA pain.

SUMMARY

Opioids produce their powerful pain-killing effects by activating opioid receptors (a type of inhibitory G protein–coupled receptor [GPCR]) located on both sensory pain neurons (nociceptors, cell bodies that reside in the dorsal root ganglia [DRGs]) and neurons in the central nervous system (CNS). Because many of the side effects of opiates are mediated by the CNS, there have been efforts to produce novel opioids that do not enter the CNS but act only peripherally. To assess the potential for GPCRs selectively localized in peripheral nociceptors to inhibit pain associated with osteoarthritis (OA), a mouse genetic approach was used to express inhibitory designer receptors exclusively activated by designer drug (DREADD) receptors in a major subgroup of nociceptors that express the voltage-gated sodium channel 1.8 ($Na_V1.8$). Activation of DREADD receptors with the use of clozapine *N*-oxide (CNO) inhibited the activity of these neurons and blocked hypersensitivity to mechanical stimuli in early experimental OA but not in the later stages. In contrast, morphine blocked pain responses during the entire course of the disease. The use of inhibitory and excitatory DREADD receptors expressed by different subtypes of neurons represents an exciting new approach to determining the role of the nervous system in the symptoms of OA. Importantly, the present observations indicate that activation of inhibitory GPCRs located solely outside the CNS may be ineffective in treating chronic OA pain.

ARTHRITIS & RHEUMATOLOGY
Vol. 69, No. 7, July 2017, pp 1343–1345
DOI 10.1002/art.40126

Arthritis & Rheumatology
An Official Journal of the American College of Rheumatology
www.arthritisrheum.org and wileyonlinelibrary.com

EDITORIAL

Arthritis Pain: Moving Between Early- and Late-Stage Disease

David A. Walsh

Joint pain remains the main problem for people with arthritis, despite availability of an increasing range of analgesic medications acting through discrete molecular targets. Existing treatments can relieve pain for some but not all people with arthritis, some but not all of the time. There remains a pressing need for better treatments to reduce the distress and disability of arthritis pain. Pain, however, also importantly warns us about and protects us from injury, and painkillers therefore need to target pathologic pain in the right people at the right times. In this issue of *Arthritis & Rheumatology*, Miller et al (1) provide important evidence that different types of pain might respond differently to the pharmacologic manipulation of a single analgesic target at various stages in the development of experimental osteoarthritis (OA) in mice. These preclinical findings resonate with observations in people with arthritis, and they point the way to how animal models and sophisticated interventional and measurement techniques might lead to new treatments and to more effective use of existing treatments in the foreseeable future.

Miller et al chose to explore pain transmitted through the abundant subset of articular sensory primary afferents that express voltage-gated sodium channel 1.8 ($Na_V1.8$). Using designer receptors exclusively activated by a designer drug technology, they selectively stimulated $G_{i/o}$ protein signaling in order to reduce peripheral sensory nerve activity. They found that they could reduce pain behaviors at various time points after surgical destabilization of the medial meniscus (DMM) in mice, sometimes to an extent similar to the analgesic effects observed with morphine. Morphine also activates $G_{i/o}$ proteins, but across a wider range of nerve types in the peripheral and central nervous systems. All of this is as might have been expected. Perhaps more importantly, Miller and colleagues' carefully conducted studies reveal that the effects of pharmacologic activation of $G_{i/o}$ varied according to the type of pain behavior measured and the time since DMM surgery. Indeed, significant analgesic effects were only observed before 12 weeks after surgery, and not at 16 weeks, a time point generally considered to represent late-stage OA in humans. In contrast, an analgesic acting on both peripheral and central nerves was able to inhibit pain behaviors at all time points.

Pain is not a single and homogeneous experience, and people with arthritis describe different types of pain, including pain on weight bearing, joint movement, or at rest, as well as aching pains or burning pains. Different pain qualities might well reflect different underlying pain mechanisms (2). Pain quality is not measurable in animal models, but various pain behaviors have also been associated with different pathophysiologic mechanisms. A reduced threshold for paw withdrawal from a normally non-noxious punctate stimulus has been associated with evidence of central sensitization in rodents and is consistent with low pain thresholds to mechanical stimuli distal to an OA joint in humans (3). Reduced threshold to mechanical pressure on a mouse's knee might model increased joint line tenderness in human arthritis, a characteristic interpreted in rheumatoid arthritis as a sign of active synovitis. Miller and colleagues' data suggest that both of these types of pain might at least sometimes be dependent on $Na_V1.8$-expressing peripheral sensory nerves and suppressible by $G_{i/o}$ activation.

Unfortunately, many analgesic interventions that have shown great promise in animal models have failed to impress through randomized controlled trials in arthritis in humans. Many explanations have been proposed for this

David A. Walsh, PhD, FRCP: Arthritis Research UK Pain Centre, University of Nottingham, Nottingham, UK.
Address correspondence to David A. Walsh, PhD, FRCP, Arthritis Research UK Pain Centre, University of Nottingham Clinical Sciences Building, City Hospital, Hucknall Road, Nottingham NG5 1PB, UK. E-mail: David.walsh@nottingham.ac.uk.
Submitted for publication March 27, 2017; accepted in revised form April 11, 2017.

lack of translational success from laboratory to clinic. Clearly, humans are different from mice, and pain mechanisms in humans might differ fundamentally from those in rodents. Animal models of arthritis pain are designed to minimize suffering of the animal, and the protracted time course of human arthritis is ideally avoided in experimental studies. Miller and colleagues' data highlight that findings in mouse models might also not translate to other time points within the same model. In the same way, effective analgesics in acute pain in humans might not provide benefit for chronic arthritis pain. Opiates, which also act through $G_{i/o}$ proteins, are effective in acute musculoskeletal pain but have limited and typically only very partial benefit for chronic pain in humans, for example, in OA or low back pain. Their underwhelming benefit might partly be attributed to tolerance with chronic use and to adverse events. It is also important to consider that they might not work simply because different pain mechanisms are at play.

So what additional mechanisms might contribute to chronic arthritis pain? Miller et al rightly draw attention to possible central pain mechanisms. Arthritis pain is probably not often centrally initiated, in contrast to chronic pain after cerebrovascular accident. Central mechanisms can, however, importantly augment evoked pain, both allodynia (pain in response to a normally non-noxious stimulus) and hyperalgesia (increased pain experienced with a standardized noxious stimulus). Evoked pain requires an intact peripheral sensory system, and therefore allodynia and hyperalgesia can be inhibited by peripherally acting analgesics as well as by agents targeting central pain processing. Inhibiting $Na_V1.8$-expressing neurons increased paw withdrawal thresholds during the early phases of the DMM model, again demonstrating that at least some centrally augmented pain might be improved by peripherally acting analgesics. Evidence of central sensitization is commonly observed in severe, late-stage OA in humans but does not preclude pain relief from joint replacement surgery, an intervention specifically designed to reduce peripheral nociceptive inputs. However, not all people undergoing arthroplasty experience adequate pain relief, suggesting that non-nociceptive inputs from the postsurgical joint might continue to be sufficient to activate central pain pathways (allodynia). With increasing chronicity, central pain augmentation might lose its dependence on peripheral nociceptive input, perhaps due to structural change within the central nervous system (4) or long-lasting functional change, as might be driven by epigenetic modifications (5). Identifying these mechanisms of chronicity could lead to novel interventions that maintain capacity for neuronal plasticity and permit reversal of chronic pain.

Another possibility is that peripheral pain mechanisms change during the progression of arthritis. Miller et al comment on a predominant role of inflammation in the early stages of the DMM model. Synovitis is also a characteristic of established OA in humans; it is associated with OA pain (6), and pain relief may be achieved at least in some patients through antiinflammatory medications (either delivered systemically or by intraarticular injection). The contribution of subchondral bone to OA pain might vary between early and late disease, when the osteochondral junction is breached and bone marrow lesions are associated with regions of cartilage defects (7). Sensory nerve terminals might eventually grow into articular structures that are not innervated in the normal joint, for example, in the inner regions of knee menisci or in noncalcified articular cartilage, becoming exposed to unaccustomed mechanical or chemical stimuli (8). Gene expression patterns in dorsal root ganglia also change through the development of arthritis (9,10), and $G_{i/o}$ activation might have less potential to inhibit nociceptive drive once different nerve types and signaling pathways become recruited. Better understanding of peripheral pain mechanisms might lead to novel treatments for chronic arthritis pain. If those mechanisms are specific for chronic (pathologic) rather than acute pain, analgesics might be developed that do not impair normal protective responses (and might even lack acute analgesic efficacy) despite offering relief to those with chronic arthritis.

Animal models are developed to mimic a particular human condition, and the DMM model was devised to resemble human OA. It reflects how internal derangement in human knees can lead to OA, although the time course for OA development in humans is usually much more protracted than that observed in mice. Indeed, by 16 weeks, the histologic, molecular, and behavioral characteristics of the DMM model closely resemble those of late-stage human OA. It is less clear, however, to what extent pathologic changes shortly after surgery reflect those in the more common, idiopathic forms of OA seen in humans. Despite these reservations, the early time points in the pathogenesis of the DMM model might give useful insights into other painful articular conditions, for example, sports injuries and inflammatory joint disease. Specific analgesic approaches might only be effective at specific times for specific symptoms in OA, but they might additionally be effective for other diagnostic groups that share discrete pain mechanisms.

Miller and colleagues are to be congratulated for their well-designed and thought-provoking research. Like much of the best research, it might raise more questions than are answered, but the direction of travel is clear. Each increment to our understanding is leading us to better explain why different people might respond differently to the same intervention and, ultimately, who will be most likely to benefit from which interventions and when. What can be seen by some as inconsistency or lack of

robust translational validity in animal models might better be seen as modeling the heterogeneity of the human experience of arthritis pain. Understanding this heterogeneity should lead us ever closer to a more effective and personalized approach to rheumatology.

AUTHOR CONTRIBUTIONS

Dr. Walsh drafted the article, revised it critically for important intellectual content, and approved the final version to be published.

REFERENCES

1. Miller RE, Ishihara S, Bhattacharyya B, Delaney A, Menichella DM, Miller RJ, et al. Chemogenetic inhibition of pain neurons in a mouse model of osteoarthritis. Arthritis Rheumatol 2017;69: 1429–39.
2. Moreton BJ, Tew V, das Nair R, Wheeler M, Walsh DA, Lincoln NB. Pain phenotype in patients with knee osteoarthritis: classification and measurement properties of painDETECT and self-report Leeds assessment of neuropathic symptoms and signs scale in a cross-sectional study. Arthritis Care Res (Hoboken) 2015;67:519–28.
3. Suokas AK, Walsh DA, McWilliams DF, Condon L, Moreton B, Wylde V, et al. Quantitative sensory testing in painful osteoarthritis: a systematic review and meta-analysis. Osteoarthritis Cartilage 2012; 20:1075–85.
4. Gwilym SE, Filippini N, Douaud G, Carr AJ, Tracey I. Thalamic atrophy associated with painful osteoarthritis of the hip is reversible after arthroplasty: a longitudinal voxel-based morphometric study. Arthritis Rheum 2010;62:2930–40.
5. Geranton SM, Tochiki KK. Regulation of gene expression and pain states by epigenetic mechanisms. Prog Mol Biol Transl Sci 2015;131:147–83.
6. Yusuf E, Kortekaas MC, Watt I, Huizinga TW, Kloppenburg M. Do knee abnormalities visualised on MRI explain knee pain in knee osteoarthritis? A systematic review. Ann Rheum Dis 2011;70:60–7.
7. Xu L, Hayashi D, Roemer FW, Felson DT, Guermazi A. Magnetic resonance imaging of subchondral bone marrow lesions in association with osteoarthritis. Semin Arthritis Rheum 2012;42:105–18.
8. Ashraf S, Wibberley H, Mapp PI, Hill R, Wilson D, Walsh DA. Increased vascular penetration and nerve growth in the meniscus: a potential source of pain in osteoarthritis. Ann Rheum Dis 2011;70:523–9.
9. Fernihough J, Gentry C, Bevan S, Winter J. Regulation of calcitonin gene-related peptide and TRPV1 in a rat model of osteoarthritis. Neurosci Lett 2005;388:75–80.
10. Miller RE, Tran PB, Das R, Ghoreishi-Haack N, Ren D, Miller RJ, et al. CCR2 chemokine receptor signaling mediates pain in experimental osteoarthritis. Proc Natl Acad Sci U S A 2012;109: 20602–7.

ARTHRITIS & RHEUMATOLOGY
Vol. 69, No. 7, July 2017, pp 1346–1349
DOI 10.1002/art.40095

EDITORIAL

Rituximab in the Treatment of Sjögren's Syndrome: Is It the Right or Wrong Drug?

Hendrika Bootsma, Frans G. M. Kroese, and Arjan Vissink

The presence of anti-SSA/Ro and/or anti-SSB/La autoantibodies, elevated plasma levels of gamma globulins and rheumatoid factor (RF), higher expression levels of Bruton's tyrosine kinase in B cells, and an increased risk of developing lymphomas, particularly mucosa-associated lymphoid tissue (MALT) lymphomas, all point toward a major role of B cells in the pathogenesis of primary Sjögren's syndrome (SS) (1). Because of this role, rituximab, a chimeric anti-CD20 monoclonal antibody, has been considered a potentially potent biologic disease-modifying antirheumatic drug to reduce disease activity in primary SS. Rituximab results in significant depletion of CD20+ B cells via several mechanisms. Open-label and smaller randomized placebo-controlled trials (2) as well as the larger Tolerance and Efficacy of Rituximab in Primary Sjögren's Syndrome (TEARS) trial (3) revealed that rituximab treatment shows beneficial effects in patients with primary SS. However, as reported in this issue of *Arthritis & Rheumatology*, rituximab treatment showed no beneficial effects at all in a new larger multicenter placebo-controlled trial, the Trial of Anti–B Cell Therapy in Patients with Primary Sjögren's Syndrome (TRACTISS) (4).

The question now arises as to whether rituximab is indeed a failing drug or is effective in only a selected category of patients with primary SS. In other words, should patients with primary SS who are treated with rituximab be better defined to enhance success of this promising treatment modality, given that beneficial effects have been reported at clinical, biologic, histologic, and ultrasonographic levels (2,3,5)? Moreover, post hoc analyses have identified possible predictors of response (6). As currently classified (7), primary SS is a heterogeneous disease (8), while rituximab might be of value to a particular, yet to be identified, subgroup of patients with primary SS and thus should not be used as a general treatment for primary SS. Therefore, before rituximab can be considered a successful or failing drug, it is necessary to assess whether it is effective in a specific subgroup of patients with primary SS (precision medicine).

Effects of rituximab on B cell hyperactivity in primary SS

Rituximab treatment of patients with primary SS results consistently in an almost complete depletion of B cells and plasmablasts in peripheral blood, which lasts up to 24–36 weeks posttreatment (9). Accordingly, a significant reduction of B cells and plasma cells was seen in minor and major salivary glands, without affecting the number of T cells (9). High absolute numbers of B cells in parotid glands have even been shown to predict responsiveness to rituximab (6). This reduction in B cells and antibody-secreting cells explains the observed decrease in total IgG and autoantibodies (RF, anti-SSA, anti-SSB) in serum. Also, other B cell activation markers, such as β_2-microglobulin and free light chains, decrease as a consequence of B cell depletion. Clearly not all plasma cells in salivary gland tissue are depleted, since most plasma cells are long-lived and are not directly targeted by rituximab. Persisting plasma cells have been found in parotid glands up to 1 year after treatment. B cells are also indirectly affected by the effect of B cell depletion on the T cell compartment. Circulating follicular helper T (Tfh) cells and to a lesser extent Th17 cells decrease after treatment, together with serum levels of their signature cytokines interleukin-21 (IL-21) and IL-17. The lower Tfh cell activity may be responsible for significantly reduced numbers of germinal centers in salivary glands after treatment with rituximab (6).

Hendrika Bootsma, MD, PhD, Frans G. M. Kroese, PhD, Arjan Vissink, DMD, MD, PhD: University of Groningen and University Medical Center Groningen, Groningen, The Netherlands.

Dr. Bootsma has received consulting fees and/or honoraria from Bristol-Myers Squibb, GlaxoSmithKline, Roche, and UCB (less than $10,000 each) and research grants from these companies. Dr. Kroese has received consulting fees and/or honoraria from Bristol-Myers Squibb (less than $10,000).

Address correspondence to Hendrika Bootsma, MD, PhD, Department of Rheumatology and Clinical Immunology, AA21, University Medical Center Groningen, PO Box 30.001, 9700 RB Groningen, The Netherlands. E-mail: h.bootsma@umcg.nl.

Submitted for publication February 13, 2017; accepted in revised form March 7, 2017.

The central position of B cells as a target of therapy is further illustrated by positive results of other recent trials of biologic agents that are not based on the direct depletion of B cells but that do target these cells either directly or indirectly (2). These biologic agents comprise belimumab, which binds to BAFF (10), resulting in less survival and less activation of B cells, and abatacept (11), which blocks costimulation of T cells and, consequently, T cell–dependent activation of B cells (1). Although several cytokines and chemokines decrease after rituximab treatment, BAFF levels increase, likely as the result of the relative unavailability of B cells, which express BAFF-binding receptors. Since high BAFF levels have been associated with humoral autoimmunity, a current trial is assessing whether the addition of belimumab enhances the efficacy of rituximab (ClinicalTrials.gov identifier: NCT02631538).

An important finding is that rituximab is the only biologic agent yet applied to the treatment of primary SS that also results in restoration of salivary gland tissue (6,12). This is reflected by the declining number and severity of lymphoepithelial lesions in glandular tissue (6). Taken together, these biologic findings provide a rationale for the clinical effects observed after rituximab treatment.

Clinical efficacy of rituximab

Effects of rituximab treatment on salivary flow are inconsistent. Although several studies showed improvement or stabilization of saliva production (13–15), other studies (3,16) did not show such an effect. A possible explanation for this discrepancy is that the studies showing no effect on saliva production also included patients who had very low saliva production at baseline. Based on the secretion of unstimulated whole saliva at baseline, the patients in the study by Meijer et al (14) were apparently less heterogeneous than those in the TEARS trial (3). St.Clair et al (16) even included patients without unstimulated whole saliva secretion at baseline, and such patients are presumably not likely to show functional improvement. The TRACTISS trial showed that unstimulated whole saliva secretion by rituximab-treated patients remained stable, while it deteriorated in placebo-treated patients. The latter was the only affirmative observation in the TRACTISS trial. Thus, rituximab treatment may have a beneficial effect on salivary gland function, as the various studies provide evidence of at least a stabilization of the salivary flow rate. These observations are consistent with recovery of salivary gland parenchyma as observed in histopathology studies (6,12) and with improved parotid parenchyma echostructure (17).

The effect of rituximab on tear gland function has not been established, since with the exception of the study by Carubbi et al (15) and the TEARS trial, most studies do not show an effect on the Schirmer I test score. The Schirmer I test is not sufficiently sensitive to detect small changes in tear production. However, rituximab has been shown to improve corneal integrity, as measured by lissamine green and rose bengal staining (13,14). This apparent recovery of corneal integrity also indicates the beneficial effect of rituximab. Except for the TRACTISS trial (4), positive results with regard to symptoms of oral and ocular dryness were reported in all studies of primary SS (2).

Extraglandular manifestations are common in primary SS, of which fatigue is the most common. Again, with the exception of the TRACTISS trial, fatigue was shown to be reduced in rituximab-treated patients with primary SS (2). The effect of rituximab on systemic disease activity, as reflected in scores on the European League Against Rheumatism (EULAR) Sjögren's Syndrome Disease Activity Index (ESSDAI) (18) and clinESSDAI (the clinical ESSDAI without the biologic domain) (19), was assessed in some studies. Importantly, baseline ESSDAI scores varied greatly between studies. Generally, studies of patients with rather high baseline ESSDAI scores showed a significant reduction of disease activity following rituximab treatment (15,20). Patients in the TRACTISS trial had low baseline ESSDAI scores, which may explain why there was no significant effect reported for the ESSDAI score. Notwithstanding comparable baseline scores (3,15,20), the TEARS trial also did not demonstrate an effect on the ESSDAI score. The lack of an effect on the ESSDAI score in the TEARS trial might possibly be explained by relatively low involvement of domains that showed the largest reductions in the other studies (articular, glandular, constitutional, hematologic, and biologic domains) (15,20,21). Furthermore, the ESSDAI score was assessed retrospectively in the TEARS trial. It is possible that different patient characteristics may account for the observed apparent differences in study outcomes based upon the ESSDAI score. In addition to being effective in the treatment of systemic disease activity in primary SS, rituximab has been shown to be an effective treatment for MALT lymphomas in primary SS (22).

Lack of consistency between studies in the efficacy of rituximab

Variations in the efficacy of rituximab in the treatment of primary SS can result from differences in patient populations in the various studies and the outcome parameters applied, as well as from heterogeneity of primary SS. For example, a major difference between the TRACTISS trial (4) with its negative results and other trials (2) with

positive results is the inclusion of a more heterogeneous cohort of patients with primary SS in the TRACTISS trial, which resulted in fewer selected patients with primary SS. In the TEARS trial (3), the other large placebo-controlled trial that also had a broader range of patients, efficacy of rituximab was shown after application of a composite outcome parameter (5).

An important inclusion criterion is the use of background immunosuppressive therapy and other comedication. In the TEARS and TRACTISS trials, patients were allowed to continue their use of corticosteroids, hydroxychloroquine, nonsteroidal antiinflammatory drugs, pilocarpine, and antidepressants, all drugs that can affect treatment outcome. Furthermore, the minimal residual unstimulated whole saliva flow of the included patients was simply defined as greater than zero, which does not guarantee that the salivary glands have some remaining function. It is also unknown how many of the subjects in the TRACTISS trial (4) had a positive salivary gland biopsy result. Thus, it is not clear what subcategories of patients with primary SS were included in the various studies (7). The evidence that there are both responders and nonresponders in terms of ESSDAI score change strongly supports the notion that there is heterogeneity between patients with primary SS included in the various trials, some of whom do and some of whom do not respond to treatment (6). Thus, yet unspecified patient characteristics may influence treatment response. The current applied classification criteria are too broad to select targeted patients with primary SS for trials (7). In an exciting new development, Lendrem et al (8) identified 4 distinct primary SS clinical phenotypes. These phenotypes were defined on the basis of hierarchical cluster analysis of patient-reported pain, fatigue, dryness, anxiety, and depression. Importantly, these 4 phenotypes exhibited marked differences in a variety of biologic parameters. Patients within these clusters may respond differently to rituximab treatment, in terms of both subjective and objective parameters.

The discrepancy between studies may also be related to the variety of outcome measures. The TEARS and TRACTISS trials have used changes in visual analog scale (VAS) scores as primary outcome measures of subjective symptoms. Although targeting subjective symptoms is important to improve quality of life, these VAS scores may not be sensitive to change. The response goals were set quite high (≥30 mm change in 2 of 4 VAS scores in the TEARS trial, 30% change of either oral dryness or fatigue VAS score in the TRACTISS trial). Such a response goal is probably too high, as a decrease of at least 15% in the EULAR Sjögren's Syndrome Patient Reported Index (ESSPRI) score (23) has been reported as a minimal clinically important improvement in primary SS (21). Interestingly, Cornec et al (5) proposed a new data-driven composite outcome measure that combines objective manifestations and subjective symptoms. Applying this outcome measure showed that rituximab had a beneficial effect in the TEARS trial. An effort by the EULAR Sjögren's Task Force to formulate a new response index is currently underway.

How to design, and select patients for, rituximab trials

As we have noted earlier (7), the 2016 American College of Rheumatology/EULAR classification criteria for primary SS (24) do not guarantee that the proper patients with primary SS are selected for studies. These criteria need refinement. Therefore, when designing a trial to show efficacy of rituximab or other biologic agents, the first step should be to define what specific baseline characteristics a subject with primary SS should have in order to be included in a particular trial. The information from the studies performed with rituximab or other biologic agents could be used to identify the subpopulation of patients with primary SS who will likely respond to a particular biologic agent. There is also a difficulty in applying strict inclusion criteria when recruiting eligible patients for trials. For example, Oni et al (25) showed that when applying specific outcome measures, such as an ESSPRI score of ≥5 and an ESSDAI score of ≥5, with requirements for unstimulated whole saliva flow greater than zero and anti-Ro positivity, the pool of eligible participants will be greatly reduced. However, if the inclusion criteria are too general, the result will be a failing trial unless the biologic agent tested has such a general beneficial action that it is effective in most subcategories of patients with primary SS.

Another critical step in trial design is to identify centers that have the tools to properly select patients with primary SS who have the required specific characteristics; these centers must also have the experience to apply the outcome parameters reliably. For many outcome parameters, specifically trained pathologists (experienced in performing targeted histologic evaluation), ophthalmologists (trained in scoring ocular staining), oral and maxillofacial surgeons/specialists in oral medicine (experienced in assessing salivary gland function and obtaining the required type of salivary gland biopsy specimen), and rheumatologists (experienced in scoring the ESSDAI) are needed. It is recommended that these expert centers perform trials that are able to include reasonable numbers of SS patients. Finally, particularly in multicenter trials, the inherent interindividual variations in applying inclusion criteria and assessment tools cannot be overcome by training and calibration if only a few subjects are included.

Based on the results of the TRACTISS trial, one might be reluctant to use rituximab to treat patients with

primary SS. However, some studies show that rituximab has a beneficial effect in a subgroup of patients, i.e., non-responders to rituximab treatment can be characterized, and rituximab has objective biologic effects (6). In other words, rituximab is not the wrong drug in primary SS, but it has to be applied in a particular subgroup of patients with the disease. The same will probably hold true for other biologic agents that are tested in primary SS. The better we can identify the specific characteristics of a patient with primary SS, the better we can prescribe a particular targeted biologic agent. Precision medicine is about to become a reality in primary SS!

AUTHOR CONTRIBUTIONS

All authors were involved in drafting the article or revising it critically for important intellectual content, and all authors approved the final version to be published.

REFERENCES

1. Kroese FG, Abdulahad WH, Haacke E, Bos NA, Vissink A, Bootsma H. B-cell hyperactivity in primary Sjögren's syndrome. Expert Rev Clin Immunol 2014;10:483–99.
2. Van Nimwegen JF, Moerman RV, Sillevis Smitt N, Brouwer E, Bootsma H, Vissink A. Safety of treatments for primary Sjögren's syndrome. Expert Opin Drug Saf 2016;15:513–24.
3. Devauchelle-Pensec V, Mariette X, Jousse-Joulin S, Berthelot JM, Perdriger A, Puéchal X, et al. Treatment of primary Sjögren syndrome with rituximab: a randomized trial. Ann Intern Med 2014;160:233–42.
4. Bowman SJ, Everett CC, O'Dwyer JL, Emery P, Pitzalis C, Ng WF, et al. Randomized controlled trial of rituximab and cost-effectiveness analysis in treating fatigue and oral dryness in primary Sjögren's syndrome. Arthritis Rheumatol 2017;69:1440–50.
5. Cornec D, Devauchelle-Pensec V, Mariette X, Jousse-Joulin S, Berthelot JM, Perdriger A, et al. Development of the Sjögren's Syndrome Responder Index, a data-driven composite endpoint for assessing treatment efficacy. Rheumatology (Oxford) 2015;54:1699–708.
6. Delli K, Haacke EA, Kroese FG, Pollard RP, Ihrler S, van der Vegt B, et al. Towards personalised treatment in primary Sjögren's syndrome: baseline parotid histopathology predicts responsiveness to rituximab treatment. Ann Rheum Dis 2016;75:1933–8.
7. Vissink A, Bootsma H. Connective tissue diseases: refining the classification criteria for primary Sjögren syndrome. Nat Rev Rheumatol 2017;13:10–2.
8. Lendrem D, Howard Tripp N, Mariette X, Johnsen SJ, Tarn J, Hackett K, et al. Rethinking primary Sjögren's syndrome: stratification by clinical phenotypes to improve understanding of disease pathogenesis, trial design, clinical management and prospective health gains? [abstract]. Arthritis Rheumatol 2016;68 Suppl 10. URL: http://acrabstracts.org/abstract/rethinking-primary-sjogrens-syndrome-stratification-by-clinical-phenotypes-to-improve-understanding-of-disease-pathogenesis-trial-design-clinical-management-and-prospective-health-gains/.
9. Verstappen GM, Kroese FG, Meiners PM, Corneth OB, Huitema MG, Haacke EA, et al. B-cell depletion therapy normalizes circulating follicular Th cells in primary Sjögren syndrome. J Rheumatol 2017;44:49–58.
10. De Vita S, Quartuccio L, Seror R, Salvin S, Ravaud P, Fabris M, et al. Efficacy and safety of belimumab given for 12 months in primary Sjögren's syndrome: the BELISS open-label phase II study. Rheumatology (Oxford) 2015;54:2249–56.
11. Meiners PM, Vissink A, Kroese FG, Spijkervet FK, Smitt-Kamminga NS, Abdulahad WH, et al. Abatacept treatment reduces disease activity in early primary Sjögren's syndrome (open-label proof of concept ASAP study). Ann Rheum Dis 2014;73:1393–6.
12. Pijpe J, Meijer JM, Bootsma H, van der Wal JE, Spijkervet FK, Kallenberg CG, et al. Clinical and histologic evidence of salivary gland restoration supports the efficacy of rituximab treatment in Sjögren's syndrome. Arthritis Rheum 2009;60:3251–6.
13. Pijpe J, van Imhoff GW, Spijkervet FK, Roodenburg JL, Wolbink GJ, Mansour K, et al. Rituximab treatment in patients with primary Sjögren's syndrome: an open-label phase II study. Arthritis Rheum 2005;52:2740–50.
14. Meijer JM, Meiners PM, Vissink A, Spijkervet FK, Abdulahad W, Kamminga N, et al. Effectiveness of rituximab treatment in primary Sjögren's syndrome: a randomized, double-blind, placebo-controlled trial. Arthritis Rheum 2010;62:960–8.
15. Carubbi F, Cipriani P, Marrelli A, Benedetto P, Ruscitti P, Berardicurti O, et al. Efficacy and safety of rituximab treatment in early primary Sjögren's syndrome: a prospective, multi-center, follow-up study. Arthritis Res Ther 2013;15:R172.
16. St.Clair EW, Levesque MC, Prak ET, Vivino FB, Alappatt CJ, Spychala ME, et al. Rituximab therapy for primary Sjögren's syndrome: an open-label clinical trial and mechanistic analysis. Arthritis Rheum 2013;65:1097–106.
17. Cornec D, Jousse-Joulin S, Costa S, Marhadour T, Marcorelles P, Berthelot JM, et al. High-grade salivary-gland involvement, assessed by histology or ultrasonography, is associated with a poor response to a single rituximab course in primary Sjögren's syndrome: data from the TEARS randomized trial. PLoS One 2016b;11:e0162787.
18. Seror R, Ravaud P, Bowman SJ, Baron G, Tzioufas A, Theander E, et al, on behalf of the EULAR Sjögren's Task Force. EULAR Sjögren's Syndrome Disease Activity Index: development of a consensus systemic disease activity index for primary Sjögren's syndrome. Ann Rheum Dis 2010;69:1103–9.
19. Seror R, Meiners P, Baron G, Bootsma H, Bowman SJ, Vitali C, et al, EULAR Sjögren Task Force. Development of the ClinESSDAI: a clinical score without biological domain. A tool for biological studies. Ann Rheum Dis 2016;75:1945–50.
20. Moerman RV, Arends S, Meiners PM, Brouwer E, Spijkervet FK, Kroese FG, et al. EULAR Sjögren's Syndrome Disease Activity Index (ESSDAI) is sensitive to show efficacy of rituximab treatment in a randomised controlled trial. Ann Rheum Dis 2014;73:472–4.
21. Seror R, Bootsma H, Saraux A, Bowman SJ, Theander E, Brun JG, et al. Defining disease activity states and clinically meaningful improvement in primary Sjögren's syndrome with EULAR Primary Sjögren's Syndrome Disease Activity (ESSDAI) and Patient-Reported Indexes (ESSPRI). Ann Rheum Dis 2016;75:382–9.
22. Pollard RP, Pijpe J, Bootsma H, Spijkervet FK, Kluin PM, Roodenburg JL, et al. Treatment of mucosa-associated lymphoid tissue lymphoma in Sjögren's syndrome: a retrospective clinical study. J Rheumatol 2011;38:2198–208.
23. Seror R, Ravaud P, Mariette X, Bootsma H, Theander E, Hansen A, et al. EULAR Sjögren's Syndrome Patient Reported Index (ESSPRI): development of a consensus patient index for primary Sjögren's syndrome. Ann Rheum Dis 2011;70:968–72.
24. Shiboski CH, Shiboski SC, Seror R, Criswell LA, Labetoulle M, Lietman TM, et al, and the International Sjögren's Syndrome Criteria Working Group. 2016 American College of Rheumatology/European League Against Rheumatism classification criteria for primary Sjögren's syndrome: a consensus and data-driven methodology involving three international patient cohorts. Arthritis Rheumatol 2017;69:35–45.
25. Oni C, Mitchell S, James K, Ng WF, Griffiths B, Hindmarsh V, et al. Eligibility for clinical trials in primary Sjögren's syndrome: lessons from the UK Primary Sjögren's Syndrome Registry. Rheumatology (Oxford) 2016;55:544–52.

ARTHRITIS & RHEUMATOLOGY
Vol. 69, No. 7, July 2017, pp 1350–1362
DOI 10.1002/art.40076

REVIEW

Extracellular Vesicles in Joint Inflammation

Andrew D. Foers,[1] Lesley Cheng,[2] Andrew F. Hill,[2] Ian P. Wicks,[1] and Ken C. Pang[3]

Introduction

The pathologic mechanisms underlying the development and maintenance of rheumatoid arthritis (RA) are incompletely understood but broadly involve persistent joint inflammation that can lead to irreversible joint damage. In recent years, extracellular vesicles (EVs) have attracted increasing attention for potential roles in inflammation, including in inflammatory arthritis (1).

EVs are released from cells and are found in all types of bodily fluids. They are typically classified as exosomes, microvesicles, or apoptotic bodies, according to the mode of biogenesis (Figure 1). Exosomes and microvesicles are continually released from cells, whereas apoptotic bodies are released only when cells undergo apoptosis. The majority of research investigating EVs has been on exosomes and microvesicles, and these will be the focus of this review. EV nomenclature tends to be inconsistent within the literature, since it is technically difficult to isolate specific classes of EVs, leading to methodologic variability and a lack of consensus on not only optimal isolation techniques, but also what types of EVs are enriched (2). To ensure consistency within this review, we have therefore reviewed the isolation techniques within each study and adopted a consistent nomenclature. If a technique does not convincingly enrich for a particular class of EV, the general term EV is used.

EVs contain a heterogeneous collection of proteins, RNAs and lipids, which reflect the state of the particular cells from which EVs are derived. Interactions between EVs and other cells can occur in several ways (Figure 2), enabling the molecular cargo of an EV to exert functional effects on recipient cells. It is clear that EVs can deliver molecules that drive disease. For example, EVs have been implicated in neurodegenerative disease through traffic of infectious, prion-like proteins (for review, see ref. 3), and in cancer through the transfer of oncoproteins to promote metastasis (4). EVs can also functionally impact recipient cells though the transfer of RNAs, such as microRNAs (miRNAs), which can influence the expression of target genes, including those involved in inflammatory processes (5,6).

In the context of inflammation, EVs have been shown to exert both pro- and antiinflammatory effects. For example, exosomes from heat-stressed hepatocytes potently stimulate tumor necrosis factor (TNF) expression in recipient macrophages via exosome-associated Hsp70 (7). Similarly, EVs from neuronal stem/precursor cells exposed to Th1 cytokines can activate STAT-1 signaling via the delivery of EV-bound interferon-γ (IFNγ) to its cognate receptor on recipient cells (8). Moreover, exosomes purified from human amniotic fluid or malignant ascites fluid can promote STAT-3 and NF-κB signaling in recipient monocytes, through activation of the Toll-like receptors (TLRs) TLR-2 and TLR-4, leading to the release of cytokines such as TNF, interleukin-1β (IL-1β), and IL-6 (9). Similarly, exosomes derived from tumor cells contain specific miRNAs that act as agonists for endosomal TLRs in recipient immune cells (10). In contrast, some EVs have antiinflammatory effects. Suppressor of cytokine signaling (SOCS) family proteins are key suppressors of inflammation through inhibition of JAK/STAT signaling (11). Exosomes and microvesicles isolated from alveolar macrophages contain SOCS-1 and SOCS-3, respectively, both of which can attenuate STAT signaling

Supported by the National Health and Medical Research Council (grant 1064591) and the Reid Family Trust.

[1]Andrew D. Foers, BSc (Hons), Ian P. Wicks, MBBS, FRACP, PhD: The Walter & Eliza Hall Institute of Medical Research and The University of Melbourne, Parkville, Victoria, Australia; [2]Lesley Cheng, BMsc (Hons), PhD, Andrew F. Hill, BSc (Hons), DIC, PhD: Latrobe University, Bundoora, Victoria, Australia; [3]Ken C. Pang, MBBS (Hons), BMedSc, PhD, FRACP: Murdoch Childrens Research Institute and The University of Melbourne, Parkville, Victoria, Australia.

Address correspondence to Ian P. Wicks, MBBS, FRACP, PhD, The Walter & Eliza Hall Institute, Parkville, Victoria 3052, Australia (e-mail: wicks@wehi.edu.au); or to Ken C. Pang, MBBS (Hons), BMedSc, PhD, FRACP, Murdoch Childrens Research Institute, Parkville, Victoria 3052, Australia (e-mail: ken.pang@mcri.edu.au).

Submitted for publication November 14, 2016; accepted in revised form February 14, 2017.

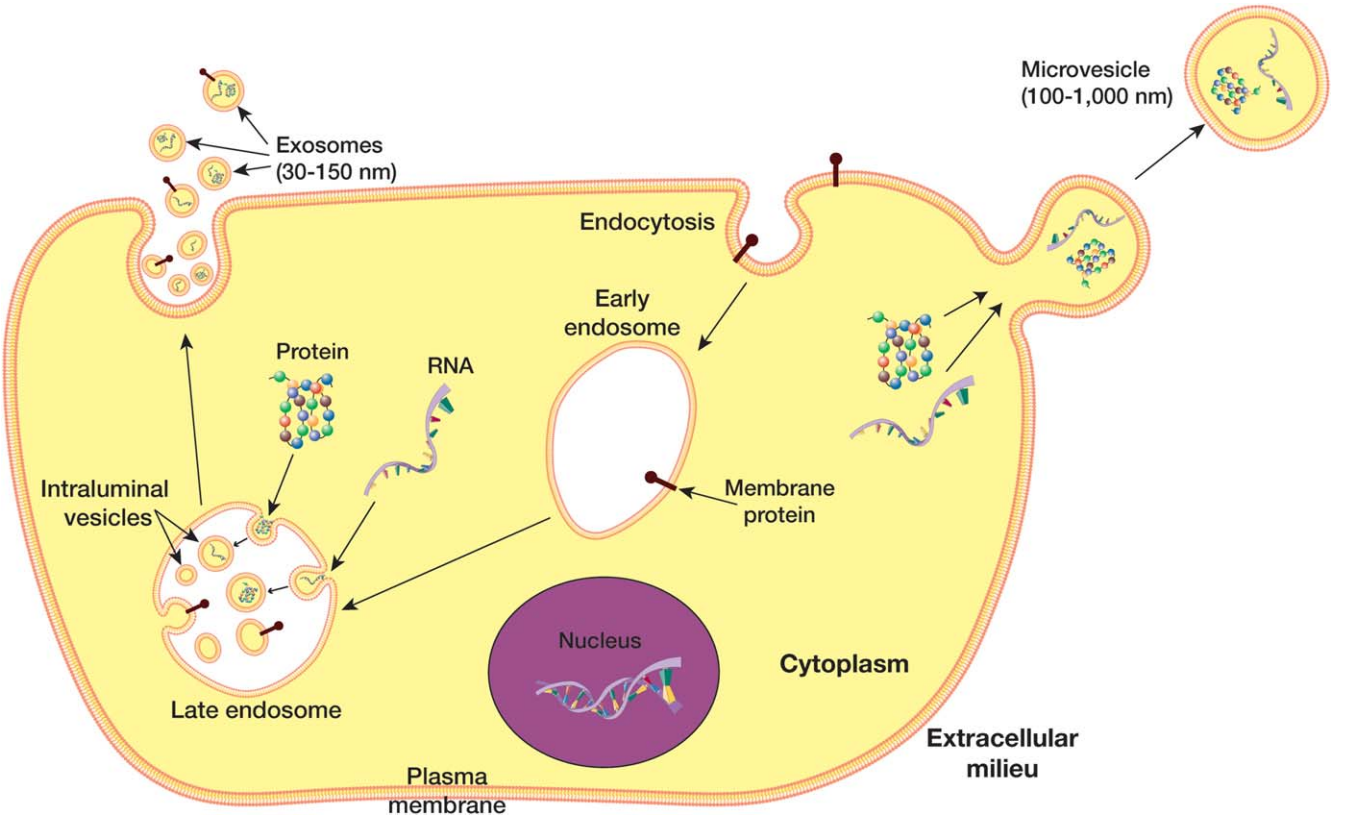

Figure 1. Biogenesis of exosomes and microvesicles. Invagination of the late endosome forms intraluminal vesicles ranging from 30 to 150 nm. Fusion of the late endosome (also known as a multivesicular body) with the plasma membrane releases the vesicles into the extracellular milieu, and the vesicles are then termed "exosomes." Microvesicles are formed by outward protrusion of the plasma membrane and are typically larger than exosomes at 100–1,000 nm. (Note that some groups use the term "microparticle" synonymously with "microvesicle," whereas others use "microparticle" as a general term that encompasses exosomes, microvesicles, and nonvesicular particulate of a similar size and/or density. To avoid confusion, we have used the term "microvesicle.") Both exosomes and microvesicles contain a range of molecules from the cell of origin, including proteins and RNAs.

(12). EVs derived from malignant ascites fluid can promote CD25 and FoxP3 expression in recipient T cells, leading to the expansion of immunosuppressive, regulatory cells that release inhibitory cytokines and increase resistance to apoptosis (13).

Separate from biologic effects, EVs are also proving to be an important source of novel biomarkers, since the molecular cargo of EVs provides information about the cell of origin. Released EVs can be isolated from readily accessible fluids such as blood and urine. Together, these properties make EVs well suited as sources of biomarkers, as elegantly demonstrated by the finding of cancer-specific messenger RNA in serum microvesicles isolated from patients with glioblastoma (14). More recently, serum exosomes containing glypican 1 were found to distinguish between patients with pancreatic cancer, those with benign pancreatic disease, and healthy controls with absolute sensitivity and specificity. Interestingly, the presence of glypican 1 in circulating exosomes preceded the appearance of lesions detectable by magnetic resonance imaging in a mouse model of pancreatic cancer, prompting hope that exosomal glypican 1 might form the basis for an early diagnostic test (15). Indeed, there is now optimism regarding the use of exosomes for "liquid biopsies" in the oncology field, and the first exosome-based diagnostic test was recently brought to market. Exosomal biomarkers may also be useful outside of oncology. Cheng et al (16) recently showed that serum EV miRNAs distinguished patients with Alzheimer's disease from healthy controls, with high sensitivity and specificity. Moreover, this miRNA signature also showed promise in identifying apparently healthy subjects who developed Alzheimer's disease at a later stage.

Therapeutically, exosomes are being investigated for drug delivery, taking advantage of a natural role in transporting biologic cargo between cells within the body. For example, small interfering RNA (siRNA)–based therapies have undergone clinical trials for a broad range of

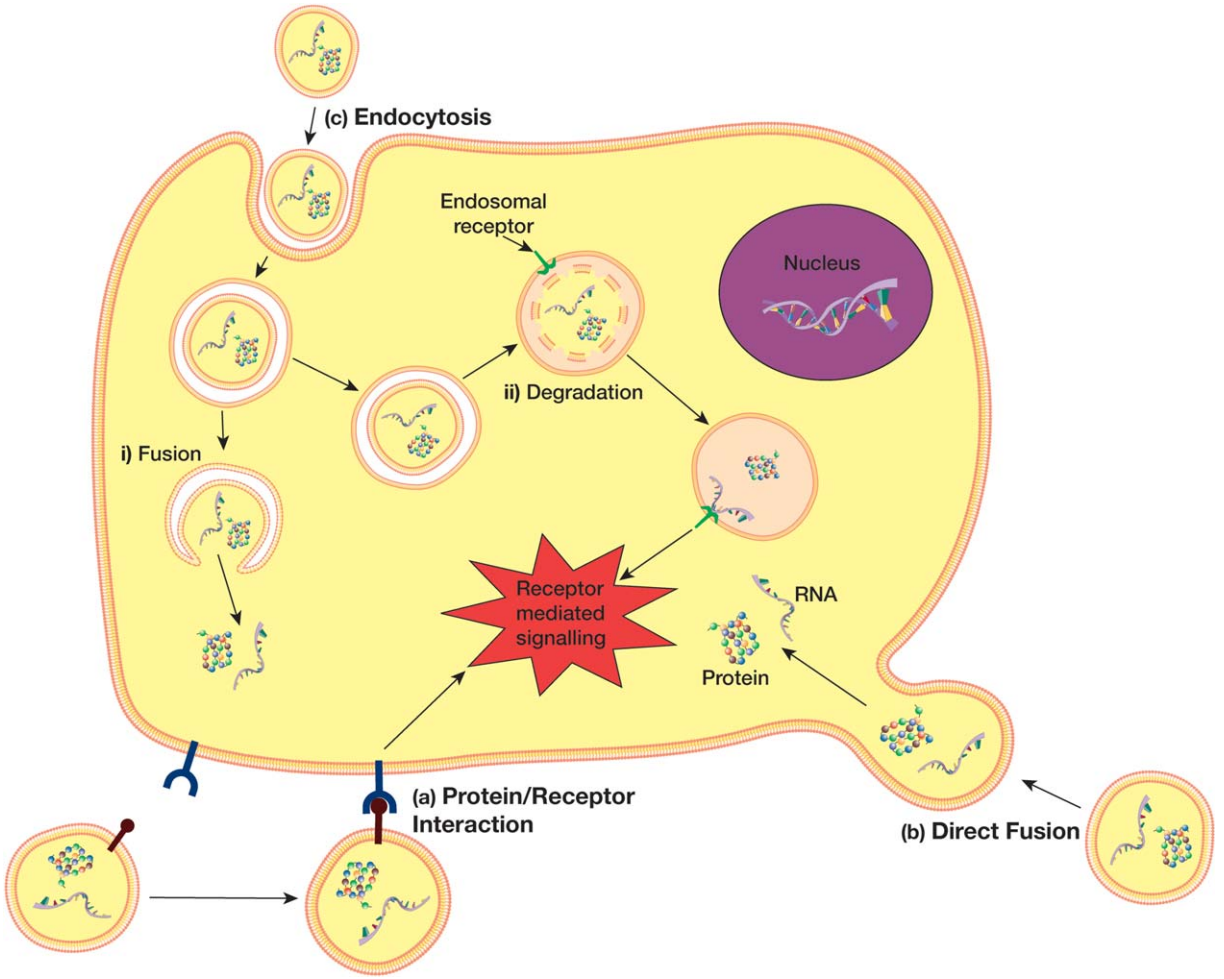

Figure 2. Mechanisms of extracellular vesicle (EV) interaction with recipient cells. EVs can interact with recipient cells in a number of ways. **a,** EV membrane proteins (including tumor necrosis factor) are capable of stimulating recipient cells via cognate receptors on the surface of target cells. **b,** Direct fusion of an EV membrane and the plasma membrane of a recipient cell results in the release of EV cargo into the cytosol. **c, i,** Endocytosis of EVs can lead to fusion of the endosomal and EV membranes to release EV contents into the cytosol. **ii,** Alternatively, the membrane of an endocytosed EV can degrade upon endosomal acidification, resulting in the release of EV cargo that can interact with endosomal receptors such as Toll-like receptors 7 and 8.

human diseases, but delivery has proven challenging for a variety of reasons, including extracellular RNases that rapidly degrade RNA and difficulty with specific targeting to the desired tissue or cell type. In this regard, EVs not only offer protection from RNases via a lipid membrane, but can also be modified to express surface proteins that allow targeting. As an example, exosomes have been loaded with siRNAs against β-site amyloid precursor protein–cleaving enzyme (BACE-1), a therapeutic target in Alzheimer's disease, and then successfully targeted to neurons after being engineered to express the neuron-specific peptide RVG. Intravenous injection of these exosomes into mice successfully knocked down BACE-1 expression within the brain (17). Similarly, another group used EVs displaying a peptide sequence that acts as an epidermal growth factor receptor (EGFR) ligand to specifically target EGFR-expressing breast cancer cells, with inhibition of tumor development in mice via delivery of a synthetic small RNA cargo (18).

Finally, it is worth noting that the ability of EVs to deliver a defined molecular cargo to specific sites is analogous to liposome-based pharmaceuticals. Liposomes are small vesicles generated from synthetic lipid formulations. Liposomes can be engineered to express specific surface molecules for cellular targeting and to carry defined cargo (19). Currently, there are a number of therapies available that make use of liposomal delivery methods (20). For example, Doxil uses a liposomal delivery system to improve

the targeting of doxorubicin to tumor cells, and has been approved by the Food and Drug Administration for the treatment of Kaposi's sarcoma, ovarian cancer, metastatic breast cancer, and multiple myeloma (21). Clinical trials involving liposomes or EVs are in progress (19,22).

Origin and abundance of EVs in arthritis

Synovial fluid contains EVs that originate from a variety of local and infiltrating cells within the synovial joint. In one study, platelet-derived EVs were identified as the most abundant type of EVs in synovial fluid from RA and other inflammatory arthritides, and were shown to be scarce in synovial fluid obtained from patients with noninflammatory osteoarthritis (OA) (23). However, Berckmans et al (24) reported that the most abundant microvesicles in both RA and non-RA synovial fluid were derived from granulocytes and monocytes, with platelet-derived microvesicles only detectable at low levels. Consistent with this, Headland et al (25) found high levels of neutrophil-derived EVs in RA synovial fluid (25). Meanwhile, another group observed that the majority of EVs in RA synovial fluid were derived from B and T cells, and noted that the levels of EVs derived from T cells in RA synovial fluid were elevated when compared with OA and strongly correlated with levels of rheumatoid factor (26). Conflicting reports such as these could be due to methodologic factors, including variations in collection, isolation, and analysis of EVs (Table 1). For example, Boilard and colleagues (23) demonstrated that platelet-derived EVs are more readily detected through the presence of CD41, as opposed to CD61, which was used by Berckmans et al (24), and this might explain their lower estimates. Moreover, methods to avoid platelet activation and aggregation were not uniformly employed across all of these studies. Such inconsistencies highlight the importance of detailed method reporting in studies involving EVs, as well as the inherent limitations that result from an absence of standardized isolation and analysis techniques (27,28).

In terms of abundance, there have been suggestions that RA promotes an increase in EV numbers within the synovial fluid. For example, increased EV concentrations have been observed in synovial fluid from individuals with RA compared to those with psoriatic arthritis (PsA), but not OA (26,29). In this situation, EV abundance in synovial fluid appears to be a function of cellular activation state rather than cell number as indicated by poor correlations between the numbers of EVs and cell counts (26). Treatment of fibroblast-like synoviocytes (FLS) derived from an RA joint with TNF resulted in large increases in exosome production, whereas FLS derived from an OA joint exhibited minimal release in response to TNF (30). Similarly, normal human FLS have been observed to increase EV production in response to IL-1β stimulation (31).

Whether circulating EVs found within the systemic circulation change in RA is unclear. For instance, one study found that plasma from RA patients contained increased numbers of EVs as well as higher proportions of platelet-derived EVs when compared to healthy controls (32), but another group failed to detect any differences (33). Interestingly, disease-modifying antirheumatic drug (DMARD) treatment has been shown to affect circulating microvesicles (34). Specifically, a decrease in the proportion of plasma microvesicles of platelet, monocyte, B cell, T cell, and endothelial origin in RA patients was observed following 4 weeks of treatment with methotrexate, sulfasalazine, and prednisone, and similar changes were also observed in urine. Consistent with this, the authors reported a significant correlation between disease activity and the proportion of plasma and urine microvesicles of platelet, monocyte, B cell, T cell, and endothelial cell origin. Interestingly, the overall numbers of circulating EVs did not change during DMARD therapy in this study (34). However, others have reported that the number of microvesicles was not significantly different after 8 weeks of treatment with methotrexate, sulfasalazine, and prednisolone, despite a reduction in disease activity (35), and plasma platelet-derived EV numbers were not significantly altered in patients who had undergone treatment with immunosuppressive or biologic drugs compared to untreated patients (32).

EVs as drivers of joint inflammation and destruction

In RA, FLS play key roles in promoting tissue inflammation and damage. Exosomes derived from RA FLS may augment these effector functions, including multiple effects on activated CD4+ T cells, such as reducing activation-induced cell death, promoting the release of IFNγ and IL-2 from these cells, increasing the activity of NF-κB and Akt, and inhibiting caspase 3 and caspase 8 cleavage. These effects were reversed by TNF inhibition (30). EVs isolated from RA FLS have also been associated with degradation of bone and cartilage through direct metalloproteinase activity (36) but also by autocrine induction of matrix metalloproteinase 1 (MMP-1) release from FLS (30). Consistent with this, another group observed that TNF stimulation of RA FLS increased secretion of exosomal miR-221-3p, which negatively regulates bone formation (37), while EVs from normal human FLS stimulated with IL-1β promoted release of glycosaminoglycans from cartilage (31). Finally, exosomes derived from RA (but not OA) FLS contained a membrane-bound form of

Table 1. Substantial methodologic variations explain discordant results across 4 studies investigating EV origins in synovial fluid

Author, year (ref.)	Predominant EV origin	Anticoagulant*	Hyaluronidase†	Sample preparation‡	EV origins assessed	Lineage marker§	Flow cytometer¶	Comments
Boilard et al, 2010 (23)	Platelet	No	No	Centrifuged 2 times at 600*g* for 30 minutes (depletes cells). Supernatant analyzed.	T cell Monocyte/macrophage Granulocyte/neutrophil Platelet	CD3 CD14 CD15 CD41	BD FACS-Canto	Synovial fluid analyzed neat following depletion of cells. A combination of exosomes, microvesicles, and apoptotic bodies likely in preparation. High levels of platelet-derived EVs were detected in synovial fluid using CD41 as a platelet lineage marker, as opposed to CD61 where negligible levels were observed.
Berckmans et al, 2002 (24)	Monocyte/macrophage	Yes (sodium citrate)	No	Centrifuged at 1,550*g* for 20 minutes (depletes cells and apoptotic bodies). Supernatant centrifuged at 17,570*g* for 15 minutes (pellets microvesicles). Microvesicle-enriched pellet analyzed.	T helper cell T suppressor cell Monocyte/macrophage B cell Platelet Granulocyte/neutrophil Erythrocyte	CD4 CD8 CD14 CD20 CD61 CD66b Glycophorin A	BD FACScan	Preparation enriched for microvesicles. Inhibition of platelet activation by sodium citrate may reduce levels of platelet-derived EVs. Low levels of the platelet lineage marker CD61 are described on platelet-derived EVs in synovial fluid (see ref. 23).
Headland et al, 2015 (25)	Granulocyte/neutrophil	No	Yes	Centrifuged at 3,000*g* for 25 minutes (depletes cells and apoptotic bodies). Supernatant centrifuged at 10,000*g* for 10 minutes (depletes microvesicles). Supernatant analyzed.	T cell Monocyte/macrophage Granulocyte/neutrophil	CD3 CD14 CD66b	Amnis ImageStreamX Mark II	Synovial fluid analyzed neat following depletion of cells, apoptotic bodies, and dense microvesicles. Hyaluronidase treatment may have depleted microvesicles in supernatant following centrifugation at 10,000g. Preparation likely to predominantly contain exosomes. Use of a pan-EV label (BODIPY-maleimide dye) may have prevented false-positive events from being identified.

Table 1. *(Cont'd)*

Author, year (ref.)	Predominant EV origin	Anticoagulant*	Hyaluronidase†	Sample preparation‡	EV origins assessed	Lineage marker§	Flow cytometer¶	Comments
György et al, 2012 (26)	B cell	No	No	Centrifuged at 650*g* for 20 minutes (depletes cells). Supernatant analyzed.	T cell T helper cell T suppressor cell Monocyte/macrophage B cell Platelet	CD3 CD4 CD8 CD14 CD19 CD41a	BD FACS-Calibur	Synovial fluid analyzed neat following depletion of cells. A combination of exosomes, microvesicles, and apoptotic bodies likely in preparation. Differential detergent lysis used to remove false-positive events.

* Platelet aggregation increases extracellular vesicle (EV) production (65).
† Hyaluronidase treatment of synovial fluid can influence levels of EVs in preparations (66).
‡ Centrifugal force, duration, and whether EVs are analyzed with or without selective enrichment affects the type and number of EVs present (27).
§ Lineage markers and antibody clones can vary in ability to accurately detect EVs (23).
¶ Ability to detect EVs by flow cytometry can vary depending on instrument and calibration settings (67).

TNF that can activate NF-κB pathway signaling in recipient FLS in an autocrine, TNF-dependent manner (30).

As well as acting as a source of EVs, RA FLS can be targets for EVs derived from other cells. For example, upon treatment with EVs from activated T cells and monocytes, RA FLS display increased release of not only MMPs, but also cytokines and chemokines, such as IL-6, IL-8, monocyte chemotactic protein 1 (MCP-1), and MCP-2. Interestingly, similar results were observed when OA FLS and nondiseased FLS were stimulated, suggesting that FLS are inherently equipped to respond to proinflammatory signals from EVs (38). Another group found that exposure of FLS to EVs isolated from RA synovial fluid results in increased transcription of chemokine CXCL1, CXCL2, CXCL3, CXCL5, and CXCL6 genes (39). Consistent with this finding, supernatant from FLS treated with EVs caused chemokine-induced migration of human microvascular endothelial cells and angiogenesis in vivo (39).

Although somewhat controversial, as noted above, platelet-derived EVs have been observed in the synovial fluid of inflamed joints and thus may contribute to the development of RA. Evidence for this was provided by Boilard et al (23), who found that platelet-derived EVs from RA synovial fluid caused activation of FLS via the IL-1 receptor and subsequent release of IL-6 and IL-8. Both IL-1α and IL-1β were associated with RA synovial fluid platelet-derived EVs, but IL-1α was more abundant and was found on the surface of platelet-derived EVs. Importantly, blocking both IL-1α and IL-1β was required to prevent FLS activation. Interestingly, that study also identified the collagen receptor glycoprotein VI as an important mediator in the genesis of platelet-derived EVs and—in a finding that might be exploited for therapeutic purposes—showed that loss of glycoprotein VI significantly reduced arthritic symptoms in the K/BxN serum transfer mouse model of RA (23).

More recently, using the K/BxN serum transfer model, Duchez et al (40) reported that intravenously injected platelet-derived EVs are preferentially taken up by activated joint neutrophils and that this internalization is dependent on both platelet-type 12-LO (an enzyme required for metabolizing arachidonic acid) and secretory phospholipase A_2 IIA ($sPLA_2$-IIA; an enzyme involved in releasing lysophospholipids and fatty acids from EV phospholipids) (40). Notably, mouse recipients of K/BxN serum developed more pronounced joint inflammation when both 12-LO and $sPLA_2$-IIA were present, providing further support for a pathogenic role of platelet-derived EVs in arthritis.

EVs may be functionally important, even if the cell of origin is unclear. For example, RA synovial fluid EVs have elevated levels of RANK and RANKL, which can drive osteoclast activity and bone destruction (26). Microvesicles from the plasma of RA patients with high disease activity induced the release of proinflammatory IL-1, TNF, and IL-17 from autologous peripheral blood mononuclear cells (34). Microvesicles from RA plasma also contained elevated levels of C1q, suggesting that circulating microvesicles in RA propagate inflammation through transport of complement components (35).

Immune complexes play an important pathogenic role in RA. EVs can form macromolecular structures in association with immune complexes, and such complexes may contribute to joint inflammation. Cloutier et al (29) identified EV–immune complex aggregates in RA synovial fluid using high-resolution flow cytometry and transmission electron microscopy, which revealed, in addition to the standard population of microvesicles ~100–300 nm in diameter, larger structures of ~700–3,000 nm in diameter that consisted of both microvesicles and immune complexes (29). This was in contrast to synovial fluid from patients with PsA, which contained a single distinct population of 100–300-nm microvesicles. The majority of immune complexes in RA synovial fluid were associated with microvesicles (including platelet-derived microvesicles), and contained citrullinated autoantigens, such as vimentin and fibrinogen. Platelet-derived microvesicles containing citrullinated proteins bound IgG from RA synovial fluid, but not IgG from PsA synovial fluid, to form microvesicle–immune complex structures in vitro, suggesting that anti–citrullinated protein antibodies in RA synovial fluid facilitate the formation of microvesicle immune complexes (29). Upon incubation with microvesicle immune complexes isolated from RA synovial fluid, human neutrophils released proinflammatory leukotrienes more robustly than when they were incubated with microvesicles alone (29). Whether synovial fluid exosomes are also able to form complexes with immune complexes remains unknown, but the observation that synovial fluid exosomes also contain citrullinated peptides suggests this possibility (41).

Drawing together the above findings, we propose a model, shown in Figure 3, wherein immune cells infiltrate the RA joint and, in conjunction with resident synoviocytes such as FLS, release large numbers of EVs into the synovial tissue and surrounding synovial fluid. Subsequently, synovial fluid EVs might trigger synoviocytes to release proinflammatory cytokines and chemokines that promote cell proliferation and survival as well as angiogenesis, leading to further immune cell infiltration. In this way, a positive feedback loop mediated by EVs might sustain joint inflammation.

Protective roles of EVs during joint inflammation

Although much work indicates that EVs have a proinflammatory role in RA, there is also growing evidence

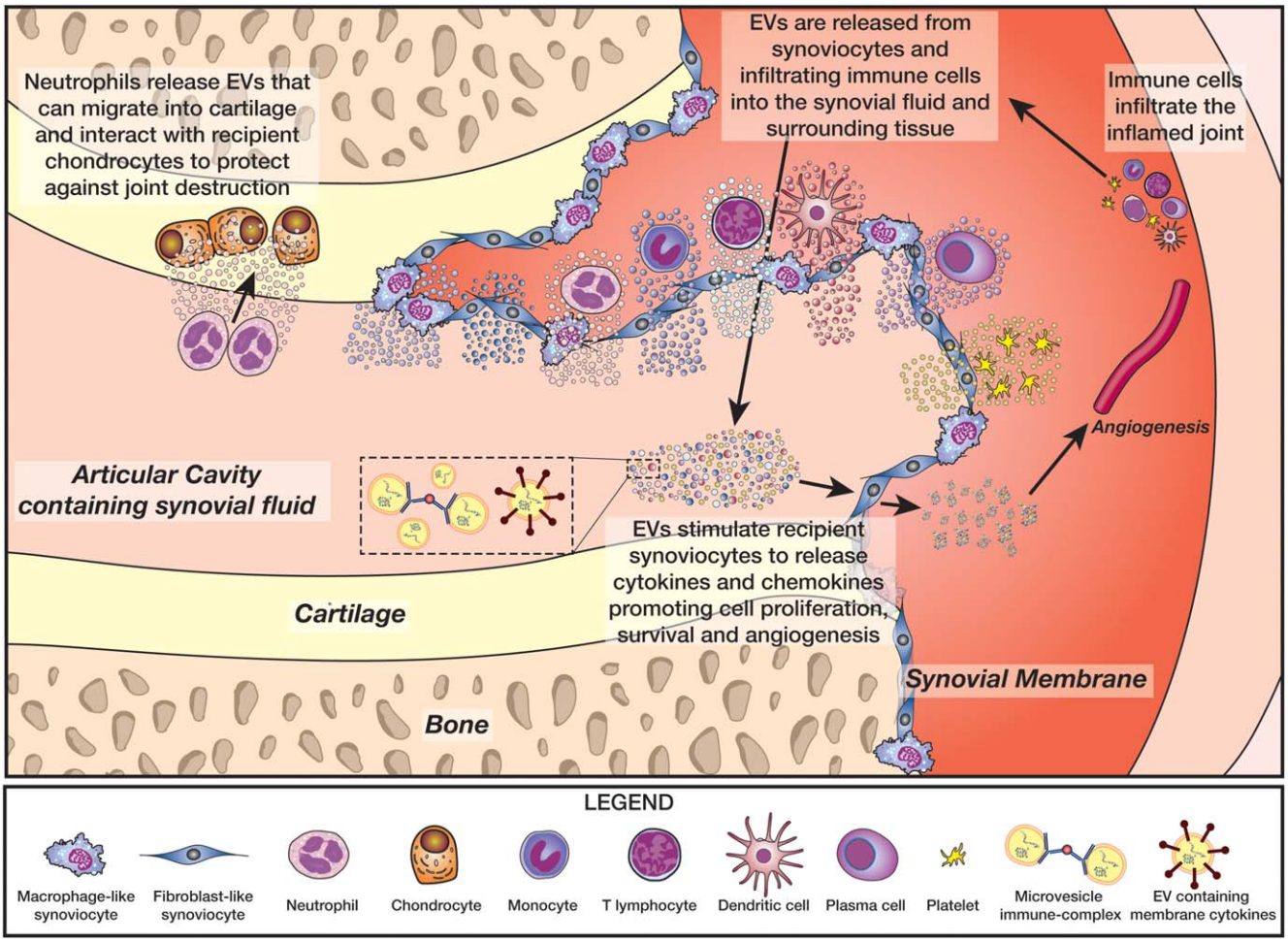

Figure 3. Potential roles of extracellular vesicles (EVs) in joint inflammation. Resident synoviocytes and infiltrating immune cells release EVs into synovial fluid and synovial tissue. Synovial EVs contain molecules capable of driving inflammation and joint destruction. Furthermore, anti–citrullinated peptide antibodies recognize EV-associated citrullinated peptides to form potent proinflammatory complexes. A positive feedback loop is proposed, whereby EVs derived from synoviocytes and various infiltrating leukocytes trigger proinflammatory responses in resident synoviocytes, including fibroblast-like synoviocytes, leading to synovial hypertrophy, angiogenesis, and further immune cell infiltration. Conversely, some EVs may regulate joint inflammation. For example, neutrophil-derived EVs can migrate into cartilage and stimulate protective effects in recipient chondrocytes, including transcription of genes involved in cartilage repair.

that EVs protect joints. For example, Martínez-Lorenzo et al (42) found that the depletion of EVs abrogated the ability of synovial fluid to induce cell death in immortalized T cells, suggesting that EVs might play a role in limiting T cell–driven inflammation. These investigators observed that synovial fluid from RA patients contains relatively few exosomes compared to synovial fluid from patients with traumatic arthritis and that RA synovial fluid displays a correspondingly reduced ability to initiate apoptosis in synovial T cells (42).

Meanwhile, Headland et al (25) described a role of neutrophil-derived EVs in mitigating cartilage damage. They showed that neutrophil-derived EVs contain the antiinflammatory protein annexin A1 and are present in high abundance in RA synovial fluid. Neutrophils derived from healthy blood were stimulated with TNF, and EVs similar to those found in RA synovial fluid were generated. These EVs were able to act upon chondrocytes to limit IL-1β–mediated repression of cartilage matrix proteins, increase transcription of transforming growth factor β1 (which stimulates extracellular matrix accumulation), inhibit release of IL-8 and prostaglandin E_2 (PGE_2) (which are involved in cartilage degradation), and limit chondrocyte apoptosis. Blocking the annexin A1 receptor, FPR2/ALX, abrogated these protective effects, providing further support for the importance of EV-bound annexin A1. Interestingly, using rat cartilage explants, the authors showed that neutrophil-derived EVs migrated into

cartilage, and that this migration was more pronounced when cartilage was prestimulated with IL-1β, whereas monocyte-derived EVs did not migrate into cartilage. Furthermore, in mouse models of RA, intraarticular injections of EVs from TNF-stimulated neutrophils abrogated loss of sulfated glycosaminoglycans from cartilage, while mice deficient in TMEM16F (a protein involved in EV formation) had greater loss of sulfated glycosaminoglycans (25).

Taken together, these findings support a model wherein inflammation within cartilage might facilitate infiltration of neutrophil-derived EVs, which could interact with recipient chondrocytes and protect against further cartilage degradation in RA (Figure 3). Such a model obviously runs counter to a large body of evidence indicating that neutrophils act to promote inflammation and joint damage, but is consistent with recent work indicating an important role of neutrophils in resolving inflammation (43).

EVs may also help to protect joints in conditions other than RA. In one recent study, neutrophil-derived EVs hastened the resolution of gout (44). Specifically, Cumpelik and colleagues (44) observed that in a monosodium urate monohydrate (MSU)–induced murine model of gout, an increase in IL-1β was closely followed by an increase in neutrophil-derived EVs. It has previously been shown that MSU-induced IL-1β production via the inflammasome is regulated by complement C5a (45), and Cumpelik et al interestingly discovered that neutrophil-derived EVs from human gout exudates suppressed complement C5a-mediated inflammasome activation in recipient macrophages (44). This suggests a negative feedback model wherein neutrophil-derived EVs help to limit the extent of joint inflammation. Along similar lines, EVs derived from mature osteoclasts have been found to inhibit osteoclast differentiation in 1,25-dihydroxyvitamin D_3–stimulated bone marrow cultures (46). In this case, inhibition was paradoxically dependent on the presence of EV-associated RANK, which may competitively bind RANKL and thereby prevent RANK/RANKL interactions in precursor cells to attenuate osteoclast differentiation (46). Finally, EVs may also help to promote joint repair, since intraarticular injection of exosomes from mesenchymal stem cells, which have important roles in tissue repair (47,48) and are normally found within the synovium (49,50), was demonstrated to promote cartilage repair in a rat model of osteochondral damage (51).

Finally, EVs might also facilitate the beneficial effects of some arthritis therapies. In one study of immortalized synovial cells, treatment with methotrexate and sulfasalazine induced changes in the protein content of released exosomes (52). Interestingly, many of the altered exosomal proteins had immunosuppressive functions, raising the possibility that treatment-induced EVs might augment the response to certain DMARDs.

EVs as biomarkers in arthritis

As noted earlier, EVs are proving of interest as novel biomarkers in a variety of diseases. One study in RA identified dysregulated long noncoding RNAs, HOTAIR and LUST, in circulating exosomes obtained from the serum of patients with established RA, compared to healthy donors (53). Other circulating biomarker studies in RA have focused on miRNAs, but these all assessed total serum or plasma RNA, without enriching for EVs. Given that the majority of circulating miRNAs in plasma and serum are associated with EVs and methods used to isolate circulating miRNAs also enrich for EV miRNAs (54,55), these studies only provide indirect information on EV miRNA content. Several circulating miRNAs appear to be promising biomarkers in RA. For example, one study identified 3 miRNAs—miR-24, miR-30a-5p, and miR-125a-5p—that in combination were able to differentiate patients with RA from healthy controls and patients with systemic lupus erythematosus or OA. Furthermore, miR-24 levels were found to correlate with the Disease Activity Score in 28 joints (56), C-reactive protein, visual analog pain scales, and erythrocyte sedimentation rate (57).

Other studies have shown that circulating miRNAs might help to predict the response to biologic agents. For example, levels of miR-23-3p and miR-223-3p in serum were good indicators of response to anti-TNF/DMARD combination therapy (58), while high pretreatment serum levels of miR-125b were associated with a good clinical response to rituximab (59). Inclusion of an EV purification step in such miRNA biomarker studies might enrich for disease-specific miRNAs and improve the signal-to-noise ratio by eliminating more abundant circulating RNAs (e.g., ribosomal RNA) (55).

Apart from RNA, other components of EVs, such as protein, lipids, and metabolites, might also prove to be useful biomarkers in RA, but minimal research has been conducted to date in this area.

Therapeutic use of EVs in inflammatory joint disease

Engineering of EVs for treatment of inflammatory joint disease is currently being explored using several different approaches in preclinical animal models (Figure 4). In the collagen-induced arthritis (CIA) mouse model, intravenous injection of exosomes from bone marrow–derived dendritic cells (BMDCs), either transduced to express a viral-encoded homolog of IL-10, or treated with recombinant murine IL-10, dramatically repressed the

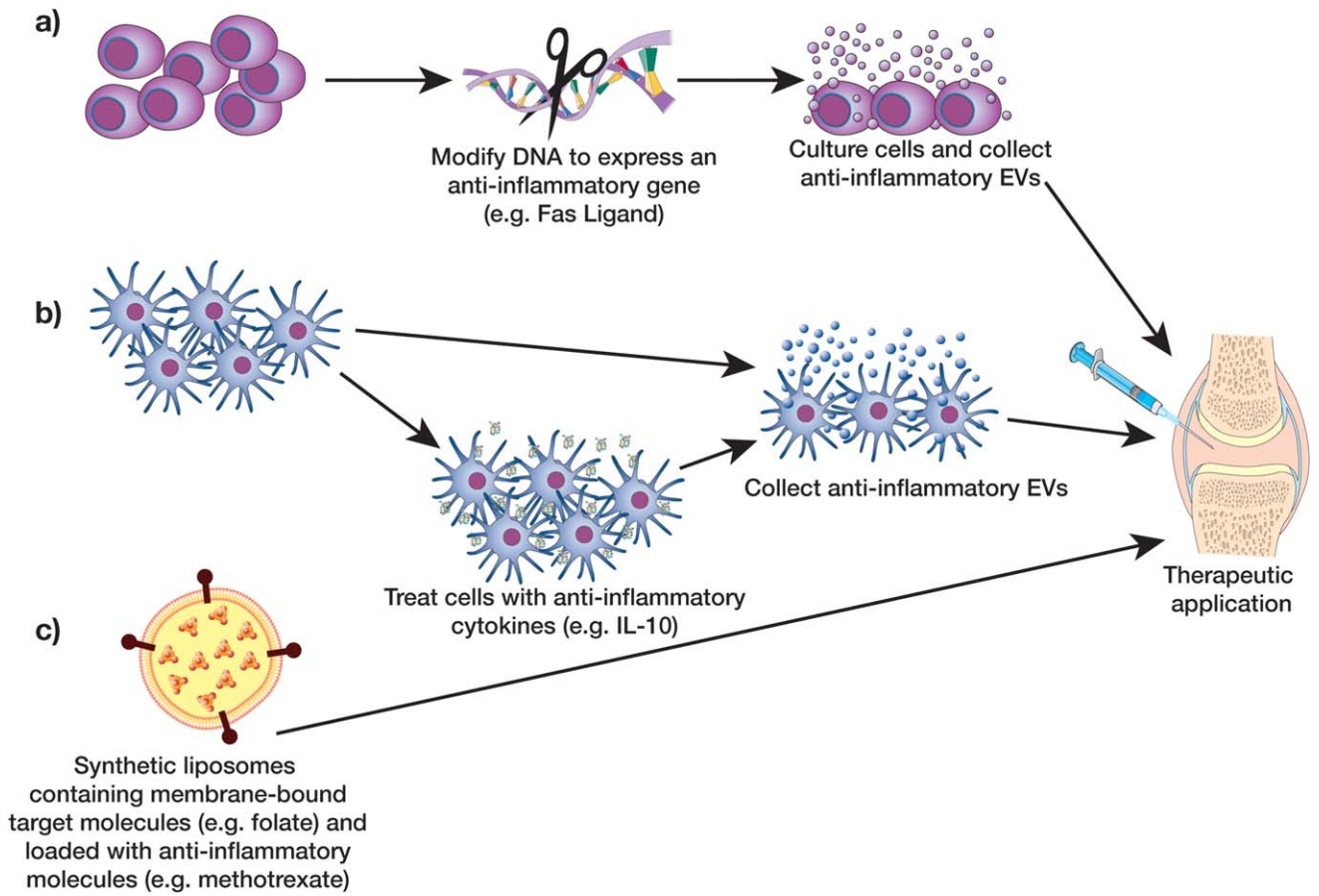

Figure 4. Generation of antiinflammatory extracellular vesicles (EVs) and liposomes for the treatment of inflammatory arthritis. **a,** Cells genetically modified to express antiinflammatory genes produce EVs with antiinflammatory properties. **b,** Cells are stimulated to generate endogenously derived EVs containing an antiinflammatory cargo. IL-10 = interleukin-10. **c,** Synthetic liposomes deliver drugs by integrating molecules into the liposome membrane that target an encapsulated drug to a specific cell type.

onset of arthritis (60). Moreover, these exosomes were also able to reduce the severity of established CIA. Interestingly, these effects were not observed with injection of IL-10, suggesting that the role of IL-10 might not be as a direct ligand in vivo, but rather to promote the production of antiinflammatory exosomes (60). Similar results in CIA have been observed using a single systemic injection of EVs generated from BMDCs genetically engineered to express Fas ligand, IL-4, the immunosuppressing enzyme indoleamine 2,3-dioxygenase, or its inducer, CTLA-4 immunoglobulin (61).

Loading of EVs with other antiinflammatory molecules may hold promise for the treatment of joint inflammation. For example, recent work suggests that EVs containing SOCS proteins may regulate proinflammatory STAT signaling, which is increased in RA. Exposing alveolar macrophages to IL-10 or PGE_2 rapidly increased SOCS-1 and SOCS-3 secretion in exosomes and microvesicles, respectively. By treating alveolar epithelial cells with SOCS-containing EVs, STAT signaling was successfully suppressed (12). In this way, SOCS-loaded EVs generated from autologous cells could represent a novel therapeutic strategy for reducing joint inflammation. Finally, as mechanisms for selectively loading RNAs into EVs are being discovered (62), the possibility of loading EVs with therapeutic siRNAs might also become an option in arthritis.

As noted above, the ability of EVs to deliver a defined molecular cargo is being exploited in liposome-based therapeutics. In one study, liposomes were loaded with a membrane-bound form of APO2L/TRAIL and then injected into the knee in a rabbit model of RA (63). This greatly reduced joint inflammation, with decreased inflammatory infiltrate, vascularity, and exudate. Another group engineered liposomes to contain not only methotrexate but also surface-bound folate (64). The latter modification targeted the liposomes to activated macrophages, and CIA was much less

pronounced following intraperitoneal injection of these liposomes compared with injection of methotrexate alone.

Conclusions

Research interest in EVs has increased dramatically in recent years. Although much work has occurred in the fields of cancer biology and oncology, efforts to improve our understanding of EVs in RA are gaining momentum. High sensitivity 'omics' approaches to detect changes in protein, RNA, lipid, and metabolite profiles of EVs may facilitate diagnosis and selection of therapies. Modulating EV biogenesis or uptake might also hold promise for treating RA. Potential molecular targets include 12-LO and $sPLA_2$-IIA, or glycoprotein VI to block uptake or biogenesis, respectively. An alternative strategy might be to prevent the formation of autoantibodies with EV-associated citrullinated peptides in order to reduce EV–immune complex formation. Finally, and excitingly, EVs may provide a new way to deliver and better target therapeutic agents in RA.

AUTHOR CONTRIBUTIONS

All authors drafted the article, revised it critically for important intellectual content, and approved the final version to be published.

REFERENCES

1. Buzas EI, Gyorgy B, Nagy G, Falus A, Gay S. Emerging role of extracellular vesicles in inflammatory diseases. Nat Rev Rheumatol 2014;10:356–64.
2. Gardiner C, Vizio DD, Sahoo S, Théry C, Witwer KW, Wauben M, et al. Techniques used for the isolation and characterization of extracellular vesicles: results of a worldwide survey. J Extracell Vesicles 2016;5:32945.
3. Coleman BM, Hill AF. Extracellular vesicles: their role in the packaging and spread of misfolded proteins associated with neurodegenerative diseases [review]. Semin Cell Dev Biol 2015;40: 89–96.
4. Peinado H, Aleckovic M, Lavotshkin S, Matei I, Costa-Silva B, Moreno-Bueno G, et al. Melanoma exosomes educate bone marrow progenitor cells toward a pro-metastatic phenotype through MET. Nat Med 2012;18:883–91.
5. Valadi H, Ekstrom K, Bossios A, Sjostrand M, Lee JJ, Lotvall JO. Exosome-mediated transfer of mRNAs and microRNAs is a novel mechanism of genetic exchange between cells [letter]. Nat Cell Biol 2007;9:654–9.
6. Alexander M, Hu R, Runtsch MC, Kagele DA, Mosbruger TL, Tolmachova T, et al. Exosome-delivered microRNAs modulate the inflammatory response to endotoxin. Nat Commun 2015;6: 7321.
7. Vega VL, Rodríguez-Silva M, Frey T, Gehrmann M, Diaz JC, Steinem C, et al. Hsp70 translocates into the plasma membrane after stress and is released into the extracellular environment in a membrane-associated form that activates macrophages. J Immunol 2008;180:4299–307.
8. Cossetti C, Iraci N, Mercer TR, Leonardi T, Alpi E, Drago D, et al. Extracellular vesicles from neural stem cells transfer IFN-γ via Ifngr1 to activate Stat1 signaling in target cells. Mol Cell 2014;56:193–204.
9. Bretz NP, Ridinger J, Rupp AK, Rimbach K, Keller S, Rupp C, et al. Body fluid exosomes promote secretion of inflammatory cytokines in monocytic cells via Toll-like receptor signaling. J Biol Chem 2013;288:36691–702.
10. Fabbri M, Paone A, Calore F, Galli R, Gaudio E, Santhanam R, et al. MicroRNAs bind to Toll-like receptors to induce prometastatic inflammatory response. Proc Natl Acad Sci U S A 2012;109: E2110–6.
11. Liu X, Croker BA, Campbell IK, Gauci SJ, Alexander WS, Tonkin BA, et al. Key role of suppressor of cytokine signaling 3 in regulating gp130 cytokine–induced signaling and limiting chondrocyte responses during murine inflammatory arthritis. Arthritis Rheumatol 2014;66:2391–402.
12. Bourdonnay E, Zasłona Z, Penke LR, Speth JM, Schneider DJ, Przybranowski S, et al. Transcellular delivery of vesicular SOCS proteins from macrophages to epithelial cells blunts inflammatory signaling. J Exp Med 2015;212:729–42.
13. Szajnik M, Czystowska M, Szczepanski MJ, Mandapathil M, Whiteside TL. Tumor-derived microvesicles induce, expand and up-regulate biological activities of human regulatory T cells (Treg). PLoS One 2010;5:e11469.
14. Skog J, Wurdinger T, van Rijn S, Meijer D, Gainche L, Sena-Esteves M, et al. Glioblastoma microvesicles transport RNA and protein that promote tumor growth and provide diagnostic biomarkers [letter]. Nat Cell Biol 2008;10:1470–6.
15. Melo SA, Luecke LB, Kahlert C, Fernandez AF, Gammon ST, Kaye J, et al. Glypican-1 identifies cancer exosomes and detects early pancreatic cancer. Nature 2015;523:177–82.
16. Cheng L, Doecke JD, Sharples RA, Villemagne VL, Fowler CJ, Rembach A, et al. Prognostic serum miRNA biomarkers associated with Alzheimer's disease shows concordance with neuropsychological and neuroimaging assessment. Mol Psychiatry 2015;20: 1188–96.
17. Alvarez-Erviti L, Seow Y, Yin H, Betts C, Lakhal S, Wood MJ. Delivery of siRNA to the mouse brain by systemic injection of targeted exosomes [letter]. Nat Biotechnol 2011;29:341–45.
18. Ohno SI, Takanashi M, Sudo K, Ueda S, Ishikawa A, Matsuyama N, et al. Systemically injected exosomes targeted to EGFR deliver antitumor MicroRNA to breast cancer cells. Mol Ther 2013;21: 185–91.
19. Allen TM, Cullis PR. Liposomal drug delivery systems: from concept to clinical applications [review]. Adv Drug Deliv Rev 2013; 65:36–48.
20. Pattni BS, Chupin VV, Torchilin VP. New developments in liposomal drug delivery [review]. Chem Rev 2015;115:10938–66.
21. Barenholz Y. Doxil—the first FDA-approved nano-drug: lessons learned [review]. J Control Release 2012;160:117–34.
22. Lener T, Gioma M, Aigner L, Börger V, Buzas E, Camussi G, et al. Applying extracellular vesicles based therapeutics in clinical trials: an ISEV position paper. J Extracell Vesicles 2015;4:30087.
23. Boilard E, Nigrovic PA, Larabee K, Watts GF, Coblyn JS, Weinblatt ME, et al. Platelets amplify inflammation in arthritis via collagen-dependent microparticle production. Science 2010; 327:580–3.
24. Berckmans RJ, Nieuwland R, Tak PP, Böing AN, Romijn FP, Kraan MC, et al. Cell-derived microparticles in synovial fluid from inflamed arthritic joints support coagulation exclusively via a factor VII–dependent mechanism. Arthritis Rheum 2002;46: 2857–66.
25. Headland SE, Jones HR, Norling LV, Kim A, Souza PR, Corsiero E, et al. Neutrophil-derived microvesicles enter cartilage and protect the joint in inflammatory arthritis. Sci Transl Med 2015;7: 315ra190.
26. György B, Szabó TG, Turiák L, Wright M, Herczeg P, Lédeczi Z, et al. Improved flow cytometric assessment reveals distinct microvesicle (cell-derived microparticle) signatures in joint diseases. PLoS One 2012;7:e49726.
27. Witwer KW, Buzás EI, Bemis LT, Bora A, Lässer C, Lötvall J, et al. Standardization of sample collection, isolation and analysis

methods in extracellular vesicle research. J Extracell Vesicles 2013;2:20360.
28. Lotvall J, Hill AF, Hochberg F, Buzas EI, Di Vizio D, Gardiner C, et al. Minimal experimental requirements for definition of extracellular vesicles and their functions: a position statement from the International Society for Extracellular Vesicles [editorial]. J Extracell Vesicles 2014;3:26913.
29. Cloutier N, Tan S, Boudreau LH, Cramb C, Subbaiah R, Lahey L, et al. The exposure of autoantigens by microparticles underlies the formation of potent inflammatory components: the microparticle-associated immune complexes. EMBO Mol Med 2013;5:235–49.
30. Zhang HG, Liu C, Su K, Yu S, Zhang L, Zhang S, et al. A membrane form of TNF-α presented by exosomes delays T cell activation-induced cell death. J Immunol 2006;176:7385–93.
31. Kato T, Miyaki S, Ishitobi H, Nakamura Y, Nakasa T, Lotz MK, et al. Exosomes from IL-1β stimulated synovial fibroblasts induce osteoarthritic changes in articular chondrocytes. Arthritis Res Ther 2014;16:R163.
32. Sellam J, Proulle V, Jüngel A, Ittah M, Miceli Richard C, Gottenberg JE, et al. Increased levels of circulating microparticles in primary Sjögren's syndrome, systemic lupus erythematosus and rheumatoid arthritis and relation with disease activity. Arthritis Res Ther 2009;11:R156.
33. Biró É, Nieuwland R, Tak PP, Pronk LM, Schaap MC, Sturk A, et al. Activated complement components and complement activator molecules on the surface of cell-derived microparticles in patients with rheumatoid arthritis and healthy individuals. Ann Rheum Dis 2007;66:1085–92.
34. Viñuela-Berni V, Doníz-Padilla L, Figueroa-Vega N, Portillo-Salazar H, Abud-Mendoza C, Baranda L, et al. Proportions of several types of plasma and urine microparticles are increased in patients with rheumatoid arthritis with active disease. Clin Exp Immunol 2015;180:442–51.
35. Van Eijk IC, Tushuizen ME, Sturk A, Dijkmans BA, Boers M, Voskuyl AE, et al. Circulating microparticles remain associated with complement activation despite intensive anti-inflammatory therapy in early rheumatoid arthritis. Ann Rheum Dis 2010;69:1378–82.
36. Lo Cicero A, Majkowska I, Nagase H, Di Liegro I, Troeberg L. Microvesicles shed by oligodendroglioma cells and rheumatoid synovial fibroblasts contain aggrecanase activity. Matrix Biol 2012;31:229–33.
37. Maeda Y, Farina NH, Matzelle MM, Fanning PJ, Lian JB, Gravallese EM. Synovium-derived microRNAs regulate bone pathways in rheumatoid arthritis. J Bone Miner Res 2017;32:461–72.
38. Distler JH, Jüngel A, Huber LC, Seemayer CA, Reich CF III, Gay RE, et al. The induction of matrix metalloproteinase and cytokine expression in synovial fibroblasts stimulated with immune cell microparticles. Proc Natl Acad Sci U S A 2005;102:2892–7.
39. Reich N, Beyer C, Gelse K, Akhmetshina A, Dees C, Zwerina J, et al. Microparticles stimulate angiogenesis by inducing ELR$^+$ CXC-chemokines in synovial fibroblasts. J Cell Mol Med 2011;15:756–62.
40. Duchez AC, Boudreau LH, Bollinger J, Belleannée C, Cloutier N, Laffont B, et al. Platelet microparticles are internalized in neutrophils via the concerted activity of 12-lipoxygenase and secreted phospholipase A2-IIA. Proc Natl Acad Sci U S A 2015;112:E3564–73.
41. Skriner K, Adolph K, Jungblut PR, Burmester GR. Association of citrullinated proteins with synovial exosomes. Arthritis Rheum 2006;54:3809–14.
42. Martínez-Lorenzo MJ, Anel A, Saez-Gutierrez B, Royo-Cañas M, Bosque A, Alava MA, et al. Rheumatoid synovial fluid T cells are sensitive to APO2L/TRAIL. Clin Immunol 2007;122:28–40.
43. Jones HR, Robb CT, Perretti M, Rossi AG. The role of neutrophils in inflammation resolution. Semin Immunol 2016;28:137–45.
44. Cumpelik A, Ankli B, Zecher D, Schifferli JA. Neutrophil microvesicles resolve gout by inhibiting C5a-mediated priming of the inflammasome. Ann Rheum Dis 2016;75:1236–45.
45. An LL, Mehta P, Xu L, Turman S, Reimer T, Naiman B, et al. Complement C5a potentiates uric acid crystal-induced IL-1β production. Eur J Immunol 2014;44:3669–79.
46. Huynh N, VonMoss L, Smith D, Rahman I, Felemban MF, Zuo J, et al. Characterization of regulatory extracellular vesicles from osteoclasts. J Dent Res 2016;95:673–9.
47. Lai RC, Yeo RW, Lim SK. Mesenchymal stem cell exosomes [review]. Semin Cell Dev Biol 2015;40:82–8.
48. Toh WS, Lai RC, Hui JH, Lim SK. MSC exosome as a cell-free MSC therapy for cartilage regeneration: implications for osteoarthritis treatment [review]. Semin Cell Dev Biol 2016. E-pub ahead of print.
49. De Bari C, Dell'Accio F, Tylzanowski P, Luyten FP. Multipotent mesenchymal stem cells from adult human synovial membrane. Arthritis Rheum 2001;44:1928–42.
50. Ando W, Kutcher JJ, Krawetz R, Sen A, Nakamura N, Frank CB, et al. Clonal analysis of synovial fluid stem cells to characterize and identify stable mesenchymal stromal cell/mesenchymal progenitor cell phenotypes in a porcine model: a cell source with enhanced commitment to the chondrogenic lineage. Cytotherapy 2014;16:776–88.
51. Zhang S, Chu WC, Lai RC, Lim SK, Hui JH, Toh WS. Exosomes derived from human embryonic mesenchymal stem cells promote osteochondral regeneration. Osteoarthritis Cartilage 2016;24:2135–40.
52. Tsuno H, Suematsu N, Sato T, Arito M, Matsui T, Iizuka N, et al. Effects of methotrexate and salazosulfapyridine on protein profiles of exosomes derived from a human synovial sarcoma cell line of SW982. Proteomics Clin Appl 2016;10:164–71.
53. Song J, Kim D, Han J, Kim Y, Lee M, Jin EJ. PBMC and exosome-derived Hotair is a critical regulator and potent marker for rheumatoid arthritis. Clin Exp Med 2015;15:121–6.
54. Gallo A, Tandon M, Alevizos I, Illei GG. The majority of microRNAs detectable in serum and saliva is concentrated in exosomes. PLoS One 2012;7:e30679.
55. Cheng L, Sharples RA, Scicluna BJ, Hill AF. Exosomes provide a protective and enriched source of miRNA for biomarker profiling compared to intracellular and cell-free blood. J Extracell Vesicles 2014;3:23743.
56. Prevoo ML, van 't Hof MA, Kuper HH, van Leeuwen MA, van de Putte LB, van Riel PL. Modified disease activity scores that include twenty-eight–joint counts: development and validation in a prospective longitudinal study of patients with rheumatoid arthritis. Arthritis Rheum 1995;38:44–8.
57. Murata K, Furu M, Yoshitomi H, Ishikawa M, Shibuya H, Hashimoto M, et al. Comprehensive microRNA analysis identifies miR-24 and miR-125a-5p as plasma biomarkers for rheumatoid arthritis. PLoS One 2013;8:e69118.
58. Castro-Villegas C, Perez-Sanchez C, Escudero A, Filipescu I, Verdu M, Ruiz-Limon P, et al. Circulating miRNAs as potential biomarkers of therapy effectiveness in rheumatoid arthritis patients treated with anti-TNFα. Arthritis Res Ther 2015;17:49.
59. Duroux-Richard I, Pers YM, Fabre S, Ammari M, Baeten D, Cartron G, et al. Circulating miRNA-125b is a potential biomarker predicting response to rituximab in rheumatoid arthritis. Mediators Inflamm 2014;2014:342524.
60. Kim SH, Lechman ER, Bianco N, Menon R, Keravala A, Nash J, et al. Exosomes derived from IL-10-treated dendritic cells can suppress inflammation and collagen-induced arthritis. J Immunol 2005;174:6440–8.
61. Robbins PD, Dorronsoro A, Booker CN. Regulation of chronic inflammatory and immune processes by extracellular vesicles [review]. J Clin Invest 2016;126:1173–80.

62. Villarroya-Beltri C, Baixauli F, Gutiérrez-Vázquez C, Sánchez-Madrid F, Mittelbrunn M. Sorting it out: regulation of exosome loading [review]. Semin Cancer Biol 2014;28:3–13.
63. Martinez-Lostao L, García-Alvarez F, Basáñez G, Alegre-Aguarón E, Desportes P, Larrad L, et al. Liposome-bound APO2L/TRAIL is an effective treatment in a rabbit model of rheumatoid arthritis. Arthritis Rheum 2010;62:2272–82.
64. Nogueira E, Lager F, Le Roux D, Nogueira P, Freitas J, Charvet C, et al. Enhancing methotrexate tolerance with folate tagged liposomes in arthritic mice. J Biomed Nanotechnol 2015;11:2243–52.
65. Aatonen MT, Öhman T, Nyman TA, Laitinen S, Grönholm M, Siljander PR. Isolation and characterization of platelet-derived extracellular vesicles. J Extracell Vesicles 2014;3:24692.
66. Boere J, van de Lest CH, Libregts SF, Arkesteijn GJ, Geerts WJ, Nolte-'t Hoen EN, et al. Synovial fluid pretreatment with hyaluronidase facilitates isolation of CD44+ extracellular vesicles. J Extracell Vesicles 2016;5:31751.
67. Lacroix R, Robert S, Poncelet P, Dignat-George F. Overcoming limitations of microparticle measurement by flow cytometry [review]. Semin Thromb Hemost 2010;36:807–18.

ARTHRITIS & RHEUMATOLOGY
Vol. 69, No. 7, July 2017, pp 1363–1373
DOI 10.1002/art.40094

REVIEW

Interventions for Cartilage Disease

Current State-of-the-Art and Emerging Technologies

Luiz Felipe Ambra,[1] Laura de Girolamo,[2] Brian Mosier,[3] and Andreas H. Gomoll[4]

Introduction

Articular cartilage has limited intrinsic repair capabilities, and cartilage defects can progress to osteoarthritis (OA) over time (1,2). Although several other factors are involved in the development of OA, this review will focus on cartilage defects (2). Even knee joints with asymptomatic cartilage defects have shown twice the rate of further cartilage loss compared with intact knees, and worsening was demonstrated in 81% of chondral defects over only 2 years (1). Young patients with cartilage defects are frequently as symptomatic as older patients presenting with established OA (3). OA is a common cause of knee pain and disability (4), with almost half the population becoming symptomatic within their lifetimes (5), and the rates of arthritis-related joint replacement surgery continue to steadily increase. OA presents a major economic burden, being among the leading causes of disability in developed countries (6). The risk of disability attributable to knee OA is as great as that due to cardiovascular disease (7). It causes considerable pain, functional limitation, deterioration of health-related quality of life, and in some cases, symptoms of depression (8). For those who fail to respond to conservative treatment, there are several options for biologic repair and reconstruction that may ideally treat definitively or at least "bridge" the patient until he or she reaches an age that is more appropriate for arthroplasty.

While overall the outcomes of primary joint replacement are among the best of any orthopedic procedure, both satisfaction with the procedure and implant survival are significantly lower in younger patients (9). One study in patients younger than age 40 years showed good and excellent Knee Society knee function scores in only 50% of patients and a failure rate of 12.5% at 8 years (10). Subsequent revision surgery is technically more challenging and less successful than a primary procedure, with a patient satisfaction rate as low as 59% (11) and 5-year survival in younger patients as low as 82% (12). Last, revision surgery is extremely costly, with average charges of $73,000 (13). It therefore appears worthwhile to invest in procedures, such as cartilage repair, with the potential for reducing disability and delaying arthroplasty as long as possible, especially in young patients.

Current recommendations for cartilage repair include treatment of symptomatic defects in patients up to age 55 years (14). Moreover, the development of concomitant surgical procedures, such as meniscus transplantation, to address articular comorbidities that previously were considered contraindications for cartilage repair have further expanded the indications (15). While providing relief for many patients who otherwise would have no treatment, cartilage repair and biologic reconstruction continue to evolve, overcoming the limitations of current technology. The major challenges concern the restoration of a biomechanically and biochemically competent extracellular matrix and intimate integration of the newly synthesized matrix with the resident surrounding tissue. This explains the special interest in biologic augmentation, such as the use of growth factors, platelet concentrates, and stem cells (for review, see ref. 16). The potential of these biologic products is based on their antiinflammatory,

[1]Luiz Felipe Ambra, MD: Universidade Federal de São Paulo, Sao Paulo, Brazil, and Brigham and Women's Hospital, Boston, Massachusetts; [2]Laura de Girolamo, PhD: Galeazzi Orthopaedic Institute, Milan, Italy; [3]Brian Mosier, MD: Allegheny Health Network, Pittsburgh, Pennsylvania; [4]Andreas H. Gomoll, MD: Harvard Medical School and Brigham and Women's Hospital, Boston, Massachusetts.

Drs. Ambra and Girolamo contributed equally to this work.

Dr. Gomoll has received research funding from JRF, Vericel, NuTech, and SBM.

Address correspondence to Luiz Felipe Ambra, MD, Universidade Federal de SaGomollo Paulo, Rua Borges Lagoa 783, Fifth Floor, Sao Paulo 04023–900, Brazil. E-mail: felipeambra71@gmail.com.

Submitted for publication July 11, 2016; accepted in revised form March 7, 2017.

immunomodulatory, and paracrine properties, with the goal of enhanced regenerative potential.

Here, we provide a review of the current state of cartilage repair, focusing mainly on current clinically established techniques, as well as briefly discussing emerging technologies for the treatment of cartilage defects in the most commonly treated joint, the knee.

Indications for cartilage repair

Cartilage repair is indicated to treat symptoms of pain and functional limitation during activities of daily living. Before surgical intervention is considered, attempts at first-line conservative management should have failed. Exceptions to this rule can be considered in younger patients with large cartilage defects that are likely to progress. In these cases, earlier and more aggressive interventions are justified based on the premise that conservative management is unlikely to provide symptomatic relief possibly for decades prior to reaching an age appropriate for treatment with arthroplasty, which is a likely outcome for many patients with OA.

Articular comorbidities

Cartilage defects are commonly associated with, and frequently the result of, malalignment, ligamentous instability, and meniscal deficiency. Therefore, any evaluation performed prior to cartilage repair must include an assessment of any comorbidities that have the potential to negatively impact treatment outcomes. Lower-extremity malalignment is a major contributing factor to compartment overload (17), and uncorrected malalignment can lead to failure of cartilage restoration and more rapid progression of OA (18). Thus, malalignment is a contraindication for tibiofemoral and patellofemoral cartilage repair surgery (19), unless the malalignment is corrected in a staged or concurrent manner to prevent overload on the repaired tissue. The meniscus is critical for load distribution in the knee. Subtotal and total meniscectomy directly lead to increased contact pressure, resulting in the accelerated development of OA, with an increase in relative risk of >20 times that for normal controls (20). Meniscus transplantation can be considered in patients who are meniscus deficient, who are candidates for cartilage repair within the same compartment (19).

Surgical interventions for cartilage repair

There are several techniques used to repair full-thickness cartilage defects, each of which has specific indications and results. Table 1 summarizes the main clinical studies regarding surgical procedures for focal cartilage lesion that are available.

Marrow stimulation techniques (MSTs)/microfracture. Marrow stimulation is the most common arthroscopic procedure aimed at the treatment of smaller cartilage defects. It involves mechanical perforation of the subchondral plate through drilling or use of an arthroscopic awl, allowing bone marrow elements and blood to collect in the defect. The resultant clot slowly matures over time to form a fibrocartilaginous repair tissue (21,22).

Although up to 80% of patients experience initial improvement in symptoms (23), these improvements tend to deteriorate over time, especially after treatment of defects that are larger or located in the patellofemoral joint (24). A systematic review of level I and II studies (25) showed that independent of patient characteristics, deterioration of clinical improvement is to be expected after 5 years. Several studies have delineated patient- and defect-specific factors to define the optimal indications for microfracture: defect size of <4 cm^2 (24,26,27), patients younger than age 40 years (23,24), defect location on the femoral condyle (24), body mass index of <30 kg/m^2, and symptom duration of <12 months (26). Serious complications after microfracture are rare but include arthrofibrosis and persistent pain in up to 16% of patients (28) and formation of intralesional osteophytes in 30–50% of defects (26).

Next-generation marrow stimulation techniques. A potential limitation of microfracture is that the mechanically weak marrow clot is dislodged from the defect and lost into the joint. Therefore, several procedures have been developed that aim to stabilize the marrow clot by adding mechanically more durable scaffolds to the defect.

Autologous matrix-induced chondrogenesis adds a bilayer porcine type I/III collagen membrane to a defect treated with marrow stimulation techniques (29). Autologous matrix-induced chondrogenesis provides significant functional improvement without deterioration of results up to 5 years after surgery (30). Moreover, magnetic resonance imaging (MRI) revealed moderate-to-complete filling of all chondral defects (30). The use of this scaffold in combination with platelet-rich plasma (PRP) has been shown in some studies to enhance chondrogenesis and the formation of hyaline-like tissue to fill the defect (31).

Investigators in the field of tissue engineering have explored the use of advanced scaffolds that incorporate specific cell sources and/or bioactive molecules to aid in tissue maturation (32). The BST-CarGel (Smith & Nephew) procedure uses a gel matrix composed of chitosan and autologous blood that is implanted into a defect treated by marrow stimulation techniques. The matrix has been shown to enhance early healing processes such as cell

Table 1. Clinical studies of cartilage repair techniques*

Author, year (ref.)	Type of study	LE	Cartilage repair technique	No. of patients in study group/no. of patients in control group	Follow-up, years†	Defect size, mean cm^2	Results
Shive et al, 2015 (34)	RCT	II	BST-CarGel vs. MFX	34/26	5	2.24	Sustained and significantly superior repair tissue quantity and quality with BST-CarGel; no clinical differences
Gobbi et al, 2014 (37)	Case series	IV	BMAC associated with type I/III collagen matrix	25	3.4	8.3	Significant improvement in all clinical scores; complete filling of the defect in 80% of patients
Saris et al, 2014 (74)	RCT	II	MACI vs. MFX	72/72	2	4.8	Significantly better clinical outcome with MACI
Basad et al, 2010 (41)	RCT	II	MACI vs. MFX	40/20	2	4–10	Significantly better outcome with MACI
Van Assche et al, 2009 (75)	RCT	II	ACI vs. MFX	33/34	2	2.4	No significant differences between groups
Cole et al, 2011 (43)	RCT	II	CAIS vs. MFX	20/9	2	3.11	Significantly higher incidence of intralesional osteophyte formation with MFX; no clinical difference between groups
Bentley et al, 2012 (76)	RCT	II	OAT vs. ACI	42/58	2	4.2	Significantly better functional outcome and graft survival with ACI
Ulstein et al, 2014 (77)	RCT	II	MFX vs. OAT	11/14	9.8	2.8	No significant clinical differences
Levy et al, 2013 (78)	Case series	IV	OCA	122	13.5	8.1	Improvement of pain and function; 85% survival at 10 years

* LE = level of evidence; RCT = randomized controlled trial; MFX = microfracture; BMAC = bone marrow aspirate concentrate; MACI = matrix-induced autologous chondrocyte implantation; ACI = autologous chondrocyte implantation; CAIS = cartilage autograft implantation system procedure; OAT = osteochondral autologous transplantation; OCA = osteochondral allograft.
† Values in the studies by Ulstein et al (77) and Levy et al (78) are the median; values in the other studies are the mean.

recruitment, vascularization of the repair tissue, and subchondral bone remodeling (33). A study comparing BST-CarGel with isolated microfracture demonstrated superiority of the former technique by MRI and histologic evaluation; however, there were no statistically significant clinical differences after 5 years of follow-up (34).

Another recently developed technique is Bio-Cartilage (Arthrex), a modified microfracture technique that uses micronized allogenic cartilage in combination with PRP to create a biochemically active scaffold populated by mesenchymal stem cells (MSCs) from the microfractured bed (35). Despite several investigators having

Table 2. Controlled trial on the use of PRP in cartilage repair procedures*

Author, year (ref.)	Type of study	LE	Patient age, years	Type of PRP	Follow-up, months	Defect	Treatment	Total no. of patients (no. in study group/no. in control group	Results
Lee et al, 2013 (80)	Randomized prospective comparative	II	40–50	Leukocyte	Up to 24	Cartilage defects of the femoral condyle up to 4 cm^2	1 PRP injection in association with microfracture	49 (24/25)	Significantly better clinical results in the study group than in the control group at 24 months after surgery
Manunta et al, 2013 (79)	Randomized prospective comparative	II	30–55	Leukocyte	Up to 24	Outerbridge grade II and III cartilage defects of the femoral condyle	3 PRP injections in association with microfracture	20 (10/10)	Faster functional recovery and resolution of pain in PRP-treated patients; better IKDC score although not statistically significant

* PRP = platelet-rich plasma; LE = level of evidence; IKDC = International Knee Documentation Committee.

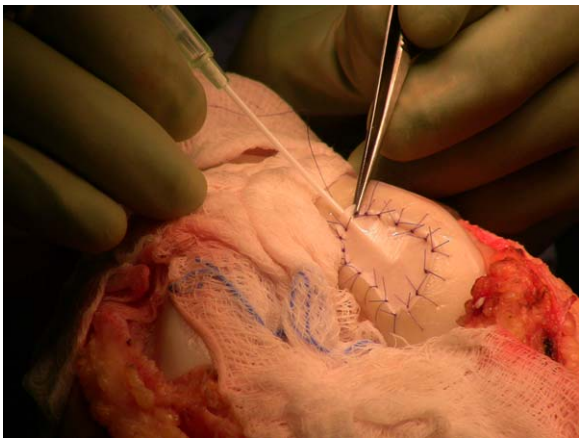

Figure 1. Injection of the chondrocyte suspension in the autologous chondrocyte implantation procedure. The defect has been debrided and covered with a collagen membrane.

suggested a valid and additive effect of PRP for cartilage repair in association with chondral matrix or osteochondral scaffolds (31,36), only few randomized clinical trials have been completed (Table 2).

Bone marrow aspirate concentrate (BMAC). An alternative to traditional microfracture is the use of BMAC obtained from either the iliac crest or the knee itself. Similar to the autologous matrix-induced chondrogenesis technique, a collagen membrane scaffold is secured over the defect, but the marrow cells are brought into the defect with the BMAC clot, not only obviating the need to injure the subchondral plate, but also allowing substantially higher numbers of MSCs into the defect compared with the number allowed using the microfracture technique. Medium-term results in small series have demonstrated durable clinical and imaging improvement (37).

Cell-based techniques

Autologous chondrocyte implantation (ACI). ACI is a cell-based approach in which a cartilage biopsy specimen is harvested from a lesser-weight-bearing region of the joint during an initial arthroscopic procedure. Chondrocytes are isolated from the biopsy sample, and the culture is expanded. The cells are either reimplanted directly after a 4-week culture process or cryogenically preserved and stored for up to 5 years. The technique as originally described was performed using a periostal flap to cover the defect; currently, however, a collagen membrane is used. The chondrocyte suspension is injected into the created space (Figure 1). ACI has demonstrated improvement in pain and functional outcomes in up to 80% of patients at 10–20 years (14,38). A systematic review showed that patients with specific factors, such as a defect size of >4 cm^2, higher activity level, and age >30 years, seem to benefit more from ACI (39). In another systematic review, Harris et al (40) observed that in patients with a defect size of >4 cm^2, ACI resulted in better outcomes compared with other cartilage repair procedures. The inherent limitations of ACI, however, include the need for 2 procedures and a comparatively long recovery time of 6–12 months. Overall, ACI is mainly reserved for the treatment of large chondral lesions (>4 cm^2) and patients who have high activity demands (i.e., those who regularly engage in athletic activities).

Matrix-induced autologous chondrocyte implantation (MACI). MACI (Vericel) is a third-generation ACI technique whereby the chondrocytes are also first grown in 2-dimensional culture but then are seeded onto a collagen scaffold prior to shipping by the supplier. Implantation can be performed through an open incision or arthroscopically. Although MACI is not yet approved in the US, it has been used in Europe since 1999, demonstrating short-term and

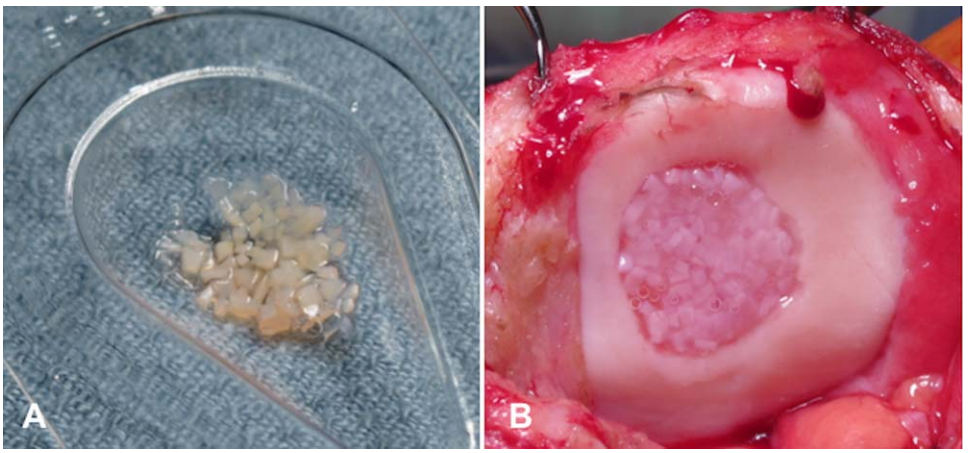

Figure 2. **A,** Particulated allograft cartilage pieces. **B,** Final aspect of the fibrin glue/cartilage construct in a patellar defect.

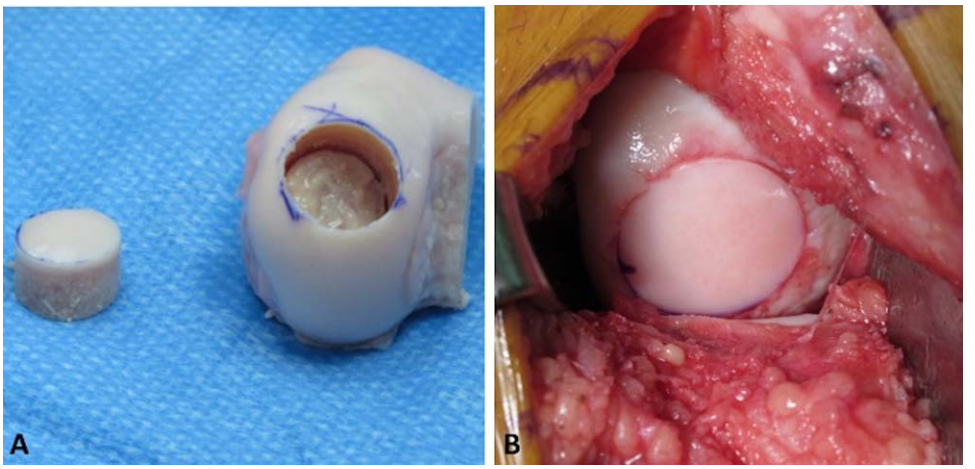

Figure 3. **A,** Osteochondral plug harvested from a donor hemicondyle. **B,** Plug seated in the lateral femoral condyle.

medium-term outcomes equal to those associated with the standard ACI technique with which it shares the same indications.

Use of the MACI technique for full-thickness cartilage lesions of the knee has consistently demonstrated good results at short-term follow-up (2). MACI has also shown superior clinical outcomes compared with microfracture at 2-year and 3-year follow-up (4,25). Medium-term outcomes have also been promising, with 98% of patients reporting satisfactory pain relief and 86% reporting improvement in activities of daily living (41).

Particulated cartilage procedures. Particulated autograft and allograft (DeNovo NT Natural Tissue Graft; Zimmer) procedures involve implantation of particulated articular cartilage from either autograft or juvenile allograft cartilage, respectively. For the autograft procedure, cartilage is arthroscopically harvested from a lesser-weight-bearing region of the joint. This cartilage is mechanically minced and then reimplanted into the defect with fibrin glue. Preclinical studies have shown formation of hyaline-like repair tissue (42), and a clinical study has demonstrated favorable outcomes (43).

Particulated juvenile allograft cartilage consists of articular cartilage obtained from juvenile donors that has been cut into ~1-mm cubes (Figure 2A). It is secured in the debrided defect with fibrin glue (Figure 2B). Case series of patients treated with particulated juvenile allograft cartilage demonstrated results comparable with those for other cartilage repair procedures at short-term follow-up (44).

Osteochondral techniques

Osteochondral procedures differ from the above-described techniques by their bilayer nature, consisting of both cartilage and subchondral bone. They are primarily indicated for the treatment of defects associated with abnormalities of the subchondral bone, such as cysts and extensive edema.

Osteochondral autograft transfer (OAT). OAT is a technique in which osteochondral cylinders are harvested from lesser-weight-bearing areas of the knee and transferred to correct chondral, as well as osteochondral, defects, mostly in the same knee but also in other joints such as the elbow, ankle, and foot. The advantages of this technique include the transfer of autologous mature hyaline cartilage with maintenance of its histologic architecture, single-stage application, and relatively low cost. Chondral defects ($<$2–3 cm^2) of the femoral condyles are most amenable to OAT. The treatment of larger lesions is limited by donor-site morbidity. Harvesting too many plugs results in the creation of defects elsewhere in the knee, which, when greater than a certain size, can become symptomatic on their own. The OAT technique is usually performed arthroscopically or through a mini open incision. The lesion is sized, and a cylindrical recipient site is created that is 10–15 mm in depth. Next, a donor plug of corresponding diameter is obtained and implanted into the recipient site via a press–fit technique. The application of OAT for small lesions has shown good-to-excellent results in $>$80% of patients and complete graft integration in 75% of cases, with 60% graft survival beyond 9-year follow-up (45).

Osteochondral allograft (OCA) transplantation. OCA transplantation is an extension of the OAT technique but harvests grafts from donated knee joints rather than using the patient's own tissue, thus eliminating donor-site morbidity. Currently, grafts are harvested within 48 hours of asystole and usually involve donors age

<40 years who have passed a very detailed screening process. The viability of chondrocytes within the graft remains at acceptable levels for ~28 days (46). The use of OCA transplantation has steadily increased, and it is used not only for the treatment of primary defects but also to salvage failed cartilage restoration procedures and posttraumatic deformities. In general, OCA transplantation is used to treat larger primary defects (>4 cm^2), especially osteochondral defects associated with subchondral edema or a damaged subchondral plate. Focal defects from osteochondritis dissecans or avascular necrosis as well as larger posttraumatic defects, such as tibial plateau fractures, are amenable to OCA transplantation.

Typically, OCAs are placed via a mini arthrotomy, and a reamer is used to create a recipient slot of ~6–8 mm in depth. Next, the osteochondral plug is prepared and inserted via the same method as that used for the OAT technique (Figure 3). The success of OCA transplantation is highly dependent on incorporation of the bony portion of the graft. The chondral portion of the graft remains isolated from the host immune system due to the dense extracellular matrix; however, the bony portion remains susceptible to immune reactions, with antibody-negative patients having a better outcome compared with antibody-positive patients. Therefore, the use of "shell grafts" with a composite thickness of only 6–8 mm is favored, minimizing the immunogenic bony component. OCA transplantation has demonstrated good-to-excellent results at long-term follow-up. Studies have shown graft survival rates of 91% at 5 years, 76% at 15 years, and 66% at 20 years (47,48).

Cell-free implants

The use of 3-dimensional artificial scaffolds for guided growth of regenerative tissue is an emerging treatment strategy in cartilage repair, stimulated by increased cost-consciousness of health care systems worldwide that are no longer able to afford the high cost of cell-cultured products or even allograft tissue. These constructs are multilayered to promote the formation of a regenerative tissue structure that more closely matches the native organization of the osteochondral unit. Two examples of these scaffolds include Agili-C (CartiHeal) and MaioRegen (Finceramica), neither of which is currently available in the US.

Agili-C is a bilayered plug made from coral. The cartilage portion is composed of aragonite and hyaluronic acid (HA) to allow for immigration of chondrocytes from the surrounding cartilage, as well as differentiation of MSCs from the subchondral bone into chondrocytes. The bony portion is composed of an aragonite crystalline structure to allow for invasion of native osteoblasts.

MaioRegen is a tri-layered collagen and hydroxyapatite scaffold consisting of a cartilaginous layer, intermediate layer, and mineralized layer with varying compositions of collagen and hydroxyapatite to recreate the structure of the entire osteochondral unit (49). The largest clinical series evaluating this technique demonstrated statistically significant improvement in clinical scores at 2 years and 5 years, with 78% of patients showing complete fill of the defect by MRI, which was maintained at 5 years (50).

Emerging technologies for biologic augmentation procedures for cartilage repair

The cartilage repair techniques discussed above are limited to filling a focal chondral or osteochondral defect and do not otherwise influence the biologic environment of the joint. It is becoming increasingly apparent that joint homeostasis plays an important role in the success of cartilage repair. Therefore, biologic augmentation of the joint environment is increasingly being explored, both as a concurrent procedure in cartilage repair and as a stand-alone treatment option.

Growth factors. Growth factors play a major role in the regulation of cell interactions and cell behavior, including that of chondrocytes. Among them, insulin-like growth factor 1 (IGF-1), fibroblast growth factor 2 (FGF-2), FGF-18, and transforming growth factor β1 (TGFβ1) are the most influential for articular cartilage. They can be regulated genetically or epigenetically, cross-talk with a variety of signaling pathways, and regulate multiple catabolic and anabolic processes in cartilage tissue. Several in vitro and preclinical studies have demonstrated the ability of growth factors to provide symptom relief and enhance the quality of tissue fill when used in combination with cartilage regeneration (51). Their effects depend on many variables, including dose, formulation, delivery mode, treatment protocol, intraarticular environment, and integration (52). However, despite the vast knowledge about the effects of growth factors demonstrated in in vitro and preclinical models, there are very few completed human clinical trials. In particular, the only clinical trials available focus on the injection of recombinant growth factors in patients with knee OA. Although definitive conclusions cannot be drawn yet, limited results demonstrate the potential of this approach in slowing degenerative processes.

Platelet concentrates. Although the use of recombinant growth factors requires specific regulatory approval, autologous growth factors obtained after minimal manipulation do not. For this reason, blood derivatives are considered safe, easy, cost-effective, and minimally invasive agents to exploit the effectiveness of bioactive molecules to improve the joint environment and possibly facilitate

Table 3. Controlled studies of MSCs (either expanded or concentrated) in cartilage repair*

Author, year (ref.)	Type of study	LE	Patient age, years†	Source of MSCs	Follow-up, months	Defect	Treatment	Total no. of patients (no. in study group/no. in control group)	Results
Nejadnik et al, 2010 (64)	Nonrandomized cohort	III	44	Bone marrow (expanded)	24	ICRS grade III/IV cartilage defect of the femoral condyle‡	BMSC with collagen membrane vs. ACI (concomitant procedures: PF realignment, HTO, ACLR, meniscectomy)	72 (36/36)	Significant improvement from baseline in both groups; no significant clinical differences between groups
Lee et al, 2012 (80)	Nonrandomized cohort	III	44	Bone marrow (expanded)	24§	More than 1 full-thickness cartilage defect	BMSC/HA injection associated with MFX vs. BMSC open implantation with patch for chondral defects	70 (35/35)	Significant improvement from baseline in both groups; no significant clinical differences between groups
Wong et al, 2013 (83)	RCT	II	51 (36–54)	Bone marrow (expanded)	24	Medial compartment OA	HTO and BMSC intrarticular injection vs. HTO	56 (28/28)	Significantly better clinical and MRI results with BMSC
Koh et al, 2014 (81)	Prospective comparative	II	54	Adipose tissue (concentrated SVF)	24	Isolated medial knee compartment OA, up to K/L grade 3	HTO in association with SVF and PRP injection vs. HTO with PRP injection	44 (21/23)	Better clinical score and cartilage regeneration in the SVF group
Koh et al, 2016 (82)	Randomized prospective comparative	II	39 (18–50)	Adipose tissue (concentrated SVF)	24	ICRS grade III/IV cartilage defect >3 cm^2 on the femoral condyle	SVF in fibrin glue and MFX vs. MXT alone	80 (40/40)	Radiologic and clinical improvement with SVF in fibrin glue and MFX
Saw et al, 2013 (72)	Randomized prospective comparative	II	45 (22–60)	Peripheral blood (apheresis after filgrastim stimulation)	24¶	ICRS grade III/IV cartilage defect	8 intraarticular injections of stem cells and HA vs. 8 intraarticular injections of HA after arthroscopic drilling and abrasion	50 (25/25)	No significant differences in clinical outcomes; better quality of articular cartilage repair in the stem cells group
Akgun et al, 2015 (70)	Randomized prospective comparative	II	32 (18–41)	Synovial membrane	24	Isolated chondral defect >2 cm^2	Matrix-induced autologous MSC implantation vs. matrix-induced autologous chondrocyte implantation	14 (7/7)	Significantly better clinical outcomes in the MSC group

* LE = level of evidence; MSCs = mesenchymal stem cells; ICRS = International Cartilage Repair Society Scale; BMSC = bone marrow stem cell; ACI = autologous chondrocyte implantation; PF = patellofemoral; HTO = high tibial osteotomy; ACLR = anterior cruciate ligament reconstruction; HA = hyaluronic acid; MFX = microfracture; RCT = randomized controlled trial; OA = osteoarthritis; SVF = stromal vascular fraction; K/L = Kellgren/Lawrence; PRP = platelet-rich plasma.
† Values in the studies by Nejadnik et al (64), Lee et al (80), and Koh et al (81) are the mean; values in the other studies are the median (range).
‡ Mean size 4.6 cm^2 in the bone marrow stem cell (BMSC) group.
§ Magnetic resonance imaging (MRI) was performed at 12 months.
¶ Arthroscopy was performed at 18 months.

cartilage healing. Among blood derivatives, PRP is the most studied. PRP contains multiple growth factors, including platelet-derived growth factor, TGFβ, FGF, IGF-1, connective tissue growth factor, epidermal growth factor, and hepatocyte growth factor (53,54), as well as various microRNAs involved in mesenchymal tissue regeneration and differentiation of MSCs into chondrocytes (55). In vitro and preclinical study findings have demonstrated that PRP exerts different actions on cartilage: a chemotactic effect on MSCs and human subchondral progenitor cells together with stimulation of proliferation, antiinflammatory action, and potential antiapoptotic effects (56). These properties are desirable in a degenerative joint environment, especially the antiinflammatory effects, whereby decreasing inflammation in the synovial tissue leads to a reduction in matrix metalloproteinases, which have a detrimental effect on cartilage matrix (53).

MSCs. MSCs can differentiate into chondrocyte-like cells when appropriately stimulated. Moreover, MSCs possess trophic, immunomodulatory, and antiinflammatory properties exhibited through direct cell–cell interaction or secretion of bioactive molecules (57). Therefore, through either direct involvement in the repair process or their function as growth factor "drug stores," MSCs may enhance cartilage repair and regeneration. Numerous recent in vitro and preclinical studies have demonstrated the feasibility and efficacy of MSCs for the treatment of cartilage disease (58). Due to the versatility of MSCs, their potential can be exploited in different ways, such as direct surgical repair, augmentation of other cartilage repair procedures, or an injection-only approach. In recent years, the number of clinical studies concerning the use of MSCs for the treatment of cartilage repair has dramatically increased, although only very few randomized clinical trials are currently available (Table 3). The abundant literature regarding MSCs can be classified according to several parameters, including the source of MSCs (bone marrow versus adipose tissue), their origin with respect to the recipient patient (autologous versus allogenic), the procurement procedure (expanded versus concentrated cells), and the manner of administration (surgical implantation versus injection).

Source. MSCs derived from bone marrow (BMSCs) are the most frequently investigated and still represent the de facto standard. Recently, the use of subcutaneous adipose tissue has been explored, and this tissue is increasingly being used as a source of MSCs due to its ready availability, simplicity, and minimally invasive method of harvesting. Moreover, it has been demonstrated that the frequency as well as the immunomodulatory capacity of adipose tissue–derived stem cells (ASCs) is higher than that of BMSCs (59), and that their properties are less likely to be affected by patient age (60).

However, thus far no significant differences have been observed using these 2 types of MSCs regarding clinical outcomes of cartilage defect treatment. Both expanded BMSCs (61,62) and ASCs (63) have been used for cartilage repair, mainly in association with different scaffolds. Most of these studies showed clinical improvement and a complete defect fill with a follow-up period ranging from 1 year to 5 years (61) and good integration with the surrounding healthy cartilage (62). From a histologic perspective, some studies showed the presence of hyaline-like tissue (63,64), fibrocartilage (61), or a mixture of both (65). A cohort study comparing the efficacy of ACI with the use of expanded BMSCs showed that BMSCs were as effective as chondrocytes at 2 year follow-up (64). However, particularly for ASCs, conclusive clinical results have yet to be published.

Administration. The benefit of a focal cartilage defect is that it is contained within healthy cartilage, and the surgical delivery of MSCs or other biologic agents can be more effective than nondirected use within the whole joint through injection for the treatment of early OA. In patients with early OA, MSCs are injected intraarticularly, with the aim of delaying or obviating progression toward worsening joint degeneration. Given the inflammatory features of OA, the trophic, immunomodulatory and antiinflammatory effects of MSCs may prove particularly beneficial (63).

Use of expanded or concentrated MSCs. From the biologic point of view, the main difference between the use of expanded MSCs or progenitor cell concentrates is the homogeneity of the cell population. When using a homogeneous expanded MSC population, the technique is more reproducible, because it allows calculation of the precise number of cells used for each treatment, facilitating conclusions regarding correlations between clinical outcomes and the number of cells used. However, treatment with expanded cells is a necessarily more expensive 2-step procedure and is considered an advanced-therapy medicinal product that is subject to more rigorous regulatory requirements prior to clinical use. Therefore, progenitor cell concentrates, from either BMAC or adipose tissue (stromal vascular fraction or micro-fragmented adipose tissue), seem to be a valid alternative, because they combine the potential of MSCs with the advantages of a 1-step procedure. Conversely, these concentrates contain a lower number of MSCs in comparison with an expanded cell suspension and cannot be considered a homogeneous product (58), but rather a bone marrow or adipose tissue niche composed of different cell types (66).

Treatment with allogenic or autologous cells. An emerging technique in biologics is the introduction of allogenic cells for the treatment of cartilage disease. Although it is well known that MSCs are nonimmunogenic due to their low expression of antigen-presenting molecules (67), and despite the number of preclinical studies demonstrating the feasibility and safety of their use in the treatment of cartilage injuries (68), few clinical studies have explored the application of allogenic MSCs for cartilage repair. Improvements in clinical scores, with satisfactory cartilage repair confirmed by MRI and arthroscopy, have been reported (69,70). Due to the increased interest in this approach, several trials are ongoing, including phase I/II clinical trials in the US and The Netherlands, investigating umbilical cord blood MSCs and allogenic BMSCs in combination with autologous chondrocytes together with their pericellular matrix (chondrons), respectively. Cartistem injection (Medipost), an emerging technique currently undergoing a Food and Drug Administration phase I/II trial, utilizes culture-expanded allogenic umbilical cord blood MSCs that are surgically implanted with an HA scaffold into a microfractured defect (52).

In a separate study, Saw and colleagues investigated the use of peripheral blood MSCs injected postoperatively after arthroscopic drilling (71). The injections of autologous stem cells mixed with HA were performed at weekly intervals for 4 weeks, starting on postoperative day 7. In a subsequent randomized controlled trial by the same group of investigators evaluating article cartilage regeneration, postoperative injections of autologous peripheral blood MSCs in combination with HA resulted in improvement of the quality of articular cartilage repair compared with the same treatment without peripheral MSCs, as demonstrated by histologic and MRI evaluation (72).

Failure

The goal of cartilage repair surgery is functional (and secondarily, also structural) improvement of the joint. Recurrence of clinical symptoms and inability to recover function are the main manifestations of clinical failure, usually associated with graft failure. Three main mechanisms of failure have been identified: mechanical/traumatic, biologic, and progression of disease. Mechanical failure is characterized by delamination, in which an initially well-formed graft becomes detached from the subchondral bone. Biologic failure is related to tissue formation and integration with the adjacent cartilage and subchondral bone. Progression of disease beyond the borders of the original defect can be focal or diffuse, the latter of which is characterized by progression toward OA. These mechanisms generally apply to all repair techniques. However, each procedure has specific intrinsic healing characteristics, and the exact mechanism of failure may vary depending on the technique used. A more in-depth discussion of failure mechanisms is outside the scope of this article, but treatment failure has been the topic of a recent detailed review (73).

Conclusions

The field of cartilage repair and regeneration remains a vibrant and rapidly evolving part of orthopedic surgery. Current techniques are successful in 70–85% of patients presenting with cartilage defects in the knee. The ultimate goal of avoiding knee replacement surgery remains elusive at this time, although studies have demonstrated success in delaying the need for arthroplasty. Clearly, there is a need for further improvements in efficacy, associated morbidity, and cost. Biologic augmentation of current techniques by use of bone marrow, stem cells, and growth factors is currently being investigated in preclinical and early clinical studies, as is the use of injection therapy for established OA.

AUTHOR CONTRIBUTIONS

All authors were involved in drafting the article or revising it critically for important intellectual content, and all authors approved the final version to be published.

REFERENCES

1. Davies-Tuck ML, Wluka AE, Wang Y, Teichtahl AJ, Jones G, Ding C, et al. The natural history of cartilage defects in people with knee osteoarthritis. Osteoarthritis Cartilage 2008;16:337–42.
2. D'Anchise R, Manta N, Prospero E, Bevilacqua C, Gigante A. Autologous implantation of chondrocytes on a solid collagen scaffold: clinical and histological outcomes after two years of follow-up. J Orthop Traumatol 2005;6:36–43.
3. Heir S, Nerhus TK, Røtterud JH, Løken S, Ekeland A, Engebretsen L, et al. Focal cartilage defects in the knee impair quality of life as much as severe osteoarthritis: a comparison of knee injury and osteoarthritis outcome score in 4 patient categories scheduled for knee surgery. Am J Sports Med 2010;38: 231–7.
4. Saris DB, Vanlauwe J, Victor J, Almqvist KF, Verdonk R, Bellemans J, et al. Treatment of symptomatic cartilage defects of the knee: characterized chondrocyte implantation results in better clinical outcome at 36 months in a randomized trial compared to microfracture. Am J Sports Med 2009;37 Suppl:10–9S.
5. Felson DT. Risk factors for osteoarthritis: understanding joint vulnerability. Clin Orthop Relat Res 2004;427 Suppl:S16–21.
6. Bitton R. The economic burden of osteoarthritis. Am J Manag Care 2009;15 Suppl:S230–5.
7. Guccione AA, Felson DT, Anderson JJ, Anthony JM, Zhang Y, Wilson PW, et al. The effects of specific medical conditions on the functional limitations of elders in the Framingham study. Am J Public Health 2011;84:351–8.
8. Dexter P, Brandt K. Distribution and predictors of depressive symptoms in osteoarthritis. J Rheumatol 1994;21:279–86.
9. Vazquez-Vela Johnson G, Worland RL, Keenan J, Norambuena N. Patient demographics as a predictor of the ten-year survival

rate in primary total knee replacement. J Bone Joint Surg Br 2003;85:52–6.
10. Lonner JH, Hershman S, Mont M, Lotke PA. Total knee arthroplasty in patients 40 years of age and younger with osteoarthritis. Clin Orthop Relat Res 2000;380:85–90.
11. Robertsson O, Dunbar M, Pehrsson T, Knutson K, Lidgren L. Patient satisfaction after knee arthroplasty: a report on 27,372 knees operated on between 1981 and 1995 in Sweden. Acta Orthop Scand 2000;71:262–7.
12. Sheng PY, Konttinen L, Lehto M, Ogino D, Jämsen E, Nevalainen J, et al. Revision total knee arthroplasty: 1990 through 2002. J Bone Joint Surg Am 2006 1;88:1425–30.
13. Lavernia C, Lee DJ, Hernandez VH. The increasing financial burden of knee revision surgery in the United States. Clin Orthop Relat Res 2006;446:221–6.
14. Minas T, von Keudell A, Bryant T, Gomoll AH. The John Insall Award: a minimum 10-year outcome study of autologous chondrocyte implantation. Clin Orthop Relat Res 2013;472:41–51.
15. Farr J, Rawal A, Marberry KM. Concomitant meniscal allograft transplantation and autologous chondrocyte implantation: minimum 2-year follow-up. Am J Sports Med 2007;35:1459–66.
16. Lotz MK, Otsuki S, Grogan SP, Sah R, Terkeltaub R, D'Lima D. Cartilage cell clusters [review]. Arthritis Rheum 2010;62:2206–18.
17. Coventry MB. Upper tibial osteotomy for gonarthrosis: the evolution of the operation in the last 18 years and long term results. Orthop Clin North Am 1979;10:191–210.
18. Cerejo R, Dunlop DD, Cahue S, Channin D, Song J, Sharma L. The influence of alignment on risk of knee osteoarthritis progression according to baseline stage of disease. Arthritis Rheum 2002;46:2632–6.
19. Gomoll AH, Farr J, Gillogly SD, Kercher J, Minas T. Surgical management of articular cartilage defects of the knee. J Bone Joint Surg Am 2010;92:2470–90.
20. Englund M, Guermazi A, Lohmander LS. The meniscus in knee osteoarthritis. Rheum Dis Clin North Am 2009;35:579–90.
21. Shapiro F, Koide S, Glimcher MJ. Cell origin and differentiation in the repair of full-thickness defects of articular cartilage. J Bone Joint Surg Am 1993;75:532–53.
22. Steadman JR, Rodkey WG, Singleton SB, Briggs KK. Microfracture technique for full-thickness chondral defects: technique and clinical results. Oper Tech Orthop 1997;7:300–4.
23. Steadman JR, Briggs KK, Rodrigo JJ, Kocher MS, Gill TJ, Rodkey WG. Outcomes of microfracture for traumatic chondral defects of the knee: average 11-year follow-up. Arthroscopy 2003;19:477–84.
24. Kreuz PC, Steinwachs MR, Erggelet C, Krause SJ, Konrad G, Uhl M, et al. Results after microfracture of full-thickness chondral defects in different compartments in the knee. Osteoarthritis Cartilage 2006;14:1119–25.
25. Goyal D, Keyhani S, Lee EH, Hui JH. Evidence-based status of microfracture technique: a systematic review of level I and II studies. Arthroscopy 2013;29:1579–88.
26. Mithoefer K, McAdams T, Williams RJ, Kreuz PC, Mandelbaum BR. Clinical efficacy of the microfracture technique for articular cartilage repair in the knee: an evidence-based systematic analysis. Am J Sports Med 2009;37:2053–63.
27. Gracitelli GC, Moraes VY, Franciozi CE, Luzo MV, Belloti JC. Surgical interventions (microfracture, drilling, mosaicplasty, and allograft transplantation) for treating isolated cartilage defects of the knee in adults. Cochrane Database Syst Rev 2016;9:CD010675.
28. Miller BS, Steadman JR, Briggs KK, Rodrigo JJ, Rodkey WG. Patient satisfaction and outcome after microfracture of the degenerative knee. J Knee Surg 2004;17:13–7.
29. Benthien JP, Behrens P. Autologous matrix-induced chondrogenesis (AMIC): a one-step procedure for retropatellar articular resurfacing. Acta Orthop Belg 2010;76:260–3.
30. Gille J, Schuseil E, Wimmer J, Gellissen J, Schulz AP, Behrens P. Mid-term results of autologous matrix-induced chondrogenesis for treatment of focal cartilage defects in the knee. Knee Surg Sports Traumatol Arthrosc 2010;18:1456–64.
31. Dhollander AA, de Neve F, Almqvist KF, Verdonk R, Lambrecht S, Elewaut D, et al. Autologous matrix-induced chondrogenesis combined with platelet-rich plasma gel: technical description and a five pilot patients report. Knee Surg Sports Traumatol Arthrosc 2011;19:536–42.
32. Daher RJ, Chahine NO, Greenberg AS, Sgaglione NA, Grande DA. New methods to diagnose and treat cartilage degeneration. Nat Rev Rheumatol 2009;5:599–607.
33. Chevrier A, Hoemann CD, Sun J, Buschmann MD. Chitosan-glycerol phosphate/blood implants increase cell recruitment, transient vascularization and subchondral bone remodeling in drilled cartilage defects. Osteoarthritis Cartilage 2007;15:316–27.
34. Shive MS, Stanish WD, McCormack R, Forriol F, Mohtadi N, Pelet S, et al. BST-CarGel® treatment maintains cartilage repair superiority over microfracture at 5 years in a multicenter randomized controlled trial. Cartilage 2015;6:62–72.
35. Meretoja VV, Dahlin RL, Kasper FK, Mikos AG. Enhanced chondrogenesis in co-cultures with articular chondrocytes and mesenchymal stem cells. Biomaterials 2012;33:6362–9.
36. Buda R, Vannini F, Cavallo M, Baldassarri M, Luciani D, Mazzotti A, et al. One-step arthroscopic technique for the treatment of osteochondral lesions of the knee with bone-marrow-derived cells: three years results. Musculoskelet Surg 2013;97:145–51.
37. Gobbi A, Karnatzikos G, Sankineani SR. One-step surgery with multipotent stem cells for the treatment of large full-thickness chondral defects of the knee. Am J Sports Med 2014;42:648–57.
38. Peterson L, Vasiliadis HS, Brittberg M, Lindahl A. Autologous chondrocyte implantation: a long-term follow-up. Am J Sports Med 2010;38:1117–24.
39. Bekkers JE, Inklaar M, Saris DB. Treatment selection in articular cartilage lesions of the knee: a systematic review. Am J Sports Med 2009;37 Suppl 1:148–155S.
40. Harris JD, Siston RA, Pan X, Flanigan DC. Autologous chondrocyte implantation: a systematic review. J Bone Joint Surg Am 2010;92:2220–33.
41. Basad E, Ishaque B, Bachmann G, Stürz H, Steinmeyer J. Matrix-induced autologous chondrocyte implantation versus microfracture in the treatment of cartilage defects of the knee: a 2-year randomised study. Knee Surg Sports Traumatol Arthrosc 2010;18:519–27.
42. Frisbie DD, Lu Y, Kawcak CE, DiCarlo EF, Binette F, McIlwraith CW. In vivo evaluation of autologous cartilage fragment-loaded scaffolds implanted into equine articular defects and compared with autologous chondrocyte implantation. Am J Sports Med 2009;37 Suppl:71–80S.
43. Cole BJ, Farr J, Winalski CS, Hosea T, Richmond J, Mandelbaum B, et al. Outcomes after a single-stage procedure for cell-based cartilage repair: a prospective clinical safety trial with 2-year follow-up. Am J Sports Med 2011;39:1170–9.
44. Farr J, Tabet SK, Margerrison E, Cole BJ. Clinical, radiographic, and histological outcomes after cartilage repair with particulated juvenile articular cartilage: a 2-year prospective study. Am J Sports Med 2014;42:1417–25.
45. Hangody L, Füles P. Autologous osteochondral mosaicplasty for the treatment of full-thickness defects of weight-bearing joints. J Bone Joint Surg Am 2003;85 Suppl 2:25–32.
46. Bugbee WD, Pallante-Kichura AL, Görtz S, Amiel D, Sah R. Osteochondral allograft transplantation in cartilage repair: graft storage paradigm, translational models, and clinical applications. J Orthop Res 2015;34:31–8.
47. Tetta C, Busacca M, Moio A, Rinaldi R, Delcogliano M, Kon E, et al. Knee osteochondral autologous transplantation: long-term MR findings and clinical correlations. Eur J Radiol 2010;76:117–23.
48. Emmerson BC, Gortz S, Jamali AA, Chung C, Amiel D, Bugbee WD. Fresh osteochondral allografting in the treatment of

osteochondritis dissecans of the femoral condyle. Am J Sports Med 2007;35:907–14.
49. Tampieri A, Sandri M, Landi E, Pressato D, Francioli S, Quarto R, et al. Design of graded biomimetic osteochondral composite scaffolds. Biomaterials 2008;29:3539–46.
50. Kon E, Filardo G, Di Martino A, Busacca M, Moio A, Perdisa F, et al. Clinical results and MRI evolution of a nano-composite multilayered biomaterial for osteochondral regeneration at 5 years. Am J Sports Med 2014;42:158–65.
51. Fortier LA, Barker JU, Strauss EJ, McCarrel TM, Cole BJ. The role of growth factors in cartilage repair. Clin Orthop Relat Res 2011;469:2706–15.
52. Yanke AB, Chubinskaya S. The state of cartilage regeneration: current and future technologies. Curr Rev Musculoskelet Med 2015;8:1–8.
53. Bendinelli P, Matteucci E, Dogliotti G, Corsi MM, Banfi G, Maroni P, et al. Molecular basis of anti-inflammatory action of platelet-rich plasma on human chondrocytes: mechanisms of NF-κB inhibition via HGF. J Cell Physiol 2010;225:757–66.
54. Mussano F, Genova T, Munaron L, Petrillo S, Erovigni F, Carossa S. Cytokine, chemokine, and growth factor profile of platelet-rich plasma. Platelets 2016;27:467–71.
55. Ham O, Song BW, Lee SY, Choi E, Cha MJ, Lee CY, et al. The role of microRNA-23b in the differentiation of MSC into chondrocyte by targeting protein kinase A signaling. Biomaterials 2012;33:4500–7.
56. Marmotti A, Rossi R, Castoldi F, Roveda E, Michielon G, Peretti GM. PRP and articular cartilage: a clinical update. Biomed Res Int 2015;2015:542502.
57. Murphy MB, Moncivais K, Caplan AI. Mesenchymal stem cells: environmentally responsive therapeutics for regenerative medicine. Exp Mol Med 2013;45:e54.
58. De Girolamo L, Kon E, Filardo G, Marmotti AG, Soler F, Peretti GM, et al. Regenerative approaches for the treatment of early OA. Knee Surg Sports Traumatol Arthrosc 2016;24:1826–35.
59. Melief SM, Zwaginga JJ, Fibbe WE, Roelofs H. Adipose tissue-derived multipotent stromal cells have a higher immunomodulatory capacity than their bone marrow-derived counterparts. Stem Cells Transl Med 2013;2:455–63.
60. Parker AM, Katz AJ. Adipose-derived stem cells for the regeneration of damaged tissues. Expert Opin Biol Ther 2006;6:567–78.
61. Wakitani S, Nawata M, Tensho K, Okabe T, Machida H, Ohgushi H. Repair of articular cartilage defects in the patello-femoral joint with autologous bone marrow mesenchymal cell transplantation: three case reports involving nine defects in five knees. J Tissue Eng Regen Med 2007;1:74–9.
62. Haleem AM, Singergy AA, Sabry D, Atta HM, Rashed LA, Chu CR, et al. The clinical use of human culture-expanded autologous bone marrow mesenchymal stem cells transplanted on platelet-rich fibrin glue in the treatment of articular cartilage defects: a pilot study and preliminary results. Cartilage 2010;1:253–61.
63. Jo CH, Lee YG, Shin WH, Kim H, Chai JW, Jeong EC, et al. Intra-articular injection of mesenchymal stem cells for the treatment of osteoarthritis of the knee: a proof-of-concept clinical trial. Stem Cells 2014;32:1254–66.
64. Nejadnik H, Hui JH, Feng Choong EP, Tai BC, Lee EH. Autologous bone marrow-derived mesenchymal stem cells versus autologous chondrocyte implantation: an observational cohort study. Am J Sports Med 2010;38:1110–6.
65. Kasemkijwattana C, Hongeng S, Kesprayura S, Rungsinaporn V, Chaipinyo K, Chansiri K. Autologous bone marrow mesenchymal stem cells implantation for cartilage defects: two cases report. J Med Assoc Thai 2011;94:395–400.
66. Woo DH, Hwang HS, Shim JH. Comparison of adult stem cells derived from multiple stem cell niches. Biotechnol Lett 2016;38:751–9.
67. Prockop DJ. Repair of tissues by adult stem/progenitor cells (MSCs): controversies, myths, and changing paradigms. Mol Ther 2009;17:939–46.
68. Bekkers JE, Tsuchida AI, van Rijen MH, Vonk LA, Dhert WJ, Creemers LB, et al. Single-stage cell-based cartilage regeneration using a combination of chondrons and mesenchymal stromal cells: comparison with microfracture. Am J Sports Med 2013;41:2158–66.
69. Sekiya I, Muneta T, Horie M, Koga H. Arthroscopic transplantation of synovial stem cells improves clinical outcomes in knees with cartilage defects. Clin Orthop Relat Res 2015;473:2316–26.
70. Akgun I, Unlu MC, Erdal OA, Ogut T, Erturk M, Ovali E, et al. Matrix-induced autologous mesenchymal stem cell implantation versus matrix-induced autologous chondrocyte implantation in the treatment of chondral defects of the knee: a 2-year randomized study. Arch Orthop Trauma Surg 2015;135:251–63.
71. Saw KY, Anz A, Merican S, Tay YG, Ragavanaidu K, Jee CS, et al. Articular cartilage regeneration with autologous peripheral blood progenitor cells and hyaluronic acid after arthroscopic subchondral drilling: a report of 5 cases with histology. Arthroscopy 2011;27:493–506.
72. Saw KY, Anz A, Siew-Yoke Jee C, Merican S, Ching-Soong Ng R, Roohi SA, et al. Articular cartilage regeneration with autologous peripheral blood stem cells versus hyaluronic acid: a randomized controlled trial. Arthroscopy 2013;29:684–94.
73. Dhollander A, Verdonk P, Tirico L. Treatment of failed cartilage repair: state of the art. J ISAKOS. In press.
74. Saris D, Price A, Widuchowski W, Bertrand-Marchand M, Caron J, Drogset JO, et al. Matrix-applied characterized autologous cultured chondrocytes versus microfracture: two-year follow-up of a prospective randomized trial. Am J Sports Med 2014;42:1384–94.
75. Van Assche D, Staes F, van Caspel D, Vanlauwe J, Bellemans J, Saris DB, et al. Autologous chondrocyte implantation versus microfracture for knee cartilage injury: a prospective randomized trial, with 2-year follow-up. Knee Surg Sports Traumatol Arthrosc 2009;18:486–95.
76. Bentley G, Biant LC, Vijayan S, Macmull S, Skinner JA, Carrington RW. Minimum ten-year results of a prospective randomised study of autologous chondrocyte implantation versus mosaicplasty for symptomatic articular cartilage lesions of the knee. J Bone Joint Surg Br 2012;94:504–9.
77. Ulstein S, Arøen A, Røtterud JH, Løken S, Engebretsen L, Heir S. Microfracture technique versus osteochondral autologous transplantation mosaicplasty in patients with articular chondral lesions of the knee: a prospective randomized trial with long-term follow-up. Knee Surg Sports Traumatol Arthrosc 2014;22:1207–15.
78. Levy YD, Görtz S, Pulido PA, McCauley JC, Bugbee WD. Do fresh osteochondral allografts successfully treat femoral condyle lesions? Clin Orthop Relat Res 2013;471:231–7.
79. Manunta AF, Manconi A. The treatment of chondral lesions of the knee with the microfracture technique and platelet-rich plasma. Joints 2013;1:167–70.
80. Lee GW, Son JH, Kim JD, Jung GH. Is platelet-rich plasma able to enhance the results of arthroscopic microfracture in early osteoarthritis and cartilage lesion over 40 years of age? Eur J Orthop Surg Traumatol 2012;23:581–7.
81. Koh YG, Kwon OR, Kim YS, Choi YJ. Comparative outcomes of open-wedge high tibial osteotomy with platelet-rich plasma alone or in combination with mesenchymal stem cell treatment: a prospective study. Arthroscopy 2014;30:1453–60.
82. Koh YG, Kwon OR, Kim YS, Choi YJ, Tak DH. Adipose-derived mesenchymal stem cells with microfracture versus microfracture alone: 2-year follow-up of a prospective randomized trial. Arthroscopy 2016;32:97–109.
83. Wong KL, Lee KB, Tai BC, Law P, Lee EH, Hui JH. Injectable cultured bone marrow-derived mesenchymal stem cells in varus knees with cartilage defects undergoing high tibial osteotomy: a prospective, randomized controlled clinical trial with 2 years' follow-up. Arthroscopy 2013;29:2020–8.

ARTHRITIS & RHEUMATOLOGY
Vol. 69, No. 7, July 2017, pp 1374–1380
DOI 10.1002/art.40111

Implementation of Treat-to-Target in Rheumatoid Arthritis Through a Learning Collaborative

Results of a Randomized Controlled Trial

Daniel H. Solomon,[1] Elena Losina,[1] Bing Lu,[1] Agnes Zak,[1] Cassandra Corrigan,[1] Sara B. Lee,[1] Jenifer Agosti,[2] Asaf Bitton,[3] Leslie R. Harrold,[4] Theodore Pincus,[5] Helga Radner,[6] Zhi Yu,[1] Josef S. Smolen,[6] Liana Fraenkel,[7] and Jeffrey N. Katz[1]

Objective. **Treat-to-target (TTT) is an accepted paradigm for the management of rheumatoid arthritis (RA), but some evidence suggests poor adherence. The purpose of this study was to test the effects of a group-based multisite improvement learning collaborative on adherence to TTT.**

Methods. **We conducted a cluster-randomized quality-improvement trial with waitlist control across 11 rheumatology sites in the US. The intervention entailed a 9-month group-based learning collaborative that incorporated rapid-cycle improvement methods. A composite TTT implementation score was calculated as the percentage of 4 required items documented in the visit notes for each patient at 2 time points, as evaluated by trained staff. The mean change in the implementation score for TTT across all patients for the intervention sites was compared with that for the control sites after accounting for intracluster correlation using linear mixed models.**

Results. **Five sites with a total of 23 participating rheumatology providers were randomized to intervention and 6 sites with 23 participating rheumatology providers were randomized to the waitlist control. The intervention included 320 patients, and the control included 321 patients. At baseline, the mean TTT implementation score was 11% in both arms; after the 9-month intervention, the mean TTT implementation score was 57% in the intervention group and 25% in the control group (change in score of 46% for intervention and 14% for control; $P = 0.004$). We did not observe excessive use of resources or excessive occurrence of adverse events in the intervention arm.**

Conclusion. **A learning collaborative resulted in substantial improvements in adherence to TTT for the management of RA. This study supports the use of an educational collaborative to improve quality.**

Randomized controlled clinical trials have consistently demonstrated that a strategy of treating to target (TTT) results in better outcomes compared with usual care in rheumatoid arthritis (RA). Specifically, this strategy is implemented by using disease activity measures at every visit and escalating therapy in eligible patients with disease activity above the target level (1–8). This strategy is similar to those recommended for diabetes mellitus and hypertension: setting a target for treatment, measuring progress toward achieving the target regularly, altering treatments until reaching the target, and maintaining the target. The TTT strategy for RA is based on a number of principles and recommendations articulated by an international working group and embraced by a US-based professional

ClinicalTrials.gov identifier: NCT02260778.

Supported by the NIH (National Institute of Arthritis and Musculoskeletal and Skin Diseases grant NIH-P60-AR-047782 and grant NIH-K24-AR-060231).

[1]Daniel H. Solomon, MD, Elena Losina, PhD, Bing Lu, PhD, Agnes Zak, BA, Cassandra Corrigan, BA, Sara B. Lee, MPH, Zhi Yu, MPH, Jeffrey N. Katz, MD: Brigham and Women's Hospital, Boston, Massachusetts; [2]Jenifer Agosti, MPP: JRA Consulting, Boston, Massachusetts; [3]Asaf Bitton, MD: Brigham and Women's Hospital and Ariadne Labs, Boston, Massachusetts; [4]Leslie R. Harrold, MD: University of Massachusetts Medical School, Worcester; [5]Theodore Pincus, MD: Rush Medical School, Chicago, Illinois; [6]Helga Radner, MD, Josef S. Smolen, MD: Medical University of Vienna, Vienna, Austria; [7]Liana Fraenkel, MD: Yale School of Medicine and VA Connecticut Healthcare System, New Haven, Connecticut.

Dr. Solomon has received research grants from Amgen, Lilly, Pfizer, Genentech, and the Consortium of Rheumatology Researchers of North America (CORRONA; to Brigham and Women's Hospital). Dr. Smolen has received research grants from AbbVie.

Address correspondence to Daniel H. Solomon, MD, Brigham and Women's Hospital, Division of Rheumatology, 75 Francis Street, PBB-B3, Boston, MA 02120. E-mail: dhsolomon@partners.org.

Submitted for publication October 24, 2016; accepted in revised form March 23, 2017.

society (9–11). These include identification of a disease activity target, recording of a disease activity score using a validated measure, and when appropriate, documentation of shared decision-making and reasons why TTT was not implemented.

Several lines of evidence suggest that TTT is not practiced consistently across rheumatology settings. The Consortium of Rheumatology Researchers of North America (CORRONA), the largest US-based RA registry, examined the management of patients at high risk of poor outcomes (i.e., with moderate disease activity and a poor prognosis or with high disease activity) (12,13). Despite having active disease, only one-third to one-half of patients, depending on their level of disease activity, received treatment changes over the subsequent 6–12 months. A large Australian cross-sectional study identified various reasons rheumatologists do not adjust RA treatments at visits where patients were found to have moderate or high levels of disease activity, such as irreversible joint damage and patient preferences (14).

Most attempts to align physician behavior with recommended management in chronic illnesses have demonstrated marginal benefits (15). While many studies have evaluated educational interventions for providers, methods are generally weak, and studies rarely report on adherence to guideline-based treatment (16). However, there is some limited evidence that quality collaboratives produce improvement (17). These collaboratives often include setting out principles that characterize best practices, forming teams that include health care providers and staff, rapid-cycle testing of changes in care that align with the agreed upon principles, frequent measurement of key indicators for care improvement, and collaboration across practice sites to share best practices (18). This process has been tested in many clinical settings and is often conducted as part of a group-based multisite educational collaborative, often described as a learning collaborative (19). Despite prior success with the care of diabetes mellitus (20), HIV (21), and childhood asthma (22), learning collaboratives have not been widely pursued in subspecialty medical care. We designed a learning collaborative for the purpose of improving care in patients with RA.

Since implementing TTT broadly requires health care delivery redesign across practices with different workflows and team members, we pursued a trial of a learning collaborative across 11 practices, the Treat-to-Target in RA: Collaboration to Improve Adoption and Adherence (TRACTION) trial. The goal of the TRACTION trial was to test the effectiveness of a learning collaborative for improving implementation of TTT principles in RA.

PATIENTS AND METHODS

Trial design. We conducted a cluster-randomized waitlist-controlled clinical trial to test the effects of the learning collaborative for TTT between January 2014 and October 2015. (The waitlist control sites received the intervention subsequent to October 2015.) We made contact with over 70 sites by e-mail and then interviewed 25 sites by telephone. Eleven US rheumatology practice sites were recruited to participate (see Appendix A); 9 were affiliated with academic medical centers, and 5 participated in rheumatology fellowship training programs. The 11 sites were diverse in geography, patient populations, and organization (for further site details, see Supplementary Table 1, available on the *Arthritis & Rheumatology* web site at http://onlinelibrary.wiley.com/doi/10.1002/art.40111/abstract). None was actively engaged in TTT at baseline according to a baseline interview of the team leaders by the Principal Investigator (DHS), who asked about the 4 aspects of the outcome measure (see below).

Sites were randomized to active intervention or waitlist control. Four sites described using disease activity measures at baseline, and these were evenly distributed across arms through stratified randomization, which was achieved through a random-number generator provided by the study statistician (BL). Randomization occurred at the site level since the intervention targeted practice sites, not patients or individual providers. Sites and providers were not blinded with regard to their treatment assignment.

Research activities were approved by the Institutional Review Board of Partners Healthcare.

Patient sample. All study sites were given the same instructions for selecting patients. A sample of at least 40 patients with RA was provided by each site, representing patients from providers who attended at least 1 learning session and contributed to the monthly medical record review. A minimum of 5 patients per provider was required. Visits had to have occurred within the baseline and follow-up periods described below. The medical records of these patients were included in the final review by study staff, not local site personnel. Baseline visits were defined as the first visit during the 4-month period prior to the start of the intervention: September 1, 2014 to December 31, 2014. The follow-up visits were defined as the first visit during the last 4 months of the study period: September 1, 2015 to December 31, 2015.

Intervention. The intervention consisted of a learning collaborative, which we have described elsewhere (23). Briefly, the learning collaborative involved the faculty developing a set of principles and associated concepts that describe the goals for implementing TTT principles, referred to herein as just TTT (see Supplementary Figure 1, available at http://onlinelibrary.wiley.com/doi/10.1002/art.40111/abstract). The concepts were used by the study sites to guide rapid-cycle tests of change. The principles and concepts were taught in the first learning session, which was conducted as a face-to-face 1-day meeting. The first learning session also aimed to facilitate team building by sites and cross-site collaborative relationships, and 8 subsequent monthly learning sessions were conducted via webinar. Each learning session included sites sharing a set of agreed upon metrics collected through a local medical record review. As well, a learning collaborative faculty member presented a question-and-answer session regarding the principles and concepts of TTT. More details of the learning sessions are provided in Supplementary Table 2 (available at http://onlinelibrary.wiley.com/doi/10.1002/art.40111/abstract).

We asked all team members from each site to attend all learning sessions, but this was not always possible. All learning sessions were recorded and made available on a web-based collaborative tool. The tool was developed using commercially available software (SharePoint by Microsoft) that helped manage contents being shared across teams (i.e., key resources, rapid-cycle tests of change), displayed monthly improvement metrics, and provided a discussion board with conversation "threads."

We reviewed the medical records (including visit notes, laboratory and radiology orders, and medication lists) of RA patients seen at the rheumatology practices involved in the learning collaborative from each site.

Outcome assessments. The primary trial outcome was the change in the composite TTT implementation score. The score included 4 items directly stemming from the principles and concepts of TTT: 1) specifying a disease activity target; 2) recording RA disease activity using 1 of 4 recommended measures (e.g., the Disease Activity Score in 28 joints, Simplified Disease Activity Index, Clinical Disease Activity Index [CDAI], or Routine Assessment of Patient Index Data 3 [RAPID3]), with results described numerically or by category (i.e., remission, low, moderate, or high) (24); 3) documenting shared decision-making when a decision was made (i.e., change in target or change in treatment); and 4) basing treatment decisions on the target and disease activity measure or describing reasons why TTT was not adhered to. Each item was recorded as absent or present based on a medical record review by trained study staff (interrater reliability $\kappa = 94\%$ [95% confidence interval (95% CI) 90–99], and intrarater reliability $\kappa = 98\%$ [95% CI 95–99]). We calculated the TTT implementation score for each patient as a percentage of TTT items noted in the visit notes at the baseline and follow-up visits.

Secondary outcomes were as follows: 1) percentage of patients with any positive change in implementation score between baseline and follow-up, and 2) proportion of patients with full implementation of all TTT items at follow-up. We assessed resource use by examining all visits for RA by patients in the sample over the 9-month study period. We examined the RA treatments used, the monitoring laboratory tests performed (i.e., complete blood cell count, liver function tests, or serum creatinine level), the levels of acute-phase reactants measured (i.e., erythrocyte sedimentation rate or C-reactive protein), and the diagnostic imaging performed (i.e., dual x-ray absorptiometry, plain radiographs, computed tomography scans, or magnetic resonance imaging). We also examined all visits during the study period for possible medication-related adverse events, such as rashes, oral ulcers, alopecia, infections requiring antibiotics, liver toxicity as manifested by abnormal findings on liver function tests and/or liver imaging studies, cytopenias as manifested by complete blood cell counts below the lower limits of normal, renal insufficiency as defined by a 50% decrease in creatinine clearance, cancer, gastrointestinal symptoms (e.g., nausea, vomiting, diarrhea, unexplained weight loss/gain, abdominal pain, or dyspepsia), and other miscellaneous side effects.

Post hoc secondary outcomes included the percentage of visits at which there was a change in disease-modifying antirheumatic drug and the percentage of patients in the different disease activity categories at follow-up.

Statistical power considerations. This trial was powered based on the primary outcome: the estimated difference in change in the TTT implementation score between the intervention sites and the control sites. Several assumptions underpinned our sample size calculations. First, we assumed that the control group would have no or only a small change (5%) in the TTT implementation score during the 9-month period compared with a change in the intervention group of ~20%. These assumptions were based on the improvement level observed in a similar trial using a learning collaborative (25). Second, we knew that the average number of providers at each of the 11 practice sites would be 4 and that there would be moderate intracluster correlation among patients within a given provider and site; we assumed an intracluster correlation of ~0.2 based on previous work (26). Finally, the statistically significant alpha level was set at a 2-sided P value of 0.05. Based on these assumptions, we estimated that to ensure 80% power, the required number of patients per provider would be 5.

Statistical analysis. We hypothesized that adherence to the TTT would improve to a greater extent in patients seen at rheumatology sites randomized to the learning collaborative intervention as compared with control patients seen at the waitlist sites. Thus, the primary analysis compared the mean change in the TTT implementation score over 9 months across patients in the intervention sites as compared with the mean change for the patients in the control sites after accounting for intrasite and intraprovider correlation using linear mixed models (27). Any patient covariates that were imbalanced at the baseline visit were considered for the model, including age, sex, baseline disease activity, baseline RA drugs, and disease duration. For the secondary binary outcomes (e.g., improvement versus no improvement

Table 1. Baseline characteristics of the patients included in the TRACTION trial*

	Control (n = 321)	Intervention (n = 320)
Age, mean ± SD years	59.7 ± 14.3	60.2 ± 27.5
BMI, mean ± SD kg/m^2	30.1 ± 7.5	29.4 ± 7.5
Female	250 (77.9)	253 (79.1)
RA duration, years		
≤2	22 (16.1)	50 (25.6)
2–5	39 (28.5)	49 (25.1)
6–10	30 (21.9)	47 (24.1)
>10	46 (33.6)	49 (25.1)
Serologic status		
Positive	193 (76.3)	216 (81.5)
Negative	60 (23.7)	49 (18.5)
Use of DMARDs		
Synthetic	248 (77.3)	259 (80.9)
Biologic	131 (40.8)	148 (46.3)
Comorbidity index, mean ± SD	1.33 ± 0.6	1.28 ± 0.5
Joint erosion		
Yes	109 (53.4)	142 (59.7)
No	95 (46.6)	96 (40.3)
Total medications		
0	0 (0)	1 (0.3)
1–5	42 (13.1)	53 (16.6)
6–10	104 (32.4)	117 (36.6)
10+	175 (54.5)	149 (46.6)

* Except where indicated otherwise, values are the number (%). Data were missing for the following variables (similar distribution across treatment arms): age (n = 64), body mass index (BMI; n = 52), rheumatoid arthritis (RA) duration (n = 309), serologic status (n = 123), and joint erosions (n = 199). TRACTION = Treat-to-Target in RA: Collaboration to Improve Adoption and Adherence; DMARDs = disease-modifying antirheumatic drugs.

Table 2. Implementation of treat-to-target and components at patient visits in the TRACTION trial*

	Control (n = 321)			Intervention (n = 320)			*P* for difference in change
	Baseline	Follow-up	Change	Baseline	Follow-up	Change	
Primary outcome							
Implementation score	11.0	24.7	13.7	11.1	57.1	46.0	0.004
Visits with components present							
Treatment target	0	12.5	12.5	0.6	45.6	45.0	0.065
Disease activity measure	30.2	52.3	22.1	20.0	89.1	69.1	0.002
Shared decision-making†	24.5	43.0	18.5	51.3	85.9	34.6	<0.001
Treatment decision‡	0	8.4	8.4	0.6	27.8	27.2	0.064

* Values are the percentage. *P* values were calculated using linear mixed models for the primary outcome and generalized linear mixed models for binary outcomes for the components; both sets of models accounted for clustering within sites and within providers (28). TRACTION = Treat-to-Target in RA: Collaboration to Improve Adoption and Adherence.
† The shared decision-making criteria did not apply to all visits when no decisions were being made about changing targets or changing treatments. The number of visits when shared decision-making applied was 102 baseline visits and 100 follow-up visits for the control group and 115 baseline visits and 184 follow-up visits for the intervention group.
‡ Treatment decision based on target and disease activity measure.

and complete implementation versus incomplete implementation), we used generalized linear mixed models for binary outcomes that accounted for clustering within sites and within providers (28). Analysis of adverse events and resource utilization was performed using Poisson regressions for resource use and adverse events as the outcome variables. Similar to the primary analyses, we adjusted for intrasite and intraprovider correlations.

RESULTS

Study population. The Consolidated Standards of Reporting Trials (CONSORT) diagram in Supplementary Figure 2 (available at http://onlinelibrary.wiley.com/doi/10.1002/art.40111/abstract) shows that 1 site dropped out after randomization but before any activities began, leaving a total of 11 participating sites. The characteristics of the 641 patients with RA included in the trial are shown in Table 1. They represent a typical RA population, with a mean age of 60 years, 78% female, and 79% with at least 1 positive serologic test for RA. Patient characteristics were well-balanced across treatment arms. The structure, staff, and insurance mix were diverse and also well-balanced (see Supplementary Table 1, available at http://onlinelibrary.wiley.com/doi/10.1002/art.40111/abstract).

Trial outcomes. At baseline, the mean TTT implementation score was 11% in both arms. After the 9-month intervention, the TTT implementation score was 57% in the intervention arm and 25% in the control arm. The mean change was 46% in the intervention arm and 14% in control (*P* for difference in change = 0.004 from a linear mixed model) (Table 2). Each component of the TTT implementation score improved in the intervention arm, but not all improved to the same extent (Table 2). The proportion of participants for whom the presence of a treatment target was documented went from 0.6% at baseline to 45.6% at follow-up in the intervention arm. Recording of the disease activity increased from 20.0% to 89.1%; all sites used the CDAI or RAPID3 instrument. Shared decision-making started out at 51.3% in the intervention group and increased to 85.9%. While there was some improvement noted over time in the waitlist control arm, the improvement in implementation of each component of the TTT was not as large as it was in the intervention arm.

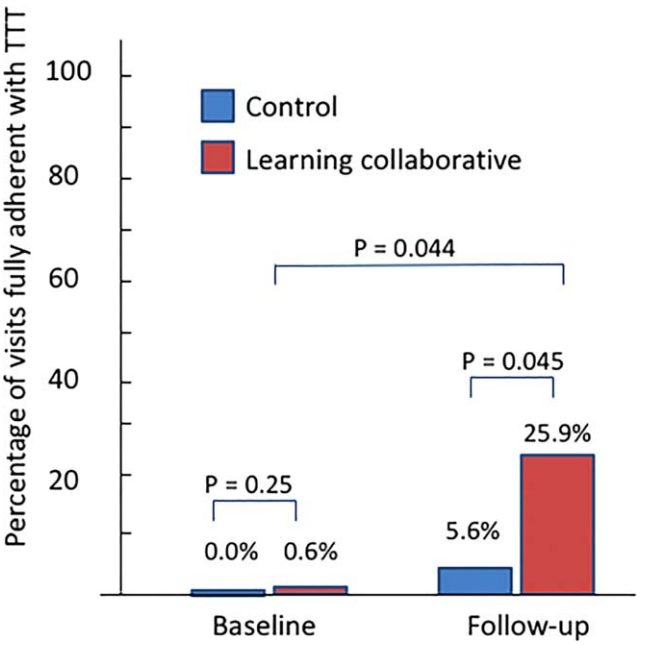

Figure 1. Percentage of visits at baseline and follow-up that were in full adherence to the treat-to-target (TTT) protocol, the secondary outcome of the Treat-to-Target in RA: Collaboration to Improve Adoption and Adherence (TRACTION) trial.

Table 3. Resource use and adverse events during the TRACTION trial*

	No. of tests or adverse events (mean no. per patient)	
	Control group (n = 321)	Intervention group (n = 320)
Monitoring laboratory tests†	2,614 (8.14)	2,591 (8.10)
C-reactive protein or erythrocyte sedimentation rate	788 (2.45)	607 (1.90)
Plain radiography of the musculoskeletal system	308 (0.96)	247 (0.77)
Computed tomography of the musculoskeletal system	6 (0.019)	12 (0.038)
Magnetic resonance imaging of the musculoskeletal system	14 (0.044)	16 (0.050)
Rheumatology visits	922 (2.87)	753 (2.35)
Adverse events‡	138 (0.43)	83 (0.26)

* *P* values were calculated using Poisson regression for the count data after accounting for clustering within sites and within providers (28). None of the *P* values were significant. TRACTION = Treat-to-Target in RA: Collaboration to Improve Adoption and Adherence.
† Consisted of a complete blood cell count and/or a basic metabolic panel and/or liver function tests.
‡ Adverse events in the intervention group and the control group included infections (n = 14 and n = 34, respectively), cutaneous reactions (n = 13 and n = 21, respectively), liver test abnormalities (n = 9 and n = 10, respectively), renal test abnormalities (n = 1 in the intervention group), gastrointestinal symptoms (n = 22 and n = 28, respectively), and other miscellaneous (n = 24 and n = 45, respectively).

Secondary outcomes differed across treatment arms. A positive change (of any magnitude) in the TTT adherence score was noted in 83.8% of patients in the intervention arm sites (268 of 320) and 36.8% in the control arm sites (118 of 321) ($P = 0.0001$). A similar trend was observed when visits were analyzed for having all components of TTT present versus fewer than all components (Figure 1). At baseline, almost no patient visits in either arm were adherent to all components of the TTT. At follow-up, the percentage of visits adherent to all 4 components was 25.9% in the intervention arm and 5.6% in the control arm ($P = 0.045$).

The number of orders for drug-monitoring laboratory tests was similar across the control (8.14 tests per patient) and intervention (8.10 tests per patient) arms ($P = 0.67$) (Table 3). Radiology orders were also very similar between the control (0.96 per patient) and intervention (0.77 per patient) arms ($P = 0.96$). Patients in the intervention arm were noted to have fewer adverse events (0.26 per patient) than those in the control arm (0.43 per patient) ($P = 0.043$) (Table 3).

We abstracted information on disease activity measures at follow-up visits from medical records when available and found that a numerically greater percentage of patients in the intervention arm were in remission: 40.5% in the intervention arm versus 26.1% in the control arm ($P = 0.07$). However, since the control arm was not instructed on disease activity measurement, this was measured in only 69 patients in the control arm but 284 patients in the intervention arm.

DISCUSSION

Treatment for RA does not always follow the recommended TTT approach. The TRACTION trial focused on improving implementation of TTT principles for RA using a learning collaborative approach to adopting new strategies and improving workflow. While TTT is a proven strategy in the care of RA, many areas of health care require a similar team approach for effective care. In this study, we found large benefits, despite using a relatively low-intensity approach to the learning collaborative, with only 1 face-to-face meeting.

The success of the TRACTION trial has potential implications beyond the care of RA. Effective management of diabetes mellitus and hypertension also requires a similar treatment approach: setting a treatment target (i.e., hemoglobin A_{1c} or blood pressure), with patient involvement, regular measurement of progress toward the target, and modification of treatments until the target is reached and maintained. While our learning collaborative focused on RA, it seems clear that the principles and concepts underlying this approach could be transferred to other chronic diseases. In fact, our model is consistent with the goals and strategy of the Million Hearts campaign to reduce cardiovascular disease burden across the US by targeting 5 areas of goal-based therapy (29). The program we used for this learning collaborative included only 1 face-to-face meeting but still produced excellent results. Further evaluation of learning collaboratives of different intensities will improve our understanding of how to best fit these improvement programs into the lives of busy health care workers.

While the TRACTION learning collaborative improved the use of TTT for RA, implementation remained far lower than desired, and several previous studies suggest potential reasons. A survey of Australian rheumatologists found that they preferred not to adjust medications for symptoms when they were perceived to be associated with irreversible joint damage (14). Some might argue that this is a defensible position that could avoid overtreatment. They also cited patient preferences as justification for not adjusting treatments. It may be the case that more engagement of patients regarding the choosing

of targets and identifying the best treatments would affect patient preferences.

The TRACTION trial was a pragmatic cluster-randomized controlled trial, with a waitlist for the control arm. This design is often used in quality improvement, and it has associated strengths and limitations. While the trial was appropriately powered, it included only 11 rheumatology practice sites in the US. The sites were geographically diverse and represented different types of practices (academic and non-academic); however, the ability of the TRACTION learning collaborative to produce similar changes in other settings requires further testing. The majority of TRACTION sites were affiliated with an academic medical center, and the results may not be generalizable across all types of practices. In addition, the intervention required ~20 hours per provider over 9 months, which may limit its generalizability.

The primary outcome of the TRACTION trial was a process measure and does not reflect clinical outcomes. The process measure appears to be valid, however, as at least 7 prior trials have demonstrated improved outcomes in RA using a TTT approach (30). We appreciate that the outcome measure for implementation of TTT was developed for this trial since no valid measures for TTT have been published. However, the 4 items were based on the original TTT recommendations to ensure face validity. The developer of the TTT recommendations (JSS) agreed that the 4 aspects of TTT that we were able to measure from chart review were essential to assuring content validity (i.e., the extent that a measure represents the full range of the construct). The measure had good reliability, as indicated by the interrater and intrarater kappa values ($\kappa > 0.9$), but it is a clear limitation that the primary outcome of the trial was not based on a previously validated measure. Disease activity was measured at baseline in only a minority of patients, which limits our understanding of whether implementation of TTT significantly improved disease activity over the course of the trial.

The TRACTION trial staff reviewed medical records to avoid the potential bias of self-assessment. However, the staff was not blinded with regard to the assignment of sites to the intervention or control arms. The high intrarater and interrater reliability values suggest that the outcomes measure, which was assessed at 2 visits, was highly reproducible. A final limitation is that adverse events were collected from chart review and thus could have been biased if providers in different treatment arms differentially reported adverse events. Since providers were not aware of our hypotheses regarding adverse events, this seems unlikely.

In summary, we found significant improvements in adherence to TTT principles in rheumatology practices participating in a learning collaborative. Future work will include dissemination activities with professional organizations to make this opportunity more widely available for other interested rheumatology practice sites. Similar efforts with learning collaboratives for RA are ongoing (31), and our results support considering this approach for other chronic diseases that benefit from TTT strategies.

AUTHOR CONTRIBUTIONS

All authors were involved in drafting the article or revising it critically for important intellectual content, and all authors approved the final version to be published. Dr. Solomon had full access to all of the data in the study and takes responsibility for the integrity of the data and the accuracy of the data analysis.

Study conception and design. Solomon, Losina, Lu, Agosti, Bitton, Harrold, Pincus, Radner, Smolen, Fraenkel, Katz.

Acquisition of data. Solomon, Zak, Corrigan, Lee, Agosti, Bitton, Pincus, Radner, Smolen, Fraenkel, Katz.

Analysis and interpretation of data. Solomon, Losina, Lu, Yu, Katz.

REFERENCES

1. Grigor C, Capell H, Stirling A, McMahon AD, Lock P, Vallance R, et al. Effect of a treatment strategy of tight control for rheumatoid arthritis (the TICORA study): a single-blind randomised controlled trial. Lancet 2004;364:263–9.
2. Verstappen SM, Jacobs JW, van der Veen MJ, Heurkens AH, Schenk Y, ter Borg EJ, et al. Intensive treatment with methotrexate in early rheumatoid arthritis: aiming for remission. Computer Assisted Management in Early Rheumatoid Arthritis (CAMERA, an open-label strategy trial). Ann Rheum Dis 2007; 66:1443–9.
3. Fransen J, Moens HB, Speyer I, van Riel PL. Effectiveness of systematic monitoring of rheumatoid arthritis disease activity in daily practice: a multicentre, cluster randomised controlled trial. Ann Rheum Dis 2005;64:1294–8.
4. Möttönen T, Hannonen P, Korpela M, Nissilä M, Kautiainen H, Ilonen J, et al. Delay to institution of therapy and induction of remission using single-drug or combination–disease-modifying antirheumatic drug therapy in early rheumatoid arthritis. Arthritis Rheum 2002;46:894–8.
5. Saunders SA, Capell HA, Stirling A, Vallance R, Kincaid W, McMahon AD, et al. Triple therapy in early active rheumatoid arthritis: a randomized, single-blind, controlled trial comparing step-up and parallel treatment strategies. Arthritis Rheum 2008; 58:1310–7.
6. Goekoop-Ruiterman YP, de Vries-Bouwstra JK, Allaart CF, van Zeben D, Kerstens PJ, Hazes JM, et al. Comparison of treatment strategies in early rheumatoid arthritis: a randomized trial. Ann Intern Med 2007;146:406–15.
7. Symmons D, Tricker K, Roberts C, Davies L, Dawes P, Scott DL. The British Rheumatoid Outcome Study Group (BROSG) randomised controlled trial to compare the effectiveness and cost-effectiveness of aggressive versus symptomatic therapy in established rheumatoid arthritis. Health Technol Assess 2005;9: iii-iv, ix-x, 1–78.
8. Van Tuyl LH, Lems WF, Voskuyl AE, Kerstens PJ, Garnero P, Dijkmans BA, et al. Tight control and intensified COBRA combination treatment in early rheumatoid arthritis: 90% remission in a pilot trial. Ann Rheum Dis 2008;67:1574–7.
9. Smolen JS, Aletaha D, Bijlsma JW, Breedveld FC, Boumpas D, Burmester G, et al. Treating rheumatoid arthritis to target: recommendations of an international task force. Ann Rheum Dis 2010;69:631–7.

10. Smolen JS, Breedveld FC, Burmester GR, Bykerk V, Dougados M, Emery P, et al. Treating rheumatoid arthritis to target: 2014 update of the recommendations of an international task force. Ann Rheum Dis 2016;75:3–15.
11. Singh JA, Furst DE, Bharat A, Curtis JR, Kavanaugh AF, Kremer JM, et al. 2012 update of the 2008 American College of Rheumatology recommendations for the use of disease-modifying antirheumatic drugs and biologic agents in the treatment of rheumatoid arthritis. Arthritis Care Res (Hoboken) 2012;64:625–39.
12. Kotak S, Koenig AS, Collier DH, Saunders KC, He P, Kremer JM, et al. Disease activity and treatment strategies in moderate rheumatoid arthritis patient population: data from the Consortium of Rheumatology Researchers of North America [abstract]. Arthritis Rheum 2012;64 Suppl:S783.
13. Harrold LR, Harrington JT, Curtis JR, Furst DE, Bentley MJ, Shan Y, et al. Prescribing practices in a US cohort of rheumatoid arthritis patients before and after publication of the American College of Rheumatology treatment recommendations. Arthritis Rheum 2012;64:630–8.
14. Tymms K, Zochling J, Scott J, Bird P, Burnet S, de Jager J, et al. Barriers to optimal disease control for rheumatoid arthritis patients with moderate and high disease activity. Arthritis Care Res (Hoboken) 2014;66:190–6.
15. Tsai AC, Morton SC, Mangione CM, Keeler EB. A meta-analysis of interventions to improve care for chronic illnesses. Am J Manag Care 2005;11:478–88.
16. Reeves S, Perrier L, Goldman J, Freeth D, Zwarenstein M. Interprofessional education: effects on professional practice and healthcare outcomes (update). Cochrane Database Syst Rev 2013:CD002213.
17. Schouten LM, Hulscher ME, van Everdingen JJ, Huijsman R, Grol RP. Evidence for the impact of quality improvement collaboratives: systematic review. BMJ 2008;336:1491–4.
18. Institute for Healthcare Improvement. Science of improvement. URL: http://www.ihi.org/about/Pages/ScienceofImprovement.aspx.
19. Leape LL, Kabcenell AI, Gandhi TK, Carver P, Nolan TW, Berwick DM. Reducing adverse drug events: lessons from a breakthrough series collaborative. Jt Comm J Qual Improv 2000;26:321–31.
20. Benedetti R, Flock B, Pedersen S, Ahern M. Improved clinical outcomes for fee-for-service physician practices participating in a diabetes care collaborative. Jt Comm J Qual Saf 2004;30:187–94.
21. Landon BE, Wilson IB, McInnes K, Landrum MB, Hirschhorn L, Marsden PV, et al. Effects of a quality improvement collaborative on the outcome of care of patients with HIV infection: the EQHIV study. Ann Intern Med 2004;140:887–96.
22. Homer CJ, Forbes P, Horvitz L, Peterson LE, Wypij D, Heinrich P. Impact of a quality improvement program on care and outcomes for children with asthma. Arch Pediatr Adolesc Med 2005;159:464–9.
23. Solomon DH, Lee SB, Zak A, Corrigan C, Agosti J, Bitton A, et al. Implementation of treat-to-target in rheumatoid arthritis through a learning collaborative: rationale and design of the TRACTION trial. Semin Arthritis Rheum 2016;46:81–7.
24. Anderson J, Caplan L, Yazdany J, Robbins ML, Neogi T, Michaud K, et al. Rheumatoid arthritis disease activity measures: American College of Rheumatology recommendations for use in clinical practice. Arthritis Care Res (Hoboken) 2012;64:640–7.
25. Mangione-Smith R, Schonlau M, Chan KS, Keesey J, Rosen M, Louis TA, et al. Measuring the effectiveness of a collaborative for quality improvement in pediatric asthma care: does implementing the chronic care model improve processes and outcomes of care? Ambul Pediatr 2005;5:75–82.
26. Knox SA, Chondros P. Observed intra-cluster correlation coefficients in a cluster survey sample of patient encounters in general practice in Australia. BMC Med Res Methodol 2004;4:30.
27. Lumley T, Diehr P, Emerson S, Chen L. The importance of the normality assumption in large public health data sets. Annu Rev Public Health 2002;23:151–69.
28. McCullagh P, Nelder JA. Generalized linear models. 2nd ed. New York: CRC Press; 1989.
29. Centers for Disease Control and Prevention. Million hearts. URL: https://millionhearts.hhs.gov/.
30. Schoels M, Knevel R, Aletaha D, Bijlsma JW, Breedveld FC, Boumpas DT, et al. Evidence for treating rheumatoid arthritis to target: results of a systematic literature search. Ann Rheum Dis 2010;69:638–43.
31. AMGA. Best practices in managing patients with rheumatoid arthritis (RA) collaborative. URL: https://www.amga.org/wcm/COL/RA/wcm/PI/Collabs/RA/index_ra.aspx?hkey=57a0f319-3117-474e-9abf-107041becd64.

APPENDIX A: RHEUMATOLOGY SITES PARTICIPATING IN THE TRACTION TRIAL

The following rheumatology sites and their teams participated in the TRACTION trial: Cedars Sinai Medical Center (Los Angeles, CA): Venturapali, Gaggi, Uy, Bustos, and Vasquez; Loyola University Medical Center (Maywood, IL): Tehrani, Ostrowski, Briones, and Murphy; NorthShore University Health System (Evanston, IL): Grober, Malik, Woodrick, Lynn, Sun, Drevlow, Zaacks, Bilbrey, Chavez, Casey, Gan, and Myers; Park Nicollet Health Services (St. Louis Park, MN): Paisansinsup, Shousboe, Glickstein, and Steele; University of Texas (Houston, TX): Scholz, McCray, Barnes, Tan, and Homann; Kansas University Medical Center (Kansas City, KS): Lindsley, Schmidt, Colbert, Springer, Bhadbhade, Parker, Estephan, McMillian, and Heneghan; University of Kentucky (Lexington, KY): Lohr, Hanaoka, Lightfoot, Jenkins, Baker, Bisono, Wafford, Wiard, Lenert, and Howard; University of Vermont (Burlington, VT): Hynes, Bethina, Kennedy, Lau, Edwards, Libman, and Farely; University of Virginia (Charlottesville, VA): Kimpel, Lewis, D'Souza, Potter, Carlson, Mosteanu, Khalique, Khurana, and Swamy; University of Texas Medical Branch (Galveston, TX): Murthy, Musty, Rudrangi, Ganti, Gonzalez, and McCullum; and Vanderbilt University (Nashville, TN): Annapureddy, Kroop, and Hayden.

ARTHRITIS & RHEUMATOLOGY
Vol. 69, No. 7, July 2017, pp 1381–1386
DOI 10.1002/art.40098

BRIEF REPORT

Anti–Carbamylated Protein Antibodies in Rheumatoid Arthritis Patients Are Reactive With Specific Epitopes of the Human Fibrinogen β-Chain

Jonathan D. Jones,[1] B. JoNell Hamilton,[2] and William F. C. Rigby[1]

Objective. **Anti–carbamylated protein (anti-CarP) antibodies are associated with the risk and severity of rheumatoid arthritis (RA) and are primarily directed against fibrinogen. The lack of understanding of anti-CarP antibody reactivity has limited analysis of the immunopathogenic associations in RA. To address this shortcoming, we mapped anti-CarP antibody epitope reactivity in RA patient sera.**

Methods. **Immunoblotting identified a patient serum sample with specific reactivity to the carbamylated human fibrinogen β-chain. Liquid chromatography mass spectrometry (LC-MS) identified sites of homocitrullines (carbamylated lysines) present in the human fibrinogen β-chain. The reactivity of an anti-CarP antibody–positive cohort to specific peptides containing carbamylated lysines was determined by enzyme-linked immunosorbent assay, through direct binding (n = 63 sera) and by competition assays (n = 40 sera).**

Results. **Serum with specific reactivity to carbamylated, but not citrullinated, fibrinogen β-chain was identified in a specimen obtained from an RA patient. LC-MS identified carbamylation of 9 of 34 lysines in the human fibrinogen β-chain. Mapping of immunoreactivity to tryptic peptide fragments demonstrated several candidate carbamylated epitopes that were confirmed by competition experiments. Peptides containing a homocitrulline at position 83 appeared to be an immunodominant epitope in some RA patient sera, with additional reactivity to peptides containing homocitrullines at positions 52, 264, 351, 367, and 374.**

Conclusion. **Anti-CarP antibodies appear to preferentially target specific regions of the human fibrinogen β-chain that contain homocitrullines. Interestingly, humoral immunoreactivity appears to be relatively restricted in some patients, which may enable detection of specific relationships with disease phenotype.**

The breaking of tolerance to citrullinated proteins, represented by the emergence of anti–citrullinated protein antibodies (ACPAs), is strongly associated with the risk of rheumatoid arthritis (RA). ACPAs can be present for many years before the onset of clinical disease (1). Curiously, ACPAs appear to be specifically directed against many different citrullinated proteins (fibrinogen, vimentin, α-enolase, filaggrin, and histone) as well as being polyreactive through citrulline binding (2,3). Thus, ACPAs serve as a marker of disease risk, although no specific reactivity is associated with the onset of joint inflammation (2,4). With the onset of clinical disease, ACPA production can be demonstrated in the joint, with evidence of synovial affinity maturation (3,5). Clinically, the presence of ACPAs predicts a greater likelihood of erosive and extraarticular disease (6).

In this context, homocitrullination of lysines (also referred to as carbamylation), a posttranslational modification similar to citrullination, has additionally been shown to be a target of autoantibodies (anti–carbamylated protein [anti-CarP] antibodies) in RA (7,8). This modification is similar to citrullination, with the same ureido functional group added to the primary amine group of lysine rather than arginine. In contrast to the enzymatic catalysis of arginine to citrulline mediated by peptidylarginine deiminase (PAD), the chemical carbamylation of lysine to homocitrulline occurs spontaneously through a reaction with cyanate that is enhanced through cyanate production mediated by myeloperoxidase (9). Both PADI4 and myeloperoxidase reside in the azurophilic granules of neutrophils. Thus, both modifications are likely to occur in concert at sites of inflammation.

Supported by the Hitchcock Foundation and the Aspire Program.

[1]Jonathan D. Jones, MD, William F. C. Rigby, MD: Dartmouth–Hitchcock Medical Center, Lebanon, New Hampshire; [2]B. JoNell Hamilton, MS: Dartmouth College, Hanover, New Hampshire.

Address correspondence to Jonathan D. Jones, MD, Section of Rheumatology, 1 Medical Center Drive, Lebanon, NH 03756. E-mail: jonathan.d.jones@dartmouth.edu.

Submitted for publication August 24, 2016; accepted in revised form March 9, 2017.

Anti-CarP antibodies were discovered using an enzyme-linked immunosorbent assay (ELISA) with immobilized carbamylated fetal calf serum (FCS) in ACPA-positive and ACPA-negative RA sera (7). Similar to ACPAs, anti-CarP antibodies were shown to precede the onset of synovitis as well as predict radiographic progression (7,10). In contrast to ACPAs, anti-CarP antibodies appear to be primarily directed against carbamylated human fibrinogen (11).

The notion that an autoantibody against a single posttranslationally modified protein (fibrinogen) is associated with disease risk and progression would potentially give anti-CarP antibodies an advantage as a biomarker relative to the polyreactivity seen with ACPAs. However, advancement in the understanding of anti-CarP antibodies has been limited by the lack of understanding of their cross-reactivity with ACPAs. Given the similarity of the posttranslational modification, with the ureido functional group added to the primary amine group of a basic (lysine versus arginine) amino acid, it would not be surprising to observe that anti-CarP antibodies and ACPAs cross-react (12). Nevertheless, adsorption and competition studies have suggested the presence of antibodies that appear to be specific for each posttranslational modification (13).

These issues impact the ability to fully assess the role of anti-CarP antibodies in RA pathogenesis or as a biomarker of disease severity. Are the anti-CarP antibodies that appear in a preclinical setting a subset of cross-reactive ACPAs? Similarly, is the association of anti-CarP antibodies with radiographic disease enhanced or diminished by the presence of cross-reactive ACPAs? Do specific anti-CarP antibodies change with disease activity, in contrast to ACPAs? Moreover, is the apparent restriction of anti-CarP antibodies to carbamylated fibrinogen inherent or a function of an assay biased toward examining fibrinogen? Each of these issues would be best addressed by understanding the specificity and selectivity of anti-CarP antibodies. In this report, we present data that lays the foundation for addressing these questions by demonstrating that anti-CarP antibodies include highly specific antibodies directed against a homocitrullinated peptide in the fibrinogen β-chain. Surprisingly, in some patients, this peptide appears to constitute an immunodominant epitope.

PATIENTS AND METHODS

Patient samples. Approval to collect patient samples and clinical data was obtained from the Dartmouth College Committee for the Protection of Human Subjects. Serum samples (n = 63) were obtained from patients seen at the Rheumatology Clinic of the Dartmouth–Hitchcock Medical Center who were classified as having RA seropositive for rheumatoid factor (RF) and/or ACPAs (with the exception of 2 seronegative RA patients who were strongly positive for anti-CarP antibodies). Serum samples were stored at −80°C as part of the Dartmouth Rheumatic Disease Biorepository. Samples that had high anti-CarP antibody reactivity were chosen, along with several others having a range of low anti-CarP antibody reactivity to no anti-CarP antibody reactivity.

Reagents, antibodies, and peptides. Fibrinogen (≥98% purity) isolated from human plasma was obtained from Hyphen-BioMed (catalog no. PP001B). Citrullinated human fibrinogen was purchased from Cayman Chemical. Fibrinogen or FCS was carbamylated by treating with 1*M* KCN (Sigma) at 37°C for 12 hours followed by extensive dialysis, as previously described (14). Rabbit anti–carbamyl-lysine (anti-CBL) polyclonal antibody was purchased from Cell Biolabs. Horseradish peroxidase (HRP)–conjugated goat anti-human fibrinogen was purchased from Novus Biologicals (catalog no. NB600-927). Human fibrinogen β-chain peptides (GenBank accession no. P02675) with specified lysine or homocitrulline were synthesized (LifeTein) as either cyclized (using a cysteine-cysteine disulfide bond) or linear (see Table 1).

Fibrinogen analysis. The β-chain of carbamylated fibrinogen was resolved by sodium dodecyl sulfate–polyacrylamide gel electrophoresis (SDS-PAGE), and the band was cut out. In-gel tryptic digestion was performed, and analysis by liquid chromatography mass spectrometry (LC-MS) performed at the Yale Mass Spectrometry (MS) and Proteomics Resource of the W. M. Keck Foundation Biotechnology Resource Laboratory revealed 9 homocitrullines among 34 lysines. Subsequently, tryptic digestion was performed, and the peptides were purified by reverse-phase high-performance liquid chromatography (HPLC). Fractions were tested for reactivity by ELISA, using index patient serum. The identity of the peptides in fractions with reactivity were determined by MS/MS.

Anti-CarP antibodies and peptide ELISA. An anti-CarP antibody ELISA was performed as previously described (14). The antigen of interest (carbamylated FCS, noncarbamylated FCS, or peptide [10 μg/ml]) was incubated overnight at 4°C in flat-bottomed 96-well microplates (R&D Systems) and then washed and blocked using 1% bovine serum albumin. Serum specimens (1:100 dilution) were incubated for 2 hours at room temperature and washed, followed by incubation with HRP-conjugated goat anti-human IgG (Bio-Rad). Following washing, tetramethylbenzidine substrate (R&D Systems) was added, and absorbance was measured with a BioTek spectrophotometer using wavelengths of 450–570 nm. Values obtained from noncarbamylated FCS were subtracted from carbamylated FCS values to yield the final antibody concentration. The positive cutoff was defined as 2 SD above the mean for 65 healthy controls.

In competition experiments, the peptide was preincubated with diluted serum at room temperature for 1 hour prior to addition to the wells. Initially, peptides were also added to noncarbamylated FCS, but because no change in background signal was observed, subsequent experiments used only noncarbamylated FCS without peptides as background. Maximal inhibition of reactivity occurred at peptide concentrations of 20 μg/ml; therefore, to ensure saturating conditions, a concentration of 50 μg/ml was used.

Immunoblots. Carbamylated fibrinogen, citrullinated fibrinogen, and native fibrinogen were loaded (1 μg) onto 12% SDS-PAGE gels, resolved by electrophoresis, and then were transferred to nitrocellulose and blocked overnight in 3% BSA in Tris buffered saline–Tween 20. The blots were incubated with CBL (1:1,000), HRP-conjugated goat anti-human fibrinogen (1 μg/ml), or patient sera at specified dilutions for 2 hours, washed,

Table 1. Human fibrinogen β-chain peptides used in the capture and competition ELISAs*

Peptide†	Form	Sequence‡
Fib 77–87	Cyclized	CKAAATQKKVERCARRR *Bovine* T-TVG------
Fib 77–87 Δ83	Cyclized	CKAAATQ**K**KVERCARRR *Bovine* T-TVG------
Fib 43–56 Δ52	Linear	Biotin-ARGHRPLDK**K**REEA *Bovine* ------Y---K---
Fib 76–90 Δ83	Linear	Biotin-AKAAATQ**K**KVERKAP *Bovine* -T-TVG-------P-
Fib 248–270 Δ264	Linear	Biotin-GGETSEMYLIQPDSSV**K**PYRVYC *Bovine* ----------
Fib 343–358 Δ351	Linear	Biotin-EMEDWKGD**K**VKAHYGG *Bovine* ----------T-----
Fib 363–377 Δ367, 374	Linear	Biotin-NEAN**K**YQISVN**K**YRG *Bovine* -------L--S--K-

* Variation in the bovine fibrinogen (Fib) sequence is shown. ELISAs = enzyme-linked immunosorbent assays.
† Homocitrullinated lysine is indicated by Δ in the peptide name and by boldface K in the amino acid sequence.
‡ Dashes in the bovine sequences represent conserved amino acids. Amino acids found in fibrinogen are underlined.

incubated with HRP-conjugated goat anti-human IgG secondary antibody (1:6,000), and then treated with SuperSignal West Pico Chemiluminescent Substrate (Thermo Fisher). Fluorescence was captured using an Alpha Innotech MultiImage III cabinet.

RESULTS

Anti-CarP antibodies specific for carbamylated fibrinogen. We identified a unique patient with refractory and erosive RA who had been persistently ACPA and RF negative yet exhibited strong anti-CarP antibody reactivity. We hypothesized that serum from this patient could be used to map epitopes of carbamylated fibrinogen without concern for ACPA cross-reactivity. Immunoblotting was performed against native, citrullinated, and carbamylated human fibrinogen, using this serum (Figure 1A). Human fibrinogen is a hexameric protein made up of 2 copies of the α-chain, β-chain, and γ-chain. Using antisera (anti-CBL) specific for homocitrullines, we demonstrated reactivity in the α-chain, β-chain, and γ-chain in carbamylated fibrinogen but not in native or citrullinated fibrinogen. Blotting with this serum exhibited specificity for carbamylated but not citrullinated or native fibrinogen β-chain (minor staining seen below the β-chain was likely a splice variant) (15).

We blotted carbamylated fibrinogen or native fibrinogen with 11 additional anti-CarP antibody–positive RA patient sera to evaluate the commonality of β-chain specificity. Five sera did not have reactivity by immunoblotting (data not shown). The remaining 6 sera had reactivity to carbamylated but not native fibrinogen (see Supplementary Figure 1, available on the *Arthritis & Rheumatology* web site at http://onlinelibrary.wiley.com/doi/10.1002/art.40098/abstract). Most of these patients had specific reactivity with the β-chain (patients 2, 12, 13, 14, and 15), while serum from 1 patient (patient 3) exhibited preferential binding of the α-chain.

Mapping homocitrullines and anti-CarP antibody reactivity in the human fibrinogen β-chain. The carbamylation sites in the fibrinogen β-chain were analyzed. Carbamylated human fibrinogen was resolved by SDS-PAGE, and the band corresponding to the fibrinogen β-chain was cut out, subjected to in-gel tryptic digestion, and analyzed by LC-MS. Of 34 lysines, 9 (52, 83, 160, 163, 264, 351, 353, 367, and 374) (26.5%) were identified as homocitrullines (see Supplementary Figure 2, available on the *Arthritis & Rheumatology* web site at http://onlinelibrary.wiley.com/doi/10.1002/art.40098/abstract). Following tryptic digestion, peptides of the fibrinogen β-chain were purified by reverse-phase HPLC and analyzed by ELISA for reactivity, using serum from the index patient. One fraction had reactivity 2–4 times that of other reactive fractions and contained a single peptide (A_{78}AATQ**K**K$_{84}$) with a single carbamylated lysine at position 83 (designated Δ83).

Frequency of anti-CarP antibody reactivity with fibrinogen 77–87 Δ83. Cyclized peptides corresponding to amino acids 77–87 with or without homocitrulline at position 83 (Table 1) were analyzed by ELISA. RA patient sera (n = 63) were analyzed for specific reactivity to the carbamylated peptide (values obtained for peptide 77–87 were subtracted from values obtained for peptide 77–87 Δ83) in relation to anti-CarP antibody reactivity (Figures 1B and C). We identified a value of >0 (a positive cutoff was not determined) in 22 patients (35%). Interestingly, although reactivity with this peptide did not correlate with anti-CarP

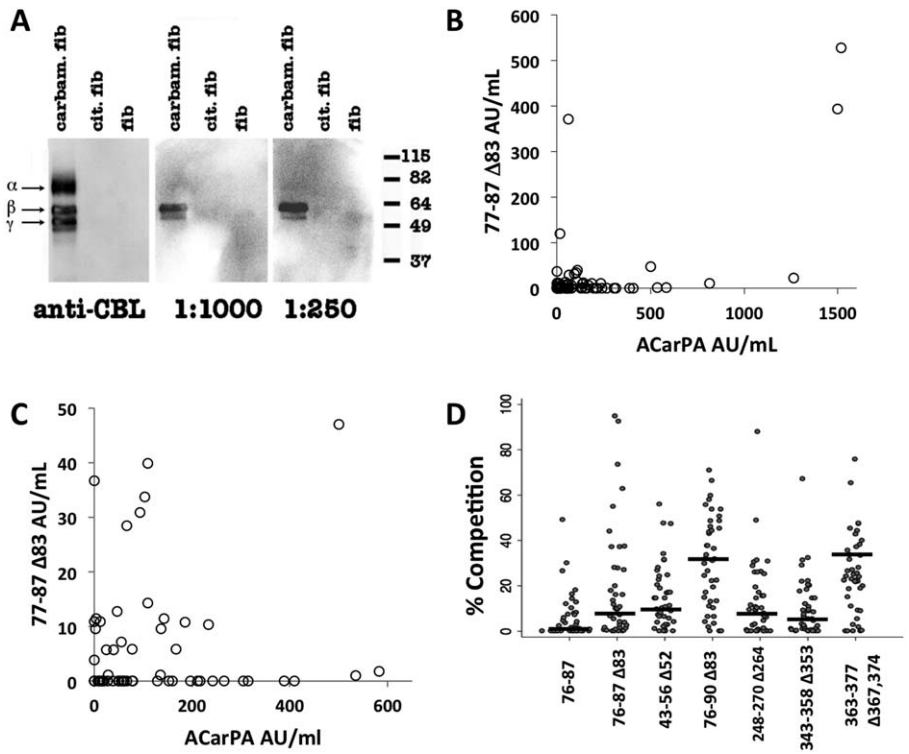

Figure 1. Reactivity of patient sera to fibrinogen (fib). **A,** Carbamylated (carbam.) fibrinogen, citrullinated (cit.) fibrinogen, and native fibrinogen (1 μg/lane) were resolved by sodium dodecyl sulfate–polyacrylamide gel electrophoresis, and immunoblotting was performed. Anti–carbamyl-lysine (anti-CBL) antibody detected carbamylated α-, β-, and γ-chains of fibrinogen, while serum from the index patient, at 2 dilutions, identified specific reactivity to the β-chain of carbamylated, but not citrullinated or native, fibrinogen. **B,** Sera from patients with rheumatoid arthritis (n = 63) were tested for reactivity to a specific fibrinogen β-chain peptide (peptide 77–87), with or without homocitrullinated lysine 83, by enzyme-linked immunosorbent assay (ELISA). Specific anti–carbamylated protein antibody (ACarPA) reactivity (with reactivity to native fetal calf serum [FCS] values subtracted) in relation to reactivity to fibrinogen 77–87 Δ83 (with reactivity to noncarbamylated peptide subtracted) is shown. **C**, Using the same data as that described in **B,** 6 outliers were removed in order to better see the distribution in patients with lower fibrinogen 77–87 Δ83 reactivity. **D,** The ability of the indicated peptides (at saturating concentrations of 50 μg/ml) to compete for binding with anti-CarP antibody–FCS was analyzed by ELISA, using patient sera (n = 40) with the best anti-CarP reactivity. Horizontal lines show the median.

antibody–FCS (reactivity to carbamylated FCS) (R = 0.12) (Figures 1B and C), some patient sera had much stronger peptide reactivity than that seen with anti-CarP antibody–FCS. The bovine and human fibrinogen β-chains share identity in 7 of 11 amino acids in this region (bovine, TATVGQKKVER [GenBank accession no. P02676]; human, KAAATQKKVER [GenBank accession no. P02675]), including the site of homocitrullination in the C-terminal half of this peptide, suggesting that the N-terminal amino acids are necessary for optimal antibody reactivity with this site in some patients.

Competition ELISA of peptides derived from the human fibrinogen β-chain. We studied the ability of carbamylated fibrinogen β-chain peptides to compete with binding to carbamylated FCS. We synthesized linear peptides with homocitrullines corresponding to sites conserved between human and bovine fibrinogen β-chain (Table 1). The ability of linear and cyclized peptides (at saturating concentrations of 50 μg/ml) to compete for binding to anti-CarP antibody–FCS was analyzed using patient sera (n = 40) with the highest anti-CarP antibody–FCS reactivity (Figure 1D). Little or no inhibition of anti-CarP antibody–FCS binding was seen in the absence of homocitrulline with peptide 77–87. Peptides corresponding to 76–90 Δ83 and 363–377 Δ367, 374 were superior at competing for binding to anti-CarP antibody–FCS. The 76–90 Δ83 or cyclized 77–87 Δ83 peptide mediated >30% inhibition in 26 (65%) of 40 sera tested. In this regard, the linear 76–90 Δ83 peptide was superior to the cyclized 76–87 Δ83 peptide for inhibiting anti-CarP antibody–FCS reactivity in this cohort (Figure 1D). These data potentially indicate the importance of additional C-terminal amino acids (amino acids 88–90) in anti-CarP antibody–FCS reactivity. In 12 sera (30%), none of the peptides mediated >30% inhibition.

Several patterns of peptide competition were observed. Some sera had competition with all carbamylated peptides (Figure 2A, patient 3), suggesting reactivity against homocitrullines independent of context. One serum

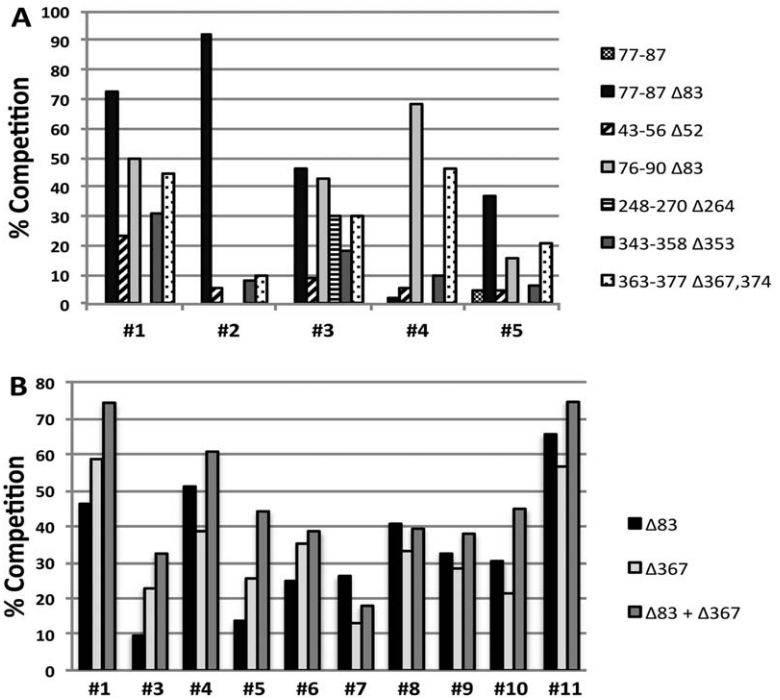

Figure 2. Competition analysis of anti-CarP antibody reactivity using human fibrinogen β-chain peptides. **A,** Five select patient sera with high reactivity were analyzed, and the percent competition with the indicated peptides was determined. Patient 1 represents the index patient described in Figure 1A. **B,** Competition analysis using peptides 76–90 Δ83, 363–377 Δ367, 374 or the combination in 10 patients with reactivity to both peptides. Each peptide concentration was 50 μg/ml (previous studies indicated that this concentration was maximally inhibitory) and was incubated for 1 hour with sera prior to adding to the ELISA. See Figure 1 for definitions.

specimen exhibited striking specificity with near-complete inhibition of all anti-CarP antibody reactivity with the cyclized 77–87 Δ83 peptide (Figure 2A, patient 2), but not with linear peptide 76–90 Δ83. There was little or no inhibition with the cyclized 77–87 peptide lacking homocitrulline. Along with other patient sera (patients 1, 4, and 5), either the cyclized 77–87 Δ83 peptide or the linear peptide 76–90 Δ83 peptide inhibited >50% of anti-CarP antibody–FCS reactivity.

These results suggest that in some patients, the carbamylated lysine at position 83 on the fibrinogen β-chain in this specific context represents a dominant epitope. This specificity was narrowed to amino acids 82–87 (QKKVER) given the poor conservation at the N-terminus in the bovine fibrinogen β-chain peptide. We also observed that the 363–377 Δ367, 374 peptide also provided significant competition. Inhibition by the 76–90 Δ83 peptide strongly correlated with that seen with 363–377 Δ367, 374 ($R = 0.59$, $P = 0.0001$) (see Supplementary Figure 3, available on the *Arthritis & Rheumatology* web site at http://onlinelibrary.wiley.com/doi/10.1002/art.40098/abstract).

We then evaluated competition of these 2 peptides, singly or in combination, to determine whether these represent unique or cross-reactive epitopes (Figure 2B). Despite the use of saturating levels of peptides, some patient sera were inhibited in an additive manner (patients 1, 3, 5, and 10), suggesting reactivity with distinct epitopes.

DISCUSSION

In the current study, we present data showing that specific peptides in the fibrinogen β-chain are a common target of anti-CarP antibodies. Using serum from an RA patient with anti-CarP antibodies specific to the β-chain of fibrinogen (Figure 1A), we identified strong reactivity to a homocitrulline at position 83. However, this was not the dominant reactive site in all RA patients, because we observed that only 35% of the RA patient sera had some level of reactivity to this peptide (Figures 1B and C). Therefore, we identified other peptides corresponding to carbamylated sites to which the index patient serum was reactive and evaluated their ability to compete with anti-CarP antibody–FCS (Figure 1D). Most sera with anti-CarP antibodies displayed reactivity to specific peptide sequences, e.g., they were not polyreactive with homocitrullines. This was also shown by immunoblotting (Figure 1A and Supplementary Figure 1, available on the *Arthritis & Rheumatology* web site at http://onlinelibrary.

wiley.com/doi/10.1002/art.40098/abstract), which additionally demonstrated predominant specificity for the fibrinogen β-chain in an additional 5 of 11 sera. Next, homocitrulline at position 83 of fibrinogen β-chain appeared to be a dominant epitope in several RA patients, most notably patients 1, 2, and 4 (Figure 2A). Finally, carbamylated lysines at positions 367 and 374 appeared to represent another dominant epitope, but only in patients whose serum also showed reactivity to the carbamylated lysine at position 83.

These observations prompt comment on anti-CarP antibody specificity. First, although some anti-CarP antibodies exhibit homocitrulline polyreactivity, most react with this posttranslational modification in the specific peptides found in the fibrinogen β-chain. Peptide competition studies demonstrated that 65% of all sera reactive with anti-CarP antibody–FCS could be competed with at least 1 of 5 homocitrulline-containing peptides (Figures 1D and Figure 2). The degree of competition between peptides was variable, but in some patients this repertoire was remarkably specific and restricted to 1 or 2 epitopes. While an analysis of all possible carbamylated peptides in both linear and cyclized forms was not performed, the conclusions reached about fibrinogen β-chain specificity remain. It is possible that the remaining 35% of sera react with other homocitrullines found on the α-chain or γ-chain of fibrinogen, but this has not been tested. Importantly, although these results suggest some degree of specificity, they do not directly address the issue of polyreactivity of individual anti-CarP antibodies, which would be more fully answered through the use of single anti-CarP monoclonal antibodies obtained from patients. Furthermore, our studies evaluated only IgG reactivity; studies of IgM or IgA antibodies may provide different perspectives.

Competition studies using intact fibrinogen have indicated that some, but not all, anti-CarP antibodies and ACPAs cross-react (13). This notion of specific anti-CarP antibodies is consistent with their presence in ACPA-negative patients (9) as well as a lack of cross-reactivity, as shown by immunoblotting (Figure 1A). This study builds on these findings by demonstrating restriction of anti-CarP antibody reactivity to specific peptides in the human fibrinogen β-chain, thereby suggesting that some patients have antibodies specific for certain homocitrullinated peptides. Thus, we can now begin to ask questions about the specificity of the anti-CarP antibody response and its relationship to disease phenotype and outcome.

AUTHOR CONTRIBUTIONS

All authors were involved in drafting the article or revising it critically for important intellectual content, and all authors approved the final version to be published. Dr. Jones had full access to all of the data in the study and takes responsibility for the integrity of the data and the accuracy of the data analysis.

Study conception and design. Jones, Hamilton, Rigby.
Acquisition of data. Jones, Hamilton, Rigby.
Analysis and interpretation of data. Jones, Hamilton, Rigby.

REFERENCES

1. Nielen MM, van Schaardenburg D, Reesink HW, van de Stadt RJ, van der Horst-Bruinsma IE, de Koning MH, et al. Specific autoantibodies precede the symptoms of rheumatoid arthritis: a study of serial measurements in blood donors. Arthritis Rheum 2004;50:380–6.
2. Sokolove J, Bromberg R, Deane KD, Lahey LJ, Derber LA, Chandra PE, et al. Autoantibody epitope spreading in the preclinical phase predicts progression to rheumatoid arthritis. PLoS One 2012;7:e35296.
3. Corsiero E, Bombardieri M, Carlotti E, Pratesi F, Robinson W, Migliorini P, et al. Single cell cloning and recombinant monoclonal antibodies generation from RA synovial B cells reveal frequent targeting of citrullinated histones of NETs. Ann Rheum Dis 2016;75:1866–75.
4. Johansson L, Pratesi F, Brink M, Arlestig L, D'Amato C, Bartaloni D, et al. Antibodies directed against endogenous and exogenous citrullinated antigens pre-date the onset of rheumatoid arthritis. Arthritis Res Ther 2016;18:127.
5. Amara K, Steen J, Murray F, Morbach H, Fernandez-Rodriguez BM, Joshua V, et al. Monoclonal IgG antibodies generated from joint-derived B cells of RA patients have a strong bias toward citrullinated autoantigen recognition. J Exp Med 2013;210:445–55.
6. Kastbom A, Strandberg G, Lindroos A, Skogh T. Anti-CCP antibody test predicts the disease course during 3 years in early rheumatoid arthritis (the Swedish TIRA project). Ann Rheum Dis 2004;63:1085–9.
7. Shi J, Knevel R, Suwannalai P, van der Linden MP, Janssen GM, van Veelen PA, et al. Autoantibodies recognizing carbamylated proteins are present in sera of patients with rheumatoid arthritis and predict joint damage. Proc Natl Acad Sci U S A 2011;108:17372–7.
8. Li L, Deng C, Chen S, Zhang S, Wu Z, Hu C, et al. Meta-analysis: diagnostic accuracy of anti-carbamylated protein antibody for rheumatoid arthritis. PLoS One 2016;11:e0159000.
9. Shi J, van Veelen PA, Mahler M, Janssen GM, Drijfhout JW, Huizinga TW, et al. Carbamylation and antibodies against carbamylated proteins in autoimmunity and other pathologies. Autoimmun Rev 2014;13:225–30.
10. Brink M, Verheul MK, Ronnelid J, Berglin E, Holmdahl R, Toes RE, et al. Anti-carbamylated protein antibodies in the presymptomatic phase of rheumatoid arthritis, their relationship with multiple anti-citrulline peptide antibodies and association with radiological damage. Arthritis Res Ther 2015;17:25.
11. Scinocca M, Bell DA, Racape M, Joseph R, Shaw G, McCormick JK, et al. Antihomocitrullinated fibrinogen antibodies are specific to rheumatoid arthritis and frequently bind citrullinated proteins/peptides. J Rheumatol 2014;41:270–9.
12. Reed E, Jiang X, Kharlamova N, Ytterberg AJ, Catrina AI, Israelsson L, et al. Antibodies to carbamylated α-enolase epitopes in rheumatoid arthritis also bind citrullinated epitopes and are largely indistinct from anti-citrullinated protein antibodies. Arthritis Res Ther 2016;18:96.
13. Shi J, Willemze A, Janssen GM, van Veelen PA, Drijfhout JW, Cerami A, et al. Recognition of citrullinated and carbamylated proteins by human antibodies: specificity, cross-reactivity and the 'AMC-Senshu' method. Ann Rheum Dis 2013;72:148–50.
14. Challener GJ, Jones JD, Pelzek AJ, Hamilton BJ, Boire G, de Brum-Fernandes AJ, et al. Anti-carbamylated protein antibody levels correlate with anti-Sa (citrullinated vimentin) antibody levels in rheumatoid arthritis. J Rheumatol 2016;43:273–81.
15. Henschen-Edman AH. Fibrinogen non-inherited heterogeneity and its relationship to function in health and disease. Ann N Y Acad Sci 2001;936:580–93.

ARTHRITIS & RHEUMATOLOGY
Vol. 69, No. 7, July 2017, pp 1387–1395
DOI 10.1002/art.40117

Antibodies to Cyclic Citrullinated Peptides in Patients With Juvenile Idiopathic Arthritis and Patients With Rheumatoid Arthritis

Shared Expression of the Inherently Autoreactive 9G4 Idiotype

Hannah Peckham,[1] Geraldine Cambridge,[2] Lauren Bourke,[1] Debajit Sen,[1] Anna Radziszewska,[1] Maria Leandro,[2] and Yiannis Ioannou[1]

Objective. **Antibodies to cyclic citrullinated peptides (anti-CCP) in rheumatoid arthritis (RA) can express the inherently autoreactive gene V_H4–34, detected using the rat monoclonal antibody 9G4. Patients with the polyarticular subtype of juvenile idiopathic arthritis (JIA) share some but not all of the features of adult patients with RA. This study was undertaken to compare serologic findings for rheumatoid factor (RF), anti-CCP, and 9G4-expressing anti-CCP in a large JIA cohort with a cohort of adult RA patients.**

Methods. **Serum from 88 patients with polyarticular JIA, 29 patients with enthesitis-related arthritis, 38 patients with extended oligoarthritis, 31 adolescent controls, 35 patients with RA, and 30 adult controls were tested for RF, for IgG, IgA, and IgM anti-CCP, and for 9G4-expressing anti-CCP by enzyme-linked immunosorbent assay. Total serum 9G4-positive IgM was also measured.**

Results. **Of 65 patients with RF-negative polyarticular JIA, 4 (6.2%) were IgG anti-CCP positive. Sera from 20 of 23 patients with RF-positive polyarticular JIA (87.0%), 24 of 35 patients with RA (68.6%), and 1 patient with extended oligoarthritis contained IgG anti-CCP. IgA and IgM anti-CCP levels were lower in the adolescent group ($P < 0.01$). Levels of 9G4-expressing anti-CCP were higher in patients with RF-positive polyarticular JIA than in those with RF-negative polyarticular JIA ($P < 0.0001$). Median levels of 9G4-expressing anti-CCP in patients with RF-positive polyarticular JIA and those with RA did not differ. Expression of 9G4 on serum total IgM was greater in patients with RF-positive polyarticular JIA than other adolescent groups ($P < 0.01$), but similar to adult RF-positive RA.**

Conclusion. **In healthy individuals, 9G4-positive B cells comprise 5–10% of the peripheral blood pool but serum immunoglobulins utilizing V_H4–34 are disproportionately low. The idiotope recognized by 9G4 was detected on anti-CCP antibodies in >80% of patients with RF-positive polyarticular JIA. V_H4–34 usage by anti-CCP in both JIA and RA patients suggest elicitation of these autoantibodies through shared pathogenic B cell selection processes.**

Juvenile idiopathic arthritis (JIA), as defined by the updated International League of Associations for Rheumatology (ILAR) classification criteria (1), is an umbrella term encompassing different subtypes of arthritis with onset in those age <16 years. Rheumatoid factor (RF)–positive polyarticular JIA is one of the more severe subtypes of JIA. It is associated with older onset (being more frequently seen in adolescents) and more disability compared to other subtypes, and more frequently progresses into adulthood, requiring continuing treatment (2). Clinically, of all of the subtypes of JIA, RF-positive polyarticular

Supported by Arthritis Research UK (grant 20164).
[1]Hannah Peckham, MSc, Lauren Bourke, PhD, Debajit Sen, MB BS, FRCP, Anna Radziszewska, MSc, Yiannis Ioannou, MB BS, FRCP, PhD: Arthritis Research UK Centre for Adolescent Rheumatology, University College London, London, UK; [2]Geraldine Cambridge, PhD, Maria Leandro, MD, PhD: University College London, London, UK.

Ms Peckham and Dr. Cambridge contributed equally to this work.

Address correspondence to Geraldine Cambridge, PhD, or Yiannis Ioannou, MB BS, FRCP, PhD, both c/o Arthritis Research UK Centre for Adolescent Rheumatology, Rayne Building, 5 University Street, London WC1E 6JF, UK. E-mail: g.cambridge@ucl.ac.uk or y.ioannou@ucl.ac.uk.

Submitted for publication December 13, 2016; accepted in revised form March 30, 2017.

JIA most closely resembles that of adult-onset rheumatoid arthritis (RA). However, there are subtle differences in the clinical pattern of disease in addition to the difference in the age at onset. Young people with RF-positive polyarticular JIA tend to have more frequent involvement of the temporomandibular joints and ankles. This is captured by the Juvenile Arthritis Disease Activity Score (3) but excluded from the Disease Activity Score in 28 joints (4), which is used in routine practice in patients with RA (5). Hence, it is uncertain to what extent RF-positive polyarticular JIA represents early-onset RA, or whether it represents a type of inflammatory arthritis of childhood onset that has pathogenic pathways that are distinct from those of adult-onset RA.

The consensus now is that RF-positive polyarticular JIA is associated with a high frequency of IgG class antibodies to citrullinated proteins, as measured in the clinic using commercial cyclic citrullinated peptides (CCPs) as the substrate. The frequency of anti-CCP positivity in RF-positive polyarticular JIA has been shown to be comparable to that seen in adult seropositive RA (6–11). However, most of those studies were of relatively small numbers of patients, most did not include separate diagnostic cohorts within the global categorization of "JIA," and very few compared their findings with those in local adult cohorts of RA. Importantly, previous studies have not investigated upstream pathways of autoantibody production in order to better understand the pathogenesis of RF-positive polyarticular JIA and to what extent this overlaps with RA. One method to investigate this research question is to define the genes that encode for anti-CCP antibody expression and determine whether they are shared by RF-positive polyarticular JIA and seropositive RA.

Although the variable regions of the heavy chain of immunoglobulins are encoded by a total of 123 heavy-chain variable region (Ig V_H) genes, with nearly half expressed as V_H segments, there is a degree of skewing toward the usage of certain V_H genes in autoimmunity and B cell malignancy. The use of particular genes encoding Ig V_H has been associated with the development of autoantibodies (12,13), with those encoded by V_H4–34 being the prototype in autoimmune diseases (14,15). Immunoglobulins derived from this gene, even in a germline configuration, are inherently autoreactive and can recognize a number of self antigens in the absence of antigen-driven selection. The rat monoclonal antibody 9G4 binds a unique conformational epitope confined largely within framework region 1 of the V_H region of immunoglobulins derived from the V_H4–34 gene. The availability of the 9G4 reagent thus allows the tracking of an autoimmune subset of B cells utilizing V_H4–34 in the B cell receptor and the identification of soluble antibodies derived from this Ig V_H gene.

V_H4–34–derived 9G4-positive B cells are present across all ethnic groups, comprising up to 10% of peripheral blood B cells. Their phenotype is consistent with being predominantly within naive B cell populations (IgD+CD27–). In contrast, except for transient increases in the context of infection (especially with Epstein-Barr virus, cytomegalovirus, and pneumococcus), serum levels of predominantly IgM class V_H4–34–derived immunoglobulins are disproportionately low in normal individuals. The 9G4-positive B cells are also not commonly seen within germinal centers, but are capable of some degree of class-switch recombination since small amounts of 9G4 IgG can be detected in serum (16,17).

In autoimmunity, however, V_H4–34–derived sequences are overrepresented in autoantibodies. V_H4–34 usage is, for example, obligatory for most cold agglutinins (18), utilized by some IgG anti–double-stranded DNA antibodies in serum, and also found deposited in renal biopsy specimens from patients with systemic lupus erythematosus (SLE) (19) and used by antimyeloperoxidase antibodies in systemic vasculitis (20). More recently, we have described 9G4-positive autoantibodies specific for CCP in patients with early RA (<6 weeks of joint symptoms) and those with established RA (21). Investigating the isotype distribution and presence of the 9G4 idiotope on anti-CCP antibodies in RF-positive polyarticular JIA and comparing this to a local seropositive adult RA population may therefore further our understanding of potential common pathways for autoreactive B cell selection in RF-positive polyarticular JIA.

PATIENTS AND METHODS

Patients. Table 1 shows the demographic and clinical characteristics of adolescent and adult patients, all of whom were seen at University College London Hospital. A total of 88 patients with polyarticular JIA, 29 patients with enthesitis-related arthritis (ERA), 38 patients with extended oligoarticular JIA, 31 age- and sex-matched healthy individuals (median age 21 years [range 13–23 years]), 35 sex-matched adult patients with RA, and 30 healthy adult controls (74% female; median age 38 years [range 24–72 years]) were included. None of the patients had received rituximab

Table 1. Demographic and clinical characteristics of the patients*

	Polyarticular JIA (n = 88)	ERA (n = 29)	Extended oligoarthritis (n = 38)	RA (n = 35)
Age, median (range) years	17 (13–23)	17 (14–27)	18 (15–29)	56 (36–80)
Sex, % female	80.1	31.0	55.7	77.1
Disease duration, median (range) years	7.9 (0.3–22.5)	4.5 (1.3–20.9)	13.4 (1.9–27.5)	13.2 (1.1–52.8)

* JIA = juvenile idiopathic arthritis; ERA = enthesitis-related arthritis; RA = rheumatoid arthritis.

at any time before sampling. In the juvenile cohorts, approximately two-thirds of the patients with polyarticular JIA (53 of 88) and those with extended oligoarticular JIA (22 of 38) were receiving methotrexate (MTX), with equal proportions in each group (36%) receiving biologic therapies (tumor necrosis factor [TNF] inhibition). Two-thirds of the patients with ERA (19 of 29) were receiving MTX, 6 were receiving additional or alternative disease-modifying antirheumatic drugs (DMARDs) (sulfasalazine [SSZ] or hydroxychloroquine [HCQ]), and 17% (n = 5) were receiving biologic agents. These were mainly TNF inhibitors, with 1 patient receiving abatacept and 2 patients receiving tocilizumab. Of 35 adult RA patients, 2 were not receiving treatment, 33 were receiving DMARDs, usually MTX (n = 18), SSZ (n = 8), and HCQ (n = 7), 13 were receiving biologic agents (all anti-TNF), and 9 were receiving oral prednisolone (all <20 mg/day).

Sera were obtained from collections within The Centre for Rheumatology, and the Arthritis Research UK Centre for Adolescent Rheumatology, University College London and selected on the basis that they fulfilled the ILAR classification criteria for JIA (1) or the American College of Rheumatology and European League Against Rheumatism (EULAR) classification criteria for RA (22). All subjects donated blood after informed consent, and the study was approved by the local ethics committee (REC 11/LO/0330 [adolescent cohorts] and REC 08/H0714/18 [adult cohorts]).

Measurement of anti-CCP antibodies. Anti-CCP antibodies in patient and control sera diluted 1:200 were measured using a commercial 96-well enzyme-linked immunosorbent assay (ELISA), using plates precoated with second-generation citrullinated peptides (CCP2) (FCCP600; Axis-Shield Diagnostics). IgG anti-CCP were measured according to kit protocol with a cutoff for positivity of 5 units/ml.

Horseradish peroxidase (HRP)–conjugated sheep anti-human IgA or IgM (The Binding Site) was used to detect anti-CCP antibodies of the given isotype using the same ELISA plates as for IgG anti-CCP.

Levels of IgA anti-CCP antibodies were calculated with reference to an in-house standard (representing 100 arbitrary units [AU]) included on each ELISA test plate as well as negative controls. Results were expressed as a proportion of the positive control following subtraction of background binding of HRP conjugate and normalization between different ELISA plates. IgA anti-CCP are rarely observed in healthy control sera (21) and cutoff was therefore based on calculations using the mean + 3SD of binding by 60 sera from healthy controls across all age groups (giving a value of 11 AU/ml) (21). In contrast, IgM class antibodies to CCP are commonly observed in sera from healthy adult controls, and since we had no reference for a cutoff level to cover both adolescent and adult IgM anti-CCP levels in samples, results are expressed as optical density (OD) (×1,000) given by serum samples following subtraction of background binding of conjugate alone to CCP-coated wells.

Determination of IgM-RF status. For JIA patients, IgM-RF status was obtained from historical clinical data from standard laboratory tests (RA particle agglutination assay). An in-house protocol was used to determine RF status in healthy adult and adolescent controls using affinity-purified rabbit IgG (Sigma-Aldrich) as the substrate. Briefly, binding of sera (diluted 1:200) to affinity-purified rabbit IgG–coated wells and to uncoated wells was measured using goat anti-human IgM-HRP conjugate (The Binding Site). After subtracting background binding (to uncoated wells), arbitrary units of binding were calculated by reference to a standard curve constructed from a commercial source (Cambridge Life Sciences) with values of >23 AU/ml considered positive.

Detection of 9G4 expression on anti-CCP and on serum total IgM. For detection of 9G4 expression on antibodies to CCP, sera (diluted 1:50 in RD6Q diluent; R&D Systems) were added to antigen-coated wells of ELISA plates. Following incubation, the 9G4 reagent (IGM Bioscience) was added at a concentration of 2 μg/ml to one side of the plate, and the duplicate serum-incubated wells received diluent buffer containing equivalent affinity-purified normal rat IgG1 (Sigma-Aldrich) instead of 9G4. An affinity-purified HRP-conjugated goat anti-rat IgG reagent (Amersham) was used to detect 9G4 recognition of CCP2-binding antibodies. Results were calculated and presented as OD × 100 at 450 nm following the subtraction of any background binding in wells in the absence of the 9G4 reagent. To assess 9G4 binding to total serum IgM, sera diluted 1:250 were added to each side of ELISA plates that were either left uncoated or coated with 2 μg/ml murine Fab_2 anti-human IgM (eBioscience). Following blocking with 1% bovine serum albumin, the rat 9G4 reagent was added at 2 μg/ml. Subsequently, goat anti-rat HRP conjugate (Abcam) was used for detection, and tetramethylbenzidine was used for development. Background binding to the uncoated side of the plates was subtracted, and results were expressed as the OD at 450 nm.

Statistical analysis. GraphPad Prism was used for all statistical analyses. Nonparametric statistics for populations not following a normal distribution (Mann-Whitney U test) were used to compare groups. For determination of relationships between variables, linear regression (Pearson's correlation) was used. *P* values less than 0.01 were considered significant.

RESULTS

Elevated levels of IgG anti-CCP in patients with RF-positive polyarticular JIA and patients with RF-positive RA. Table 2 summarizes the RF status and frequency of class-switched anti-CCP antibodies in the adult RA, JIA, extended oligoarthritis, and ERA patient groups. In the adult RA patients, 20 of 26 RF-positive serum samples (77%) also contained IgG anti-CCP. Of 88 patients diagnosed as having polyarticular JIA, 65 were RF negative.

Table 2. Autoantibody profiles of the patient groups*

	RF positive	IgG anti-CCP positive	IgA anti-CCP positive
RF-positive polyarticular JIA (n = 23)	23 (100.00)	20 (86.96)	7 (30.43)
RF-negative polyarticular JIA (n = 65)	0 (0.00)	4 (6.15)	0 (0.00)
ERA (n = 29)	0 (0.00)	0 (0.00)	1 (3.45)
Extended oligoarthritis (n = 38)	2 (5.26)	1 (2.63)	2 (5.26)
RF-positive RA (n = 26)	26 (100.00)	20 (76.92)	17 (65.37)
RF-negative RA (n = 9)	0 (0.00)	4 (44.44)	2 (22.22)

* Values are the number (%) of patients. RF = rheumatoid factor; anti-CCP = anti–cyclic citrullinated peptide; JIA = juvenile idiopathic arthritis; ERA = enthesitis-related arthritis; RA = rheumatoid arthritis.

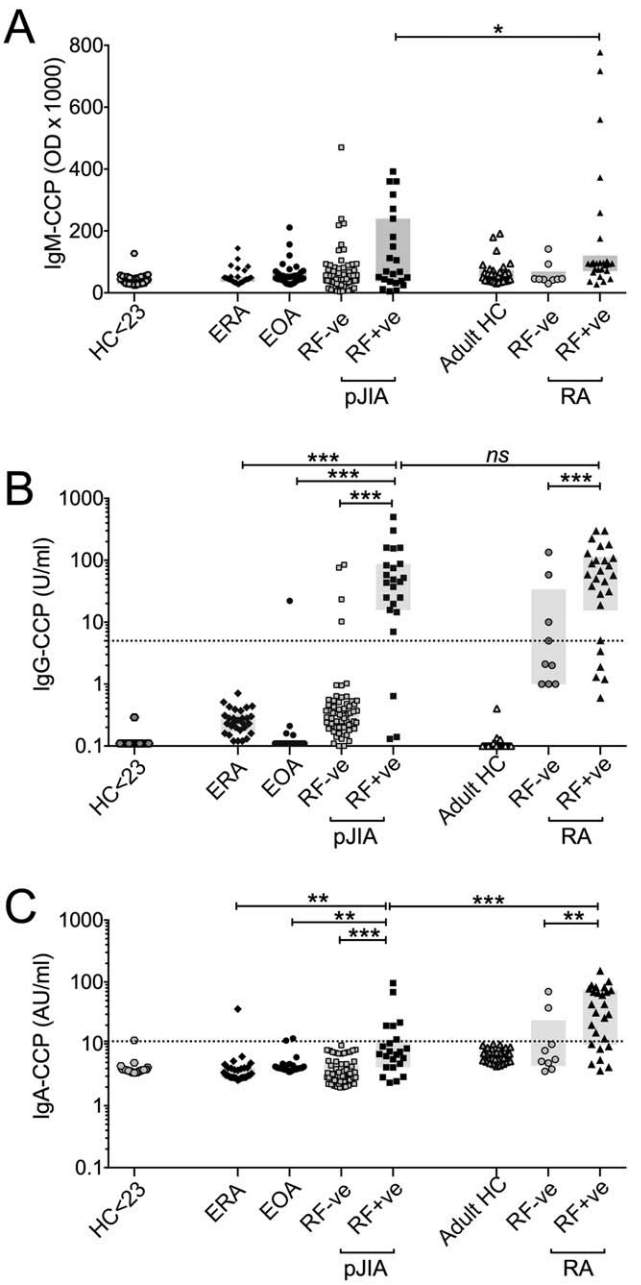

Figure 1. Levels of IgM anti–cyclic citrullinated peptide (anti-CCP) (**A**), IgG anti-CCP (**B**), and IgA anti-CCP (**C**) in healthy controls (HC) age <23 years (n = 31), patients with enthesitis-related arthritis (ERA; n = 29), patients with extended oligoarthritis (EOA; n = 38), patients with rheumatoid factor (RF)–negative polyarticular juvenile idiopathic arthritis (pJIA; n = 65), patients with RF-positive polyarticular JIA (n = 23), healthy adult controls (n = 26), patients with RF-negative rheumatoid arthritis (RA; n = 9), and patients with RF-positive RA (n = 26). Symbols represent individual patients; shaded areas show the 25th to 75th percentiles. Broken lines in **B** and **C** indicate the upper limit of normal. * = $P < 0.01$; ** = $P < 0.001$; *** = $P < 0.0001$, by Mann-Whitney U test. Only selected comparisons are shown to preserve clarity. NS = not significant.

Only 4 (6%) of these patients had levels of IgG anti-CCP above the cutoff for a positive result (>5 units/ml). In the RF-positive polyarticular JIA group, 20 of 23 samples (87%) contained IgG anti-CCP. These findings validate the suggestion that IgG anti-CCPs are frequently seen in the RF-positive polyarticular subset of JIA, with a specificity of 96.9% (95% confidence interval 92.99–99.00%). Only 1 patient in the other adolescent patient groups (in the extended oligoarthritis cohort) had a positive result for IgG anti-CCP.

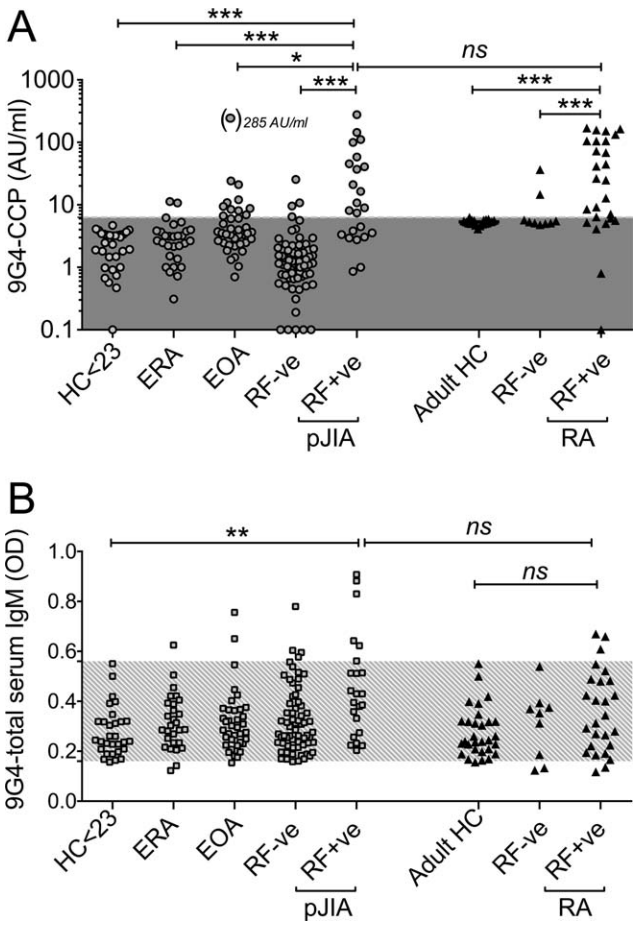

Figure 2. Binding of the rat monoclonal antibody 9G4 to anti-CCP antibodies (**A**) and to serum total IgM (**B**) in healthy controls age <23 years (n = 31), patients with ERA (n = 38), patients with extended oligoarthritis (n = 38), patients with RF-negative polyarticular JIA (n = 65), patients with RF-positive polyarticular JIA (n = 23), healthy adult controls (n = 26), patients with RF-negative RA (n = 9), and patients with RF-positive RA (n = 26). Symbols represent individual patients. In **A**, the shaded area indicates the mean + SD in healthy adolescent control samples. In **B**, the shaded area indicates the minimum and maximum OD of results of binding in healthy adolescent controls. * = $P < 0.01$; ** = $P < 0.001$; *** = $P < 0.0001$, by Mann-Whitney U test. Only selected comparisons are shown to preserve clarity. See Figure 1 for definitions.

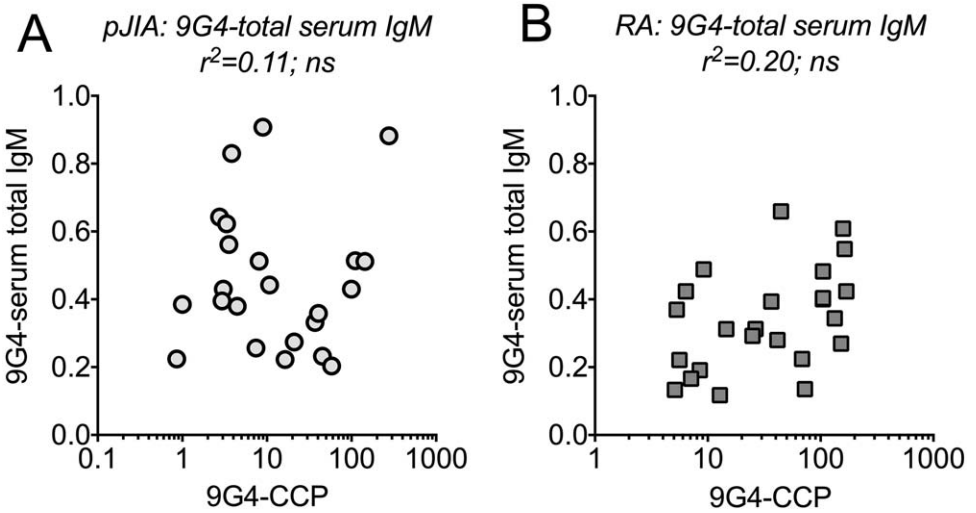

Figure 3. Lack of correlation between 9G4-expressing anti–cyclic citrullinated peptide (9G4-CCP) and 9G4 on serum total IgM in patients with polyarticular juvenile idiopathic arthritis (pJIA) (**A**) and adult patients with rheumatoid arthritis (RA) (**B**). Symbols represent individual patients. Linear regression results (Pearson's correlation coefficient) and significance at 5% are indicated. NS = not significant.

Figure 1B shows the comparative levels of IgG anti-CCP antibodies across all disease and control groups and illustrates that patients with RF-positive polyarticular JIA had significantly higher levels of IgG anti-CCP antibodies than patients with RF-negative polyarticular JIA ($P < 0.0001$), patients with extended oligoarthritis ($P < 0.0001$), patients with ERA ($P < 0.0001$), and healthy adolescent controls ($P < 0.0001$). No significant difference in IgG anti-CCP antibody levels was seen between the adolescent RF-positive polyarticular JIA and adult RF-positive RA patient cohorts (median 44.1 units/ml [interquartile range (IQR) 15.4–87.3] versus median 58.3 units/ml [IQR 15.4–113.7]; $P = 0.21$). Adult patients with RF-positive RA had significantly higher levels of IgG anti-CCP than patients with RF-negative RA and age- and sex-matched controls (both $P < 0.0001$).

Presence of IgM and IgA anti-CCP antibodies in patients with RF-positive polyarticular JIA. Figures 1A and C show the comparative levels of IgM and IgA anti-CCP, respectively, across all patient and control groups. Although levels of IgG anti-CCP were similar between adolescent patients with RF-positive polyarticular JIA and adult patients with RF-positive RA, both IgM and IgA anti-CCP levels were significantly lower in the adolescent group.

The differences in IgA anti-CCP levels were mirrored when sera from healthy adolescents (median 3.4 AU/ml [IQR 3.6–3.9]) and sera from adults (median 6.3 AU/ml [IQR 5.2–7.7]) were compared ($P < 0.0001$), but the levels in most samples from adolescents were well below the cutoff for positivity. Healthy adults also had significantly higher median levels of IgM anti-CCP (59.0 [IQR 38.5–73.6]) than healthy controls who were age <23 years (42.4 [IQR 28.4–52.7) ($P = 0.001$).

Although healthy adult controls and patients with RA were not matched for age, there was no correlation between levels of any isotype of anti-CCP with disease duration or age within either the juvenile or adult cohorts (data not shown).

Anti-CCP antibodies in RF-positive polyarticular JIA and RF-positive RA share an inherently autoreactive germline gene as detected by 9G4 binding. Usage of the V_H4–34 immunoglobulin gene by autoantibodies recognizing CCP was tracked using binding of the antiidiotope rat monoclonal antibody 9G4 (Figure 2A). The expression of 9G4 on anti-CCP antibodies was significantly higher in patients with RF-positive RA than in patients with RF-negative RA (median 25.7 [IQR 6.0–105.0] versus 5.2 [IQR 5.0–8.0]) ($P < 0.0001$). Similarly, binding of 9G4 antibodies to anti-CCP was significantly higher in the patients with RF-positive polyarticular JIA than in those with RF-negative polyarticular JIA (median 9.8 [IQR 3.3–41.8]) versus 1.2 [IQR 0.7–2.0]) ($P < 0.0001$), and those with extended oligoarthritis ($P < 0.01$) and ERA ($P < 0.0001$). Similar median levels of 9G4-expressing anti-CCP were present in patients with RF-positive polyarticular JIA and RF-positive adult RA ($P = 0.13$).

One explanation for the detection of 9G4 expression on antibodies to CCP in patients with RF-positive polyarticular JIA is that there is a general expansion of usage of this V_H gene in adolescents. Since serum IgM contains virtually all 9G4-expressing immunoglobulin

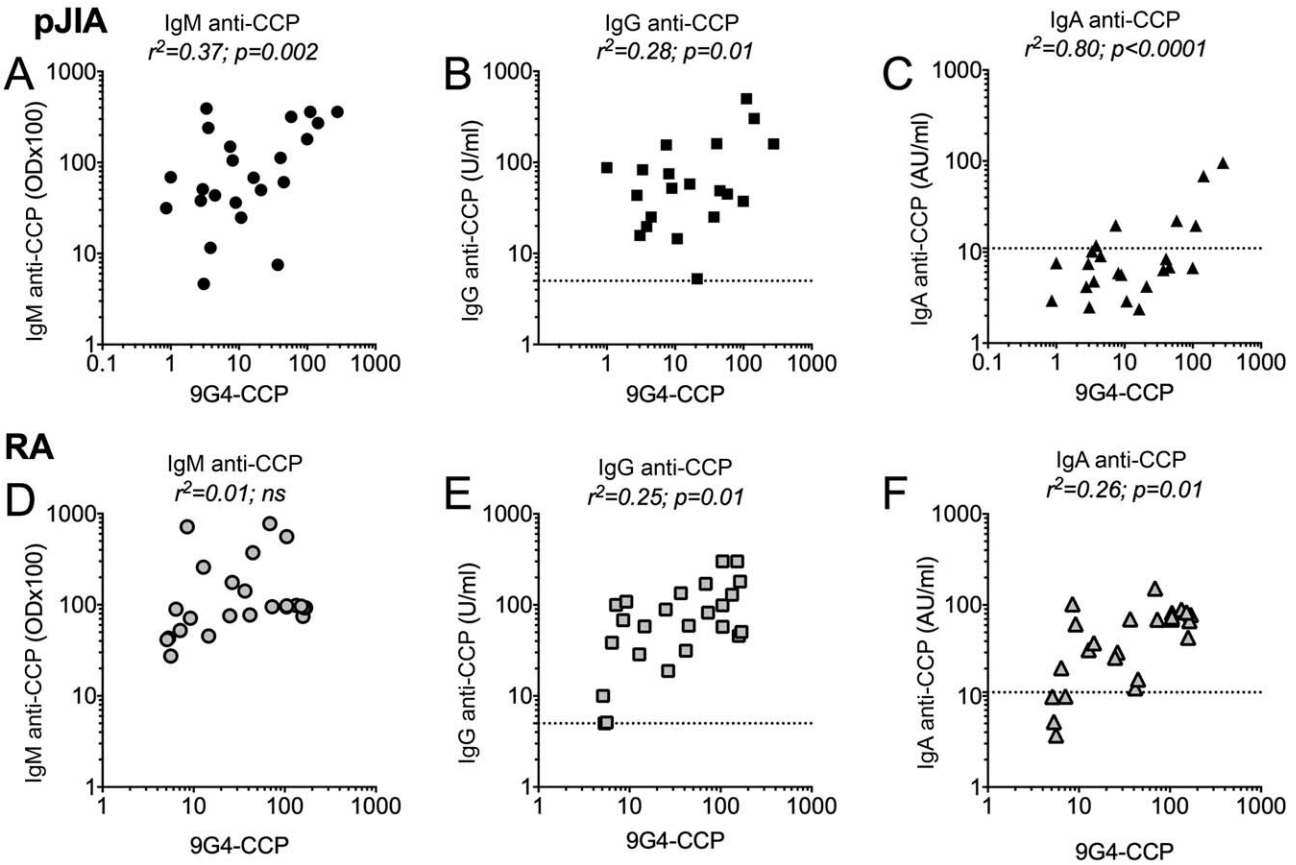

Figure 4. **A–C**, Relationships between levels of 9G4-expressing anti–cyclic citrullinated peptide (9G4-CCP) and IgM anti-CCP (**A**), IgG anti-CCP (**B**), and IgA anti-CCP (**C**) in patients with rheumatoid factor–positive polyarticular juvenile idiopathic arthritis (pJIA). **D–F**, Relationships between levels of 9G4-expressing anti-CCP and IgM anti-CCP (**D**), IgG anti-CCP (**E**), and IgA anti-CCP (**F**) in adult patients with rheumatoid arthritis (RA). All patients included were seropositive for IgG anti-CCP antibodies. Linear regression results (Pearson's correlation coefficient) and significance at 5% are indicated. NS = not significant.

species, we compared levels of 9G4 IgM between patients with RF-positive polyarticular JIA and other adolescent cohorts (Figure 2B). Expression of 9G4 on serum total IgM was significantly higher in patients with RF-positive polyarticular JIA than in healthy adolescent controls ($P < 0.001$), but similar to that found in RF-positive adult RA (Figure 2B). However, only 5 of 19 samples exceeded the upper limit of the range in sera from healthy controls age <23 years (Figure 2B), and there was no correlation between 9G4-expressing anti-CCP and 9G4 on serum total IgM as determined by capture ELISA (Figure 3A) (Pearson's correlation coefficient $r^2 = 0.11$; $P = 0.15$), suggesting that despite a possible increase in 9G4 IgM, 9G4-positive B cells committed to anti-CCP antibody production may have undergone differentiation by a different pathway of activation. There was no correlation between 9G4-expressing anti-CCP and 9G4 binding to serum total IgM in adult RA patients (Figure 3B).

With respect to the Ig class distribution of 9G4-expressing anti-CCP antibodies in adult RA patients, the results of our previous experiments suggested that 9G4 expression was associated with IgM anti-CCP but that a small proportion may also be of IgG class (21). We have yet to undertake similar experiments using adolescent patient samples, but analyzed possible correlations between the levels of the different classes of anti-CCP in adult RA and RF-positive polyarticular JIA and 9G4-expressing anti-CCP, using linear regression analysis (Figure 4). Interestingly, differences were found between patients with polyarticular JIA and adult RA patients. Binding of 9G4 to anti-CCP antibodies was strongly correlated with levels of IgM anti-CCP in adolescent but not adult patients (Figures 4A and D). IgG anti-CCP antibody levels, however, were similarly correlated, albeit weakly, with 9G4-expressing anti-CCP in both diseases (Figures 4B and E). The strongest correlation was between IgA anti-CCP and 9G4-expressing anti-CCP in polyarticular

JIA (Figure 4C). A much weaker correlation between IgA anti-CCP and 9G4-expressing anti-CCP was observed in adult RA patients (Figure 4F). However, IgA anti-CCP levels were only positive in 5 (25%) of 20 samples from patients with JIA compared with 20 samples from adult RA patients.

DISCUSSION

Class-switched (IgG) anti-CCP antibodies, while rare in JIA patients overall, were found to occur predominantly in the subset of patients with polyarticular JIA who also tested positive for RF, supporting previous findings in smaller cohorts (6–11). We also confirmed that the IgG anti-CCP antibody profile of patients with RF-positive polyarticular JIA was significantly distinct from both age- and sex-matched healthy controls and patients with other subtypes of JIA. Only 3.1% (5 of 163) of all disease controls or age- and sex-matched healthy controls tested positive for IgG anti-CCP antibodies. IgG anti-CCP isotype serology in serum samples from RF-positive adolescent patients with polyarticular JIA was compared directly with that in serum samples from RF-positive adults with RA. Although the prevalence of anti-CCP antibodies in RA has been widely studied, for the purposes of this investigation we included a random sample of our own adult cohort, to eliminate discrepancies in methodology or cutoffs for positivity. No significant difference was found between the levels of IgG anti-CCP antibodies in RF-positive polyarticular JIA and RF-positive RA. This suggests that the IgG anti-CCP antibody phenotypes of the two diseases are similar, consistent with the parallels seen in other diagnostic criteria between these two conditions.

IgG anti-CCP antibodies are routinely tested upon clinician's request, but are not included in the current diagnostic criteria for RF-positive polyarticular JIA (1). The confirmation of the specificity of IgG anti-CCP antibodies for RF-positive polyarticular JIA, in contrast to both healthy controls and JIA disease controls, suggests that IgG anti-CCP levels could also prove a worthwhile formal addition to existing criteria for RF-positive polyarticular JIA.

Levels of IgA anti-CCP antibodies were significantly higher in patients with RF-positive polyarticular JIA than in all control groups, but values were very low, with the median and the value for most samples (14 of 19 [74%]) within the normal range in our assay. Adult RA patients also had significantly higher levels of IgM anti-CCP compared with the adolescent patients with RF-positive polyarticular JIA, despite their comparable IgG anti-CCP levels. Most patients in all of the disease groups were receiving DMARDs, and many were also receiving biologic agents, so it was difficult to attribute any significant effects of treatment on differences in autoantibody isotype between patient groups. This presents the interesting question as to whether anti-CCP antibodies follow the same pathway of class-switching that is seen in adult RA patients. The lower IgA anti-CCP antibody levels in JIA may also indicate that the class switch to IgG anti-CCP precedes the possible accumulation of switched B cells of IgA isotype in juvenile versus adult patients. As we and others have shown, IgM autoantibodies can persist at high levels alongside class-switched species and therefore do not follow the patterns that would be expected in a normal humoral response to immunization or some infectious insults (23).

In RA, it is well established that the presence of anti-CCP antibodies can predate clinical symptoms by up to 10 years (24–26). If the case is put forward that RF-positive polyarticular JIA *does* represent very early onset RA, following up patients with RF-positive polyarticular JIA into adulthood should show that they develop the same profile as patients with RF-positive RA. Although it would be very difficult to ascertain whether anti-CCP positivity antedates symptoms in children with RF-positive polyarticular JIA, the question arises as to why these patients develop symptoms at a much younger age, while adult RA patients may be anti-CCP positive for many years before the onset of disease. The time at which treatment with biologic agents is initiated can influence the duration and severity of symptoms, as well as a patient's chances of remission (27). Both the Trial of Early Aggressive Therapy (TREAT) (28) and the Aggressive Combination Drug Therapy in Very Early Polyarticular Juvenile Idiopathic Arthritis (ACUTE-JIA) study (29) demonstrated that in polyarticular JIA, early and aggressive treatment induced significantly higher clinical remission rates and significantly reduced joint erosion and narrowing (30,31). Early detection of autoimmunity may therefore aid in exploiting such a window of opportunity in patients with polyarticular JIA.

It has been postulated that what begins as an abnormal immune response, with anti-CCP positivity, requires a "second event" in order to convert this response into active disease (32). Indeed, the number of citrullinated epitopes recognized by patient antibodies was shown to increase over time, and anti-CCP levels to markedly increase 2–4 years prior to an RA diagnosis, but then to plateau after onset, suggestive of a second stage in disease development (26). We also found that few new epitope specificities arose after B cell depletion with rituximab in adult RA patients (33). In future studies, it could prove interesting to explore whether this process is accelerated in RF-positive polyarticular JIA, and if so, what drives this occurrence.

In addition to defining antibodies by the antigens that they detect, immunoglobulins may also be distinguished

by hypervariable region structures known as idiotypes. The idiotope recognized by the 9G4 rat monoclonal antibody forms a hydrophobic patch that binds to *N*-acetyllactosamine residues that are present on a number of self and microbial glycoproteins and glycolipids (34,35). The ability to recognize *N*-acetyllactosamine is potentially advantageous in assisting the clearance of damaged, apoptotic, or neoplastic cells but may also risk autoimmunity if excessive mutation in the antigen-combining site, located predominantly within the complementarity-determining regions, confers additional binding to a self-specificity.

If a particular idiotype is found in different patients, but on a particular group of antibodies (e.g., anti-CCP), this is a strong indication that the unrelated individuals share usage of the same immunoglobulin-encoding gene (19). The V_H4–34 gene, which is strongly associated with autoimmunity (12), has been demonstrated to be utilized by anti-CCP antibodies in patients with (adult-onset) RA (21). This was seen both in patients with early RA and in those with established RA, but not in those with early polyarthritis not evolving into RA. It also suggests a notable restriction in V_H gene usage that biases the development of their immunoglobulin repertoire, which may be instrumental in the production of autoantibodies to citrullinated proteins (12). In this study we have confirmed that this inherently autoreactive idiotope is also found on anti-CCP antibodies in patients with RF-positive polyarticular JIA.

In conclusion, this study has demonstrated the novel finding that adolescent patients with RF-positive polyarticular JIA have an anti-CCP antibody phenotype that is distinct from that of patients with other clinical subtypes of JIA and age- and sex-matched healthy controls. Patients with RF-positive polyarticular JIA have levels of IgG anti-CCP comparable to those in RF-positive adult patients, and both express the same inherently autoreactive 9G4 idiotype. However, it was found that the adult group had significantly higher levels of IgA and IgM anti-CCPs than the adolescent group, suggesting that further investigation is needed to fully elucidate the extent to which these two conditions may be seen as one.

AUTHOR CONTRIBUTIONS

All authors were involved in drafting the article or revising it critically for important intellectual content, and all authors approved the final version to be published. Dr. Cambridge had full access to all of the data in the study and takes responsibility for the integrity of the data and the accuracy of the data analysis.

Study conception and design. Peckham, Cambridge, Bourke, Leandro, Ioannou.

Acquisition of data. Peckham, Cambridge, Bourke, Sen, Radziszewska, Ioannou.

Analysis and interpretation of data. Peckham, Cambridge, Bourke, Ioannou.

REFERENCES

1. Petty RE, Southwood TR, Manners P, Baum J, Glass DN, Goldenberg J, et al. International League of Associations for Rheumatology classification of juvenile idiopathic arthritis: second revision, Edmonton, 2001. J Rheumatol 2004;31:390–2.
2. Fisher C, Sen D. Juvenile idiopathic arthritis: in adolescence and beyond. Br J Hosp Med (Lond) 2012;73:564–70.
3. Consolaro A, Ruperto N, Bazso A, Pistorio A, Magni-Manzoni S, Filocamo G, et al, for the Paediatric Rheumatology International Trials Organisation. Development and validation of a composite disease activity score for juvenile idiopathic arthritis. Arthritis Rheum 2009;61:658–66.
4. Prevoo ML, van 't Hof MA, Kuper HH, van Leeuwen MA, van de Putte LB, van Riel PL. Modified disease activity scores that include twenty-eight–joint counts: development and validation in a prospective longitudinal study of patients with rheumatoid arthritis. Arthritis Rheum 1995;38:44–8.
5. Wu Q, Chaplin H, Ambrose N, Sen D, Leandro MJ, Wing C, et al. Juvenile arthritis disease activity score is a better reflector of active disease than the disease activity score 28 in adults with polyarticular juvenile idiopathic arthritis. Ann Rheum Dis 2016;75:635–6.
6. Van Rossum M, van Soesbergen R, de Kort S, ten Cate R, Zwinderman AH, de Jong B, et al. Anti-cyclic citrullinated peptide (anti-CCP) antibodies in children with juvenile idiopathic arthritis. J Rheumatol 2003;30:825–8.
7. Low JM, Chauhan AK, Kietz DA, Daud U, Pepmueller PH, Moore TL. Determination of anti-cyclic citrullinated peptide antibodies in the sera of patients with juvenile idiopathic arthritis. J Rheumatol 2004;31:1829–33.
8. Brunner J, Sitzmann F. The diagnostic value of anti-cyclic citrullinated peptide (CCP) antibodies in children with juvenile idiopathic arthritis. Clin Exp Rheumatol 2006;24:449–51.
9. Syed R, Gilliam B, Moore T. Prevalence and significance of isotypes of anti-cyclic citrullinated peptide antibodies in juvenile idiopathic arthritis. Ann Rheum Dis 2008;67:1049–51.
10. Gupta R, Thabah M, Vaidya B, Gupta S, Lodha R, Kabra S. Anti-cyclic citrullinated peptide antibodies in juvenile idiopathic arthritis. Indian J Pediatr 2010;77:41–4.
11. Tebo AE, Jaskowski T, Davis KW, Whiting A, Clifford B, Zeft A, et al. Profiling anti-cyclic citrullinated peptide antibodies in patients with juvenile idiopathic arthritis. Pediatr Rheumatol Online J 2012;10:29.
12. Dörner T, Lipsky PE. Immunoglobulin variable-region gene usage in systemic autoimmune diseases [review]. Arthritis Rheum 2001;44:2715–27.
13. Pascal V, Viktor K, Randen I, Thompson K, Steinitz M, Forre O, et al. Nucleotide sequence analysis of rheumatoid factors and polyreactive antibodies derived from patients with rheumatoid arthritis reveals diverse use of VH and VL gene segments and extensive variability in CDR-3. Scand J Immunol 1992;36:349–62.
14. Rahman A, Latchman DS, Isenberg DA. Immunoglobulin variable region sequences of human monoclonal anti-DNA antibodies. Semin Arthritis Rheum 1998;28:141–54.
15. Pugh-Bernard AE, Silverman GJ, Cappione AJ, Villano ME, Ryan DH, Insel RA, et al. Regulation of inherently autoreactive VH4-34 B cells in the maintenance of human B cell tolerance. J Clin Invest 2001;108:1061–70.
16. Bhat NM, Kshirsagar MA, Bieber MM, Teng NN. IgG subclasses and isotypes of VH4-34 encoded antibodies. Immunol Invest 2015;44:400–10.
17. Cappione A III, Anolik JH, Pugh-Bernard A, Barnard J, Dutcher P, Silverman G, et al. Germinal center exclusion of autoreactive B cells is defective in human systemic lupus erythematosus. J Clin Invest 2005;115:3205–16.
18. Pascual V, Victor K, Spellerberg M, Hamblin TJ, Stevenson F, Capra J. VH restriction among human cold agglutinins: the VH4-21 gene segment is required to encode anti-I and anti-i specificities. J Immunol 1992;149:2337–44.

19. Isenberg D, Spellerberg M, Williams W, Griffiths M, Stevenson F. Identification of the 9G4 idiotope in systemic lupus erythematosus. Br J Rheumatol 1993;32:876–82.
20. Locke IC, Leaker B, Cambridge G. A comparison of the characteristics of circulating anti-myeloperoxidase autoantibodies in vasculitis with those in non-vasculitic conditions. Clin Exp Immunol 1999;115:369–76.
21. Cambridge G, Moura RA, Santos T, Khawaja AA, Polido-Pereira J, Canhao H, et al. Expression of the inherently autoreactive idiotope 9G4 on autoantibodies to citrullinated peptides and on rheumatoid factors in patients with early and established rheumatoid arthritis. PloS One 2014;9:e107513.
22. Arnett FC, Edworthy SM, Bloch DA, McShane DJ, Fries JF, Cooper NS, et al. The American Rheumatism Association 1987 revised criteria for the classification of rheumatoid arthritis. Arthritis Rheum 1988;31:315–24.
23. Verpoort K, Jol-van der Zijde C, Papendrecht-van der Voort E, Ioan-Facsinay A, Drijfhout J, van Tol M, et al. Isotype distribution of anti–cyclic citrullinated peptide antibodies in undifferentiated arthritis and rheumatoid arthritis reflects an ongoing immune response. Arthritis Rheum 2006;54:3799–808.
24. Jansen AL, van der Horst-Bruinsma I, van Schaardenburg D, van de Stadt RJ, de Koning MH, Dijkmans BA. Rheumatoid factor and antibodies to cyclic citrullinated peptide differentiate rheumatoid arthritis from undifferentiated polyarthritis in patients with early arthritis. J Rheumatol 2002;29:2074–6.
25. Nielen MM, van Schaardenburg D, Reesink HW, van de Stadt RJ, van der Horst-Bruinsma IE, de Koning MH, et al. Specific autoantibodies precede the symptoms of rheumatoid arthritis: a study of serial measurements in blood donors. Arthritis Rheum 2004;50:380–6.
26. Van de Stadt LA, de Koning MH, van de Stadt RJ, Wolbink G, Dijkmans BA, Hamann D, et al. Development of the anti–citrullinated protein antibody repertoire prior to the onset of rheumatoid arthritis. Arthritis Rheum 2011;63:3226–33.
27. Zhao Y, Wallace C. Judicious use of biologicals in juvenile idiopathic arthritis. Curr Rheumatol Rep 2014;16:454.
28. Wallace CA, Giannini EH, Spalding SJ, Hashkes PJ, O'Neil KM, Zeft AS, et al. Trial of early aggressive therapy in polyarticular juvenile idiopathic arthritis. Arthritis Rheum 2012;64:2012–21.
29. Tynjälä P, Vähäsalo P, Tarkiainen M, Kröger L, Aalto K, Malin M, et al. Aggressive combination drug therapy in very early polyarticular juvenile idiopathic arthritis (ACUTE–JIA): a multicentre randomised open-label clinical trial. Ann Rheum Dis 2011;70:1605–12.
30. Van Jaarsveld CH, Jacobs JW, van der Veen MJ, Blaauw AA, Kruize AA, Hofman DM, et al. Aggressive treatment in early rheumatoid arthritis: a randomised controlled trial. Ann Rheum Dis 2000;59:468–77.
31. Smolen JS, van der Heijde DM, Keystone EC, van Vollenhoven RF, Goldring MB, Guérette B, et al. Association of joint space narrowing with impairment of physical function and work ability in patients with early rheumatoid arthritis: protection beyond disease control by adalimumab plus methotrexate. Ann Rheum Dis 2013;72:1156–62.
32. Kinloch AJ, Lundberg KE, Moyes D, Venables PJ. Pathogenic role of antibodies to citrullinated proteins in rheumatoid arthritis. Expert Rev Clin Immunol 2006;2:365–75.
33. Cambridge G, Stohl W, Leandro MJ, Migone TS, Hilbert DM, Edwards JC. Circulating levels of B lymphocyte stimulator in patients with rheumatoid arthritis following rituximab treatment: relationships with B cell depletion, circulating antibodies, and clinical relapse. Arthritis Rheum 2006;54:723–32.
34. Bhat NM, Bieber MM, Chapman CJ, Stevenson FK, Teng NN. Human antilipid A monoclonal antibodies bind to human B cells and the i antigen on cord red blood cells. J Immunol 1993;151:5011–21.
35. Richardson C, Chida AS, Adlowitz D, Silver L, Fox E, Jenks SA, et al. Molecular basis of 9G4 B cell autoreactivity in human systemic lupus erythematosus. J Immunol 2013;191:4926–39.

ARTHRITIS & RHEUMATOLOGY
Vol. 69, No. 7, July 2017, pp 1396–1406
DOI 10.1002/art.40102

Regional Differences Between Perisynovial and Infrapatellar Adipose Tissue Depots and Their Response to Class II and Class III Obesity in Patients With Osteoarthritis

Natalia S. Harasymowicz, Nick D. Clement, Asim Azfer, Richard Burnett, Donald M. Salter, and A. Hamish W. R. Simpson

Objective. **Obesity is associated with an increased risk of developing osteoarthritis (OA), which is postulated to be secondary to adipose tissue–dependent inflammation. Periarticular adipose tissue depots are present in synovial joints, but the association of this tissue with OA has not been extensively explored. The aim of this study was to investigate differences in local adipose tissue depots in knees with OA and characterize the changes related to class II and class III obesity in patients with end-stage knee OA.**

Methods. **Synovium and the infrapatellar fat pad (IPFP) were collected during total knee replacement from 69 patients with end-stage OA. Histologic changes, changes in gene and protein expression of adiponectin, peroxisome proliferator–activated receptor γ (PPARγ), and Toll-like receptor 4 (TLR-4), and immune cell infiltration into the adipose tissue were investigated.**

Results. **IPFP and synovium adipose tissue depots differed significantly and were influenced by the patient's body mass index. Compared to adipocytes from the IPFP and synovium of lean patients, adipocytes from the IPFP of obese patients were significantly larger and the synovium of obese patients displayed marked fibrosis, increased macrophage infiltration, and higher levels of TLR4 gene expression. The adipose-related markers PPARγ in the IPFP and adiponectin and PPARγ in the synovium were expressed at lower levels in obese patients compared to lean patients. Furthermore, there were increased numbers of CD45+ hematopoietic cells, CD45+CD14+ total macrophages, and CD14+CD206+ M2-type macrophages in both the IPFP and synovial tissue of obese patients.**

Conclusion. **These differences suggest that IPFP and synovium may contain 2 different white adipose tissue depots and support the theory of inflammation-induced OA in patients with class II or III obesity. These findings warrant further investigation as a potentially reversible, or at least suppressible, cause of OA in obese patients.**

The prevalence of obesity (defined as a body mass index [BMI] of ≥30 kg/m^2) has significantly increased within developed societies over the last decade. It has been estimated that more than 50% of adults in the US will be obese by 2030 (1). Obesity, characterized by an excess of white adipose tissue due to an imbalance between calories consumed and calories expended, is associated with an increased risk of a number of diseases, including type 2 diabetes mellitus (DM), atherosclerosis (2), and some types of cancer (3). There is also a recognized association between obesity and osteoarthritis (OA) (4), with obese individuals having a higher risk of developing OA in both the weight-bearing and non–weight-bearing joints.

Several mechanisms by which obesity may initiate or accelerate the progression of OA have been postulated. Biomechanical factors are likely to be important, since the weight-bearing joints are overloaded. However, the increased incidence of OA in non–weight-bearing joints indicates that other factors are also involved. It has been postulated that venous outlet obstruction in the subchondral bone might impair nutrient supply, making articular cartilage more susceptible to damage (5). It is now becoming clear, however, that adipose tissue may create a systemic inflammatory milieu via the release of various cytokines and adipokines, which have the potential to damage articular cartilage directly (6). Furthermore, increasing BMI is

Natalia S. Harasymowicz, PhD, Nick D. Clement, PhD, FRCS, Asim Azfer, PhD, Richard Burnett, FRCS, Donald M. Salter, MD, FRCPath, A. Hamish W. R. Simpson, DM, MA, FRCS: University of Edinburgh, Edinburgh, UK.

Address correspondence to Natalia S. Harasymowicz, PhD, University of Edinburgh, Orthopaedics and Trauma Surgery, Chancellor's Building, 49 Little France Crescent, EH16 4SB Edinburgh, UK. E-mail: n.harasymowicz@gmail.com.

Submitted for publication July 14, 2016; accepted in revised form March 14, 2017.

correlated with a higher content of free glycosaminoglycans in synovial fluid (7), and both hypercholesterolemia and hypertriglyceridemia have been hypothesized to interfere with cartilage metabolism (8).

White adipose tissue depots are predominantly present in subcutaneous sites (as subcutaneous adipose tissue [SAT]) or within the abdomen (as omental/visceral adipose tissue [VAT]). In a healthy subject of normal weight, the majority of adipose tissue (up to 80%) is represented by SAT, and only 10–20% is represented by VAT. These depots differ in a number of features, such as adipocyte size, blood vessel density, and immune cell content (9,10). Adiponectin and peroxisome proliferator–activated receptor γ (PPARγ) are 2 important adipose tissue–related proteins. Adiponectin is a secretory protein that is postulated to have antiatherogenic and antiinflammatory properties (11). PPARγ is a nuclear receptor crucial for the differentiation of mesenchymal stem cells into mature adipocytes and is important in fatty acids and glucose metabolism.

Adipose tissue in healthy adults is dynamic, and its size and function may change depending on the level of incoming energy. Extracellular matrix (ECM) remodeling is essential to allow rapid adipose tissue responses to a nutrient deficiency or surplus. As such, there is constant matrix remodeling, with a balance between ECM production and ECM degradation. In obese individuals, hypertrophic adipocytes, which are unable to store additional triglycerides, start a process of lipolysis with associated tissue fibrosis (12). These events lead to enhanced free fatty acid release. These free fatty acids may accumulate in other tissues, such as the liver, skeletal muscle, or joints, with consequent organ lipotoxicity (13,14).

Impaired adipocyte function in fat depots, in turn, leads to adipocyte necrosis, which triggers an influx of proinflammatory cells, including hematopoietic cells such as macrophages, mast cells, and subtypes of T cells (15). Significantly, up to 30% of up-regulated genes in adipose tissue in obese individuals are related to macrophage function (16). Increased levels of circulating saturated fatty acids, which are potent agonists of Toll-like receptors (TLRs) including TLR-2 and TLR-4, may also contribute to the production of a range of proinflammatory and profibrotic mediators recognized as being potential targets in the pathogenesis of OA (17).

In synovial joints, adipose tissue is present in the subsynoviocyte intimal layer and in periarticular depots such as the infrapatellar fat pad (IPFP) of the knee joint. The physiologic role of these fat deposits and their origin are not well described. It has been suggested that fat deposits in the IPFP are similar in type to those in the SAT (18) due to the fibrous tissue surrounding adipocytes, whereas others support the notion that fat deposits in the IPFP are similar to those in the VAT (19).

The aim of this study was to ascertain whether there are differences in the adipose tissue depots in the knee joints between obese and nonobese patients with end-stage knee OA. Additionally, we analyzed differences in the characteristics of the SAT and VAT and their potential to act as sites of local proinflammatory mediator production, a process that might contribute to the progression of OA.

PATIENTS AND METHODS

Sample collection. Ethics approval for the study was granted by the Lothian Research Ethics Committee and UK National Health Service Lothian Research and Development Management, which provided consent for the use of surgical discard tissue for this study. The tissue was obtained from patients (n = 69) during primary total knee replacement surgery for knee OA. Patients were divided into a lean group (with a BMI of <25 kg/m^2) and an obese group (patients with class II or class III obesity, with a BMI of ≥ 35 kg/m^2). The analyzed samples were isolated by the same surgeon (RB) with the same incision technique of harvesting synovial punch biopsy specimens from the suprapatellar synovial region and from the IPFP in the infrapatellar region. The synovial membrane was not separated from the adipose tissue.

Hematoxylin and eosin (H&E)–stained sections of knee joint tissue from each patient were analyzed; samples with increased synovial membrane inflammation were not analyzed in this study. In general, samples from OA patients had no more than 10–15% of total synovial membrane per whole-tissue biopsy sample. Representative results of histologic assessments are presented in Supplementary Figure 1, available on the *Arthritis & Rheumatology* web site at http://onlinelibrary.wiley.com/doi/10.1002/art.40102/abstract.

Reagents. All reagents were obtained from Sigma-Aldrich unless otherwise stated. Antibodies for immunohistochemical analyses were obtained from Dako or as otherwise stated. Antibodies for flow cytometry were obtained from ImmunoTool. Cell culture reagents were from Life Technologies. The primary and secondary antibodies used in these analyses, as well as the negative controls, are summarized in Supplementary Tables 1 and 2 (available on the *Arthritis & Rheumatology* web site at http://onlinelibrary.wiley.com/doi/10.1002/art.40102/abstract).

Histologic assessment, measurement of adipocyte area, and tissue staining with picrosirius red S. Tissue samples were fixed in 4% paraformaldehyde, embedded in paraffin, and cut into 4-μm sections. The sections were deparaffinized, rehydrated, and stained with H&E or picrosirius red S. Images of 10 different regions (representing 50–150 adipocytes) in each sample (n = 12 samples per group) were obtained at 20 × magnification (for adipocyte size measurement) and 60 × magnification (for picrosirius red S staining) on a Nikon Eclipse E800 microscope. Adipocyte size was then assessed by measuring the longest diameter (designated a) and the shortest diameter (designated b) for the area of an ellipse to calculate the area of the cell (designated A), using the following mathematical formula:

$$A = \pi\left(\frac{a}{2} \times \frac{b}{2}\right)$$

For quantification of fibrosis, images of picrosirius red S–stained sections were converted into an 8-bit image with the

exclusion of the background, and the percentage area of fibrosis was calculated. For measurements of the adipocyte size and area of fibrosis, ImageJ software was used.

Immunohistochemical analyses. Immunohistochemical analyses were performed by incubating the tissue sections (n = 10 samples per group) with the primary antibody (anti-human CD45 and anti-human CD206 antibodies [R&D Systems], and anti-human TLR4 antibodies [Bioss]) followed by a secondary antibody conjugated with horseradish peroxidase. The chromogenic substrate 3,3′-diaminobenzidine was used to develop the color. Counterstaining was performed with Harris' hematoxylin.

Tissue explant cultures and enzyme-linked immunosorbent assays (ELISAs). Tissue sections (n = 5 samples per group) were cut into 1–3-mm^3 fragments, weighed, and cultured for 24 hours in Iscove's modified Dulbecco's medium (IMDM) supplemented with 10% fetal bovine serum and penicillin/streptomycin. Explants were then cultivated (in duplicate) for 3 days in serum-free IMDM with penicillin/streptomycin. Thereafter, supernatants were collected and total adiponectin levels in the medium were assessed using an Adiponectin/Arcp30 Quantikine ELISA kit (R&D Systems). This kit allowed analysis of total adiponectin. The concentration of the protein produced was adjusted for the weight (in mg) of the wet tissue explant.

Western blotting. Tissue samples (n = 7 samples per group) were snap-frozen in liquid nitrogen and homogenized. Protein concentrations were measured using a Bradford assay (Bio-Rad). In total, 25 μg of protein from each sample was subjected to 12% sodium dodecyl sulfate–polyacrylamide gel electrophoresis and transferred to a PVDF membrane (Immobilon-FL) using a Bio-Rad Wet Transfer system. Blots were blocked by Odyssey Blocking buffer (1:1 with phosphate buffered saline [PBS]) and incubated with the appropriate antibody cocktail (mouse anti-human adiponectin antibodies [1:500; PeproTech] and rabbit anti-human GAPDH antibodies [1:10,000; Sigma-Aldrich], or rabbit anti-human PPARγ antibodies [1:1,000; Santa Cruz Biotechnology] and mouse anti-human β-actin antibodies [1:10,000; Bioss]) diluted in Odyssey Blocking buffer (1:1 with PBS–Tween) overnight at 4°C. Immunoblots were visualized by incubation with a cocktail of fluorescent dye–conjugated secondary antibodies (anti-rabbit IRDYE 800CW and anti-mouse IRDYE 680RD, both 1:10,000; Li-Cor) and scanned under an infrared Odyssey FC Imaging System for detection by Western blotting. For semiquantitative analysis of protein expression, densitometric analyses of the bands on Western blots were performed using Image Studio Lite 3.1 software. Denaturing conditions allowed the analysis of total adiponectin in the investigated blots.

RNA isolation, complementary DNA (cDNA) synthesis, and real-time quantitative polymerase chain reaction (qPCR) analysis. RNA from IPFP and synovium samples (n = 7 samples per group) was obtained using a combined QIAzol and Qiagen Mini RNA isolation kit technique. Stability of the RNA was established by gel electrophoresis, and 2 bands (28S RNA and 18S RNA) were detected. RNA purity was assessed by NanoDrop absorbance measurement with 260 nm/280 nm and 260 nm/230 nm absorbance ratios of >1.9. One microgram of RNA was treated with DNAse I (Invitrogen) and reverse transcribed using iSCRIPT (Bio-Rad) in accordance with the instructions of the suppliers. Real-time PCR was conducted on a LightCycler 96 (Roche). Ten nanograms of cDNA was analyzed. The primer concentration was 10 μ*M*.

The reactions were performed in triplicate for each analyzed gene. Reactions using SYBR Green chemistry were also subjected to melting curve analysis. The amplification curves and efficiency of amplification of each gene were validated, and the efficiency values ranged from 95% to 105%. Values for target gene expression were normalized to those of the β_2-microglobulin (B2M) reference gene. Relative messenger RNA (mRNA) expression was assessed using the $2^{-\Delta\Delta C_t}$ method, with the lowest C_t value serving as a calibrator (according to the method described by Schmittgen and Livak [20]). In order to analyze the fold change in mRNA levels, values in the samples from lean patients were used as the reference level, being set at 1.0. The primer sequences used for assessment of gene expression were as follows: for ADIPOQ, forward GCA-TTC-AGT-GTG-GGA-TTG-GA and reverse TAA-AGC-GAA-TGG-GCA-TGT-TG (product size 80 kb); for PPARG, forward GCT-GTG-CAG-GAG-ATC-ACA-GA and reverse GGG-CTC-CAT-AAA-GTC-ACC-AA (product size 225 kb); for TLR4, forward AGC-TGT-ACC-GCC-TTC-TCA-GC and reverse CCT-GCC-AAT-TGC-ATC-CTG-TA (product size 152 kb); and for B2M, forward TGT-GCT-CGC-GCT-ACT-CTC-TC and reverse CCA-TTC-TCT-GCT-GGA-TGA-CG (product size 90 kb).

Flow cytometry. The stromovascular fraction from each tissue explant was obtained as follows. First, 1–3 gm of tissue was intensively washed with sterile PBS and minced into 1–2-mm^3 pieces, and then incubated for 1.5 hours at 37°C in 2 mg/ml of type I and type II collagenases in 0.5% bovine serum albumin in Hanks' balanced salt solution with Ca^{2+} and Mg^{2+}. The cell fraction was filtered and lysed using Red Cell Lysis buffer (Millipore). Cells were then incubated in the dark for 30 minutes at 4°C with anti-human CD45, anti-human CD14, and anti-human CD206 antibodies or isotype control antibodies (each at 1:100 dilution; ImmunoTool) and TLR4 antibodies (1:100 dilution; BioLegend) and analyzed by flow cytometry (Beckman Coulter XL). Details regarding the gating strategy are shown in Supplementary Figures 2–6, available on the *Arthritis & Rheumatology* web site at http://onlinelibrary.wiley.com/doi/10.1002/art.40102/abstract.

Statistical analysis. All statistical analyses were performed using GraphPad Prism software (version 6.0). The Mann-Whitney U test and Wilcoxon's matched pairs test were used to compare linear variables between groups, and Spearman's rho correlation was used to assess the association between nonparametric linear variables. A Mann-Whitney U test was performed for comparison of linear variables between groups (lean versus obese), and a Wilcoxon's matched pairs analysis was used to assess differences in linear variables between anatomic sites in the same group (IPFP versus synovium from the same donor). *P* values less than 0.05 were considered significant.

RESULTS

Association of obesity with changes in adipocyte size and fibrosis in knee joint fat depots. Histomorphometric analyses of the knee joint tissue demonstrated differences in adipocyte size and in the extent of fibrosis in knee joint fat depots between lean patients and obese patients (Figures 1A–D). In lean patients, the size of adipocytes in the synovial adipose tissue was greater than that in the IPFP (median 5.52 μm^2, interquartile range [IQR] 3.41–8.21

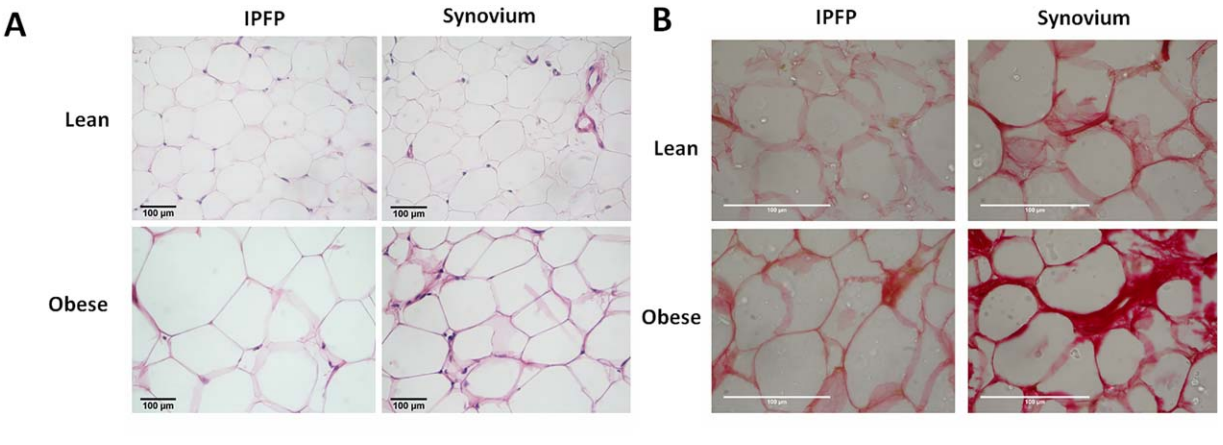

C

Group	Fat Pad		Synovium		Difference	p-value*
	Median	IQR	Median	IQR		
Lean	4.89	3.00 to 7.87	5.52	3.41 to 8.21	0.63	0.003
Obese	6.54	3.82 to 9.90	5.75	3.29 to 9.03	0.79	<0.0001
Difference	1.65		0.23			
p-value*	<0.0001		0.17			

IQR Interquartile range

* Mann Whitney U test

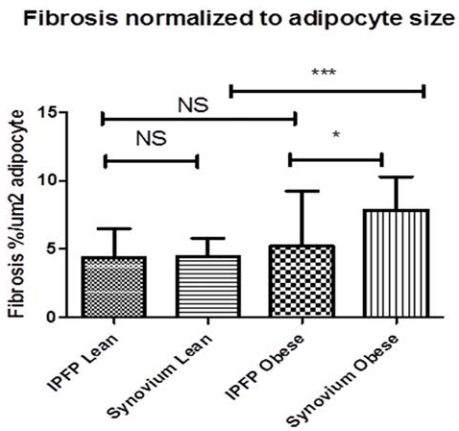

Figure 1. **A** and **B,** Representative hematoxylin and eosin staining (**A**) and picrosirius red S staining (**B**) of adipose tissue depots in the infrapatellar fat pad (IPFP) and synovium from lean and obese patients with end-stage knee osteoarthritis (OA) (n = 10 samples per group). **C,** Differences in median adipocyte cell size between lean and obese OA patients and between anatomic locations. **D,** Percentage area of fibrosis, normalized to median adipocyte size, in the IPFP and synovium of lean and obese OA patients. Results are the mean ± SD. * = $P < 0.05$; *** = $P < 0.001$. NS = not significant.

versus median 4.89 μm^2, IQR 3.00–7.87; $P = 0.003$). This difference was reversed in obese patients, whose synovial adipose tissue contained smaller adipocytes than those in the IPFP (median 5.75 μm^2, IQR 3.29–9.03 versus median 6.54 μm^2, IQR 3.82–9.90; $P < 0.0001$) (Figures 1A–C). Furthermore, in the synovium, there was no significant difference between lean and obese patients in the median size of adipocytes ($P = 0.17$), whereas in the IPFP, the median adipocyte size was significantly higher in obese patients compared to lean patients ($P < 0.0001$).

Analysis of pericellular fibrosis showed that the percentage area of fibrosis in the synovial tissue did not differ from that in the IPFP in knee joint samples from lean individuals (Figure 1D). Similarly, there was no difference in pericellular fibrosis seen between the IPFP and synovium of obese individuals. However, there was a significantly greater area of matrix deposition in the synovial adipose tissue of obese individuals (mean ± SD 24.66 ± 5.62%) compared to that of lean individuals (14.44 ± 5.21%) ($P < 0.005$), whereas there was no significant difference in the area of matrix deposition in the IPFP (20.91 ± 8.1% in obese patients versus 16.89 ± 3.35% in lean patients). The mean area of adipocyte fibrosis was normalized to the median adipocyte size in each patient, to adjust for differences in adipocyte size.

Association of obesity with changes in adipose tissue–related gene and protein expression in knee joint fat depots. Real-time qPCR and Western blot analyses showed differential expression of adipose tissue–related genes and proteins in the synovium and IPFP of lean and obese individuals (Table 1 and Figures 2A–D).

The expression levels of the ADIPOQ gene and adiponectin protein were not different in paired synovium and IPFP samples from lean patients, whereas in obese patients, their levels were significantly lower in the synovium compared to the IPFP ($P = 0.02$ in qRT-PCR, $P = 0.04$ in ELISA, and $P = 0.03$ in Western blotting). Furthermore, synovium from lean patients expressed

Table 1. Quantitative polymerase chain reaction analysis of ADIPOQ, PPARG, and TLR4 gene expression in the IPFP and synovium obtained from lean and obese patients with osteoarthritis*

	ADIPOQ	PPARG	TLR4
IPFP			
Lean	1 ± 0.75	1 ± 0.43	1 ± 0.13
Obese	0.74 ± 0.56†	0.35 ± 0.9†‡	1.01 ± 0.12
Synovium			
Lean	0.41 ± 0.51	0.25 ± 0.53†	1.85 ± 0.13
Obese	0.09 ± 0.04†‡	0.06 ± 0.62†‡	3.65 ± 0.14‡

* Expression value of each gene. The adiponectin (ADIPOQ), peroxisome proliferator–activated receptor γ (PPARG), and Toll-like receptor 4 (TLR4) genes were normalized to the values for the β_2-microglobulin gene. The $2^{-\Delta\Delta C_t}$ method was used to investigate the fold change in gene expression. The control values (from the infrapatellar fat pad [IPFP] of lean patients) were expressed as 1 to indicate a precise fold change value for each gene of interest. Values are the mean ± SEM fold change (n = 7 samples per group).
† $P < 0.05$ in IPFP/synovium paired-sample analysis (tissue samples from the same donor).
‡ $P < 0.05$ in unpaired analysis (obese patients versus lean patients).

significantly higher levels of the ADIPOQ gene and adiponectin protein compared to synovium from obese subjects ($P = 0.04$ in qRT-PCR, $P = 0.03$ in ELISA, and $P = 0.004$ in Western blotting), but there was no such difference between lean and obese patients in the IPFP (Table 1 and Figures 2A and C).

Analysis of the expression of the PPARG gene and PPARγ protein showed significantly lower expression levels in the synovium than in the IPFP in lean patients ($P = 0.02$ in qRT-PCR and $P = 0.01$ in Western blotting), but this difference between the synovium and the IPFP was not seen in obese patients. PPARγ was also expressed at a significantly lower level in obese patients as compared to lean patients, both in the IPFP ($P = 0.02$ in qRT-PCR and $P = 0.03$ in Western blotting) and in the synovium ($P = 0.04$ in qRT-PCR and $P = 0.03$ in Western blotting) (Table 1 and Figures 2B and D).

Increased numbers of CD45+ hematopoietic cells and macrophage content in the knee joint synovium and IPFP with obesity. Immunohistochemical and flow cytometric analyses of samples from lean individuals showed that the number of CD45+ hematopoietic cells was significantly greater in the synovial adipose tissue than in the IPFP (mean ± SD 18.7 ± 6.9% versus 15.02 ± 6.7%; $P = 0.03$) (Figures 3A and B). In obese patients, the number of CD45+ hematopoietic cells was elevated, as compared to that in lean patients, in both the IPFP (19.4 ± 3.4%) and the synovium (26.6 ± 8.7%) ($P = 0.04$ for the IPFP, P 0.004 for the synovium). However, there was no difference in the number of CD45+ hematopoietic cells between the IPFP and synovium of obese patients.

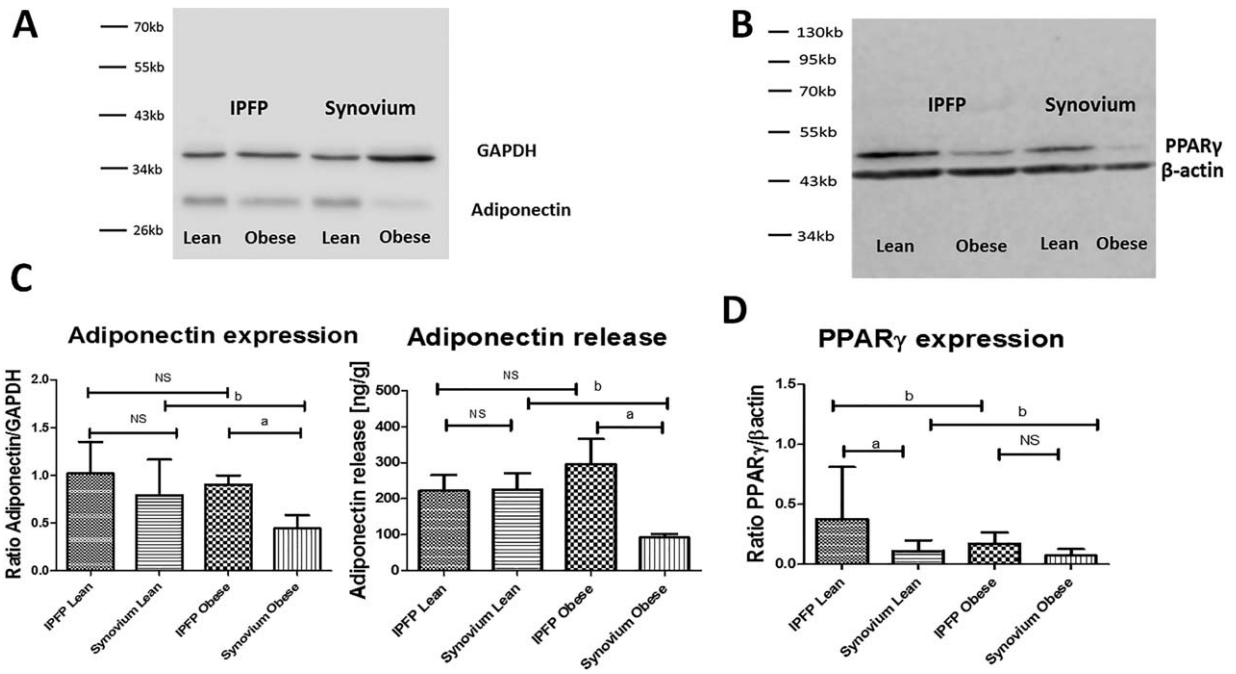

Figure 2. **A** and **B,** Representative Western blots of adiponectin protein expression **(A)** and peroxisome proliferator–activated receptor γ (PPARγ) protein expression **(B)** in the IPFP and synovium of lean and obese patients with end-stage knee OA. **C** and **D,** Semiquantitative Western blot analyses of total adiponectin expression and ex vivo adiponectin release **(C)** and PPARγ expression **(D)** in the IPFP and synovium of lean and obese OA patients. Densitometry data are presented as the mean ± SD adiponectin-to-GAPDH expression ratio and PPARγ-to–β-actin expression ratio in 7 samples per group. a = $P < 0.05$ for paired analyses; b = $P < 0.05$ for obese patients versus lean patients. See Figure 1 for other definitions.

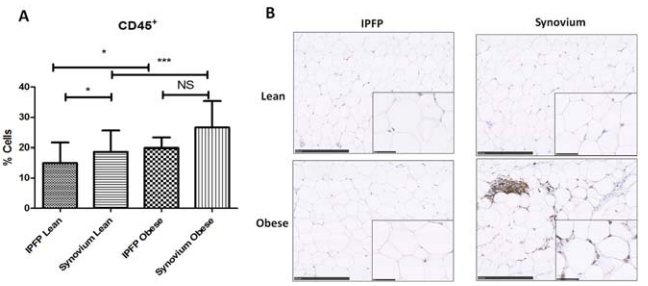

Figure 3. Expression of CD45+ hematopoietic cells in the IPFP and synovium of patients with end-stage OA, as assessed by flow cytometry **(A)** and immunohistochemical analysis **(B)**. **A,** Stromovascular fractions from the IPFP and synovium of lean and obese OA patients were analyzed for CD45+ cell expression; isotype controls were analyzed at the same time. Results are the mean ± SD percentage of CD45+ hematopoietic cells in 7 samples per group. $* = P < 0.05$; $*** = P < 0.001$. **B,** Representative images of immunohistochemical staining for the CD45 marker in the IPFP and synovium of lean and obese OA patients. **Insets**, Higher-magnification views. Bars in main images = 250 μm; bars in boxed areas = 50 μm. See Figure 1 for definitions. Color figure can be viewed in the online issue, which is available at http://onlinelibrary.wiley.com/doi/10.1002/art.40102/abstract.

Cell profiling by flow cytometry showed that the frequency of CD45+CD14+ total macrophages (mean ± SD 8.2 ± 3.5% in the IPFP, 8.84 ± 2.15% in the synovium) and the frequency of CD14+CD206+ M2-type macrophages (6.8 ± 2.2% in the IPFP, 5.7 ± 1.6% in the synovium) was not different between the synovium and IPFP of lean individuals (Figures 4A–C). However, in obese individuals, the percentage of CD45+CD14+ total macrophages (10.6 ± 4.1% in the IPFP, 12.5 ± 2.8% in the synovium) and percentage of CD14+CD206+ M2-type macrophages (8.9 ± 3.2% in the IPFP, 9.5 ± 2.6% in the synovium) were higher than that in lean individuals, both in the IPFP ($P = 0.02$) and in the synovium ($P = 0.0001$). The percentages of CD45+ CD14+ total macrophages and CD14+CD206+ M2-type macrophages correlated significantly with the BMI score, as summarized in Figures 4A and B.

Increased TLR4 expression in the synovium of obese patients, and correlation with BMI. Real-time PCR analysis showed that TLR4 gene expression was not different between the synovium and IPFP of lean individuals (Table 1). There was a significantly higher expression of TLR4 in the synovium of obese patients compared to

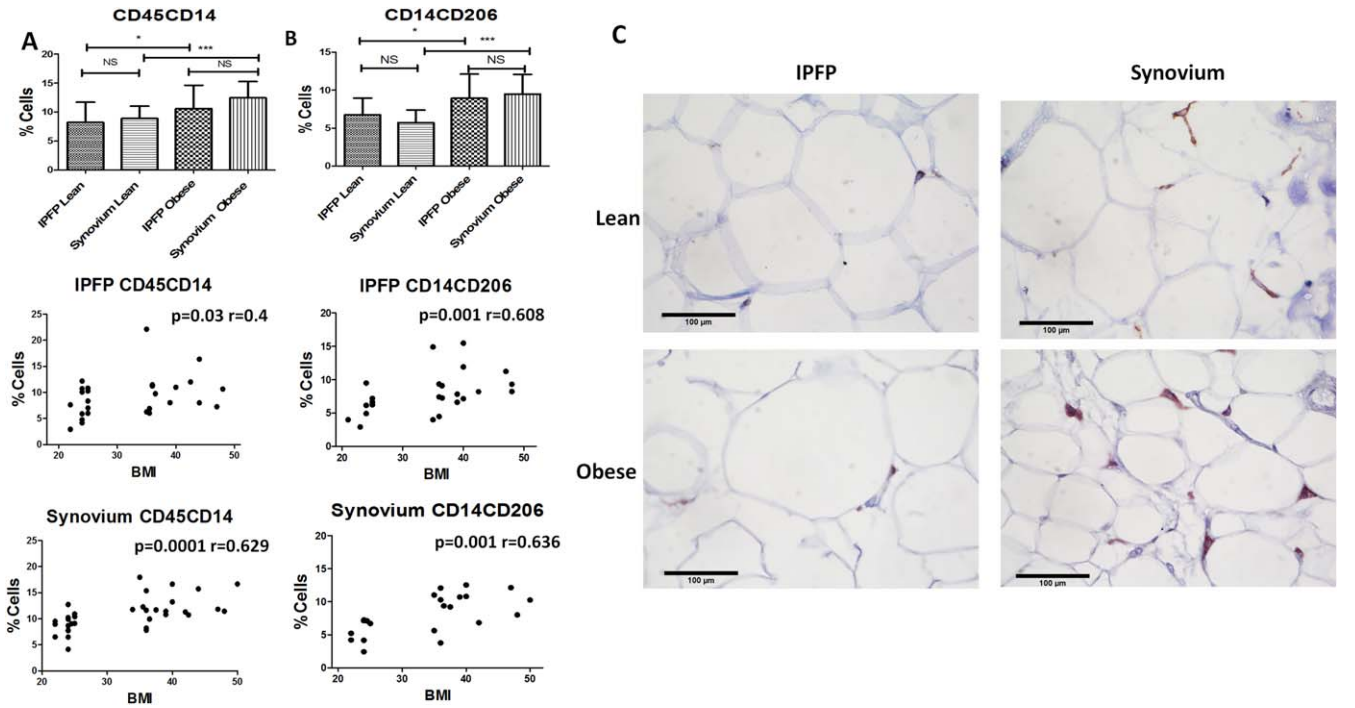

Figure 4. **A** and **B,** Percentages of CD45+CD14+ cells **(A)** and CD14+CD206+ cells **(B)** were determined in the stromovascular fraction of paired synovium and IPFP samples from lean and obese OA patients. Results are the mean ± SD of 10 samples from lean patients and 14 samples from obese patients (top). Percentages of CD45+CD14+ cells and CD14+CD206+ cells were assessed for correlation with the body mass index (BMI) score in the IPFP (n = 26) (middle) and synovium (n = 33) (bottom). $* = P < 0.05$; $*** P < 0.001$. **C,** Representative results of immunohistochemical staining for CD206 are shown in the IPFP and synovium of lean and obese OA patients. See Figure 1 for other definitions. Color figure can be viewed in the online issue, which is available at http://onlinelibrary.wiley.com/doi/10.1002/art.40102/abstract.

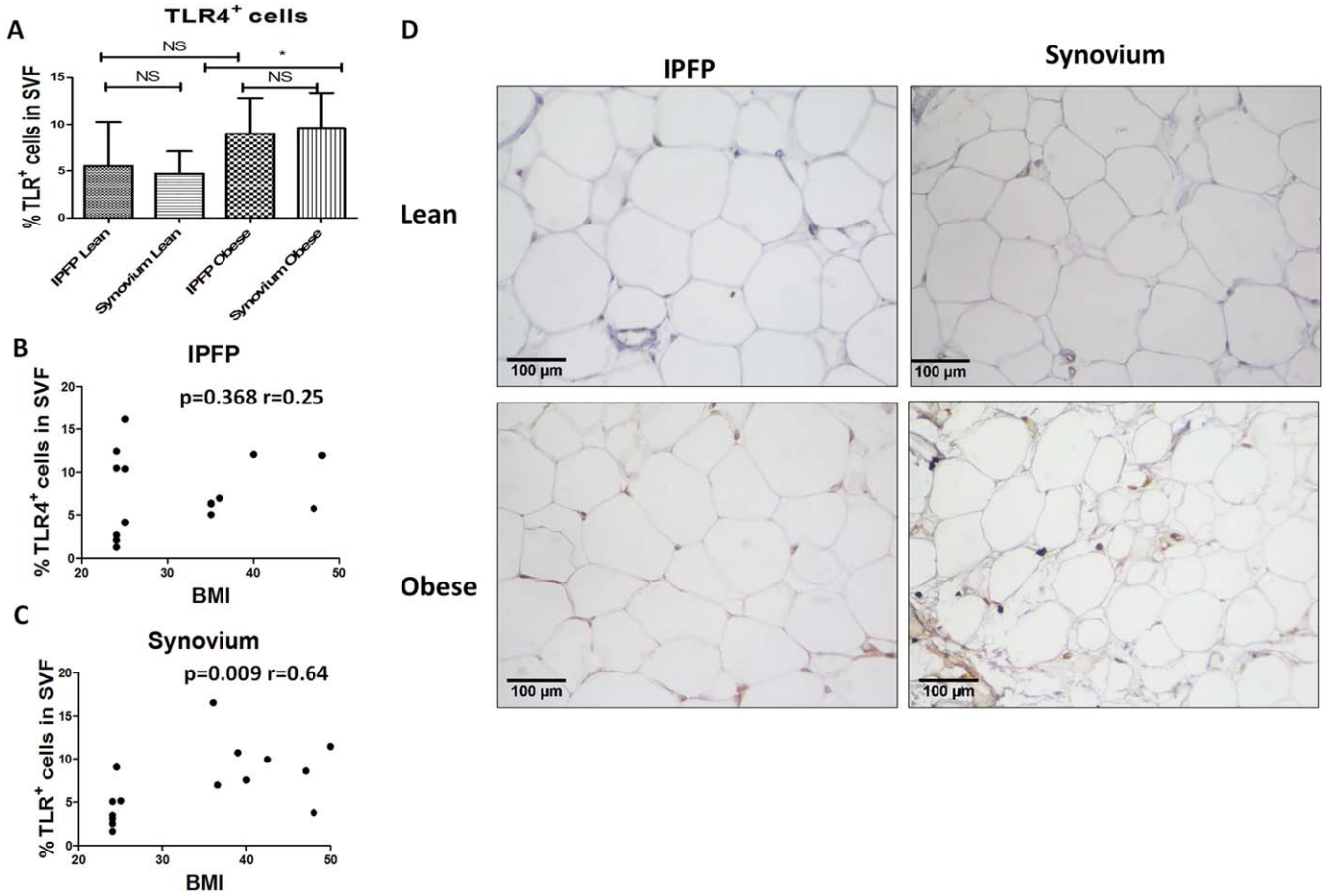

Figure 5. **A,** The percentage of cells positive for TLR4 gene expression were determined in the stromovascular fraction (SVF) of paired synovium and IPFP samples from lean and obese OA patients. Results are the mean ± SD of 5 samples per group. $* = P < 0.05$. **B** and **C,** The percentage of TLR4+ cells was assessed for correlation with the body mass index (BMI) score in the IPFP (n = 15) **(B)** and synovium (n = 15) **(C)** of lean and obese OA patients. **D,** Representative results of immunohistochemical staining are shown for TLR4 gene expression in IPFP and synovium from lean and obese OA patients. See Figure 1 for other definitions. Color figure can be viewed in the online issue, which is available at http://onlinelibrary.wiley.com/doi/10.1002/art.40102/abstract.

the synovium of lean patients ($P = 0.03$). However, no difference in TLR4 expression was seen in the IPFP between lean and obese patients or between the IPFP and synovium of obese patients.

Flow cytometric analysis showed that the percentage of TLR4+ cells did not differ between the synovium and the IPFP of lean patients (mean ± SD 4.7 ± 2.3% and 5.5 ± 4.7%, respectively), but was significantly higher in the synovium of obese patients (9.6 ± 3.7%) compared to the synovium of lean patients ($P = 0.009$) (Figures 5A and D). The percentage of TLR4+ cells in the synovium correlated with the BMI score (Figure 5C). There was no significant difference in the percentage of TLR4+ cells in the IPFP between lean patients and obese patients (mean ± SD 5.54 ± 4.73% versus 9.0 ± 3.81%), and there was no correlation of the percentage of TLR4+ cells in the IPFP with BMI (Figures 5B and D).

DISCUSSION

Obesity is a strong risk factor for the development of OA. The association of OA with obesity in both the load-bearing and non–load-bearing joints suggests that excessive or abnormal loading of the joints does not explain this relationship entirely. As such, an hypothesis suggesting that systemic/metabolic factors may play a role supports the notion that metabolic factors related to obesity act directly or indirectly on chondrocytes, leading to the increased risk of developing OA (21). In the current study, we assessed whether there were any differences in the intraarticular fat deposits within the knee joint (namely, the synovium and the IPFP) of lean and obese individuals undergoing arthroplasty, which may indicate a local, in addition to a systemic, contribution to the development and progression of OA. We found that in lean individuals, the adipocytes were

larger in the synovial adipose tissue than in the IPFP. Furthermore, there was no difference in the extent of pericellular fibrosis or in the levels of adiponectin, but expression of PPARγ was significantly lower in the synovium compared to the IPFP of these patients.

A significantly higher content of CD45+ hematopoietic cells was identified in the synovium compared to the IPFP, but no differences in macrophage numbers (characterized by the expression of CD45+CD14+ and CD14+CD206+ cells) and no differences in the expression of TLR4+ cells were seen in the fat deposits in lean individuals. In comparison, in obese patients, the size of adipocytes was larger in the IPFP than in the synovium, and pericellular fibrosis was greater in the synovial fat. In the synovium compared to the IPFP of obese patients with end-stage knee OA, the expression levels of adiponectin and PPARγ were lower, whereas the expression of TLR4 was higher. In both the IPFP and synovium of obese patients, there was a significantly higher content of CD45+ hematopoietic cells, CD45+CD14+ total macrophages, and CD14+CD206+ M2-type macrophages, as compared to the IPFP and synovium of lean subjects.

In a previous study, immunohistochemical and flow cytometric analyses identified the presence of CD86 (M1-type marker) and CD206 (M2-type marker) in the IPFP, but did not find an influence of BMI on the numbers of these cells (22). A recent study also demonstrated no differences in immune cell populations between paired IPFP and synovium samples; however, those authors investigated individuals with a mean BMI of 28.9 kg/m^2 (BMI range no more than 32 kg/m^2), and this may explain the contrasting results in comparison to those of the current study (23).

Studies of fat deposits in obesity indicate that, with weight gain, adipocytes in the SAT increase in size significantly more than those in the VAT (9). Results of the current study demonstrated that in obese patients, the size of adipocytes in the IPFP was significantly increased, whereas there was no change in the size of adipocytes in the synovium.

Fibrosis, a hallmark of metabolically dysfunctional white adipose tissue with resident adipocytes being surrounded by a network of ECM, is a typical feature of the visceral fat in obese patients (24). Results of the current study, which demonstrated an increase in adipocyte size in the IPFP and augmented pericellular fibrosis in the synovial fat, support the theory that synovial and IPFP adipose tissue depots may each represent a different subtype of white adipose tissue. The synovial adipose tissue demonstrated characteristics akin to those of the VAT, whereas the characteristics of the IPFP were more in keeping with those of the SAT. Conversely, findings reported by other investigators have suggested a profibrotic role of the IPFP, which is independent of the BMI of the patient (25). The extent of fibrosis and the deposition of collagen could have been quantified further in this study with the use of picrosirius red staining accompanied by polarized light to evaluate birefringence.

Adiponectin has been postulated to be both procatabolic (26,27) and proanabolic (28) in OA. As such the influence of adiponectin on the OA pathogenetic pathway is not clear. The adiponectin concentration has been reported to be elevated in the serum of OA patients compared to healthy individuals (29); however, the levels of adiponectin in the synovial fluid are significantly lower than those in the peripheral blood of OA patients (30). However, adiponectin levels in synovial fluid have been shown to correlate with proteoglycan catabolism (31). The IPFP has been shown to produce more adiponectin than that produced by subcutaneous depot fat from the same donor (6,32), consistent with the observation of differential expression and production of adiponectin by the IPFP and the synovium in the current study. However, a negative correlation between adiponectin expression by the IPFP and the BMI of OA patients was not observed in the current study, as has been suggested by other authors (33).

Differential expression of adiponectin has also been reported in various kinds of adipose tissue depots. SAT produces more adiponectin than VAT (34,35), and during weight gain, a significant down-regulation of adiponectin production in VAT, but not in SAT, has been reported (31). We observed a decrease in adiponectin gene expression and protein production ex vivo by the synovium, but not the IPFP, of obese individuals. Although, in the present study, synovial membrane was not dissected from the adjacent adipose tissue, we hypothesize that the results obtained may indicate a difference in the origin of the 2 fatty tissue depots analyzed.

PPARγ is a ligand-activated transcription factor that plays a key role in lipid homeostasis. Our data indicate that PPARγ expression was significantly lower in both the IPFP and synovium of obese patients. Such changes are likely to have a proinflammatory/procatabolic effect in the joint, as PPARγ activation in adipose tissue is associated with beneficial effects on the expression and secretion of a range of factors, including adiponectin by adipocytes and suppression of production of inflammatory mediators such as resistin, interleukin-6, and tumor necrosis factor by macrophages (36). Notably, mice with cartilage-specific knockout of PPARγ spontaneously develop OA (37), indicating a role for this transcription factor in the regulation of chondrocyte function, including inhibition of procatabolic pathways through support of autophagy (38). PPARγ agonists have potent antiinflammatory and

anticatabolic activity when applied to articular chondrocytes and synovial fibroblasts (39), and have been shown to have some degree of efficacy in instability-induced OA models in guinea pigs and dogs (40,41). Although the effects of these agents have not yet been shown in human studies, the lower expression of PPARγ in tissue samples from the knee joints of obese patients indicates that targeted therapy for this subgroup of OA patients might be beneficial.

Leukocyte numbers increase with obesity, both in the circulation and in local adipose tissue depots, and are correlated with such proinflammatory diseases as type 2 DM (42) and liver steatosis (43). Our flow cytometry and immunohistochemistry data indicate that the frequency of hematopoietic cells was significantly higher in the synovium than in the IPFP from lean patients with OA, with a further increase in the number of CD45+ cells being seen in those with obesity, suggesting a more proinflammatory profile of both tissues. The main hematopoietic cells present in adipose tissue are macrophages, which are postulated to play an important role in obesity-related exacerbation of inflammation and organ fibrosis (44). In the current study, we observed, for the first time, an increased frequency of CD14+CD206+ M2-type macrophages in both knee joint synovial deposits and IPFP deposits from obese patients with OA, which correlated significantly with the patients' BMI. CD206 is considered to be an antiinflammatory macrophage marker. However, M2-type macrophages also play a role in profibrotic processes during wound healing and are an important source of the profibrotic factor transforming growth factor β (TGFβ) (45). This is a limitation of the current study and could be a very interesting future goal for further investigation, to determine the expression of TGFβ in fatty tissue deposits in obesity-driven OA.

The expression levels of TLR4 and the number of TLR4+ cells were significantly increased in the knee joint synovium from obese patients compared to lean patients in the current study. In keeping with this, the findings from our immunohistochemical analyses of TLR4 gene expression indicated that TLR4 was expressed at a significantly higher level in the synovial adipose tissue of obese patients compared to lean patients. In humans, expression of TLR4 is up-regulated in the VAT, but not in the SAT, from obese patients (46), consistent with our premise that synovial fat deposits in the knee have characteristics of VAT. TLR-4 plays a crucial role the accumulation of macrophages in adipose tissue of obese patients (47). TLR-4 ligands activate fibroblasts and promote their differentiation into collagen-producing cells (48). Moreover, in adipose tissue, it is proposed that interactions between adipocytes and macrophages through TLR-4/myeloid differentiation protein 2 will aggravate adipose tissue inflammation (49), and therefore possibly by such mechanisms, the progression of OA could be potentiated.

Our analysis of end-stage knee OA, the exclusion of patients with a BMI of between 30 and 35 kg/m^2, and no separation of synovial membrane from adipose tissue are potential limitations of this study. However, recent studies and observations suggest that BMI is not a perfect index. People classified as obese with a BMI of 30 kg/m^2 have been shown to have the same health profile, or even a better health profile, than that of individuals of normal weight (50). A further limitation was the effect of comorbidities, such as type 2 DM, which, given the number of patients and subgroups, was not possible to evaluate fully in the current study.

Thus, the findings of this study show that there are significant differences between synovial and IPFP adipose tissue in patients undergoing joint arthroplasty for knee OA, which supports the theory that synovial fat has characteristics of VAT, while the IPFP is more akin to SAT. Obesity is associated with changes in these fat depots, with synovial fat, in particular, showing changes typical of VAT, which is likely to be associated with a proinflammatory and catabolic phenotype. Nevertheless, there is an increased number of CD45+ hematopoietic cells and CD45+CD14+ and CD14+CD206+ macrophages in both adipose tissue depots in obese patients, which supports the idea that, in addition to biomechanical factors, local inflammation-produced mediators probably contribute to the development of OA in obese individuals. Targeting of this adipose tissue–dependent inflammation by novel therapies, such as PPARγ agonists, may have a benefit and delay the progression of OA in obese patients.

AUTHOR CONTRIBUTIONS

All authors were involved in drafting the article or revising it critically for important intellectual content, and all authors approved the final version to be published. Dr. Harasymowicz had full access to all of the data in the study and takes responsibility for the integrity of the data and the accuracy of the data analysis.

Study conception and design. Harasymowicz, Burnett, Salter, Simpson.

Acquisition of data. Harasymowicz, Clement, Azfer, Burnett.

Analysis and interpretation of data. Harasymowicz, Clement, Salter, Simpson.

REFERENCES

1. Wang YC, Mcpherson K, Marsh T, Gortmaker SL, Brown M. Health and economic burden of the projected obesity trends in the USA and the UK. Lancet 2011;378:815–25.
2. Saydah S, Bullard KM, Cheng Y, Ali MK, Gregg EW, Geiss L, et al. Trends in cardiovascular disease risk factors by obesity level in adults in the United States, NHANES 1999–2010. Obesity (Silver Spring) 2014;22:1888–95.

3. Bianchini F, Kaaks R, Vainio H. Overweight, obesity, and cancer risk. Lancet Oncol 2002;3:565–74.
4. Sturmer T, Gunther KP, Brenner H. Obesity, overweight and patterns of osteoarthritis: the Ulm Osteoarthritis Study. J Clin Epidemiol 2000;53:307–13.
5. Conaghan P, Vanharanta H, Dieppe P. Is progressive osteoarthritis an atheromatous vascular disease? Ann Rheum Dis 2005; 64:1539–41.
6. Klein-Wieringa IR, Kloppenburg M, Bastiaansen-Jenniskens YM, Yusuf E, Kwekkeboom JC, El-Bannoudi H, et al. The infrapatellar fat pad of patients with osteoarthritis has an inflammatory phenotype. Ann Rheum Dis 2011;70:851–7.
7. Buchholz AL, Niesen MC, Gausden EB, Sterken DG, Hetzel SJ, Baum SZ, et al. Metabolic activity of osteoarthritic knees correlates with BMI. Knee 2010;17:161–6.
8. Zainal Z, Longman AJ, Hurst S, Duggan K, Caterson B, Hughes CE, et al. Relative efficacies of omega-3 polyunsaturated fatty acids in reducing expression of key proteins in a model system for studying osteoarthritis. Osteoarthritis Cartilage 2009;17:896–905.
9. Tchernof A, Bélanger C, Morisset AS, Richard C, Mailloux J, Laberge P, et al. Regional differences in adipose tissue metabolism in women: minor effect of obesity and body fat distribution. Diabetes 2006;55:1353–60.
10. Meyer LK, Ciaraldi TP, Henry RR, Wittgrove AC, Phillips SA. Adipose tissue depot and cell size dependency of adiponectin synthesis and secretion in human obesity. Adipocyte 2013;2: 217–26.
11. Li, Wang Z, Wang C, Ma Q, Zhao Y. Perivascular adipose tissue-derived adiponectin inhibits collar-induced carotid atherosclerosis by promoting macrophage autophagy. PLoS One 2015; 10:e0124031.
12. Suganami T, Tanaka M, Ogawa Y. Adipose tissue inflammation and ectopic lipid accumulation. Endocr J 2012;59:849–57.
13. Neuschwander-Tetri BA. Hepatic lipotoxicity and the pathogenesis of nonalcoholic steatohepatitis: the central role of nontriglyceride fatty acid metabolites. Hepatology 2010;52:774–88.
14. Alvarez-Garcia O, Rogers NH, Smith RG, Lotz MK. Palmitate has proapoptotic and proinflammatory effects on articular cartilage and synergizes with interleukin-1. Arthritis Rheumatol 2014;66:1779–88.
15. Kanneganti TD, Dixit VD. Immunological complications of obesity. Nat Immunol 2012;13:707–12.
16. Weisberg SP, Mccann D, Desai M, Rosenbaum M, Leibel RL, Ferrante AW Jr. Obesity is associated with macrophage accumulation in adipose tissue. J Clin Invest 2003;112:1796–808.
17. Sohn DH, Sokolove J, Sharpe O, Erhart JC, Chandra PE, Lahey LJ, et al. Plasma proteins present in osteoarthritic synovial fluid can stimulate cytokine production via Toll-like receptor 4. Arthritis Research Ther 2012;14:R7.
18. Vahlensieck M, Linneborn G, Schild H, Schmidt HM. Hoffa's recess: incidence, morphology and differential diagnosis of the globular-shaped cleft in the infrapatellar fat pad of the knee on MRI and cadaver dissections. Eur Radiol 2002;12:90–3.
19. Ioan-Facsinay A, Kloppenburg M. An emerging player in knee osteoarthritis: the infrapatellar fat pad. Arthritis Res Ther 2013; 15:225.
20. Schmittgen TD, Livak KJ. Analyzing real-time PCR data by the comparative C(T) method. Nat Protoc 2008;3:1101–8.
21. Loeser RF. Systemic and local regulation of articular cartilage metabolism: where does leptin fit in the puzzle? Arthritis Rheum 2003;48:3009–12.
22. Bastiaansen-Jenniskens YM, Clockaerts S, Feijt C, Zuurmond AM, Stojanovic-Susulic V, Bridts C, et al. Infrapatellar fat pad of patients with end-stage osteoarthritis inhibits catabolic mediators in cartilage. Ann Rheum Dis 2012;71:288–94.
23. Klein-Wieringa IR, de Lange-Brokaar BJ, Yusuf E, Andersen SN, Kwekkeboom JC, Kroon HM, et al. Inflammatory cells in patients with endstage knee osteoarthritis: a comparison between the synovium and the infrapatellar fat pad. J Rheumatol 2016; 43:771–8.
24. Sun K, Tordjman J, Clement K, Scherer PE. Fibrosis and adipose tissue dysfunction. Cell Metab 2013;18:470–7.
25. Bastiaansen-Jenniskens YM, Wei W, Feijt C, Waarsing JH, Verhaar JA, Zuurmond AM, et al. Stimulation of fibrotic processes by the infrapatellar fat pad in cultured synoviocytes from patients with osteoarthritis: a possible role for prostaglandin $F_{2\alpha}$. Arthritis Rheum 2013;65:2070–80.
26. Lago R, Gomez R, Otero M, Lago F, Gallego R, Dieguez C, et al. A new player in cartilage homeostasis: adiponectin induces nitric oxide synthase type II and pro-inflammatory cytokines in chondrocytes. Osteoarthritis Cartilage 2008;16:1101–9.
27. Francin PJ, Abot A, Guillaume C, Moulin D, Bianchi A, Gegout-Pottie P, et al. Association between adiponectin and cartilage degradation in human osteoarthritis. Osteoarthritis Cartilage 2014;22:519–26.
28. Chen T, Chen L, Hsieh MS, Chang CP, Chou DT, Tsai SH. Evidence for a protective role for adiponectin in osteoarthritis. Biochim Biophys Acta 2006;1762:711–8.
29. De Boer TN, van Spil WE, Huisman AM, Polak AA, Bijlsma JW, Lafeber FP, et al. Serum adipokines in osteoarthritis; comparison with controls and relationship with local parameters of synovial inflammation and cartilage damage. Osteoarthritis Cartilage 2012;20:846–53.
30. Hao D, Li M, Wu Z, Duan Y, Li D, Qiu G. Synovial fluid level of adiponectin correlated with levels of aggrecan degradation markers in osteoarthritis. Rheumatol Int 2011;31:1433–7.
31. Drolet R, Belanger C, Fortier M, Huot C, Mailloux J, Legare D, et al. Fat depot-specific impact of visceral obesity on adipocyte adiponectin release in women. Obesity (Silver Spring) 2009;17: 424–30.
32. Distel E, Cadoudal T, Durant S, Poignard A, Chevalier X, Benelli C. The infrapatellar fat pad in knee osteoarthritis: an important source of interleukin-6 and its soluble receptor. Arthritis Rheum 2009;60:3374–7.
33. Clockaerts S, Bastiaansen-Jenniskens YM, Feijt C, de Clerck L, Verhaar JA, Zuurmond AM, et al. Cytokine production by infrapatellar fat pad can be stimulated by interleukin 1β and inhibited by peroxisome proliferator activated receptor α agonist. Ann Rheum Dis 2012;71:1012–8.
34. Hernandez-Morante JJ, Milagro FI, Larque E, Lujan J, Martinez JA, Zamora S, et al. Relationship among adiponectin, adiponectin gene expression and fatty acids composition in morbidly obese patients. Obes Surg 2007;17:516–24.
35. Lihn AS, Bruun JM, He G, Pedersen SB, Jensen PF, Richelsen B. Lower expression of adiponectin mRNA in visceral adipose tissue in lean and obese subjects. Mol Cell Endocrinol 2004;219:9–15.
36. Sharma AM, Staels B. Peroxisome proliferator-activated receptor γ and adipose tissue: understanding obesity-related changes in regulation of lipid and glucose metabolism [review]. J Clin Endocrinol Metab 2007;92:386–95.
37. Vasheghani F, Monemdjou R, Fahmi H, Zhang Y, Perez G, Blati M, et al. Adult cartilage-specific peroxisome proliferator-activated receptor γ knockout mice exhibit the spontaneous osteoarthritis phenotype. Am J Pathol 2013;182:1099–106.
38. Vasheghani F, Zhang Y, Li YH, Blati M, Fahmi H, Lussier B, et al. PPARγ deficiency results in severe, accelerated osteoarthritis associated with aberrant mTOR signalling in the articular cartilage. Ann Rheum Dis 2015;74:569–78.
39. Fahmi H, Martel-Pelletier J, Pelletier JP, Kapoor M. Peroxisome proliferator-activated receptor γ in osteoarthritis. Mod Rheumatol 2011;21:1–9.
40. Kobayashi T, Notoya K, Naito T, Unno S, Nakamura A, Martel-Pelletier J, et al. Pioglitazone, a peroxisome proliferator–activated receptor γ agonist, reduces the progression of experimental osteoarthritis in guinea pigs. Arthritis Rheum 2005;52:479–87.
41. Boileau C, Martel-Pelletier J, Fahmi H, Mineau F, Boily M, Pelletier JP. The peroxisome proliferator–activated receptor γ

agonist pioglitazone reduces the development of cartilage lesions in an experimental dog model of osteoarthritis: in vivo protective effects mediated through the inhibition of key signaling and catabolic pathways. Arthritis Rheum 2007;56:2288–98.
42. Wensveen FM, Jelencic V, Valentic S, Sestan M, Wensveen TT, Theurich S, et al. NK cells link obesity-induced adipose stress to inflammation and insulin resistance. Nat Immunol 2015;16:376–85.
43. Yoshimura A, Ohnishi S, Orito C, Kawahara Y, Takasaki H, Takeda H, et al. Association of peripheral total and differential leukocyte counts with obesity-related complications in young adults. Obes Facts 2015;8:1–16.
44. Bourlier V, Zakaroff-Girard A, Miranville A, de Barros S, Maumus M, Sengenes C, et al. Remodeling phenotype of human subcutaneous adipose tissue macrophages. Circulation 2008;117:806–15.
45. Mahdavian Delavary B, van der Veer WM, van Egmond M, Niessen FB, Beelen RH. Macrophages in skin injury and repair. Immunobiology 2011;216:753–62.
46. Catalan V, Gomez-Ambrosi J, Rodriguez A, Ramirez B, Rotellar F, Valenti V, et al. Increased tenascin C and Toll-like receptor 4 levels in visceral adipose tissue as a link between inflammation and extracellular matrix remodeling in obesity. J Clin Endocrinol Metab 2012;97:E1880–9.
47. Nagareddy PR, Kraakman M, Masters SL, Stirzaker RA, Gorman DJ, Grant RW, et al. Adipose tissue macrophages promote myelopoiesis and monocytosis in obesity. Cell Metab 2014;19:821–35.
48. Bhattacharyya S, Kelley K, Melichian DS, Tamaki Z, Fang F, Su Y, et al. Toll-like receptor 4 signaling augments transforming growth factor-β responses: a novel mechanism for maintaining and amplifying fibrosis in scleroderma. Am J Pathol 2013;182:192–205.
49. Suganami T, Ogawa Y. Adipose tissue macrophages: their role in adipose tissue remodeling. J Leukoc Biol 2010;88:33–9.
50. Rothman KJ. BMI-related errors in the measurement of obesity. Int J Obes (Lond) 2008;32 Suppl 3:S56–9.

ARTHRITIS & RHEUMATOLOGY
Vol. 69, No. 7, July 2017, pp 1407–1417
DOI 10.1002/art.40101

Effects of Treadmill Exercise on Advanced Osteoarthritis Pain in Rats

Joshua Allen,[1] Ian Imbert,[1] Joshua Havelin,[1] Terry Henderson,[2] Glenn Stevenson,[1] Lucy Liaw,[2] and Tamara King[1]

Objective. **Exercise is commonly recommended for patients with osteoarthritis (OA) pain. However, whether exercise is beneficial in ameliorating ongoing pain that is persistent, resistant to nonsteroidal antiinflammatory drugs (NSAIDs), and associated with advanced OA is unknown.**

Methods. **Rats treated with intraarticular (IA) monosodium iodoacetate (MIA) or saline underwent treadmill exercise or remained sedentary starting 10 days postinjection. Tactile sensory thresholds and weight bearing were assessed, followed by radiography at weekly intervals. After 4 weeks of exercise, ongoing pain was assessed using conditioned place preference (CPP) to IA or rostral ventromedial medulla (RVM)–administered lidocaine. The possible role of endogenous opioids in exercise-induced pain relief was examined by systemic administration of naloxone. Knee joints were collected for micro–computed tomography (micro-CT) analysis to examine pathologic changes to subchondral bone and metaphysis of the tibia.**

Results. **Treadmill exercise for 4 weeks reversed MIA-induced tactile hypersensitivity and weight asymmetry. Both IA and RVM lidocaine D35, administered post-MIA, induced CPP in sedentary but not exercised MIA-treated rats, indicating that exercise blocks MIA-induced ongoing pain. Naloxone reestablished weight asymmetry in MIA-treated rats undergoing exercise and induced conditioned place aversion, indicating that exercise-induced pain relief is dependent on endogenous opioids. Exercise did not alter radiographic evidence of OA. However, micro-CT analysis indicated that exercise did not block lateral subchondral bone loss or trabecular bone loss in the metaphysis, but did block MIA-induced medial bone loss.**

Conclusion. **These findings support the conclusion that exercise induces pain relief in advanced, NSAID-resistant OA, likely through increased endogenous opioid signaling. In addition, treadmill exercise blocked MIA-induced bone loss in this model, indicating a potential bone-stabilizing effect of exercise on the OA joint.**

Osteoarthritis (OA) is the most prevalent chronic joint disease worldwide, with incidence predicted to rise due to the aging population and the impact of obesity (1–5). OA is characterized by cartilage degradation and bone remodeling, observable on radiographs as diminished joint space and bony growths within the joint (6). Micro–computed tomography (micro-CT) analysis of OA joints indicates development of subchondral bone remodeling that corresponds to cartilage loss (7). Notably, the degree of joint pain does not correlate with radiographic evidence of pathology, although other imaging modalities such as magnetic resonance imaging (MRI) demonstrate that development of synovitis correlates with the presence of knee pain even in the absence of radiographic signs of OA (3,8,9).

OA can be a debilitating condition, with pain being the most common OA symptom for which patients present to primary care practitioners (10). OA pain is typically characterized by predictable sharp pain that is associated with movement or use of the joint (10). Some patients develop advanced OA, which is characterized by nonsteroidal antiinflammatory drug (NSAID)–resistant, constant, dull, and aching pain, interspersed with short unpredictable episodes of intense pain (10,11).

Supported by the NIH (National Institute of General Medical Sciences COBRE grant P20-GM-103643 to Dr. King). Micro–computed tomography was supported by the NIH (COBRE grant in vascular biology 5P30-GM-103392 to the Maine Medical Center Research Institute).

[1]Joshua Allen, BS, Ian Imbert, MPH, Joshua Havelin, BS, Glenn Stevenson, PhD, Tamara King, PhD: University of New England, Biddeford, Maine; [2]Terry Henderson, BS, Lucy Liaw, PhD: Center for Molecular Medicine, Maine Medical Center Research Institute, Scarborough.

Address correspondence to Tamara King, PhD, Department of Biomedical Sciences, College of Osteopathic Medicine, Center for Excellence in the Neurosciences, 11 Hills Beach Road, Biddeford, ME 04005. E-mail: tking6@une.edu.

Submitted for publication August 31, 2016; accepted in revised form March 14, 2017.

Current treatments focus on alleviating pain and stiffness (12). Oral NSAIDs or duloxetine are the most common pharmacologic treatments (13,14). Surgery consists primarily of joint replacement options that are successful for most patients (15). However, the prevalence of OA is increasing in younger populations for whom total

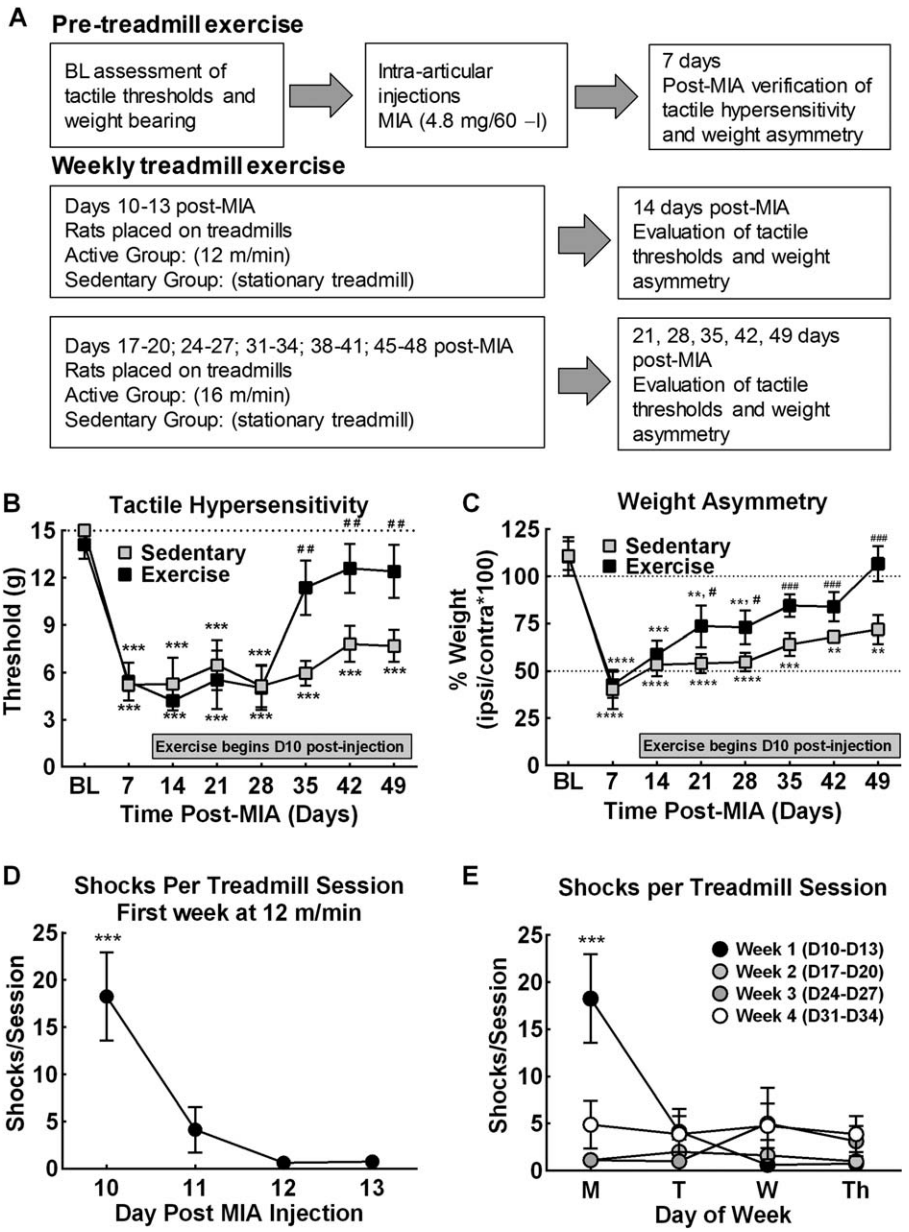

Figure 1. Alleviation of monosodium iodoacetate (MIA)–induced weight asymmetry and tactile hypersensitivity following treadmill exercise. **A,** Experimental procedure used to examine the effects of treadmill exercise on MIA-induced tactile hypersensitivity and weight asymmetry. **B,** Selective reversal of tactile hypersensitivity in exercised rats. Treadmill exercise starting 10 days post–MIA injection selectively reversed tactile hypersensitivity in exercised rats by day 35 after MIA treatment, corresponding to 4 weeks of exercise. $* = P < 0.05$; $** = P < 0.01$; $*** = P < 0.001$ versus baseline (BL); $\#\# = P < 0.01$ versus week 1. **C,** Reversal of weight asymmetry in exercised rats. Treadmill exercise starting 10 days post–MIA injection into the knee joint reversed weight asymmetry in exercised but not sedentary rats, with improvement observed by day 21 after treatment, corresponding to 2 weeks of exercise, and continued improvement between days 35 and 49 after treatment. $* = P < 0.05$; $** = P < 0.01$; $*** = P < 0.001$ versus BL; $\# = P < 0.05$; $\#\# = P < 0.01$; $\#\#\# = P < 0.001$ versus week 1. **D,** Average number of shocks per weekly treadmill session in MIA-treated rats. During the first week of treadmill exercise, the average number of shocks per weekly session demonstrates quick adaptation to running on the treadmill. $*** = P < 0.05$ versus days 11, 12, and 13. **E,** Average number of shocks per daily treadmill session in MIA-treated rats. Across the 4-week treatment period, the average number of shocks per daily session demonstrates elevation only during the first day of the first week of treadmill training. Values are the mean ± SEM.

knee replacement may not be optimal, as this procedure was originally designed for patients age >70 years old (15).

Exercise is the most commonly recommended method of nonpharmacologic intervention (14). Clinical studies have demonstrated that aerobic and strengthening exercises improve joint function and pain in patients with OA (16). Preclinical studies have demonstrated that exercise across a period of weeks alleviated hypersensitivity in a variety of rodent models of chronic pain (17–24). Blockade of opioid signaling has been shown to reverse exercise-induced pain relief in models of nerve injury (17). The present study examined the hypothesis that treadmill exercise blocks weight asymmetry and ongoing pain through enhanced opioidergic signaling in a rat model of advanced knee OA pain, previously shown to produce persistent NSAID-resistant ongoing pain (25).

MATERIALS AND METHODS

Animals. Male Sprague-Dawley rats (Harlan) weighing 175–200 gm were housed with a 12-hour light/dark cycle, with food and water available ad libitum. Rats were group housed, except those that had undergone cannulation surgery of the rostral ventromedial medulla (RVM), which were individually housed starting immediately postsurgery. All experiments were performed in accordance with policies and recommendations of the International Association for the Study of Pain and the National Institutes of Health guidelines for the handling and use of laboratory animals. All experimental protocols received approval from the Institutional Animal Care and Use Committee of the University of New England.

Study design. *Tactile hypersensitivity and weight asymmetry.* Figure 1A demonstrates the protocol used to determine the impact of exercise on MIA-induced tactile hypersensitivity and weight asymmetry. Pre–MIA treatment (baseline) assessment of tactile sensory thresholds was performed, followed by assessment of hind limb weight bearing. MIA (4.8 mg/60 μl) was injected intra-articularly (IA) through the infrapatellar ligament of the left knee under isoflurane (2% in O_2), as previously described (25–27). Tactile sensory thresholds and, subsequently, weight asymmetry were assessed 7 days postinjection to verify initiation of MIA-induced tactile hypersensitivity and weight asymmetry.

Starting 10 days after IA injection of MIA or saline, rats were randomly assigned to the exercise or sedentary treatment groups. Treadmill sessions were performed using a 3-lane treadmill (Columbus Instruments) for 30 minutes daily over a sequential 4-day period, as previously described (17). For exercise rats, treadmill speed was 12 meters/minute during the first week of exercise (postinjection days 10–13), increased to 16 meters/minute starting the second week (postinjection days 17–20), and continued at this rate through the remainder of the study. Sedentary control rats were placed on the treadmill at the stationary setting for 30 minutes. The treadmill was cleaned with 70% ethanol between groups of rats. Weight bearing and then tactile sensory thresholds were determined the fifth day of each week, 20–24 hours after the last treadmill session. No exercise or behavioral testing occurred during days 6 or 7 of each week.

The experiments included 6 exercise and 6 sedentary rats treated with MIA for tactile sensory testing, and 11 exercise and 10 sedentary rats treated with MIA for analysis of weight bearing (33 rats total). Three of 36 rats were removed as they failed to show MIA-induced weight asymmetry (defined as weight distribution [left/right × 100] of 85% or higher) and tactile hypersensitivity (defined as failure to respond at cutoff von Frey filament of 15 gm). The experimenters (JA and IA) were aware of the treatment condition of each rat during behavioral testing.

Conditioned place preference (CPP) measure of ongoing pain. Figure 2A shows the protocol used to determine the impact of exercise on MIA-induced ongoing pain. Rats received IA injections of MIA (4.8 mg/60 μl) or an equal volume of saline, followed by verification of development of weight asymmetry 7 days later. Rats that failed to show weight asymmetry were removed from the study (7 of 75 rats that had received IA lidocaine; 0 of 65 rats that had received RVM lidocaine). Saline- and MIA-treated rats were randomly divided into the treadmill exercise or sedentary treatment groups, resulting in a 2 × 2 experimental design ([saline, MIA] × [exercise, sedentary]). CPP in response to pain relief, induced by IA or RVM administration of lidocaine, was assessed using a single-trial conditioning protocol on days 34–36 after IA injection, which corresponded to week 4 of treadmill exercise.

On day 34 (during the preconditioning period), rats were placed into the CPP apparatus with access to all 3 chambers, and baseline time spent in each chamber was measured for 15 minutes using webcams and video analysis (performed with the computer program Any-maze [Stoelting]). Rats spending <180 or >720 seconds in a pairing chamber during baseline testing were removed from the study (1 of 55 rats in the IA lidocaine experiment and 9 of 65 rats in the intra-RVM lidocaine experiment). Drug-chamber pairings were counterbalanced across subjects. On day 35, single-trial conditioning was performed for either the IA lidocaine or the RVM lidocaine experiment.

IA lidocaine. While under isoflurane anesthesia, rats received IA saline (200 μl) injected into the ipsilateral knee joint and were immediately confined to the pre-assigned pairing chamber for 30 minutes (within 2 minutes of injection). They were then returned to their home cages. Four hours later, rats received IA lidocaine (200 μl 4% [weight/volume]) while under isoflurane anesthesia, and were immediately confined to the opposite pairing chamber for 30 minutes. All rats awoke prior to placement into the pairing chambers. Of the saline-treated rats, a total of 10 sedentary and 9 exercise rats were tested and of the MIA-treated rats, a total of 18 sedentary and 18 exercise rats were tested.

RVM lidocaine. Rats received RVM microinjection of sterile saline (0.5 μl/minute), with the injector remaining in place for 1 minute postinjection to prevent backflow. Rats were immediately confined to the pre-assigned pairing chamber for 30 minutes (within 2 minutes of injection) and then returned to their home cages. Four hours later, rats received a microinjection of RVM lidocaine (4% [w/v], 0.5 μl/minute) and were immediately confined to the opposite pairing chamber for 30 minutes. Following verification of cannula placement, a total of 9 saline-treated sedentary, 10 saline-treated exercise, 11 MIA-treated sedentary, and 9 MIA-treated exercise rats were included in the data analysis. Seventeen of 56 rats were eliminated from the data analysis due to missed cannula placement. On day 36, rats were placed in the 3-chamber apparatus with access to all chambers for 15 minutes and time in each chamber was recorded.

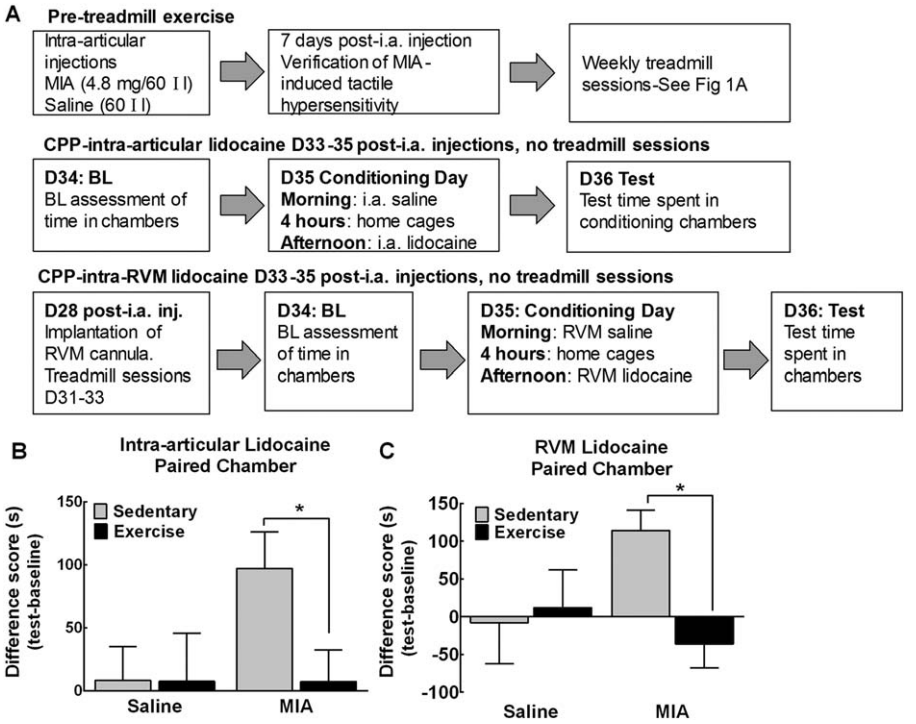

Figure 2. Alleviation of monosodium iodoacetate (MIA)–induced ongoing pain following treadmill exercise. **A,** Experimental procedure used to examine the effects of treadmill exercise on MIA-induced ongoing pain using conditioned place preference (CPP) from baseline (BL) to intraarticular (IA) or rostral ventromedial medulla (RVM) lidocaine injections (inj.). **B,** Amount of time spent in the IA lidocaine paired chamber. This time was significantly increased in sedentary MIA-treated rats. Exercised MIA-treated rats had no increase in time spent in the IA lidocaine paired chamber. Time spent in the IA lidocaine paired chamber for rats treated with IA saline was not altered. Values are the mean ± SEM. **C,** Amount of time spent in the chamber paired with RVM lidocaine. This time was significantly increased in sedentary MIA-treated rats. Exercised MIA-treated rats had no increase in time spent in the RVM lidocaine paired chamber. Time spent by IA saline–treated rats in the RVM lidocaine paired chamber was not altered, irrespective of whether rats were sedentary or exercised. Values are the mean ± SEM. $* = P < 0.05$.

Effects of systemic administration of naloxone on place preference and weight bearing. Following preinjection assessment of weight bearing, rats were injected intraarticularly with MIA and were tested for weight asymmetry weekly throughout the treadmill exercise, as described above. On day 35, rats underwent pre-naloxone testing followed by injection of naloxone (3 mg/kg, intraperitoneally [IP]). Weight-bearing measurements were then repeated 30 minutes after naloxone treatment. A total of 6 MIA-treated sedentary and 6 MIA-treated exercise rats were tested. The experimenter was blinded with regard to the treatment condition during behavioral testing.

A single-trial conditioning protocol was performed 34–36 days post-IA injection, with baseline (day 34) and test (day 36) procedures performed as described above. On day 35 (conditioning day), rats underwent systemic administration of saline (IP) and were immediately confined to the pre-assigned pairing chamber for 30 minutes. They were returned to their home cages and underwent systemic administration of naloxone (3 mg/kg, IP) 4 hours later, followed immediately by confinement to the opposite pairing chamber for 30 minutes. A total of 12 saline-treated sedentary, 16 saline-treated exercise, 20 MIA-treated sedentary, and 15 MIA-treated exercise rats were tested.

Experimental procedures. *Tactile hypersensitivity.* Tactile sensory thresholds were assessed using calibrated von Frey filaments (ranging from 0.41 to 15 gm) and the up-down method, analyzed by Dixon nonparametric test, and expressed as the mean withdrawal threshold on the ipsilateral hind paw, as previously described (28,29).

Weight asymmetry. Baseline testing was performed prior to IA MIA injections and at weekly intervals through 49 days postinjection. Changes in hind paw weight distribution between the left (MIA) and right (contralateral) limbs were measured using an incapacitance tester (Stoelting) and were used as an index of joint discomfort in the MIA-treated knee (26). Rats were placed in an angled plexiglass chamber, and positioned so that each hind paw rested on a separate force plate. The force exerted by each hind limb was determined over a 5-second period. Each data point is the mean of 3 readings. As previously described (26), data were normalized as the percent injured/uninjured weight bearing, with equal weight distribution indicated by 100% and sensitivity on the injured side indicated by values of $<100\%$.

Rostral ventromedial medulla cannula surgery. Rats underwent RVM cannula surgery under anesthesia (100 mg/kg

ketamine and 10 mg/kg xylazine, administered IP) 28 days postinjection using stereotaxic techniques as previously described (26). Bilateral 26-gauge guide cannulas, separated by 1.2 mm, were directed toward the lateral portions of the RVM (anteroposterior, 11.0 mm from the bregma; lateral ± 0.6 mm; dorsoventral 8.5 mm from the skull), according to Paxinos and Watson (30). Guide cannulas were secured to the skull by small stainless steel machine screws and cemented in place. Animals were allowed to recover 3 days postsurgery before returning to the treadmill for the fourth week of exercise, days 31–33 postinjection. RVM microinjections (0.5 μl) were administered over a period of 1 minute through a 33-gauge injector that protruded 1 mm beyond the end of the guide cannula and into fresh tissue to prevent backflow. Cannula placement was verified at the end of the study by microinjection (0.5 μl/1 minute) of Evans blue dye (50 mg/ml; Sigma Aldrich).

Radiographic imaging. Through day 28 post-IA injection, radiographic images were obtained on a weekly basis following behavioral testing. Radiography was not performed during CPP in order to avoid disruption of the learning process. To limit movement during the imaging, rats were lightly anesthetized with a 2% isoflurane/O_2 mixture, and radiographic images of the knee joint were captured using a digital x-ray system (Fujifilm Medical Systems).

Micro–computed tomography (micro-CT). Following behavioral analyses for the naloxone-induced weight asymmetry experiment (day 42 post–MIA injection), rats were euthanized and knee joints dissected and fixed in 10% neutral buffered formalin for 3 days. The joints were then transferred to 70% ethanol. To characterize exercise-induced changes in joint microarchitecture, the proximal tibias were analyzed with a Scanco VivaCT-40 scanner. Joints were loaded into 12.3 mm–diameter scanning tubes. Scans were integrated into 3-dimensional voxel images (2,048 × 2,048–pixel matrices for trabecular and 1,024 × 1,024–pixel matrices for all other individual planar stacks). Rat tibias were scanned at low resolution, at an energy level of 55 kVp and intensity of 145 μA.

Trabecular bone volume fraction and microarchitecture of the proximal metaphyseal region were evaluated below the growth plate. Approximately 375 consecutive slices were made at 10.5-μm intervals at the distal end of the growth plate, extending in a proximal direction, and 250 contiguous slices were selected for analysis. Subchondral trabecular bones were scanned at low resolution, at an energy level of 55kVp and intensity of 145 μA at 10.5 μm.

Subchondral trabecular bone in the medial and lateral tibial plateau was analyzed over 50 cross-sections. The volume of interest included the subchondral trabecular bone starting below the subchondral plate, extending distally toward the growth plate. The images were segmented using a threshold of 260. The 3-dimensional morphometric parameters were calculated for the medial, lateral, and total subchondral trabecular bone. A total of 6 joints per group (6 MIA-treated sedentary rats, 5 saline-treated sedentary rats, 6 MIA-treated sedentary rats, and 4 MIA-treated exercise rats) were analyzed for the subchondral bones. For the metaphysis, some samples were not analyzed due to an insufficient area of analysis.

Statistical analysis. All statistical analyses were performed using GraphPad Prism. Sample sizes for all experiments were based on those typically reported in the literature. MIA-induced changes in weight bearing and tactile hypersensitivity were examined using two-way repeated measures analysis of variance (ANOVA) (exercise treatment × time), followed by analysis of exercise effects at each time point compared to day 7 (pre-exercise) using Bonferroni's post hoc test. Shock data were analyzed by using two-way repeated-measures ANOVA, followed by post hoc analysis using Tukey's multiple comparison test.

For the CPP and CPA experiments, the effects of exercise and conditioning chamber were analyzed using the Holm-Sidak test (at an alpha level of 5%). Computations were made under the assumption that all rows were samples from populations with the same scatter (standard deviation). Differences between groups were assessed using difference scores that were calculated as post-conditioning (test) or pre-conditioning (baseline) time spent in the treatment-paired chamber. Statistical analyses for group comparisons were performed by one-way ANOVA, followed by analysis using the Holm-Sidak post hoc test. Micro-CT data were analyzed by two-way ANOVA, followed by post hoc analysis using Fisher's least significant difference test.

RESULTS

Tactile hypersensitivity and weight asymmetry. In sedentary rats, MIA-induced tactile hypersensitivity and weight asymmetry were present 7 days post–MIA treatment, and persisted for 7 weeks (Figures 1B and C, respectively). Exercise reversed the MIA-induced tactile hypersensitivity, with withdrawal thresholds returning to pre–MIA treatment values 35 days postinjection, corresponding to 4 weeks of exercise (Figure 1B). Exercise also reversed MIA-induced weight asymmetry, with significant improvement observed by day 21 post–MIA injection, and continued improvement seen between days 35 and 49. MIA-treated rats showed greatly diminished exposure to the shock pad after the first day on the treadmill (Figure 1D). Analysis of shocks per weekday across 4 weeks showed an elevated number on the first day of week 1, but only in exercised rats (Figure 1E).

Exercise blocks MIA-induced ongoing pain. IA lidocaine produced CPP selectively in the sedentary MIA-treated rats, but not in exercised MIA–treated rats (Figure 2B). IA lidocaine did not alter time spent in the lidocaine paired chamber in sedentary rats or in exercised rats that had been administered IA saline. RVM lidocaine also produced CPP in the sedentary MIA-treated rats but not in exercised MIA-treated rats (Figure 2C). RVM lidocaine failed to alter the amount of time spent in the lidocaine paired chambers in the IA saline–treated rats. Any rats with missed injections, defined by ink marks outside of the RVM (Figure 2C), were excluded from data analysis.

Naloxone induces CPA and unmasks weight asymmetry. In sedentary rats, MIA-induced weight asymmetry was present 35 days post–MIA treatment. MIA-treated rats that had undergone exercise for 4 weeks demonstrated normal weight bearing, with weight-bearing ratios equivalent to pre-MIA baseline values ($P > 0.05$). Treatment with systemic naloxone (3 mg/kg, administered

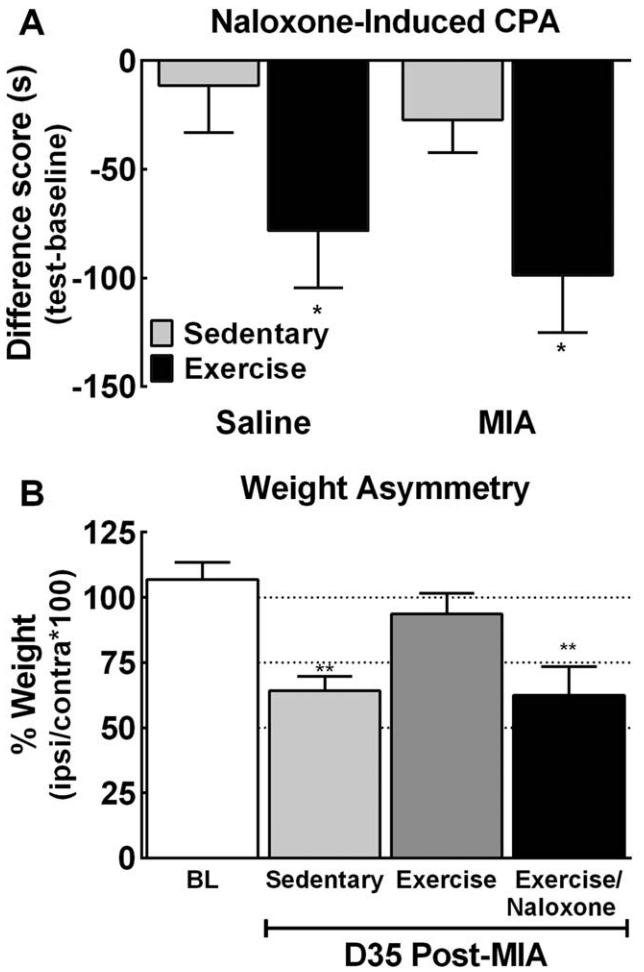

Figure 3. Increased opioid tone following treadmill exercise for 4 weeks starting 10 days after injection. **A,** Analysis of difference scores shows that exercised rats had equivalent decreases in time spent in the naloxone paired chamber (* = P < 0.05 versus sedentary rats), whereas sedentary rats failed to show significant conditioned place aversion (CPA), irrespective of whether they received intraarticular saline or monosodium iodoacetate (MIA). **B,** MIA-induced weight asymmetry (ipsilateral [ipsi]/contralateral [contra]) persisted for 35 days in sedentary rats. Exercise starting 10 days post–MIA injection blocked MIA-induced weight asymmetry. In exercised rats, treatment with naloxone (3 mg/kg intraperitoneally) reestablished the weight asymmetry at 30 minutes post-injection (** = $P < 0.01$ versus baseline; n = 6 MIA-treated sedentary rats and 5 MIA-treated exercised rats). Values are the mean ± SEM.

IP) revealed weight asymmetry in MIA-treated exercised rats, with values returning to those observed in sedentary control rats (Figure 3A). To examine whether blocking of endogenous opioid signaling also unmasked ongoing pain, we investigated whether exercised rats that had received IA-MIA injections showed CPA to a chamber paired with naloxone (3 mg/kg, IP). Naloxone produced CPA in rats that had undergone 4 weeks of exercise, but not in sedentary rats (Figure 3B). Of interest, the naloxone-induced CPA was observed in exercised rats irrespective of whether they had received IA saline or MIA (Figure 3A).

Effects of exercise on MIA-induced joint pathology. Weekly radiography of the femorotibial (knee) joint demonstrated a time-dependent progression of MIA-induced joint pathology in both the sedentary and exercise treatment groups (Figure 4). There were no apparent differences between exercised and sedentary rats.

Exercise-induced blockade of MIA-induced joint pathology demonstrated by micro-CT analysis. Three-dimensional images from micro-CT scans revealed extensive bone remodeling within the femorotibial joint, with clear development of osteophytes as well as apparent pitting and lesions of the cortical bone (Figure 5A). Reconstructed images showing trabecular bone within the subchondral bone and metaphysis revealed diminished trabecular bone, particularly in the metaphysis of sedentary MIA-treated rats (Figure 5A). Exercise appeared to ameliorate the MIA-induced trabecular bone loss within the metaphysis (Figure 5A).

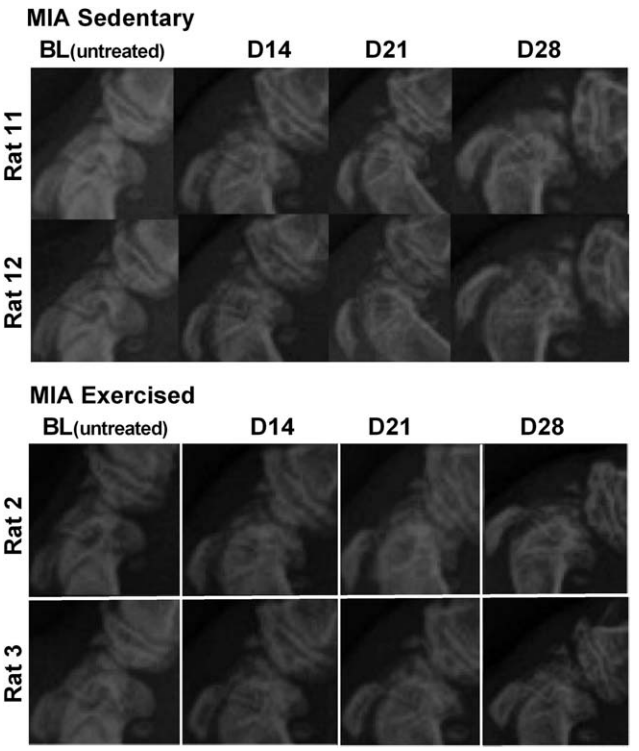

Figure 4. Representative radiographic images obtained at baseline (BL) and on days 14, 21, 28 in sedentary or exercised monosodium iodoacetate (MIA)–treated rats. Pathologic changes in the joint were evident within 14 days post–MIA injection in both treatment groups. Radiographs indicate equivalent levels of MIA-induced joint pathology, irrespective of whether the rats remained sedentary or underwent exercise.

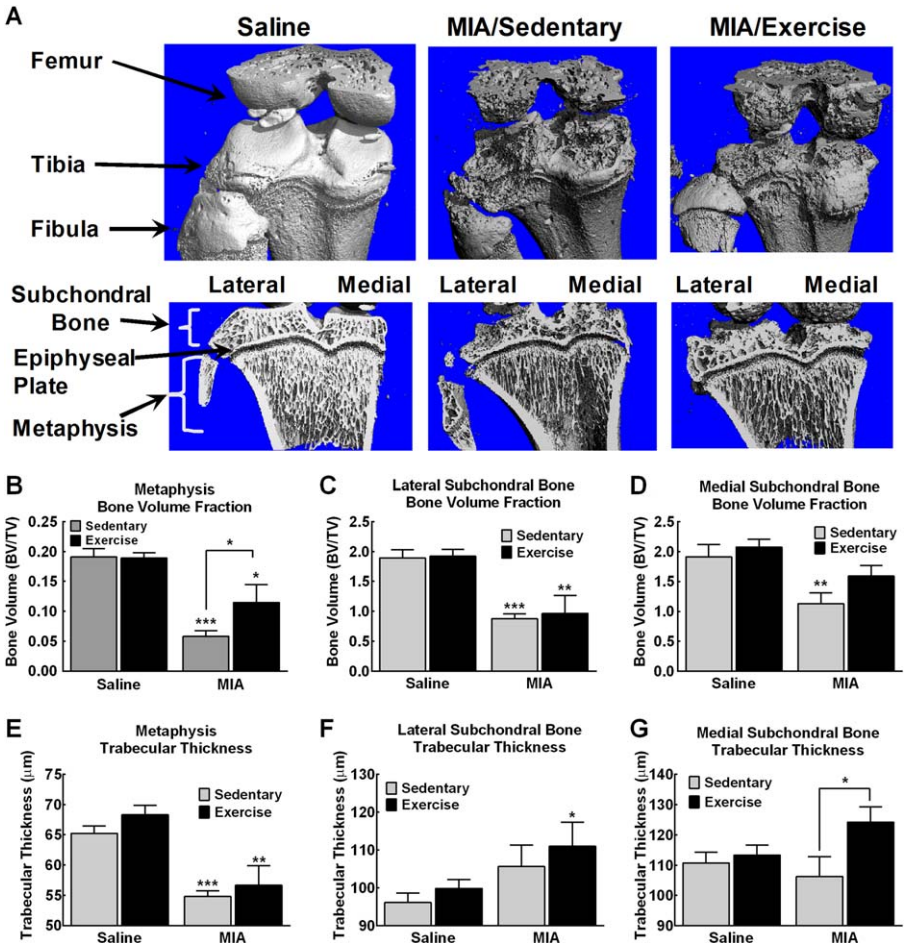

Figure 5. Blocking of monosodium iodoacetate (MIA)–induced pathologic changes in the subchondral bone and metaphysis by 4 weeks of treadmill exercise. **A,** Representative micro–computed tomography images demonstrating MIA-induced remodeling of the exterior bone, with development of osteophytes and bone deformities. Trabecular bone loss within the subchondral bone and metaphysis. **B,** Significant reduction in bone volume (bone volume [BV]/trabecular volume [TV]) in the medial subchondral bone of MIA-treated sedentary, but not MIA-treated exercised, rats. **C,** Significant reduction in bone volume in the lateral subchondral bone of MIA-treated sedentary and exercised rats. **D,** Diminished bone volume in the trabecular region of the metaphysis in MIA-treated sedentary rats, which is attenuated in MIA-treated rats that underwent treadmill exercise. **E,** Significant reduction of trabecular bone thickness in the metaphysis of MIA-treated rats. **F,** Increased trabecular thickness in the lateral subchondral bone of MIA-treated rats. **G,** Increased trabecular thickness within the medial subchondral bone in MIA-treated rats that underwent exercise. $* = P < 0.05$; $** = P < 0.01$; $*** = P < 0.001$ for the indicated comparisons or versus saline-treated sedentary rats.

Quantitative analysis of bone volume demonstrated that MIA-induced pathologic changes in sedentary rats occurred both in the metaphysis just below the epiphyseal plate and in both the lateral and medial subchondral bones (Figures 5B–D). Within the metaphysis, MIA treatment diminished total trabecular bone volume in sedentary rats, but this was attenuated in exercised MIA-treated rats (Figure 5B). MIA-treated rats demonstrated a significant decrease in bone volume of the lateral subchondral bone (measured 35 days post–MIA treatment) that was not altered by exercise (Figure 5C). Sedentary MIA-treated rats also had decreased trabecular bone volume in the medial subchondral bone (Figure 5D). This MIA-induced bone loss was blocked by exercise (Figure 5D). MIA treatment diminished trabecular thickness within the metaphysis of sedentary and exercised rats (Figure 5E). In the medial subchondral bone, MIA induced increased trabecular thickness in exercised rats compared to saline-treated rats (Figure 5F). Similarly, a significant increase in trabecular thickness was observed in the lateral subchondral bone of exercised MIA-treated rats compared to sedentary saline-treated control rats (Figure 5G).

Within the metaphysis, MIA treatment reduced the number of trabecular bone and increased trabecular spacing

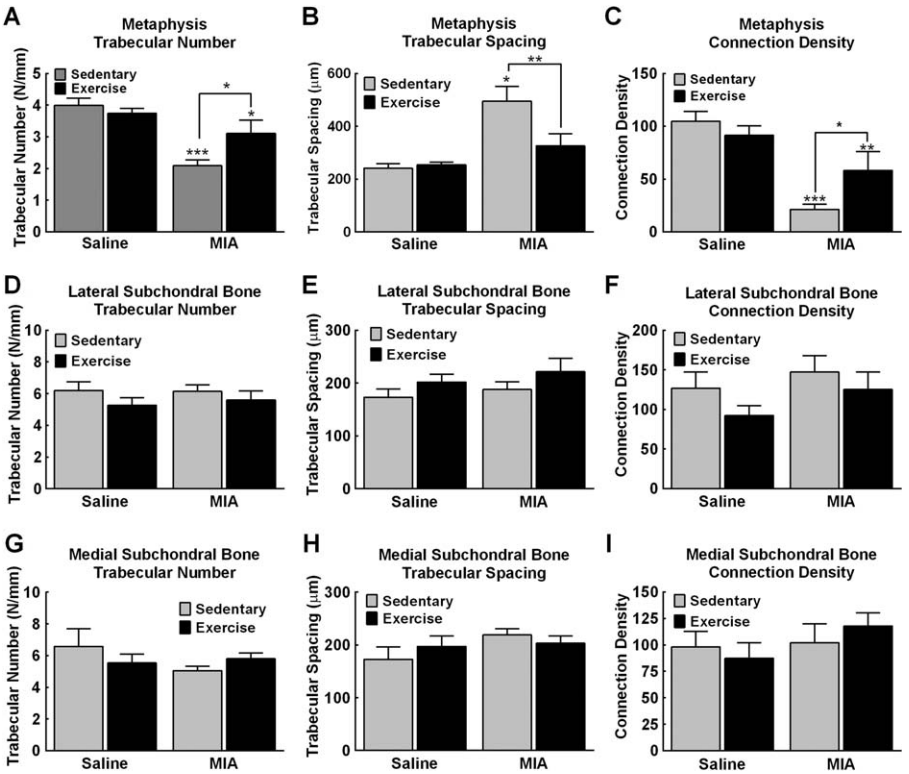

Figure 6. Micro–computed tomography (micro-CT) confirmation of the blocking of monosodium iodoacetate (MIA)–induced pathologic changes in the subchondral bone and metaphysis by treadmill exercise. **A,** Analysis of the number of trabeculae within the metaphysis demonstrated decreased trabeculae in MIA-treated sedentary rats. Exercise blocked the MIA-induced decrease in trabecular number, but the number was still significantly lower compared to saline-treated sedentary control rats. **B,** Analysis of trabecular spacing demonstrated increased space between trabecular bone within the metaphysis in sedentary MIA-treated rats. Exercise blocked the MIA-induced increase in trabecular spacing, with trabecular spacing similar to that in saline-treated sedentary control rats. **C,** MIA treatment reduced the connection density of trabecular bone within the metaphysis. Exercise attenuated the MIA-induced reduction in connection density of trabecular bone. **D–F,** Neither MIA treatment nor exercise altered the number (**D**), spacing (**E**), or connection density (**F**) of the trabecular bone within the lateral subchondral bone. **G–I**, Neither MIA treatment nor exercise altered the number (**G**), spacing (**H**), or connection density (**I**) of the trabecular bone within the medial subchondral bone. Values are the mean ± SEM. $* = P < 0.05$; $** = P < 0.01$; $*** = P < 0.001$ for the indicated comparisons or versus saline-treated sedentary rats.

in sedentary rats that was blocked by 4 weeks of exercise (Figures 6A and B). MIA treatment reduced connectivity density of trabecular bone in sedentary rats, but this was also blocked by 4 weeks of exercise (Figure 6C). Within the lateral and medial subchondral bone, no changes in trabecular number (Figures 6D and G), trabecular spacing (Figures 6E and H), or connectivity density (Figures 6F and I) were observed in sedentary or exercised MIA-treated rats.

DISCUSSION

In our study we demonstrated that 4 weeks of treadmill exercise alleviates ongoing pain, restores weight bearing on the osteoarthritic knee, and alleviates hind paw tactile hypersensitivity in a rat model of advanced OA pain. The exercise-induced pain relief was dependent on endogenous opioids, illustrated by the ability of systemic administration of the opioid receptor antagonist naloxone to unmask weight asymmetry and produce CPA in exercised rats that had OA. Naloxone also produced CPA in control rats that had received IA saline, indicating that exercise increases endogenous opioid signaling in the absence of joint pathology and that blocking this signal is aversive.

Exercise also attenuated MIA-induced bone remodeling within the subchondral bone and metaphysis, indicating a potentially stabilizing effect of exercise. Notably, our observations that naloxone unmasked pain behaviors in the exercised rats indicates that these protective effects of exercise on the bone were likely independent of the pain-alleviating effects of exercise.

Our observation that 4 weeks of treadmill exercise reversed OA-induced tactile hypersensitivity and weight asymmetry is consistent with clinical studies demonstrating that exercise can improve joint function and diminish pain in

patients with OA (16). The reversal of weight asymmetry indicates an increased willingness of MIA-treated rats that had undergone exercise to load the joint, potentially reflecting improved use and function. Analysis of joint use and weight bearing while running warrants further study.

We further demonstrated that exercise reversed MIA-induced ongoing pain. IA lidocaine produced CPP in sedentary MIA-treated rats, consistent with previous observations that this concentration of MIA produces ongoing pain that is dependent on peripheral input from the joint (25). In contrast, lidocaine treatment failed to induce CPP in exercised rats, indicating that the exercise blocked ongoing pain following MIA pain. This conclusion is further supported by the observation that RVM lidocaine produced CPP in sedentary but not exercised MIA-treated rats. RVM lidocaine–induced CPP in sedentary rats is consistent with our previous observations that blockade of descending (presumably facilitatory) output from the RVM induces CPP and supports the conclusion that advanced OA pain is dependent on descending pain-facilitatory pathways (9,26).

Together, the data from previous observations and the present study indicate that MIA-induced knee joint pain is reversed by 4 weeks of treadmill exercise. An important aspect of these observations is that administration of lidocaine to the knee joint or RVM failed to alter the time spent in the lidocaine-paired chamber in control rats irrespective of treatment group. This suggests that lidocaine-induced CPP is specific to relief of OA-induced ongoing pain.

The findings in this model of OA suggest that exercise-induced pain relief may be observed in patients who develop persistent, NSAID-resistant joint pain. It has been suggested that development of moderate-to-severe pain in advanced OA is due to central sensitization and to neuropathic pain likely arising from damage to nerves (9,31–33). Several studies have demonstrated signs of central sensitization in preclinical studies of MIA-induced joint pain (9,26,34–36). Electrophysiologic studies have demonstrated enhanced evoked responses of dorsal horn neurons in response to pinch and noxious mechanical stimuli within the spinal cord (34). Other studies demonstrate that rats with MIA-induced knee joint OA show glial activation in the spinal cord (35), a marker of spinal sensitization associated with release of proinflammatory cytokines and brain-derived neurotrophic factor (BDNF) (37).

Whether exercise-induced pain relief may be due in part to suppression of proinflammatory factors released by spinal glia remains to be determined. In support of this possibility, several studies have demonstrated that exercise reduced proinflammatory factors including BDNF, glial activation, macrophage infiltration, and proinflammatory cytokines within the spinal cord in rat models of neuropathic pain (38–40). Furthermore, exercise might be beneficial in that it diminishes proinflammatory cytokines within the dorsal root ganglion and the brain (39). Further studies are needed to determine whether exercise decreases central microglial activation and associated proinflammatory factors that promote chronic pain.

Clinical observations indicate elevated levels of the endogenous opioid β-endorphin while running (41). Animal studies have shown elevated levels of endogenous opioids in the serum (42) and brain regions (43) of rats, including elevated β-endorphin and met-enkephalin within the RVM and proliferation-associated gene protein (17), key components of the descending pain modulatory pathways (44). Endogenous opioids may block pain through multiple mechanisms including actions on μ-opioid receptors in the cortex as well as in subcortical regions, the spinal cord, and the periphery (44). Moreover, spinal naloxone was demonstrated to block analgesia in Nav1.7 mutant mice, suggesting that tonic opioid signaling can maintain analgesia at the level of the spinal cord (45). The release of endogenous opioids in the anterior cingulate cortex has been suggested as a general mechanism of pain relief (46), consistent with the present observations.

Endogenous opioids may also improve both pain and bone remodeling through indirect actions by blocking proinflammatory responses by glia or peripheral immune cells (39,47). Our observations that naloxone blocked the exercise-induced weight asymmetry is consistent with other studies demonstrating that naloxone blocked exercise-induced reversal of thermal and tactile hypersensitivity in models of nerve injury and muscle pain (17,20). Previous studies have indicated that this is likely through descending pain-inhibitory pathways from the RVM, as administration of a peripherally restricted antagonist failed to block the exercise-induced blockade of evoked hypersensitivity, and RVM-administered naloxone reestablished the nerve-injury induced thermal and tactile hypersensitivity (17). These observations suggest that exercise normalizes the balance of descending pain modulation, overcoming OA-induced net descending pain-facilitatory drive. RVM lidocaine in the MIA-treated exercised rats failed to induce CPA, likely because lidocaine inactivates both descending pain-inhibitory and pain-facilitatory pathways within the RVM (44).

In addition to reestablishing weight asymmetry, naloxone produced CPA in MIA-treated exercised rats. This is consistent with the hypothesis that blockade of the opioid signaling unmasks ongoing pain, thereby creating an aversion to the naloxone paired chamber. However, naloxone also produced CPA in the exercised control rats that did not have knee OA. These observations indicate that treadmill exercise produces a tonic endogenous opioid signaling that, when blocked, creates a contrasting aversive state.

This is consistent with observations that exercise stimulates the release of endogenous opioid peptides and increases nociceptive thresholds in human and animal studies (48). In addition, chronic long-term exercise has been demonstrated to decrease sensitivity to morphine and other μ-opioid receptor agonists, suggesting that exercise may lead to cross-tolerance to exogenously administered opioid agonists and dependence (48). Supporting this idea, naloxone has been reported to precipitate a mild withdrawal syndrome in exercised, but not sedentary, rats (48). The CPA observed in MIA-treated rats may result from unmasking knee joint pain, a conclusion supported by the observation that naloxone also produces weight asymmetry. However, we acknowledge that other, non–pain-associated factors may contribute to naloxone-induced CPA.

Preclinical studies have demonstrated that MIA causes time- and concentration-dependent cartilage loss (25,49) and progressive changes to subchondral bone in a time-dependent manner (50–52). Micro-CT analysis of tibias indicates that treadmill exercise blocked MIA-induced trabecular bone loss. Thus, exercise has protective effects on trabecular bone degradation in this model of advanced OA pain. Our data are consistent with reports that interval training on a treadmill prevents MIA-induced decreased bone mineral density in the proximal tibia (52). Moreover, these data are consistent with other observations that light-to-moderate, but not intense, exercise has a protective effect on joint pathology in a surgical model of OA (53). The potential protective effects of exercise on bone remodeling and joint pathology support the conclusion of a recent meta-analysis indicating that running has protective effects against knee joint surgery in OA (54).

Our data demonstrate that naloxone reestablished pain behaviors characteristic of OA pain, indicating that the protective effects of exercise on bone remodeling within the tibia are likely to be independent of the pain-alleviating effects of exercise. The mechanism by which exercise ameliorates degeneration of trabecular bone deserves further study. Potential contributing factors may include the antiinflammatory effects of endogenous opioids, as indicated by the antiinflammatory effects of met-enkephalin demonstrated in a model of inflammation-associated arthritis (47). With regard to exercise, both clinical and preclinical studies have demonstrated that regular exercise diminishes proinflammatory markers in peripheral tissue (39).

Whether endogenous opioids mediate potential exercise-associated antiinflammatory effects that diminish advanced OA-induced bone remodeling and joint pain deserves further exploration. It should be noted that other factors, such as potential increased weight bearing on the joint during exercise, may also contribute to the protective effects observed in the exercised rats. Additionally, future studies examining other aspects of joint function and use, such as joint stiffness and range of motion, are warranted to further explore potential protective effects of exercise on the joint.

In conclusion, our studies indicate that exercise may improve pain in patients with advanced OA, resulting in an overall improvement in the quality of life of these patients. In addition, the protective effects of exercise on OA-associated bone remodeling may be able to prevent or delay joint replacement therapy in patients with OA. Taken together, these studies indicate potential protective effects of exercise in advanced OA joint pathology.

AUTHOR CONTRIBUTIONS

All authors were involved in drafting the article or revising it critically for important intellectual content, and all authors approved the final version to be published. Dr. Allen has full access to all of the data in the study and takes responsibility for the integrity of the data and the accuracy of the data analysis.

Study conception and design. Allen, Stevenson, King.
Acquisition of data. Allen, Imbert, Havelin, Henderson, Liaw.
Analysis and interpretation of data. Allen, Liaw.

REFERENCES

1. Dillon CF, Rasch EK, Gu Q, Hirsch R. Prevalence of knee osteoarthritis in the United States: arthritis data from the Third National Health and Nutrition Examination Survey 1991–94. J Rheumatol 2006;33:2271–9.
2. Hugle T, Geurts J, Nuesch C, Muller-Gerbl M, Valderrabano V. Aging and osteoarthritis: an inevitable encounter? J Aging Res 2012;2012:950192.
3. Hunter DJ, McDougall JJ, Keefe FJ. The symptoms of osteoarthritis and the genesis of pain. Rheum Dis Clin North Am 2008;34:623–43.
4. Mobasheri A, Batt M. An update on the pathophysiology of osteoarthritis. Ann Phys Rehabil Med 2016;59:333–9.
5. Neogi T, Zhang Y. Epidemiology of OA. Rheum Dis Clin North Am 2013;39:1–19.
6. Lane NE, Brandt K, Hawker G, Peeva E, Schreyer E, Tsuji W, et al. OARSI-FDA initiative: defining the disease state of osteoarthritis. Osteoarthritis Cartilage 2011;19:478–82.
7. Finnila MA, Thevenot J, Aho OM, Tiitu V, Rautiainen J, Kauppinen S, et al. Association between subchondral bone structure and osteoarthritis histopathological grade. J Orthop Res 2016. E-pub ahead of print.
8. Hill CL, Hunter DJ, Niu J, Clancy M, Guermazi A, Genant H, et al. Synovitis detected on magnetic resonance imaging and its relation to pain and cartilage loss in knee osteoarthritis. Ann Rheum Dis 2007;66:1599–603.
9. Thakur M, Dickenson AH, Baron R. Osteoarthritis pain: nociceptive or neuropathic? Nat Rev Rheumatol 2014;10:374–80.
10. Hawker GA, Stewart L, French MR, Cibere J, Jordan JM, March L, et al. Understanding the pain experience in hip and knee osteoarthritis: an OARSI/OMERACT initiative. Osteoarthritis Cartilage 2008;16:415–22.
11. Liu A, Kendzerska T, Stanaitis I, Hawker G. The relationship between knee pain characteristics and symptom state acceptability in people with knee osteoarthritis. Osteoarthritis Cartilage 2014; 22:178–83.
12. Bijlsma JW, Berenbaum F, Lafeber FP. Osteoarthritis: an update with relevance for clinical practice. Lancet 2011;377:2115–26.
13. Maserejian NN, Fischer MA, Trachtenberg FL, Yu J, Marceau LD, McKinlay JB, et al. Variations among primary care

physicians in exercise advice, imaging, and analgesics for musculoskeletal pain: results from a factorial experiment. Arthritis Care Res (Hoboken) 2014;66:147–56.
14. McAlindon TE, Bannuru RR, Sullivan MC, Arden NK, Berenbaum F, Bierma-Zeinstra SM, et al. OARSI guidelines for the non-surgical management of knee osteoarthritis. Osteoarthritis Cartilage 2014;22:363–88.
15. Ravi B, Croxford R, Reichmann WM, Losina E, Katz JN, Hawker GA. The changing demographics of total joint arthroplasty recipients in the United States and Ontario from 2001 to 2007. Best Pract Res Clin Rheumatol 2012;26:637–47.
16. Semanik PA, Chang RW, Dunlop DD. Aerobic activity in prevention and symptom control of osteoarthritis. PM R 2012;4 Suppl:S37–44.
17. Stagg NJ, Mata HP, Ibrahim MM, Henriksen EJ, Porreca F, Vanderah TW, et al. Regular exercise reverses sensory hypersensitivity in a rat neuropathic pain model: role of endogenous opioids. Anesthesiology 2011;114:940–8.
18. Leung A, Gregory NS, Allen LA, Sluka KA. Regular physical activity prevents chronic pain by altering resident muscle macrophage phenotype and increasing interleukin-10 in mice. Pain 2016;157:70–9.
19. Sabharwal R, Rasmussen L, Sluka KA, Chapleau MW. Exercise prevents development of autonomic dysregulation and hyperalgesia in a mouse model of chronic muscle pain. Pain 2016;157:387–98.
20. Bement MK, Sluka KA. Low-intensity exercise reverses chronic muscle pain in the rat in a naloxone-dependent manner. Arch Phys Med Rehab 2005;86:1736–40.
21. Sluka KA, Danielson J, Rasmussen L, DaSilva LF. Exercise-induced pain requires NMDA receptor activation in the medullary raphe nuclei. Med Sci Sports Exerc 2012;44:420–7.
22. Chen YW, Hsieh PL, Chen YC, Hung CH, Cheng JT. Physical exercise induces excess hsp72 expression and delays the development of hyperalgesia and allodynia in painful diabetic neuropathy rats. Anesth Analg 2013;116:482–90.
23. Shankarappa SA, Piedras-Renteria ES, Stubbs EB Jr. Forced-exercise delays neuropathic pain in experimental diabetes: effects on voltage-activated calcium channels. J Neurochem 2011;118:224–36.
24. Kuphal KE, Fibuch EE, Taylor BK. Extended swimming exercise reduces inflammatory and peripheral neuropathic pain in rodents. J Pain 2007;8:989–97.
25. Okun A, Liu P, Davis P, Ren J, Remeniuk B, Brion T, et al. Afferent drive elicits ongoing pain in a model of advanced osteoarthritis. Pain 2012;153:924–33.
26. Havelin J, Imbert I, Cormier J, Allen J, Porreca F, King T. Central sensitization and neuropathic features of ongoing pain in a rat model of advanced osteoarthritis. J Pain 2016;17:374–82.
27. Liu P, Okun A, Ren J, Guo RC, Ossipov MH, Xie J, et al. Ongoing pain in the MIA model of osteoarthritis. Neurosci Lett 2011;493:72–5.
28. Chaplan SR, Bach FW, Pogrel JW, Chung JM, Yaksh TL. Quantitative assessment of tactile allodynia in the rat paw. J Neurosci Methods 1994;53:55–63.
29. Xie JY, Qu C, Patwardhan A, Ossipov MH, Navratilova E, Becerra L, et al. Activation of mesocorticolimbic reward circuits for assessment of relief of ongoing pain: a potential biomarker of efficacy. Pain 2014;155:1659–66.
30. Paxinos G, Watson C. The rat brain in stereotaxic coordinates. London: Academic Press; 1998.
31. Arendt-Nielsen L, Nie H, Laursen MB, Laursen BS, Madeleine P, Simonsen OH, et al. Sensitization in patients with painful knee osteoarthritis. Pain 2010;149:573–81.
32. Schaible HG. Mechanisms of chronic pain in osteoarthritis. Curr Rheumatol Rep 2012;14:549–56.
33. Thakur M, Rahman W, Hobbs C, Dickenson AH, Bennett DL. Characterisation of a peripheral neuropathic component of the rat monoiodoacetate model of osteoarthritis. PLoS One 2012;7:e33730.
34. Harvey VL, Dickenson AH. Behavioural and electrophysiological characterisation of experimentally induced osteoarthritis and neuropathy in C57Bl/6 mice. Mol Pain 2009;5.
35. Sagar DR, Burston JJ, Hathway GJ, Woodhams SG, Pearson RG, Bennett AJ, et al. The contribution of spinal glial cells to chronic pain behaviour in the monosodium iodoacetate model of osteoarthritic pain. Mol Pain 2011;7.
36. Rahman W, Bauer CS, Bannister K, Vonsy JL, Dolphin AC, Dickenson AH. Descending serotonergic facilitation and the antinociceptive effects of pregabalin in a rat model of osteoarthritic pain. Mol Pain 2009;5:45.
37. Tsuda M, Beggs S, Salter MW, Inoue K. Microglia and intractable chronic pain. Glia 2013;61:55–61.
38. Almeida C, DeMaman A, Kusuda R, Cadetti F, Ravanelli MI, Queiroz AL, et al. Exercise therapy normalizes BDNF upregulation and glial hyperactivity in a mouse model of neuropathic pain. Pain 2015;156:504–13.
39. Cooper MA, Kluding PM, Wright DE. Emerging relationships between exercise, sensory nerves, and neuropathic pain. Front Neurosci 2016;10:372.
40. Grace PM, Fabisiak TJ, Green-Fulgham SM, Anderson ND, Strand KA, Kwilasz AJ, et al. Prior voluntary wheel running attenuates neuropathic pain. Pain 2016;157:2012–23.
41. Colt EW, Wardlaw SL, Frantz AG. The effect of running on plasma β-endorphin. Life Sci 1981;28:1637–40.
42. Debruille C, Luyckx M, Ballester L, Brunet C, Odou P, Dine T, et al. Serum opioid activity after physical exercise in rats. Physiol Res 1999;48:129–33.
43. Blake MJ, Stein EA, Vomachka AJ. Effects of exercise training on brain opioid peptides and serum LH in female rats. Peptides 1984;5:953–8.
44. Ossipov MH, Morimura K, Porreca F. Descending pain modulation and chronification of pain. Curr Opin Support Palliat Care 2014;8:143–51.
45. Minett MS, Pereira V, Sikandar S, Matsuyama A, Lolignier S, Kanellopoulos AH, et al. Endogenous opioids contribute to insensitivity to pain in humans and mice lacking sodium channel Nav1.7. Nat Commun 2015;6:8967.
46. Navratilova E, Xie JY, Meske D, Qu C, Morimura K, Okun A, et al. Endogenous opioid activity in the anterior cingulate cortex is required for relief of pain. J Neurosci 2015;35:7264–71.
47. Lu Y, McNearney TA, Wilson SP, Yeomans DC, Westlund KN. Joint capsule treatment with enkephalin-encoding HSV-1 recombinant vector reduces inflammatory damage and behavioural sequelae in rat CFA monoarthritis. Eur J Neurosci 2008;27:1153–65.
48. Smith MA, Yancey DL. Sensitivity to the effects of opioids in rats with free access to exercise wheels: μ-opioid tolerance and physical dependence. Psychopharmacology (Berl) 2003;168:426–34.
49. Pomonis JD, Boulet JM, Gottshall SL, Phillips S, Sellers R, Bunton T, et al. Development and pharmacological characterization of a rat model of osteoarthritis pain. Pain 2005;114:339–46.
50. Morenko BJ, Bove SE, Chen L, Guzman RE, Juneau P, Bocan TM, et al. In vivo micro computed tomography of subchondral bone in the rat after intra-articular administration of monosodium iodoacetate. Contemp Top Lab Anim Sci 2004;43:39–43.
51. Xie L, Lin AS, Kundu K, Levenston ME, Murthy N, Guldberg RE. Quantitative imaging of cartilage and bone morphology, reactive oxygen species, and vascularization in a rodent model of osteoarthritis. Arthritis Rheum 2012;64:1899–908.
52. Boudenot A, Presle N, Uzbekov R, Toumi H, Pallu S, Lespessailles E. Effect of interval-training exercise on subchondral bone in a chemically-induced osteoarthritis model. Osteoarthritis Cartilage 2014;22:1176–85.
53. Galois L, Etienne S, Grossin L, Watrin-Pinzano A, Cournil-Henrionnet C, Loeuille D, et al. Dose-response relationship for exercise on severity of experimental osteoarthritis in rats: a pilot study. Osteoarthritis Cartilage 2004;12:779–86.
54. Timmins KA, Leech RD, Batt ME, Edwards KL. Running and knee osteoarthritis: a systematic review and meta-analysis. Am J Sports Med 2017;45:1447–57.

ARTHRITIS & RHEUMATOLOGY
Vol. 69, No. 7, July 2017, pp 1418–1428
DOI 10.1002/art.40104

Regulated in Development and DNA Damage Response 1 Deficiency Impairs Autophagy and Mitochondrial Biogenesis in Articular Cartilage and Increases the Severity of Experimental Osteoarthritis

Oscar Alvarez-Garcia, Tokio Matsuzaki, Merissa Olmer, Lars Plate, Jeffery W. Kelly, and Martin K. Lotz

Objective. **Regulated in development and DNA damage response 1 (REDD1) is an endogenous inhibitor of mechanistic target of rapamycin (mTOR) that regulates cellular stress responses. REDD1 expression is decreased in aged and osteoarthritic (OA) cartilage, and it regulates mTOR signaling and autophagy in articular chondrocytes in vitro. This study was undertaken to investigate the effects of REDD1 deletion in vivo using a mouse model of experimental OA.**

Methods. **OA severity was histologically assessed in 4-month-old wild-type and REDD1$^{-/-}$ mice subjected to surgical destabilization of the medial meniscus (DMM). Chondrocyte autophagy, apoptosis, mitochondrial content, and expression of mitochondrial biogenesis markers were determined in cartilage and cultured chondrocytes from wild-type and REDD1$^{-/-}$ mice.**

Results. **REDD1 deficiency increased the severity of changes in cartilage, menisci, subchondral bone, and synovium in the DMM model of OA. Chondrocyte death was increased in the cartilage of REDD1$^{-/-}$ mice and in cultured REDD1$^{-/-}$ mouse chondrocytes under oxidative stress conditions. Expression of key autophagy markers (microtubule-associated protein 1A/1B light chain 3 and autophagy protein 5) was markedly reduced in cartilage from REDD1$^{-/-}$ mice and in cultured human and mouse chondrocytes with REDD1 depletion. Mitochondrial content, ATP levels, and expression of the mitochondrial biogenesis markers peroxisome proliferator–activated receptor γ coactivator 1α (PGC-1α) and transcription factor A, mitochondrial (TFAM) were also decreased in REDD1-deficient chondrocytes. REDD1 was required for AMP-activated protein kinase–induced PGC-1α in chondrocytes.**

Conclusion. **Our findings suggest that REDD1 is a key mediator of cartilage homeostasis through regulation of autophagy and mitochondrial biogenesis and that REDD1 deficiency exacerbates the severity of injury-induced OA.**

Osteoarthritis (OA) is the most prevalent joint disease and causes pain and disability (1). Although OA is considered a disease of the whole synovial joint, degradation of articular cartilage is a critical event in disease initiation and progression. Cartilage damage is a result of an imbalance between anabolic and catabolic processes that compromise the function of articular chondrocytes, the cells that maintain tissue homeostasis (2). OA is a multifactorial disease, and aging is its main risk factor (2). Despite the fact that not all persons develop OA with age, there are significant age-related changes in articular cartilage that may serve as a basis for OA development (3). These changes include reduced thickness and cell density, abnormal secretory activity, cell senescence, and defective cellular defense mechanisms (3). Understanding the molecular mechanisms that drive cartilage aging has become a main focus of OA research.

Macroautophagy (hereinafter referred to as autophagy) is a conserved process that recycles defective cellular organelles and macromolecules and is activated during hypoxic and energy stress to provide energy for the cell (4). Our group has shown that autophagy is constitutively active in articular chondrocytes and that there is a reduction in the expression of key autophagy markers during aging and OA (5). A major regulator of autophagy is the serine/threonine kinase mechanistic target of rapamycin

Supported by the NIH (US Department of Health and Human Services grant AG-007996 and grant AG-049617).

Oscar Alvarez-Garcia, PhD, Tokio Matsuzaki, MD, PhD, Merissa Olmer, MA, Lars Plate, PhD, Jeffery W. Kelly, PhD, Martin K. Lotz, MD: The Scripps Research Institute, La Jolla, California.

Address correspondence to Martin K. Lotz, MD, Department of Molecular and Experimental Medicine, MEM-161, The Scripps Research Institute, 10550 North Torrey Pines Road, La Jolla, CA 92037. E-mail: mlotz@scripps.edu.

Submitted for publication September 27, 2016; accepted in revised form March 16, 2017.

(mTOR) (6). Under nutrient-replete conditions, mTOR suppresses autophagy through phosphorylation of Unc-51–like kinase 1 and autophagy protein 13 (ATG-13) (6). As part of the normal cellular response to stress, endogenous regulators such as FOXO, AMP-activated protein kinase (AMPK), or regulated in development and DNA damage response 1 (REDD1) inhibit mTOR to arrest cell growth and proliferation while enhancing stress resistance and cell survival (6). However, these regulatory mechanisms seem to be defective in articular cartilage during aging and OA. We and others have reported a reduction in FOXO, AMPK, and REDD1 expression and activity in cartilage during aging and OA (7–10), and there is evidence of increased mTOR expression in OA cartilage (11). Moreover, genetic or pharmacologic inhibition of mTOR signaling results in autophagy activation and protection against experimental OA in mice (11,12). These findings suggest that increased mTOR signaling may compromise autophagy in chondrocytes and contribute to the development of OA.

REDD1 (encoded by *DDIT4*) is an evolutionarily conserved protein that is ubiquitously expressed in adult tissue and regulates cellular stress responses. REDD1 expression is induced by hypoxia and other stresses (13,14) and acts primarily as a canonical mTOR inhibitor (15–17). Interestingly, REDD1 regulates autophagy through an mTOR-independent mechanism that involves a direct interaction with thioredoxin-interacting protein to induce reactive oxygen species (ROS) production and activation of ATG-4B, a key component of the autophagic machinery (18). We have previously reported that REDD1 is abundantly expressed in human and mouse knee articular cartilage and that its expression is reduced during aging and OA (10). Moreover, REDD1 positively regulates autophagy in human and mouse articular chondrocytes, also in an mTOR-independent manner (10), suggesting that reduced REDD1 expression in cartilage may contribute to the increased mTOR activity and autophagy deficiency that are characteristic of OA pathophysiology.

The present study was designed to evaluate the role of REDD1 in OA development in vivo using a mouse model of experimental OA. Our results show that genetic disruption of REDD1 impairs autophagy in cartilage and exacerbates the severity of experimental OA. Furthermore, we identified a novel function of REDD1 as a regulator of mitochondrial biogenesis in articular chondrocytes.

MATERIALS AND METHODS

Mice. All animal experiments were performed in compliance with protocols approved by the Institutional Animal Care and Use Committee at The Scripps Research Institute. Global REDD1-knockout mice (REDD1$^{-/-}$) on a C57BL/6J background (19) are the property of Quark Pharmaceuticals, were provided by the company, and were generated specifically for Quark by Lexicon Genetics. For examination of joint and skeletal development and of growth and maturation, mice were euthanized after 7 days (on postnatal day 7), or at 1, 2, or 6 months of age. For aging studies, wild-type mice were euthanized at 6 or 27 months of age. For the surgical OA model, 4-month-old male mice (n = 12 per genotype) were anesthetized, and transection of the medial meniscotibial ligament (destabilization of the medial meniscus [DMM]) and the medial collateral ligament was performed in the right knee as previously described (12,20). For a control, sham surgery was performed on the left knee and consisted of a small incision in the medial side, opening of the joint capsule, and closing with surgical suture. Animals were euthanized 10 weeks after surgery, and knee joints were embedded in a standardized fixed angle of the femur relative to the tibia so that the sections that were scored represented the center of the weight-bearing areas of the tibial plateau and femoral condyle (9).

Five-micrometer–thick sagittal sections of the medial compartment of the knee were stained with Safranin O–fast green (9), and OA-related changes were scored in one section per animal as previously described for articular cartilage (summed Osteoarthritis Research Society International [OARSI] score for femur and tibia) (21), synovium (22), anterior and posterior meniscal horns (23), and subchondral bone (24). Samples were graded by 2 individuals who were blinded with regard to mouse genotype.

Mouse cell culture. Immature mouse articular chondrocytes were isolated from the knees and hips of 6-day-old wild-type and REDD1$^{-/-}$ mice (19) following the protocol described by Gosset et al (25). Synovial membranes were obtained from the knee joints of 4-month-old REDD1$^{+/+}$ and REDD1$^{-/-}$ mice (n = 4 per genotype), and synoviocytes were isolated after a 4-hour digestion with collagenase (2 mg/ml; Sigma) at 37°C. Cells were maintained in medium containing 10% calf serum, and second-passage cells were plated at a density of 10^5 cells/ml, incubated overnight, and treated for 24 hours with *tert*-butyl-hydroperoxide (tBHP; Sigma), 1 n*M* interleukin-1β (IL-1β; PeproTech), chloroquine (25 μM; Sigma), or 1 m*M* 5-aminoimidazole-4-carboxamide ribonucleotide (AICAR; Sigma) as indicated.

Human chondrocyte culture. Human primary chondrocytes were isolated as previously described (8) and maintained in Dulbecco's modified Eagle's medium containing 10% calf serum at 37°C in 5% CO_2. First-passage chondrocytes were used in all experiments. For REDD1 knockdown, chondrocytes were grown to confluence and transfected with small interfering RNA (siRNA) for DDIT4/REDD1 (Life Technologies) using Lipofectamine RNAiMAX (Life Technologies) in media containing 1% calf serum for 48 hours.

Immunohistochemistry. Paraffin-embedded knees from REDD1$^{+/+}$ mice were processed as previously described (9), and sections were incubated overnight with antibodies against REDD1 (1:100; Proteintech), microtubule-associated protein 1A/1B light chain 3 (LC3) (1:50; MBL), or ATG-5 (1:100, Abcam). After washing with phosphate buffered saline (PBS), sections were incubated for 30 minutes with ImmPRESS-AP anti-rabbit IgG polymer detection reagent (Vector), dehydrated, and mounted. Positive cells were quantified in the articular cartilage and both meniscal horns of the proximal tibial plateau in 2 different pictures per section taken at 20× magnification. Results are reported as the percentage of immunopositive cells.

TUNEL staining. Five-micrometer–thick sections were digested with pepsin (Dako) for 8 minutes at 37°C, and endogenous peroxidase was blocked using Vector's Bloxall solution at

room temperature for 10 minutes. TUNEL staining was completed using an in situ detection kit with fluorescein (Roche). Cartilage cellularity and TUNEL-positive cells were measured in 2 different fields per section, and results are expressed as cells per mm^2 and percentage of fluorescent cells, respectively.

Cell viability. Articular chondrocytes from REDD1$^{+/+}$ and REDD1$^{-/-}$ mice were cultured in 96-well plates and treated with the oxidant tBHP at 0, 50, 100, or 250 μM for 24 hours. Cell viability was assessed using a RealTime-Glo MT Cell Viability Assay (Promega). Four independent experiments were performed in triplicate. Results are expressed as relative cell viability with respect to untreated chondrocytes from REDD1$^{+/+}$ mice.

Intracellular ATP measurement. Mouse articular chondrocytes were cultured in 96-well plates in media containing 25 mM glucose or galactose for 24 hours, and intracellular ATP levels were measured using a CellTiter-Glo assay (Promega).

DNA isolation and mitochondrial DNA (mtDNA) quantification. Knee cartilage, spleen, and brain were collected from 6-month-old mice, flash-frozen in liquid nitrogen, and DNA was isolated using a Blood and Tissue DNA isolation kit (Qiagen). To quantify mtDNA content, quantitative polymerase chain reaction (qPCR) was performed for mtDNA-encoded cytochrome c oxidase subunit 2 (MT-CO2) and nucleus-encoded 18S ribosomal DNA as previously described (26). The MT-CO2:18S ratio represents the relative mtDNA copy number (26).

RNA isolation and gene expression analysis. Mouse and human cartilage were homogenized in QIAzol Lysis Reagent (Qiagen), and RNA was isolated using an RNeasy Mini kit (Qiagen). In cultured cells, RNA was collected using a Direct-zol RNA Miniprep kit (Zymo Research).

Gene expression was measured by qPCR using predesigned TaqMan gene expression assays for MAP1LC3, ATG5, PPARGC1A, and TFAM. GAPDH was measured as a reference gene.

Protein isolation and Western blotting. Cultured cells were washed twice in PBS and lysed in ice-cold radioimmunoprecipitation assay buffer (Pierce) supplemented with protease and phosphatase inhibitor cocktail (Thermo Scientific). Twenty

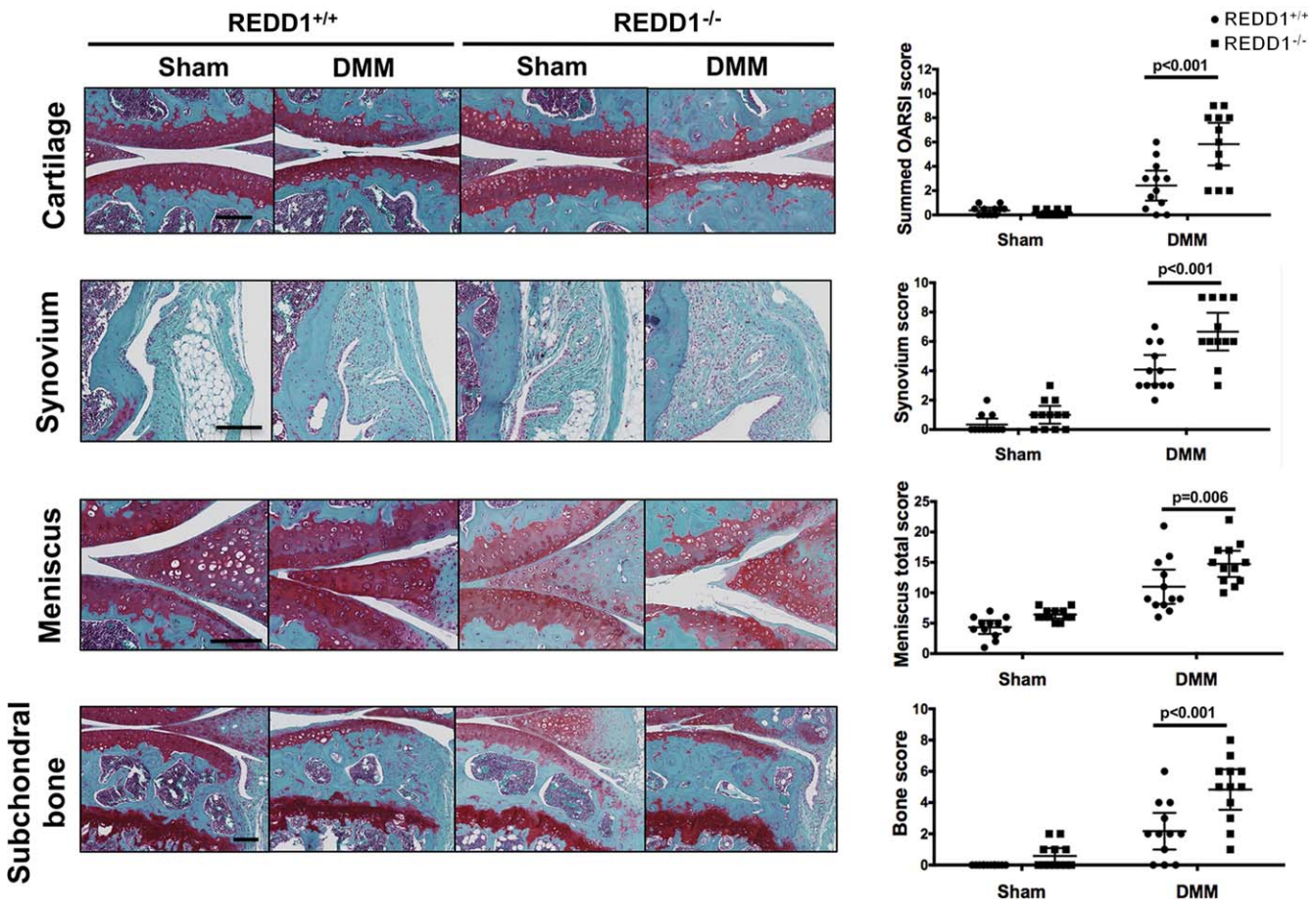

Figure 1. Increased severity of experimental osteoarthritis (OA) in REDD1$^{-/-}$ mice. Left, Representative images showing histologic changes in the medial articular cartilage, synovium, meniscus, and subchondral bone of the knees of 6.5-month-old REDD1$^{+/+}$ and REDD1$^{-/-}$ mice subjected to destabilization of the medial meniscus (DMM) or sham procedure. Bars = 100 μm. Right, Quantification of the histologic scores for each mouse joint tissue. Symbols represent individual mice (n = 12 per group); horizontal lines and error bars show the mean ± SD. OARSI = Osteoarthritis Research Society International.

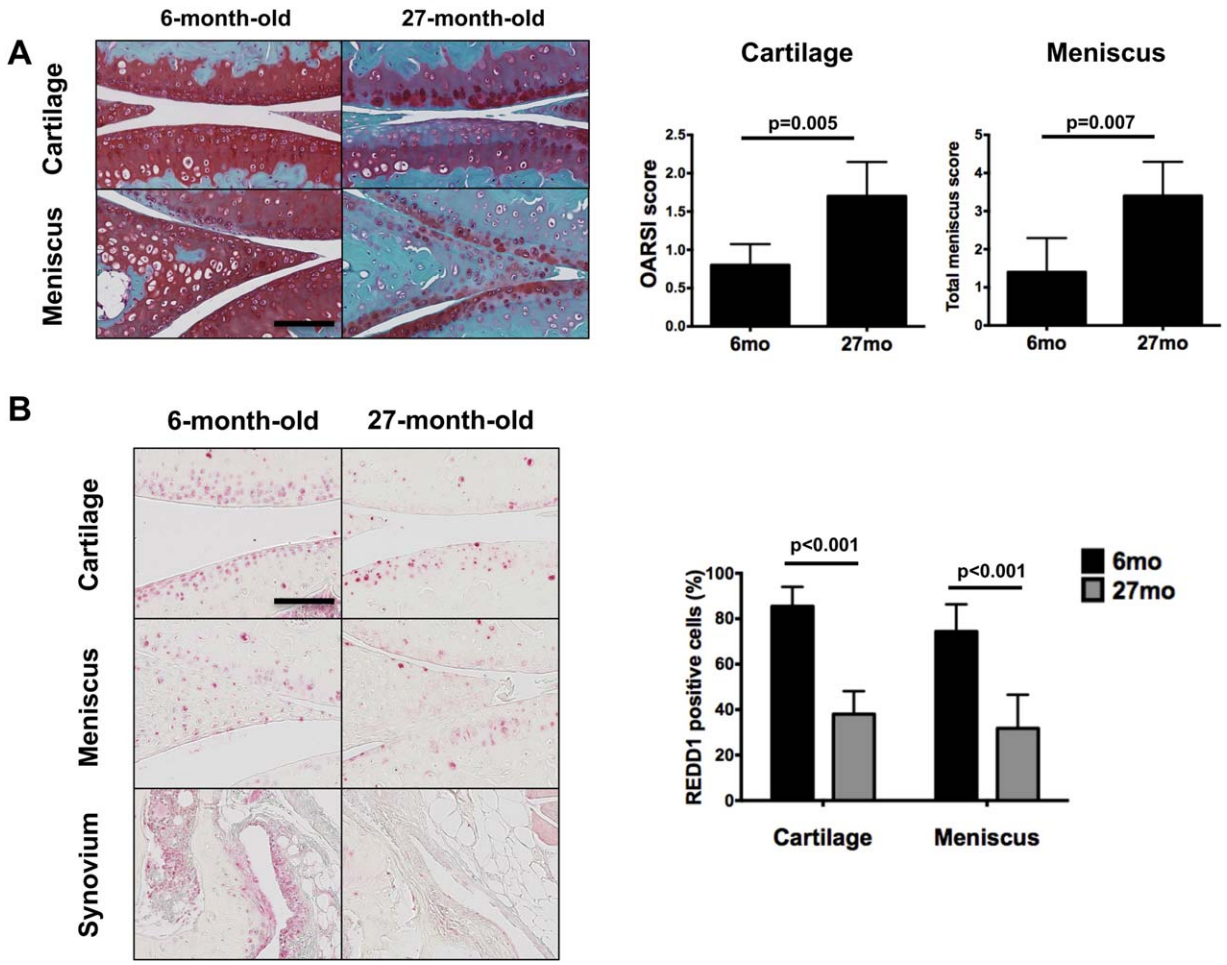

Figure 2. Reduced expression of regulated in development and DNA damage response 1 (REDD1) in the joint tissue of aging wild-type mice. **A,** Left, Representative histologic images of the medial articular cartilage and meniscus of the knees of 6-month-old and 27-month-old mice. Bar = 100 μm. Right, Quantification of histologic scores for the mouse cartilage and meniscus. Values are the mean ± SD (n = 5 mice per group). OARSI = Osteoarthritis Research Society International. **B,** Left, Representative images of immunohistochemical staining for REDD1 in knee joint tissue from 6-month-old and 27-month-old mice. Bar = 100 μm. Right, Quantification of REDD1-positive cells in the mouse cartilage and meniscus. Values are the mean ± SD (n = 5 mice per group). Color figure can be viewed in the online issue, which is available at http://onlinelibrary.wiley.com/doi/10.1002/art.40104/abstract.

micrograms of protein was resolved in 4–12% acrylamide gels, transferred to nitrocellulose membranes, and blotted overnight with antibodies against REDD1 (1:500; Proteintech), cleaved caspase 3 (1:500; Cell Signaling Technology), LC3 (1:1,000; Cell Signaling Technology), p62 (1:1,000; Cell Signaling Technology), oxidative phosphorylation cocktail (1:1,000; Abcam), peroxisome proliferator–activated receptor γ coactivator 1α (PGC-1α) (1:1,000; BioVision), transcription factor A, mitochondrial (TFAM) (1:500; Cell Signaling Technology), and GAPDH (1:5,000; Abcam). After incubating with secondary antibodies for 1 hour at room temperature, blots were visualized using a Li-Cor Odyssey infrared imaging system. Intensity values were analyzed using ImageStudioLite software and normalized to those of GAPDH.

Statistical analysis. Data are shown as the mean ± SD. Differences between groups were assessed by one-way analysis of variance followed by a post hoc Tukey test. Comparisons between 2 groups were assessed by an unpaired, 2-tailed *t*-test after testing for equal variance using an F test. All statistical analyses were performed using Prism 6 software (GraphPad). *P* values less than 0.05 were considered significant.

RESULTS

Normal embryonic skeletal development and postnatal growth and maturation in REDD1-deficient mice. Mice with global deletion of REDD1 developed normally and had similar weight and length as their wild-type littermates (see Supplementary Figure 1, available on the *Arthritis & Rheumatology* web site at http://onlinelibrary.wiley.com/doi/10.1002/art.40104/abstract). Histologic analysis of the knees showed no differences in articular cartilage morphology between REDD1$^{+/+}$ and REDD1$^{-/-}$ mice up to 6 months of age.

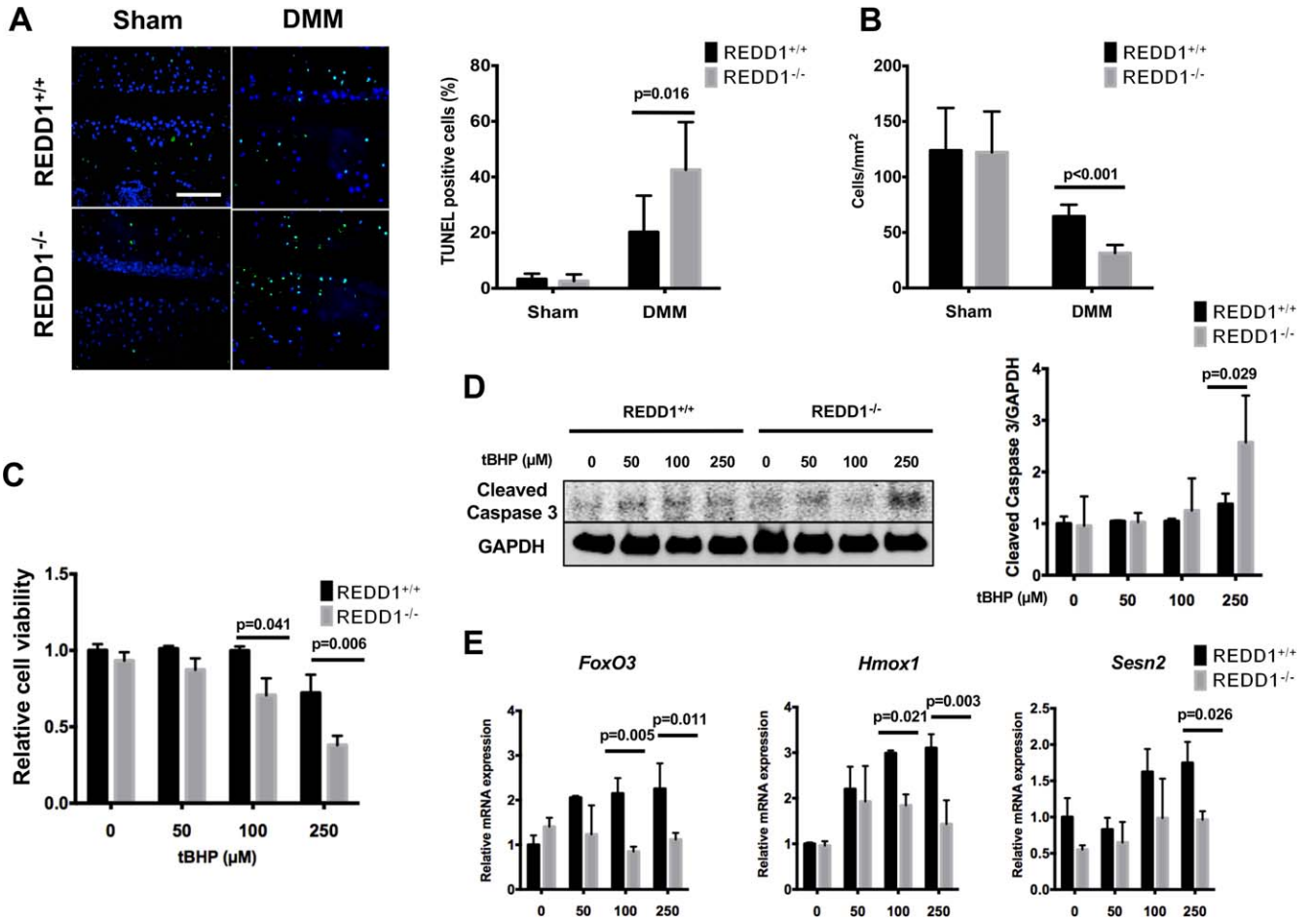

Figure 3. Increased chondrocyte death in REDD1$^{-/-}$ mice with experimental osteoarthritis (OA). **A,** Left, Representative images showing chondrocyte apoptosis in knee articular cartilage from 6.5-month-old REDD1$^{+/+}$ and REDD1$^{-/-}$ mice subjected to destabilization of the medial meniscus (DMM) or sham procedure and assessed by TUNEL staining. Bar = 100 μm. Right, Quantification of TUNEL-positive cells. Values are the mean ± SD (n = 6 mice per group). **B,** Quantification of articular cartilage cellularity in knees from 6.5-month-old REDD1$^{+/+}$ and REDD1$^{-/-}$ mice subjected to DMM or sham procedure. Values are the mean ± SD (n = 6 mice per group). **C,** Cell viability in cultured mouse articular chondrocytes treated with 0, 50, 100, or 250 μM *tert*-butyl-hydroperoxide (tBHP) for 24 hours. Data are expressed as relative cell viability with respect to untreated chondrocytes from REDD1$^{+/+}$ mice. Values are the mean ± SD from 4 independent experiments performed in triplicate. **D,** Left, Western blot analysis of cleaved caspase 3 in cultured chondrocytes isolated from REDD1$^{+/+}$ and REDD1$^{-/-}$ mice treated with different doses of tBHP to induce oxidative stress. Right, Quantification of cleaved caspase 3. Values are the mean ± SD from 3 different experiments. **E,** Quantitative polymerase chain reaction analysis of *FoxO3*, *Hmox1*, and *Sesn2* expression in cultured chondrocytes isolated from REDD1$^{+/+}$ and REDD1$^{-/-}$ mice treated with the indicated doses of tBHP. Values are the mean ± SD from 3 different experiments performed in duplicate. Color figure can be viewed in the online issue, which is available at http://onlinelibrary.wiley.com/doi/10.1002/art.40104/abstract.

Increased OA severity in mice deficient in REDD1. To evaluate the role of REDD1 in cartilage homeostasis during OA pathogenesis, we induced OA in REDD1$^{-/-}$ and wild-type mice by DMM. REDD1$^{-/-}$ mice showed increased articular cartilage degradation and had significantly higher histopathologic scores than wild-type mice 10 weeks after DMM surgery ($P < 0.001$) (Figure 1). In addition, REDD1$^{-/-}$ mice had significantly higher synovitis scores ($P < 0.001$) with increased synovial hyperplasia and abundant cell infiltration, increased meniscus degeneration ($P = 0.006$) with loss of meniscus cells and Safranin O staining and partial erosion of tissue, and more severe bone pathology ($P < 0.001$) with thickening of subchondral bone, reduction of medullary cavities, and increased osteophyte formation (Figure 1).

Reduced REDD1 expression in aging mouse joint tissue. REDD1 deficiency resulted in widespread pathologic changes in the joint during experimental OA. Our previous work focused on articular cartilage only, and we showed decreased expression of REDD1 with aging (10). In this study, we sought to evaluate the changes in REDD1 expression during aging in different tissues of the knee joint from 6- and 27-month-old mice. Histologic analysis of knees from older mice revealed OA-like changes with aging that resulted in significantly increased

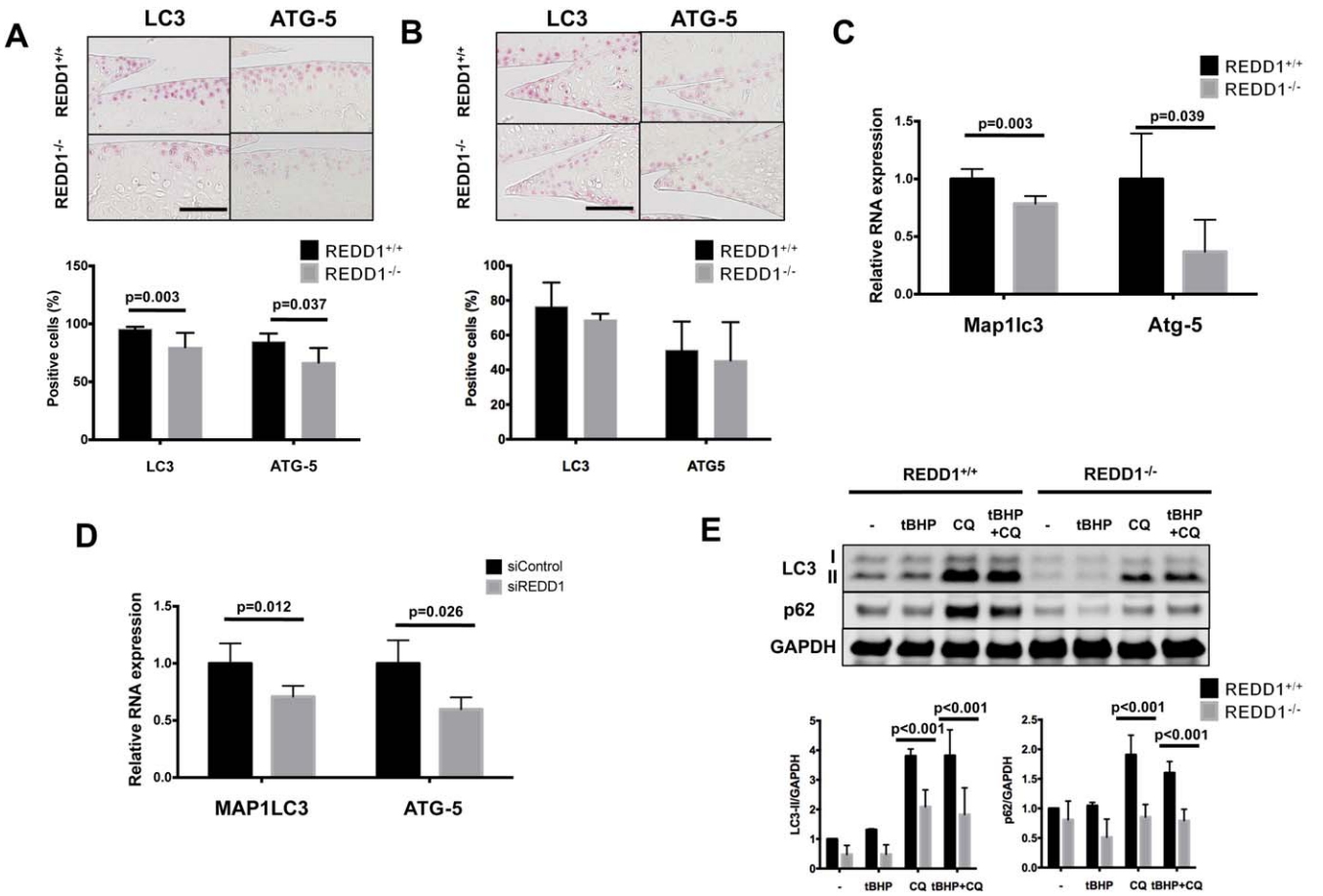

Figure 4. Reduced expression of autophagy markers in regulated in development and DNA damage response 1 (REDD1)–deficient articular chondrocytes. **A,** Top, Representative images of immunohistochemical staining for microtubule-associated protein 1A/1B light chain 3 (LC3) and autophagy protein 5 (ATG-5) in knee articular cartilage from 6-month-old REDD1$^{+/+}$ and REDD1$^{-/-}$ mice. Bar = 100 μm. Bottom, Quantification of LC3- and ATG-5–positive cells. Values are the mean ± SD (n = 6 mice per genotype). **B,** Top, Representative images of immunohistochemical staining for LC3 and ATG-5 in the medial meniscus of 6-month-old REDD1$^{+/+}$ and REDD1$^{-/-}$ mice. Bar = 100 μm. Bottom, Quantification of LC3- and ATG-5–positive cells. Values are the mean ± SD (n = 6 mice per genotype). **C,** Quantitative polymerase chain reaction (PCR) analysis of Map1lc3 and Atg5 expression in cultured chondrocytes isolated from REDD1$^{+/+}$ and REDD1$^{-/-}$ mice. Values are the mean ± SD from 3 different experiments. **D,** Quantitative PCR analysis of MAP1LC3 and ATG5 expression in human cultured chondrocytes transfected with control small interfering RNA (siRNA; siControl) or siRNA against REDD1. Values are the mean ± SD (n = 4 donors). **E,** Top, Western blot analysis of p62 and LC3 in cultured chondrocytes isolated from REDD1$^{+/+}$ and REDD1$^{-/-}$ mice and treated with *tert*-butyl-hydroperoxide (tBHP) or chloroquine (CQ). Bottom, Quantification of LC3 and p62. Values are the mean ± SD from 3 different experiments. Color figure can be viewed in the online issue, which is available at http://onlinelibrary.wiley.com/doi/10.1002/art.40104/abstract.

histopathologic scores compared with young controls (Figure 2A). Immunohistochemical staining for REDD1 was abundant in the cartilage, meniscus, and synovium of 6-month-old mice. However, REDD1 expression was significantly reduced in the articular cartilage and medial meniscus of 27-month-old mice when compared with 6-month-old controls (Figure 2B), and a similar reduction in REDD1 staining was observed in the synovium.

Increased chondrocyte death in REDD1-deficient mice. Chondrocyte death following injury is a pivotal event that is closely linked to cartilage degradation (27). We next evaluated whether REDD1 deficiency altered chondrocyte viability. TUNEL staining revealed an increased rate of chondrocyte apoptosis in the knee articular cartilage of REDD1$^{-/-}$ mice compared with controls, and there was a concomitant reduction in cartilage cellularity ($P < 0.001$) (Figures 3A and B). To test whether articular chondrocytes with REDD1 depletion are more susceptible to apoptotic cell death, cultured primary chondrocytes from REDD1$^{-/-}$ and wild-type mice were treated with increasing concentrations of tBHP to induce oxidative stress (Figure 3C). Cells from mutant mice showed significantly higher rates of cell death than wild-type cells and a significant increase in cleaved caspase 3, an indicator of

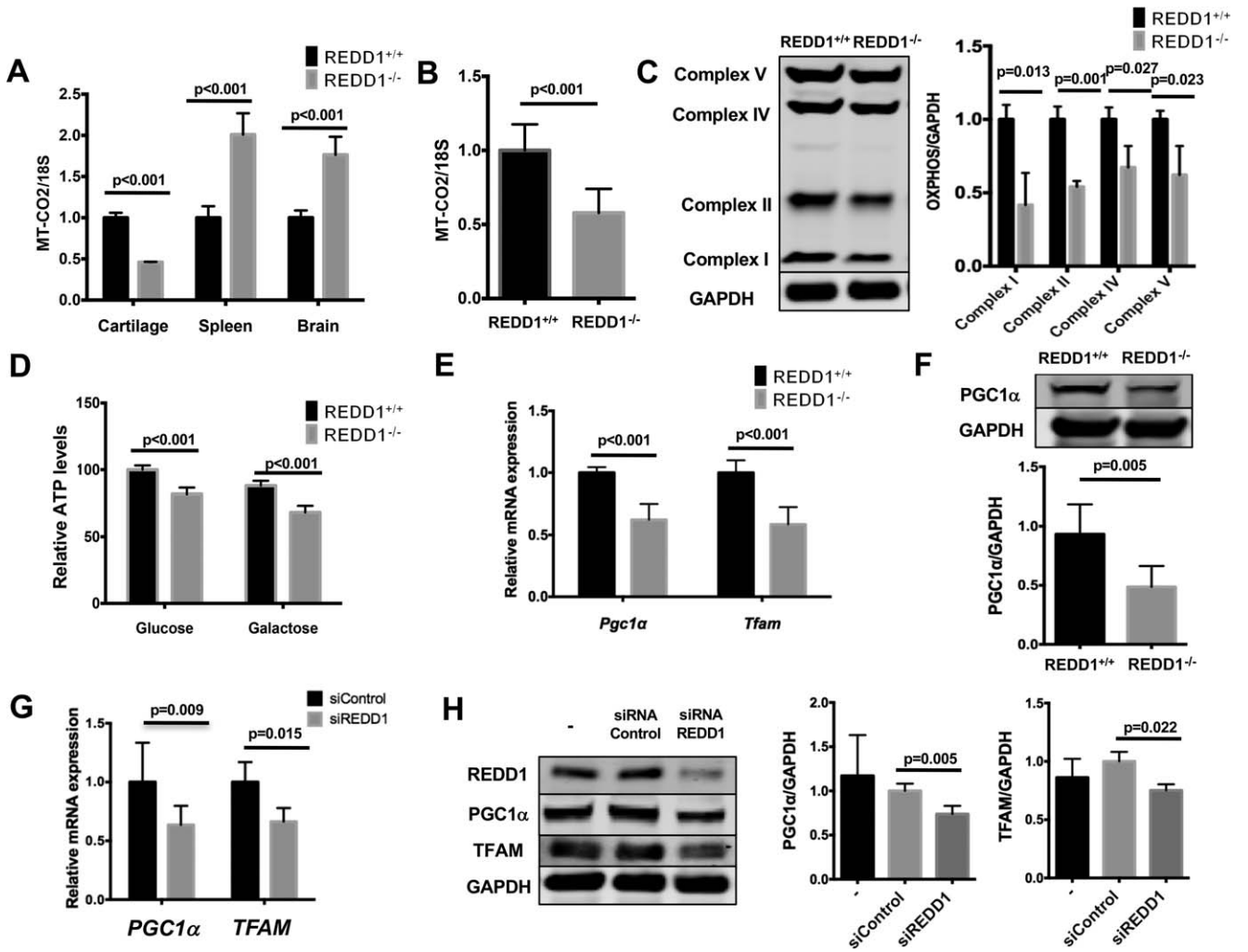

Figure 5. Reduced mitochondrial biogenesis in regulated in development and DNA damage response 1 (REDD1)–deficient articular chondrocytes. **A,** Mitochondrial DNA copy number in cartilage, spleen, and brain from 6-month-old REDD1$^{+/+}$ and REDD1$^{-/-}$ mice. Data are shown as the ratio of cytochrome c oxidase subunit 2 (MT-CO2) to 18S DNA, measured by quantitative polymerase chain reaction (qPCR). Values are the mean ± SD (n = 4 mice per genotype). **B,** Mitochondrial DNA copy number in cultured articular chondrocytes isolated from REDD1$^{+/+}$ and REDD1$^{-/-}$ mice. Data are shown as the ratio of MT-CO2 to 18S DNA, measured by qPCR. Values are the mean ± SD from 3 different experiments. **C,** Left, Western blot analysis of mitochondrial complex protein expression in cultured chondrocytes isolated from REDD1$^{+/+}$ and REDD1$^{-/-}$ mice. Right, Quantification of mitochondrial complex protein expression. Values are the mean ± SD from 3 different experiments. **D,** Intracellular ATP levels in cultured chondrocytes isolated from REDD1$^{+/+}$ and REDD1$^{-/-}$ mice in the presence of 25 m*M* glucose or galactose. Values are the mean ± SD from 4 different experiments. **E,** Quantitative PCR analysis of *Pgc1α* and *Tfam* expression in cultured chondrocytes isolated from REDD1$^{+/+}$ and REDD1$^{-/-}$ mice. Values are the mean ± SD from 3 different experiments. **F,** Top, Western blot analysis of peroxisome proliferator–activated receptor γ coactivator 1α (PGC-1α) expression in cultured chondrocytes isolated from REDD1$^{+/+}$ and REDD1$^{-/-}$ mice. Bottom, Quantification of PGC-1α expression. Values are the mean ± SD from 3 different experiments. **G,** Quantitative PCR analysis of *PGC1α* and *TFAM* expression in human cultured chondrocytes transfected with control small interfering RNA (siRNA; siControl) or siRNA against REDD1. Values are mean ± SD from 4 different donors. **H,** Left, Western blot analysis of PGC-1α and TFAM expression in human cultured chondrocytes transfected with control siRNA or siRNA against REDD1. Right, Quantification of PGC-1α and TFAM expression. Values are the mean ± SD from 4 different donors.

apoptotic cell death (Figure 3D). In addition, REDD1-deficient chondrocytes exhibited a significant reduction in the expression of key antioxidant genes (*FoxO3, Hmox1,* and *Sesn2*) when treated with tBHP as compared with wild-type cells (Figure 3E). In contrast, REDD1 deficiency did not alter IL-1β–induced expression of inflammatory mediators or apoptosis induction by tBHP (data not shown). Taken together, these results indicate that articular chondrocytes lacking REDD1 are more susceptible to apoptotic cell death under oxidative stress.

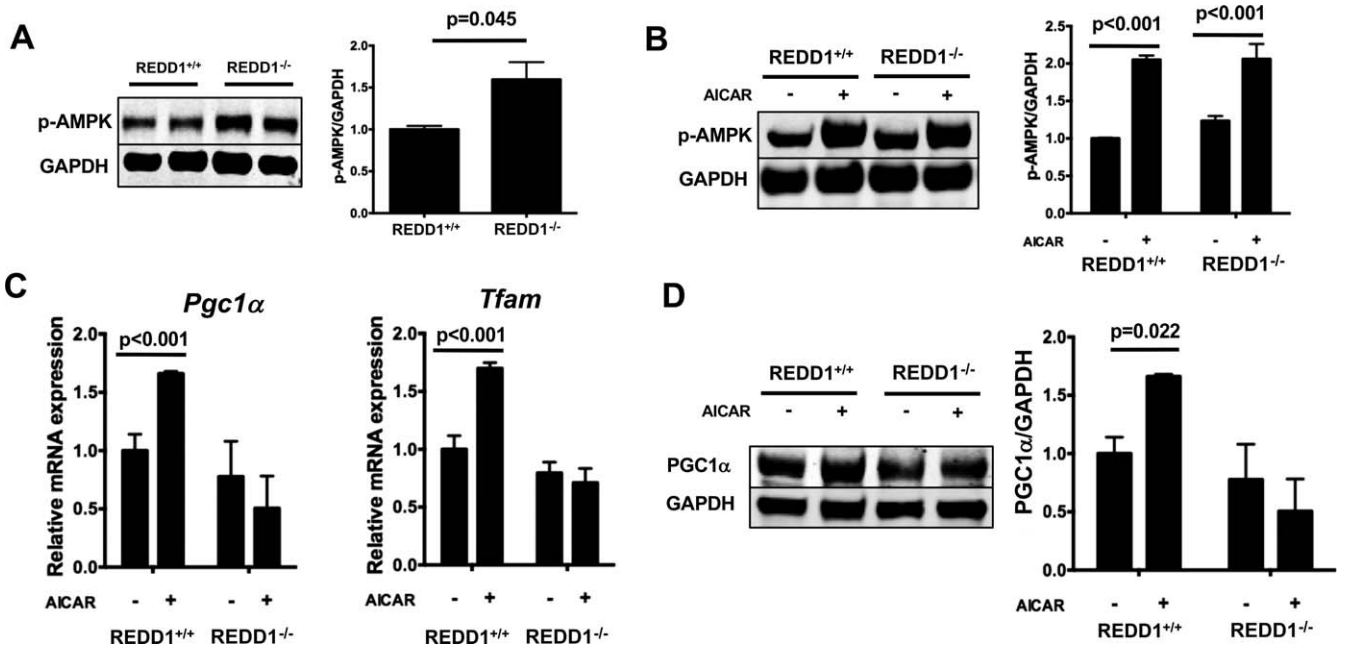

Figure 6. Regulated in development and DNA damage response 1 (REDD1) is required for AMP-activated protein kinase (AMPK)–dependent peroxisome proliferator–activated receptor γ coactivator 1α (PGC-1α) expression. **A**, Left, Western blot analysis of AMPK phosphorylation in cultured chondrocytes isolated from REDD1$^{+/+}$ and REDD1$^{-/-}$ mice. Right, Quantification of p-AMPK. Values are the mean ± SD from 3 different experiments. **B**, Left, Western blot analysis of AMPK phosphorylation in cultured chondrocytes isolated from REDD1$^{+/+}$ and REDD1$^{-/-}$ mice and treated with aminoimidazole carboxamide ribonucleotide (AICAR) or vehicle for 24 hours. Right, Quantification of AMPK phosphorylation. Values are the mean ± SD from 3 different experiments. **C**, Quantitative polymerase chain reaction analysis of *Pgc1α* and *Tfam* expression in cultured chondrocytes isolated from REDD1$^{+/+}$ and REDD1$^{-/-}$ mice and treated with AICAR or vehicle for 24 hours. Values are the mean ± SD from 3 different experiments. **D**, Left, Western blot analysis of PGC-1α expression in cultured chondrocytes isolated from REDD1$^{+/+}$ and REDD1$^{-/-}$ mice and treated with AICAR or vehicle for 24 hours. Right, Quantification of PGC-1α expression. Values are the mean ± SD from 3 different experiments.

REDD1 deficiency reduces autophagy protein expression. The levels of 2 key autophagy proteins, LC3 and ATG-5, were significantly lower in the cartilage of 6-month-old REDD1$^{-/-}$ mice than wild-type mice (Figure 4A). No differences in LC3 or ATG-5 expression were seen in the medial meniscus (Figure 4B) or synovium (Supplementary Figure 2A, available on the *Arthritis & Rheumatology* web site at http://onlinelibrary.wiley.com/doi/10.1002/art.40104/abstract). In cultured primary chondrocytes, LC3 and ATG-5 messenger RNA (mRNA) levels were significantly lower in cells from REDD1$^{-/-}$ mice compared with wild-type cells (Figure 4C), and this effect was mimicked by siRNA-mediated REDD1 knockdown in human articular chondrocytes (Figure 4D), but it was not present in primary mouse synoviocytes (Supplementary Figure 2B). In addition, autophagy flux analysis by Western blotting revealed a significant reduction in LC3 processing and p62 protein levels in REDD1-deficient chondrocytes compared with wild-type cells under normal and stress conditions (Figure 4E). These results suggest that REDD1 is a key regulator of articular cartilage autophagy in vivo and in vitro.

REDD1 controls mitochondrial biogenesis through PGC-1α signaling. It has recently been reported that REDD1 deficiency results in accumulation of dysfunctional mitochondria (18). We measured the levels of mtDNA and nuclear DNA in the cartilage of REDD1$^{-/-}$ and wild-type mice to estimate the number of mitochondria. Surprisingly, whereas there was a significant increase in the ratio of mtDNA to nuclear DNA in the spleen and brain of mutant mice, consistent with previous reports (18), we found a marked reduction in mtDNA in the cartilage of REDD1$^{-/-}$ mice (Figure 5A), suggesting that REDD1 controls mitochondrial number in a tissue-specific manner. Moreover, REDD1$^{-/-}$ primary chondrocytes had significantly lower mtDNA content (Figure 5B), mitochondrial complex proteins (Figure 5C), and ATP levels (Figure 5D) than wild-type mouse cells.

These findings prompted us to investigate whether mitochondrial biogenesis was impaired in the absence of

REDD1. REDD1$^{-/-}$ mouse chondrocytes, but not synoviocytes, had significantly lower levels of mRNA for *Pgc1a* and *Tfam*, 2 key regulators of mitochondrial biogenesis (Figure 5E and Supplementary Figure 2C). PGC-1α protein levels were also reduced in chondrocytes from mutant mice (Figure 5F), but not in synoviocytes (Supplementary Figure 2D). In a similar manner, knockdown of REDD1 in cultured human articular chondrocytes resulted in a significant decrease in PGC-1α and TFAM mRNA and protein levels (Figures 5G and H). These data indicate that REDD1 controls mitochondrial biogenesis in articular chondrocytes through transcriptional regulation of PGC-1α and TFAM.

AMPK signaling is known to act upstream of PGC-1α to promote mitochondrial biogenesis and regulate energy metabolism (28). To elucidate whether AMPK signaling is involved in REDD1-induced PGC-1α expression, levels of p-AMPK were measured in cultured chondrocytes from REDD1$^{+/+}$ and REDD1$^{-/-}$ mice by Western blotting. Chondrocytes from mutant mice showed higher levels of p-AMPK than control cells (Figure 6A). Upon treatment with AICAR, p-AMPK levels were similar in REDD1$^{+/+}$ and REDD1$^{-/-}$ mouse chondrocytes (Figure 6B), indicating that REDD1 is not required for AMPK activation by AICAR. However, AMPK activation induced expression of PGC-1α and TFAM mRNA (Figure 6C) and protein levels (Figure 6D) in normal chondrocytes but not in REDD1-deficient cells. These findings suggest that REDD1 acts downstream of AMPK and is required for AMPK-mediated transcriptional control of PGC-1α.

DISCUSSION

The main finding of the present study is that REDD1 deficiency increases the severity of experimental OA in mice. Articular cartilage damage was more severe in REDD1$^{-/-}$ mice than in wild-type mice, and similar differences were observed in the synovium, meniscus, and subchondral bone. These findings are of particular relevance in the context of joint aging, since REDD1 expression is reduced in human and mouse cartilage (10) and in mouse meniscus and synovium with age.

Another important finding of this study is that cartilage cellularity in REDD1$^{-/-}$ mice was significantly reduced. Extensive death of chondrocytes is a hallmark of posttraumatic OA pathophysiology and is linked to tissue damage (29–31). After the initial injury that leads to disruption of the cartilage matrix and death of chondrocytes in the affected area, multiple factors are generated in response to the trauma that can contribute to the activation of apoptotic pathways, further extending the zone of chondrocyte death. These factors include inflammatory cytokines, ROS, nitric oxide, and various damage-associated molecular patterns (32,33).

Our data showed that REDD1 preserves chondrocyte viability in vivo and in vitro and supports the notion that this function of REDD1 partly mediates the effects of REDD1 in posttraumatic OA. While the precise molecular mechanisms underlying this function of REDD1 in cartilage remain to be entirely elucidated, our data support the role of REDD1 as an important survival factor against oxidative stress in chondrocytes by activating the expression of important antioxidant genes and protecting cells against apoptotic cell death. Consistent with this finding, it has been reported that a fraction of REDD1 is located in the mitochondria, and that mitochondrial localization is required for REDD1 to suppress mitochondrial ROS production (34). REDD1-deficient murine embryonic fibroblasts exhibit increased levels of ROS, and ectopic expression of REDD1 is sufficient to normalize cellular ROS production (34). Furthermore, treatment with antioxidant prevents hydrogen peroxide–induced apoptosis of human umbilical vein endothelial cells in a REDD1-dependent manner (35). Taken together, these findings highlight the role of REDD1 as a pivotal factor in the cellular defense mechanisms against oxidative stress.

Autophagy is an essential cellular process that maintains organismal homeostasis by degradation and turnover of the defective organelles within the cell. Mounting evidence supports the notion that autophagy is an important regulator of articular cartilage homeostasis and may play a key role in OA pathogenesis (5,12). REDD1 regulates autophagy in an mTOR-independent manner involving redox-dependent regulation of ATG-4B, a key enzyme in autophagosome assembly and maturation (18). In the absence of REDD1, ATG-4B activity is high and prevents the correct processing of LC3, thereby decreasing autophagic flux. In addition to our previous findings that REDD1 is essential for autophagy in articular chondrocytes (10), we showed in the present study that MAP1LC3 and ATG-5 expression is reduced in cartilage from REDD1$^{-/-}$ mice and in human chondrocytes with REDD1 knockdown, indicating that REDD1 also regulates autophagy at the transcriptional level. This finding sheds additional light on the mechanisms that regulate autophagy in cartilage and underscores the importance of REDD1 as a regulator of autophagy at multiple levels.

Mitochondrial dysfunction has been well characterized in OA chondrocytes (26,36–38), and alterations in mitochondrial biogenesis have recently been reported in OA (26). Emerging evidence suggests that REDD1 is a key regulator of mitochondrial integrity and oxidative capacity (39–41). REDD1$^{-/-}$ murine embryonic fibroblasts exhibited decreased basal oxygen consumption,

oxidative ATP generation, and maximal respiratory capacity (18). Modulation of mitochondrial biogenesis can also be tissue specific and might vary depending on the cell-specific metabolic state (42). We found large differences in the relative content of mtDNA in spleen, brain, and chondrocytes of REDD1$^{-/-}$ mice when compared with wild-type controls, suggesting that REDD1 functions in mitochondrial biogenesis may be tissue dependent.

Since cartilage is an avascular tissue with low oxygen tension (43), the role of hypoxia in controlling mitochondrial biogenesis might be particularly relevant to cartilage biology. The chief mediator of hypoxic response is the transcription factor hypoxia-inducible factor 1α (HIF-1α) (44). Although its role in mitochondrial biogenesis has not yet been studied in cartilage, HIF-1α has been reported to regulate mitochondrial biogenesis in adipose tissue (45), skeletal muscle (46), and neurons (47). Since REDD1 is induced by hypoxia in an HIF-1α–dependent manner (48) and basal REDD1 expression is high in articular cartilage under normal conditions, it could be hypothesized that the HIF-1α–REDD1 pathway is a regulator of mitochondrial biogenesis in cartilage. Based on this rationale, it is thus conceivable that the impact of REDD1 deficiency is more severe in articular cartilage than in other tissue.

In this study, we showed that articular chondrocytes from REDD1$^{-/-}$ mice have decreased mtDNA content, mitochondrial complex proteins, and ATP levels compared with wild-type littermates. Expression of PGC-1α and TFAM, two regulators of mitochondrial biogenesis, was significantly reduced in the absence of REDD1 in human and mouse chondrocytes, but not in mouse synoviocytes. Importantly, activation of the AMPK–PGC-1α pathway by AICAR required REDD1, which indicates that REDD1 acts downstream of AMPK to transcriptionally regulate PGC-1α expression (Supplementary Figure 3, available on the *Arthritis & Rheumatology* web site at http://onlinelibrary.wiley.com/doi/10.1002/art.40104/abstract). Thus, the present study provides a novel mechanism whereby REDD1 controls mitochondrial biogenesis in articular chondrocytes.

In summary, our study identifies REDD1 as a novel regulator of autophagy and mitochondrial biogenesis in articular chondrocytes and demonstrates that REDD1 deficiency increases the severity of experimental OA. The present results thus support the notion that the reduced REDD1 expression in human aging and OA-affected joints is a factor that contributes to OA progression and severity. These findings suggest that REDD1 is a central mediator of articular cartilage homeostasis and a potential target for the development of novel therapeutic strategies for OA.

ACKNOWLEDGMENTS

We thank Josan Chung, Stuart Duffy, and Lilo Creighton for technical assistance. We also thank Drs. Irina Budunova and Rubin Tuder for kindly providing the REDD1$^{-/-}$ mice.

AUTHOR CONTRIBUTIONS

All authors were involved in drafting the article or revising it critically for important intellectual content, and all authors approved the final version to be published. Dr. Lotz had full access to all of the data in the study and takes responsibility for the integrity of the data and the accuracy of the data analysis.

Study conception and design. Alvarez-Garcia, Kelly, Lotz.
Acquisition of data. Alvarez-Garcia, Matsuzaki, Olmer, Plate.
Analysis and interpretation of data. Alvarez-Garcia, Matsuzaki, Lotz.

REFERENCES

1. Hunter DJ, Schofield D, Callander E. The individual and socioeconomic impact of osteoarthritis. Nat Rev Rheumatol 2014;10:437–41.
2. Loeser RF, Goldring SR, Scanzello CR, Goldring MB. Osteoarthritis: a disease of the joint as an organ. Arthritis Rheum 2012;64:1697–707.
3. Lotz M, Loeser RF. Effects of aging on articular cartilage homeostasis. Bone 2012;51:241–8.
4. Choi AM, Ryter SW, Levine B. Autophagy in human health and disease. N Engl J Med 2013;368:1845–6.
5. Carames B, Taniguchi N, Otsuki S, Blanco FJ, Lotz M. Autophagy is a protective mechanism in normal cartilage, and its aging-related loss is linked with cell death and osteoarthritis. Arthritis Rheum 2010;62:791–801.
6. Laplante M, Sabatini DM. mTOR signaling in growth control and disease. Cell 2012;149:274–93.
7. Terkeltaub R, Yang B, Lotz M, Liu-Bryan R. Chondrocyte AMP-activated protein kinase activity suppresses matrix degradation responses to proinflammatory cytokines interleukin-1β and tumor necrosis factor α. Arthritis Rheum 2011;63:1928–37.
8. Akasaki Y, Alvarez-Garcia O, Saito M, Caramés B, Iwamoto Y, Lotz MK. FoxO transcription factors support oxidative stress resistance in human chondrocytes. Arthritis Rheumatol 2014;66:3349–58.
9. Akasaki Y, Hasegawa A, Saito M, Asahara H, Iwamoto Y, Lotz MK. Dysregulated FOXO transcription factors in articular cartilage in aging and osteoarthritis. Osteoarthritis Cartilage 2014;22:162–70.
10. Alvarez-Garcia O, Olmer M, Akagi R, Akasaki Y, Fisch KM, Shen T, et al. Suppression of REDD1 in osteoarthritis cartilage, a novel mechanism for dysregulated mTOR signaling and defective autophagy. Osteoarthritis Cartilage 2016;24:1639–47.
11. Zhang Y, Vasheghani F, Li YH, Blati M, Simeone K, Fahmi H, et al. Cartilage-specific deletion of mTOR upregulates autophagy and protects mice from osteoarthritis. Ann Rheum Dis 2015;74:1432–40.
12. Carames B, Hasegawa A, Taniguchi N, Miyaki S, Blanco FJ, Lotz M. Autophagy activation by rapamycin reduces severity of experimental osteoarthritis. Ann Rheum Dis 2012;71:575–81.
13. Ellisen LW, Ramsayer KD, Johannessen CM, Yang A, Beppu H, Minda K, et al. REDD1, a developmentally regulated transcriptional target of p63 and p53, links p63 to regulation of reactive oxygen species. Mol Cell 2002;10:995–1005.
14. Shoshani T, Faerman A, Mett I, Zelin E, Tenne T, Gorodin S, et al. Identification of a novel hypoxia-inducible factor 1-responsive gene, RTP801, involved in apoptosis. Mol Cell Biol 2002;22:2283–93.
15. Brugarolas J, Lei K, Hurley RL, Manning BD, Reiling JH, Hafen E, et al. Regulation of mTOR function in response to

hypoxia by REDD1 and the TSC1/TSC2 tumor suppressor complex. Genes Dev 2004;18:2893–904.
16. Corradetti MN, Inoki K, Guan KL. The stress-inducted proteins RTP801 and RTP801L are negative regulators of the mammalian target of rapamycin pathway. J Biol Chem 2005;280: 9769–72.
17. DeYoung MP, Horak P, Sofer A, Sgroi D, Ellisen LW. Hypoxia regulates TSC1/2-mTOR signaling and tumor suppression through REDD1-mediated 14-3-3 shuttling. Genes Dev 2008;22: 239–51.
18. Qiao S, Dennis M, Song X, Vadysirisack DD, Salunke D, Nash Z, et al. A REDD1/TXNIP pro-oxidant complex regulates ATG4B activity to control stress-induced autophagy and sustain exercise capacity. Nat Commun 2015;6:7014.
19. Brafman A, Mett I, Shafir M, Gottlieb H, Damari G, Gozlan-Kelner S, et al. Inhibition of oxygen-induced retinopathy in RTP801-deficient mice. Invest Ophthalmol Vis Sci 2004;45: 3796–805.
20. Glasson SS, Blanchet TJ, Morris EA. The surgical destabilization of the medial meniscus (DMM) model of osteoarthritis in the 129/SvEv mouse. Osteoarthritis Cartilage 2007;15:1061–9.
21. Glasson SS, Chambers MG, van den Berg WB, Little CB. The OARSI histopathology initiative: recommendations for histological assessments of osteoarthritis in the mouse. Osteoarthritis Cartilage 2010;18 Suppl 3:S17–23.
22. Krenn V, Morawietz L, Haupl T, Neidel J, Petersen I, Konig A. Grading of chronic synovitis: a histopathological grading system for molecular and diagnostic pathology. Pathol Res Pract 2002; 198:317–25.
23. Kwok J, Onuma H, Olmer M, Lotz MK, Grogan SP, D'Lima DD. Histopathological analyses of murine menisci: implications for joint aging and osteoarthritis. Osteoarthritis Cartilage 2016; 24:709–18.
24. Caramés B, Olmer M, Kiosses WB, Lotz MK. The relationship of autophagy defects to cartilage damage during joint aging in a mouse model. Arthritis Rheumatol 2015;67:1568–76.
25. Gosset M, Berenbaum F, Thirion S, Jacques C. Primary culture and phenotyping of murine chondrocytes. Nat Protoc 2008;3: 1253–60.
26. Wang Y, Zhao X, Lotz M, Terkeltaub R, Liu-Bryan R. Mitochondrial biogenesis is impaired in osteoarthritis chondrocytes but reversible via peroxisome proliferator–activated receptor γ coactivator 1α. Arthritis Rheumatol 2015;67:2141–53.
27. Olson SA, Horne P, Furman B, Huebner J, Al-Rashid M, Kraus VB, et al. The role of cytokines in posttraumatic arthritis. J Am Acad Orthop Surg 2014;22:29–37.
28. Liang H, Ward WF. PGC-1α: a key regulator of energy metabolism. Adv Physiol Educ 2006;30:145–51.
29. Borrelli J Jr. Chondrocyte apoptosis and posttraumatic arthrosis. J Orthop Trauma 2006;20:726–31.
30. Buckwalter JA, Brown TD. Joint injury, repair, and remodeling: roles in post-traumatic osteoarthritis. Clin Orthop Relat Res 2004:7–16.
31. Furman BD, Olson SA, Guilak F. The development of posttraumatic arthritis after articular fracture. J Orthop Trauma 2006;20: 719–25.
32. Lieberthal J, Sambamurthy N, Scanzello CR. Inflammation in joint injury and post-traumatic osteoarthritis. Osteoarthritis Cartilage 2015;23:1825–34.
33. Martin JA, Buckwalter JA. Post-traumatic osteoarthritis: the role of stress induced chondrocyte damage. Biorheology 2006;43:517–21.
34. Horak P, Crawford AR, Vadysirisack DD, Nash ZM, DeYoung MP, Sgroi D, et al. Negative feedback control of HIF-1 through REDD1-regulated ROS suppresses tumorigenesis. Proc Natl Acad Sci U S A 2010;107:4675–80.
35. Xu MC, Shi HM, Wang H, Gao XF. Salidroside protects against hydrogen peroxide-induced injury in HUVECs via the regulation of REDD1 and mTOR activation. Mol Med Rep 2013;8:147–53.
36. Blanco FJ, Rego I, Ruiz-Romero C. The role of mitochondria in osteoarthritis. Nat Rev Rheumatol 2011;7:161–9.
37. Coleman MC, Ramakrishnan PS, Brouillette MJ, Martin JA. Injurious loading of articular cartilage compromises chondrocyte respiratory function. Arthritis Rheumatol 2016;68:662–71.
38. Lane RS, Fu Y, Matsuzaki S, Kinter M, Humphries KM, Griffin TM. Mitochondrial respiration and redox coupling in articular chondrocytes. Arthritis Res Ther 2015;17:54.
39. Lipina C, Hundal HS. Is REDD1 a metabolic éminence grise? Trends Endocrinol Metab 2016;27:868–80.
40. Regazzetti C, Dumas K, Le Marchand-Brustel Y, Peraldi P, Tanti JF, Giorgetti-Peraldi S. Regulated in development and DNA damage responses -1 (REDD1) protein contributes to insulin signaling pathway in adipocytes. PloS One 2012;7:e52154.
41. Dungan CM, Wright DC, Williamson DL. Lack of REDD1 reduces whole body glucose and insulin tolerance, and impairs skeletal muscle insulin signaling. Biochem Biophys Res Commun 2014;453:778–83.
42. Wenz T. Regulation of mitochondrial biogenesis and PGC-1α under cellular stress. Mitochondrion 2013;13:134–42.
43. Schipani E, Ryan HE, Didrickson S, Kobayashi T, Knight M, Johnson RS. Hypoxia in cartilage: HIF-1α is essential for chondrocyte growth arrest and survival. Genes Dev 2001;15:2865–76.
44. Semenza GL, Wang GL. A nuclear factor induced by hypoxia via de novo protein synthesis binds to the human erythropoietin gene enhancer at a site required for transcriptional activation. Mol Cell Biol 1992;12:5447–54.
45. Zhang X, Lam KS, Ye H, Chung SK, Zhou M, Wang Y, et al. Adipose tissue-specific inhibition of hypoxia-inducible factor 1α induces obesity and glucose intolerance by impeding energy expenditure in mice. J Biol Chem 2010;285:32869–77.
46. O'Hagan KA, Cocchiglia S, Zhdanov AV, Tambuwala MM, Cummins EP, Monfared M, et al. PGC-1α is coupled to HIF-1α–dependent gene expression by increasing mitochondrial oxygen consumption in skeletal muscle cells. Proc Natl Acad Sci U S A 2009;106:2188–93.
47. Zhao J, Li L, Pei Z, Li C, Wei H, Zhang B, et al. Peroxisome proliferator activated receptor (PPAR)-γ co-activator 1-α and hypoxia induced factor-1α mediate neuro- and vascular protection by hypoxic preconditioning in vitro. Brain Res 2012;1447:1–8.
48. Schwarzer R, Tondera D, Arnold W, Giese K, Klippel A, Kaufmann J. REDD1 integrates hypoxia-mediated survival signaling downstream of phosphatidylinositol 3-kinase. Oncogene 2005;24:1138–49.

ARTHRITIS & RHEUMATOLOGY
Vol. 69, No. 7, July 2017, pp 1429–1439
DOI 10.1002/art.40118

Chemogenetic Inhibition of Pain Neurons in a Mouse Model of Osteoarthritis

Rachel E. Miller,[1] Shingo Ishihara,[1] Bula Bhattacharyya,[2] Ada Delaney,[1] Daniela M. Menichella,[2] Richard J. Miller,[2] and Anne-Marie Malfait[1]

Objective. **To determine the ability of drugs that activate inhibitory G protein–coupled receptors (GPCRs) expressed in peripheral voltage-gated sodium channel 1.8 ($Na_V1.8$)–positive sensory neurons to control osteoarthritis (OA)–associated pain.**

Methods. **We used designer receptors exclusively activated by a designer drug (DREADD) technology, which employs engineered GPCRs to activate or inhibit neurons upon binding the synthetic ligand clozapine *N*-oxide (CNO). $Na_V1.8$-Pdi C57BL/6 mice were generated to express the inhibitory DREADD receptor Pdi in $Na_V1.8$-expressing sensory neurons. Destabilization of the medial meniscus (DMM) surgery was performed in 10-week-old male mice. Four, 8, 12, or 16 weeks after surgery, knee hyperalgesia or hind paw mechanical allodynia was tested. Subsequently, CNO or vehicle was administered, and the effect on pain-related behaviors was measured by a blinded observer. Morphine was used as a control.**

Results. **Immunohistochemistry and electrophysiology confirmed functional expression of the inhibitory DREADD receptor Pdi by $Na_V1.8$-positive sensory neurons. Acute inhibition of $Na_V1.8$-expressing neurons in mice treated with CNO reduced knee hyperalgesia 4 weeks after DMM surgery and reduced mechanical allodynia 8 weeks after DMM surgery. Inhibition had no effect on pain-related behaviors 12 and 16 weeks after DMM surgery. Morphine, a drug that activates GPCRs in the peripheral and central nervous systems, was still effective in the later stage of experimental OA.**

Conclusion. **Chemogenetic inhibition of $Na_V1.8$-expressing neurons blocks knee hyperalgesia and mechanical allodynia in early experimental OA, but is no longer efficacious in the later stages. These data indicate that activation of inhibitory GPCRs located solely outside the central nervous system may be ineffective in treating chronic OA pain.**

Pain is one of the most debilitating symptoms associated with progressive osteoarthritis (OA), yet few options exist for efficacious treatment of chronic OA pain. Conventional treatment options for OA pain rely mainly on nonsteroidal antiinflammatory drugs (NSAIDs) (1,2), but these drugs are only moderately effective and are associated with serious long-term risks (3). The development of more efficacious and safer pharmacologic therapies will depend on gaining a better understanding of the basic mechanisms that underlie OA pain.

G protein–coupled receptors (GPCRs) constitute one of the largest groups of drug targets, with an estimated 30–40% of approved drugs targeting these receptors (4). Drugs such as opioids produce analgesic effects in a wide variety of circumstances by activating opioid receptors, which are GPCRs coupled to inhibitory $G_{i/o}$ proteins (5). $G_{i/o}$ proteins then cause downstream signaling, resulting in reduced nerve excitability and inhibition of neurotransmission (5). As such, opioids have been recommended as an alternative for treating OA pain when NSAIDs are ineffective (1,2). These and other inhibitory GPCRs, such as the cannabinoid receptors, are localized both peripherally on nociceptive neurons in the dorsal root ganglion (DRG) (6) and in the central nervous system (CNS), at several different levels of the neuraxis (5–7). Because the psychoactive, respiratory, and gastrointestinal side effects associated

Dr. R. E. Miller's work was supported by grants F32-AR-062927 and K01-AR-070328 from the National Institute of Arthritis and Musculoskeletal and Skin Diseases (NIAMS), NIH. Dr. R. J. Miller's work was supported by grant R01-AR-064251 from NIAMS. Dr. Malfait's work was supported by grants R01-AR-064251 and R01-AR-060364 from NIAMS.

[1]Rachel E. Miller, PhD, Shingo Ishihara, MS, Ada Delaney, PhD, Anne-Marie Malfait, MD, PhD: Rush University Medical Center, Chicago, Illinois; [2]Bula Bhattacharyya, PhD, Daniela M. Menichella, MD, Richard J. Miller, PhD: Northwestern University, Chicago, Illinois.

Address correspondence to Anne-Marie Malfait, MD, PhD, Rush University Medical Center, 1611 West Harrison Street, Suite 510, Chicago, IL 60612. E-mail: anne-marie_malfait@rush.edu.

Submitted for publication October 18, 2016; accepted in revised form March 30, 2017.

with many of the drugs that target inhibitory GPCRs are mediated by the CNS (5,8–10), there have been efforts to produce agonists that do not enter the CNS and that selectively activate peripheral receptors. Indeed, a recent study using a conditional knockout mouse approach supports this idea by demonstrating that removing peripheral neuron expression of the μ-opioid receptor reduces, but does not abolish, the analgesic effectiveness of morphine in a model of inflammatory pain (11). However, the effectiveness of peripheral activation of opioid, cannabinoid, or other novel inhibitory GPCR targets in the production of analgesia remains to be fully tested in the context of a specific disease (9,12).

A potentially important factor to be considered in the design of novel OA pain therapeutics is the long-term and variable nature of the disease. Pain experienced in association with OA has been characterized qualitatively and may be classified by 3 main stages (13). In early OA, pain is associated with high-impact activity. As disease progresses, low-impact activities such as walking and climbing stairs become painful. Finally, late-stage OA is characterized by chronic pain accompanied by acute, unpredictable pain episodes (13). This chronic OA pain differs from other types of chronic pain since the tissue injury never resolves (14). It is unclear whether targeting inhibitory GPCRs solely localized in the periphery may be analgesic in these different stages.

The chronic disease course of OA can be recapitulated in mice by surgical destabilization of the medial meniscus (DMM) (15), which induces a mild instability in the knee and results in joint damage that develops slowly over the course of 16 weeks or longer (16–18). By 2–4 weeks after DMM surgery, mild cartilage lesions, subchondral bone sclerosis, and osteophytes are evident (15,19–21), while synovitis has recently been reported to peak during this time as well (16). As the disease progresses, cartilage lesions worsen, osteophytes mature, and synovitis resolves, but not completely (16,22). We and others have shown that mice develop pain-related behaviors associated with this progressive joint damage, with each behavior developing on a unique time course. Mechanical allodynia in the ipsilateral hind paw appears by week 4 after DMM (but not sham) surgery and is maintained through 16 weeks (17,23–25). Herein we describe another measure of sensitivity, hyperalgesia of the knee, which is more strongly associated with the early stage of disease prior to 8 weeks. Previous studies in other OA models have used vocalization in response to pressure applied to the knee by hand as a means of assessing knee hyperalgesia (26,27); in the present study, we used a device previously validated in models of inflammatory arthritis (28,29) to apply a range of forces to the knee in order to determine a quantitative withdrawal threshold. Decreases in locomotive behaviors (distance traveled, climbing, rearing) (17,30), changes in gait (31), and decreases in weight bearing on the operated limb (30) only develop with the onset of moderate-to-severe joint damage (>8 weeks after surgery).

One way of investigating whether inhibitory GPCRs on peripheral neurons can be targeted to modulate these pain-related behaviors at different stages of the DMM model is through chemogenetic procedures. The most widely used chemogenetic approach is a platform termed designer receptors exclusively activated by designer drugs (DREADD) (32). DREADD technology uses engineered GPCRs to activate or inhibit neurons based on the binding of synthetic chemicals (for review, see ref. 33). In the present study, we used a neuronal inhibitory DREADD based on an engineered M_4 muscarinic acetylcholine receptor, which exerts its effects through activation of the inhibitory $G_{i/o}$ protein pathway (32). Activation of the engineered receptor (termed Pdi) with the synthetic chemical agonist clozapine *N*-oxide (CNO) has been shown to inhibit neuronal activity (34), mimicking the actions of analgesics that target this inhibitory GPCR pathway. In order to genetically target expression of this engineered Pdi receptor to the peripheral nervous system, we used voltage-gated sodium channel 1.8 ($Na_V1.8$) as a marker, since this channel is expressed by a large subset of sensory neurons in the DRG (35). Approximately 75% of DRG sensory neurons have been shown to express $Na_V1.8$, which includes >90% of C-fiber nociceptors (pain-sensing neurons) and C-fiber low-threshold mechanoreceptors, as well as a lower percentage of Aδ-fiber nociceptors and Aβ-fiber afferents (35). Previous studies in experimental models of OA have shown the $Na_V1.8$ channel itself to be important for the transmission of nociceptive information at both the peripheral (36) and central (37) levels.

The overall aim of this study was to examine the analgesic effects of peripheral activation of inhibitory GPCRs on pain-related behaviors at different stages after DMM surgery, using novel $Na_V1.8$-Pdi mice. We focused on two pain-related behaviors, knee hyperalgesia and mechanical allodynia in the hind paw. Findings were compared to analgesia produced by morphine, a commonly used opioid for pain management, which exerts its effects through activation of inhibitory GPCRs in both the peripheral nervous system and CNS (5).

MATERIALS AND METHODS

Animals. A total of 91 mice were used. All animal experiments were approved by the Institutional Animal Care and

Use Committees at Rush University Medical Center and Northwestern University. Animals were housed with food and water ad libitum and kept on 12-hour light cycles. $Na_V1.8$-Cre and $Na_V1.8$-Cre-TdTomato mice were obtained as a gift from Dr. John Wood (University College London, London, UK) (on the C57BL/6 background) (35,38); hM_4Di-loxP mice in which the hM_4Di (inhibitory DREADD receptor) had also been tagged with a human influenza hemagglutinin (HA) epitope (HA tag) (termed Pdi mice) were obtained as a gift from Dr. Susan Dymecki (Harvard Medical School, Boston, MA) (on the C57BL/6 background) (34). Dr. Dymecki's laboratory has previously characterized these mice and verified that CNO suppressed action potential firing in neurons expressing Pdi (34). $Na_V1.8$-Cre or $Na_V1.8$-Cre-TdTomato mice were crossed with Pdi mice in order to generate $Na_V1.8$-Pdi or $Na_V1.8$-TdTomato-Pdi mice. All experiments used mice heterogeneous for both $Na_V1.8$ and Pdi.

Surgery. DMM surgery was performed in the right knee of 10-week-old male mice (25–30 gm) under isoflurane anesthesia, as previously described (15,17). Briefly, after medial parapatellar arthrotomy, the anterior fat pad was dissected to expose the anterior medial meniscotibial ligament, which was severed. The knee was flushed with saline and the incision was closed. Sham surgery followed the same procedure to expose the anterior medial meniscotibial ligament, but the ligament was left intact. Mice were not administered analgesia after surgery.

Knee hyperalgesia. Knee hyperalgesia was measured using a Pressure Application Measurement (PAM) device (Ugo Basile) by adapting the methods previously established by Barton et al (28) and Leuchtweis et al (29). Mice were manually restrained, and the hind paw was lightly pinned with a finger in order to hold the knee in flexion at a similar angle for each mouse. With the knee in flexion, the PAM transducer was pressed against the medial side of the ipsilateral knee while the operator's thumb lightly held the lateral side of the knee. The PAM software guided the user to apply an increasing amount of force at a constant rate (30 gm/second), up to a maximum of 450 gm. If the mouse tried to withdraw its knee, the force at which this occurred was recorded. If the mouse did not try to withdraw, the maximum possible force of 450 gm was assigned. Two measurements were obtained per knee, and the withdrawal force data were averaged. Knee hyperalgesia was assessed before surgery and at weeks 2, 4, 8, 12, and 16 after sham surgery (n = 6–7 mice per time point) or DMM surgery (n = 6–8 mice per time point) in wild-type (WT) mice. Four weeks after DMM surgery, a second set of WT mice was tested using morphine (10 mg/kg using 10 mg/ml morphine in saline, subcutaneously [SC]) (Rush University pharmacy) (n = 4) or vehicle (saline) (n = 5) to establish that knee hyperalgesia was a pain-related behavior. Finally, knee hyperalgesia was assessed before surgery and at weeks 4, 8, 12, and 16 after DMM surgery in $Na_V1.8$-Pdi mice. In all cases, the assessor (SI) was blinded to the experimental groups.

Mechanical allodynia. $Na_V1.8$-Pdi mice were tested for secondary mechanical allodynia of the ipsilateral hind paw using von Frey filaments and the up-down staircase method, as previously described (17). Withdrawal thresholds were assessed before surgery and weeks 4, 8, 12, and 16 after DMM surgery or 4 and 8 weeks after sham surgery.

Drug administration. CNO (10 mg/kg in saline, intraperitoneally; Sigma-Aldrich) or vehicle (phosphate buffered saline [PBS]) was administered to test the effect of neuronal inhibition on knee hyperalgesia or mechanical allodynia in $Na_V1.8$-Pdi mice (n = 6–7 receiving vehicle, n = 6–7 receiving CNO). At each time point, $Na_V1.8$-Pdi mice were tested for mechanical allodynia, allowed to rest for 2 days, and then tested for knee hyperalgesia. Between tests, treatment of mice was alternated between vehicle and CNO. A separate set of $Na_V1.8$-Pdi mice was tested for mechanical allodynia for the first time 16 weeks after DMM surgery (n = 2 receiving vehicle, n = 2 receiving CNO). Morphine (10 mg/kg in saline, SC) or vehicle (saline) was used to test reversibility of knee hyperalgesia (n = 6 receiving morphine, n = 6 receiving saline) or mechanical allodynia (n = 4 receiving morphine, n = 4 receiving saline) in the late stage of the DMM model (>12 weeks after surgery) in WT mice. Behaviors were tested 2 hours prior to injection and at the indicated times after injection by a blinded observer (SI or REM).

Histopathology of the knee. Sixteen weeks after sham surgery (n = 11 WT mice, n = 8 $Na_V1.8$-Pdi mice) or DMM surgery (n = 10 WT mice, n = 8 $Na_V1.8$-Pdi mice), histopathology of the knee was evaluated by Dr. Alison Bendele (Bolder BioPATH) based on modified Osteoarthritis Research Society International recommendations, as previously described (21,39). Joints were fixed in 10% formalin, decalcified, embedded in the frontal plane, sectioned (8 μm), and stained with toluidine blue (0.04% weight/volume). A section from the mid-joint (area of maximal damage [15]) was used to score the medial femoral condyles and tibial plateaus for severity of cartilage degeneration. For each cartilage surface, scores were assigned individually to each of 3 zones (inner, middle, outer) on a scale of 0–5, with 5 representing the most damage (maximal summed score of 30 for femoral plus tibial cartilage degeneration). The largest osteophyte (medial tibia or femur) was measured using an ocular micrometer.

Immunofluorescence. For DRG analyses, naive $Na_V1.8$-Pdi male mice age >10 weeks (n = 3) were used. For spinal cord analyses, naive $Na_V1.8$-Pdi (n = 3) or $Na_V1.8$-TdTomato reporter (n = 3) male and female mice age >10 weeks were used. Mice were anesthetized with ketamine and xylazine, killed, and perfused transcardially with PBS followed by 4% paraformaldehyde in PBS. The spinal column was dissected and postfixed in 4% paraformaldehyde overnight followed by cryopreservation in 30% sucrose in PBS. Individual L3–L5 DRGs or corresponding levels of the spinal cord were embedded in OCT compound (Tissue-Tek), frozen with dry ice, and cut into 12-μm (DRG) or 20-μm (spinal cord) sections. DRG sections were stained with the primary antibodies anti-$Na_V1.8$ (1:250 dilution, no. 75-166; Antibodies Incorporated) and anti–HA tag (1:250 dilution, no. 3724S; Cell Signaling Technology). Spinal cord sections were stained with anti–HA tag primary antibody and DAPI. A no-primary control was included to confirm specificity. Isotype-specific Alexa Fluor 405–, Alexa Fluor 488–, or Alexa Fluor 633–conjugated secondary antibodies (1:300 dilution; Invitrogen) were used. Images were captured using an Olympus FV10i confocal microscope, and images were adjusted using Olympus software to the brightness and contrast needed to reflect true colors.

Electrophysiology. Electrophysiologic recording from cultured DRG neurons isolated from naive $Na_V1.8$-TdTomato-Pdi mice was performed using current clamp recordings employing patch electrodes with a resistance of 5–7 MΩ filled with 140 m*M* KCl, 0.5 m*M* EGTA, 5 m*M* HEPES, and 3 m*M* Mg-ATP, pH 7.3 (300 mOsm). Action potentials were evoked from (≤25-mm diameter) $Na_V1.8$-positive neurons by using 700-msec depolarizing current (1×, 2×, or 3×) injections from the resting membrane potential (approximately −55 mV) before or after application of CNO (2.5 μM). Control experiments were performed in the presence of pertussis toxin (1 μg/ml overnight).

Statistical analysis. For mechanical allodynia data, paw withdrawal thresholds were log-transformed prior to further analyses (40). For mechanical allodynia and knee hyperalgesia analgesic time courses, a repeated-measures two-way analysis of variance (ANOVA) with Bonferroni post tests was used to compare mice treated with vehicle to mice treated with a particular drug at each time point. For knee hyperalgesia time courses in WT mice, a two-way ANOVA with Bonferroni post tests was used to compare responses of sham-operated and DMM-operated mice at each time point. For knee histopathology and electrophysiology, data were analyzed using the Mann-Whitney test. All analyses were carried out using GraphPad Prism software version 6.07 for Windows. Results are presented as the mean ± SEM.

RESULTS

$Na_V1.8$-Pdi mice express functional DREADD receptors in $Na_V1.8$-expressing neurons. In order to ascertain that the DREADD receptor was expressed in $Na_V1.8$-expressing neurons in $Na_V1.8$-Pdi mice, immunofluorescence was performed in L3–L5 DRGs obtained from naive $Na_V1.8$-Pdi mice (n = 3). As anticipated, nearly all (>90%) $Na_V1.8$-expressing neurons also stained for the DREADD receptor; no expression of the DREADD receptor was detected in non–$Na_V1.8$-expressing neurons (representative images shown in Figure 1A). Colocalization of $Na_V1.8$ and Pdi was observed in small- to medium-diameter neurons (83–600 μm^2), consistent with the expected size of $Na_V1.8$-expressing neurons (35). Interestingly, no DREADD expression was observed in the dorsal horn of the spinal cord (Figure 1B) in the area where nociceptive DRG neurons, including $Na_V1.8$-expressing neurons, terminate (Figure 1C). This was presumably due to the lack of an axonal targeting motif in the DREADD used in these experiments (41).

In order to confirm that the DREADD receptors were functional, patch-clamp electrophysiology was performed on cultured DRG cells from $Na_V1.8$-Pdi mice in

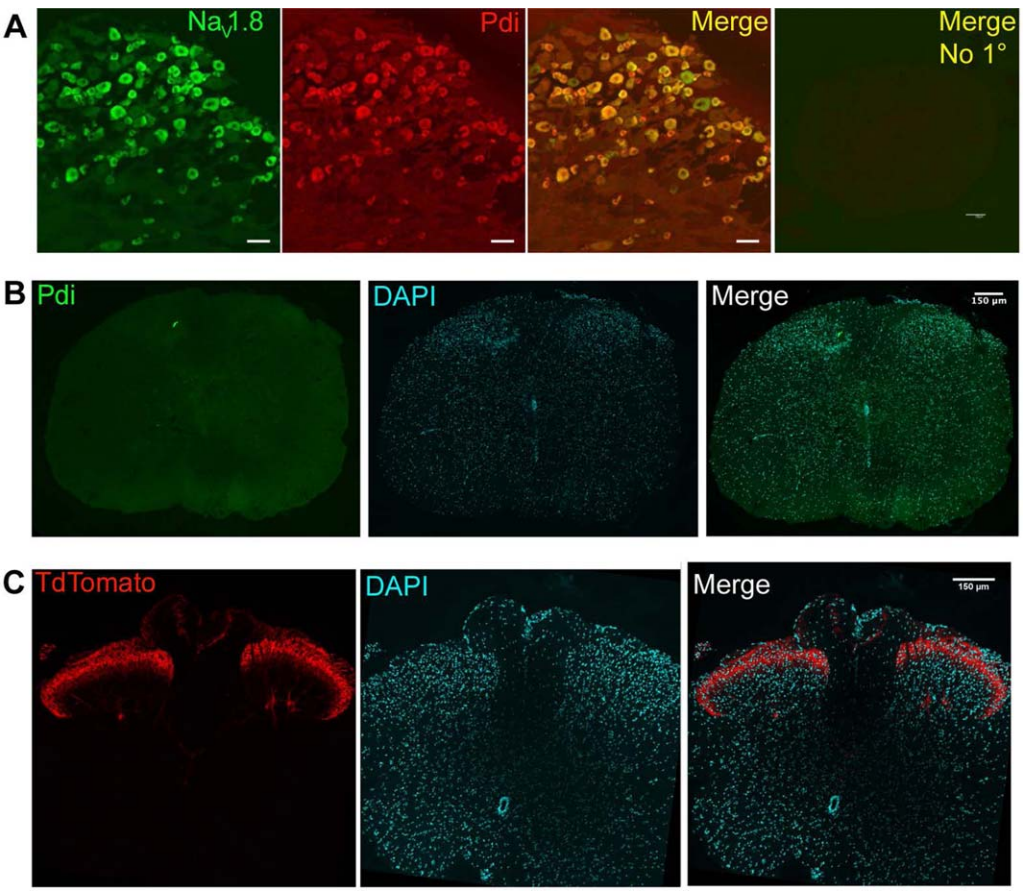

Figure 1. The inhibitory receptor Pdi, which was engineered with designer receptors exclusively activated by designer drugs technology, is expressed in dorsal root ganglion (DRG) neurons expressing voltage-gated sodium channel 1.8 ($Na_V1.8$), but not in the spinal cord. **A,** Representative immunohistochemical images for $Na_V1.8$ and human influenza hemagglutinin (HA) epitope tag (HA tag) (Pdi) in DRG L3–L5 sections obtained from naive $Na_V1.8$-Pdi mice (n = 3). Merge No 1° = no primary antibody. Bars = 50 μm. **B,** Representative immunohistochemical images for HA tag (Pdi) in spinal cord L3–L5 sections obtained from naive $Na_V1.8$-Pdi mice (n = 3). Bar = 150 μm. **C,** Representative immunohistochemical images showing $Na_V1.8$ expression in spinal cord L3–L5 sections obtained from naive $Na_V1.8$-TdTomato reporter mice (n = 3). Bar = 150 μm.

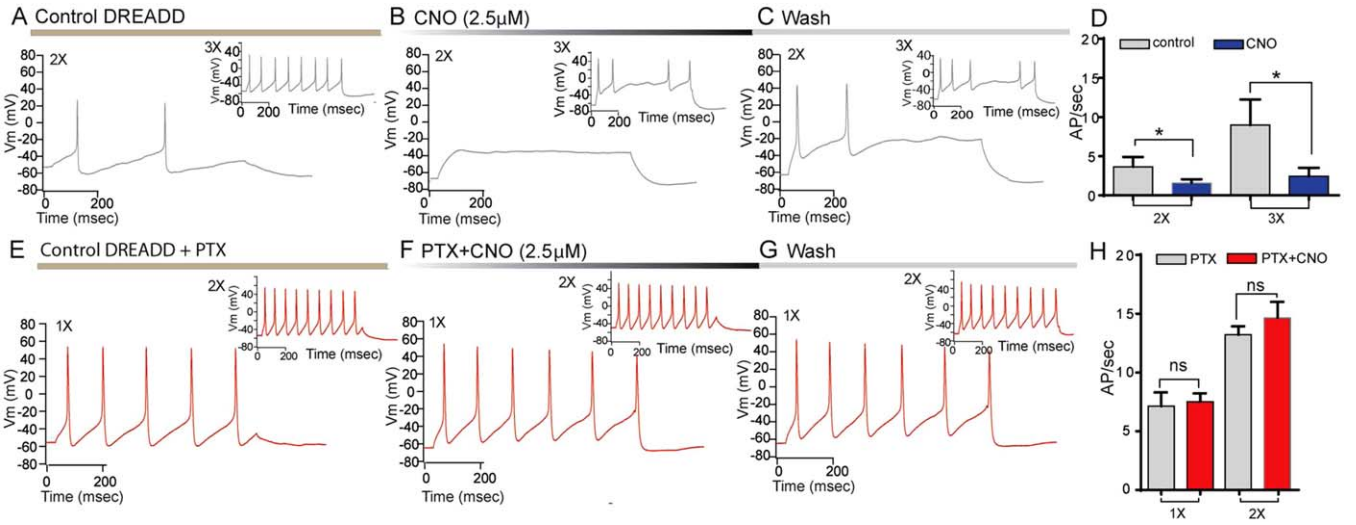

Figure 2. The inhibitory receptor Pdi, which was engineered with designer receptors exclusively activated by designer drugs (DREADD) technology, is functional. **A,** Representative trace showing action potentials (APs) induced by 2× and 3× threshold current injection in an untreated naive neuron cultured from a voltage-gated sodium channel 1.8 ($Na_V1.8$)–TdTomato-Pdi mouse. **B,** Representative trace showing APs induced by 2× and 3× threshold current injection blocked by pretreatment with clozapine *N*-oxide (CNO). **C,** Representative trace showing restoration of APs following a 5-minute wash period. **D,** Reduced frequency of APs after CNO treatment (>7 neurons per group). Values are the mean ± SEM. * = $P < 0.05$. **E,** Representative trace showing APs induced by 1× and 2× threshold current injection in an untreated naive neuron cultured from a $Na_V1.8$-TdTomato-Pdi mouse pretreated overnight with 1 μg/ml pertussis toxin (PTX). **F,** Representative trace showing effects of CNO blocked by pretreatment with pertussis toxin. **G,** Representative trace showing no effect of washing on results in **F**. **H,** No effect on frequency of APs by CNO treatment in the presence of pertussis toxin (4 neurons per group). Values are the mean ± SEM. Vm = membrane potential; NS = not significant. Color figure can be viewed in the online issue, which is available at http://onlinelibrary.wiley.com/doi/10.1002/art.40118/abstract.

which $Na_V1.8$-expressing cells were labeled with a Tomato reporter. Injection of current induced a series of action potentials in $Na_V1.8$-expressing DRG neurons (Figure 2A). When neurons were incubated with CNO, action potential generation in $Na_V1.8$-expressing neurons was suppressed and the rheobase (the amount of current required to elicit an action potential) was increased, indicating that the DREADD receptors were functional (Figures 2B and D); washing restored functionality of the neurons (Figure 2C). The effects of CNO were not observed if DREADD-expressing neurons were incubated overnight with pertussis toxin, indicating that the effects were mediated by DREADD-activated $G_{i/o}$ signaling (Figures 2E–H). Addition of CNO had no effect on the behavior of neurons cultured from WT, non–DREADD-expressing mice (data not shown).

Chemogenetic inhibition of $Na_V1.8$-expressing neurons reverses hind paw mechanical allodynia 8 weeks after DMM surgery, but not at later time points. We have previously demonstrated that WT mice develop mechanical allodynia by 4 weeks after DMM surgery and maintain this allodynia through 16 weeks (17,21,25). Sham-operated mice develop initial mechanical allodynia that resolves by 8 weeks after surgery (17). Likewise, $Na_V1.8$-Pdi mice displayed a baseline 50% withdrawal threshold of 0.64 ± 0.05 gm prior to surgery, developed mechanical allodynia by 4 weeks after DMM surgery (50% withdrawal threshold of 0.03 ± 0.004 gm), and maintained the same level of allodynia through week 16 (0-hour time points in Figure 3). Sham surgery induced some initial mechanical allodynia in $Na_V1.8$-Pdi mice 4 weeks after surgery (50% withdrawal threshold of 0.14 ± 0.03 gm; n = 5) ($P = 0.0001$ versus before surgery) that resolved by 8 weeks after surgery (50% withdrawal threshold of 0.45 ± 0.05 gm) ($P = 0.41$ versus before surgery), as in WT mice. Histology performed 16 weeks after DMM surgery confirmed that $Na_V1.8$-Pdi mice developed similar levels of cartilage degeneration ($P = 0.50$) (see Supplementary Figure 1A, available on the *Arthritis & Rheumatology* web site at http://onlinelibrary.wiley.com/doi/10.1002/art.40118/abstract) and osteophytes ($P = 0.32$) (Supplementary Figure 1B) in the medial knee compartment compared to WT mice, while sham surgery did not cause joint damage (Supplementary Figure 1).

Administering CNO to $Na_V1.8$-Pdi mice 4 weeks after DMM surgery partially inhibited mechanical allodynia for 1 hour ($P = 0.09$) (Figure 3A). Administering CNO to mice 8 weeks after DMM surgery had a more robust effect on mechanical allodynia, inhibiting allodynia for 2 hours ($P < 0.0001$) (Figure 3B); allodynia returned to predrug baseline levels by 4 hours after injection. In contrast, CNO had no effect on mechanical allodynia when administered to $Na_V1.8$-Pdi mice 12 or 16 weeks after DMM surgery (Figures 3C and D). CNO had no effect on mice not expressing

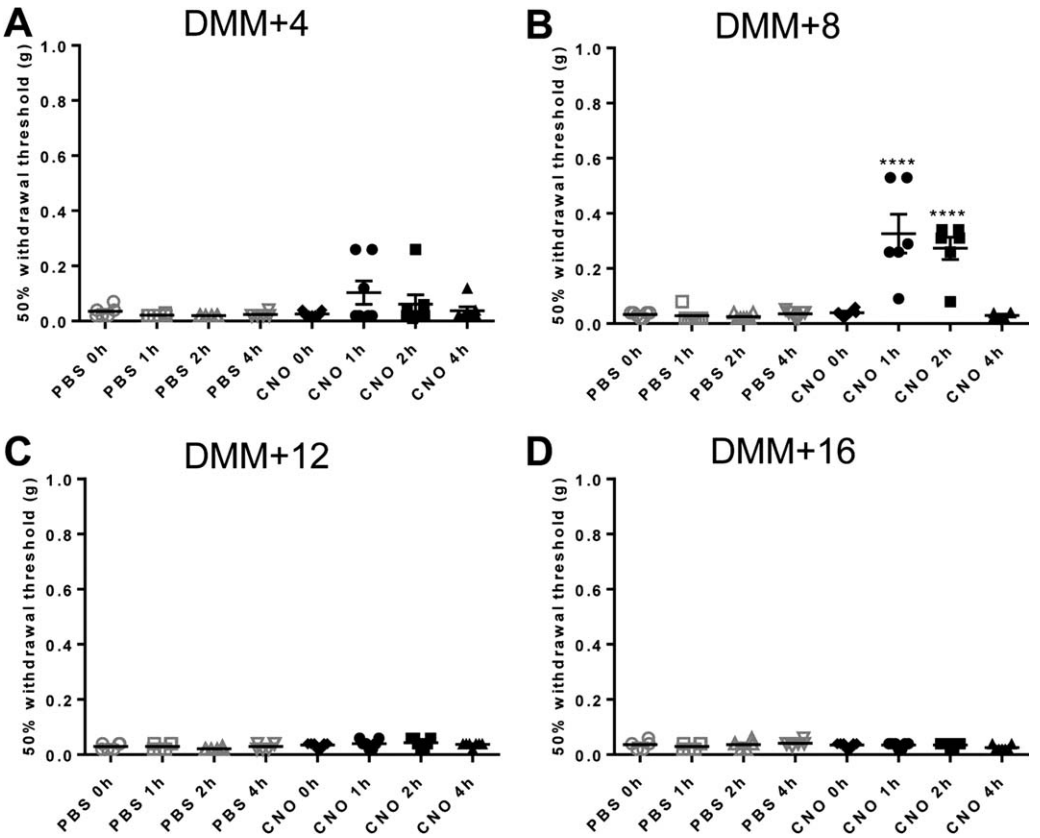

Figure 3. Clozapine *N*-oxide (CNO) temporarily reverses mechanical allodynia of the hind paw in voltage-gated sodium channel 1.8 ($Na_V1.8$)–Pdi mice 8 weeks after destabilization of the medial meniscus surgery (DMM+8) (**B**) but has no statistically significant effect 4 weeks (**A**), 12 weeks (**C**), or 16 weeks (**D**) after DMM surgery. Symbols represent individual mice; bars show the mean ± SEM. **** = $P < 0.0001$ versus vehicle (phosphate buffered saline [PBS]) at the same time point.

the Pdi receptor (see Supplementary Figure 2, http://onlinelibrary.wiley.com/doi/10.1002/art.40118/abstract).

Knee hyperalgesia following DMM surgery in WT mice. In addition to assessing the effects of neuronal inhibition on secondary mechanical allodynia of the hind paw, we sought to measure primary knee hyperalgesia using a previously validated PAM device (28,29), in order to apply a specific range of forces directly to the knee joint to determine a quantitative withdrawal threshold. Both sham and DMM surgeries induced knee hyperalgesia in WT mice, but DMM surgery caused more pronounced hyperalgesia 2–12 weeks after surgery (Figure 4A). Four

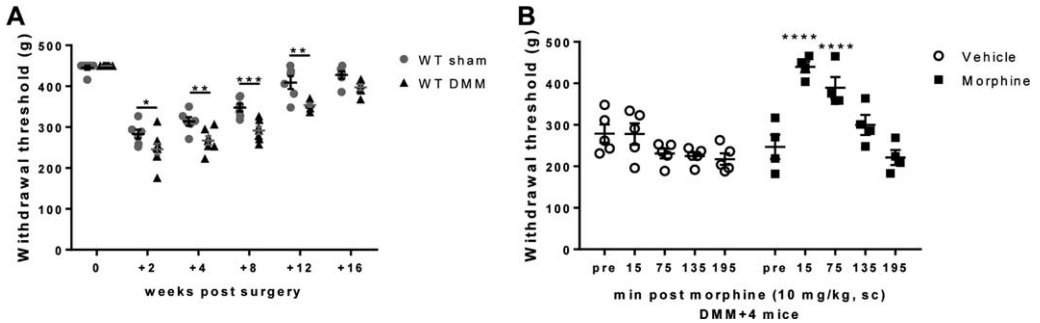

Figure 4. **A,** Wild-type (WT) mice develop more severe and more prolonged knee hyperalgesia after destabilization of the medial meniscus (DMM) surgery than after sham surgery. * = $P < 0.05$; ** = $P < 0.01$; *** = $P < 0.001$. **B,** Morphine administered subcutaneously (SC) is able to transiently reverse knee hyperalgesia 4 weeks after DMM surgery (DMM+4) in WT mice. **** = $P < 0.0001$ versus vehicle (saline) at the same time point. Symbols represent individual mice; bars show the mean ± SEM.

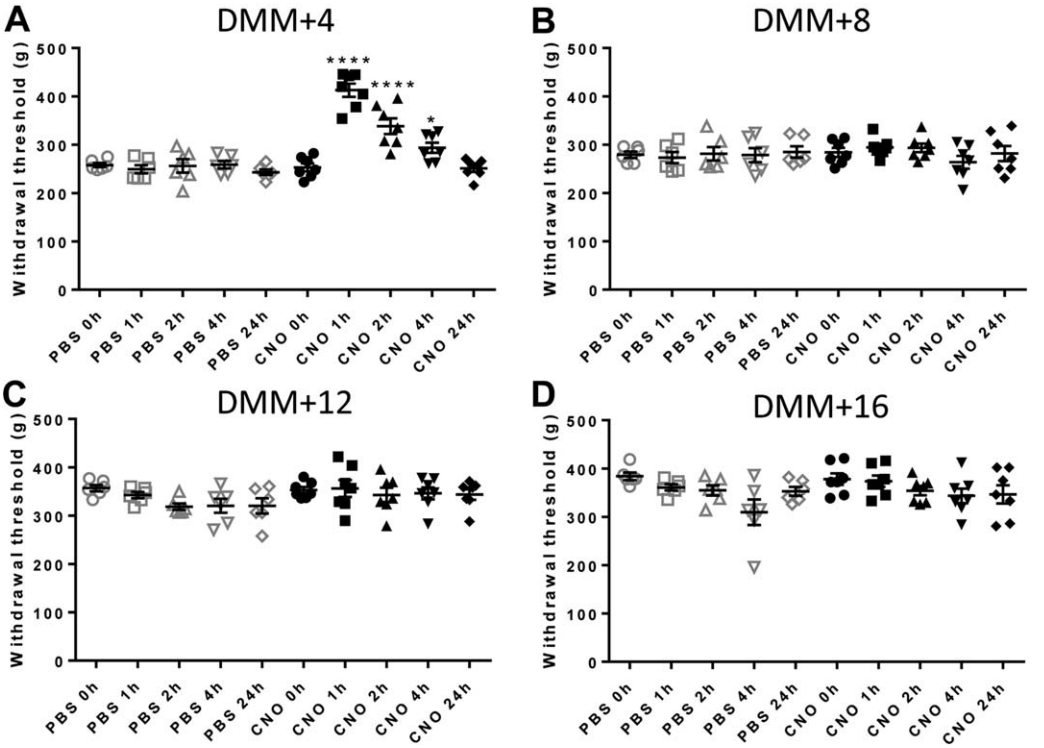

Figure 5. Clozapine *N*-oxide (CNO) temporarily reverses knee hyperalgesia in voltage-gated sodium channel 1.8 ($Na_V1.8$)–Pdi mice 4 weeks after destabilization of the medial meniscus surgery (DMM+4) (**A**) but has no statistically significant effect 8 weeks (**B**), 12 weeks (**C**), or 16 weeks (**D**) after DMM surgery. Symbols represent individual mice; bars show the mean ± SEM. $* = P < 0.05$; $**** = P < 0.0001$ versus vehicle (phosphate buffered saline [PBS]) at the same time point.

weeks after surgery, knee hyperalgesia was reversible with SC injection of morphine (86 ± 23% inhibition) (Figure 4B), suggesting that it is a pain-related behavior.

Chemogenetic inhibition of $Na_V1.8$-expressing neurons reverses knee hyperalgesia 4 weeks after DMM surgery, but not at later time points. $Na_V1.8$-Pdi mice and WT mice developed similar levels of knee hyperalgesia 4 through 16 weeks after DMM surgery (baseline time 0 in Figure 5 compared to Figure 4A). Administering CNO to mice 4 weeks after DMM surgery inhibited knee hyperalgesia for 1 to 4 hours (65 ± 9% inhibition at 1 hour) (Figure 5A); by 24 hours after injection of CNO, knee hyperalgesia had returned to predrug baseline levels. Inhibition by CNO at this time point (Figure 5A) was comparable to that seen with morphine (Figure 4B). In contrast, injection of CNO had no effect 8 weeks (4 ± 3% inhibition), 12 weeks (1 ± 5% inhibition), or 16 weeks (−1 ± 1% inhibition) after DMM surgery (Figures 5B–D).

Effects of the centrally acting analgesic, morphine, on late-stage pain. In order to assess whether late-stage pain behaviors are susceptible to the effects of a centrally acting analgesic, we tested the effects of morphine, which is known to act centrally through the GPCR pathway. Although knee hyperalgesia was mild 12 weeks after surgery, morphine was still able to significantly reverse hyperalgesia (44 ± 13% inhibition) in WT mice (Figure 6A). Similarly, mechanical allodynia was inhibited by morphine in WT mice tested between 13 and 16 weeks after DMM surgery (Figure 6B).

DISCUSSION

We used a chemogenetic approach employing DREADD receptors (Pdis) to examine whether activation of peripherally expressed inhibitory GPCRs was effective in reversing two pain-related behaviors, knee hyperalgesia and mechanical allodynia, at different stages after DMM surgery. We demonstrated that activation of Pdis expressed in the $Na_V1.8$-positive population of DRG neurons was effective in inhibiting the firing of these neurons, something that is shared with naturally occurring inhibitory GPCRs such as opioid receptors expressed in these cells. It is thought that inhibition of neuronal excitability and synaptic transmission constitutes the basis for the analgesic effects of drugs such as morphine, and so we imagined that

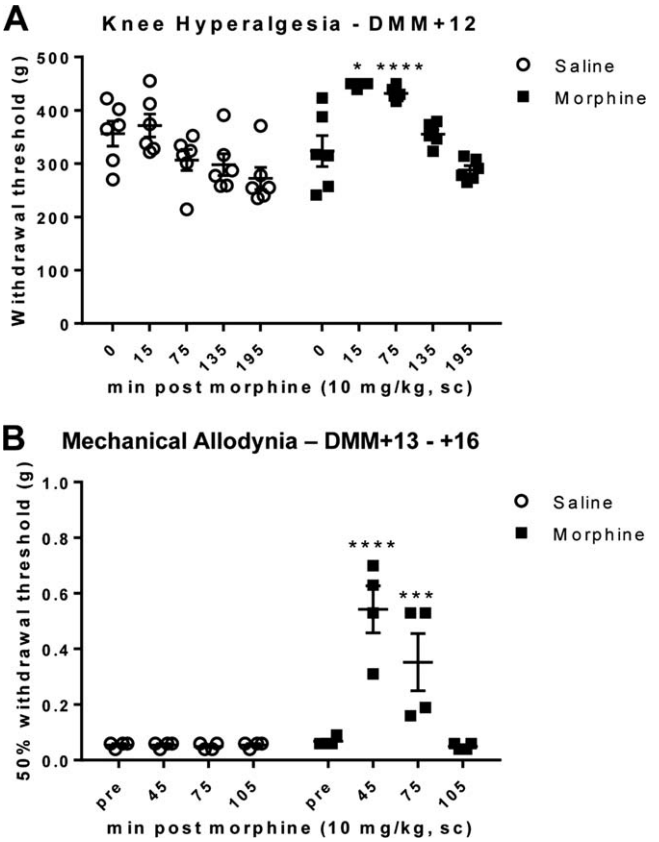

Figure 6. Morphine administered subcutaneously (SC) temporarily reverses knee hyperalgesia in wild-type (WT) mice 12 weeks after destabilization of the medial meniscus surgery (DMM+12) (**A**) and mechanical allodynia of the hind paw in WT mice 13–16 weeks after DMM surgery (**B**). Symbols represent individual mice; bars show the mean ± SEM. $* = P < 0.05$; $*** = P < 0.001$; $**** = P < 0.0001$ versus vehicle (saline) at the same time point.

this would also be true for appropriately expressed Pdis. Indeed, we might expect that activation of peripherally expressed Pdis in our experiments might actually be more effective than activation of peripherally expressed μ-opioid receptors, as the $Na_V1.8$-expressing population of DRG neurons is more extensive than the population that expresses μ-opioid receptors (42).

The current study is also the first to show the pattern of knee hyperalgesia after surgery. Knee hyperalgesia developed as soon as 2 weeks after sham or DMM surgery and then slowly resolved over time. It was more pronounced after DMM surgery than after sham surgery, and this difference was still clear at week 12. The time course of resolution paralleled the resolution of synovitis in this model (16) and was similar to the knee hyperalgesia and synovitis pattern reported in the antigen-induced arthritis model (29). Hence, while early OA changes in the joint may contribute to the establishment of knee hyperalgesia after DMM surgery, it should be considered that this assay failed to demonstrate differences in hyperalgesia between DMM-operated and sham-operated animals at week 16; thus, knee hyperalgesia may indicate postsurgical or postinjury pain more than OA-related pain. The finding that chemogenetic inhibition of $Na_V1.8$-expressing neurons blocks knee hyperalgesia 4 weeks after surgery might, in fact, suggest analgesic strategies for early post–joint surgery pain or postinjury pain, even though the relevance to OA remains unclear and further work needs to be done to establish which pathologic features contribute to knee hyperalgesia.

Chemogenetic inhibition of $Na_V1.8$-expressing sensory neurons blocked knee hyperalgesia and secondary mechanical allodynia at early stages of experimental OA, but DREADD activation was no longer effective during the later stages (>8 weeks after DMM surgery). In contrast, morphine, a drug that normally activates inhibitory GPCRs expressed in both the peripheral and central components of the pain pathway, was still effective at the later stage.

These results support work performed in other experimental OA models, which have noted a time-dependent effect of pharmacologic modulation of pain. For example, in the rat monoiodoacetate model, NSAIDs are effective in reversing weight-bearing deficits, paw hyperalgesia, and knee hyperalgesia in the first 2 weeks after induction (43–45), but by day 21, only drugs which are associated with powerful central analgesic mechanisms, such as morphine and gabapentin, are effective (44–47). Similarly, in the mouse partial meniscectomy model, an NSAID was effective in reversing paw and knee hyperalgesia in an early stage (day 7) but not in a late stage (day 42), while morphine could reverse both behaviors in the late phase (27). Together with the results presented herein, these data suggest that therapies targeted at the peripheral nervous system alone may no longer be sufficient for analgesia in the late stage of OA. This is not because peripheral mechanisms of pain inhibition are ineffective in all types of pain. Sole activation of peripherally expressed μ-opioid receptors using either genetic techniques or opioids that do not enter the CNS can inhibit pain in some circumstances (11,48). Similarly, activation of Pdis uniquely expressed in the $Na_V1.8$-expressing DRG population, as described in the current report, is effective in blocking pain in other situations such as painful diabetic neuropathy (Menichella DM, Miller RJ: unpublished observations). Nevertheless, our data do indicate that there must be changes in the way that the pathways signaling pain are organized in later stages of OA.

In the current study, we used $Na_V1.8$ as a marker to target a specific population of sensory neurons. Two

studies tested the efficacy of targeting the ion channel itself by using a small-molecule inhibitor of $Na_V1.8$, A-803467, in the rat monoiodoacetate model (36,37). Both studies focused on day 14, which is in the NSAID-sensitive phase of the model. This inhibitor was able to reduce the mechanosensitivity of joint afferent fibers during noxious rotation of the joint (36), reverse weight bearing, and mechanical allodynia (36), and it could block spinal neuron responses to mechanical and thermal stimuli (37). These results suggest that at least some of the observed effects may in fact be mediated by $Na_V1.8$ itself. Future work will be directed toward testing this hypothesis.

There are several potential explanations for our findings indicating that blocking the firing of action potentials in peripheral $Na_V1.8$-positive sensory neurons is not sufficient to reverse pain-related behaviors in the late stage of the DMM model. GPCRs, such as those for opioids and cannabinoids, expressed by DRG neurons inhibit the transmission of information into the spinal cord by several mechanisms. Receptors expressed in the DRG can inhibit spike firing, while those on terminals in the dorsal horn reduce transmitter release through inhibition of voltage-dependent calcium influx into nerve terminals (49). It is possible that this latter mechanism becomes more important during later phases of the disease, and the lack of DREADD receptors in the dorsal horn is reflected by their inability to affect pain at later time points.

While it is also possible that the lack of efficacy in the late stage is due to the development of tolerance, the development of tolerance in this case is unlikely for the following reasons. We administered CNO in 1-month intervals, and the effect of chronic CNO administration has been shown to wash out within 48 hours (50). In addition, we tested a separate set of mice at only the +16-week time point and found that CNO still had no effect on mechanical allodynia (see Supplementary Figure 3, http://onlinelibrary.wiley.com/doi/10.1002/art.40118/abstract). Our results can also be compared with those of another recent study that used a non–drug-based strategy: optogenetic silencing of $Na_V1.8$-expressing nociceptors was achieved by using a light-activated inhibitory proton pump to study the effects on pain in a nerve injury mouse model (51). Although—in contrast to the current approach—expression of the pump was demonstrated both in the DRG cell bodies as well as in the axons in the periphery and the dorsal horn, the authors reported findings very similar to our current results: inhibiting $Na_V1.8$-positive sensory neurons in the spared nerve injury neuropathic pain model reversed mechanical allodynia of the hind paw in the early phase (3–4 weeks after surgery) but not in the late phase (6–9 weeks after surgery) (51).

These results suggest that expression of the DREADD receptor in the axons might not improve inhibition in the late phase of experimental OA. It is also possible that during the later stages of this experimental OA model, central sensitization may contribute to the observed pain-related behaviors. Little is known regarding central sensitization in experimental mouse models of OA, but our results suggest that it will be important to investigate how central pathways contribute to chronic OA pain. There is ample clinical evidence to support the notion that OA pain is generated and maintained through continuous nociceptive input from the damaged joint, which is underscored by the fact that the majority of patients are free of pain after total knee replacement (52). Clearly, it is an important limitation of the current study that chemogenetic inhibition of $Na_V1.8$-expressing neurons was only transient. The effects of extended administration of CNO—early, late, or continuous—will be tested in future studies.

Another possibility is that the lack of efficacy in the late phase of the DMM model may indicate phenotypic changes in the non–$Na_V1.8$-expressing sensory neuron population (a subset of Aδ-fibers and Aβ-fibers). Normally, myelinated Aβ-fibers convey low-threshold stimuli as light touch. Clinical studies have suggested that, under pathologic conditions, neuronal plasticity results in these Aβ-fibers now interpreting light touch as being painful (mechanical allodynia) (53–55). Recently, targeted silencing of Aβ-fibers was shown to reduce persistent mechanical allodynia associated with neuropathic pain models (56), but the exact sensory neuron subsets that mediate mechanical allodynia associated with different types of neurons remain to be fully identified (57). Therefore, it is possible that the behaviors related to mechanical sensitivity tested in the present study may involve a mixture of $Na_V1.8$- and non–$Na_V1.8$-expressing sensory neurons, and the roles of each population may change over the course of the model. This will be a focus of future research.

A limitation of the studies reported here is that we focused on two evoked behaviors, mechanical hyperalgesia of the knee and mechanical allodynia of the hind paw. In order to assess effects of silencing $Na_V1.8$-expressing neurons on spontaneous behaviors, such as locomotion deficits, future work will focus on delivering CNO in a chronic manner. Chronic administration of CNO will also allow us to determine whether long-term suppression of $Na_V1.8$-expressing cells is sufficient to prevent the onset of chronic pain in this model.

In conclusion, we have demonstrated that using the inhibitory $G_{i/o}$ protein pathway to transiently inhibit the majority of sensory neurons is only able to inhibit knee hyperalgesia and mechanical allodynia of the hind paw in

the early stage of the DMM mouse model of OA. Importantly, our results set limits on the mechanisms of any new drugs designed to treat OA pain that target inhibitory GPCRs using the same $G_{i/o}$ protein pathway. Our data suggest that activation of inhibitory GPCRs solely expressed in peripheral sensory neurons may not be effective in treating chronic OA pain, although the effects of long-term inhibition need to be studied. This work may lead to a better understanding of which analgesics are effective in different stages of OA, and may also lead to novel therapeutics targeting specific subsets of neurons in different stages of disease.

AUTHOR CONTRIBUTIONS

All authors were involved in drafting the article or revising it critically for important intellectual content, and all authors approved the final version to be published. Dr. Malfait had full access to all of the data in the study and takes responsibility for the integrity of the data and the accuracy of the data analysis.

Study conception and design. R. E. Miller, Menichella, R. J. Miller, Malfait.

Acquisition of data. R. E. Miller, Ishihara, Bhattacharyya, Delaney.

Analysis and interpretation of data. R. E. Miller, Bhattacharyya, R. J. Miller, Malfait.

REFERENCES

1. Hochberg MC, Altman RD, April KT, Benkhalti M, Guyatt G, McGowan J, et al. American College of Rheumatology 2012 recommendations for the use of nonpharmacologic and pharmacologic therapies in osteoarthritis of the hand, hip, and knee. Arthritis Care Res (Hoboken) 2012;64:465–74.
2. McAlindon TE, Bannuru RR, Sullivan MC, Arden NK, Berenbaum F, Bierma-Zeinstra SM, et al. OARSI guidelines for the non-surgical management of knee osteoarthritis. Osteoarthritis Cartilage 2014;22:363–88.
3. Da Costa BR, Reichenbach S, Keller N, Nartey L, Wandel S, Juni P, et al. Effectiveness of non-steroidal anti-inflammatory drugs for the treatment of pain in knee and hip osteoarthritis: a network meta-analysis. Lancet 2016;387:2093–105.
4. Roth BL, Kroeze WK. Integrated approaches for genome-wide interrogation of the druggable non-olfactory G protein-coupled receptor superfamily. J Biol Chem 2015;290:19471–7.
5. Al-Hasani R, Bruchas MR. Molecular mechanisms of opioid receptor-dependent signaling and behavior. Anesthesiology 2011; 115:1363–81.
6. Stein C, Clark JD, Oh U, Vasko MR, Wilcox GL, Overland AC, et al. Peripheral mechanisms of pain and analgesia. Brain Res Rev 2009;60:90–113.
7. Erbs E, Faget L, Scherrer G, Matifas A, Filliol D, Vonesch JL, et al. A mu-delta opioid receptor brain atlas reveals neuronal co-occurrence in subcortical networks. Brain Struct Funct 2015; 220:677–702.
8. Da Costa BR, Nuesch E, Kasteler R, Husni E, Welch V, Rutjes AW, et al. Oral or transdermal opioids for osteoarthritis of the knee or hip. Cochrane Database Syst Rev 2014;CD003115.
9. Manzanares J, Julian M, Carrascosa A. Role of the cannabinoid system in pain control and therapeutic implications for the management of acute and chronic pain episodes. Curr Neuropharmacol 2006;4:239–57.
10. Mackie K. Cannabinoid receptors: where they are and what they do. J Neuroendocrinol 2008;20 Suppl 1:10–4.
11. Weibel R, Reiss D, Karchewski L, Gardon O, Matifas A, Filliol D, et al. Mu opioid receptors on primary afferent nav1.8 neurons contribute to opiate-induced analgesia: insight from conditional knockout mice. PLoS One 2013;8:e74706.
12. Sehgal N, Smith HS, Manchikanti L. Peripherally acting opioids and clinical implications for pain control. Pain Physician 2011; 14:249–58.
13. Hawker GA, Stewart L, French MR, Cibere J, Jordan JM, March L, et al. Understanding the pain experience in hip and knee osteoarthritis: an OARSI/OMERACT initiative. Osteoarthritis Cartilage 2008;16:415–22.
14. Neogi T. The epidemiology and impact of pain in osteoarthritis. Osteoarthritis Cartilage 2013;21:1145–53.
15. Glasson SS, Blanchet TJ, Morris EA. The surgical destabilization of the medial meniscus (DMM) model of osteoarthritis in the 129/SvEv mouse. Osteoarthritis Cartilage 2007;15:1061–9.
16. Jackson MT, Moradi B, Zaki S, Smith MM, McCracken S, Smith SM, et al. Depletion of protease-activated receptor 2 but not protease-activated receptor 1 may confer protection against osteoarthritis in mice through extracartilaginous mechanisms. Arthritis Rheumatol 2014;66:3337–48.
17. Miller RE, Tran PB, Das R, Ghoreishi-Haack N, Ren D, Miller RJ, et al. CCR2 chemokine receptor signaling mediates pain in experimental osteoarthritis. Proc Natl Acad Sci U S A 2012;109: 20602–7.
18. Glasson SS, Hopkins B, Attipoe S, Schelling S, Morris EA. ADAMTS-5 KO mice are protected in a long-term instability model of osteoarthritis [poster]. Presented at the 53rd Annual Meeting of the Orthopaedic Research Society; 2007; San Diego, California.
19. Bateman JF, Rowley L, Belluoccio D, Chan B, Bell K, Fosang AJ, et al. Transcriptomics of wild-type mice and mice lacking ADAMTS-5 activity identifies genes involved in osteoarthritis initiation and cartilage destruction. Arthritis Rheum 2013;65: 1547–60.
20. Loeser RF, Olex AL, McNulty MA, Carlson CS, Callahan M, Ferguson C, et al. Disease progression and phasic changes in gene expression in a mouse model of osteoarthritis. PLoS One 2013;8:e54633.
21. Miller RE, Tran PB, Ishihara S, Larkin J, Malfait AM. Therapeutic effects of an anti-ADAMTS-5 antibody on joint damage and mechanical allodynia in a murine model of osteoarthritis. Osteoarthritis Cartilage 2016;24:299–306.
22. Fang H, Beier F. Mouse models of osteoarthritis: modelling risk factors and assessing outcomes. Nat Rev Rheumatol 2014;10: 413–21.
23. Malfait AM, Ritchie J, Gil AS, Austin JS, Hartke J, Qin W, et al. ADAMTS-5 deficient mice do not develop mechanical allodynia associated with osteoarthritis following medial meniscal destabilization. Osteoarthritis Cartilage 2010;18:572–80.
24. Bradley EW, Carpio LR, McGee-Lawrence ME, Castillejo Becerra C, Amanatullah DF, Ta LE, et al. Phlpp1 facilitates post-traumatic osteoarthritis and is induced by inflammation and promoter demethylation in human osteoarthritis. Osteoarthritis Cartilage 2016;24:1021–8.
25. Miller RE, Belmadani A, Ishihara S, Tran PB, Ren D, Miller RJ, et al. Damage-associated molecular patterns generated in osteoarthritis directly excite murine nociceptive neurons through Toll-like receptor 4. Arthritis Rheumatol 2015;67:2933–43.
26. Ferreira-Gomes J, Adaes S, Castro-Lopes JM. Assessment of movement-evoked pain in osteoarthritis by the knee-bend and CatWalk tests: a clinically relevant study. J Pain 2008;9:945–54.
27. Knights CB, Gentry C, Bevan S. Partial medial meniscectomy produces osteoarthritis pain-related behaviour in female C57BL/6 mice. Pain 2012;153:281–92.
28. Barton NJ, Strickland IT, Bond SM, Brash HM, Bate ST, Wilson AW, et al. Pressure application measurement (PAM): a novel behavioural technique for measuring hypersensitivity in a rat model of joint pain. J Neurosci Methods 2007;163:67–75.

29. Leuchtweis J, Imhof AK, Montechiaro F, Schaible HG, Boettger MK. Validation of the digital pressure application measurement (PAM) device for detection of primary mechanical hyperalgesia in rat and mouse antigen-induced knee joint arthritis. Methods Find Exp Clin Pharmacol 2010;32:575–83.
30. Inglis JJ, McNamee KE, Chia SL, Essex D, Feldmann M, Williams RO, et al. Regulation of pain sensitivity in experimental osteoarthritis by the endogenous peripheral opioid system. Arthritis Rheum 2008;58:3110–9.
31. Muramatsu Y, Sasho T, Saito M, Yamaguchi S, Akagi R, Mukoyama S, et al. Preventive effects of hyaluronan from deterioration of gait parameters in surgically induced mice osteoarthritic knee model. Osteoarthritis Cartilage 2014;22:831–5.
32. Armbruster BN, Li X, Pausch MH, Herlitze S, Roth BL. Evolving the lock to fit the key to create a family of G protein-coupled receptors potently activated by an inert ligand. Proc Natl Acad Sci U S A 2007;104:5163–8.
33. Urban DJ, Roth BL. DREADDs (Designer Receptors Exclusively Activated by Designer Drugs): chemogenetic tools with therapeutic utility. Annu Rev Pharmacol Toxicol 2015;55: 399–417.
34. Ray RS, Corcoran AE, Brust RD, Kim JC, Richerson GB, Nattie E, et al. Impaired respiratory and body temperature control upon acute serotonergic neuron inhibition. Science 2011; 333:637–42.
35. Shields SD, Ahn HS, Yang Y, Han C, Seal RP, Wood JN, et al. Nav1.8 expression is not restricted to nociceptors in mouse peripheral nervous system. Pain 2012;153:2017–30.
36. Schuelert N, McDougall JJ. Involvement of Nav 1.8 sodium ion channels in the transduction of mechanical pain in a rodent model of osteoarthritis. Arthritis Res Ther 2012;14:R5.
37. Rahman W, Dickenson AH. Osteoarthritis-dependent changes in antinociceptive action of Nav1.7 and Nav1.8 sodium channel blockers: an in vivo electrophysiological study in the rat. Neuroscience 2015;295:103–16.
38. Stirling LC, Forlani G, Baker MD, Wood JN, Matthews EA, Dickenson AH, et al. Nociceptor-specific gene deletion using heterozygous NaV1.8-Cre recombinase mice. Pain 2005;113: 27–36.
39. Glasson SS, Chambers MG, Van Den Berg WB, Little CB. The OARSI histopathology initiative—recommendations for histological assessments of osteoarthritis in the mouse. Osteoarthritis Cartilage 2010;18 Suppl 3:S17–23.
40. Mills C, Leblond D, Joshi S, Zhu C, Hsieh G, Jacobson P, et al. Estimating efficacy and drug ED50's using von Frey thresholds: impact of Weber's law and log transformation. J Pain 2012;13: 519–23.
41. Sciolino NR, Plummer NW, Chen YW, Alexander GM, Robertson SD, Dudek SM, et al. Recombinase-dependent mouse lines for chemogenetic activation of genetically defined cell types. Cell Rep 2016;15:2563–73.
42. Scherrer G, Imamachi N, Cao YQ, Contet C, Mennicken F, O'Donnell D, et al. Dissociation of the opioid receptor mechanisms that control mechanical and heat pain. Cell 2009; 137:1148–59.
43. Bove SE, Calcaterra SL, Brooker RM, Huber CM, Guzman RE, Juneau PL, et al. Weight bearing as a measure of disease progression and efficacy of anti-inflammatory compounds in a model of monosodium iodoacetate-induced osteoarthritis. Osteoarthritis Cartilage 2003;11:821–30.
44. Fernihough J, Gentry C, Malcangio M, Fox A, Rediske J, Pellas T, et al. Pain related behaviour in two models of osteoarthritis in the rat knee. Pain 2004;112:83–93.
45. Rashid MH, Theberge Y, Elmes SJ, Perkins MN, McIntosh F. Pharmacological validation of early and late phase of rat monoiodoacetate model using the Tekscan system. Eur J Pain 2013; 17:210–22.
46. Bove SE, Laemont KD, Brooker RM, Osborn MN, Sanchez BM, Guzman RE, et al. Surgically induced osteoarthritis in the rat results in the development of both osteoarthritis-like joint pain and secondary hyperalgesia. Osteoarthritis Cartilage 2006; 14:1041–8.
47. Ivanavicius SP, Ball AD, Heapy CG, Westwood FR, Murray F, Read SJ. Structural pathology in a rodent model of osteoarthritis is associated with neuropathic pain: increased expression of ATF-3 and pharmacological characterisation. Pain 2007;128: 272–82.
48. Stein C, Machelska H. Modulation of peripheral sensory neurons by the immune system: implications for pain therapy. Pharmacol Rev 2011;63:860–81.
49. Stein C, Lang LJ. Peripheral mechanisms of opioid analgesia. Curr Opin Pharmacol 2009;9:3–8.
50. Carvalho Poyraz F, Holzner E, Bailey MR, Meszaros J, Kenney L, Kheirbek MA, et al. Decreasing striatopallidal pathway function enhances motivation by energizing the initiation of goal-directed action. J Neurosci 2016;36:5988–6001.
51. Daou I, Beaudry H, Ase AR, Wieskopf JS, Ribeiro-da-Silva A, Mogil JS, et al. Optogenetic silencing of Nav1.8-positive afferents alleviates inflammatory and neuropathic pain. eNeuro 2016;3.
52. Malfait AM, Schnitzer TJ. Towards a mechanism-based approach to pain management in osteoarthritis. Nat Rev Rheumatol 2013;9:654–64.
53. Campbell JN, Raja SN, Meyer RA, Mackinnon SE. Myelinated afferents signal the hyperalgesia associated with nerve injury. Pain 1988;32:89–94.
54. Von Hehn CA, Baron R, Woolf CJ. Deconstructing the neuropathic pain phenotype to reveal neural mechanisms. Neuron 2012;73:638–52.
55. Koltzenburg M, Lundberg LE, Torebjork HE. Dynamic and static components of mechanical hyperalgesia in human hairy skin. Pain 1992;51:207–19.
56. Xu ZZ, Kim YH, Bang S, Zhang Y, Berta T, Wang F, et al. Inhibition of mechanical allodynia in neuropathic pain by TLR5-mediated A-fiber blockade. Nat Med 2015;21:1326–31.
57. Seal RP. Do the distinct synaptic properties of VGLUTs shape pain? Neurochem Int 2016;98:82–8.

ARTHRITIS & RHEUMATOLOGY
Vol. 69, No. 7, July 2017, pp 1440–1450
DOI 10.1002/art.40093

Randomized Controlled Trial of Rituximab and Cost-Effectiveness Analysis in Treating Fatigue and Oral Dryness in Primary Sjögren's Syndrome

Simon J. Bowman,[1] Colin C. Everett,[2] John L. O'Dwyer,[2] Paul Emery,[3] Costantino Pitzalis,[4] Wan-Fai Ng,[5] Colin T. Pease,[3] Elizabeth J. Price,[6] Nurhan Sutcliffe,[7] Nagui S. T. Gendi,[8] Frances C. Hall,[9] Sharon P. Ruddock,[2] Catherine Fernandez,[2] Catherine Reynolds,[2] Claire T. Hulme,[2] Kevin A. Davies,[10] Christopher J. Edwards,[11] Peter C. Lanyon,[12] Robert J. Moots,[13] Euthalia Roussou,[14] Ian P. Giles,[15] Linda D. Sharples,[16] and Michele Bombardieri[4]

Objective. **To investigate whether rituximab, an anti–B cell therapy, improves symptoms of fatigue and oral dryness in patients with primary Sjögren's syndrome (SS).**

Methods. **We conducted a multicenter, randomized, double-blind, placebo-controlled, parallel-group trial that included health economic analysis. Anti-Ro–positive patients with primary SS, symptomatic fatigue, and oral dryness were recruited from 25 UK rheumatology clinics from August 2011 to January 2014. Patients were centrally randomized to receive either intravenous (IV) placebo (250 ml saline) or IV rituximab (1,000 mg in 250 ml saline) in 2 courses at weeks 0, 2, 24, and 26, with pre- and postinfusion medication including corticosteroids. The primary end point was the proportion of patients achieving a 30% reduction in either fatigue or oral dryness at 48 weeks, as measured by visual analog scale. Other outcome measures included salivary and lacrimal flow rates, quality of life, scores on the European League Against Rheumatism (EULAR) Sjögren's Syndrome Patient Reported Index and EULAR Sjögren's Syndrome Disease Activity Index, symptoms of ocular and overall dryness, pain, globally assessed disease activity, and cost-effectiveness.**

Results. **All 133 patients who were randomized to receive placebo (n = 66) or rituximab (n = 67) were included in the primary analysis. Among patients with**

ISRCTN: 65360827. EudraCT database no. 2010-021430-64.
Supported by Arthritis Research UK.

[1]Simon J. Bowman, PhD, FRCP: University Hospitals Birmingham NHS Foundation Trust, Birmingham, UK; [2]Colin C. Everett, MSc, John L. O'Dwyer, MSc, Sharon P. Ruddock, BSc (Hons), Catherine Fernandez, PhD, Catherine Reynolds, BSc (Hons), Claire T. Hulme, PhD: University of Leeds, Leeds, UK; [3]Paul Emery, MA, MD, FRCP, FMedSci, Colin T. Pease, MD, FRCP: Chapel Allerton Hospital, Leeds, UK; [4]Costantino Pitzalis, MD, PhD, FRCP, Michele Bombardieri, MD, PhD, FRCP: Barts and The London School of Medicine and Dentistry, London, UK; [5]Wan-Fai Ng, FRCP, PhD: University of Newcastle, Newcastle-upon-Tyne, UK; [6]Elizabeth J. Price, MBBCh, FRCP, MD: Great Western Hospital, Swindon, UK; [7]Nurhan Sutcliffe, MD, FRCP: Royal London Hospital (Mile End), London, UK; [8]Nagui S. T. Gendi, MSc, FRCP: Basildon and Thurrock University Hospital, Essex, UK; [9]Frances C. Hall, BM, BCh, DPhil, RCP(UK): University of Cambridge, Addenbrookes Hospital, Cambridge, UK; [10]Kevin A. Davies, MD: University of Sussex, Brighton, UK; [11]Christopher J. Edwards, MBBS, MD, FRCP: NIHR Wellcome Trust Clinical Research Facility, University Hospital Southampton, Southampton, UK; [12]Peter C. Lanyon, MB, ChB, DM: University of Nottingham and Circle Nottingham, Nottingham NHS Treatment Centre, Nottingham, UK; [13]Robert J. Moots, MD, PhD: Aintree University Hospital, Liverpool, UK; [14]Euthalia Roussou, MD, DM: King George Hospital, Barking Havering and Redbridge University Hospitals NHS Trust, Essex, UK; [15]Ian P. Giles, BSc, MBBS, PhD, FRCP: University College London Hospital, London, UK; [16]Linda D. Sharples, PhD: London School of Hygiene and Tropical Medicine, London, UK.

Prof. Bowman has received consulting fees from AstraZeneca/MedImmune, Bristol-Myers Squibb, Celgene, Eli Lilly, Glenmark, GlaxoSmithKline, MTPharma, Novartis, Ono, Pfizer, Takeda, UCB, and XTLBio (less than $10,000 each). Dr. Emery has received consulting fees, speaking fees, and/or honoraria from Pfizer, MSD, AbbVie, BMS, UCB, Roche, Novartis, Samsung, Sandoz, and Lilly (less than $10,000 each). Dr. Ng has received consulting fees, speaking fees, and/or honoraria from Pfizer, Regeneron, Takeda, AstraZeneca, and Roche (less than $10,000 each) and research grants from UCB Foundation. Dr. Gendi has received consulting fees, speaking fees, and/or honoraria from Celgene (less than $10,000). Dr. Hall has received research grants from Actelion. Dr. Hulme has received research grants from Arthritis Research UK. Dr. Bombardieri has received consulting fees, speaking fees, and/or honoraria from MedImmune and GlaxoSmithKline (less than $10,000 each) and research grants from MedImmune.

Address correspondence to Simon J. Bowman, PhD, FRCP, University Hospitals Birmingham NHS Foundation Trust, Mindelsohn Way, Edgbaston, Birmingham B15 2TH, UK. E-mail: Simon.Bowman@uhb.nhs.uk.

Submitted for publication July 28, 2016; accepted in revised form March 7, 2017.

complete data, 21 of 56 placebo-treated patients and 24 of 61 rituximab-treated patients achieved the primary end point. After multiple imputation of missing outcomes, response rates in the placebo and rituximab groups were 36.8% and 39.8%, respectively (adjusted odds ratio 1.13 [95% confidence interval 0.50, 2.55]). There were no significant improvements in any outcome measure except for unstimulated salivary flow. The mean ± SD costs per patient for rituximab and placebo were £10,752 ± 264.75 and £2,672 ± 241.71, respectively. There were slightly more adverse events (AEs) reported in total for rituximab, but there was no difference in serious AEs (10 in each group).

***Conclusion*. The results of this study indicate that rituximab is neither clinically effective nor cost-effective in this patient population.**

Primary Sjögren's syndrome (SS) is the second most common autoimmune rheumatic disease after rheumatoid arthritis (RA) (1). Patients with primary SS are typically women (9:1 female:male ratio), and the prevalence of the disease is estimated to be 1–6 per 1,000 adult women. Typical symptoms of primary SS are oral and ocular dryness, fatigue, and pain. Fibromyalgia is also reported in 5% of patients with primary SS, comparable to its frequency in systemic lupus erythematosus (2). Organ-specific systemic involvement is observed in 5–20% of patients and includes cutaneous involvement, peripheral neuropathy, nonerosive arthritis, interstitial cystitis, and lung and renal disease. Patients with primary SS almost always have evidence of B cell hyperreactivity, with anti-Ro/anti-La antibodies and hypergammaglobulinemia.

Currently, treatment of primary SS focuses on relieving symptoms rather than altering the course of the disease. For ocular dryness, artificial tears are reasonably effective. For oral dryness, however, symptomatic therapies (sprays, lozenges, pastilles) have limited efficacy. Pilocarpine has been shown to alleviate symptoms of dryness (3,4). However, the usefulness of pilocarpine is generally considered to be limited, and its side effects reduce the risk/benefit profile. There is no effective therapy for fatigue.

In the absence of positive clinical trial data, treatment of systemic primary SS is empirical. Hydroxychloroquine and/or low-dose prednisolone are often used in mild disease (although recent findings from the Randomized Evaluation of Hydroxychloroquine in Primary Sjögren's Syndrome study suggest limited benefit [5]). For severe disease, such as progressive neuropathy, intravenous (IV) methylprednisolone, cyclophosphamide, azathioprine, cyclosporine, mycophenolate mofetil, or chlorambucil may be used. In B cell lymphoma, it is routine to treat with combination chemotherapy plus rituximab.

Rituximab is a monoclonal antibody against CD20 (a cell surface antigen expressed on B cells). Treatment with rituximab induces a rapid and sustained depletion of B cells. Rituximab is currently approved for the treatment of relapsed or refractory non-Hodgkin's lymphoma, chronic lymphocytic leukemia, and in combination with methotrexate for the treatment of RA.

Evidence from small prospective, uncontrolled, open-label studies of rituximab in primary SS has shown improvements in patient-reported levels of dryness, pain, fatigue, and disease activity (patient's global assessment) as well as improvements in Short Form 36 (SF-36) health survey scores (6,7), stimulated salivary flow (8), and physician's global assessment of disease activity (9). A prospective study comparing symptom levels over 120 weeks of follow-up between patients receiving rituximab in one hospital and disease-modifying antirheumatic drugs (DMARDs) in another showed superior improvements for rituximab compared to DMARD therapy (10).

Findings from small double-blind, randomized, placebo-controlled trials have also provided some cause for optimism in terms of reduced fatigue (11) and improvements in ocular dryness (12). More recently, however, in the Tolerance and Efficacy of Rituximab in Primary Sjögren's Syndrome (TEARS) study (13), there was no significant difference in the proportions of patients achieving the primary end point (absolute improvement of ≥30 mm on 2 of 4 visual analog scales [VAS] measuring fatigue, dryness, pain, and patient's global assessment of disease activity) at 24 weeks, although a greater response in terms of fatigue was demonstrated at earlier time points.

As evidence from randomized trials has only addressed the efficacy of a single course of rituximab, we are still missing the clinical knowledge that could be obtained from a randomized, double-blind evaluation of a follow-up dose of rituximab in patients with primary SS. The Trial of Anti–B cell Therapy in Patients with Primary Sjögren's Syndrome (TRACTISS) was designed to determine the effectiveness of rituximab in improving symptoms of fatigue or oral dryness in patients with primary SS following 2 courses of therapy.

PATIENTS AND METHODS

Trial design and patients. TRACTISS (ISRCTN: 65360827/European Clinical Trials database no. 2010-021430-64) is a multicenter, randomized, 1:1, double-blind, placebo-controlled, parallel-group trial to determine the effectiveness of rituximab in alleviating patient-reported symptoms of fatigue and oral dryness in patients with primary SS. The trial was carried out in accordance with Good Clinical Practice and the Declaration of

Helsinki. Ethics approval and governance approval were obtained from the Leeds West Ethics Committee (ref. 10/H1307/99) and the Leeds Teaching Hospitals NHS Trust, respectively. An independent Data Monitoring and Ethics Committee had access to ongoing unblinded reports of safety and compliance, and a Trial Steering Committee had overall oversight of the study. Appendix A lists the Site Principal Investigators as well as members of the Trial Steering Committee, Data Monitoring and Ethics Committee, and Clinical Trials Research Unit.

The TRACTISS protocol has been reported (14). Briefly, between August 2011 and January 2014, participants were recruited from 25 UK rheumatology clinics and were eligible if they had primary SS, were ages 18–80 years, were positive for anti-Ro autoantibodies, and had some (greater than zero) unstimulated salivary flow, symptomatic fatigue, and oral dryness worse than 5 of 10 on a self-completed Likert scale. Eligible participants had to be receiving a stable dose of corticosteroids, nonsteroidal antiinflammatory drugs, DMARDs, pilocarpine, and antidepressants for 4 weeks prior to and throughout the study, and they had to provide written informed consent to participate. Exclusion criteria included secondary SS, hepatitis B or C infection, tuberculosis, HIV infection or other immunodeficiency, prior use of rituximab or a monoclonal antibody, malignancies within the previous 5 years, recent organ transplant, major surgery either planned or within the previous 3 months, pregnancy/lactation, and unwillingness to use contraception throughout the study. Eligibility criteria were changed after the 37th randomization to reduce the required period of stable hydroxychloroquine use (where applicable) from 6 months to 4 weeks and to allow patients with benign ethnic neutropenia to take part rather than being excluded due to neutropenia. There was no difference in characteristics between patients randomized before and those randomized after this change.

Intervention and outcome measures. Rituximab was provided free of charge to the study by Hoffmann-La Roche. Participants received either intravenous (IV) rituximab (1,000 mg in 250 ml saline) or IV placebo (250 ml saline) in 2 courses at weeks 0, 2, 24, and 26. To reduce risk of infusion reactions, patients received methylprednisolone, acetaminophen, and chlorpheniramine preinfusion and oral prednisolone postinfusion, tapering from 60 mg/day to 15 mg/day over 7 days postinfusion (14).

At baseline and at weeks 16, 24, 36, and 48, patients completed VAS questionnaires recording fatigue, overall dryness, oral dryness, ocular dryness, pain, and disease activity (global assessment) (average symptom level over previous 2 weeks: 0 = none, 100 mm = severe), as well as the European League Against Rheumatism (EULAR) Sjögren's Syndrome Patient Reported Index (ESSPRI) (15). The Profile of Fatigue and Discomfort Sicca Symptoms Inventory (PROFAD-SSI) (16), SF-36, and EuroQol 5-domain 3L (EQ-5D-3L) (17) questionnaires were completed at baseline and at weeks 24 and 48. Unstimulated and stimulated (using 2% citric acid solution) salivary flow was measured at these visits, as was lacrimal flow using the Schirmer I test. Physicians completed the EULAR Sjögren's Syndrome Disease Activity Index (ESSDAI) (18) and global assessment of disease activity at all visits, and they completed the Sjögren's Syndrome Disease Activity Index (19), Sjögren's Syndrome Damage Index (20), Sjögren's Syndrome Disease Damage Index (19), Sjögren's Syndrome Clinical Activity Index (21), and global assessment of damage at baseline and at weeks 24 and 48 (14).

Randomization and blinding. Randomization was by 24-hour central telephone service operated by the Clinical Trials Research Unit. Consenting participants were registered before undergoing further clinical tests to ensure eligibility. Once eligibility was confirmed, participants were allocated by minimization, which assigned a patient with 80% probability to the arm that reduced the between-group imbalance in randomizing center, age category, years since diagnosis, consent for ultrasound, and consent for biopsy substudies.

Each site's dispensing pharmacy received details of the participant allocation, by fax, to facilitate infusion preparation. On the day of infusion, the pharmacy provided either a bag of pure saline (placebo) or a bag of saline to which rituximab had been added. A small volume of saline was withdrawn from bags containing rituximab to ensure that no difference in bag volume was detected. Placebo and rituximab infusion bags were otherwise identical.

Sample size. The predefined minimum clinically important effect of rituximab was an increase in treatment response rate from 20% in the placebo arm to 50% in the rituximab arm. For a 2-sided continuity-corrected chi-square test, 50 patients with complete data in each treatment arm were needed in order to have 80% power to detect this difference at a 5% significance level. To allow for noncompletion, 110 patients (55 per treatment arm) were needed. In July 2013, the Data Monitoring and Ethics Committee recommended extending recruitment until the end of the planned recruitment period and, to reduce loss to follow-up, a protocol amendment allowed participants to complete the final primary end point questionnaire at home rather than attending clinic.

Statistical analysis. The primary end point was the achievement of a reduction of at least 30% relative to the baseline measurement in the patient-completed VAS assessments of either fatigue or oral dryness at week 48. Secondary end points included the patient-completed and physician-completed assessments at other time points and measurements of salivary and lacrimal flow. The primary end point was modeled using mixed-effects logistic regression, with a fixed effect for the randomized treatment arm and terms for the minimization factors (age category, disease duration category, and consent for substudies as fixed effects and randomizing center as a random effect). All patients were included in this primary analysis, even if the patient had incomplete outcome data. For patients with incomplete primary end point questionnaire data (fatigue and oral dryness each at baseline and week 48), we used multiple imputation by chained equations (22) to impute plausible missing VAS values; the imputation function included fixed randomization factors (for baseline values) and also the baseline values (for week 48 values). Missing values were imputed separately for each scale, both for placebo-treated patients and for rituximab-treated patients, to produce 1 full data set. This was repeated n times, where n is the number of patients with incomplete data. Analysis was performed for each data set, and the results were combined to estimate treatment effects and appropriate 95% confidence intervals (95% CIs) using Rubin's rules (23).

To assess sensitivity of results to alternative assumptions about missing data, we repeated the analysis using a last observation carried forward approach, a complete-case analysis, and a per-protocol population analysis. In order to calculate adjusted absolute differences in response rates, we fitted a linear probability model (binary error structure with identity link function); we excluded the random center effect from this model to ensure model convergence.

Secondary end points were analyzed by fitting a random-coefficients mixed-effects linear regression model, with fixed effects for baseline value, age, disease duration, the substudy

consent, time, and time-by-treatment interaction, and random effects for patient and patient-by-time interaction, taking the time to be the number of weeks since randomization. Most end points were analyzed on their original scale, although we log-transformed the salivary and lacrimal flow rates and the ESSDAI score (including an offset to avoid zero values) to better approximate normality. We repeated this longitudinal analysis using a covariance pattern type mixed model, treating assessments as discrete sequential observations (relaxing the assumption of a linear treatment effect) so as to provide graphical summaries of group means at each time point using least squares means. Adverse event (AE) data were reported throughout the trial duration and collated after completion of follow-up at 48 weeks.

Economic analyses. An economic evaluation was conducted alongside the clinical trial to assess the cost-effectiveness of rituximab compared to placebo over 48 weeks. Incremental cost-effectiveness ratios were calculated and assessed against a willingness-to-pay threshold of £20,000 per quality-adjusted life-year (QALY) gain (24). QALYs were calculated using utility weights derived from the EQ-5D-3L collected 16, 24, 36, and 48 weeks postrandomization (17). Resource use was captured using bespoke patient-completed forms and nurse records of medications and hospital visits. Costs were attached to individuals by using NHS reference costs and Personal Social Services Research Unit and British National Formulary databases (price year 2014) (25–27). Analyses were conducted from the perspective of the health care provider. The probability of cost-effectiveness was determined by bootstrapping and constructing cost-effectiveness acceptability curves using a range of willingness-to-pay thresholds for QALY gains (28). Multiple imputation was used to account for missing cost and EQ-5D data (29). No discounting was undertaken due to the short follow-up duration of 48 weeks per patient.

RESULTS

Recruitment. Between August 2011 and January 2014, 133 participants were randomized 1:1 to receive either rituximab or placebo (Figure 1) (also see Supplementary Figures A1 and A2, available on the *Arthritis & Rheumatology* web site at http://onlinelibrary.wiley.com/doi/10.1002/art.40093/abstract). The final follow-up visit was completed by January 2015. The mean ± SD age of randomized patients was 54.4 ± 11.5 years, and 30 of 133 patients (22.6%) were age ≥65 years. The mean ± SD years since diagnosis was 5.7 ± 5.4 (24 of 133 [18.0%] had been diagnosed ≥10 years previously), and 124 (93.2%) were women. Baseline characteristics of the patients are presented in Table 1.

Primary end point analysis. All 66 placebo-treated patients and 67 rituximab-treated patients were included in the primary end point analysis. Sixteen participants (12.0%) had incomplete fatigue or oral dryness measurements at baseline (1 in each group) or at week 48 (9 in the placebo group and 5 in the rituximab group). The primary end point response rates among patients with complete data were 37.5% for placebo-treated patients (21 of 56) and 39.3% for rituximab-treated patients (24 of 61). After multiple imputation of missing responses, the mean response rates were 36.8% and 39.8% for the placebo and rituximab treatment arms, respectively (unadjusted absolute

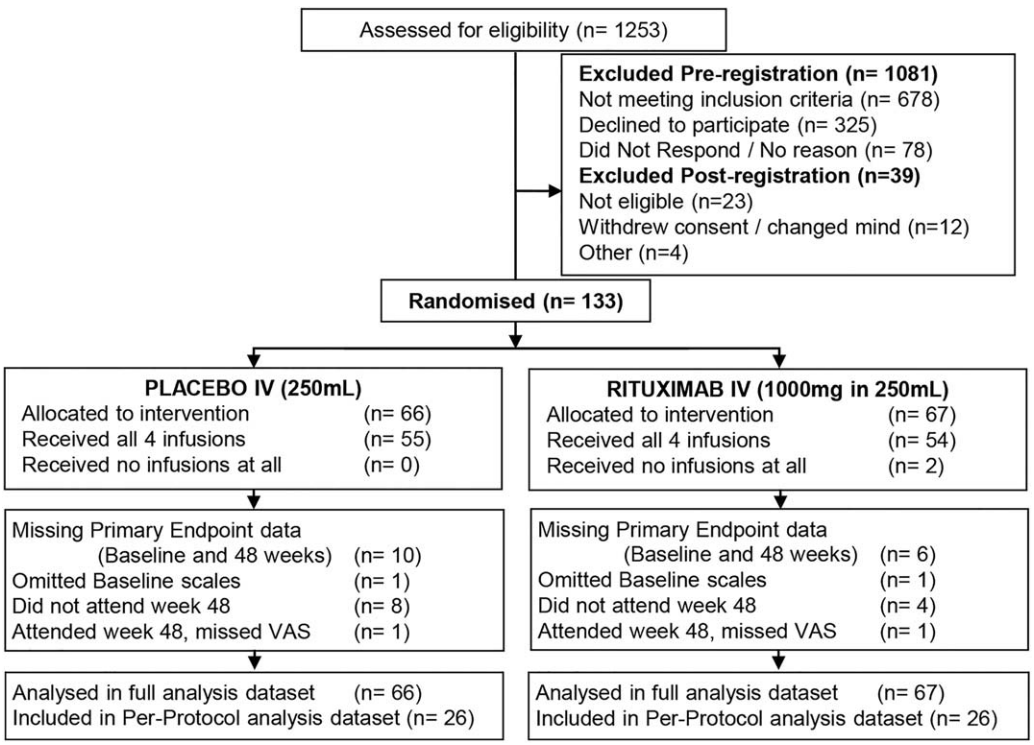

Figure 1. Flow diagram showing the distribution of the study participants. IV = intravenous; VAS = visual analog scale.

Table 1. Selected baseline characteristics of the study patients*

	Placebo (n = 66)	Rituximab (n = 67)	All (n = 133)
Age, years	54.4 ± 11.6	54.3 ± 11.5	54.4 ± 11.5
Age ≥65 years, no. (%)	15 (22.7)	15 (22.4)	30 (22.6)
Years since diagnosis	6.2 ± 5.8	5.3 ± 4.9	5.7 ± 5.4
Ten or more years since diagnosis, no. (%)	13 (19.7)	11 (16.4)	24 (18.0)
Women, no. (%)	61 (92.4)	63 (94.0)	124 (93.2)
Current medications (prior to randomization), no. (%)			
Pilocarpine	3 (4.5)	11 (16.4)	14 (10.5)
Hydroxychloroquine	35 (53.0)	39 (58.2)	74 (55.6)
Corticosteroids	12 (18.2)	7 (10.4)	19 (14.3)
NSAIDs	16 (24.2)	19 (28.4)	35 (26.3)
Unstimulated salivary flow, ml per 15 minutes	1.2 ± 1.8	1.2 ± 1.2	1.2 ± 1.5
Mean lacrimal flow, mm per 5 minutes†	8.2 ± 11.3	6.6 ± 8.8	7.4 ± 10.2
IgG, gm/liter	17.7 ± 7.9	18.4 ± 7.3	18.0 ± 7.5
IgA, gm/liter	3.4 ± 2.2	3.0 ± 0.9	3.2 ± 1.7
IgM, gm/liter	1.2 ± 0.6	1.3 ± 0.6	1.2 ± 0.6
Anti-Ro positive, no. (%)	66 (100.0)	66 (98.5)	132 (99.2)
Reduced C4, no. (%)	9 (13.6)	10 (14.9)	19 (14.3)
Current smoker, no. (%)	8 (12.1)	3 (4.5)	11 (8.3)
Patient-completed VAS values over last 2 weeks, 0–100 mm‡			
Fatigue	74.6 ± 15.3	71.2 ± 16.8	72.8 ± 16.1
Oral dryness	77.3 ± 17.0	75.3 ± 15.3	76.3 ± 16.2
Ocular dryness	72.0 ± 19.6	69.4 ± 20.9	70.7 ± 20.2
Overall dryness	76.3 ± 16.3	74.2 ± 15.4	75.2 ± 15.8
Joint pain	57.5 ± 28.7	52.0 ± 27.2	54.7 ± 28.0
Global assessment of disease activity§	70.7 ± 17.8	68.6 ± 18.0	69.7 ± 17.9
ESSPRI score¶	6.7 ± 1.6	6.4 ± 1.6	6.6 ± 1.6
ESSDAI score#	6.0 ± 4.3	5.3 ± 4.7	5.7 ± 4.5
SF-36 physical component summary score	35.6 ± 10.9	36.6 ± 9.8	36.1 ± 10.3
SF-36 mental component summary score	40.7 ± 12.3	39.2 ± 11.6	40.0 ± 11.9

* Except where indicated otherwise, values are the mean ± SD. NSAIDs = nonsteroidal antiinflammatory drugs; VAS = visual analog scale; ESSPRI = European League Against Rheumatism (EULAR) Sjögren's Syndrome Patient Reported Index; ESSDAI = EULAR Sjögren's Syndrome Disease Activity Index; SF-36 = Short Form 36.
† By Schirmer I test.
‡ Score of 100 = severe, except for global assessment of disease activity.
§ Score of 100 = very active Sjögren's syndrome.
¶ Score of 10 = maximal symptom severity.
# Score of 123 = maximal disease activity.

difference 3.0% [95% CI −14.5, 20.5]). In the primary analysis, rituximab-treated patients were not significantly more likely than placebo-treated patients to achieve 30% reduction in fatigue or oral dryness (odds ratio [OR] 1.13 [95% CI 0.50, 2.55], $P = 0.76$). The baseline-adjusted absolute difference in response rates (rituximab–placebo) was 1.7% (95% CI −16.5, 19.1) ($P = 0.84$). The lack of significant treatment effect remained even when using different end point imputation strategies or a complete-case analysis. A per-protocol population analysis (excluding patients found to be ineligible, those not receiving all 4 doses within a reasonable time frame, and those with incomplete primary end point data) also did not yield significant results (OR 0.9 [95% CI 0.1, 6.5], $P = 0.95$).

Secondary end points. Longitudinal analyses of patient VAS values did not reveal significant differences in change over time between randomized treatment arms for any of the 6 VAS scores. Figures 2A and B illustrate the levels of symptomatic fatigue and oral dryness reported over time; there were no significant differences between the groups at any time point for these or any of the other symptom scales (see Supplementary Figure B1, http://onlinelibrary.wiley.com/doi/10.1002/art.40093/abstract).

Composite disease activity scores and patient-reported outcome measures showed no benefit conferred by rituximab. There was no significant difference between the 2 groups over time in average ESSPRI or ESSDAI scores (except for a small relative difference in ESSDAI scores at week 36 in favor of rituximab) (Table 2) (also see Supplementary Tables C1–C12, http://onlinelibrary.wiley.com/doi/10.1002/art.40093/abstract). There was no improvement conferred by rituximab in any domain of the SF-36 or in the SF-36 component scores. There was also no improvement conferred by rituximab in the PROFAD-SSI domains at any time point.

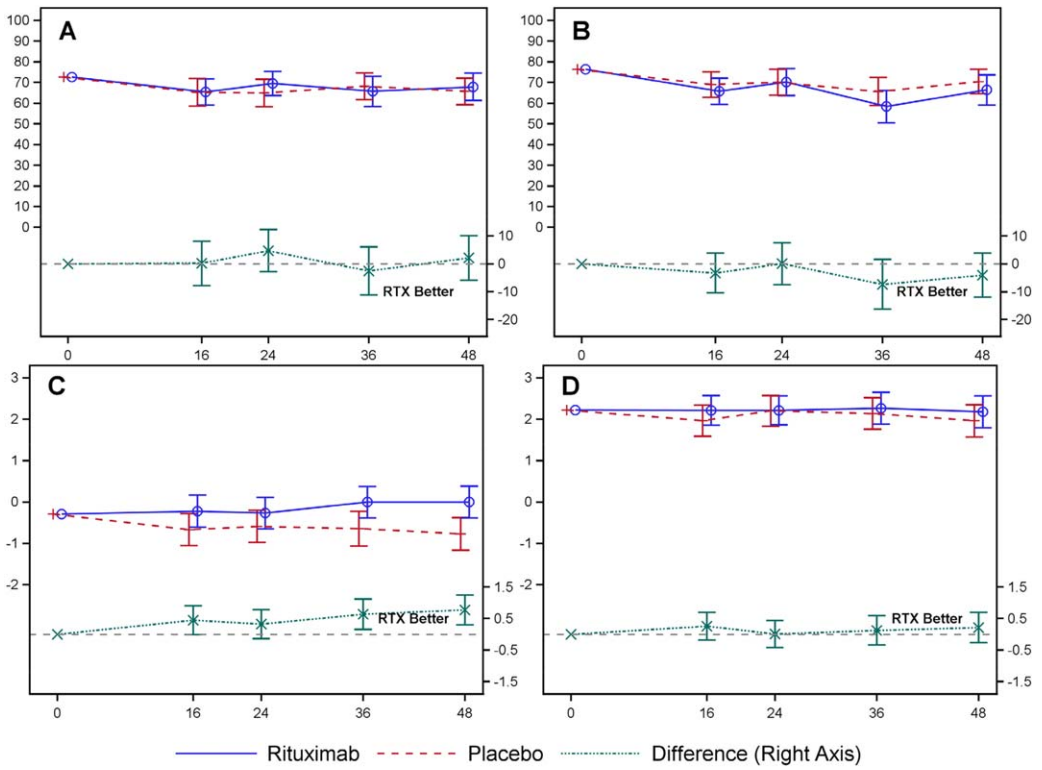

Figure 2. Values for fatigue (in mm on a visual analog scale [VAS]) (**A**), oral dryness (in mm on a VAS) (**B**), unstimulated salivary flow (in ml per 15 minutes) (**C**), and lacrimal flow (in mm per 5 minutes) (**D**). Values are the least squares means and 95% confidence intervals adjusted for baseline values, age, disease duration, and substudy consent (left y-axes) and between-group differences (right y-axes) at each visit (baseline and weeks 16, 24, 36, and 48). Salivary and lacrimal flow are plotted on a $\log_2$ scale. Higher VAS values indicate worse symptom severity; higher log flow rates indicate greater salivary or lacrimal flow. The region in which a difference favors rituximab (RTX) is annotated.

We did observe a difference between treatment arms in unstimulated salivary flow. Over the duration of follow-up, we found that the log-transformed unstimulated salivary flow values seemed to hold constant for rituximab-treated patients and to deteriorate for placebo-treated patients. Although the treatment-by-time interaction effect was not statistically significant at traditional thresholds (estimate 0.013 [95% CI −0.001, 0.028], $P = 0.066$), the between-group differences between the mean values of unstimulated salivary flow at weeks 36 and 48 were statistically significant (Table 2 and Figure 2C). No similar benefit was seen in stimulated salivary flow or in mean lacrimal flow (Figure 2D).

We performed 4 post hoc subgroup analyses to investigate treatment modification effect due to baseline ESSDAI scores (using 2 different thresholds), baseline ESSPRI scores, and disease duration since diagnosis (Table 3). No significant treatment modification effect was observed in any of these subgroup analyses.

Cost-effectiveness. The mean costs and QALY estimates by treatment arm at 48 weeks are included in Supplementary Table D1, http://onlinelibrary.wiley.com/doi/10.1002/art.40093/abstract. When we excluded the rituximab infusion, no significant difference was observed in resource use between treatment arms. However, including the rituximab infusion conferred significant differences in costs between treatment arms. The mean ± SD cost per patient in the rituximab arm was £10,752 ± 264.75, compared to £2,672 ± 241.71 in the placebo arm. Mean ± SD QALYs were 0.55 ± 0.003 and 0.56 ± 0.004 in the rituximab and placebo groups, respectively. The higher mean costs and lower QALYs mean that placebo dominates rituximab (see Supplementary Figure D1, http://onlinelibrary.wiley.com/doi/10.1002/art.40093/abstract). Bootstrapping the mean costs and QALYs suggested that rituximab had a 0% probability of being cost-effective at any threshold from £0 to £200,000.

Safety. Rituximab was well-tolerated among patients. There were no deaths in either treatment arm. There were 10 serious AEs (SAEs) among 9 patients in each treatment arm, of which 3 events in 3 patients in each treatment arm were serious adverse reactions (Table 4). One participant randomized to receive rituximab did not receive any rituximab prior to having an SAE. One serious

Table 2. Summaries of secondary outcome measures adjusted for baseline measurements*

Outcome measure, time point, weeks	Placebo, mean ± SEM†	RTX, mean ± SEM†	Mean difference, RTX – placebo (95% CI)†	*P*‡
Fatigue VAS				
16	65.2 ± 3.4	65.4 ± 3.2	0.16 (−7.79, 8.10)	0.9693
24	64.9 ± 3.4	69.5 ± 3.0	4.67 (−2.87, 12.22)	0.2241
36	68.2 ± 3.3	65.7 ± 3.7	−2.54 (−11.19, 6.11)	0.5639
48	65.8 ± 3.3	67.9 ± 3.3	2.10 (−5.89, 10.09)	0.6053
Oral dryness VAS				
16	69.0 ± 3.1	65.7 ± 3.2	−3.28 (−10.50, 3.94)	0.3725
24	70.1 ± 3.2	70.2 ± 3.3	0.09 (−7.46, 7.64)	0.9821
36	65.7 ± 3.4	58.3 ± 4.0	−7.33 (−16.35, 1.69)	0.1110
48	70.5 ± 3.0	66.4 ± 3.7	−4.06 (−12.01, 3.89)	0.3157
ESSDAI score (log-transformed)§				
16	4.1 ± 1.1	3.4 ± 1.1	0.85 (0.64, 1.11)	0.2234
24	4.4 ± 1.1	4.1 ± 1.1	0.94 (0.73, 1.22)	0.6549
36	4.8 ± 1.1	3.5 ± 1.1	0.74 (0.55, 0.98)	0.0352
48	4.5 ± 1.1	3.4 ± 1.1	0.75 (0.55, 1.03)	0.0721
ESSPRI score				
16	6.3 ± 0.3	6.5 ± 0.3	0.19 (−0.45, 0.82)	0.5682
24	5.8 ± 0.2	6.3 ± 0.2	0.55 (0.01, 1.09)	0.0458
36	6.4 ± 0.3	6.2 ± 0.3	−0.21 (−0.90, 0.49)	0.5622
48	5.7 ± 0.2	6.3 ± 0.3	0.54 (−0.12, 1.20)	0.1087
Unstimulated salivary flow, ml per 15 minutes (log-transformed)§				
16	0.6 ± 1.1	0.9 ± 1.1	1.36 (0.99, 1.88)	0.0583
24	0.7 ± 1.1	0.8 ± 1.1	1.25 (0.91, 1.72)	0.1742
36	0.6 ± 1.2	1.0 ± 1.1	1.56 (1.11, 2.18)	0.0103
48	0.6 ± 1.1	1.0 ± 1.1	1.71 (1.23, 2.37)	0.0015
Mean lacrimal flow, mm per 5 minutes (log-transformed)§¶				
16	2.0 ± 0.2	2.2 ± 0.2	1.19 (0.88, 1.61)	0.2624
24	2.2 ± 0.2	2.2 ± 0.2	1.01 (0.75, 1.35)	0.9642
36	2.1 ± 0.2	2.3 ± 0.2	1.09 (0.79, 1.51)	0.5926
48	2.0 ± 0.2	2.2 ± 0.2	1.16 (0.84, 1.61)	0.3698
SF-36 physical component summary score				
24	38.2 ± 1.0	36.3 ± 1.1	−1.86 (−4.15, 0.43)	0.1107
48	37.9 ± 1.0	37.1 ± 1.1	−0.79 (−3.25, 1.67)	0.5246
SF-36 mental component summary score				
24	41.7 ± 1.4	41.0 ± 1.4	−0.64 (−3.81, 2.54)	0.6924
48	41.0 ± 1.6	41.1 ± 1.5	0.12 (−3.58, 3.82)	0.9495

* RTX = rituximab; 95% CI = 95% confidence interval; VAS = visual analog scale; ESSDAI = European League Against Rheumatism (EULAR) Sjögren's Syndrome Disease Activity Index; ESSPRI = EULAR Sjögren's Syndrome Patient Reported Index; SF-36 = Short Form 36.
† From the covariance pattern model.
‡ By Wald's test.
§ Raw values were highly positively skewed; therefore, they were log-transformed prior to analysis, and the results were back-transformed for presentation. Treatment effects presented for these comparisons are ratios on the original scale rather than differences on the logarithmic scale.
¶ By Schirmer I test.

infusion reaction was reported in 1 patient receiving rituximab, and 1 serious anaphylaxis event was reported in 1 patient receiving placebo. For nonserious AEs, 275 were reported in 55 placebo-treated patients, of which 61 (22.2%) were suspected to be related to treatment, 24 (8.7%) resulted in delayed or modified treatment administration, and 5 (1.8%) resulted in cessation of treatment; 325 nonserious AEs were reported in 61 rituximab-treated patients, of which 82 (25.2%) were suspected to be related to treatment, 33 (10.2%) resulted in delayed or modified treatment administration, and 10 (3.1%) resulted in cessation of treatment.

Table 3. ORs for the effect of RTX relative to placebo on the primary outcome measure and for the interaction between subgroup and treatment effect for selected post hoc subgroups*

Categorization	Adjusted OR of primary end point response, RTX vs. placebo (95% CI)	*P* for interaction†
Baseline ESSDAI score		
≥5	0.55 (0.18, 1.73)	
0–4	2.16 (0.65, 7.16)	
Interaction effect (relative OR)	0.26 (0.05, 1.33)	0.1044
Baseline ESSDAI score		
≥14	1.27 (0.06, 26.44)	
0–13	1.13 (0.49, 2.63)	
Interaction effect (relative OR)	1.12 (0.05, 26.01)	0.9441
Years since diagnosis		
≥5	1.10 (0.31, 3.90)	
0–4	1.11 (0.38, 3.23)	
Interaction effect (relative OR)	1.00 (0.19, 5.35)	0.9969
Baseline ESSPRI score		
5–10	1.16 (0.48, 2.80)	
0–4	1.02 (0.14, 7.62)	
Interaction effect (relative OR)	1.14 (0.13, 10.07)	0.9086

* ORs = odds ratios; RTX = rituximab; 95% CI = 95% confidence interval; ESSDAI = European League Against Rheumatism (EULAR) Sjögren's Syndrome Disease Activity Index; ESSPRI = EULAR Sjögren's Syndrome Patient Reported Index.
† By Wald's test.

DISCUSSION

TRACTISS is the largest randomized, placebo-controlled trial of rituximab in patients with primary SS to date. After 2 courses of treatment, each comprising 2 doses of 1,000 mg of rituximab, patients were not significantly more likely to report a response to treatment at the 48-week time point (in terms of a reduction of 30% of baseline measurement in either oral dryness or fatigue on a VAS questionnaire) than those randomized to receive placebo. These and other patient-reported outcomes of ocular and overall dryness, joint pain, and global assessment of disease activity were not significantly improved by rituximab at any time point. We also did not observe a significant benefit in terms of lacrimal flow or in any of the composite patient-reported outcomes or disease activity indices, except for a one-off significant difference between groups in the ESSDAI score at week 36. We did observe significant differences between the groups in average unstimulated salivary flow rates; rituximab-treated patients maintained their baseline flow rate, while the rate decreased in placebo-treated patients. However, given the many statistical tests performed in these secondary outcome analyses, this may well be a Type I error and should not be overinterpreted. No difference in the safety profile was observed between the 2 treatment arms.

In the economic analyses, a small nonsignificant difference in QALYs was observed between treatment arms in favor of placebo. The main driver of costs was the rituximab infusion, which incurred a cost of £1,746 per 1,000 mg and a significantly higher overall cost compared to placebo. There was no significant difference in costs when rituximab was excluded. Further analysis revealed that even at a willingness-to-pay threshold 10 times higher than the current recommendation of the National Institute for Health and Care Excellence (24), rituximab was not cost-effective; even with a relatively large reduction in price the use of rituximab is unlikely to be cost-effective.

TRACTISS is the fourth double-blind, placebo-controlled, randomized trial of rituximab in primary SS reported to date, bringing the total number of patients included in such studies to 302. The first study, a pilot randomized controlled trial (RCT) in 17 patients (11), showed a greater reduction in fatigue among patients randomized to receive rituximab compared to those receiving placebo, but showed no significant difference in the proportions of

Table 4. Summary of the numbers of serious adverse events and serious adverse reactions observed*

	Placebo	Rituximab
Serious adverse events		
Cardiac: myocardial infarction	1	–
Endocrine: hydatid disease	1	–
Gastrointestinal		
Diarrhea and abdominal pain	1	–
Diarrhea	–	1
Abdominal pain	–	1
Infections and infestations: pneumonia	1	–
Metabolism and nutrition: episode of hypotension	–	1
Musculoskeletal and connective tissue		
Fractured bone	–	1†
Swollen ankle	–	1
Chest pain	1	–
Neoplasms: pancreatic tumor	–	1
Renal and urinary: EUA cystoscopy and TVT release	1	–
Respiratory, thoracic, and mediastinal: pulmonary embolism	1	–
Skin and subcutaneous tissue: malignant melanoma	–	1
Serious adverse reactions		
Infections and infestations		
Chest infection	1	–
Sepsis	–	1
Urinary tract infection	–	1
Injury, poisoning, and procedural complications		
Anaphylaxis	1	–
Serious infusion reaction	–	1
Respiratory, thoracic, and mediastinal: epiglottitis	1	–
Total	10	10

* One patient in the placebo arm and 1 patient in the rituximab arm each reported 2 serious adverse events. EUA = examination under anesthesia; TVT = tension-free vaginal tape.
† One patient randomized to receive rituximab withdrew prior to the first infusion. Subsequently, the patient reported a fall that resulted in a bone fracture.

patients achieving either a 20% or a 30% reduction from baseline in fatigue at 6 months. A later RCT in 30 patients (12) showed significant changes from baseline for most variables (including salivary flow rates and patient-reported measures of fatigue and oral and ocular dryness) in both treatment arms, but the 20 rituximab-treated patients differed significantly from the 10 placebo-treated patients in only stimulated salivary flow at 12 weeks and ocular dryness at 36 and 48 weeks.

Most recently, the TEARS study (13) analyzed 120 patients randomized to receive either rituximab or placebo in a multicenter trial and did not reveal a significant difference in numbers of patients achieving the primary end point (reductions of 30 mm on at least 2 VAS for dryness, pain, fatigue, and global assessment of disease activity). Although a significant response was detected at 6 weeks, particularly in fatigue, this was not sustained by the 24-week time point. Signs of efficacy in fatigue and dryness were evident when these outcome data were analyzed longitudinally, but symptoms of pain and globally assessed disease activity were not significantly improved. As in previous studies, the TEARS study showed no significant difference in safety profiles between the treatment arms.

The TRACTISS trial differed from these randomized trials in that patients were randomized to receive 2 doses of the trial drug in a double-blinded manner. It was hoped that signals of efficacy observed in earlier studies would be seen at the same time points in the TRACTISS trial, and that a second dose would demonstrate long-term efficacy of rituximab. However, early efficacy measured by fatigue at 16 weeks (the TEARS study) and late efficacy in terms of ocular dryness (Meijer et al [12]) were not observed in the TRACTISS trial. Similarly, although we observed significant deterioration in unstimulated salivary flow with placebo compared to rituximab at later time points, no such effect was reported from other RCTs.

Early evidence from nonrandomized trials and uncontrolled studies was more promising. In an open-label prospective study (10), 19 patients at one center received rituximab and 22 patients at another center received DMARD therapy with follow-up over 120 weeks. Patients in that study had higher disease activity (mean baseline ESSDAI score of 20). Significant differences between the 2 treatment arms were demonstrated in fatigue and dryness VAS scores (mean ± SEM fatigue score 51.8 ± 4.5 in the DMARD group versus 41.1 ± 4.2 in the rituximab group at week 120; mean ± SEM dryness score 51.8 ± 11.1 in the DMARD group versus 25.1 ± 7.7 in the rituximab group at week 120) as well as in the ESSDAI score (8.8 ± 1.7 in the DMARD group versus 5.2 ± 0.9 in the rituximab group at week 120), unstimulated salivary flow (0.1 ± 0.08 in the DMARD group versus 0.4 ± 0.04 in the rituximab group at week 120), and lacrimal flow (5.5 ± 0.8 in the DMARD group versus 7.3 ± 0.8 in the rituximab group at week 120). However, bias due to potential differences between practices at the centers, the open-label nature of one study, and the differing additional study medications (DMARDs and prednisone versus methylprednisolone, acetaminophen, and chlorpheniramine) cannot be ruled out. Sixteen patients who received rituximab in an uncontrolled study (30) showed significant improvements from baseline in SF-36 component scores (mean physical and mental component summary score improvements of 16.9 and 31.2, respectively), but no such improvement was found either in our study (Table 2) or in the TEARS study.

Researchers have previously suggested (5,13) that outcome measures used in studies of these patients are not sufficiently sensitive to changes in the patient's condition after successful treatment. To that end, composite outcome measures to be completed by the physician (18) and by the patient (15) were developed by EULAR. These outcome measures were developed in patient populations of an age similar to those in the TEARS study and TRACTISS trial, but the development population profiles for both tools involved patients with slightly longer disease durations (~8.5 years) than seen here. Moerman et al computed ESSDAI scores for all patients in one RCT (31) and concluded that the ESSDAI was sensitive enough to detect a treatment effect of rituximab despite low average ESSDAI scores. In both the TEARS study and the TRACTISS trial, patients had low ESSDAI scores at baseline (relative to the maximum score of 123), and mean improvement in ESSDAI score was not different between the 2 treatment arms. The ESSPRI did not have the same problem as the ESSDAI in the TRACTISS trial, but no significant difference was detected overall, nor did the ESSPRI define a subgroup that demonstrated a benefit. A recent reanalysis of data from the TEARS study (32) proposed a data-driven composite outcome measure, the Sjögren's Syndrome Responder Index (SSRI), rooted in the assumption that rituximab is effective. Data from the TRACTISS trial may assist in the external validation of the SSRI.

A post hoc analysis of data from the TEARS study (33) to estimate the required sample size to detect a significant difference in response rates suggested that the most sensitive end point by which response to treatment can be assessed would be change in ultrasound grading. However, the observed improvement on ultrasonography in the TEARS study (34) did not translate into patient-reported symptomatic improvement. Findings of the TRACTISS ultrasound substudy will be presented at a later date, as will results of the labial gland biopsy substudy.

Despite the requirement for a minimum level of symptomatic fatigue and oral dryness in order to take part

in the TRACTISS trial, the patients mostly had disease of recent onset and had mild systemic disease activity as measured by the ESSDAI. Although the 2 courses of rituximab given constituted a treatment regimen different from the single course in other RCTs, it remains a possibility that a benefit to patients would be seen if rituximab is administered over longer periods of time, such as those seen in longer open-label comparative studies. Further, although TRACTISS is the largest trial of rituximab in primary SS to date, a sample size of 133 patients is small by the standards of phase III randomized trials, and confidence intervals around our estimates were wide. The low population prevalence of primary SS poses challenges to recruitment and emphasizes the importance of patient retention to ensure that studies are adequately powered.

Despite our ambition of performing a meta-analysis with data from the TEARS study, our study omitted a 6-week assessment visit, which was the time point at which the greatest fatigue response was observed in the TEARS study. We omitted this visit to reduce the burden on patients. Although our study had low levels of patient withdrawal (and used multiple imputation to account for uncertainty due to incomplete data), it was necessary to offer to mail questionnaires to some participants to capture primary end point data at 48 weeks.

Like the TEARS study, the TRACTISS trial was designed to have power to detect a large difference in response rates between treatment arms; the possible side effects due to rituximab as well as the underlying inconvenience and costs of rituximab administration mean that a large benefit would need to be demonstrated for rituximab to be worthwhile. The existence of a smaller long-term effect cannot be ruled out—and may be identified in a possible meta-analysis—but it remains to be seen whether a smaller effect would be worthwhile or cost-effective. Moreover, in common with other studies in this context, many outcome measurements were compared at several time points, and we did not adjust our secondary end point analyses for multiple comparisons; it is possible that the relative deterioration in unstimulated salivary flow in placebo-treated patients was a false-positive finding.

Although there did not appear to be any excess risk due to rituximab, the results of the TRACTISS trial do not support the general use of rituximab in treating primary SS, particularly in patients with recent disease onset and/or low disease activity. Meta-analysis with the TEARS study may improve overall precision of findings, but it seems unlikely that the combined results will identify a worthwhile treatment benefit. The need for further large randomized trials to demonstrate longer-term benefit appears questionable, since the lack of effect of 2 courses of rituximab seems consistent with the lack of benefit of 1 course in randomized trials. Rituximab may still have a role in treating patients with primary SS who have high levels of systemic disease activity and whose disease has failed to improve following conventional immunosuppressive therapy.

ACKNOWLEDGMENTS

We acknowledge the assistance of all clinical research staff at participating sites, as well as assistance from Peter Smith, John Rout, and Luke Dawson.

AUTHOR CONTRIBUTIONS

All authors were involved in drafting the article or revising it critically for important intellectual content, and all authors approved the final version to be published. Dr. Bowman had full access to all of the data in the study and takes responsibility for the integrity of the data and the accuracy of the data analysis.

Study conception and design. Bowman, Emery, Pitzalis, Bombardieri.

Acquisition of data. Bowman, Pitzalis, Ng, Pease, Price, Sutcliffe, Gendi, Hall, Ruddock, Fernandez, Reynolds, Davies, Edwards, Lanyon, Moots, Roussou, Giles, Bombardieri.

Analysis and interpretation of data. Bowman, Everett, O'Dwyer, Emery, Ng, Pease, Price, Sutcliffe, Gendi, Hall, Ruddock, Fernandez, Reynolds, Hulme, Davies, Edwards, Lanyon, Moots, Roussou, Giles, Sharples, Bombardieri.

REFERENCES

1. Fox RI, Stern M, Michelson P. Update in Sjögren syndrome. Curr Opin Rheumatol 2000;12:391–8.
2. Bowman SJ, Booth DA, Platts RG, UK Sjögren's Interest Group. Measurement of fatigue and discomfort in primary Sjögren's syndrome using a new questionnaire tool. Rheumatology (Oxford) 2004;43:758–64.
3. Vivino FB, Al-Hashimi I, Khan Z, LeVeque FG, Salisbury PL III, Tran-Johnson TK, et al. Pilocarpine tablets for the treatment of dry mouth and dry eye symptoms in patients with Sjögren syndrome: a randomized, placebo-controlled, fixed-dose, multicenter trial. Arch Intern Med 1999;159:174–81.
4. Papas AS, Sherrer YS, Charney M, Golden HE, Medsger TA Jr, Walsh BT, et al. Successful treatment of dry mouth and dry eye symptoms in Sjögren's syndrome patients with oral pilocarpine: a randomized, placebo-controlled, dose-adjustment study. J Clin Rheumatol 2004;10:169–77.
5. Gottenberg JE, Ravaud P, Puéchal X, Le Guern V, Sibilia J, Goeb V, et al. Effects of hydroxychloroquine on symptomatic improvement in primary Sjögren syndrome: the JOQUER randomized clinical trial. JAMA 2014;312:249–58.
6. Ware JE Jr, Snow KK, Kosinski M, Gandek B. SF-36 health survey: manual and interpretation guide. Boston: The Health Institute, New England Medical Center; 1993.
7. Devauchelle-Pensec V, Pennec Y, Morvan J, Pers JO, Daridon C, Jousse-Joulin S, et al. Improvement of Sjögren's syndrome after two infusions of rituximab (anti-CD20). Arthritis Care Res (Hoboken) 2007;57:310–7.
8. Pijpe J, van Imhoff GW, Spijkervet FK, Roodenburg JL, Wolbink GJ, Mansour K, et al. Rituximab treatment in patients with primary Sjögren's syndrome: an open-label phase II study. Arthritis Rheum 2005;52:2740–50.
9. St.Clair EW, Levesque MC, Prak ET, Vivino FB, Alappatt CJ, Spychala ME, et al. Rituximab therapy for primary Sjögren's syndrome: an open-label clinical trial and mechanistic analysis. Arthritis Rheum 2013;65:1097–106.
10. Carubbi F, Cipriani P, Marrelli A, Benedetto P, Ruscitti P, Berardicurti O, et al. Efficacy and safety of rituximab treatment

in early primary Sjögren's syndrome: a prospective, multi-center, follow-up study. Arthritis Res Ther 2013;15:R172.
11. Dass S, Bowman SJ, Vital EM, Ikeda K, Pease CT, Hamburger J, et al. Reduction of fatigue in Sjögren syndrome with rituximab: results of a randomised, double-blind, placebo-controlled pilot study. Ann Rheum Dis 2008;67:1541–4.
12. Meijer JM, Meiners PM, Vissink A, Spijkervet FK, Abdulahad W, Kamminga N, et al. Effectiveness of rituximab treatment in primary Sjögren's syndrome: a randomized, double-blind, placebo-controlled trial. Arthritis Rheum 2010;62:960–8.
13. Devauchelle-Pensec V, Mariette X, Jousse-Joulin S, Berthelot JM, Perdriger A, Puéchal X, et al. Treatment of primary Sjögren syndrome with rituximab: a randomized trial. Ann Intern Med 2014;160:233–42.
14. Brown S, Navarro Coy N, Pitzalis C, Emery P, Pavitt S, Gray J, et al. The TRACTISS Protocol: a randomised double blind placebo controlled clinical TRial of Anti-B-Cell Therapy In patients with primary Sjögren's Syndrome. BMC Musculoskelet Disord 2014;15:21.
15. Seror R, Ravaud P, Mariette X, Bootsma H, Theander E, Hansen A, et al. EULAR Sjögren's Syndrome Patient Reported Index (ESSPRI): development of a consensus patient index for primary Sjögren's syndrome. Ann Rheum Dis 2011;70:968–72.
16. Bowman SJ, Hamburger J, Richards A, Barry RJ, Rauz S. Patient-reported outcomes in primary Sjögren's syndrome: comparison of the long and short versions of the Profile of Fatigue and Discomfort—Sicca Symptoms Inventory. Rheumatology (Oxford) 2009;48:140–3.
17. Hurst NP, Kind P, Ruta D, Hunter M, Stubbings A. Measuring health-related quality of life in rheumatoid arthritis: validity, responsiveness and reliability of EuroQol (EQ-5D). Br J Rheumatol 1997;36:551–9.
18. Seror R, Ravaud P, Bowman SJ, Baron G, Tzioufas A, Theander E, et al, on behalf of the EULAR Sjögren's Task Force. EULAR Sjögren's Syndrome Disease Activity Index: development of a consensus systemic disease activity index for primary Sjögren's syndrome. Ann Rheum Dis 2010;69:1103–9.
19. Vitali C, Palombi G, Baldini C, Benucci M, Bombardieri S, Covelli M, et al. Sjögren's Syndrome Disease Damage Index and Disease Activity Index: scoring systems for the assessment of disease damage and disease activity in Sjögren's syndrome, derived from an analysis of a cohort of Italian patients. Arthritis Rheum 2007;56:2223–31.
20. Barry RJ, Sutcliffe N, Isenberg DA, Price E, Goldblatt F, Adler M, et al. The Sjögren's Syndrome Damage Index—a damage index for use in clinical trials and observational studies in primary Sjögren's syndrome. Rheumatology (Oxford) 2008;47:1193–8.
21. Bowman SJ, Sutcliffe N, Isenberg DA, Goldblatt F, Adler M, Price E, et al. Sjögren's Systemic Clinical Activity Index (SCAI)–a systemic disease activity measure for use in clinical trials in primary Sjögren's syndrome. Rheumatology (Oxford) 2007;46:1845–51.
22. White IR, Royston P, Wood AM. Multiple imputation using chained equations: issues and guidance for practice. Stat Med 2011;30:377–99.
23. Rubin DB. Multiple imputation for nonresponse in surveys. New York: John Wiley & Sons; 2008.
24. National Institute for Health and Care Excellence. Guide to the methods of technology appraisal 2013. April 4, 2013. URL: https://www.nice.org.uk/process/pmg9/resources/guide-to-the-methods-of-technology-appraisal-2013-pdf-2007975843781.
25. Joint Formulary Committee. British national formulary. 67th ed. London: BMJ Group and Pharmaceutical Press; 2013.
26. Department of Health. National schedule of reference costs. URL: https://www.gov.uk/government/publications/nhs-reference-costs-2013-to-2014.
27. Curtis L. Unit costs of health & social care 2014. Canterbury: Personal Social Services Research Unit; 2014.
28. Dolan P. Modeling valuations for EuroQol health states. Med Care 1997;35:1095–108.
29. Ramsey S, Willke R, Briggs A, Brown R, Buxton M, Chawla A, et al. Good research practices for cost-effectiveness analysis alongside clinical trials: the ISPOR RCT-CEA Task Force report. Value Health 2005;8:521–33.
30. Devauchelle-Pensec V, Morvan J, Rat AC, Jousse-Joulin S, Pennec Y, Pers JO, et al. Effects of rituximab therapy on quality of life in patients with primary Sjögren's syndrome. Clin Exp Rheumatol 2010;29:6–12.
31. Moerman RV, Arends S, Meiners PM, Brouwer E, Spijkervet FK, Kroese FG, et al. EULAR Sjögren's Syndrome Disease Activity Index (ESSDAI) is sensitive to show efficacy of rituximab treatment in a randomised controlled trial. Ann Rheum Dis 2014;73:472–4.
32. Cornec D, Devauchelle-Pensec V, Mariette X, Jousse-Joulin S, Berthelot JM, Perdriger A, et al. Development of the Sjögren's Syndrome Responder Index, a data-driven composite endpoint for assessing treatment efficacy. Rheumatology (Oxford) 2015;54:1699–708.
33. Devauchelle-Pensec V, Jousse-Joulin S, Mariette X, Berthelot JM, Perdriger A, Hachulla E, et al. Impact of different end points on the patient cohort size needed to demonstrate the efficacy of a therapeutic intervention in PSS: a post hoc analysis of the TEARS study (Tolerance and Efficacy of Rituximab in Primary Sjögren Syndrome study) [abstract]. Arthritis Rheum 2013;65 Suppl:S1235.
34. Jousse-Joulin S, Devauchelle-Pensec V, Cornec D, Marhadour T, Bressollette L, Gestin S, et al. Ultrasonographic assessment of salivary gland response to rituximab in primary Sjögren's syndrome. Arthritis Rheumatol 2015;67:1623–8.

APPENDIX A: SITE PRINCIPAL INVESTIGATORS, TRIAL STEERING COMMITTEE, DATA MONITORING AND ETHICS COMMITTEE, AND CLINICAL TRIALS RESEARCH UNIT

Site Principal Investigators. Mohammed Akil, MD, FRCP, Prof. Simon J. Bowman, PhD, FRCP, Prof. Baskar Dasgupta, Kevin A. Davies, MD, Christopher J. Edwards, MBBS, MD, FRCP, Nagui S. T. Gendi, MSc, FRCP, Ian P. Giles, BSc, MBBS, PhD, FRCP, Frances C. Hall, BM, BCh, DPhil, RCP(UK), Philip Helliwell, PhD, Pauline Ho, PhD, FRCP, John Hunter, MBChB, Sanjeet Kamath, MD, FRCP, Bruce Kirkham, MD, Peter C. Lanyon, MB, ChB, DM, Prof. Neil McHugh, Devesh Mewar, MB, PhD, Robert J. Moots, MD, PhD, Diarmuid Mulherin, MD, Wan-Fai Ng, FRCP, PhD, Colin T. Pease, MD, FRCP, Elizabeth J. Price, MBBCh, FRCP, MD, Marian Regan, MB, Euthalia Roussou, MD, DM, Vadivelu Saravanan, MD, FRCP, and Nurhan Sutcliffe, MD, FRCP.

Trial Steering Committee. Prof. Ian Bruce, Ian Griffiths, MBBS, FRCP, Prof. David Isenberg, FRCP, Ashley Jones, PhD, and Linda Stone, BPharm, FRPharmS.

Data Monitoring and Ethics Committee. Marwan Bukhari, FRCP, PhD, Martyn Lewis, PhD, and Jon Packham, DM.

Clinical Trials Research Unit. Sarah Brown, MSc and Janine C. Gray, PhD.

ARTHRITIS & RHEUMATOLOGY
Vol. 69, No. 7, July 2017, pp 1451–1460
DOI 10.1002/art.40114

Mycophenolate Mofetil Versus Placebo for Systemic Sclerosis–Related Interstitial Lung Disease

An Analysis of Scleroderma Lung Studies I and II

Elizabeth R. Volkmann,[1] Donald P. Tashkin,[1] Ning Li,[1] Michael D. Roth,[1] Dinesh Khanna,[2] Anna-Maria Hoffmann-Vold,[3] Grace Kim,[1] Jonathan Goldin,[1] Philip J. Clements,[1] Daniel E. Furst,[1] and Robert M. Elashoff[1]

Objective. **To compare mycophenolate mofetil (MMF) with placebo for the treatment of systemic sclerosis (SSc)–related interstitial lung disease (ILD).**

Methods. **We included participants enrolled in the placebo arm of Scleroderma Lung Study (SLS) I and the MMF arm of SLS II. SLS I randomized participants to receive either oral cyclophosphamide (CYC) or placebo for 1 year, while SLS II randomized participants to receive either MMF for 2 years or oral CYC for 1 year followed by 1 year of placebo. Eligibility criteria for SLS I and SLS II were nearly identical. The primary outcome was % predicted forced vital capacity (FVC), and key secondary outcomes included % predicted diffusing capacity for carbon monoxide (DL$_{CO}$), the modified Rodnan skin thickness score (MRSS), and dyspnea. Joint models were created to evaluate the treatment effect on the course of these outcomes over 2 years.**

Results. **At baseline, the MMF-treated group in SLS II (n = 69) and the placebo-treated group in SLS I (n = 79) had similar percentages of men and women and similar disease duration, SSc subtype, extent of skin disease, and % predicted FVC. MMF-treated patients in SLS II were slightly older (mean ± SD age 52.6 ± 9.7 years versus 48.1 ± 12.4 years; $P = 0.0152$) and had higher % predicted DL$_{CO}$ (mean ± SD 54.0 ± 11.1 versus 46.2 ± 13.3; $P = 0.0002$) than placebo-treated patients in SLS I. After adjustment for baseline disease severity, treatment with MMF in comparison with placebo was associated with improved % predicted FVC ($P < 0.0001$), % predicted DL$_{CO}$ ($P < 0.0001$), MRSS ($P < 0.0001$), and dyspnea ($P = 0.0112$) over 2 years.**

Conclusion. **Although there are inherent limitations in comparing participants from different trials, treatment with MMF was associated with improvements in physiologic outcomes and dyspnea compared with placebo, even after accounting for baseline disease severity. These results further substantiate the use of MMF for the treatment of SSc-related ILD.**

Interstitial lung disease (ILD) accounts for the majority of deaths in patients with systemic sclerosis (SSc) (1,2). Historically, randomized controlled trials have favored the use of cyclophosphamide (CYC) for treating SSc-related ILD (3,4). Given concerns regarding the potential long-term toxicity associated with CYC use, mycophenolate mofetil (MMF) has

Supported by the NIH (National Heart, Lung, and Blood Institute grants R01-HL-089758 [to Dr. Tashkin] and R01-HL-089901 [to Dr. Elashoff], and National Center for Advancing Translational Sciences grant UL1-TR-000124 [to Dr. Li through the University of California, Los Angeles]) and the Scleroderma Foundation (Young Investigator Award to Dr. Volkmann).

[1]Elizabeth R. Volkmann, MD, MS, Donald P. Tashkin, MD, Ning Li, PhD, Michael D. Roth, MD, Grace Kim, PhD, Jonathan Goldin, MD, PhD, Philip J. Clements, MD, MPH, Daniel E. Furst, MD, Robert M. Elashoff, PhD: University of California, Los Angeles; [2]Dinesh Khanna, MD, MS: University of Michigan Medical School, Ann Arbor; [3]Anna-Maria Hoffmann-Vold, MD, PhD: Oslo University Hospital, Oslo, Norway.

Dr. Tashkin has received consulting fees, speaking fees, and/or honoraria from EMD Serono (less than $10,000). Dr. Khanna has received consulting fees, speaking fees, and/or honoraria from Bayer, Cytori, EMD Serono (Merck), Forward, Genentech/Roche (InterMune), and Lycera (less than $10,000 each) and research grants from Bristol-Myers Squibb and Genentech/Roche (InterMune). Dr. Furst has received consulting fees from AbbVie, Amgen, Bristol-Myers Squibb, Cytori, Janssen, Gilead, GlaxoSmithKline, NIH, Novartis, Pfizer, Roche/Genentech, UCB, and Actelion (less than $10,000 each) and research grants from AbbVie, Actelion, Amgen, Bristol-Myers Squibb, Gilead, GlaxoSmithKline, Novartis, Pfizer, Roche/Genentech, and UCB.

Address correspondence to Elizabeth R. Volkmann, MD, MS, 1000 Veteran Avenue, Suite 32-59, Los Angeles, CA 90095. E-mail: evolkmann@mednet.ucla.edu.

Submitted for publication November 21, 2016; accepted in revised form March 28, 2017.

emerged as an alternative treatment for SSc-related ILD (5). Uncontrolled studies have demonstrated that MMF may prevent progression of SSc-related ILD (6–12).

To further explore the safety and efficacy of MMF in SSc-related ILD, Tashkin and colleagues designed Scleroderma Lung Study (SLS) II to directly compare CYC with MMF for the treatment of SSc-related ILD (13). The study demonstrated that the majority of participants in the MMF arm (72%) showed improvements in % predicted forced vital capacity (FVC) (13). However, as the study design lacked a placebo arm, it has been difficult to interpret the absolute magnitude of the treatment effect for MMF when compared to the natural history of SSc-related ILD. A proportion of patients with SSc-related ILD exhibit intrinsically stable ILD that fails to progress even in the absence of treatment (14).

To address this shortcoming, the present study compared outcomes for patients assigned to the MMF arm of SLS II with outcomes for patients assigned to the placebo arm of SLS I. The primary objective was to determine whether patients assigned to receive MMF experienced an improvement in % predicted FVC over 24 months compared with patients assigned to receive placebo. The study also aimed to compare secondary efficacy outcomes and the safety profiles for patients in these 2 groups.

PATIENTS AND METHODS

Study participants. All participants enrolled in the MMF arm of SLS II (13) and the placebo arm of SLS I (3) were included in this analysis. Participating centers and investigators were similar for both trials. Eligibility criteria for both studies were also similar. Common inclusion criteria were age ≥18 years, duration of disease ≤7 years from onset of the first non–Raynaud's phenomenon symptom of SSc, FVC 40–85% predicted (SLS I) or 40–80% predicted (SLS II), hemoglobin-adjusted single-breath diffusing capacity for carbon monoxide (DLCO) ≥40% predicted (or 30–39% predicted if no evidence of clinically significant pulmonary hypertension), and evidence of *any* ground glass opacity (i.e., hazy parenchymal opacity) on high-resolution computed tomography (HRCT) of the chest in the presence or absence of reticular opacity or architectural distortion, as an indication of "active" disease. MMF and matching placebo were supplied at no charge through Drug Supply Grant CEL539 from Hoffmann-La Roche/Genentech.

The only difference between SLS I and SLS II entry criteria related to bronchoscopy. In SLS I, patients were encouraged to undergo a screening bronchoscopy and considered eligible if they had ≥3% neutrophils and/or ≥2% eosinophils in bronchoalveolar lavage fluid even if they had an HRCT scan that did not show any ground glass opacity. Sixteen of the 162 randomized participants (9.9%) in SLS I were included based on these criteria. Although they did not have ground glass opacity, all of these patients did exhibit evidence of fibrosis on HRCT. Bronchoscopy was not performed in SLS II, and all patients were required to have ground glass opacity on HRCT. Exclusion criteria for both studies were nearly identical (3,13).

SLS I and SLS II study design. SLS I consisted of 162 participants randomized between September 2000 and January 2004 and assigned to receive either oral CYC (titrated to 2.0 mg/kg once daily) or matching placebo for 1 year followed by an additional year of observation while not receiving treatment, as previously reported (15). In SLS II, 142 patients were randomized between September 2009 and December 2012 and assigned to receive either MMF (titrated as tolerated to 3.0 gm/day in divided doses) for 2 years or oral CYC (titrated as tolerated to 2 mg/kg once daily) for 1 year followed by an additional year receiving placebo, using a double-dummy design to maintain the blinding (13).

SLS I and SLS II assessment measurement. Baseline measurements included the following physiologic variables: spirometry (FVC, forced expiratory volume in 1 second), lung volumes (functional residual capacity, residual volume, and total lung capacity by whole-body plethysmography or helium dilution), and DLCO and DLCO corrected for alveolar volume. The FVC (primary SLS I/II end point) and DLCO (secondary SLS I/II end point) were measured every 3 months during the trials. Dyspnea was assessed using the Baseline Dyspnea Index (BDI) at baseline and using the Transition Dyspnea Index (TDI) every 3 months thereafter for SLS I and every 6 months thereafter for SLS II (16,17). In SLS I, an interview-administered paper version of the BDI/TDI was used (16), while in SLS II a self-administered computer-assisted version of the BDI/TDI was used (17). The modified Rodnan skin thickness score (MRSS) (18) was used to assess cutaneous sclerosis. The MRSS was obtained every 3 months in SLS II and every 6 months in SLS I.

HRCT thoracic imaging was obtained at baseline and at 24 months in SLS II and at baseline and at 12 months in SLS I. Both studies used similar HRCT acquisition and analysis methods (19), except that in SLS I nonvolumetric CT scans of 1–2-mm slice thickness were acquired at 10-mm increments, while in SLS II volumetric CT scans of 1–1.5-mm slice thickness were acquired contiguously. For both studies, scans were reconstructed with sharp or manufacturer-recommended overenhancing filters. After semiautomated lung segmentation, the images were entered into a quantitative image workstation to produce quantitative scores automatically as described previously (20). For the present study, we report the quantitative lung fibrosis score, which represents the percentage of counts with reticular opacity with architectural distortion, and the quantitative ILD (QILD) score, which represents the sum of all scores classified as abnormal, including scores for fibrosis, ground glass opacity, and honeycombing, defined as clustered air-filled cysts with dense walls. In both studies, scores were summed using the same methods both for the whole lung (including both lungs) and for the zone of maximal involvement.

Statistical analysis. *Baseline characteristics.* Summary statistics were generated for baseline characteristics of the 2 cohorts. Group comparisons were performed using a 2-sample *t*-test, a Wilcoxon rank sum test, and a chi-square test.

Primary outcome of FVC (% predicted). An intent-to-treat principle was applied to all analyses using an inferential joint model consisting of a mixed-effects model for longitudinal outcomes and a survival model to handle nonignorable missing data due to study dropout, treatment failure, or death (i.e., likely related to disease or treatment and therefore not random) (21,22). The joint model was used as our primary inferential approach because it can provide unbiased and efficient estimates when there are nonignorable missing data in the outcomes due to

Table 1. Baseline characteristics of the participants assigned to placebo in SLS I and MMF in SLS II*

Characteristic (n)	Placebo (n = 79)	MMF (n = 69)	*P*
Age, mean ± SD (range) years (148)	48.1 ± 12.4 (19–83)	52.6 ± 9.7 (34–79)	0.0152†
Women, % (148)	64.6	69.6	0.5184‡
Duration of scleroderma, years (146)§			0.0742¶
Median (IQR)	3.0 (1.7–4.7)	2.1 (1.3–4.2)	
Range	0.2–6.8	0.3–6.5	
Limited/diffuse disease, % (148)	43.0/57.0	37.7/62.3	0.5079‡
FVC, mean ± SD % predicted (148)	68.6 ± 13.0	66.5 ± 8.3	0.2510†
DLco, mean ± SD % predicted (148)	46.2 ± 13.3	54.0 ± 11.1	0.0002†
BDI, mean ± SD focal score (range 0–12) (144)	5.7 ± 2.0	7.3 ± 2.1	<0.0001†
SF-36 score, mean ± SD			
Physical component summary (148)	34.3 ± 10.7	36.0 ± 10.0	0.3326†
Mental component summary (148)	50.7 ± 10.6	49.1 ± 7.9	0.2847†
MRSS (range 0–51)			
All patients (148)			0.3776¶
Median (IQR)	11 (4–21)	13 (6–24)	
Range	0–40	1–41	
Patients with dcSSc (88)			0.8351¶
Median (IQR)	19 (13–28)	20 (13–26)	
Range	6–40	4–41	
Patients with lcSSc (60)			0.4677¶
Median (IQR)	4 (3–7)	6 (4–7)	
Range	0–14	1–14	
HAQ DI score, median (IQR) (range 0–3) (148)	0.5 (0.1–1.1)	0.6 (0.1–1.1)	0.7110¶
QLF-WL score, median (IQR) (131)	8.0 (2.6–13.0)	7.1 (2.9–11.8)	0.5309¶
QLF-ZM score, median (IQR) (131)	21.4 (8.7–36.5)	18.6 (5.7–34.0)	0.5249¶
QILD-WL score, mean ± SD (131)	35.3 ± 16.9	27.2 ± 13.2	0.0027†
QILD-ZM score, mean ± SD (131)	58.0 ± 21.3	50.0 ± 20.9	0.0321†

* SLS = Scleroderma Lung Study; MMF = mycophenolate mofetil; IQR = interquartile range; FVC = forced vital capacity; DLco = diffusing capacity for carbon monoxide; BDI = Baseline Dyspnea Index (lower scores indicate worse dyspnea); SF-36 = Short Form 36; MRSS = modified Rodnan skin thickness score (higher scores indicate more severe thickening); dcSSc = diffuse cutaneous systemic sclerosis; lcSSc = limited cutaneous SSc; HAQ DI = Health Assessment Questionnaire disability index (higher scores indicate greater disability); QLF-WL = quantitative lung fibrosis (on high-resolution computed tomography [HRCT]) for the whole lung; QLF-ZM = QLF (on HRCT) for zone of maximal involvement; QILD-WL = quantitative interstitial lung disease (score includes scores for fibrosis, ground-glass opacity, and honeycombing) for the whole lung; QILD-ZM = QILD for zone of maximal involvement.
† By *t*-test.
‡ By chi-square test.
§ Based on onset of the first non–Raynaud's phenomenon symptom attributable to SSc.
¶ By Wilcoxon's rank sum test.

dropouts, treatment failures, and deaths. The complete-case analysis was not believed to be a valid approach in this scenario since it assumes data are missing completely at random. Consistent with the intent-to-treat principle, those for whom treatment had failed and others who withdrew prematurely from the double-blind treatment phase were encouraged to return for outcome monitoring up until 24 months for both studies.

Repeated measurements of % predicted FVC were characterized by a linear mixed-effects submodel in the joint model, and intrasubject data correlation among multiple measurements over time was accounted for by random intercept and random time trend. Fixed effects were prespecified covariates for the primary outcome including baseline % predicted FVC, baseline whole lung QILD score, a time trend, treatment assignment, treatment assignment–time trend interactions, and treatment assignment–QILD score interaction. The time trend was modeled by linear splines with knots at 12 and 21 months. The location of knots was determined by preliminary examination of the data using descriptive statistics. Treatment assignment was coded as a binary variable with placebo as the reference by convention. Thus, the model estimates 3 piecewise linear trends for the placebo group at 3–12 months, 12–21 months, and 21–24 months as well as change in these time trends in the MMF group when compared to placebo.

Secondary outcomes of DLco (% predicted), TDI, MRSS, and safety. Secondary efficacy end points were also analyzed using a joint model with no adjustment for multiple comparisons. For safety analyses, descriptive statistics were used to compare the incidence of adverse events (AEs) and serious AEs (SAEs) between treatment arms. The definitions of specific AEs (leukopenia, anemia, etc.) were identical between SLS I and SLS II (3,13).

All tests were 2-sided. Group comparisons of baseline characteristics were performed using SAS 9.4 (SAS Institute). The joint model was implemented in C, which calls functions in the GNU Scientific Library (http://www.gnu.org/software/gsl).

RESULTS

Baseline characteristics of the study patients. Patients assigned to MMF in SLS II and placebo in SLS I

exhibited similar baseline demographic features except for a slight difference in age (Table 1). The extent of lung disease, as measured by % predicted FVC, and skin involvement, as measured by the MRSS, were also similar. Patients assigned to placebo had a lower % predicted DLCO and more extensive QILD than those in the MMF arm. Patients assigned to placebo reported more dyspnea at baseline than those assigned to MMF, although, as mentioned above, different versions of the BDI were used in SLS I and SLS II.

Disposition of the study participants. In SLS II, 20 patients (29.0%) in the MMF arm prematurely stopped study drug treatment (due to 1 death, no treatment failures, and 19 withdrawals for other reasons) over 24 months. An additional 4 deaths in the MMF arm occurred in subjects who had already withdrawn for other reasons. In SLS I, during the initial 12 months, 24 patients (30.4%) in the placebo arm prematurely stopped study drug treatment (due to 3 deaths, 5 treatment failures, and 16 withdrawals for other reasons). Of the 55 patients in the placebo arm who remained at the conclusion of the 12-month treatment period, 45 completed visits up to and including the 24-month visit. An additional 11 patients in the placebo arm returned for the 24-month visit after having withdrawn or after treatment had failed at earlier time points in the study. Among the 56 patients in the placebo arm who were followed up for the entire 24 months, an additional 10 withdrew from the study during the second year of follow-up (due to 1 death, 3 treatment failures, and 6 withdrawals from the study) (for patient disposition details, see Supplementary Figure 1, available on the *Arthritis & Rheumatology* web site at http://onlinelibrary.wiley.com/doi/10.1002/art.40114/abstract).

Use of potential disease-modifying therapy in the placebo arm. Of the 56 patients in the placebo arm who were followed up during year 2 of SLS I, 14 began treatment with immunosuppressive agents during this year of observation while not receiving the study drug. Therapies included prednisone at >10 mg daily (mean dose 11.6 mg daily) in 12 patients and oral CYC (mean dose 72.5 mg daily) in 2 patients. No patients received MMF or azathioprine during this time. Our previous study found that neither prednisone nor oral CYC had an independent effect on any of the outcome measures at 24 months in SLS I (15).

Association of MMF treatment with improved course of FVC. After controlling for baseline % predicted FVC and baseline whole lung QILD score, treatment with MMF was associated with improved % predicted FVC over 24 months (Table 2 and Figure 1). The test of the overall treatment group effect for the entire model was highly significant ($P < 0.0001$). From 3 to 12 months, patients in the MMF arm experienced significant improvement in % predicted FVC compared with those in the placebo arm (Figure 1). There was continued improvement in % predicted FVC from 12 to 24 months in the MMF arm. In contrast, in the placebo arm, there was a significant decline in % predicted FVC from 3 to 12 months, with subsequent improvement from 12 to 21 months. From 12 to 21 months and from 21 to 24 months, there was no significant difference in % predicted FVC between the 2 groups (Table 2 and Figure 1); however, as depicted in Supplementary Figures 2 and 3 (http://onlinelibrary.wiley.com/doi/10.1002/art.40114/abstract), substantially more patients assigned to MMF in SLS II experienced an improvement in FVC at both 12 and 24 months compared with patients assigned to placebo.

Using the intent-to-treat population, 64.4% and 71.7% of MMF-treated patients had any improvement in % predicted FVC at 12 and 24 months, respectively, and the majority of patients who experienced improvement in % predicted FVC at 24 months had an absolute improvement of >5% (Supplementary Figures 2 and 3). Among those who completed the study, the percentage of MMF-treated patients who had any improvement in % predicted FVC at 24 months was even higher (75.5%) (13). In contrast, only 28.8% of placebo-treated patients had any improvement in % predicted FVC at 12 months, and 37.5% had any improvement in % predicted FVC at 24 months (Supplementary Figures 2 and 3).

Table 2. Association of MMF treatment with improved overall course of % predicted FVC over 24 months using a joint model analysis (n = 125)*

Covariate	Estimated effect	Standard error	*P*
Time†			
3–12 months	−0.49	0.13	0.0002
12–21 months	0.54	0.16	0.0007
21–24 months	0.17	0.36	0.64
Baseline % predicted FVC	0.97	0.02	<0.0001
Baseline QILD-WL score	0.01	0.02	0.62
Treatment arm assignment‡	0.002	1.21	0.999
Interaction of treatment arm assignment and time§			
3–12 months	0.68	0.19	0.0003
12–21 months	−0.03	0.24	0.90
21–24 months	0.38	0.56	0.50
Interaction of treatment arm assignment and baseline QILD-WL score	−0.02	0.03	0.50

* See Table 1 for definitions.
† The reference group is the placebo arm; therefore, these time trends represent the trends observed in the placebo arm. From 3 to 12 months, there was a significant decline in % predicted FVC in the placebo arm (estimated effect −0.49).
‡ Represents estimate for baseline differences in % predicted FVC by treatment arm.
§ These time trends represent trends observed in the MMF arm compared with those observed in the placebo arm. From 3 to 12 months, there was a significant improvement in % predicted FVC in the MMF arm compared with the placebo arm (estimated effect 0.68).

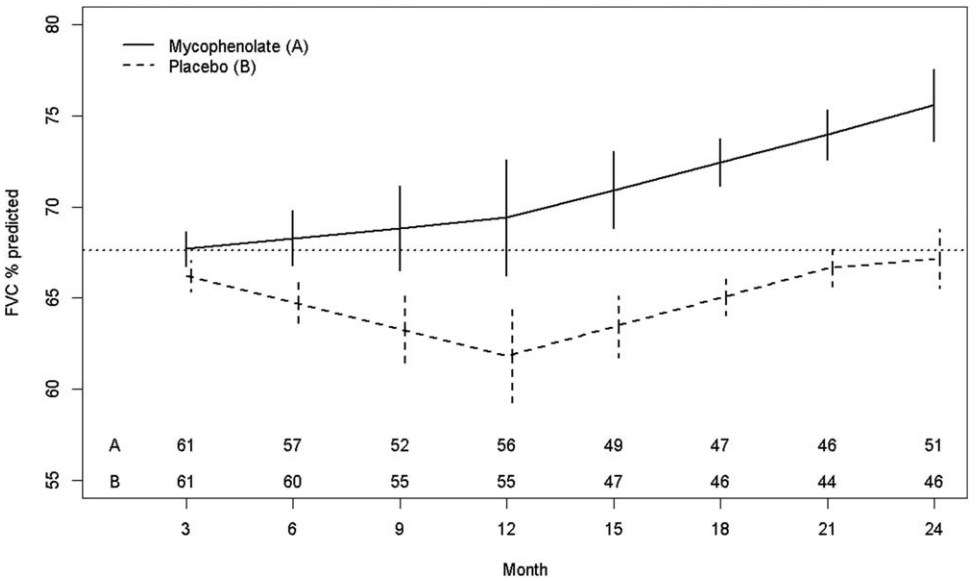

Figure 1. Course of the % predicted forced vital capacity (FVC) from 3 to 24 months in Scleroderma Lung Study (SLS) II patients assigned to receive mycophenolate mofetil versus SLS I patients assigned to receive placebo, using joint model analysis. Values are the mean (numbers of patients at time points are shown for each group). The test of the overall treatment group effect was significant at $P < 0.0001$. Prespecified covariates for this model included baseline % predicted FVC and baseline whole lung quantitative interstitial lung disease score. The dotted line represents the mean baseline value for the entire cohort.

The joint model also revealed that patients with a higher % predicted FVC at baseline had improved % predicted FVC over 24 months (Table 2). The absolute change in % predicted FVC (unadjusted) over 24 months by treatment arm appears in Supplementary Table 1A (http://onlinelibrary.wiley.com/doi/10.1002/art.40114/abstract).

Association of MMF treatment with improved course of DLco. After controlling for baseline % predicted DLco and baseline whole lung QILD score, treatment with MMF was associated with improved % predicted DLco over 24 months ($P < 0.0001$) (Figure 2). From 3 to 12 months, patients in the MMF arm experienced significant improvement in % predicted DLco compared with those in the placebo arm ($P = 0.0063$) (Figure 2), while patients in the placebo arm experienced significant decline in % predicted DLco ($P = 0.0060$) (Figure 2). From 12 to 21 months ($P = 0.38$) and from 21 to 24 months ($P = 0.99$), there was no significant difference in % predicted DLco between groups (Figure 2). While statistically significant, the improvement in % predicted DLco in the MMF arm relative to the placebo arm is of uncertain clinical significance.

The joint model also revealed that baseline % predicted DLco (estimated effect 0.95; standard error 0.03; $P < 0.0001$) and baseline whole lung QILD score (estimated effect 0.08; standard error 0.03; $P = 0.0077$) were independently associated with % predicted DLco over 24 months (see Supplementary Table 2, http://onlinelibrary.wiley.com/doi/10.1002/art.40114/abstract). The absolute change in % predicted DLco (unadjusted) over 24 months by treatment arm appears in Supplementary Table 1B (http://onlinelibrary.wiley.com/doi/10.1002/art.40114/abstract).

Association of MMF treatment with improved course of MRSS. In all patients (those with diffuse cutaneous SSc and those with limited cutaneous SSc combined), after adjustment for baseline MRSS, treatment with MMF was associated with improved MRSS over 24 months ($P < 0.0001$). From 3 to 12 months, patients in the MMF arm experienced a significant improvement (decrease) in the MRSS compared with those in the placebo arm ($P = 0.0018$) (Figure 3). There was continued improvement in the MRSS from 12 to 21 months and from 21 to 24 months in the MMF arm. Patients in the placebo arm experienced an increase (worsening) in the MRSS from 3 to 12 months, followed by a decline in the MRSS from 12 to 21 months and from 21 to 24 months. Both treatment arms had similar rates of improvement in the MRSS from 12 to 21 months ($P = 0.95$) and from 21 to 24 months ($P = 0.90$) (Figure 3) (see Supplementary Table 3, http://onlinelibrary.wiley.com/doi/10.1002/art.40114/abstract).

MMF was associated with a stronger treatment effect on the MRSS in patients with diffuse cutaneous disease (41 in the MMF arm and 45 in the placebo arm) than in all patients combined. From 3 to 12 months, the MRSS improved (declined) at a faster rate in the MMF arm

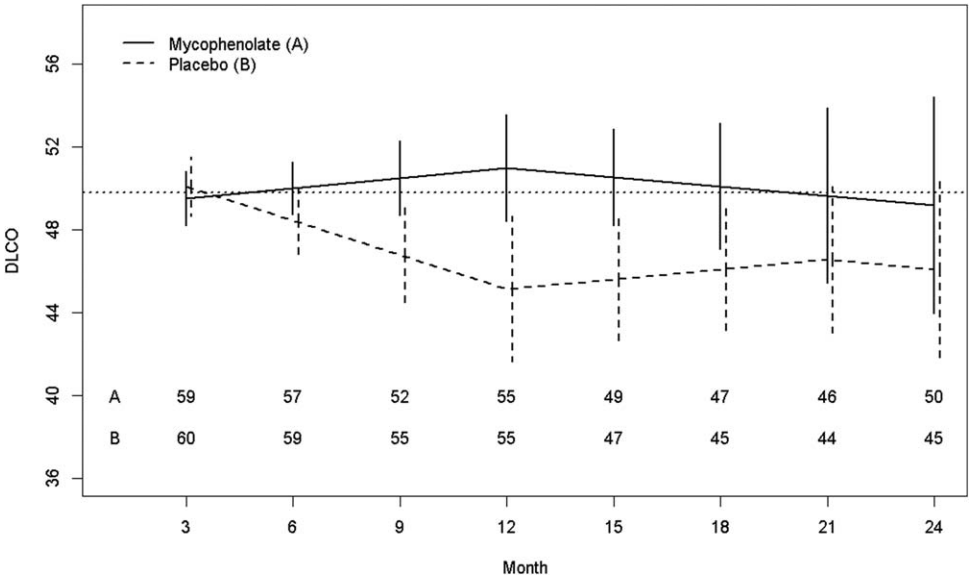

Figure 2. Course of the % predicted diffusing capacity for carbon monoxide (DLco) from 3 to 24 months in Scleroderma Lung Study (SLS) II patients assigned to receive mycophenolate mofetil versus SLS I patients assigned to receive placebo, using joint model analysis. Values are the mean (numbers of patients at time points are shown for each group). The test of the overall treatment group effect was significant at $P < 0.0001$. Prespecified covariates for this model included baseline % predicted DLco and baseline whole lung quantitative interstitial lung disease score. The dotted line represents the mean baseline value for the entire cohort.

compared with the placebo arm ($P = 0.0017$) (see Supplementary Figure 4 and Supplementary Table 4, http://onlinelibrary.wiley.com/doi/10.1002/art.40114/abstract).

In patients with limited cutaneous disease (25 in the MMF arm and 45 in the placebo arm), there was no significant difference between MMF and placebo in the MRSS over the 24-month period at any of the aforementioned time intervals (all $P > 0.2$). The absolute change in the MRSS (unadjusted) over 24 months by treatment arm appears in Supplementary Tables 1C and D (http://onlinelibrary.wiley.com/doi/10.1002/art.40114/abstract).

Association of MMF treatment with improved course of TDI. After adjustment for baseline BDI, treatment with MMF was associated with improvement in

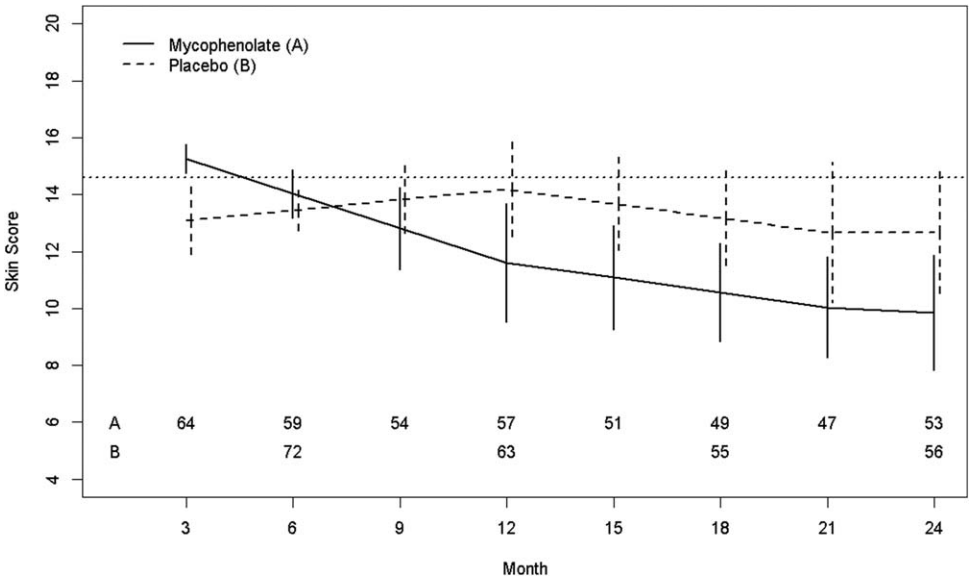

Figure 3. Course of the modified Rodnan skin thickness score from 3 to 24 months in Scleroderma Lung Study (SLS) II patients assigned to receive mycophenolate mofetil versus SLS I patients assigned to receive placebo, using joint model analysis. Values are the mean (numbers of patients at time points are shown for each group). The test of the overall treatment group effect was significant at $P < 0.0001$. The dotted line represents the mean baseline value for the entire cohort.

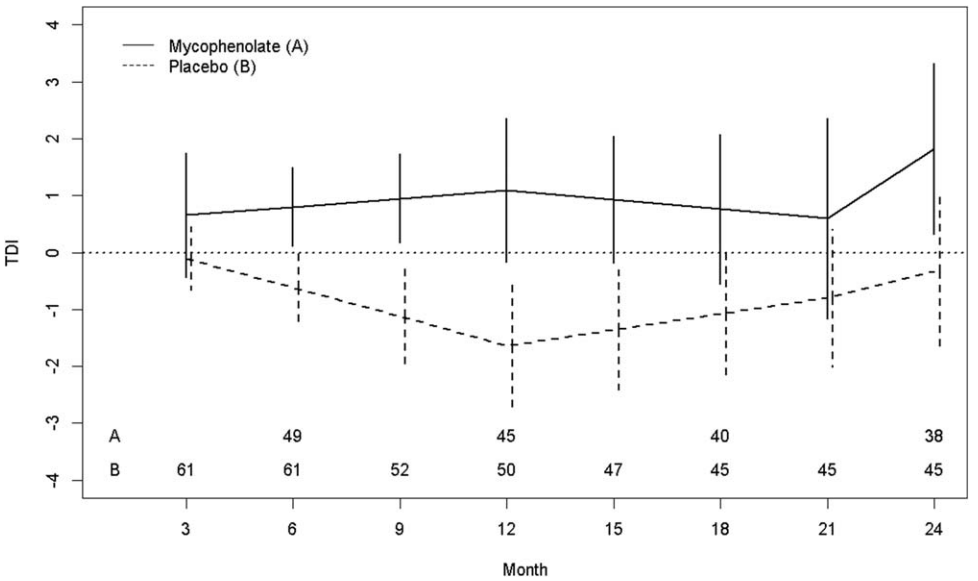

Figure 4. Course of the Transition Dyspnea Index (TDI) from 3 to 24 months in Scleroderma Lung Study (SLS) II patients assigned to receive mycophenolate mofetil versus SLS I patients assigned to receive placebo, using joint model analysis. Values are the mean (numbers of patients at time points are shown for each group). The test of the overall treatment group effect was significant at $P = 0.0112$. The dotted line represents the mean baseline value for the entire cohort.

dyspnea compared with placebo as measured by the TDI ($P = 0.0112$). From 3 to 12 months, patients in the MMF arm experienced a trend toward improvement in dyspnea compared with those in the placebo arm ($P = 0.0906$) (Figure 4). The observed improvement in the TDI in the MMF arm exceeded the minimal clinically important difference in the TDI for SSc-related ILD (23). The TDI progressively worsened in the placebo arm during the first 12 months, but during the second year trended toward progressive improvement relative to the change during the first year of the study (see Supplementary Table 5, http://onlinelibrary.wiley.com/doi/10.1002/art.40114/abstract). The absolute change in the TDI (unadjusted) over 24 months by treatment arm appears in Supplementary Table 1E (http://onlinelibrary.wiley.com/doi/10.1002/art.40114/abstract).

Safety analysis. In terms of predefined AEs that would warrant clinical intervention and a change in therapy, leukopenia (4 AEs in the MMF arm and none in the placebo arm), neutropenia (3 AEs in the MMF arm and none in the placebo arm), anemia (8 AEs in the MMF arm and 1 in the placebo arm), and pneumonia (5 AEs in the MMF arm and 1 in the placebo arm) occurred in more MMF-treated patients in SLS II than placebo-treated patients in SLS I (Table 3). However, SAEs were experienced by more placebo-treated patients in SLS I (n = 38) than MMF-treated patients in SLS II (n = 27). Seven of the SAEs occurring in the placebo arm were judged by the Morbidity and Mortality Committee to be related to treatment, compared with 3 of the SAEs in the MMF arm. Numbers of deaths

Table 3. Numbers of patients with AEs and SAEs from baseline to 24 months*

	Placebo (n = 79)	MMF (n = 69)
AEs†		
Leukopenia	0	4
Neutropenia	0	3
Anemia	1	8
Thrombocytopenia	0	0
Hematuria	5	3
Pneumonia	1	5
SAEs	38	27
No. of patients with SAEs		
Related to treatment‡	7	3
Not related to treatment‡	31	23
Death	6	5

* AEs = adverse events; SAEs = serious AEs; MMF = mycophenolate mofetil.
† Predefined by protocol as likely to be related to study drug and to warrant protocol-defined management (except for pneumonia): for leukopenia, white blood cell count $<2{,}500/mm^3$; for neutropenia, neutrophil count $<1{,}000/mm^3$; for anemia, hemoglobin value <10 gm/dl or <9 gm/dl for those with hemoglobin <11 gm/dl at enrollment; for thrombocytopenia, platelet count $<100{,}000/mm^3$; for hematuria, >25 red blood cells per mm^3 (or 10–15 red blood cells per mm^3 on more than one urinalysis) in the absence of urinary tract infection or menses.
‡ According to consensus classification by Morbidity and Mortality Committee.

in the 2 groups were similar (5 in the MMF arm and 6 in the placebo arm).

DISCUSSION

The present report describes the first analysis comparing MMF with placebo for the treatment of SSc-related ILD, although using data from 2 independent studies with nearly identical designs and similar patient populations. The results reported herein demonstrate that treatment with MMF is associated with improvements in physiologic outcomes and dyspnea, as well as with reductions in the extent of cutaneous sclerosis, in comparison with placebo.

The observed treatment effects were greatest within the first 12 months of therapy and diminished with time. Possible explanations for this observation include the use of potential disease-modifying therapy in the placebo arm during months 12 to 24. As mentioned above, 12 patients received prednisone and 2 patients received CYC in the placebo arm during this period. Given the small number of patients receiving CYC and the lack of substantial evidence that prednisone prevents progression of SSc-related ILD, additional explanations for the loss of treatment effect after 12 months may relate to the natural history of SSc-related ILD. Steen and colleagues (24) demonstrated that the greatest decline in FVC occurs within the first year among patients with severe SSc-related ILD; therefore, it is plausible that lung function, as well as dyspnea as measured by the TDI, stabilized/improved in both groups after 12 months regardless of treatment. Similarly, the MRSS also improved in the placebo arm in the second year of the study, which again likely reflects the natural history of cutaneous sclerosis progression in SSc (25). A survival bias may also contribute to the diminished MMF treatment effect in months 12 to 24, although our joint model analysis specifically adjusts for nonignorable missing data due to study dropout, treatment failure, or death.

Notably, compared with placebo, the MMF treatment effect persisted at 24 months in contrast to the CYC treatment effect observed in SLS I (3,15). In SLS I, less than half of the patients assigned to CYC had any improvement in % predicted FVC at 12 months (3), and by 24 months there was no difference in % predicted FVC between patients assigned to placebo and those assigned to CYC (15). In contrast, the percentage of patients with any improvement in % predicted FVC at 24 months was substantially higher in patients receiving MMF (71.7%; nearly 3 times higher than in those assigned to placebo). Furthermore, even though % predicted FVC in the second year improved in both study arms, MMF still conferred an advantage at 24 months.

From the standpoint of safety and tolerability, MMF appears to be well tolerated. There were 8 predefined treatment failures in the placebo arm and none in the MMF arm over 24 months. Furthermore, 30 patients in the placebo arm experienced treatment failures/drug withdrawals compared with only 19 patients in the MMF arm during this time frame. As a reference point, there were 30 treatment failures/drug withdrawals in the CYC arm of SLS I and 34 treatment failures/drug withdrawals in the CYC arm of SLS II over 24 months.

The present analysis found that numerically more patients experienced AEs in the MMF arm than in the placebo arm; however, patients in the placebo arm experienced more SAEs. It is unclear why more SAEs occurred in the placebo arm; however, this may be related to progression of the SSc disease state in the absence of disease-modifying therapy, as most of the SAEs were not attributed to study drug in both groups. When compared with placebo, CYC use in SLS I was associated with more AEs, SAEs, and deaths (3). Taken together, these observations seem to suggest that MMF introduction may pose less serious risk to the patient.

The results of our analyses should be interpreted within the context of certain limitations. Namely, comparing cohorts from 2 different trials can introduce bias. Time period bias is one concern, as enrollment for SLS I concluded in 2004 and enrollment for SLS II concluded in 2012. However, this time difference is unlikely to contribute significantly to the phenotypic expression of SSc-related ILD in each cohort, as there were no new major therapeutic discoveries during this time period.

Of greater concern are potential differences in the baseline features of these 2 groups, which may affect progression of SSc-related ILD. Patients assigned to the placebo arm had greater radiographic extent of ILD and lower DL_{CO} compared with patients assigned to the MMF arm. While we attempted to control for baseline ILD disease severity in our analyses (i.e., FVC, DL_{CO}, whole lung QILD score), without a randomization process one cannot adequately control for those "unknown" variables that may be different in the 2 groups and that may affect the study outcome.

Reassuringly, the MMF and placebo groups appeared relatively similar in terms of their baseline features. Moreover, participants in SLS I and SLS II were recruited from similar academic centers. Nine of the 13 centers for recruitment in SLS I were used in SLS II. In addition, these 9 centers recruited the majority of patients for both SLS I and SLS II. The principal investigators from these centers were also similar for SLS I and SLS II, suggesting that practice management styles were likely consistent between the 2 trials.

Aside from the inherent limitations associated with comparing groups from different trials, our study also has important strengths. First, the number of patients is relatively large for an SSc-related ILD intervention study in both trials. Second, unlike many prior studies in this area, we did not evaluate an outcome measure at a single follow-up time point. Instead, we employed sophisticated statistical techniques to examine outcomes measured at multiple time points (i.e., FVC measured at 3-month intervals over 24 months), which likely results in a more clinically meaningful characterization of progression of SSc-related ILD. Third, our analysis adjusted for missing data due to dropouts, treatment failures, and deaths and thus represents a novel approach for dealing with nonignorable missing data in clinical trials.

To conclude, in patients with symptomatic SSc-related ILD, treatment with MMF is associated with improvements in the % predicted FVC, % predicted DLco, TDI, and MRSS, compared with placebo using data from a historical study. The MMF treatment effect was greatest within the first 12 months but persisted throughout the 2-year trial. These findings support the use of MMF for the treatment of SSc-related ILD.

ACKNOWLEDGMENTS

We thank the patients, investigators, and coordinators who participated in SLS I and SLS II.

AUTHOR CONTRIBUTIONS

All authors were involved in drafting the article or revising it critically for important intellectual content, and all authors approved the final version to be published. Dr. Volkmann had full access to all of the data in the study and takes responsibility for the integrity of the data and the accuracy of the data analysis.

Study conception and design. Volkmann, Tashkin, Roth, Khanna, Goldin, Clements, Furst, Elashoff.

Acquisition of data. Volkmann, Tashkin, Kim.

Analysis and interpretation of data. Volkmann, Tashkin, Li, Hoffmann-Vold, Kim, Elashoff.

REFERENCES

1. Elhai M, Meune C, Avouac J, Kahan A, Allanore Y. Trends in mortality in patients with systemic sclerosis over 40 years: a systematic review and meta-analysis of cohort studies. Rheumatology (Oxford) 2012;51:1017–26.
2. Tyndall AJ, Bannert B, Vonk M, Airo P, Cozzi F, Carreira PE, et al. Causes and risk factors for death in systemic sclerosis: a study from the EULAR Scleroderma Trials and Research (EUSTAR) database. Ann Rheum Dis 2010;69:1809–15.
3. Tashkin DP, Elashoff R, Clements PJ, Goldin J, Roth M, Furst DE, et al. Cyclophosphamide versus placebo in scleroderma lung disease. N Engl J Med 2006;354:2655–66.
4. Hoyles RK, Ellis RW, Wellsbury J, Lees B, Newlands P, Goh NS, et al. A multicenter, prospective, randomized, double-blind, placebo-controlled trial of corticosteroids and intravenous cyclophosphamide followed by oral azathioprine for the treatment of pulmonary fibrosis in scleroderma. Arthritis Rheum 2006;54:3962–70.
5. Volkmann ER, Tashkin DP. Treatment of systemic sclerosis-related interstitial lung disease: a review of existing and emerging therapies. Ann Am Thorac Soc 2016;13:2045–56.
6. Nihtyanova SI, Brough GM, Black CM, Denton CP. Mycophenolate mofetil in diffuse cutaneous systemic sclerosis: a retrospective analysis. Rheumatology (Oxford) 2007;46:442–5.
7. Derk CT, Grace E, Shenin M, Naik M, Schulz S, Xiong W. A prospective open-label study of mycophenolate mofetil for the treatment of diffuse systemic sclerosis. Rheumatology (Oxford) 2009;48:1595–9.
8. Gerbino AJ, Goss CH, Molitor JA. Effect of mycophenolate mofetil on pulmonary function in scleroderma-associated interstitial lung disease. Chest 2008;133:455–60.
9. Simeón-Aznar CP, Fonollosa-Plá V, Tolosa-Vilella C, Selva-O'Callaghan A, Solans-Laque R, Vilardell-Tarres M. Effect of mycophenolate sodium in scleroderma-related interstitial lung disease. Clin Rheumatol 2011; 30:1393.
10. Swigris JJ, Olson AL, Fischer A, Lynch DA, Cosgrove GP, Frankel SK, et al. Mycophenolate mofetil is safe, well tolerated and preserves lung function in patients with connective tissue disease-related interstitial lung disease. Chest 2006;130:30–6.
11. Zamora AC, Wolters PJ, Collard HR, Connolly MK, Elicker BM, Webb WR, et al. Use of mycophenolate mofetil to treat scleroderma-associated interstitial lung disease. Respir Med 2008;102:150–55.
12. Fischer A, Brown KK, Du Bois RM, Frankel SK, Cosgrove GP, Fernandez-Perez ER, et al. Mycophenolate mofetil improves lung function in connective tissue disease-associated interstitial lung disease. J Rheumatol 2013;40:640–6.
13. Tashkin DP, Roth MD, Clements PJ, Furst DE, Khanna D, Kleerup EC, et al. Mycophenolate mofetil versus oral cyclophosphamide in scleroderma-related interstitial lung disease (SLS II): a randomised controlled, double-blind, parallel group trial. Lancet Respir Med 2016;4:708–19.
14. Wells AU. Interstitial lung disease in systemic sclerosis. Press Med 2014;43:e329–e343.
15. Tashkin DP, Elashoff R, Clements PJ, Roth MD, Furst DE, Silver RM, et al. Effects of 1-year treatment with cyclophosphamide on outcomes at 2 years in scleroderma lung disease. Am J Respir Crit Care Med 2007;176:1026–34.
16. Mahler DA, Weinberg DH, Wells CK, Feinstein AR. The measurement of dyspnea: contents, interobserver agreement and physiologic correlates of two new clinical indexes. Chest 1984;85: 751–8.
17. Mahler DA, Ward J, Fierro-Carrion G, Waterman LA, Lentine TF, Mejia-Alfaro R, et al. Development of self-administered versions of modified baseline and transition dyspnea indexes in COPD. COPD 2004;1:1–8.
18. Clements PJ, Lachenbruch PA, Seibold JR, Zee B, Steen VD, Brennan P, et al. Skin thickness score in systemic sclerosis (SSc): an assessment of inter-observer variability in three independent studies. J Rheumatol 1993;20:1892–6.
19. Goldin J, Elashoff R, Kim HJ, Yan X, Lynch D, Strollo D, et al. Treatment of scleroderma-interstitial lung disease with cyclophosphamide is associated with less progressive fibrosis on serial thoracic high-resolution CT scan than placebo: findings from the scleroderma lung study. Chest 2009;136:1333–40.
20. Kim HJ, Li G, Gjertson D, Elashoff R, Shah SK, Ochs R, et al. Classification of parenchymal abnormality in scleroderma lung using a novel approach to denoise images collected via a multicenter study. Acad Radiol 2008;15:1004–16.
21. Li N, Elashoff RM, Li G, Tseng CH. Joint analysis of bivariate longitudinal ordinal outcomes and competing risks survival times with nonparametric distributions for random effects. Stat Med 2012;31:1707–21.

22. Elashoff RM, Li G, Li N. A joint model for longitudinal measurements and survival data in the presence of multiple failure types. Biometrics 2008;64:762–71.
23. Khanna D, Tseng CH, Furst DE, Clements PJ, Elashoff R, Roth M, et al. Minimally important differences in the Mahler's Transition Dyspnoea Index in a large randomized controlled trial: results from the Scleroderma Lung Study. Rheumatology (Oxford) 2009;48:1537–40.
24. Steen VD, Lanz JK Jr, Conte C, Owens GR, Medsger TA Jr. Therapy for severe interstitial lung disease in systemic sclerosis. a retrospective study. Arthritis Rheum 1994;37:1290–6.
25. Clements PJ, Medsger TA Jr, Feghali CA. Cutaneous involvement in systemic sclerosis. In: Clements PJ, Furst DE, editors. Systemic sclerosis. 2nd ed. New York: Lippincott Williams and Wilkins; 2004. p. 129–50.

DOI: 10.1002/art.40092

Clinical Images: Black esophagus in antiphospholipid syndrome

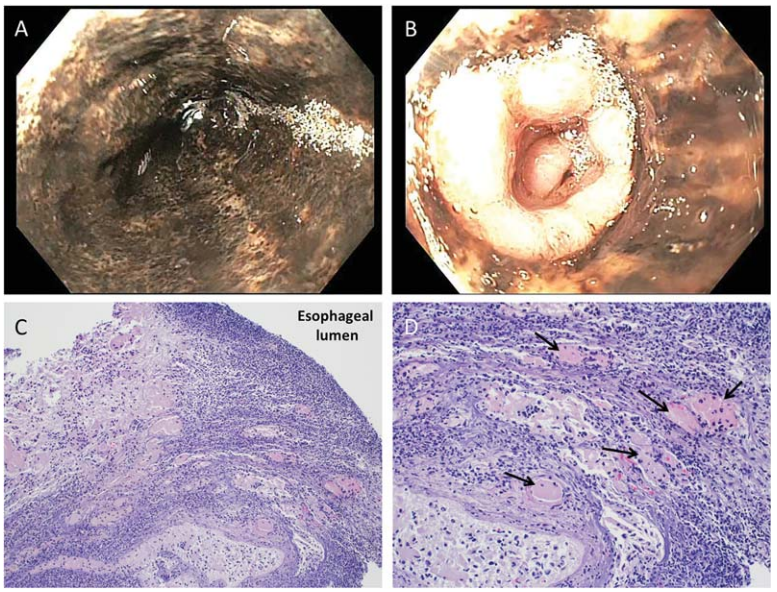

The patient, a 64-year-old woman, presented with a history of systemic lupus erythematosus characterized by antinuclear antibody and anti–double-stranded DNA positivity, chronic hypocomplementemia, polyarthritis, pericarditis, and lupus nephritis complicated by end-stage renal disease. She had been receiving hemodialysis for ~3 years and peritoneal dialysis for many years prior to that. She also had a history of antiphospholipid syndrome (APS) characterized by persistently positive lupus anticoagulant, high-titer IgG and IgM anti–β_2-glycoprotein I, and high-titer IgG and IgM anticardiolipin. She was receiving anticoagulation therapy for an episode of deep venous thrombosis complicated by pulmonary embolism. She was admitted for cachexia and found to have evidence suggestive of smoldering disseminated intravascular coagulation (DIC) (low fibrinogen and elevated D-dimer levels, prolonged prothrombin and partial thromboplastin times, low hemoglobin [Hgb] level, and low platelet count). While hospitalized, she developed coffee ground emesis, hypotension, and an acute drop in her Hgb concentration of 3 gm/dl. Upper gastrointestinal endoscopy revealed "black esophagus" involving the middle and lower portions of the esophagus (**A** and **B**) (lower third of the esophagus and gastroesophageal junction, respectively). Extensive thrombosis (**arrows**) and acute esophageal necrosis were confirmed by histopathologic examination (**C** and **D** [original magnification × 10 and × 20, respectively]). Acute esophageal necrosis appears black, circumferential, and can affect any portion of the esophagus. Risk factors include hypertension, diabetes, hyperlipidemia, and chronic kidney disease. Alcohol abuse, malnourishment, hypoalbuminemia, and history of vascular and thromboembolic disease are other risk factors. In this patient, a prothrombotic state due to APS and DIC likely contributed. Extensive evaluation did not reveal evidence of infection or malignancy. We suspect the DIC was due at least in part to APS. Evaluation of 8 cases suggests that acute esophageal necrosis is multifactorial in most patients (as in this patient) and has multiple risk factors for ischemic insult and decreased gastric mucosal defenses (1). Gastrointestinal ischemia involving the small bowel or colon has been reported in APS (2). To our knowledge, this is only the second reported case of acute esophageal necrosis in a patient with APS (3).

We would like to thank Dr. Jiaqi Shi, Department of Pathology, University of Michigan, for her help with the histopathologic examination.

1. Gurvits GE, Cherian K, Shami MN, Korabathina R, El-Nader EM, Rayapudi K, et al. Black esophagus: new insights and multicenter international experience in 2014. Dig Dis Sci 2015;60:444–53.
2. Cappell MS, Mikhail N, Gujral N. Gastrointestinal hemorrhage and intestinal ischemia associated with anticardiolipin antibodies. Dig Dis Sci 1994;39:1359–64.
3. Cappell MS. Esophageal necrosis and perforation associated with the anticardiolipin antibody syndrome. Am J Gastroenterol 1994;89:1241–5.

Amrita Padda, MD
Amar Mandalia, MD
Amr H. Sawalha, MD
University of Michigan
Ann Arbor, MI

22. Elashoff RM, Li G, Li N. A joint model for longitudinal measurements and survival data in the presence of multiple failure types. Biometrics 2008;64:762–71.
23. Khanna D, Tseng CH, Furst DE, Clements PJ, Elashoff R, Roth M, et al. Minimally important differences in the Mahler's Transition Dyspnoea Index in a large randomized controlled trial: results from the Scleroderma Lung Study. Rheumatology (Oxford) 2009;48:1537–40.
24. Steen VD, Lanz JK Jr, Conte C, Owens GR, Medsger TA Jr. Therapy for severe interstitial lung disease in systemic sclerosis. a retrospective study. Arthritis Rheum 1994;37:1290–6.
25. Clements PJ, Medsger TA Jr, Feghali CA. Cutaneous involvement in systemic sclerosis. In: Clements PJ, Furst DE, editors. Systemic sclerosis. 2nd ed. New York: Lippincott Williams and Wilkins; 2004. p. 129–50.

DOI: 10.1002/art.40092

Clinical Images: Black esophagus in antiphospholipid syndrome

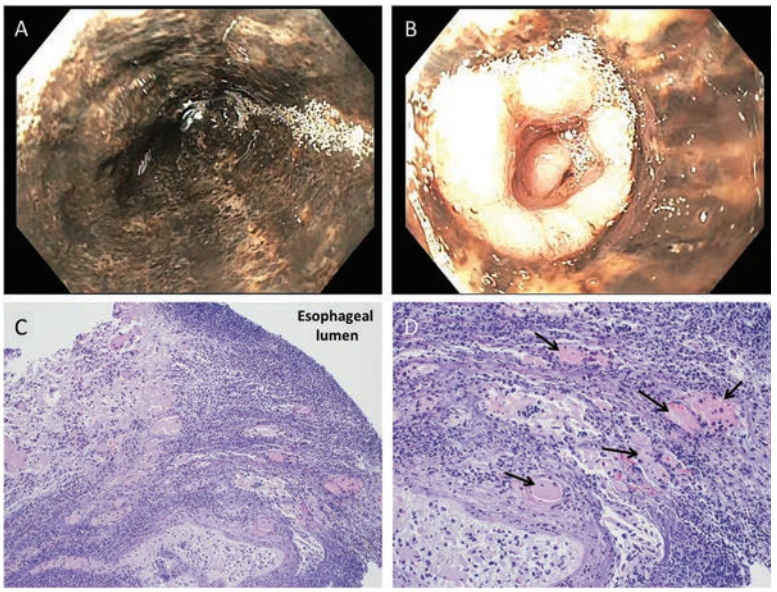

The patient, a 64-year-old woman, presented with a history of systemic lupus erythematosus characterized by antinuclear antibody and anti–double-stranded DNA positivity, chronic hypocomplementemia, polyarthritis, pericarditis, and lupus nephritis complicated by end-stage renal disease. She had been receiving hemodialysis for ~3 years and peritoneal dialysis for many years prior to that. She also had a history of antiphospholipid syndrome (APS) characterized by persistently positive lupus anticoagulant, high-titer IgG and IgM anti–β_2-glycoprotein I, and high-titer IgG and IgM anticardiolipin. She was receiving anticoagulation therapy for an episode of deep venous thrombosis complicated by pulmonary embolism. She was admitted for cachexia and found to have evidence suggestive of smoldering disseminated intravascular coagulation (DIC) (low fibrinogen and elevated D-dimer levels, prolonged prothrombin and partial thromboplastin times, low hemoglobin [Hgb] level, and low platelet count). While hospitalized, she developed coffee ground emesis, hypotension, and an acute drop in her Hgb concentration of 3 gm/dl. Upper gastrointestinal endoscopy revealed "black esophagus" involving the middle and lower portions of the esophagus (**A** and **B**) (lower third of the esophagus and gastroesophageal junction, respectively). Extensive thrombosis (**arrows**) and acute esophageal necrosis were confirmed by histopathologic examination (**C** and **D** [original magnification × 10 and × 20, respectively]). Acute esophageal necrosis appears black, circumferential, and can affect any portion of the esophagus. Risk factors include hypertension, diabetes, hyperlipidemia, and chronic kidney disease. Alcohol abuse, malnourishment, hypoalbuminemia, and history of vascular and thromboembolic disease are other risk factors. In this patient, a prothrombotic state due to APS and DIC likely contributed. Extensive evaluation did not reveal evidence of infection or malignancy. We suspect the DIC was due at least in part to APS. Evaluation of 8 cases suggests that acute esophageal necrosis is multifactorial in most patients (as in this patient) and has multiple risk factors for ischemic insult and decreased gastric mucosal defenses (1). Gastrointestinal ischemia involving the small bowel or colon has been reported in APS (2). To our knowledge, this is only the second reported case of acute esophageal necrosis in a patient with APS (3).

We would like to thank Dr. Jiaqi Shi, Department of Pathology, University of Michigan, for her help with the histopathologic examination.

1. Gurvits GE, Cherian K, Shami MN, Korabathina R, El-Nader EM, Rayapudi K, et al. Black esophagus: new insights and multicenter international experience in 2014. Dig Dis Sci 2015;60:444–53.
2. Cappell MS, Mikhail N, Gujral N. Gastrointestinal hemorrhage and intestinal ischemia associated with anticardiolipin antibodies. Dig Dis Sci 1994;39:1359–64.
3. Cappell MS. Esophageal necrosis and perforation associated with the anticardiolipin antibody syndrome. Am J Gastroenterol 1994;89:1241–5.

Amrita Padda, MD
Amar Mandalia, MD
Amr H. Sawalha, MD
University of Michigan
Ann Arbor, MI

ARTHRITIS & RHEUMATOLOGY
Vol. 69, No. 7, July 2017, pp 1461–1469
DOI 10.1002/art.40110

Population-Specific Resequencing Associates the ATP-Binding Cassette Subfamily C Member 4 Gene With Gout in New Zealand Māori and Pacific Men

Callum Tanner,[1] James Boocock,[1] Eli A. Stahl,[2] Amanda Dobbyn,[2] Asim K. Mandal,[3] Murray Cadzow,[1] Amanda J. Phipps-Green,[1] Ruth K. Topless,[1] Jennie Harré Hindmarsh,[4] Lisa K. Stamp,[5] Nicola Dalbeth,[6] Hyon K. Choi,[7] David B. Mount,[3] and Tony R. Merriman[1]

Objective. **There is no evidence for a genetic association between organic anion transporters 1–3 (*SLC22A6, SLC22A7,* and *SLC22A8*) and multidrug resistance protein 4 (MRP4; encoded by *ABCC4*) with the levels of serum urate or gout. The Māori and Pacific (Polynesian) population of New Zealand has the highest prevalence of gout worldwide. The aim of this study was to determine whether any Polynesian population–specific genetic variants in *SLC22A6–8* and *ABCC4* are associated with gout.**

Methods. **All participants had ≥3 self-reported Māori and/or Pacific grandparents. Among the total sample set of 1,808 participants, 191 hyperuricemic and 202 normouricemic individuals were resequenced over the 4 genes, and the remaining 1,415 individuals were used for replication. Regression analyses were performed, adjusting for age, sex, and Polynesian ancestry. To study the functional effect of nonsynonymous variants of *ABCC4*, transport assays were performed in *Xenopus laevis* oocytes.**

Results. **A total of 39 common variants were detected, with an *ABCC4* variant (rs4148500) significantly associated with hyperuricemia and gout. This variant was monomorphic for the urate-lowering allele in Europeans. There was evidence for an association of rs4148500 with gout in the resequenced samples (odds ratio [OR] 1.62 [$P = 0.012$]) that was replicated (OR 1.25 [$P = 0.033$]) and restricted to men (OR 1.43 [$P = 0.001$] versus OR 0.98 [$P = 0.89$] in women). The gout risk allele was associated with fractional excretion of uric acid in male individuals ($\beta = -0.570$ [$P = 0.01$]). A rare population-specific allele (P1036L) with predicted strong functional consequence reduced the uric acid transport activity of *ABCC4* by 30%.**

Conclusion. **An association between *ABCC4* and gout and fractional excretion of uric acid is consistent with the established role of MRP4 as a unidirectional renal uric acid efflux pump.**

Gout is a form of arthritis caused by an innate immune system reaction to monosodium urate crystals in patients with hyperuricemia (1). Gout is 3–4-fold more prevalent in men than in women (2). Genome-wide association studies have identified genetic variants in loci encoding renal and intestinal uric acid transporters and associated accessory molecules (*SLC2A9*/*GLUT9*, *ABCG2*, *SLC22A11*/*OAT4, SLC22A12*/*URAT1*, *SLC17A1*/*NPT1*, and *PDZK1*) that control serum urate levels in Europeans (3–5). Most of these variants are associated with serum urate and gout in other ancestral groups (6,7). However, there remain other known uric acid transporters (*SLC22A6–8*/*OAT1–3*, *ABCC4*/*MPR4*) (8–12) without evidence at a genome-wide level of significance for genetic control of urate levels and the risk of gout (13). Identifying

Supported by the NIH (grant R21-AR-065968-01 to Drs. Stahl, Choi, Mount, and Merriman and grant NIH-R01-AR-056291 to Dr. Choi) and the New Zealand Health Research Council program (grants 08/075, 11/1075, and 14/527 to Drs. Stamp, Dalbeth, and Merriman).

[1]Callum Tanner, BSc (Hons), James Boocock, MSc, Murray Cadzow, BSc, Amanda J. Phipps-Green, MSc, Ruth K. Topless, BSc, Tony R. Merriman, PhD: University of Otago, Dunedin, New Zealand; [2]Eli A. Stahl, PhD, Amanda Dobbyn, BSc: Icahn School of Medicine at Mount Sinai, New York, New York; [3]Asim K. Mandal, PhD, David B. Mount, MD: Brigham and Women's Hospital and VA Boston Healthcare System, Harvard Medical School, Boston, Massachusetts; [4]Jennie Harré Hindmarsh, PhD: Ngati Porou Hauora Charitable Trust, Te Puia Springs, New Zealand; [5]Lisa K. Stamp, MBChB, PhD: University of Otago Christchurch, Christchurch, New Zealand; [6]Nicola Dalbeth, MD: University of Auckland, Auckland, New Zealand; [7]Hyon K. Choi, MD, PhD: Massachusetts General Hospital, Harvard Medical School, Boston.

Mr. Tanner and Mr. Boocock contributed equally to this work.

Address correspondence to Tony R. Merriman, PhD, Department of Biochemistry, University of Otago, Box 56, Dunedin, New Zealand. E-mail: tony.merriman@otago.ac.nz.

Submitted for publication February 8, 2017; accepted in revised form March 23, 2017.

natural common genetic variants that are associated with urate levels and the risk of gout in the genes encoding these molecules would both increase the understanding of the molecular basis of hyperuricemia and gout and highlight the molecules as targets for urate-lowering drugs. For example, small molecules reverse the urate-raising property of the common ATP-binding cassette subfamily G member 2 (ABCG2) 141K variant (14), and lesinurad is a recently developed drug that promotes uric acid excretion via urate transporter 1 (15,16).

We hypothesized that the genome of the Māori and Pacific (Polynesian) population of New Zealand could contain genetic variants in *SLC22A6–8* and *ABCC4* (which are absent in Europeans) that control serum urate levels. This population group has the highest prevalence of gout worldwide (2), driven by inherent hyperuricemia (17,18). Furthermore, individuals of Polynesian ancestry exhibit lower urinary fractional excretion of uric acid (19–21). Therefore, these genes were resequenced in 191 Polynesian individuals with the highest serum urate levels and 202 with the lowest serum urate levels, with the aim of detecting population-specific genetic variants that are associated with gout.

PATIENTS AND METHODS

Participants. All 1,808 Polynesian gout patients and controls in this study were drawn from the New Zealand Māori and Pacific Island populations and were recruited during the years 2006 to 2013 from within New Zealand. Only individuals with ≥3 self-reported Polynesian grandparents were included (Table 1). Patients with gout fulfilled the 1977 American College of Rheumatology preliminary criteria for the classification of primary gout, as determined by clinical examination (22). Participants who self-reported no history of gout were categorized as non-gout. From this group, 191 individuals with the highest serum urate levels (average 0.539 mmoles/liter in men and 0.511 mmoles/liter in women) and 202 individuals with the lowest serum urate levels (average 0.330 mmoles/liter in men and 0.284 mmoles/liter in women) were selected for resequencing (resequence sample set [n = 393]). Of the remaining 1,415 subjects, 1,075 comprised the replication 1 sample set. The Lower South Ethics Committee (OTA/99/11/098) and New Zealand Multi-region Ethics Committee (MEC/05/10/130) granted ethics approval for analysis of these individuals.

A separate sample set (replication 2) comprised 181 individuals with gout and 159 without gout (non-gout), as ascertained using the above criteria. These participants were recruited in collaboration with Ngāti Porou Hauora Charitable Trust (NPHCT), the Māori *iwi* (tribe) health service provider located in the East Coast (Tairāwhiti) region of the North Island of New Zealand. This separate sample set is comprised nearly exclusively (99.5%) of persons of New Zealand Māori (Eastern Polynesian) ancestry. The NPHCT study was approved by the Ngāti Porou Hauora Board, and ethics approval was granted by the Northern Y Region Health Research Ethics Committee (NTY07/07/074).

Urate and creatinine levels for all sample sets were obtained using serum and a spot urine sample (nonfasting), with sampling occurring at convenient times. Serum urate values at the time of recruitment are shown for all participants in Table 1. Fractional excretion of uric acid was calculated using the Simkin index (23). Hyperuricemia was defined as ≥6 mg/dl in women and ≥7 mg/dl in men. The characteristics of the participants are shown in Table 1.

Resequencing. Illumina-indexed libraries were constructed using 250 ng of native genomic DNA according to the manufacturer's protocol (Illumina), with the following modifications: 1) DNA was fragmented, using a Covaris E220 DNA sonicator, to range in size between 100 bp and 400 bp; 2) Illumina adapter–ligated library fragments were amplified for 8 cycles; 3) solid-phase reversible immobilization bead cleanup was used for enzymatic purification throughout the library process, as well as final library size selection targeting 300–500-bp fragments. Hybridization was performed with a custom version of a Roche NimbleGen SeqCap kit, according to the manufacturer's protocol. Ninety dual-indexed samples were combined and captured as a pool and run on a lane of Illumina HiSeq 2000, which produces ~36 Gb/lane of sequence. The total target capture was 2.59 Mb of genomic space that included the *SLC22A6–8* and *ABCC4*

Table 1. Demographic characteristics of and laboratory findings in the participants, according to sample set*

	Resequencing		Replication 1		Replication 2	
Characteristic	Gout (n = 142)	Non-gout (n = 251)	Gout (n = 589)	Non-gout (n = 486)	Gout (n = 181)	Non-gout (n = 159)
Age, years	34.2 ± 0.9 (1.4)	44.2 ± 0.9 (0)	39.1 ± 0.6 (2.9)	43.9 ± 0.7 (0)	40.4 ± 1.2 (3.9)	41.8 ± 1.2 (0)
Male, %	88.0	48.2	80.6	46.7	80.1	55.3
Proportion of self-reported Polynesian grandparents	0.969 ± 0.006	0.945 ± 0.006	0.949 ± 0.004	0.943 ± 0.004	0.906 ± 0.008	0.905 ± 0.009
Serum urate level, mmoles/liter						
Men	0.549 ± 0.015 (0)	0.377 ± 0.008 (0)	0.403 ± 0.005 (19.8)	0.445 ± 0.005 (18.2)	0.441 ± 0.00 (4.29)	0.404 ± 0.008 (1.2)
Women	0.538 ± 0.015 (0)	0.309 ± 0.007 (0)	0.391 ± 0.012 (21.2)	0.389 ± 0.004 (25.3)	0.458 ± 0.022 (5.6)	0.339 ± 0.010 (0)
FEUA						
Men	2.25 ± 0.27 (33.6)	5.98 ± 0.37 (66.1)	3.64 ± 0.28 (40.0)	4.71 ± 0.25 (60.4)	4.10 ± 0.19 (15.9)	5.33 ± 0.25 (4.5)
Women	2.49 ± 0.83 (29.5)	6.10 ± 0.50 (66.9)	4.09 ± 0.46 (38.6)	4.84 ± 0.24 (59.5)	4.97 ± 0.38 (11.2)	6.21 ± 0.46 (5.6)

* Except where indicated otherwise, values are the mean ± SE (% missing). FEUA = fractional excretion of uric acid.

promoters, 5′-untranslated region (5′-UTR) and 3′-UTR, and exons (see Supplementary Table 1, available on the *Arthritis & Rheumatology* web site at http://onlinelibrary.wiley.com/doi/10.1002/art.40110/abstract). The total sequence per sample was 132.56 Mb, yielding 51.2× average coverage across the targeted space. Resequencing was performed at the McDonnell Genome Institute at Washington University in St. Louis, Missouri.

Using Genome Analysis Toolkit (GATK) best practice recommendations (24), FASTQ files were aligned to the human decoy reference genome (build GRCh37) using Burrows-Wheeler Aligner (BWA version 0.7.12 r1039) (25). Resulting BAM files were processed using Picard (version 1.114) to mark reads that originate from duplication by polymerase chain reaction. This was followed by Indel Realignment and base recalibration using GATK version 3.3.0 (26). GNU Parallel (version 20140422) (27) and GATK HaplotypeCaller (28) were used to generate genomic variant call files (GVCFs). These files were merged in batches of 100 using the GATK Merge GVCF command, followed by variant calling using the GATK Genotype GVCF command. The single-nucleotide polymorphisms (SNPs) in the resulting VCF were processed using the GATK variant quality score recalibration utility, taking quality by depth, Fisher score, mapping quality rank sum, and read position rank sum into account. This recalibration was applied to the VCF file, and SNPs with a truth sensitivity of <99.00 were removed.

Each variant was annotated using Plink/Seq (version 0.10) (https://atgu.mgh.harvard.edu/plinkseq/), and for those variants found within the boundary of a gene or genes, the variants were classified as follows: intronic, exonic-unknown, exonic-missense, exonic-silent, 3′-UTR, and 5′-UTR. Rare variants were additionally annotated (see Supplementary Table 2, available on the *Arthritis & Rheumatology* web site at http://onlinelibrary.wiley.com/doi/10.1002/art.40110/abstract) with Combined Annotation Dependent Depletion (CADD) scores (29) using Gemini (version 0.12.2) (30).

Genotyping. All samples, including those in the resequencing experiment, were genotyped using either a TaqMan rs4148500 assay or a custom TaqMan Genotyping Assay (for chromosome 13:95724019) on a Roche LightCycler 480 instrument. The genotypes were autocalled by the LightCycler 480 software, and the reported dye signal plots were visually inspected for correct genotype clustering. There was 100% concordance between genotypes determined by TaqMan assay and genotypes obtained from the resequencing VCF files. No individual or combined sample set departed from Hardy-Weinberg equilibrium ($P > 0.05$).

Association analysis. Logistic regression was performed on the resequence data using Plink/Seq, with hyperuricemia as outcome. This model was adjusted for age and sex. Association with gout was tested by logistic regression with adjustment for age, sex, self-reported number of Polynesian grandparents, and Polynesian ancestral group (Western, Eastern, mixed) in the resequence, replication, and combined sample sets using R version 3.2.0 (31). Linear regression, with the same adjustors, was used to test for association with fractional excretion of uric acid and serum urate.

ATP-binding cassette subfamily C member 4 (ABCC4) functional assay. To study the effect of the rare allele of the P1036L coding SNP on the transport function of ABCC4, the relevant point mutant was first generated using site-directed mutagenesis (QuikChange; Stratagene) of *Xenopus laevis* expression constructs in the pGEMHE vector. Point mutants were also generated for 2 additional nonsynonymous variants, G187W and G487E, which showed reduced function in a previous study (32). In each case, the fidelity of mutagenesis was assessed by sequencing the entire open reading frame. The transport function of wild-type and mutant ABCC4 was then assessed using [^{14}C] efflux in individual *X laevis* oocytes, as previously described for ABCG2 (12,33).

Collagenase-digested oocytes were thus microinjected with in vitro–transcribed complementary RNA (cRNA) (25 ng/oocyte) for each construct, followed by transport assays after 2 days in culture. For [^{14}C]-urate efflux studies, oocytes were pre-injected with 50 nl of 1,500 μM [^{14}C]-urate dissolved in efflux medium (ND96, pH 7.4). Pre-injected oocytes were then incubated in ND96 medium for 30 minutes at 16°C for recovery. After incubation, the oocytes were washed in ND96 medium 4 times to remove any external adhering [^{14}C]-urate from the oocytes and were then subjected to efflux for 1 hour at room temperature (~25°C) in ND96 medium (pH 7.4) in the absence or presence of drug; pharmacologic sensitivity was determined for tranilast, benzbromarone, and probenecid. Oocytes were then washed again 3 times with the ice-cold uptake medium to remove external radioisotope. The radioisotope content of each oocyte was measured using a scintillation counter after solubilization in 0.3 ml of 10% (volume/volume) sodium dodecyl sulfate (SDS) and the addition of 2.5 ml of scintillation fluid. The experiments included either 12–15 oocytes per group or 30 oocytes per group. Given the modest functional effects of coding mutations in ABCC4, we utilized twice the usual number of oocytes in this experiment. The radioisotope content of each oocyte was measured using a scintillation counter after solubilization in 0.3 ml of 10% (v/v) SDS and the addition of 2.5 ml of scintillation fluid. Statistical significance for individual experiments was defined as a 2-tailed P value of <0.05 by Mann-Whitney rank sum test. Results are reported as the mean ± SE.

ABCC4 Western blot analysis. Total cellular protein for Western blot analysis was prepared from groups of ~50 *X laevis* oocytes injected with relevant cRNAs that were transcribed in vitro from related constructs. After 48 hours of expression of protein from the injected cRNA, oocytes were transferred to 1.7-ml polypropylene microfuge tubes on ice and lysed using a Teflon homogenizer in lysis buffer (50 m*M* Tris HCl, pH 7.5, 50 m*M* NaCl, 1 m*M* EDTA, pH 8, 1% Triton X-100) supplemented with protease inhibitor cocktail (Roche). After clearing the lysate off yolk and cellular debris by centrifugation at 5,000 revolutions per minute for 10 minutes, the supernatant was stored at −80°C. Western blotting was performed using affinity-purified rabbit anti-ABCC4 polyclonal antibody (Cell Signaling Technology) at a titer of 1:1,000. Total lysates of proteins were fractionated using 7.5% SDS–polyacrylamide gel electrophoresis (Bio-Rad). Proteins were transferred to polyvinylidene difluoride membrane (Bio-Rad) at 100V for 3 hours. The membrane was blocked in 5% nonfat dry milk in Tris buffered saline–Tween 20 (TBST). Primary antibodies were diluted in 5% milk in TBST and incubated with the membrane at room temperature for 2 hours with continuous gentle shaking. Blots were washed in TBST and probed with a horseradish peroxidase–conjugated secondary antibody (Bio-Rad) in TBST containing 5% fat-free milk for 1 hour at room temperature. The membrane was then washed 4 times with TBST, and chemiluminescence was determined using an enhanced chemiluminescence technique (Pierce), following standard protocols.

Table 2. Association of 39 variants in *ABCC4* and *SLC22A6–A8* with hyperuricemia*

ID no.	Position (Chr.), bp	REF/ALT	Frequency			OR‡	SE	*P*	Annotation§
			Reseq	EUR†	EAS†				
rs3017670	11:62744899	A/G	0.683	0.84	0.81	0.92	0.16	0.59	SLC22A6|intronic
rs2276300	11:62748699	G/A	0.165	0	0.16	0.95	0.21	0.82	SLC22A6|intronic
rs4149171	11:62752182	T/C	0.245	0.15	0.24	1.04	0.17	0.81	SLC22A6|5′-UTR
rs4149170	11:62752289	C/T	0.239	0.08	0.23	1.11	0.17	0.56	SLC22A6|5′-UTR
rs2187384	11:62761161	C/T	0.099	0.19	0.27	1.04	0.25	0.88	SLC22A8|intronic
rs953894	11:62762422	C/T	0.182	0.21	0.30	1.25	0.20	0.26	SLC22A8|intronic
rs2276299	11:62766431	A/T	0.456	0.18	0.27	0.82	0.16	0.21	SLC22A8|exonic-silent
rs4149179	11:62782446	C/T	0.265	0.03	0.26	0.92	0.17	0.63	SLC22A8|5′-UTR
rs4963227	11:62783150	C/T	0.934	0.90	0.93	1.14	0.30	0.68	SLC22A8|intronic
rs3770	13:95672237	G/A	0.662	0.39	0.50	0.94	0.16	0.72	ABCC4|3′-UTR
rs9516519	13:95672457	T/G	0.052	0.13	0	0.94	0.36	0.86	ABCC4|3′-UTR
rs9516520	13:95672858	T/C	0.052	0.13	0	0.94	0.36	0.86	ABCC4|3′-UTR
rs1059751	13:95672950	A/G	0.272	0.48	0.49	1.07	0.18	0.69	ABCC4|3′-UTR
rs9516521	13:95673122	T/C	0.052	0.13	0	0.94	0.36	0.86	ABCC4|3′-UTR
rs4148553	13:95673135	C/T	0.272	0.48	0.49	1.07	0.18	0.69	ABCC4|3′-UTR
rs4148551	13:95673518	T/C	0.662	0.38	0.50	0.94	0.16	0.72	ABCC4|3′-UTR
rs3742106	13:95673791	A/C	0.662	0.38	0.50	0.94	0.16	0.72	ABCC4|3′-UTR
–¶	13:95714909	A/G	0.091	–	–	0.95	0.26	0.83	ABCC4|intronic
rs1751034	13:95714976	C/T	0.784	0.81	0.78	1.10	0.18	0.60	ABCC4|exonic-silent
rs1189466	13:95726541	A/G	0.810	0.94	0.80	0.99	0.20	0.96	ABCC4|exonic-silent
rs1678339	13:95727780	T/C	0.810	0.94	0.79	0.99	0.20	0.96	ABCC4|exonic-silent
rs45477596	13:95735502	C/T	0.145	0	0	0.97	0.21	0.88	ABCC4|exonic-missense
rs1189437	13:95735604	G/T	0.762	0.94	0.78	1.00	0.18	0.99	ABCC4|intronic
rs6650282	13:95748221	T/C	0.504	0.44	0.27	0.88	0.15	0.41	ABCC4|3′-UTR
rs1729770	13:95818193	C/T	0.144	0.30	0.09	0.63	0.23	0.04	ABCC4|intronic
rs4148500	13:95818288	G/C	0.290	0	0.15	1.86	0.18	6.2×10^{-4}	ABCC4|intronic
rs2274405	13:95818978	T/C	0.550	0.62	0.53	0.65	0.15	5.4×10^{-3}	ABCC4|exonic-silent
rs2274406	13:95818996	T/C	0.550	0.62	0.53	0.65	0.15	5.4×10^{-3}	ABCC4|exonic-silent
rs2274407	13:95859035	C/A	0.162	0.08	0.18	0.73	0.21	0.13	ABCC4|splice-missense
rs11568679	13:95861741	T/C	0.148	0	0	0.86	0.22	0.51	ABCC4|exonic-silent
rs899494	13:95861804	A/G	0.749	0.84	0.81	0.65	0.18	1.7×10^{-2}	ABCC4|exonic-silent
rs899496	13:95862896	A/G	0.727	0.81	0.69	0.66	0.17	1.6×10^{-2}	ABCC4|intronic
rs11568637	13:95886854	T/C	0.117	0.01	0.11	1.05	0.25	0.84	ABCC4|intronic
rs4148437	13:95899354	A/G	0.233	0.40	0.19	0.83	0.19	0.32	ABCC4|splice
rs11568681	13:95953517	G/T	0.067	0.01	0.02	1.47	0.33	0.24	ABCC4|exonic-missense
rs1574430	6:43269029	A/C	0.807	0.58	0.62	0.87	0.20	0.47	SLC22A7|intronic
rs2841648	6:43269179	C/A	0.810	0.58	0.63	0.89	0.20	0.54	SLC22A7|intronic
rs56401710	6:43269180	C/A	0.810	0.58	0.63	0.89	0.20	0.54	SLC22A7|intronic
rs2270860	6:43270151	C/T	0.180	0.34	0.37	1.20	0.20	0.36	SLC22A7|splice

* Chr. = chromosome; REF/ALT = reference/alternative; Reseq = resequence; OR = odds ratio.
† In the European (EUR) and East Asian (EAS) sample sets, reference allele frequencies were derived from 1000 Genomes data (www.ensembl.org).
‡ Adjusted for age and sex.
§ Each variant was annotated using Plink/Seq (version 0.10) (https://atgu.mgh.harvard.edu/plinkseq/); variants found within the boundary of a gene or genes were further classified as intronic, exonic-unknown, exonic-missense, exonic-silent, 3′-untranslated region (3′-UTR), and 5′-UTR.
¶ This variant is not reported in the 1000 Genomes data.

RESULTS

Identification of common variants. A total of 39 variants with a frequency of >0.05 were detected by resequencing across the 4 loci, with the majority (n = 26) in *ABCC4* (Table 2). All variants were tested for association with hyperuricemia, and 6 variants in *ABCC4* were significantly associated (2 were in complete linkage disequilibrium) (Table 2). Accounting for variants in strong linkage disequilibrium ($r^2 > 0.90$), a total of 32 tests were performed (Table 2 and Figure 1). Therefore, the corrected *P* value for significant association with hyperuricemia was $P < 1.46 \times 10^{-3}$, which only rs4148500 achieved (odds ratio [OR] 1.86, $P = 6 \times 10^{-4}$). This variant was monomorphic for the urate-lowering allele in Europeans (Table 2).

Replication of rs4148500. Variant rs4148500 was genotyped over the replication 1 and replication 2 sample sets and tested for an association with gout (Table 3). Gout rather than hyperuricemia was examined for the pragmatic reason that we had access to a large number of clinically ascertained gout patients for whom hyperuricemia could be assumed. Given the differences in allele frequency at *ABCG2* rs2231142 between Western (Samoa, Tonga, Niue, Tokelau)

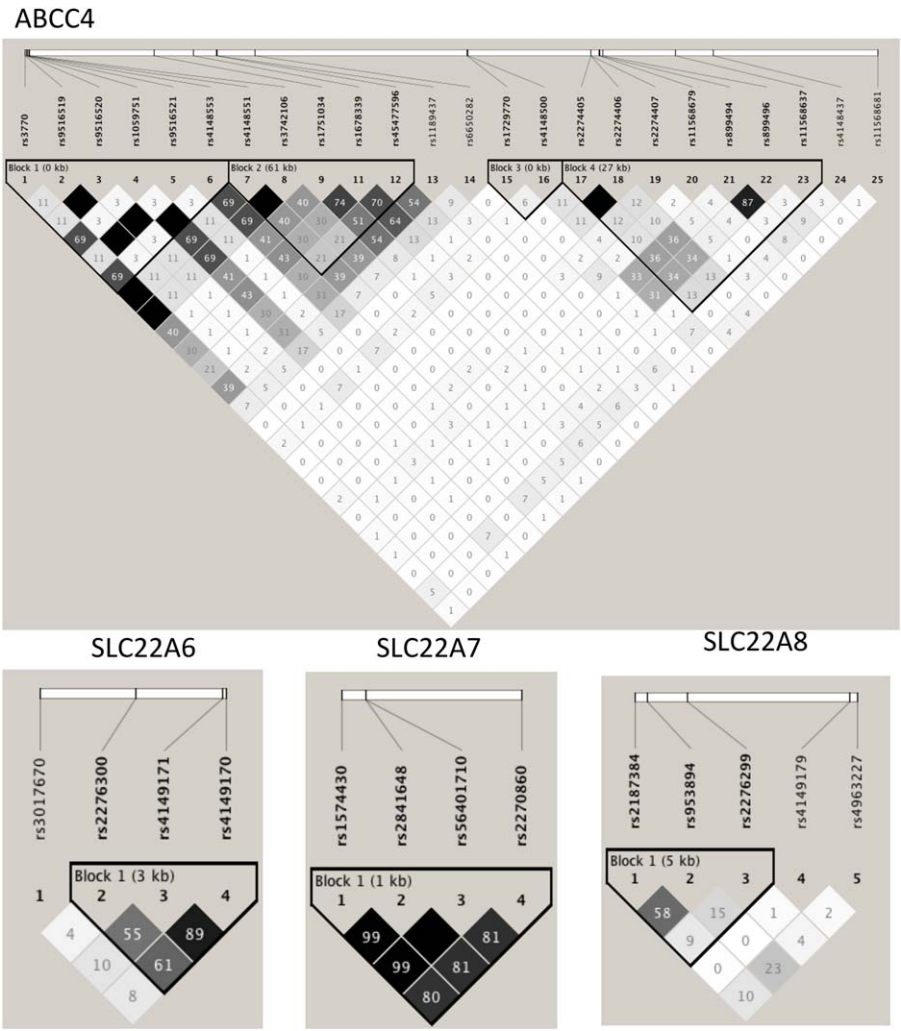

Figure 1. Linkage disequilibrium (r^2) relationships between common variants (shown in Table 2) in resequenced samples across *ABCC4*, *SLC22A6*, *SLC22A7*, and *SLC22A8*.

and Eastern (New Zealand and Cook Island Māori) Polynesians (34), the non-gout samples were first subdivided into Eastern and Western Polynesians. The A allele frequency was 0.186 in Eastern Polynesians and 0.314 in Western Polynesians. Therefore, subsequent regression analyses were performed with additional adjustment for Eastern versus Western versus mixed ancestry in order to account for any intra-Polynesian stratification. Applying the ancestry adjustment (in addition to the number of Polynesian grandparents) to the resequence data set showed evidence for association of rs4148500 with both gout (Table 3) (OR 1.62, $P = 0.012$) and hyperuricemia (OR 1.80, $P = 0.003$).

The association with gout was replicated in the combined replication sample sets (replication 1 + 2) (OR 1.25, $P = 0.033$), with significant association in replication 1 (OR 1.36, $P = 0.008$) but not replication 2 (OR 0.80, $P = 0.36$). The minor allele of rs4148500 was also associated with an increased risk of gout in the combined resequence and replication sample sets (OR 1.30, $P = 0.004$). Using the combined resequence and replication 1 and 2 sample sets, sex-stratified sample sets were generated, revealing that the association was restricted to men (OR 1.43 [$P = 0.001$] versus OR 0.98 [$P = 0.89$] in women) (Table 3). Combining the male and female sample sets by meta-analysis demonstrated evidence for a differential strength of effect (P for heterogeneity = 0.062, using a fixed-effects model). The effect size was similar between Western and Eastern Polynesian men (OR 1.41 [$P = 0.03$] and OR 1.45 [$P = 0.02$], respectively).

Association of rs4148500 with fractional excretion of uric acid. In the combined sample set, rs4148500 was tested for association with fractional excretion of uric

Table 3. Association of *ABCC4* rs4148500 with gout*

	Gout				Non-gout					
Sample set	GG	AG	AA	A	GG	AG	AA	A	OR (95% CI)†	*P*
Resequence	54 (0.380)	69 (0.486)	19 (0.134)	107 (0.377)	141 (0.562)	98 (0.390)	12 (0.048)	122 (0.243)	1.62 (1.12, 2.38)	0.012
Replication 1 and 2	407 (0.529)	298 (0.387)	65 (0.102)	428 (0.278)	371 (0.575)	244 (0.378)	30 (0.047)	304 (0.236)	1.25‡ (1.02, 1.53)	0.033
Replication 1	283 (0.480)	246 (0.418)	60 (0.102)	366 (0.311)	272 (0.560)	191 (0.393)	23 (0.047)	237 (0.244)	1.36 (1.08, 1.71)	0.0081
Replication 2	124 (0.685)	52 (0.287)	5 (0.028)	62 (0.173)	99 (0.623)	53 (0.333)	7 (0.044)	67 (0.211)	0.80 (0.49, 1.29)	0.36
All samples	461 (0.505)	367 (0.402)	84 (0.092)	535 (0.293)	512 (0.571)	342 (0.382)	42 (0.047)	426 (0.238)	1.30§ (1.09, 1.55)	0.0038
Men	365 (0.490)	303 (0.407)	77 (0.103)	457 (0.307)	253 (0.583)	163 (0.376)	18 (0.041)	199 (0.229)	1.43¶ (1.15, 1.77)	0.0011
WP	119 (0.361)	158 (0.479)	53 (0.161)	264 (0.400)	64 (0.430)	71 (0.477)	14 (0.094)	99 (0.332)	1.41 (1.04, 1.93)	0.030
EP	236 (0.608)	131 (0.338)	21 (0.054)	173 (0.223)	175 (0.681)	78 (0.304)	4 (0.016)	66 (0.167)	1.45 (1.06, 1.99)	0.020
Women	96 (0.575)	64 (0.383)	7 (0.042)	78 (0.234)	257 (0.561)	177 (0.386)	24 (0.052)	225 (0.246)	0.98# (0.70, 1.36)	0.89
WP	16 (0.432)	19 (0.514)	2 (0.054)	23 (0.311)	57 (0.500)	48 (0.421)	9 (0.079)	66 (0.289)	1.37 (0.71, 2.61)	0.34
EP	78 (0.614)	44 (0.346)	5 (0.039)	54 (0.213)	184 (0.580)	119 (0.375)	14 (0.044)	147 (0.232)	0.82 (0.54, 1.21)	0.32

* Individuals of mixed Eastern Polynesian (EP)/Western Polynesian (WP) ancestry (n = 85) were not included in the sex stratification. Individuals in the replication 2 sample set were recruited in collaboration with Ngāti Porou Hauora Charitable Trust. Values are the number (frequency). 95% CI = 95% confidence interval.
† Adjusted for age, sex, number of Polynesian grandparents, and Polynesian ancestral class (WP, EP, mixed [WP/EP]).
‡ Odds ratio (OR) 1.31, $P = 0.01$ by meta-analysis combining the replication 1 and replication 2 sample sets using a fixed-effects model, and OR 1.15, $P = 0.59$ using a random-effects model (P for heterogeneity [P_{het}] = 0.048).
§ OR 1.42, $P = 1 \times 10^{-4}$ by meta-analysis combining the resequence and replication 1 and replication 2 sample sets using a fixed-effects model, and OR 1.36, $P = 0.098$ using a random-effects model ($P_{het} = 0.036$).
¶ OR 1.43, $P = 0.0015$ by meta-analysis combining WP and EP men using a fixed-effects model, and OR 1.43, $P = 0.0015$ using a random-effects model ($P_{het} = 0.90$).
# OR 0.94, $P = 0.73$ by meta-analysis combining WP and EP women using a fixed-effects model, and OR 0.99, $P = 0.97$ using a random-effects model ($P_{het} = 0.18$).

acid in combined gout patients and non-gout controls and with serum urate in controls (Table 4). There was evidence for an association of the minor allele with reduced fractional excretion of uric acid in the combined sample set ($\beta = -0.378$ [$P = 0.03$]), an effect that was restricted to men ($\beta = -0.570$ [$P = 0.01$] in men; $\beta = 0.071$ [$P = 0.82$] in women). Among the non-gout controls, there was a strong trend toward an association with serum urate in the combined male sample set ($\beta = 0.013$ [$P = 0.07$]) (Table 4).

Identification of rare variants ABCC4 P1036L. Eighty rare variants were also detected in the resequenced Polynesian samples. These included 37 singleton variants (17 of which were not reported in 1000 Genomes), 19 variants with a prevalence of <1% in controls (5 not reported in 1000 Genomes), and 24 with a prevalence of 1–5% in controls (3 not reported in 1000 Genomes) (see Supplementary Table 2, available on the *Arthritis & Rheumatology* web site at http://onlinelibrary.wiley.com/doi/10.1002/art.40110/abstract). Of particular interest was a novel *ABCC4* missense variant found in 7 hyperuricemic Western Polynesian individuals and no controls (chromosome 13:95724019, G/A, P1036L). The mutated residue is located within the ABC transporter 2 domain with a scaled CADD score of 24 (top 0.003% of CADD scores in the genome). The chromosome 13:95724019 variant was genotyped over the replication 1 sample set, in which the A allele was restricted to individuals of Western Polynesian ancestry (see Supplementary Table 3, available on the *Arthritis & Rheumatology* web site at http://onlinelibrary.wiley.com/doi/10.1002/art.40110/abstract). Testing for association with gout revealed overrepresentation of the A allele in patients with gout, although there was no statistical evidence for association (OR 3.09 [$P = 0.15$]). Overrepresentation of the A allele in patients with gout was restricted to men (unadjusted OR 3.61 [$P = 0.23$] versus OR 1.07 [$P = 0.96$] in women).

Table 4. Change in FEUA and serum urate level per copy of the *ABCC4* rs4148500 minor allele in combined sample sets*

	Serum urate (non-gout only)			FEUA (gout and non-gout)		
	β (95% CI)	SE	*P*	β (95% CI)	SE	*P*
Combined	0.004 (−0.005, 0.014)	0.005	0.38	−0.378 (−0.729, −0.027)	0.179	0.035
Combined men	0.013 (−0.001, 0.027)	0.007	0.070	−0.570 (−1.006, −0.135)	0.222	0.011
Combined women	−0.003 (−0.016, 0.010)	0.007	0.67	0.071 (−0.529, 0.671)	0.306	0.82

* Testing was adjusted for age, sex, number of Polynesian grandparents, and Polynesian ancestral class (Western Polynesian, Eastern Polynesian, mixed). 95% CI = 95% confidence interval; FEUA = fractional excretion of uric acid.

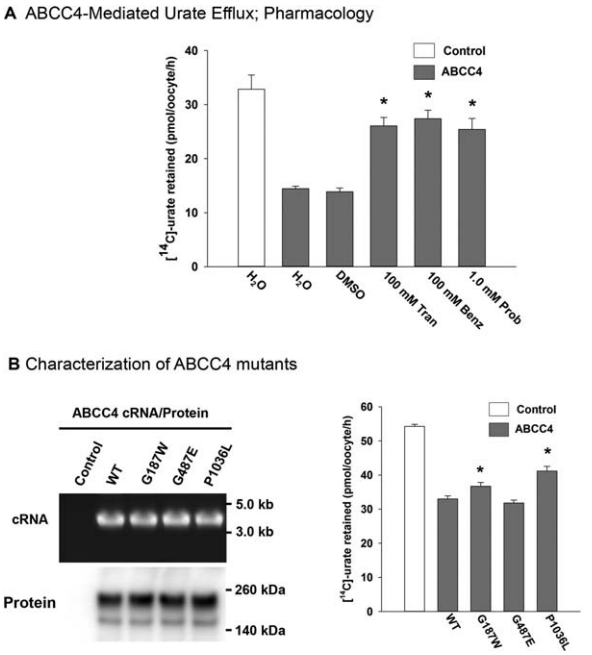

Figure 2. A, ATP-binding cassette subfamily C member 4 (ABCC4)–mediated urate efflux in *Xenopus* oocytes. Pharmacologic sensitivity was determined for tranilast (Tran), benzbromarone (Benz), and probenecid (Prob). $* = P < 0.001$, tranilast versus control and benzbromarone versus control; $P = 0.002$, probenecid versus control. **B,** Characterization of *ABCC4* mutants. Values are the mean ± SE. $* = P = 0.011$, G187W versus wild-type (WT); $P < 0.001$, P1076L versus WT.

Functional testing of P1036L. In order to evaluate any effects of P1036L on uric acid transport by ABCC4, the wild-type and mutant alleles were expressed in *Xenopus* oocytes, and efflux of [^{14}C] uric acid measured (Figure 2). ABCC4 exported uric acid at an ~2-fold slower rate compared with ABCG2 (ref. 33 and data not shown). Unlike ABCG2 (33), ABCC4 was sensitive to tranilast and benzbromarone, in addition to 1.0 m*M* probenecid (Figure 2A). The presence of a leucine residue at position 1036 led to an ~35% reduction in uric acid efflux compared with wild-type but had no effect on protein expression (Figure 2B).

In contrast to a prior study of coding SNP effects in ABCC4 (32), we observed that the G487E coding SNP mutation did not affect ABCC4 function, whereas the G187W mutant had reduced function, as reported previously (Figure 2B). Additionally, unlike in the previous study (32), in which reduced protein expression for the G187W mutant was observed, this mutant was fully expressed in oocytes, as shown by Western blotting. This discrepancy is perhaps a reflection of the different expression systems used (transient transfection of HEK 293 cells versus direct microinjection of cRNA in *X laevis* oocytes). A recent study in which transient transfection of HEK 293T cells was used also demonstrated normal expression of the 187W mutant (35).

DISCUSSION

We used a resequencing approach to detect an association between *ABCC4*, which encodes multidrug resistance protein 4 (MRP4), and hyperuricemia (OR 1.80, $P = 0.003$) and gout (OR 1.62, $P = 0.012$) in a sample set from the New Zealand Māori and Pacific population. The association with gout was replicated (OR 1.25, $P = 0.033$). These results demonstrate the utility of resequencing approaches in populations with a higher prevalence of the phenotype of interest in order to increase understanding of the molecular basis of disease. The reason for non-replication of the association of rs4148500 with gout in the replication 2 sample set could be low power: there was only 43% power to detect an effect at $\alpha = 0.05$ and (based on data for the replication 1 sample set) an OR 1.36 and a minor allele frequency of 0.244. Nevertheless, the direction of effect in men in the replication sample set (OR 1.23, $P > 0.05$) was consistent with findings in the combined data whereby the minor A allele of rs4148500 confers risk of gout in male individuals of Polynesian ancestry.

Similarly, the gout risk allele was associated with reduced fractional excretion of uric acid in men (Table 4). This finding is also important, because it provides further confirmation of MRP4 as a unidirectional efflux pump for uric acid (11,12). In avian proximal tubule epithelium, MRP4 is the dominant apical secretory uric acid transporter, and *ABCG2* apparently does not significantly contribute to uric acid secretion in the avian system (36). Interestingly, in this system, uric acid secretion is inhibited by AMP-activated protein kinase. The gene encoding the gamma-2 subunit of AMP-activated protein kinase is associated with the urate concentration and gout in European individuals (5,7). MRP4 also has been proposed as a transporter for urate excretion into the circulation because of its basolateral expression in the liver (11). It has been demonstrated that furosemide and thiazide diuretics and the urate-lowering benzbromarone inhibit, whereas the active metabolite of the urate-lowering allopurinol (oxypurinol) stimulates, MRP4-mediated renal uric acid efflux (37). Consistent with this, we observed that ABCC4 was sensitive to benzbromarone and probenecid at a higher concentration (1.0 m*M*). Thus, MRP4 may emerge as being a clinically important transporter in the management of gout and comorbid conditions.

The association of *ABCC4* with gout and fractional excretion of uric acid was restricted to male individuals (Tables 3 and 4). This finding may be of particular clinical relevance considering the very high rates of gout in Māori

and Pacific men; gout affects >25% of Māori and Pacific men older than age 60 years (2). The differential effects of an association of genetic variants with urate and gout between men and women represent a phenomenon observed at some other uric acid transporter loci. At *ABCG2*, an association of rs2231142 with gout was weaker in women (OR 1.5) than in men (OR 2.0), which at least partly reflects a 50% greater effect of rs2231142 on serum urate levels in men (5). At *SLC2A9*, there is a 70% greater effect on serum urate levels in women than in men, while the effect on gout is similar in women and men (5). At *SLC17A1*/*NPT1, SLC22A11*/*OAT4,* and *SLC22A12*/*URAT1*, however, although the effect sizes are up to one-third larger in men, any sex-specific effects remain to be established and are not of the extent observed at *SLC2A9, ABCG2*, and *ABCC4*. Understanding the molecular basis of the interaction between sex and genotype at these loci will illuminate the molecular mechanisms of control of urate levels.

The rare (~1%) Western Polynesian-specific 1036L variant selected for follow-up genotyping was not significantly associated with gout in the combined resequence and replication 1 and 2 sample sets ($P = 0.15$), although the direction of effect (OR 3.1) was consistent with overrepresentation of the 1036L variant in resequenced individuals with hyperuricemia (n = 7) compared with none in normouricemic individuals. This variant also had an extremely high CADD score, predicting a pathogenic (functional) effect. Consistent with the extremely high CADD score and with overrepresentation of the 1036L allele in hyperuricemic individuals and those with gout, the 1036L allele reduced uric acid reflux from *X laevis* oocytes by 30%. It can be predicted that individuals with this allele filter less uric acid into the urine. Residue 1036 is intracellular, being located in the second nucleotide-binding domain (32). *ABCC4* is a highly polymorphic gene; for example, >400 missense variants were reported in the Exome Aggregation Consortium database of 60,706 unrelated individuals (38), although 1036L is not reported in this database. Some of the variants have been evaluated for an effect on the functional characteristics of MRP4 (e.g., contributing to intracellular accumulation of antiviral agents [32] and methylated arsenic metabolites [35], and to lack of localization to the plasma membrane [35]). With urate control and risk of gout as clinical outcomes, it will be necessary to systematically test missense variants of *ABCC4* for association with urate concentrations and risk of gout, and to evaluate their influence on the ability of MRP4 to transport uric acid.

In the current study, an extreme sample drawn from the hyperuricemic Polynesian population was resequenced based on the hypothesis that this population has a higher prevalence of urate-raising genetic variants in the selected genes (postulated to control urinary uric acid excretion) that had not previously been associated with urate levels or gout by genome-wide association studies. In the case of *ABCC4,* the minor risk allele (A) of rs4148500 was not present in Europeans yet had a prevalence of 24% in persons of Polynesian descent. Thus, rs4148500 is a population-specific variant that highlights the relative importance of genetic variation in *ABCC4* as a risk factor for gout in the population of New Zealand Māori and Pacific men. Determining whether rs4148500 is the causal variant at the *ABCC4* locus will require sequence information from the entire region in the Polynesian genome and genotyping of variants in linkage disequilibrium. Furthermore, risk allele A was also prevalent in the Asian population (19%) (Table 2), which warrants testing for an association with gout in populations from this region, with a focus on replicating the male-specific effect observed in the Polynesian population of New Zealand.

ACKNOWLEDGMENTS

We thank Anna Gosling for helpful discussions on Polynesian migrations. We sincerely thank all participants with and those without gout who donated time and information for this study. We also thank the Genome Institute at the University of Washington St. Louis and Bob Fulton for their help. Finally, we thank Ria Akuhata, Nancy Aupouri, Carol Ford (Ngāti Porou Hauora), Jill Drake (Canterbury District Health Board), Roddi Laurence and Meaghan House (University of Auckland), and Gabrielle Sexton for their assistance in recruitment.

AUTHOR CONTRIBUTIONS

All authors were involved in drafting the article or revising it critically for important intellectual content, and all authors approved the final version to be published. Dr. Merriman had full access to all of the data in the study and takes responsibility for the integrity of the data and the accuracy of the data analysis.

Study conception and design. Stahl, Cadzow, Choi, Mount, Merriman.
Acquisition of data. Tanner, Boocock, Dobbyn, Mandal, Phipps-Green, Topless, Harré Hindmarsh, Stamp, Dalbeth, Merriman.
Analysis and interpretation of data. Boocock, Stahl, Mandal, Cadzow, Mount, Merriman.

REFERENCES

1. Dalbeth N, Merriman TR, Stamp LK. Gout [review]. Lancet 2016;388:2039–52.
2. Winnard D, Wright C, Taylor WJ, Jackson G, Te Karu L, Gow PJ, et al. National prevalence of gout derived from administrative health data in Aotearoa New Zealand. Rheumatology (Oxford) 2012;51:901–9.
3. Dehghan A, Köttgen A, Yang Q, Hwang SJ, Kao WL, Rivadeneira F, et al. Association of three genetic loci with uric acid concentration and risk of gout: a genome-wide association study. Lancet 2008;372:1953–61.
4. Merriman TR, Choi HK, Dalbeth N. The genetic basis of gout. Rheum Dis Clin North Am 2014;40:279–90.
5. Köttgen A, Albrecht E, Teumer A, Vitart V, Krumsiek J, Hundertmark C, et al. Genome-wide association analyses

identify 18 new loci associated with serum urate concentrations. Nat Genet 2013;45:145–54.
6. Merriman TR. Population heterogeneity in the genetic control of serum urate [review]. Sem Nephrol 2011;31:420–5.
7. Phipps-Green A, Merriman M, Topless R, Altaf S, Montgomery G, Franklin C, et al. Twenty-eight loci that influence serum urate levels: analysis of association with gout. Ann Rheum Dis 2016;75:124–30.
8. Aslamkhan A, Han YH, Walden R, Sweet DH, Pritchard JB. Stoichiometry of organic anion/dicarboxylate exchange in membrane vesicles from rat renal cortex and hOAT1-expressing cells. Am J Physiol 2003;285:F775–83.
9. Bakhiya N, Bahn A, Burckhardt G, Wolff NA. Human organic anion transporter 3 (hOAT3) can operate as an exchanger and mediate secretory urate flux. Cell Physiol Biochem 2003;13:249–56.
10. Sato M, Mamada H, Anzai N, Shirasaka Y, Nakanishi T, Tamai I. Renal secretion of uric acid by organic anion transporter 2 (OAT2/SLC22A7) in human. Biol Pharm Bull 2010;33:498–503.
11. Van Aubel RA, Smeets PH, van den Heuvel JJ, Russel FG. Human organic anion transporter MRP4 (ABCC4) is an efflux pump for the purine end metabolite urate with multiple allosteric substrate binding sites. Am J Physiol 2005;288:F327–33.
12. Woodward OM, Köttgen A, Coresh J, Boerwinkle E, Guggino WB, Köttgen M. Identification of a urate transporter, ABCG2, with a common functional polymorphism causing gout. Proc Natl Acad Sci U S A 2009;106:10338–42.
13. Mandal A, Mount DB. The molecular physiology of uric acid homeostasis. Annu Rev Physiol 2015;77:323–45.
14. Woodward OM, Tukaye DN, Cui J, Greenwell P, Constantoulakis LM, Parker BS, et al. Gout-causing Q141K mutation in ABCG2 leads to instability of the nucleotide-binding domain and can be corrected with small molecules. Proc Natl Acad Sci U S A 2013;110:5223–8.
15. Edwards NL, So A. Emerging therapies for gout. Rheum Dis Clin North Am 2014;40:375–87.
16. Tan PK, Liu S, Miner JN. The URAT1 uric acid transporter is important in uric acid homeostasis and its activity may be altered in gout patients and in drug-induced hyperuricemia [abstract]. Arthritis Rheumatol 2014;66 Suppl 10. URL: http://acrabstracts.org/abstract/the-urat1-uric-acid-transporter-is-important-in-uric-acid-homeostasis-and-its-activity-may-be-altered-in-gout-patients-and-in-drug-induced-hyperuricemia/.
17. Robinson P, Taylor W, Merriman T. Systematic review of the prevalence of gout and hyperuricaemia in Australia. Inter Med J 2012;42:997–1007.
18. Gosling AL, Matisoo-Smith E, Merriman TR. Hyperuricaemia in the Pacific: why the elevated serum urate levels? Rheumatol Int 2014;34:743–57.
19. Dalbeth N, House ME, Gamble GD, Horne A, Pool B, Purvis L, et al. Population-specific influence of SLC2A9 genotype on the acute hyperuricaemic response to a fructose load. Ann Rheum Dis 2013;72:1868–73.
20. Gibson T, Waterworth R, Hatfield P, Robinson G, Bremner K. Hyperuricaemia, gout and kidney function in New Zealand Maori men. Br J Rheumatol 1984;23:276–82.
21. Simmonds HA, McBride MB, Hatfield PJ, Graham R, McCaskey J, Jackson M. Polynesian women are also at risk for hyperuricaemia and gout because of a genetic defect in renal urate handling. Br J Rheumatol 1994;33:932–7.
22. Wallace SL, Robinson H, Masi AT, Decker JL, McCarty DJ, Yü TF. Preliminary criteria for the classification of the acute arthritis of primary gout. Arthritis Rheum 1977;20:895–900.
23. Simkin PA. Urate excretion in normal and gouty men. Adv Exp Med Biol 1977;76B:41–5.
24. Auwera GA, Carneiro MO, Hartl C, Poplin R, del Angel G, Levy-Moonshine A, et al. From FastQ data to high-confidence variant calls: the Genome Analysis Toolkit best practices pipeline. Curr Protoc Bioinformatics 2013;43:11.10.1–33.
25. Li H, Durbin R. Fast and accurate short read alignment with Burrows-Wheeler transform. Bioinformatics 2009;25:1754–60.
26. McKenna A, Hanna M, Banks E, Sivachenko A, Cibulskis K, Kernytsky A, et al. The Genome Analysis Toolkit: a MapReduce framework for analyzing next-generation DNA sequencing data. Genome Res 2010;20:1297–303.
27. Tange O. Gnu parallel-the command-line power tool: the USENIX Magazine 2011;36:42–7.
28. DePristo MA, Banks E, Poplin R, Garimella KV, Maguire JR, Hartl C, et al. A framework for variation discovery and genotyping using next-generation DNA sequencing data. Nat Genet 2011;43:491–8.
29. Kircher M, Witten DM, Jain P, O'Roak BJ, Cooper GM, Shendure J. A general framework for estimating the relative pathogenicity of human genetic variants. Nat Genet 2014;46:310–5.
30. Paila U, Chapman BA, Kirchner R, Quinlan AR. GEMINI: integrative exploration of genetic variation and genome annotations. PLoS Comput Biol 2013;9:e1003153.
31. R Development Core Team. R: a language and environment for statistical computing. Vienna: R Foundation for Statistical Computing; 2012.
32. Abla N, Chinn LW, Nakamura T, Liu L, Huang CC, Johns SJ, et al. The human multidrug resistance protein 4 (MRP4, ABCC4): functional analysis of a highly polymorphic gene. J Pharmacol Exp Ther 2008;325:859–68.
33. Mandal AK, Mercado A, Foster A, Zandi-Nejad K, Mount DB. Uricosuric targets of tranilast. Pharmacol Res Perspec 2017;5:e00291.
34. Phipps-Green AJ, Hollis-Moffatt J, Dalbeth N, Merriman ME, Topless R, Gow PJ, et al. A strong role for the ABCG2 gene in susceptibility to gout in New Zealand Pacific Island and Caucasian, but not Maori, case and control sample sets. Hum Mol Genet 2010;19:4813–9.
35. Banerjee M, Marensi V, Conseil G, Le XC, Cole SP, Leslie EM. Polymorphic variants of MRP4/ABCC4 differentially modulate the transport of methylated arsenic metabolites and physiological organic anions. Biochem Pharmacol 2016;120:72–82.
36. Bataille AM, Goldmeyer J, Renfro JL. Avian renal proximal tubule epithelium urate secretion is mediated by Mrp4. Am J Physiol 2008;295:R2024–33.
37. El-Sheikh AA, van Den Heuvel JJ, Koenderink JB, Russel FG. Effect of hypouricaemic and hyperuricaemic drugs on the renal urate efflux transporter, multidrug resistance protein 4. Br J Pharmacol 2008;155:1066–75.
38. Lek M, Karczewski K, Minikel E, Samocha K, Banks E, Fennell T, et al. Analysis of protein-coding genetic variation in 60,706 humans. Nature 2016;536:285–91.

ARTHRITIS & RHEUMATOLOGY
Vol. 69, No. 7, July 2017, pp 1470–1479
DOI 10.1002/art.40112

Early Outcomes in Children With Antineutrophil Cytoplasmic Antibody–Associated Vasculitis

Kimberly A. Morishita,[1] Lakshmi N. Moorthy,[2] Joanna M. Lubieniecka,[3] Marinka Twilt,[4] Rae S. M. Yeung,[5] Mary B. Toth,[6] Susan Shenoi,[7] Goran Ristic,[8] Susan M. Nielsen,[9] Raashid A. Luqmani,[10] Suzanne C. Li,[11] Tzielan Lee,[12] Erica F. Lawson,[13] Mikhail M. Kostik,[14] Marisa Klein-Gitelman,[15] Adam M. Huber,[16] Aimee O. Hersh,[17] Dirk Foell,[18] Melissa E. Elder,[19] Barbara A. Eberhard,[20] Paul Dancey,[21] Sirirat Charuvanij,[22] Susanne M. Benseler,[4] and David A. Cabral,[1]
for the ARChiVe Investigators Network within the PedVas Initiative

Objective. **To characterize the early disease course in childhood-onset antineutrophil cytoplasmic antibody (ANCA)–associated vasculitis (AAV) and the 12-month outcomes in children with AAV.**

Methods. **Eligible subjects were children entered into the Pediatric Vasculitis Initiative study who were diagnosed before their eighteenth birthday as having granulomatosis with polyangiitis (Wegener's), microscopic polyangiitis, eosinophilic granulomatosis with polyangiitis (Churg-Strauss), or ANCA-positive pauci-immune glomerulonephritis. The primary outcome measure was achievement of disease remission (Pediatric Vasculitis Activity Score [PVAS] of 0) at 12 months with a corticosteroid dosage of <0.2 mg/kg/day. Secondary outcome measures included the rates of inactive disease (PVAS of 0, with any corticosteroid dosage) and rates of improvement at postinduction (4–6 months after diagnosis) and at 12 months, presence of damage at 12 months (measured by a modified Pediatric Vasculitis Damage Index [PVDI]; score 0 = no damage, score 1 = one damage item present), and relapse rates at 12 months.**

Results. **In total, 105 children with AAV were included in the study. The median age at diagnosis was 13.8 years (interquartile range 10.9–15.8 years). Among the study cohort, 42% of patients achieved remission at 12 months, 49% had inactive disease at postinduction**

Supported by the Canadian Institutes of Health Research (grant FRN: TR-119188), the Child and Family Research Institute of British Columbia Children's Hospital, the Childhood Arthritis & Rheumatology Research Alliance, and the Vasculitis Foundation.

[1]Kimberly A. Morishita, MD, MHSc, David A. Cabral, MBBS: British Columbia Children's Hospital, University of British Columbia, Vancouver, British Columbia, Canada; [2]Lakshmi N. Moorthy, MD: Rutgers–Robert Wood Johnson Medical School, New Brunswick, New Jersey; [3]Joanna M. Lubieniecka, PhD: Simon Fraser University, Burnaby, British Columbia, Canada; [4]Marinka Twilt, MD, PhD, Susanne M. Benseler, MD, PhD: Alberta Children's Hospital, University of Calgary, Calgary, Alberta, Canada; [5]Rae S. M. Yeung, MD, PhD: The Hospital for Sick Children, University of Toronto, Toronto, Ontario, Canada; [6]Mary B. Toth, MD: Akron Children's Hospital, Akron, Ohio; [7]Susan Shenoi, MBBS, MS: Seattle Children's Hospital, Seattle, Washington; [8]Goran Ristic, MD: Mother and Child Health Care Institute of Serbia, Belgrade, Serbia; [9]Susan M. Nielsen, MD: Rigshospitalet, Copenhagen, Denmark; [10]Raashid A. Luqmani, DM, FRCP: Nuffield Orthopaedic Centre, University of Oxford, Oxford, UK; [11]Suzanne C. Li, MD, PhD: Joseph M. Sanzari Children's Hospital, Hackensack, New Jersey; [12]Tzielan Lee, MD: Stanford Children's Health, Stanford University School of Medicine, Stanford, California; [13]Erica F. Lawson, MD: University of California at San Francisco; [14]Mikhail M. Kostik, MD: Saint-Petersburg State Pediatric Medical University, Saint Petersburg, Russia; [15]Marisa Klein-Gitelman, MD, MPH: Ann & Robert H. Lurie Children's Hospital of Chicago, Chicago, Illinois; [16]Adam M. Huber, MD: IWK Health Centre and Dalhousie University, Halifax, Nova Scotia, Canada; [17]Aimee O. Hersh, MD: University of Utah, Salt Lake City; [18]Dirk Foell, MD: University Children's Hospital, Muenster, Germany; [19]Melissa E. Elder, MD: University of Florida, Gainesville; [20]Barbara A. Eberhard, MBBS, MSc: Cohen Children's Medical Center of New York, New Hyde Park, New York; [21]Paul Dancey, MD: Janeway Children's Health and Rehabilitation Centre, St. John's, Newfoundland, Canada; [22]Sirirat Charuvanij, MD: Siriraj Hospital, Mahidol University, Bangkok, Thailand.

Ms Shenoi has received consulting fees and speaking fees from Novartis (less than $10,000). Dr. Luqmani has received consulting fees and/or honoraria from GlaxoSmithKline, Roche, and MedImmune (less than $10,000 each). Dr. Foell has received honoraria from Novartis, Pfizer, Chugai-Roche, AbbVie, and Sobi (less than $10,000 each). Dr. Elder has received consulting fees from Medac Pharma (less than $10,000).

Address correspondence to Kimberly A. Morishita, MD, MHSc, Division of Rheumatology, Room K4-115, British Columbia Children's Hospital, Vancouver, British Columbia V6H 3V4, Canada. E-mail: kmorishita@cw.bc.ca.

Submitted for publication July 6, 2016; accepted in revised form March 23, 2017.

(4–6 months), and 61% had inactive disease at 12 months. The majority of patients improved, even if they did not achieve inactive disease. An improvement in the PVAS score of at least 50% from time of diagnosis to postinduction was seen in 92% of patients. Minor relapses occurred in 12 (24%) of 51 patients after inactive disease had been achieved postinduction. The median PVDI damage score at 12 months was 1 (range 0–6), and 63% of patients had ≥1 PVDI damage item scored as present at 12 months.

Conclusion. **This is the largest study to date to assess disease outcomes in pediatric AAV. Although the study showed that a significant proportion of patients did not achieve remission, the majority of patients responded to treatment. Unfortunately, more than one-half of this patient cohort experienced damage to various organ systems early in their disease course.**

Childhood antineutrophil cytoplasmic antibody (ANCA)–associated vasculitis (AAV) is rare, and studies of disease outcomes in children are limited. The AAVs include granulomatosis with polyangiitis (Wegener's) (GPA), microscopic polyangiitis (MPA), eosinophilic granulomatosis with polyangiitis (Churg-Strauss) (EGPA), and localized disease variants such as pauci-immune necrotizing glomerulonephritis (GN). Although they occur rarely, these diseases are often organ- or life-threatening. Prior to the introduction of treatment with corticosteroids and cyclophosphamide, the disease was rapidly fatal in the majority of pediatric and adult cases (1).

Evolving treatment strategies have significantly improved survival and reduced morbidity for patients with AAV. Due to the rarity of AAV in childhood, much of our knowledge about outcomes, such as remission, relapse, and damage, has come from studies in adult disease (2–9) or small pediatric case series (2,10–14). Data from AAV studies in adults have shown remission rates as high as 90% (15) and 5-year survival rates of 80% (16). Despite these advances, disease relapses occur in up to 30–50% of adult patients (17–19). In addition, even when patients achieve remission, damage can be seen early in the disease course and tends to increase over time (4). A recent retrospective study of 66 children with AAV from France assessed outcomes in children who had been followed up for a median of 5.2 years (20); 90% of the patients achieved remission after a median time of 6.7 months (interquartile range [IQR] 4.9–10.1), but 41% experienced at least 1 relapse after a median time of 29 months (IQR 14–89). To date, this French retrospective study has been the largest pediatric study of follow-up data for pediatric AAV, but because it was retrospective, remission or relapse rates at prespecified times were not reported.

A better understanding of remission rates, relapse rates, and other outcomes (ideally, using standardized pediatric-specific tools) will only be possible through international collaborations and use of international registries. Already, such initiatives have resulted in the development of pediatric-specific classification criteria (21), formulation of the Pediatric Vasculitis Activity Score (PVAS) (22), and ongoing initiatives to develop pediatric-specific vasculitis damage indices. The impact of disease (activity, severity, and damage) and its individual treatments (toxicity, safety, and efficacy) may be different in children, since their immune system is evolving, and comorbidities in children are likely to be different from those in adults. Moreover, the impact on physical and psychosocial growth and development is unique to children, and this requires long-term follow-up studies. For these reasons, research specific to pediatric patients is critically important.

The Pediatric Vasculitis Initiative (PedVas) is an international collaborative translational research initiative funded until 2017 by the Canadian Institutes of Health Research (for more details, see https://clinicaltrials.gov/ct2/show/NCT02006134) with the primary aim of improving the lives of children with chronic vasculitis. Clinical data are being collected through 2 previously established web-based registries, ARChiVe (A Registry for Children with Vasculitis) for the study of chronic systemic vasculitis (see Supplementary Appendix A for a list of the sites and investigators in the ARChiVe network, available on the *Arthritis & Rheumatology* web site at http://onlinelibrary.wiley.com/doi/10.1002/art.40112/abstract) and BRAINWORKS, a registry for the study of primary angiitis of the central nervous system. The primary objective of the current study was to describe the early disease course of children with AAV. Specifically, the aims were 1) to describe the baseline clinical features of children with AAV, including organ involvement, disease activity, and treatments initiated, and 2) to characterize the early disease course and outcomes by determining treatment response (rates of remission, improvement, and inactive disease), relapse rates, and damage in the first 12 months of disease.

PATIENTS AND METHODS

Patients. The ARChiVe registry was established in March 2007 and initially collected data from the time of diagnosis only (23), but since January 2013, with the support of PedVas, retrospective and prospective follow-up data have been collected. The current study is an inception cohort study

using data from patients entered into the ARChiVe registry from 22 international sites.

Patient eligibility criteria, the registry data set, and the strategy for establishing the time of diagnosis data set have been described previously (23). Eligible patients included were those who were diagnosed by the treating physician after January 1, 2004 and before the age of 18 years as having a primary chronic systemic vasculitis. Patient data were collected retrospectively for those diagnosed before March 2007, and prospectively for those diagnosed subsequently.

For the purpose of the present study, eligible subjects were children diagnosed before their eighteenth birthday as having GPA, MPA, EGPA, or ANCA-positive pauci-immune GN and who had complete follow-up data at postinduction (4–6 months after diagnosis) and at 12 months after diagnosis, collected through November 2015. Patients with a treating physician's diagnosis of ANCA-positive pauci-immune GN were included because, on further review, many of these children met the classification criteria for GPA or could be classified as having MPA after application of the European Medicines Agency (EMA) algorithm. Each eligible patient was reviewed and classified as follows. For EGPA, patients had to meet the American College of Rheumatology (ACR) criteria or the Lanham criteria for EGPA (24,25). For a diagnosis of GPA, patients had to meet the ACR criteria or the European League Against Rheumatism (EULAR)/Paediatric Rheumatology International Trials Organisation (PRINTO)/Paediatric Rheumatology European Society (PRES) classification criteria for GPA (21,24). For MPA, because MPA-specific classification criteria are lacking, the diagnosis was formalized by applying a pediatric modification of the EMA algorithm for classifying AAV (incorporating the EULAR/PRINTO/PRES classification criteria) (26). Patients were excluded if they could not be classified as having GPA, MPA, or EGPA after application of the above-described criteria.

The ARChiVe registry uses a web-based interface for entry of data at several time points, including the time of diagnosis, postinduction (4–6 months after diagnosis), 12 months postdiagnosis, and flare visits. The study protocol was approved by the local research ethics board at each participating center. Informed consent for participation was obtained from parents, and informed consent or assent was obtained from patients for both retrospective and prospective recruitment. Study data were collected and managed using REDCap electronic data capture tools hosted at the University of British Columbia (27).

Data collection. Categorical data collected included demographic data, treating physician's diagnosis, date of diagnosis, family and patient's medical history, presenting symptoms and interval history, clinical features, results of laboratory testing, diagnostic investigations, including diagnostic imaging or other procedures such as biopsies, medications, including the dosage of corticosteroid, the PVAS (maximum possible score of 63) (22), and a modified version of the Vasculitis Damage Index (VDI) (28) for use in pediatrics (PVDI).

Outcome assessments. The primary outcome measure was achievement of disease remission at 12 months following diagnosis. Secondary outcome measures included rates of inactive disease at postinduction (4–6 months after diagnosis) and at 12 months after diagnosis, rates of improvement at postinduction and at 12 months, presence of damage at 12 months, and rates of relapse within 12 months. Definitions from the EULAR recommendations for conducting clinical studies in AAV (29) were used to define remission, improvement, relapse, and damage. In order to apply these definitions to pediatric data, the PVAS was used in place of the Birmingham Vasculitis Activity Score (BVAS) (30), and the PVDI was used in place of the adult VDI (28).

Remission was defined as a PVAS of 0 (inactive disease) and a dosage of prednisone (or equivalent) of <0.2 mg/kg/day. Adult guidelines recommend that remission should be defined as occurring only when a patient has attained a stable low dosage of prednisone (29), which formed the basis of our weight-based criterion of <0.2 mg/kg/day for remission in this pediatric cohort. Inactive disease was defined as an absence of disease activity (PVAS of 0), regardless of corticosteroid dosage. Improvement was defined as a decrease in the PVAS score by at least 50% postinduction (at 4–6 months after diagnosis) or at 12 months after diagnosis as compared to the time of diagnosis. This level of response is consistent with the definition of a clinically important improvement according to the EULAR recommendations (29). A decrease in the PVAS of 70% or more was also studied as a measure of improvement.

Relapse was defined as recurrence or new onset of disease activity (an increase in the PVAS of ≥ 1, from 0) attributable to active inflammation. Major relapse was defined as the recurrence or new onset of potentially organ- or life-threatening disease activity requiring an escalation in treatment, in addition to treatment with corticosteroids. Other relapses were considered minor.

In adult vasculitis, damage is scored according to the VDI, which is a validated tool for assessing damage from disease, treatment, or concurrent conditions (28). Damage is considered irreversible and must be present for at least 3 months to be counted as an item in the VDI. There is no validated tool to assess disease damage in children with vasculitis. Therefore, in order to apply the VDI to our pediatric cohort of patients, we made the following modifications. 1) Hypertension in the adult VDI is defined as a diastolic blood pressure (BP) of ≥ 95 mm Hg or requiring treatment with antihypertensive agents; this was modified to a diastolic BP of $>$95th percentile for height and age or requiring treatment with antihypertensive agents. 2) Proteinuria in the adult VDI is defined as a level of ≥ 0.5 gm/24 hours; this was modified to a level of >0.3 gm/24 hours in order to be consistent with how proteinuria data are collected in this registry. The PRES Vasculitis Working Group and Childhood Arthritis & Rheumatology Research Alliance are currently working toward validating a formal pediatric modification of the VDI (31). The modifications that were made to the VDI for this study align with the proposed changes by the PRES Vasculitis Working Group. Further considerations by the Working Group include the addition of other pediatric-specific items, such as growth delay, delayed puberty, and new-onset obesity. These items were also collected in the registry but not scored. In the present study, a PVDI score of 0 indicated no damage, while a score of 1 indicated the presence of 1 damage item (of a total of 64 potential damage items on the PVDI). A copy of the modified pediatric version of the VDI used for this study is provided in Supplementary Figure 1 (available on the *Arthritis & Rheumatology* web site at http://onlinelibrary.wiley.com/doi/10.1002/art.40112/abstract).

Statistical analysis. Descriptive statistics were used for baseline characteristics, remission-induction medications, rates of improvement, rates of inactive disease, and rates of remission. Comparisons were made using the Fisher's exact test for categorical data and *t*-test or Mann-Whitney U test for quantitative variables. Statistical analysis of the data was performed using Microsoft Excel version 2007 software or R version 3.2.2 (R Core Team, 2015; available at https://www.R-project.org/).

RESULTS

Characteristics of the patients. In total, 107 patients were eligible for inclusion in the study. The diagnosis in 2 patients was not classifiable as AAV according to the defined classification criteria, and therefore these 2 patients were excluded. Of the remaining 105 children, 81% were classified as having GPA, 13% as having MPA, and 6% as having EGPA. Among the 105 patients, 68% were female and 50% were white. Fifty percent of the patients did not have complete data on ethnicity or the ethnicity was unknown. The distribution of the ethnic groups is shown in Table 1. The median age at diagnosis was 13.8 years (IQR 10.9–15.8 years). The median PVAS of disease activity at diagnosis was 19 (IQR 14–24), while the median PVAS by subtype of AAV were 20 (IQR 14–24) in patients with GPA, 17.5 (IQR 13.8–19.8) in those with MPA, and 17 (IQR 11–26.8) in those with EGPA. The median interval between symptom onset and diagnosis was 2.2 months (IQR 0.9–5.6 months). In total, 83 patients were diagnosed after March 2007 (prospective data collection), and 22 patients were diagnosed before March 2007 (retrospective data collection).

Clinical presentation and laboratory test results. The majority of patients had pulmonary disease (80%) and/or renal disease (78%). Sixty-four patients (61%) had both pulmonary and renal disease. One-third of the patient cohort had alveolar hemorrhage or massive hemoptysis at presentation, and 10% were in respiratory failure. Seventeen patients (16%) were in renal failure requiring dialysis, and 5 patients (5%) had end-stage renal disease. Other systems involved in a majority of patients were ear, nose, and throat (ENT) (56%) and musculoskeletal (53%). Additional baseline clinical features are shown in Table 1.

Of the 105 patients, 99 underwent immunofluorescence testing for ANCAs. Among these patients, 54% were positive for cytoplasmic ANCAs (cANCAs) (94% with proteinase 3 [PR3] specificity, 2% with myeloperoxidase [MPO] specificity, 4% with negative specificity), 32% were positive for perinuclear ANCAs (pANCAs) (91% with MPO specificity, 9% with PR3 specificity), 3% were mixed positive for both cANCAs and pANCAs, and 11% were negative for ANCAs. The 6 patients who did not undergo immunofluorescence testing had antigen specificity testing, which showed that 4 of the patients were PR3 positive and 2 were MPO positive.

Ninety-one patients (87%) had tissue biopsies performed as part of their diagnostic evaluation, of whom 61 patients (58%) had renal biopsies, 20 patients (19%) had skin biopsies, and 9 patients (9%) had paranasal sinus biopsies. Other biopsy sites included the gastrointestinal tract (8% of patients), upper airways (6% of patients), orbital masses (3% of patients), and other sites (7% of patients).

Treatment. For remission induction, cyclophosphamide (CYC) was used in 74 patients (70%), methotrexate (MTX) in 17 patients (16%), and rituximab (RTX) in 14 patients (13%). Four patients received both

Table 1. Baseline demographic and clinical features of the 105 children with antineutrophil cytoplasmic antibody–associated vasculitis*

Female	71 (68)
Ethnicity	
White	52 (50)
East Indian/South Asian	5 (5)
Asian	4 (4)
Hispanic	3 (3)
Aboriginal	2 (2)
African American	2 (2)
Middle Eastern	1 (1)
Mixed	10 (10)
Age at diagnosis, median (IQR) years	13.8 (10.9–15.8)
Interval between symptom onset and diagnosis, median (IQR) months	2.2 (0.9–5.6)
Clinical feature	
Constitutional symptoms	84 (80)
Pulmonary involvement	84 (80)
Alveolar hemorrhage/massive hemoptysis	34
Respiratory failure	11
Abnormal findings on chest imaging	75
Renal involvement	82 (78)
Hematuria	77
Proteinuria (>0.3 gm/24 hours)	73
Rise in creatinine >10% or fall in creatinine clearance >25%	37
Renal failure requiring dialysis	17
End-stage renal disease	5
Ear, nose, and throat involvement	59 (56)
Nasal discharge/crusts/ulcers/granuloma	38
Paranasal sinus involvement	25
Subglottic stenosis	9
Musculoskeletal involvement	56 (53)
Arthralgia/myalgia	48
Arthritis	23
Mucous membrane/ocular involvement	42 (40)
Gastrointestinal involvement	41 (39)
Cutaneous involvement	39 (37)
Nervous system involvement	20 (19)
Cardiovascular involvement	6 (6)

* Except where indicated otherwise, values are the number (%) of patients. IQR = interquartile range.

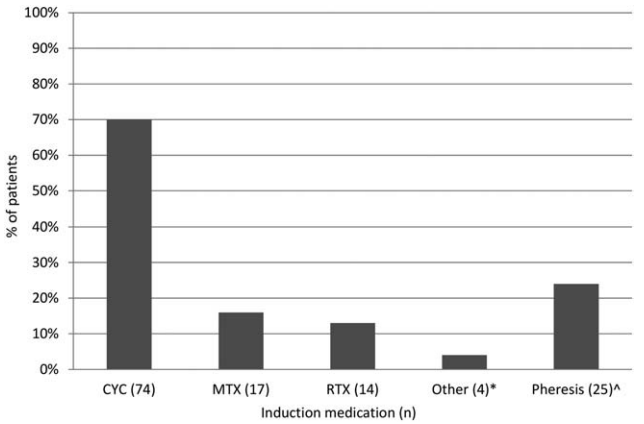

Figure 1. Primary treatments used for remission induction in children with antineutrophil cytoplasmic antibody–associated vasculitis, including cyclophosphamide (CYC), methotrexate (MTX), rituximab (RTX), plasmapheresis, and other treatments. * = Other primary remission-induction medications included azathioprine (n = 2 patients), mycophenolate mofetil (n = 1 patient), and corticosteroids only (n = 1 patient). ^ = 25 patients received plasmapheresis in the following combinations: CYC and plasmapheresis (n = 21), CYC and RTX and plasmapheresis (n = 3), and RTX and plasmapheresis (n = 1).

CYC and RTX. All patients who received RTX were diagnosed after 2010. RTX use did not appear to be center-specific, as it was used at 9 different sites; however, all sites were either in Canada or the US. Azathioprine (AZA) was used as the primary remission-induction agent in 2 patients, and mycophenolate mofetil (MMF) was used in 1 patient. One patient received corticosteroid alone for remission induction, without any other primary immunosuppressant treatment. Plasmapheresis was used in conjunction with CYC and/or RTX in 25 patients (24%). Of these 25 patients who received plasmapheresis, 24 (96%) had renal disease and 21 (84%) had both pulmonary and renal disease. All patients received oral corticosteroids as part of their remission-induction treatment. Seventy-four patients (70%) were also treated with intravenous pulses of high-dose methylprednisolone at the time of diagnosis. The dose and number of pulses used were highly variable, ranging from 10 mg/kg/dose to 30 mg/kg/dose and 1–12 pulses. Primary treatments used for remission induction are shown in Figure 1.

Treatments for remission maintenance were AZA in 45 patients (43%), MTX in 24 patients (23%), MMF in 14 patients (13%), CYC in 10 patients (9%), and RTX in 10 patients (9%) (Figure 2). At 12 months after diagnosis, 75 patients were either no longer receiving corticosteroids (32 patients [30%]) or were receiving a low dosage of corticosteroids (<0.2 mg/kg/day; 43 patients [41%]).

Outcomes. *Remission.* Forty-four patients (42%) achieved remission at 12 months (PVAS of 0, corticosteroid dosage <0.2 mg/kg/day). Twenty-one (48%) of these 44 patients who achieved remission had discontinued their corticosteroid treatment by 12 months. All but 3 patients remained on maintenance treatment at 12 months (18 receiving AZA, 9 receiving MTX, 6 receiving RTX, 5 receiving MMF, and 3 receiving CYC).

Inactive disease. Fifty-one (49%) of the 105 patients had inactive disease (PVAS of 0) at postinduction (4–6 months after diagnosis), and 64 patients (61%) had inactive disease at 12 months (of whom 44 were described as being in remission, in that they were receiving a minimal dosage of corticosteroids or had discontinued corticosteroids by 12 months, whereas the remaining 20 patients had inactive disease at 12 months while continuing to receive a higher dosage of corticosteroids). Thirty-nine of the patients who had inactive disease postinduction continued to have inactive disease at 12 months.

Improvement postinduction. The majority of patients improved even if they did not achieve inactive disease by the postinduction visit. An improvement in the PVAS of at least 50% from the time of diagnosis to postinduction was seen in 92% of patients. An improvement in the PVAS of at least 70% was seen in 85% of patients. Four patients had no improvement or a worse PVAS during the postinduction time period.

Improvement at 12 months. An improvement in the PVAS of at least 50% from the time of diagnosis to 12 months was seen in 93% of patients, and an improvement of at least 70% was seen in 90% of patients. One

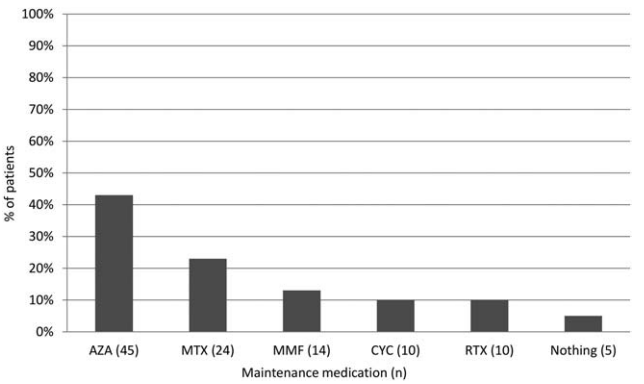

Figure 2. Primary treatments used for remission maintenance in children with antineutrophil cytoplasmic antibody–associated vasculitis, including azathioprine (AZA), methotrexate (MTX), mycophenolate mofetil (MMF), cyclophosphamide (CYC), and rituximab (RTX), or no maintenance medication.

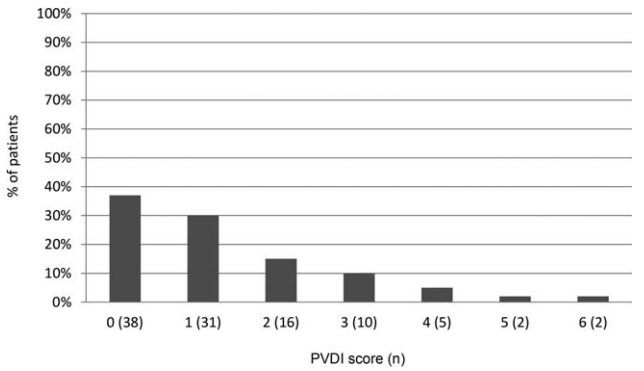

Figure 3. Percentage and number of patients with Pediatric Vasculitis Damage Index (PVDI) scores of 0–6, at 12 months after diagnosis.

patient had a worse PVAS at 12 months compared to the time of diagnosis.

Relapses. Relapses occurred in 12 (24%) of 51 patients after inactive disease had been achieved at the postinduction visit. All relapses were considered minor. Twenty-two (21%) of 105 patients had a worsening of the PVAS between the postinduction visit and the 12-month visit (PVAS worsened by 1 or more points, regardless of whether inactive disease [PVAS of 0] had been achieved at the postinduction visit).

Damage. Completed PVDI scores for damage were available for 104 patients. The median PVDI score at 12 months was 1 (range 0–6). Sixty-six (63%) of the 104 patients had ≥1 damage item scored as present at 12 months, 35 (34%) had ≥2 damage items scored as present, and 19 (18%) had ≥3 damage items scored as present. The distribution of PVDI scores is shown in Figure 3, and the specific items scored across the various organ systems are shown in Table 2.

One-third of the 104 patients had evidence of renal damage. The most frequent renal damage items scored as present were proteinuria (20%), an estimated/measured glomerular filtration rate of ≤50% of normal (18%), and end-stage renal disease (12%). Two patients had received renal transplants. ENT damage was seen in 20% of patients, and pulmonary damage was seen in 15% of patients. Investigators were given the opportunity to enter other items that they believed would represent damage but were not included in the scoring form. Items that were entered more than once included chronic cough (3 patients), new-onset obesity (3 patients), and significant striae (5 patients).

Hospitalizations and deaths. Following the time of diagnosis, 43 patients reported a hospitalization during the follow-up (total of 80 hospitalizations). Hospitalizations for routine treatments were not included. Almost one-half (46%) of the hospitalizations were in relation to disease flares, 16% were attributable to infection, and 5% were because of treatment- or medication-related adverse effects. Twelve hospitalizations (15%) were for other disease-related reasons, such as a renal biopsy or other tissue biopsy (beyond the time of diagnosis), investigational procedures such as endoscopies, or, in 1 patient, 3 admissions for physical rehabilitation. Fourteen hospitalizations (18%) were for reasons unrelated to the underlying disease or treatments, according to the site investigator. No deaths occurred.

Exploration of associations with remission at 12 months. We conducted an exploratory univariate analysis of a few selected baseline features to determine whether these features showed an association with remission at 12 months. Based on observations from

Table 2. Pediatric Vasculitis Damage Index damage items scored as present at 12 months after diagnosis among 104 patients with antineutrophil cytoplasmic antibody–associated vasculitis

System, damage item	No. (%) of patients affected
Renal	36 (35)
Proteinuria	21
Decreased glomerular filtration rate	19
End-stage renal disease	12
Hypertension	8
Ear, nose, and throat	21 (20)
Nasal bridge collapse/septal perforation	8
Nasal blockage/chronic discharge/crusting	7
Chronic sinusitis	6
Subglottic stenosis	5
Hearing loss	4
Pulmonary	16 (15)
Impaired lung function	11
Chronic asthma	6
Chronic breathlessness	2
Pulmonary fibrosis	1
Pulmonary infarct	1
Ocular	9 (9)
Cataract	8
Retinopathy	1
Visual impairment/diplopia	1
Musculoskeletal	4 (3)
Avascular necrosis	2
Osteoporosis/vertebral collapse	2
Significant muscle atrophy	1
Cardiovascular	3 (3)
Valvular disease	2
Pericarditis for ≥3 months or pericardectomy	1
Skin/mucous membranes	2 (2)
Alopecia	1
Cutaneous ulcers	1
Gastrointestinal	2 (2)
Chronic peritonitis	2
Neuropsychiatric	1 (1)
Peripheral neuropathy	1
Peripheral vascular disease	0

previous research (8,15,17,32–34), we selected, a priori, age, sex, ANCA status, the PVAS, and induction treatment as potential variables associated with remission. The reported *P* values were not corrected for multiple comparisons.

The median age of patients who achieved remission was 14 years, compared to 13 years for patients who did not achieve remission ($P = 0.04$). At 12 months, 55% of the male patients compared to 34% of the female patients achieved remission ($P = 0.06$). Treatment was dichotomized into 2 groups, aggressive versus moderate. Aggressive treatment was defined as remission-induction medications that included CYC and/or RTX, with or without plasmapheresis. Moderate treatment was defined as remission-induction medications that included MTX, AZA, or MMF. The 1 patient who received only corticosteroids for induction treatment was excluded from the treatment analysis. Rates of remission at 12 months postdiagnosis were similar between patients who received aggressive treatment and those who received moderate treatment (43% who received aggressive treatment achieved remission versus 30% who received moderate treatment; $P = 0.32$). The median baseline PVAS for the patients who received aggressive treatment was 20, compared to a median baseline PVAS of 14 for the patients who received moderate treatment ($P = 0.0001$).

There was minimal difference in the baseline PVAS score between patients who achieved remission at 12 months and those who did not achieve remission at 12 months (median baseline PVAS of 21 in the remission group versus 19 in the nonremission group; $P = 0.18$). Similarly, ANCA subtype was not associated with remission, in that 42% of cANCA/PR3-positive patients achieved remission at 12 months compared to 38% of pANCA/MPO-positive patients ($P = 0.83$).

DISCUSSION

This multicenter international study assessed the early disease course and outcomes in 105 patients with childhood-onset AAV. This is the largest cohort study to date to report pediatric outcomes in this group of diseases. Despite numerous adult-based studies and clinical trials reporting short- and long-term outcomes in AAV, our knowledge of pediatric-specific outcomes remains limited. Until now, the 2 largest pediatric studies in which outcomes have been described have included respective total sample sizes of 66 patients and 35 patients with AAV (20,35).

In our study, the majority of children had GPA. The median age at diagnosis (13.8 years) and predominance of female patients are consistent with the findings in other pediatric AAV studies (20,35). The high rates of renal disease (78%) and pulmonary disease (80%) at presentation are also consistent with those reported previously; however, children in our study had lower rates of ENT disease, at 56%, as compared to the reported rates of 70–90% in other recent studies (11,20,35,36). Treatment strategies were also consistent with those in previous studies, with the majority of patients receiving CYC in conjunction with corticosteroids for remission induction and then switching to AZA or MTX for remission maintenance (20,35). Disease activity, as measured using the PVAS, was not easily comparable to that in other studies, as it has only been reported in 1 previous study, the French Vasculitis Study Group cohort, in which the median PVAS was 9.5 for MPA, 12 for GPA, and 14.5 for EGPA (35). The median baseline PVAS in our patients was higher, at a median of 19. The use of plasmapheresis in 50% of the patients may be an indicator of severe disease; however, it may also be a reflection of more recent practices or jurisdiction-based capacity or preferences.

A significant proportion of patients were not in remission at 12 months. The 12-month remission rate of 42% in our cohort was significantly lower than the remission rates reported by Sacri et al in their cohort (20), which were 73% at postinduction and 90% for the overall remission rate (including secondary remissions after a median time of 6.7 months). In that study cohort, remission was assessed after remission-induction therapy had been initiated, but the criteria for remission did not need to be met within a specified time frame. Remission in the study by Sacri et al was defined as a Birmingham Vasculitis Activity Score (BVAS) of 0 or a BVAS for Wegener's Granulomatosis of 0 and corticosteroid dosage of $\leq$7.5 mg once daily (regardless of weight) (20), which was similar to the criteria used in this study. Differences in remission rates between our study and the study by Sacri et al might be explained by several factors. 1) The patient characteristics were different, in that there were more patients with MPA in the French cohort and fewer patients with pulmonary disease. 2) Disease activity scoring was applied retrospectively in the French cohort, compared to use of an automated online calculator in conjunction with a clinic visit for the majority of patients in the PedVas cohort. 3) The timing of assessments was different; in our study, inactive disease was assessed at postinduction (specifically, 4–6 months after diagnosis), and remission was assessed at the 12-month visit. 4) The proportion of patients receiving treatments for remission induction in the French cohort

were similar to those in our study (in the French cohort, 66% received CYC, 14% received RTX, and 17% received plasmapheresis). However, direct comparisons between the cohorts with regard to baseline disease activity, specifics of treatment regimens, and the basis behind treatment decisions could not be made.

Reported remission rates in several adult clinical trials in AAV have also shown variability, ranging between 53% and 93% (37–39). The lower reported remission rates in some trials assessing adult patients have been attributed to several potential factors, including stricter corticosteroid-weaning protocols (for example, complete weaning by 6 months versus weaning by 12 months), stricter definitions of remission (BVAS of 0 versus BVAS of <2), and longer duration of disease inactivity to define remission (3 months of inactive disease versus no minimum duration of inactive disease). For our study, the definition of remission required use of a minimum corticosteroid dosage at 12 months, and there was no minimum duration of inactive disease required; however, our criterion for disease activity was strict (PVAS of 0). These definitions were selected on the basis of recommendations for reporting outcomes in adult patients in clinical trials (29), which were introduced in an attempt to reduce heterogeneity in outcomes reporting. It is acknowledged that the strict inclusion and exclusion criteria of clinical trials, in addition to the highly systematic approach to disease assessment, medication administration, and weaning, are not directly comparable to those in observational cohorts.

Selection of patients in clinical trials and strict protocols may allow for easier attainment of remission criteria at certain time points and may also result in selection of patients who are more likely to respond to treatment. Our registry included all patients with AAV regardless of baseline disease severity, disease activity, organ involvement, or specific treatments, all of which would be important factors in determining the chance of remission. In addition, the treating physician's protocol of continuing treatment with prednisone at a dosage of either >0.2 mg/kg/day or <0.2 mg/kg/day might represent the physician's individual practice approach, rather than a patient-specific requirement to maintain control of inflammation. The remission rates reported in this study may be a better reflection of the remission rates seen in clinical practice as compared to what is reported from clinical trials.

Despite a significant proportion of patients not achieving inactive disease postinduction or not achieving remission at 12 months, the majority of patients met the definition of treatment response, with 92% of patients experiencing an improvement of at least 50% in the PVAS at postinduction. This is similar to the high rate of treatment response reported in the study by Sacri et al (20). Relapses occurred in 24% of patients who achieved inactive disease at postinduction. This rate is lower than the reported rates of 40–80% in other pediatric studies, but our duration of follow-up was only 1 year, compared to a median follow-up of 2–8 years in other studies (20,35,40). Longer-term follow-up data are needed to examine the relapse rates with current treatment regimens.

More than one-half of the patient cohort (63%) had evidence of damage by 12 months. A study by Iudici et al also assessed damage in a cohort of children with systemic necrotizing vasulitides (35). They used the VDI to score damage and reported a median VDI score of 1 at last follow-up (median follow-up time 96 months), which is the same as the median PVDI score in our cohort at 12 months after diagnosis. The percentage of patients who had evidence of damage was not reported in the study by Iudici et al, and therefore it is difficult to make further comparisons. Robson and colleagues summarized the rates of damage in adult patients with AAV from 6 European Vasculitis Study Group studies, and found a similarly high rate of damage (87%) at 12 months (4). As in other studies of adult patients, the most frequently scored damage items in the study by Robson et al were renal items such as proteinuria and reduced glomerular filtration rate, followed by ENT items (4). The fact that so many children already have evidence of renal damage within 12 months of diagnosis is concerning, considering that adults are more likely than children to have underlying preexisting renal disease, whereas we speculate that children might have some degree of renal reserve.

In our exploratory analyses, no significant associations with remission were found with regard to sex, age, ANCA status, remission-induction treatment, and the PVAS at baseline. Previous studies in adults have suggested that female sex, older age, less aggressive treatment, and PR3-ANCA status are associated with treatment resistance, reduced chance of remission, or higher relapse rates (8,17,33,34). Higher disease activity, as measured by the BVAS, has been associated with a higher chance of remission (independent of treatment) but poorer survival in adults with AAV (34,41). We recognize that disease activity, as measured by the PVAS, and treatment are likely to be related; however, due to limited patient numbers, we did not have the power to assess the effect of treatment as a modifier, nor were we able to incorporate the effects of remission-maintenance treatments. The purpose of this analysis

was to test for simple associations of baseline factors previously reported to be associated with outcome in adults. It is possible that the factors associated with remission in adults are not the same as those in pediatric patients; however, it is also possible that the sample size limited our power to detect associations. The size of the sample in the current study limited our analysis to remission as the primary outcome measure; however, predictive factors for other outcomes, such as relapse, damage, and survival, are also of interest, especially over the longer term. Increased numbers of patients will enable analyses with multiple variables and outcomes that will likely be more informative.

Our study had the following limitations. Formal training in scoring the PVAS was not required of site investigators; however, a comprehensive manual and an instructional PVAS video were provided to each site. The database was designed specifically to collect the clinical data required to calculate the PVAS; however, it is possible that items were incorrectly entered or missing. Patient data were collected at prespecified time points (time of diagnosis, postinduction, and 12 months), which meant that we were unable to capture precisely what happened between visits. For example, if a patient achieved remission after the postinduction visit but had a minor relapse prior to the 12-month visit (resulting in a PVAS of >0), then we would not have captured the remission or the relapse in such a patient. However, these instances are likely to be few, because investigators were asked at each visit whether the patient had experienced a relapse since the last visit, and all such instances were reviewed. Nevertheless, subtle relapses, according to our definition, may not necessarily have been captured, especially if the investigator did not routinely calculate the PVAS between study visits.

We used a modified version of the VDI to assess damage in this cohort, because there is currently no validated pediatric-specific VDI. It is not known whether scoring damage in this way is meaningful in the pediatric population, and further studies, including validation studies, are needed to determine the extent to which this tool will effectively capture damage accrual in pediatric vasculitis patients.

Finally, for the 22 patients in the cohort who were diagnosed before March 2007, data were entered retrospectively and may have been subject to recall bias or missing data. The reliability and utility of retrospectively entered PVAS and PVDI scores have not been studied.

This is the largest study to date to report outcomes in pediatric AAV. Although we found that a significant proportion of patients did not achieve remission, the majority of patients responded to treatment. Unfortunately, more than one-half of the patient cohort experienced damage early in the disease course. Ongoing collection of clinical and biologic data through the PedVas initiative and other international collaborations will allow for further exploration and comparison of early, as well as longer-term, outcomes. A study of outcome predictors is currently underway.

AUTHOR CONTRIBUTIONS

All authors were involved in drafting the article or revising it critically for important intellectual content, and all authors approved the final version to be published. Dr. Morishita had full access to all of the data in the study and takes responsibility for the integrity of the data and the accuracy of the data analysis.

Study conception and design. Morishita, Moorthy, Twilt, Luqmani, Benseler, Cabral.

Acquisition of data. Morishita, Moorthy, Yeung, Toth, Shenoi, Ristic, Nielsen, Li, Lee, Lawson, Kostik, Klein-Gitelman, Huber, Hersh, Elder, Eberhard, Dancey, Charuvanij, Benseler, Cabral.

Analysis and interpretation of data. Morishita, Moorthy, Lubieniecka, Twilt, Luqmani, Foell, Benseler, Cabral.

REFERENCES

1. Moorthy AV, Chesney RW, Segar WE, Groshong T. Wegener granulomatosis in childhood: prolonged survival following cytotoxic therapy. J Pediatr 1977;91:616–8.
2. Li X, Liang S, Zheng C, Zeng C, Zhang H, Hu W, et al. Clinicopathological characteristics and outcomes of pediatric patients with systemic small blood vessel vasculitis. Pediatr Nephrol 2014; 29:2365–71.
3. Furuta S, Chaudhry AN, Hamano Y, Fujimoto S, Nagafuchi H, Makino H, et al. Comparison of phenotype and outcome in microscopic polyangiitis between Europe and Japan. J Rheumatol 2014;41:325–33.
4. Robson J, Doll H, Suppiah R, Flossmann O, Harper L, Hoglund P, et al. Damage in the ANCA-associated vasculitides: long-term data from the European Vasculitis Study Group (EUVAS) therapeutic trials. Ann Rheum Dis 2015;74:177–84.
5. Marco H, Mirapeix E, Arcos E, Comas J, Ara J, Gil-Vernet S, et al. Long-term outcome of antineutrophil cytoplasmic antibody-associated small vessel vasculitis after renal transplantation. Clin Transplant 2013;27:338–47.
6. Westman K, Flossmann O, Gregorini G. The long-term outcomes of systemic vasculitis. Nephrol Dial Transplant 2015;30 Suppl 1:i60–6.
7. Specks U, Merkel PA, Seo P, Spiera R, Langford CA, Hoffman GS, et al. Efficacy of remission-induction regimens for ANCA-associated vasculitis. N Engl J Med 2013;369:417–27.
8. Miloslavsky EM, Specks U, Merkel PA, Seo P, Spiera R, Langford CA, et al. Clinical outcomes of remission induction therapy for severe antineutrophil cytoplasmic antibody–associated vasculitis. Arthritis Rheum 2013;65:2441–9.
9. Cotch MF, Fauci AS, Hoffman GS. HLA typing in patients with Wegener granulomatosis. Ann Intern Med 1995;122:635.
10. Siomou E, Tramma D, Bowen C, Milford DV. ANCA-associated glomerulonephritis/systemic vasculitis in childhood: clinical features-outcome. Pediatr Nephrol 2012;27:1911–20.
11. Akikusa JD, Schneider R, Harvey EA, Hebert D, Thorner PS, Laxer RM, et al. Clinical features and outcome of pediatric Wegener's granulomatosis. Arthritis Rheum 2007;57:837–44.

12. Yu F, Huang JP, Zou WZ, Zhao MH. The clinical features of anti-neutrophil cytoplasmic antibody-associated systemic vasculitis in Chinese children. Pediatr Nephrol 2006;21:497–502.
13. Valentini RP, Smoyer WE, Sedman AB, Kershaw DB, Gregory MJ, Bunchman TE. Outcome of antineutrophil cytoplasmic autoantibodies-positive glomerulonephritis and vasculitis in children: a single-center experience. J Pediatr 1998;132:325–8.
14. Arulkumaran N, Jawad S, Smith SW, Harper L, Brogan P, Pusey CD, et al. Long-term outcome of paediatric patients with ANCA vasculitis. Pediatr Rheumatol Online J 2011;9:12.
15. Mukhtyar C, Flossmann O, Hellmich B, Bacon P, Cid M, Cohen-Tervaert JW, et al. Outcomes from studies of anti-neutrophil cytoplasm antibody associated vasculitis: a systematic review by the European League Against Rheumatism systemic vasculitis task force. Ann Rheum Dis 2008;67:1004–10.
16. Flossmann O, Berden A, de Groot K, Hagen C, Harper L, Heijl C, et al. Long-term patient survival in ANCA-associated vasculitis. Ann Rheum Dis 2011;70:488–94.
17. Pagnoux C, Hogan SL, Chin H, Jennette JC, Falk RJ, Guillevin L, et al. Predictors of treatment resistance and relapse in antineutrophil cytoplasmic antibody–associated small-vessel vasculitis: comparison of two independent cohorts. Arthritis Rheum 2008;58:2908–18.
18. Li ZY, Chang DY, Zhao MH, Chen M. Predictors of treatment resistance and relapse in antineutrophil cytoplasmic antibody–associated vasculitis: a study of 439 cases in a single Chinese center. Arthritis Rheumatol 2014;66:1920–6.
19. Walsh M, Flossmann O, Berden A, Westman K, Höglund P, Stegeman C, et al. Risk factors for relapse of antineutrophil cytoplasmic antibody–associated vasculitis. Arthritis Rheum 2012;64:542–8.
20. Sacri AS, Chambaraud T, Ranchin B, Florkin B, See H, Decramer S, et al. Clinical characteristics and outcomes of childhood-onset ANCA-associated vasculitis: a French nationwide study. Nephrol Dial Transplant 2015;30 Suppl 1:i104–12.
21. Ozen S, Pistorio A, Iusan SM, Bakkaloglu A, Herlin T, Brik R, et al. EULAR/PRINTO/PRES criteria for Henoch-Schonlein purpura, childhood polyarteritis nodosa, childhood Wegener granulomatosis and childhood Takayasu arteritis: Ankara 2008. Part II. Final classification criteria. Ann Rheum Dis 2010;69:798–806.
22. Dolezalova P, Price-Kuehne FE, Ozen S, Benseler SM, Cabral DA, Anton J, et al. Disease activity assessment in childhood vasculitis: development and preliminary validation of the Paediatric Vasculitis Activity Score (PVAS). Ann Rheum Dis 2013;72:1628–33.
23. Cabral DA, Uribe AG, Benseler S, O'Neil KM, Hashkes PJ, Higgins G, et al. Classification, presentation, and initial treatment of Wegener's granulomatosis in childhood. Arthritis Rheum 2009;60:3413–24.
24. Fries JF, Hunder GG, Bloch DA, Michel BA, Arend WP, Calabrese LH, et al. The American College of Rheumatology 1990 criteria for the classification of vasculitis: summary. Arthritis Rheum 1990;33:1135–6.
25. Lanham JG, Elkon KB, Pusey CD, Hughes GR. Systemic vasculitis with asthma and eosinophilia: a clinical approach to the Churg-Strauss syndrome. Medicine (Baltimore) 1984;63:65–81.
26. Watts R, Lane S, Hanslik T, Hauser T, Hellmich B, Koldingsnes W, et al. Development and validation of a consensus methodology for the classification of the ANCA-associated vasculitides and polyarteritis nodosa for epidemiological studies. Ann Rheum Dis 2007;66:222–7.
27. Harris PA, Taylor R, Thielke R, Payne J, Gonzalez N, Conde JG. Research electronic data capture (REDCap): a metadata-driven methodology and workflow process for providing translational research informatics support. J Biomed Inform 2009;42:377–81.
28. Exley AR, Bacon PA, Luqmani RA, Kitas GD, Gordon C, Savage CO, et al. Development and initial validation of the Vasculitis Damage Index for the standardized clinical assessment of damage in the systemic vasculitides. Arthritis Rheum 1997;40:371–80.
29. Hellmich B, Flossmann O, Gross WL, Bacon P, Cohen-Tervaert JW, Guillevin L, et al. EULAR recommendations for conducting clinical studies and/or clinical trials in systemic vasculitis: focus on anti-neutrophil cytoplasm antibody-associated vasculitis. Ann Rheum Dis 2007;66:605–17.
30. Luqmani RA, Bacon PA, Moots RJ, Janssen BA, Pall A, Emery P, et al. Birmingham Vasculitis Activity Score (BVAS) in systemic necrotizing vasculitis. QJM 1994;87:671–8.
31. Dolezalova P. SAT0286 Paediatric Vasculitis Damage Index: a new tool for standardised disease assessment. Ann Rheum Dis 2014;73 Suppl 2:696.4–697.
32. Lionaki S, Blyth ER, Hogan SL, Hu Y, Senior BA, Jennette CE, et al. Classification of antineutrophil cytoplasmic autoantibody vasculitides: the role of antineutrophil cytoplasmic autoantibody specificity for myeloperoxidase or proteinase 3 in disease recognition and prognosis. Arthritis Rheum 2012;64:3452–62.
33. Hogan SL, Falk RJ, Chin H, Cai J, Jennette CE, Jennette JC, et al. Predictors of relapse and treatment resistance in antineutrophil cytoplasmic antibody-associated small-vessel vasculitis. Ann Intern Med 2005;143:621–31.
34. Koldingsnes W, Nossent JC. Baseline features and initial treatment as predictors of remission and relapse in Wegener's granulomatosis. J Rheumatol 2003;30:80–8.
35. Iudici M, Puechal X, Pagnoux C, Quartier P, Agard C, Aouba A, et al. Childhood-onset systemic necrotizing vasculitides: long-term data from the French Vasculitis Study Group registry. Arthritis Rheumatol 2015;67:1959–65.
36. Bohm M, Gonzalez Fernandez MI, Ozen S, Pistorio A, Dolezalova P, Brogan P, et al. Clinical features of childhood granulomatosis with polyangiitis (Wegener's granulomatosis). Pediatr Rheumatol Online J 2014;12:18.
37. Stone JH, Merkel PA, Spiera R, Seo P, Langford CA, Hoffman GS, et al. Rituximab versus cyclophosphamide for ANCA-associated vasculitis. N Engl J Med 2010;363:221–32.
38. De Groot K, Rasmussen N, Bacon PA, Tervaert JW, Feighery C, Gregorini G, et al. Randomized trial of cyclophosphamide versus methotrexate for induction of remission in early systemic antineutrophil cytoplasmic antibody–associated vasculitis. Arthritis Rheum 2005;52:2461–9.
39. De Groot K, Harper L, Jayne DR, Flores Suarez LF, Gregorini G, Gross WL, et al. Pulse versus daily oral cyclophosphamide for induction of remission in antineutrophil cytoplasmic antibody-associated vasculitis: a randomized trial. Ann Intern Med 2009;150:670–80.
40. Rottem M, Fauci AS, Hallahan CW, Kerr GS, Lebovics R, Leavitt RY, et al. Wegener granulomatosis in children and adolescents: clinical presentation and outcome. J Pediatr 1993;122:26–31.
41. Gayraud M, Guillevin L, le Toumelin P, Cohen P, Lhote F, Casassus P, et al. Long-term followup of polyarteritis nodosa, microscopic polyangiitis, and Churg-Strauss syndrome: analysis of four prospective trials including 278 patients. Arthritis Rheum 2001;44:666–75.

ARTHRITIS & RHEUMATOLOGY
Vol. 69, No. 7, July 2017, pp 1480–1494
DOI 10.1002/art.40099

Proinflammatory Cytokine Environments Can Drive Interleukin-17 Overexpression by γ/δ T Cells in Systemic Juvenile Idiopathic Arthritis

Christoph Kessel,[1] Katrin Lippitz,[1] Toni Weinhage,[1] Claas Hinze,[1] Helmut Wittkowski,[1] Dirk Holzinger,[1] Ndate Fall,[2] Alexei A. Grom,[2] Niklas Gruen,[1] and Dirk Foell[1]

Objective. **Systemic-onset juvenile idiopathic arthritis (JIA) is speculated to follow a biphasic course, with an initial systemic disease phase driven by innate immune mechanisms and interleukin-1β (IL-1β) as a key cytokine and a second chronic arthritic phase that may be dominated by adaptive immunity and cytokines such as IL-17A. Although a recent mouse model points to a critical role of IL-17–expressing γ/δ T cells in disease pathology, in humans, both the prevalence of IL-17 and the role of IL-17–producing cells are still unclear.**

Methods. **Serum samples from systemic JIA patients and healthy pediatric controls were analyzed for the levels of IL-17A and related cytokines. Whole blood samples were studied for cellular expression of IL-17 and interferon-γ (IFNγ). CD4+ and γ/δ T cells isolated from the patients and controls were assayed for cytokine secretion in different culture systems.**

Results. **IL-17A was prevalent in sera from patients with active systemic JIA, while both ex vivo and in vitro experiments revealed that γ/δ T cells overexpressed this cytokine. This was not seen with CD4+ T cells, which expressed strikingly low levels of IFNγ. Therapeutic IL-1 blockade was associated with partial normalization of both cytokine expression phenotypes. Furthermore, culturing healthy donor γ/δ T cells in serum from systemic JIA patients or in medium spiked with IL-1β, IL-18, and S100A12 induced IL-17 overexpression at levels similar to those observed in the patients' cells.**

Conclusion. **A systemic JIA cytokine environment may prime γ/δ T cells in particular for IL-17A overexpression. Thus, our observations in systemic JIA patients strongly support a pathophysiologic role of these cells, as proposed by the recent murine model.**

Systemic juvenile idiopathic arthritis (JIA) is a unique form of childhood arthritis with features of an autoinflammatory disease. Due to complications, such as macrophage activation syndrome (MAS) and destructive arthritis, systemic JIA is associated with higher morbidity compared to other JIA subtypes (1).

At disease onset, systemic JIA is characterized by quotidian fever, polyserositis, evanescent rash, and substantial systemic inflammation (2,3). High levels of interleukin-6 (IL-6), IL-18, as well as S100A8/A9 and S100A12 are detectable in serum (4), while IL-1β in particular is critically involved in initially driving inflammation. This became evident from remarkably improved disease outcome seen upon therapeutic IL-1 blockade (5), which seems particularly effective when initiated as first-line therapy (6,7). In contrast, children with established polyarthritis have been reported to have a worse clinical response to recombinant IL-1 receptor antagonist (IL-1Ra; anakinra) treatment (8,9). Current clinical trial results suggest that

Supported by the Federal Ministry of Education and Research (BMBF project 01GM08100, AID-Net) and Cells-in-Motion Cluster of Excellence (DFG EXC-1003). Dr. Grom's work was supported by the NIH (grant R01-AR-059049).

[1]Christoph Kessel, PhD, Katrin Lippitz, MD, Toni Weinhage, PhD, Claas Hinze, MD, Helmut Wittkowski, MD, Dirk Holzinger, MD, Niklas Gruen, Dirk Foell, MD: University Children's Hospital, Münster, Germany; [2]Ndate Fall, MS, Alexei A. Grom, MD: Cincinnati Children's Hospital Medical Center, Cincinnati, Ohio.

Drs. Kessel and Lippitz contributed equally to this work.

Dr. Grom has received consulting fees from Novartis and NovImmune (less than $10,000 each). Dr. Foell has received consulting fees, speaking fees, and/or honoraria from Chugai-Roche, Sobi, Novartis, and Pfizer (less than $10,000 each) and research grants from Novartis and Pfizer. Drs. Kessel and Foell have submitted a patent application relating to the use of proinflammatory S100A12 homomultimers in the diagnosis and treatment of inflammatory disorders (WO 2016/178154 A1).

Address correspondence to Christoph Kessel, PhD, or Dirk Foell, MD, Department of Pediatric Rheumatology and Immunology, University Children's Hospital, Domagkstrasse 3, 48149 Munster, Germany. E-mail: christoph.kessel@uni-muenster.de or dfoell@uni-muenster.de.

Submitted for publication June 17, 2016; accepted in revised form March 9, 2017.

these patients benefit from therapeutic IL-6 receptor (IL-6R) blockade (tocilizumab) instead (10).

It is speculated that systemic JIA may follow a biphasic clinical course, with innate immune mechanisms primarily involved in the pathology of the systemic disease stage and adaptive immune mechanisms significantly contributing to the later, chronic arthritic phenotype (11). In fact, the HLA–DRB1*11 class II molecule has been found to be associated with susceptibility to systemic JIA, although the exact mechanistic implication in the disease pathology is still unclear (12).

To date, the only data supporting involvement of adaptive immunity in systemic JIA are related to T cells. These describe skewed patterns of Th1/Th2 cells as well as increased numbers of interleukin-17 (IL-17)–producing Th17 cells (13,14). IL-17 can drive chronic arthritis (15) and can be produced by either Th17 (16), γ/δ (γ/δ T17) (17), CD8+ (18), or natural killer (NK) (19) T cells. It has been proposed that in systemic JIA, high levels of IL-1β and IL-6 during the systemic phase may favor induction of such cells (11). Interestingly, γ/δ T cells in particular have been critically implicated in the disease pathology of a recently introduced systemic JIA mouse model in which a hyperinflammatory phenotype is induced upon administration of Freund's complete adjuvant (20). This model is reported to resemble systemic JIA in a number of clinical, biologic, and histopathologic features. Phenotype induction required an IFNγ^{low} or IFNγ$^{-/-}$ background. In these animals, γ/δ T cell numbers in draining lymph nodes as well as their IL-17 expression were strongly increased (20).

The role of IL-17 in systemic JIA patients is currently unclear. Data on IL-17 serum levels are inconsistent (8,21). It has been speculated that Th17 cells contribute to local IL-17 expression (11,13), while low frequencies of peripheral γ/δ T cells in particular have been reported, as these cells are thought to predominantly reside at sites of inflammation (22). In this study, we found markedly increased IL-17A serum levels in patients with active systemic JIA, whereas both ex vivo and particularly in vitro γ/δ T cells revealed significant IL-17A overexpression.

PATIENTS AND METHODS

Study subjects and samples. Serum samples from patients with active and inactive systemic JIA (n = 12) were collected (between December 2011 and June 2014) at Cincinnati Children's Hospital Medical Center for analysis of cytokines. Samples from healthy pediatric control subjects (n = 10) were collected at St. Franziskus Hospital in Munster, Germany. All samples were stored at −20°C until analyzed. For flow cytometry studies, fresh heparinized peripheral blood was obtained from 12 systemic JIA patients and 10 familial Mediterranean fever (FMF) patients (autoinflammatory disease controls) collected at the University Children's Hospital in Munster, Germany (between August 2014 and June 2015). Samples from 13 healthy pediatric donors were obtained from St. Franziskus Hospital (Table 1). For in vitro studies, peripheral blood mononuclear cells (PBMCs) from systemic JIA patients (n = 5) as well as healthy controls (n = 5) were prepared and stored at −150°C until analyzed.

Inactive disease was defined as the absence of fever (in systemic JIA and FMF patients), rash, and arthritis (in systemic JIA patients) and a C-reactive protein level and/or an erythrocyte sedimentation rate in the range of normal (in systemic JIA [23] and FMF [24] patients).

All study subjects or their parents provided written informed consent. The study was approved by the respective local ethics committees.

Bead array assays. Serum cytokines (see below) were measured using a multiplex immunoassay as previously described (25). Serum S100A12 was detected by a combination of in-house monoclonal anti-S100A12 antibodies translated to the MagPlex microsphere platform (Luminex). Data acquisition was performed on a MagPix instrument (Merck Millipore) using xPONENT v4.2 software (Luminex). Data were analyzed using ProcartaPlex Analyst software (v1.0; eBioscience). Cell culture supernatant cytokines were quantified using ProcartaPlex panels (eBioscience) according to the manufacturer's instructions.

Cell stimulation and flow cytometry stainings. Samples of whole heparinized peripheral blood (100 μl) were surface-stained for flow cytometric analysis of the expression of CD3 (clone OKT3), CD4 (RPA-T4), and γ/δ T cell receptor (TCR; B1) (all from BioLegend). Respective antibodies were used in excess. One triplicate set (100 μl each) was stimulated with phorbol 12-myristate 13-acetate (PMA) and ionomycin in the presence of brefeldin A and monensin (cell stimulation cocktail including protein transport inhibitor; eBioscience). A second triplicate set was left untreated. After stimulation (4 hours at 37°C in an atmosphere of 5% CO_2), erythrocytes were lysed, and the remaining cells were fixed (1-step fix/lyse solution; eBioscience). Cells were permeabilized (FoxP3/transcription factor staining buffer set; eBioscience) and stained for intracellular IL-17A (BL168; BioLegend) or interferon-γ (IFNγ) (4S.B3; eBioscience). All antibodies were added at 5 μl/sample. Cells were analyzed by flow cytometry (FACSCanto flow cytometer; BD Biosciences). Collected data were analyzed using FlowJo software (v10.0.8). To evaluate cytokine expression, median fluorescence intensities (MFIs) were calculated. The flow cytometer was calibrated daily using CS&T beads (BD Biosciences) and the preset photomultiplier values were not changed throughout the whole study.

In vitro T cell stimulation. CD3+γ/δTCR+ and CD4+ T cells were isolated from PBMCs obtained from patients with systemic JIA and healthy controls with the use of human γ/δ or CD4+ T cell isolation kits (StemCell Technologies). Monocytes were isolated from PBMCs prepared from a single healthy donor (human monocyte isolation kit; StemCell Technologies). T cells (2×10^4) were cocultured with monocytes (4×10^4) in RPMI 1640 medium (Merck Millipore) or in medium supplemented with 100 pg/ml of lipopolysaccharide (LPS; Sigma-Aldrich) or recombinant LPS–free S100A12 (produced in-house). Additionally, healthy donor γ/δ T cells were either cocultured with monocytes in fetal calf serum–free RPMI 1640 medium supplemented with the endogenous γ/δ TCR ligand isopentenyl pyrophosphate (IPP; 10 μg/ml) (Sigma-Aldrich), IL-2 (100 units/ml; PeproTech), and 20% (volume/volume) systemic JIA patient or healthy pediatric control sera, or cultured with

Table 1. Characteristics of the systemic JIA and FMF patients and the healthy control subjects*

Analysis, diagnosis, disease status	Demographic and clinical features								Laboratory parameters			Treatment (no. of patients)
					Disease status							
	No. of subjects	Disease duration, median (range) years	Sex, no. male/ female	Age, median (range) years	Duration, median (range) years	No. of patients	No. of joints with active disease, mean (range)	No. of patients with fever/rash	CRP, mean (range) mg/dl	ESR, mean (range) mm/hour	S100A12, mean (range) ng/ml	
Bead array												
Systemic JIA	12	6.3 (0.2–12.6)	2/10	13 (3–27)	–	–	–	–	–	–	–	–
Active	12†	–	–	–	5.9 (0.2–11.6)	12	4.4 (0–19)	2/7	6.4 (1.6–16.0)	33.6 (16–65)	300 (100–7,080)	Ana. + pred. (3); Can. (1); pred. + MTX (1); Toc. (7)
Inactive	12†	–	–	–	6.7 (0.2–12.7)	12	0	0/0	<0.5	6.7 3–13)	22 (6–68)	Toc. (3); Can. (2); Ana. + pred. (6); Ril. (1)
Healthy controls	10	NA	4/6	11 (6–18)	–	–	–	–	<0.5	NR	52 (33–120)	NA
Flow cytometry												
Systemic JIA	12	5.2 (1.6–20.8)	4/8	15 (4–23)	–	–	–	–	–	–	–	–
Active	5‡	–	–	–	3.8 (1.6–20.8)	5	2 (1–4)	1/1	3.8 (1.2–7.0)	16.8 (2–40)	1,103 (380–5,760)	MTX (1); pred. (1); Ana. + pred. (1); Can. + NSAID (1); Can. (1)
Inactive	10‡	–	–	–	5.9 (2.9–8.6)	10	0	0/0	<0.5	5.3 (1–14)	80 (15–410)	Toc. (1) Toc. + NSAID (1); Can. + MTX (2); Can. (4); Ana. + pred. (2)
FMF	10	–	6/4	13 (6–20)	–	–	–	–	–	–	–	–
Active	3	–	–	–	–	3	0	3/0	3.9 (2.3–4.2)	27 (25–30)	720 (390–10,450)	Col. (2)
Inactive	7	–	–	–	–	7	0	0/0	<0.5	8 (3–14)	44.5 (17–98)	Col. (6)
Healthy controls	13	NA	10/3	11 (6–26)	–	–	–	–	<0.5	NR	NR	NA
In vitro, isolated cells												
Systemic JIA	5	4.5 (1.6–20.8)	2/3	15 (5–24)	–	–	–	–	–	–	–	–
Inactive	5	–	–	–	–	5	0	0/0	<0.5	2 (1–10)	51 (29–150)	Can. (3); Ana. + pred. (1); Toc. (1)
Healthy controls	5	NA	1/4	20 (18–24)	–	–	–	–	<0.5	NR	NR	NA

Table 1. *(Cont'd)*

Analysis, diagnosis, disease status	Demographic and clinical features								Laboratory parameters			Treatment (no. of patients)
					Disease status							
	No. of subjects	Disease duration, median (range) years	Sex, no. male/ female	Age, median (range) years	Duration, median (range) years	No. of patients	No. of joints with active disease, mean (range)	No. of patients with fever/rash	CRP, mean (range) mg/dl	ESR, mean (range) mm/hour	S100A12, mean (range) ng/ml	
In vitro, serum cultures												
Systemic JIA	15	4.5 (0.4–6.8)	10/5	–	–	–	–	–	–	–	–	–
Active, systemic§	5	–	3/2	14 (11–15)	0.6 (0.4–0.66)	5	0	3/2	11 (4.7–19)	27 (14–45)	926 (357–1,928)	Treatment naive (2); Ana. (3)
Active, arthritic§	5	–	4/1	13 (12–15)	0.6 (0.5–0.9)	5	7 (1–16)	0/0	3.7 (<0.5–13)	36 (4–120)	200 (71–388)	Ana. (1); pred. (1); pred. + Toc. (1); pred. + MTX (1)
Inactive	5	–	3/2	11 (9–17)	2.6 (0.9–6.8)	5	0	0.0	<0.5	4 (1–6)	65 (30–97)	None (4); pred. (1)
Healthy controls	5	NA	2/3	12 (10–16)	–	–	–	–	<0.5	NR	NR	NA

* S100A12 levels were quantified by monoclonal assay (Kessel C, et al: unpublished techniques), allowing for exact molar quantification (cutoff for healthy versus systemic inflammation 75 ng/ml). FMF = familial Mediterranean fever; CRP = C-reactive protein; ESR = erythrocyte sedimentation rate; Ana. = anakinra; pred. = prednisolone; Can. = canakinumab; MTX = methotrexate; Toc. = tocilizumab; Ril. = rilonacept; NA = not applicable; NR = not recorded; NSAID = nonsteroidal antiinflammatory drug; Col = colchicine.
† These 12 patients with systemic juvenile idiopathic arthritis (JIA) provided samples during both active and inactive disease.
‡ Three of the 12 patients with systemic JIA provided samples during both active and inactive disease. Sampling time points were at least 10 weeks apart.
§ Patients who had no joints with active disease were categorized as active, systemic disease status. Patients who had joints with active disease but no fever/rash were categorized as active, arthritic disease status.

monocytes in S100A12 (20 μg/ml) and medium treated with recombinant cytokine (10 ng/ml of IL-18, 10 ng/ml of IL-1β, or IL-18 plus IL-1β). Where indicated, cultures were further treated with 1 μg/ml of anti–IL-6 receptor (anti–IL-6R; tocilizumab; Hoffmann-La Roche), 1 μg/ml of anti–IL-1β (canakinumab; Novartis), or 10 μg/ml of anti–Toll-like receptor 4 (anti–TLR-4; clone W7C11; InvivoGen) antibodies.

On day 0 and day 3, cultures were supplemented with 100 units/ml of recombinant IL-2. An additional set of stimulations was supplemented with 1 μg/ml of canakinumab on day 0. On day 6, γ/δ T cells were restimulated with 10 μg/ml of IPP (24 hours at 37°C in an atmosphere of 5% CO_2). CD4+ T cells were superstimulated with PMA/ionomycin (6 hours at 37°C in an atmosphere of 5% CO_2). Supernatants were harvested, cleared from remnant cells, and analyzed for cytokine expression using bead array assays as described above.

Statistical analysis. Data were analyzed with GraphPad Prism software (version 6.0 for Mac OS X). Depending on data distribution, multiple group comparisons were performed using one-way analysis of variance or the Kruskal-Wallis test followed by Bonferroni's or Dunn's post test, respectively. Where indicated, group-to-group comparisons were performed using Mann-Whitney U test or Wilcoxon's signed rank test. *P* values less than or equal to 0.05 were considered statistically significant.

RESULTS

Overexpression of serum IL-17A in patients with active systemic JIA. Serum samples were analyzed for levels of the inflammatory disease activity biomarker S100A12 as well as cytokine and chemokine expression associated with the generation and propagation of IL-17A–expressing T cells (IL-1β, IL-6, IL-17A, and IL-23) as well as IFNγ expression and signaling (IL-18, IFNγ, CXCL10, and CXCL9) (Figure 1).

Levels of IL-6 were significantly elevated in sera from systemic JIA patients ($P = 0.014$) and were further increased in samples from patients with active disease ($P = 0.0002$ versus healthy controls and $P < 0.0001$ versus patients with inactive disease). Levels of IL-17, IL-18, and S100A12 changed in parallel with systemic JIA disease activity as defined by clinical parameters (Table 1) and were significantly elevated in patients with especially active systemic JIA as compared to healthy children or patients with inactive systemic JIA. Serum levels of IL-1β, IFNγ, and CXCL10 tended to follow disease activity, albeit below the significance level, while serum concentrations of IL-23 and CXCL9 remained at or even below those in healthy controls.

Reduced expression of IFNγ in CD4+ T cells from patients with systemic JIA. CD4+ T cells in freshly drawn whole blood samples were analyzed for IFNγ and IL-17A expression following PMA/ionomycin stimulation (Figure 2A). In our mixed cohort of systemic JIA patients (Table 1), the proportions of CD4+ T cells among total lymphocytes were significantly increased compared to healthy controls, both in PMA/ionomycin-

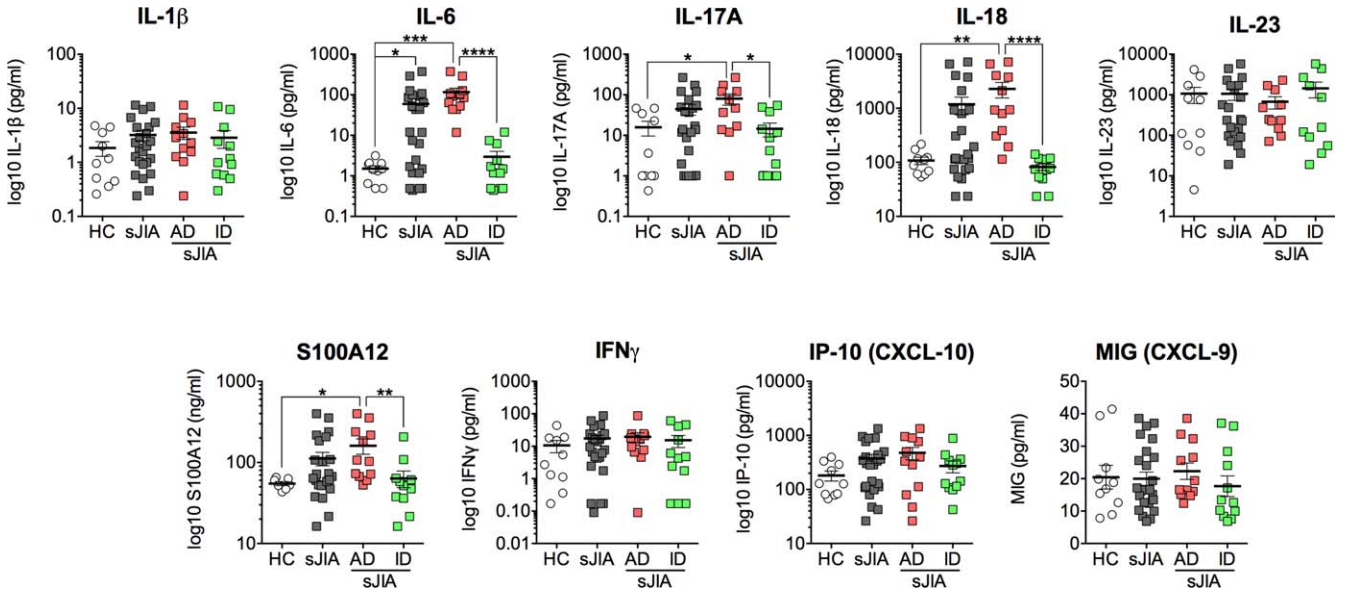

Figure 1. Serum cytokine and chemokine levels in systemic juvenile idiopathic arthritis (JIA). Interleukin-1β (IL-1β), IL-6, IL-17A, IL-18, IL-23, S100A12, interferon-γ–(IFNγ), CXCL10 (IFNγ-inducible 10-kd protein), and CXCL9 (monokine induced by IFNγ [MIG]) in the sera of systemic JIA (sJIA; n = 12) patients and healthy controls (HC; n = 10) was detected by bead array assay. Except for CXCL9, results are presented as raw data on a log-scale y-axis. Results are shown for the entire group of systemic JIA patients and for the subgroups with active disease (AD; n = 12) and inactive disease (ID; n = 12) (see Table 1 for details). Bars show the mean ± SEM. * = $P < 0.05$; ** = $P < 0.01$; *** = $P < 0.001$; **** = $P < 0.0001$, by Kruskal-Wallis test followed by Dunn's multiple comparison test.

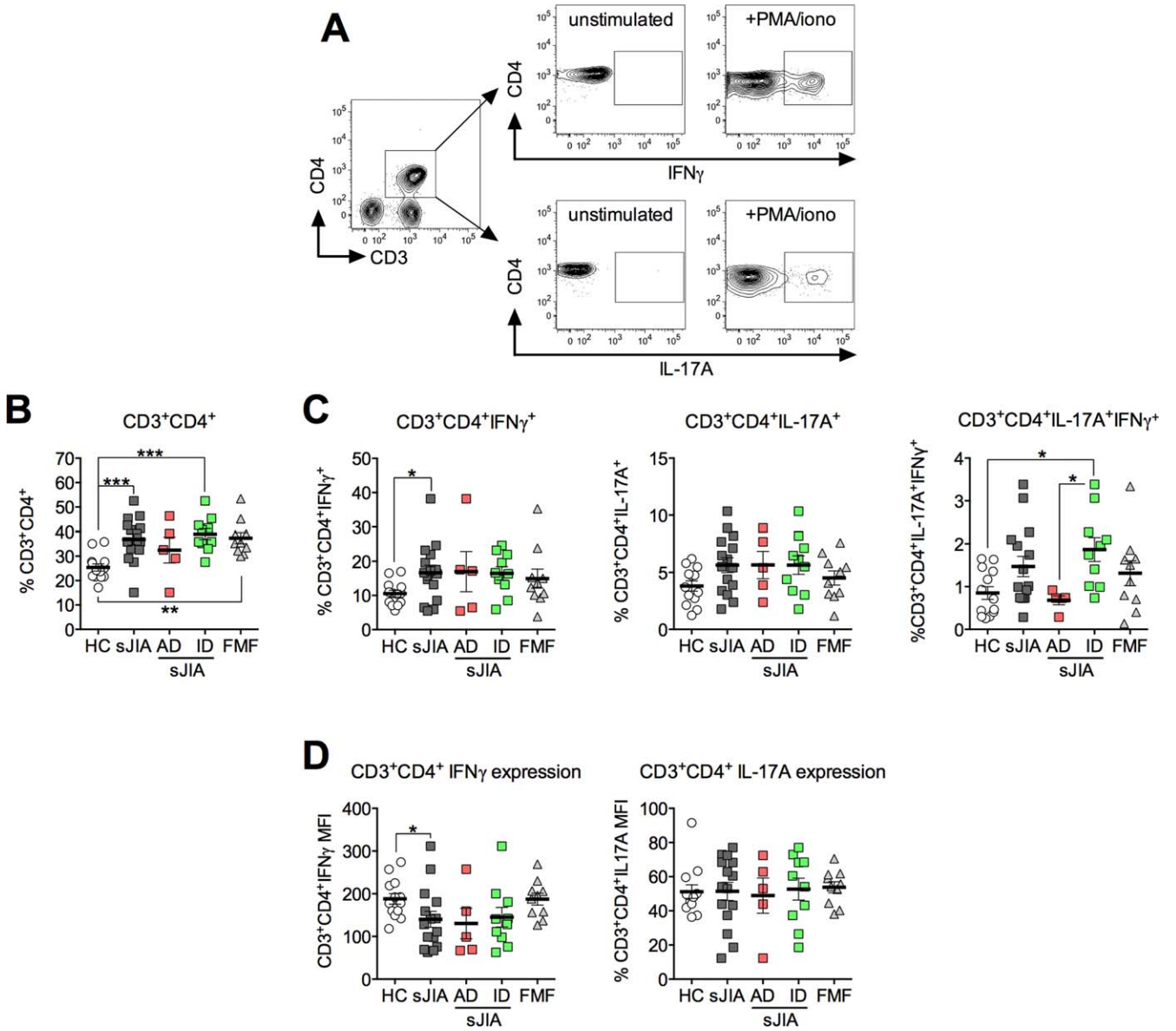

Figure 2. CD4+ T cells in whole blood from patients with systemic juvenile idiopathic arthritis (JIA). **A,** Representative flow cytometry plots identifying interferon-γ (IFNγ)– and interleukin-17A (IL-17A)–expressing cells in phorbol 12-myristate 13-acetate (PMA)/ionomycin (iono)–stimulated whole blood after 4 hours of stimulation. **B** and **C,** Frequencies of CD4+ (**B**), CD4+INFγ+ (**C**, left), CD4+IL-17A+ (**C**, middle), and CD4+IL-17A+INFγ+ (**C**, right) among total lymphocytes in PMA/ionomycin-stimulated whole blood samples from systemic JIA (sJIA; n = 12) and familial Mediterranean fever (FMF; n = 10) patients as well as healthy controls (HC; n = 13). Results are shown as scattered dot plots. FMF patients were included as an autoinflammatory disease control group. **D,** Expression of IFNγ (left) and IL-17A (right) by CD3+CD4+ cells following PMA/ionomycin stimulation of whole blood samples. Results are expressed as the median fluorescence intensity (MFI). Data are shown for the entire group of systemic JIA patients and for the subgroups with active disease (AD; n = 5) and inactive disease (ID; n = 10) (see Table 1 for details). Bars show the mean ± SEM. * = $P < 0.05$; *** = $P < 0.001$, by Kruskal-Wallis test followed by Dunn's multiple comparison test.

stimulated ($P = 0.0007$) (Figure 2B) and untreated (data not shown) samples. Circulating CD4+ T cell frequencies in FMF patients (both active and inactive disease) (Table 1), who were included as an autoinflammatory disease control group, were similarly increased ($P = 0.0014$) (Figure 2B). Although increased proportions of CD4+ T cells were observed in systemic JIA patients with both active and inactive disease, this was particularly evident in patients with inactive disease ($P = 0.0003$).

Following PMA/ionomycin stimulation, proportions of CD4+ T cells positive for IFNγ (CD3+CD4+IFNγ+) in whole blood from systemic JIA patients were significantly

increased compared to healthy controls ($P = 0.04$) (Figure 2C, left). A similar trend was observed with samples from systemic JIA patients stratified by disease activity as well as samples from FMF patients. However, when intracellular IFNγ expression levels among CD4+ T cells were assessed based on MFI values, IFNγ expression was significantly decreased in systemic JIA T cells ($P = 0.04$ versus healthy controls) (Figure 2D, left). This tendency was also seen in samples grouped according to systemic JIA disease activity, but not FMF patients' CD4+ T cells.

The proportions of IL-17+ T cells as well as IL-17/IFNγ double-expressing CD4+ T cells (IL-17A+IFNγ+) revealed a nonsignificant increase in systemic JIA patients compared to healthy controls ($P = 0.25$ for IL-17A+ and $P = 0.4$ for IL-17A+IFNγ+) (Figure 2C, middle and right). When systemic JIA samples were grouped by clinical disease activity, IL-17/IFNγ double-positive CD4+ T cell frequencies were significantly elevated during inactive disease versus active disease ($P = 0.04$) and versus healthy controls ($P = 0.02$). Both IL-17+ and IL-17/IFNγ double-expressing CD4+ T cells were also increased in samples from the FMF patients, although the difference remained below the level of statistical significance.

In contrast to IFNγ, we observed no apparent differences in intracellular IL-17A expression levels among CD4+ T cells based on the MFI values (Figure 2D, right).

Increased expression of IL-17A in γ/δ T cells from patients with systemic JIA. We also analyzed CD3+ γ/δTCR+ cells in whole blood for PMA/ionomycin-induced IFNγ and IL-17A expression (Figure 3A). In contrast to the elevated CD4+ T cell percentages observed in systemic JIA patients, the proportions of CD3+ T cells expressing γ/δ TCR (γ/δ T cells) were nonsignificantly reduced in systemic JIA patients compared to healthy controls ($P = 0.3$) (Figure 3B) as well as to FMF patients ($P = 0.7$) in both PMA/ionomycin-stimulated and untreated samples (data not shown). This reduction was not affected by the activity of the underlying systemic JIA. Similarly, frequencies of IFNγ+ γ/δ T cells were nonsignificantly reduced in whole blood from systemic JIA patients compared to healthy controls as well as to FMF patients (Figure 3C, left), while the intracellular IFNγ expression levels tended to be increased, except for those in samples obtained during active systemic JIA (Figure 3D, left).

Despite their apparent reduced frequency in the circulation, systemic JIA γ/δ T cells revealed significantly increased intracellular IL-17A expression compared to healthy control cells ($P = 0.023$) (Figure 3D, right). This seemed not to be due to an expansion of CD3+ γ/δTCR+IL-17A+ cells or IL-17/IFNγ double-expressing γ/δ T cells (Figure 3C, middle and right). Increased γ/δ T cell expression of IL-17A in systemic JIA patients was particularly evident in cells obtained during inactive disease ($P = 0.012$ versus healthy controls and $P = 0.06$ versus FMF patients), while cytokine expression levels in patients with active JIA were still elevated compared to both healthy controls and FMF patients, albeit this was below statistical significance level (Figure 3D, right).

Normalization of aberrant expression of IFNγ and IL-17A phenotypes during IL-1 blockade. IL-1β antagonists have been demonstrated to result in remarkably improved disease outcome in systemic JIA. The majority of patient samples analyzed in flow cytometry (n = 11) were obtained during anti–IL-1 therapy with either anakinra or canakinumab (Table 1). All patients had received corticosteroids prior to initiating IL-1 blockade. IL-1 blockade was introduced in the context of systemic JIA refractory to or dependent on corticosteroid therapy (26). During the time of sampling, some patients were treated with just IL-1 antagonists, while others received additional corticosteroid or conventional disease-modifying antirheumatic drug treatment (Table 1).

In this mixed systemic JIA cohort, we noted that γ/δ T cells in whole blood obtained during therapeutic IL-1 blockade revealed lower intracellular IL-17A expression compared to samples from patients receiving other treatments, including IL-6 blockade ($P = 0.011$ versus healthy controls) (Figure 3E). This seemed to be unaffected by the underlying disease activity as well as by the proportions of CD3+γ/δTCR+IL-17A+ or IL-17/IFNγ double-expressing γ/δ T cells (see Supplementary Figure 1E, available on the *Arthritis & Rheumatology* web site at http://onlinelibrary.wiley.com/doi/10.1002/art.40099/abstract).

Further, the frequencies of CD4+, CD3+γ/δTCR+, CD4+IL-17A+, IL-17/IFNγ double-expressing CD4+, and IFNγ+ γ/δ T cells as well as the respective intracellular cytokine expression (Figures 2B–D and 3B and C) were not affected by therapeutic IL-1 blockade (Supplementary Figures 1A and B and D–F). In contrast, higher frequencies of CD4+IFNγ+ cells in systemic JIA patients were observed predominantly in samples obtained from those receiving IL-1–inhibiting agents ($P = 0.012$) (Supplementary Figure 1B, middle). This was not observed in patients receiving other medication, including IL-6R blockade (Table 1). Moreover, we noted that the levels of intracellular IFNγ expression normalized over the course of therapeutic IL-1 blockade, while cytokine expression in cells from patients receiving other treatments remained significantly decreased compared to healthy controls ($P = 0.013$) (Supplementary Figure 1C, right).

Expression of IL-17A and IFNγ in culture supernatants of T cells from patients with systemic JIA. To verify the observed cytokine expression phenotypes based on MFI data, we examined IL-17A and IFNγ

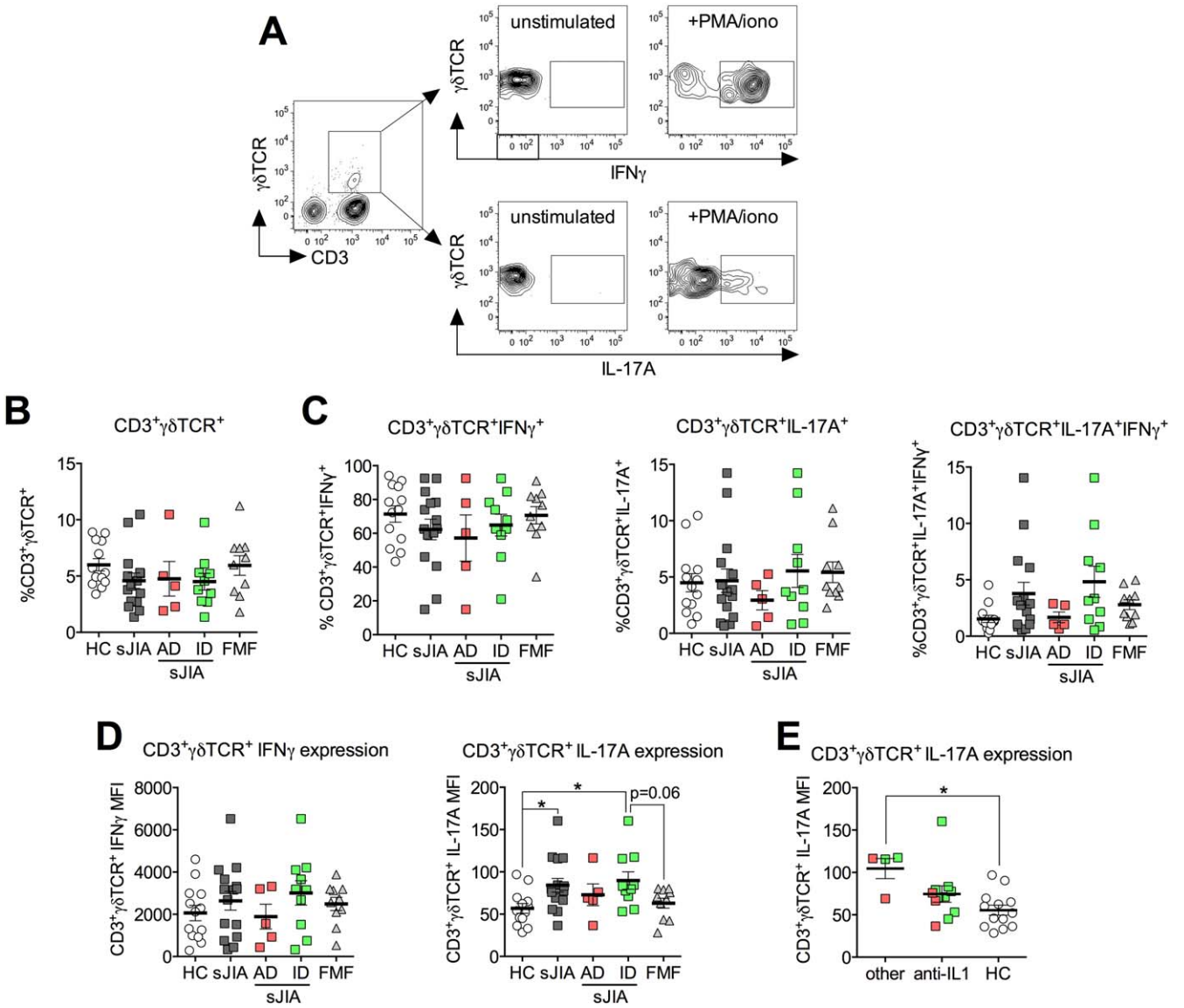

Figure 3. CD3+γ/δTCR+ T cells in whole blood from patients with systemic juvenile idiopathic arthritis (JIA). **A,** Representative flow cytometry plots identifying interferon-γ (IFNγ)– and interleukin-17A (IL-17A)–expressing cells in phorbol 12-myristate 13-acetate (PMA)/ionomycin (iono)–stimulated whole blood after 4 hours of stimulation. **B** and **C,** Frequencies of CD3+γ/δTCR+ (**B**), CD3+γ/δTCR+INFγ (**C**, left), CD3+γ/δTCR+IL-17A+ (**C**, middle), and CD3+γ/δTCR+IL-17A+INFγ+ (**C**, right) among total lymphocytes in PMA/ionomycin–stimulated whole blood from systemic JIA (sJIA; n = 12) and familial Mediterranean fever (FMF; n = 10) patients as well as healthy controls (HC; n = 13). Results are shown as scattered dot plots. **D** and **E,** Expression of IFNγ (**D**, left) and IL-17A (**D**, right and **E**) by CD3+γ/δTCR+ cells following PMA/ionomycin stimulation of whole blood samples. Results are expressed as the median fluorescence intensity (MFI). Data in **B–D** are shown for the entire group of systemic JIA patients and for the subgroups with active disease (AD; n = 5) and inactive disease (ID; n = 10) (see Table 1 for details). Data in **E** are shown for treatment at the time of blood sampling (n = 3 with active disease and n = 8 with inactive disease for other treatment; n = 2 each with active and inactive disease). Bars show the mean ± SEM. $* = P < 0.05$ by Kruskal-Wallis test followed by Dunn's multiple comparison test.

expression at the level of the secreted protein rather than analyzing transcription signatures in these partly very scarce cell populations. CD3+γ/δTCR+ cells were isolated from systemic JIA patients or healthy controls (n = 5 per group) and cultured at a 1:2 ratio with heterologous monocytes isolated from a single healthy donor, in medium supplemented with IPP and IL-2 as well as either LPS (100 pg/ml) or S100A12 (20 μg/ml), where indicated (Figures 4A and B). These experiments required coculture with viable monocytes since stimulations of γ/δ T cells alone or in coculture with fixed monocytes did not result in cytokine expression.

Upon stimulation with the common γ/δ TCR ligand IPP, only a minor increase in basal IL-17A expression by γ/δ T cells from systemic JIA patients as compared to controls was observed (Figure 4A). However, when the TLR-4 ligand LPS or S100A12 was added to the culture, IL-17A expression by γ/δ T cells from systemic JIA patients was significantly increased compared to controls ($P = 0.007$ for LPS and $P = 0.008$ for S100A12). This enhanced γ/δ T cell IL-17A secretion was strongly reduced following IL-1β neutralization ($P = 0.01$ for LPS and $P = 0.06$ for S100A12) (Figure 4A).

While we did not observe a pronounced IL-17A expression phenotype without additional TLR-4 stimulation, IFNγ secretion by systemic JIA γ/δ T cells was significantly reduced following IPP stimulation alone ($P = 0.008$ versus healthy controls) and was not affected by IL-1β neutralization ($P = 0.01$ versus healthy controls) (Figure 4B). We observed no significant changes in γ/δ T cell IFNγ expression between

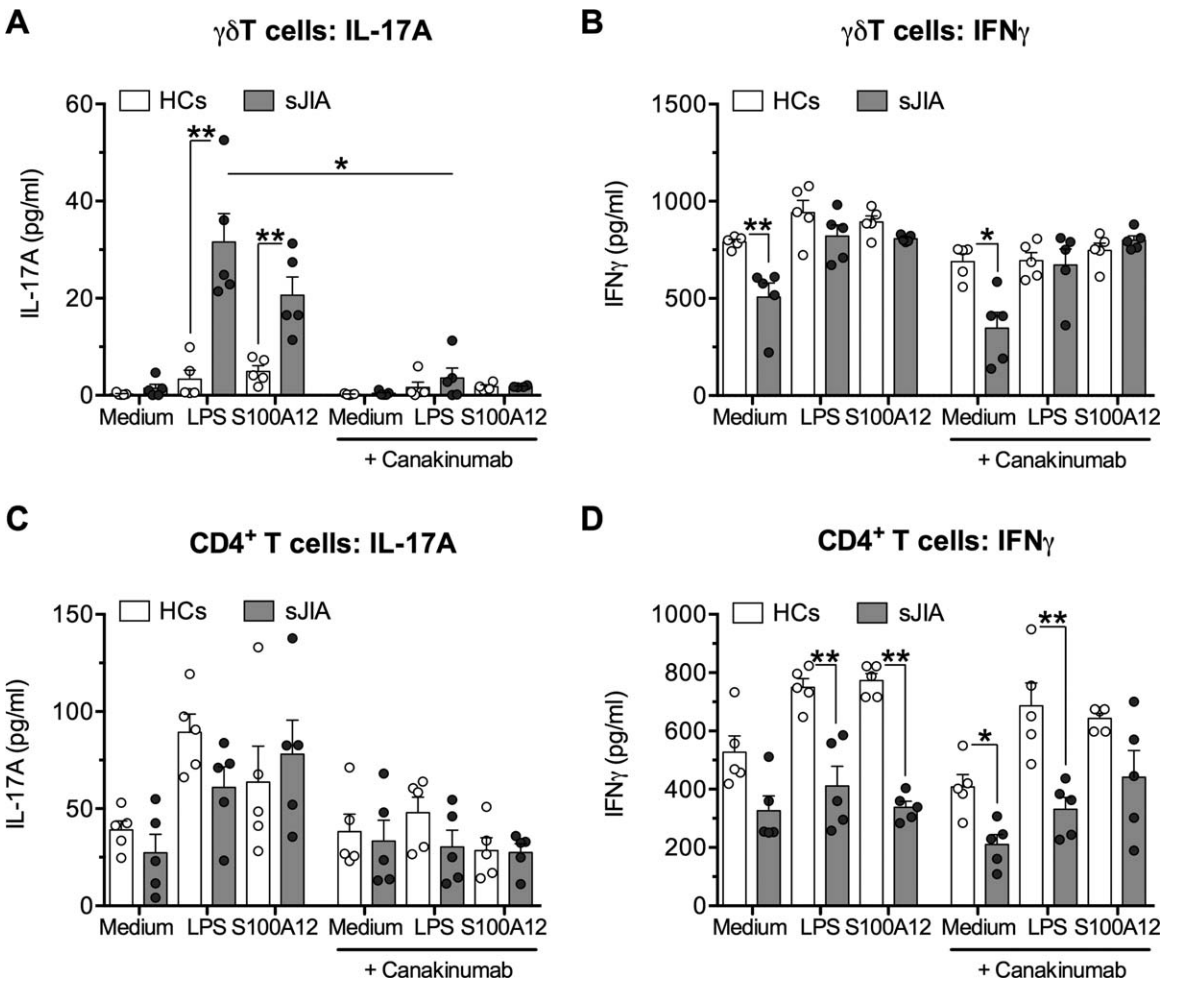

Figure 4. Cytokine expression by isolated T cells from patients with systemic juvenile idiopathic arthritis (JIA). CD3+γ/δTCR+ cells (**A** and **B**) and CD3+CD4+ cells (**C** and **D**) were isolated from peripheral blood mononuclear cells (PBMCs) from systemic JIA (sJIA) patients and healthy controls (HC; n = 5 per group) (see Table 1 for details) and cultured at a 1:2 ratio with heterologous monocytes from a single healthy donor. **A** and **B,** Cells were cultured for 6 days with 10 μg/ml of isopentenyl pyrophosphate (IPP) in medium alone or medium supplemented with 100 pg/ml of lipopolysaccharide (LPS) or 20 μg/ml of S100A12. Interleukin-2 (IL-2; 30 units/ml) was added on day 0 and day 3. In a parallel set of stimulations, cultures were supplemented with canakinumab (1 μg/ml) on day 0. On day 6, cells were restimulated with IPP, and the secretion of IL-17A (**A**) and interferon-γ (IFNγ) (**B**) into culture supernatants was quantified by bead array assay. **C** and **D,** CD4+ T cells from the same JIA patients and controls were cultured under similar conditions as above, except for the addition of IPP. On day 6, cells were superstimulated with phorbol 12-myristate 13-acetate/ionomycin for 6 hours, and the release of IL-17A (**C**) and IFNγ (**D**) into culture supernatants was quantified by bead array assay. Bars show the mean ± SEM. Values in individual subjects are shown as scattered dot blots. * = $P < 0.05$; ** = $P < 0.01$, by Mann-Whitney U test for patients versus controls and by Wilcoxon's signed rank test for the impact of anti–IL-1 blockade.

patients and controls following additional TLR-4 stimulation (Figure 4B).

In similar stimulation experiments using CD4+ T cells, we observed no differences in IL-17A expression between patients and controls (Figure 4C) following 6 days of coculture in the presence of IL-2, LPS (100 pg/ml), or S100A12 (20 μg/ml) and subsequent PMA/ionomycin superstimulation. Instead, when analyzing these cells for the release of IFNγ, this was significantly reduced in cells from the patients under all stimulation conditions tested (Figure 4D). This was not affected by IL-1β blockade except for stimulations with S100A12.

When analyzing cell culture supernatants for levels of IL-1β, IL-6, and IL-23, we observed no differences in their concentrations between cultures of γ/δ TCR+ cells (Supplementary Figures 2A–C, available at http://onlinelibrary.wiley.com/doi/10.1002/art.40099/abstract) or CD4+ T cells (Supplementary Figures 2D–F) from patients and healthy controls. No free IL-1β was detectable in supernatants of cultures treated with canakinumab (Supplementary Figures 2A and D).

Promotion of γ/δ T cell IL-17A expression by a systemic JIA serum environment. Systemic JIA serum contains elevated levels of IL-1 as well as high concentrations

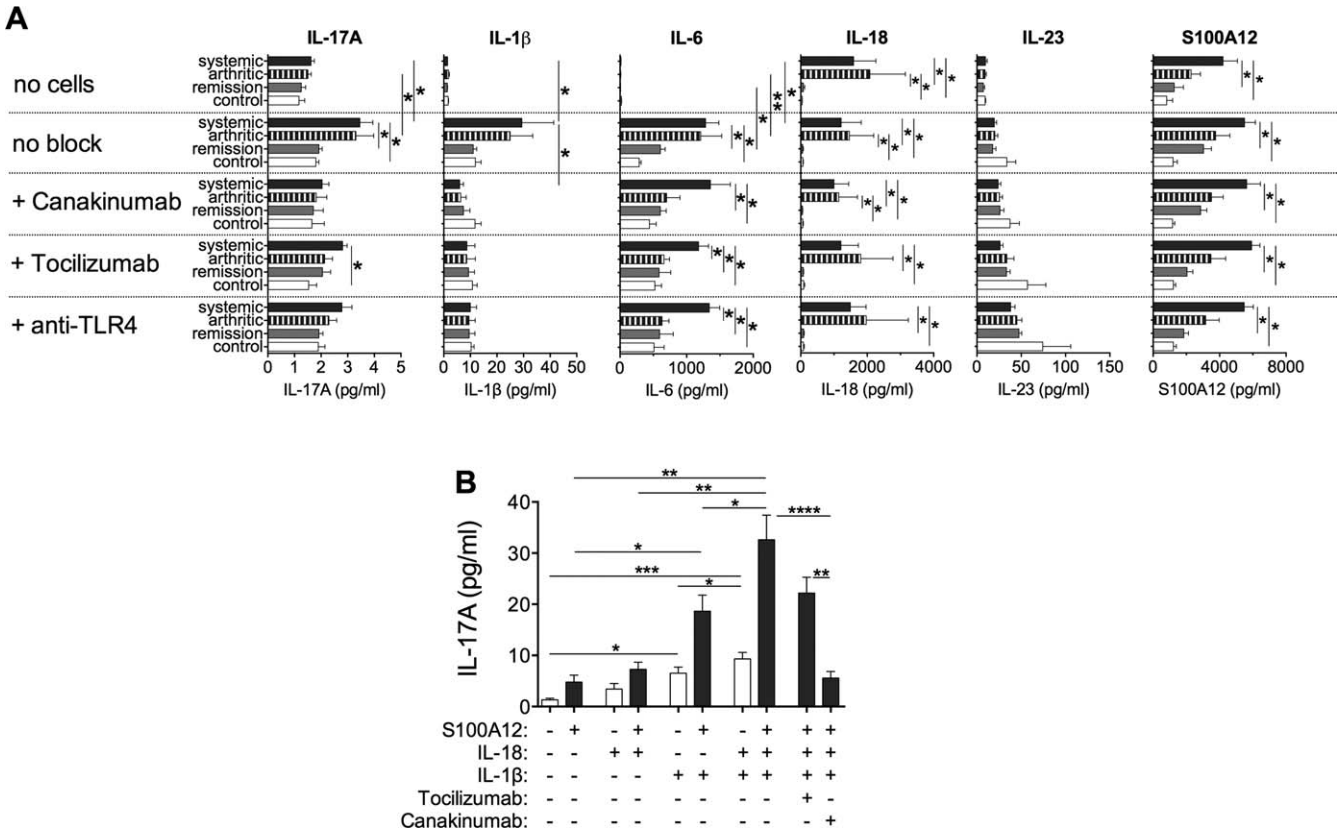

Figure 5. Promotion of γ/δ T cell interleukin-17A (IL-17A) expression by a systemic juvenile arthritis (JIA) serum factor environment. **A,** Healthy donor γ/δ T cells and monocytes together with isopentenyl pyrophosphate (IPP) and IL-2 were cultured in medium supplemented with 20% serum from systemic (fever/rash, but no active joints) or arthritis-prone systemic (no fever/rash but active joints) JIA patients as well as JIA patients in remission (no clinical symptoms) and pediatric healthy control donors (n = 5 per group) (see Table 1 for details). Where indicated, cultures were treated with anti–IL-1 (canakinumab 1 μg/ml), anti–IL-6 receptor (IL-6R; tocilizumab 1 μg/ml), or anti–Toll-like receptor 4 (anti–TLR-4; 10 μg/ml) antibody. Background cytokine levels were determined in medium supplemented with serum alone (no cells). Following IPP restimulation on day 6, levels of IL-17A, IL-1β, IL-6, IL-18, IL-23, and S100A12 in culture supernatants were quantified by bead array assay. **B,** Healthy donor γ/δ T cells (n = 6) together with monocytes, IPP, and IL-2 were left unstimulated or were stimulated with S100A12 (20 μg/ml), recombinant IL-18 (10 ng/ml), IL-1β (10 ng/ml), or IL-18 plus IL-1β where indicated. Cocultures stimulated with S100A12 plus IL-18 plus IL-1β were treated with either anti–IL-6R (tocilizumab 1 μg/ml) or IL-1β (canakinumab 1 μg/ml) blockade. Following IPP restimulation on day 6, levels of IL-17A in culture supernatants were quantified by bead array assay. (For levels of IL-1β, IL-6, and IL-23, see Supplementary Figure 4, available on the *Arthritis & Rheumatology* web site at http://onlinelibrary.wiley.com/doi/10.1002/art.40099/abstract.) Solid bars represent stimulations with S100A12; open bars indicate no S100A12 stimulation. Bars show the mean ± SEM. * = $P < 0.05$; ** = $P < 0.01$; *** = $P < 0.001$; **** = $P < 0.0001$, by Kruskal-Wallis test followed by Dunn's multiple comparison test.

of IL-6 and S100A12 (Figure 1) and may thus provide an environment in which γ/δ T cells are primed for elevated IL-17 expression. In our coculture experiments, medium supplemented with sera from patients with active systemic JIA (Table 1) induced elevated IL-17 expression by healthy donor γ/δ T cells (Figure 5A). Although the observed levels of IL-17 were generally low (Figure 5A), they revealed significant increases compared to 20% systemic JIA serum–supplemented medium without cultured cells. Blockade of IL-1β or TLR-4 reduced γ/δ T cell IL-17 expression induced by either systemic (fever/rash, but no active joints) or arthritis-prone systemic (no fever/rash but active joints) JIA patient serum–supplemented medium, while this appeared to be less pronounced following IL-6R blockade.

As observed with IL-17A, compared to serum in medium (no cells) as well as cultures additionally treated with blocking agents, we also detected increased levels of free IL-1β in cultures with systemic or arthritis-prone systemic JIA serum–supplemented medium. Similarly, IL-6, IL-18, and S100A12 were found to be strongly increased in systemic JIA sera–treated cultures, regardless of cytokine (IL-1β, IL-6) or TLR-4 blockade. High levels of both IL-18 and S100A12 were detectable even in 20% systemic JIA serum–supplemented medium without cells. No increase in IL-23 was measured in any systemic JIA serum culture.

As immunomodulatory medication in both patient serum and cells may eventually affect experimental outcome, we continued by testing IL-17A expression in healthy donor γ/δ T cells upon stimulation with recombinant IL-1β, IL-18, and S100A12 (Figure 5B). These experiments revealed that the addition of IL1β as well as a 1:1 combination of IL-18 plus IL-1β gradually increased the release of IL-17A from γ/δ T cells. This was strongly enhanced by further stimulation of cocultures with S100A12 in addition to the IL-1β or IL-1β plus IL-18. The latter combination of stimulants resulted in IL-17A expression levels comparable to those previously observed with cultured systemic JIA γ/δ T cells (Figure 4A). Similarly, IL-1 blockade reduced IL-17A secretion almost to levels as in cultures without cells, while IL-6R blockade had no such effect.

Although stimulation of cocultures with just IL-18 triggered only marginally increased IL-17A expression by γ/δ T cell, this still resulted in elevated IL-1β levels in culture supernatants as compared to cells stimulated with just IPP (Supplementary Figure 3A, available at http://onlinelibrary.wiley.com/doi/10.1002/art.40099/abstract). Compared to CD4+ cells, both healthy donor and systemic JIA γ/δ T cells revealed highly elevated IL-18 receptor expression (Supplementary Figures 4A and B, available at http://onlinelibrary.wiley.com/doi/10.1002/art.40099/abstract) and both proliferated in response to IL-18 stimulation (Supplementary Figures 4C and D).

The addition of IL-1β as well as IL-1β plus IL-18 gradually increased IL-6 expression in cocultures (Supplementary Figure 3B). Yet, this was most pronounced by stimulation with S100A12, either alone or combined with recombinant cytokines. In contrast to IL-1β and IL-6, IL-23 expression was low and appeared to be unaffected (*P* not significant) by the various stimulations (Supplementary Figure 3C).

DISCUSSION

In this study, we report ex vivo and in vitro data demonstrating a pronounced overexpression of IL-17A by γ/δ T cells from patients with systemic JIA, which seemed to occur in an environment of decreased T cell IFNγ expression. This cytokine expression pattern appeared to be partly sensitive to anti–IL-1 treatment. Thus, our patient data are strikingly similar to key pathomechanistic findings reported in a recent systemic JIA mouse model, which revealed the most pronounced clinical phenotype on an IFNγ$^{-/-}$ background and appeared to be critically dependent on IL-17 overexpression by γ/δ T cells (20).

Increased IL-17A levels in systemic JIA were already apparent at the serum level. While current published data on this feature are inconsistent (8,21), we observed IL-17A serum concentrations in systemic JIA to be significantly increased over those in healthy controls when stratifying patients for underlying disease activity (Figure 1). This observation, together with the reported findings in the systemic JIA mouse model, provided the rationale for our studies on systemic JIA patients' T cells. Although the relatively small patient cohort studied may pose a limitation, for the ex vivo T cell phenotyping as well as in vitro, we focused on well-characterized patients with both systemic and arthritis-prone disease (Table 1) available in our center.

Ex vivo T cell phenotyping indicated that systemic JIA γ/δ T cells, but not CD4+ T cells, overexpress IL-17A. Although we observed partly elevated Th17 cell (CD3+ CD4+IL-17A+) frequencies in whole blood from systemic JIA patients (Figure 2D), which is consistent with previously published data (13), these cells did not express IL-17A at higher intracellular levels than did Th17 cells from healthy controls or FMF autoinflammatory disease control patients. Similarly, IL-17 expression from isolated systemic JIA CD4+ T cells was not elevated compared to controls (Figure 4B).

In contrast to elevated Th17 cell frequencies, γ/δ T cell overexpression of IL-17A in whole blood from patients

with systemic JIA did not seem to be due to an expansion of CD3+γ/δTCR+IL-17A+ (γ/δ T17) cells (Figure 3D). Importantly, γ/δ T cell overexpression of IL-17 in systemic JIA was reproduced at the level of isolated cells. Yet, this did not readily occur upon stimulation with IPP alone, although together with IL-2, this was shown to expand γ/δ T cells in systemic JIA synovial fluid (27), but required costimulation with TLR-4 ligands such as LPS or S100A12, providing the cytokine environment (IL-1β, IL-6, IL-23) (Supplementary Figure 2, available at http://onlinelibrary.wiley.com/doi/10.1002/art.40099/abstract) for γ/δ T cells to produce IL-17. In these experiments, stimulation with S100A12 potentially generated a systemic JIA–like environment (Figure 1). The possibility that endogenous TLR-4 ligands such as S100A12 or S100A8/A9 could promote the observed elevated IL-17 expression also under sterile inflammatory conditions is intriguing (28–30).

In this context, it is striking that both in the systemic JIA mouse and in systemic JIA patients, IL-17 overexpression appears to be restricted to γ/δ T cells. In systemic JIA patients, this seemed to occur independently of clinical disease activity, although we cannot rule out an effect of disease duration on our observations (Figure 3D and Table 1). Of note, γ/δ T cell overexpression of IL-17 was not as pronounced during active systemic JIA, although serum levels of IL-1β, IL-6, and S100A12 were highest during this disease phase (Figure 3D). Consistent with this, serum from systemic JIA patients with active clinical disease was able to promote IL-17 expression in healthy donor γ/δ T cells, as compared to sera from patients in remission or healthy controls (Figure 5A).

As we did not further phenotype the γ/δ T cells for chemokine receptor expression or analyze cell distribution in inflamed tissue, we are left to hypothesize that peripheral γ/δ T cells found in active systemic JIA may reflect the recirculation of cells from sites of inflammation (Supplementary Figure 5, available at http://onlinelibrary.wiley.com/doi/10.1002/art.40099/abstract). Reduced γ/δ T17 cell frequencies in active systemic JIA, as observed by us (Figure 3C) and others (22,31,32), might in fact support the idea of the migration of human γ/δ T cells into inflamed tissues such as the synovium, where they drive local inflammation during active disease (22,31,32). Recirculation of γ/δ T17 cells via peripheral blood and lymph is thought to spread and aggravate inflammation in multiple tissues (33,34). Similar to chronic stimulation with bisphosphonate resulting in the accumulation of IPP (35,36), decreased IFNγ expression as induced by these peripheral cells during active systemic JIA (Figure 3C) may indicate exhaustion following their participation in tissue-borne inflammatory processes. Alternatively, as suggested by a study on psoriasis patients (37), a low frequency of, and reduced cytokine expression by, peripheral γ/δ T cells, particularly during active disease, reflects recruitment of a specific proinflammatory γ/δ T cell subset to drive the local inflammation. Upon disease inactivity, this again increases in the periphery due to recirculation or less migration into tissue (37).

Apart from γ/δ T cells, it remains to be discussed why, under the test conditions aimed at activation rather than de novo differentiation of Th cell subsets (38), the patients' Th17 cells did not reveal comparably increased IL-17 expression. Our data may point to a role of IL-23 in accounting for this divergence. IL-23 is strictly required for human Th17 cell differentiation and maintenance (39,40). However, in contrast to IL-1β and IL-6, serum levels of IL-23 were not elevated in systemic JIA, while the lowest concentrations were detected during active disease (Figure 1). Furthermore, in vitro experiments indicated no changes in IL-23 levels, particularly following S100A12 or cytokine stimulations (Supplementary Figures 2C and F and 3C, available at http://onlinelibrary.wiley.com/doi/10.1002/art.40099/abstract).

In contrast to IL-23 levels, systemic JIA patients had highly elevated levels of IL-18 (Figure 1) (21,41), while γ/δ TCR+, but not CD4+, T cells from both healthy donors and systemic JIA patients expressed high levels of IL-18 receptor (Supplementary Figure 4A). In our γ/δ T cell stimulation experiments, supplementing cocultures with both IL-1β and IL-18 further increased IL-17 expression by γ/δ T cells, which was most pronounced when combined with S100A12 (Figure 5B).

These data support the findings on murine cells reported earlier, which suggested that IL-18–induced γ/δ T cell IL-17 expression was mediated in part through IL-1 (42). In fact, in our cocultures, the addition of IL-18 resulted in elevated IL-1β expression (Supplementary Figure 3A) and significantly enhanced IPP-induced proliferation of γ/δ T cells from patients as well as healthy donors (Supplementary Figures 4B and C). The latter may not necessarily happen at the systemic level, as we did observe γ/δ T cell expansion in whole blood, but may be restricted to tissue, as particularly macrophages (43) and keratinocytes (44) have been suggested to be major producers of IL-18.

Further indicating the IL-1 dependence of γ/δ T cell IL-17 expression, we observed this to be reduced in whole blood from patients treated with canakinumab (Figure 3E). This seemed to occur irrespective of the patients' underlying disease activity. However, it has to be noted that these observations are based on rather small patient numbers and the groups were not normalized for median disease duration (4.5 years for anti–IL-1; 8 years for other

treatments). More importantly, IL-17A released from isolated γ/δ T cells was significantly reduced in the presence of canakinumab, efficiently neutralizing free IL-1β (Supplementary Figure 2A, available at http://onlinelibrary.wiley.com/doi/10.1002/art.40099/abstract).

A critical role of IL-1β in γ/δ T cell IL-17 expression has also been demonstrated in mice developing IL-17–dependent spontaneous arthritis due to the lack of endogenous IL-1Ra (IL-1rn$^{-/-}$ mice) expression (45,46). Recently, arthritis development in IL-1rn$^{-/-}$ mice was found to depend on both γ/δ T cells and CD4+ T cells. IL-1rn$^{-/-}$ γ/δ T cells demonstrated increased IL-1 receptor expression and thus enhanced sensitivity for IL-1. They served as the main source of IL-17 in inflamed joints but required CD4+ T cells for tissue homing (47).

In systemic JIA, the simultaneous decrease in peripheral IL-17/IFNγ–expressing CD4+ and γ/δ T cells, particularly during active disease (Figures 1C and 2C), may indicate a similar concerted action of these cells. Yet, further studies analyzing chemotaxis, phenotype, and function of T cells, especially in systemic JIA tissue, are required to prove this.

Apart from IL-1β, IL-6 serum levels were strongly elevated in systemic JIA (Figure 1), and therapeutic IL-6R blockade is a highly effective treatment option (10). IL-6 is another cytokine that is critically involved in the differentiation of IL-17–expressing T cells (48). Yet, although IL-6 concentrations were strongly increased in cultures stimulated with either LPS or S100A12 (Supplementary Figures 2B and E and 3B, available at http://onlinelibrary.wiley.com/doi/10.1002/art.40099/abstract), IL-6 is thought to be dispensable for γ/δ T cell IL-17 expression (49,50). In fact, the results of our ex vivo and in vitro experiments do not support the idea that either therapeutic or experimental IL-6R blockade might affect IL-17 expression by γ/δ T cells.

In summary, it is conceivable that a "systemic JIA serum factor environment" characterized by high levels of IL-1β and IL-18, likely induced by overexpressed endogenous TLR-4 ligands such as S100 proteins, specifically primes γ/δ T cells for IL-17 overexpression (Supplementary Figure 5). This may be further promoted by low levels of T cell IFNγ production, as IFNγ-induced STAT-1 signaling has been shown to impair human IL-17 immunity (51). While significantly increased CD4+IFNγ+ cell frequencies have been observed in whole blood (Figure 2C) and PBMCs (13) from systemic JIA patients, we now report that these cells reveal decreased IFNγ expression (Figures 2C and 4C). Although this is not readily apparent at the serum level (Figure 1) (8,21), we observed decreased CXCL9 expression, indicating weak IFNγ-signaling. CXCL10 serum levels were nonsignificantly elevated during active systemic JIA (Figure 1), although CXCL10 expression has been demonstrated to result from either IFNγ or TLR-4 signaling (52), as for example, that triggered by S100A12. Along similar lines, gene expression profiles in monocytes from active systemic JIA patients (53) failed to demonstrate strong IFNγ-induced transcriptional signatures, which can be suggestive of a limited in vivo exposure of cells to IFNγ.

IL-1 blockade efficiently abrogated IL-17 overexpression by γ/δ T cells and contributed to the normalization of T cell IFNγ expression. IFNγ has been described as a potential master switch in systemic JIA. Aberrantly low levels can contribute to the progression of autoimmune arthritis, but IFNγ overexpression may drive MAS as one of the most severe systemic JIA complications (54). As decreased IFNγ release has so far been attributed to defective NK cells in systemic JIA (55,56), investigating the mechanisms that contribute to low levels of IFNγ expression on CD4+ T cells may allow a deeper understanding of the complex pathophysiology of systemic JIA in the future.

ACKNOWLEDGMENTS

The authors thank Susanne Schleifenbaum, Melanie Saers, and Sabrina Fuehner for outstanding technical assistance. We are grateful to the patients and their families for their support of the study, and we further thank Drs. Jean Tsokas and Arnd Heiligenhaus (both of St. Franziskus Hospital, Munster, Germany) for providing samples from healthy pediatric control subjects. Bead array cytokine analysis of sera from systemic JIA patients and healthy controls was performed by Dr. Wilco de Jager (University Medical Center Utrecht, Utrecht, The Netherlands).

AUTHOR CONTRIBUTIONS

All authors were involved in drafting the article or revising it critically for important intellectual content, and all authors approved the final version to be published. Drs. Kessel and Foell had full access to all of the data in the study and take responsibility for the integrity of the data and the accuracy of the data analysis.

Study conception and design. Kessel, Foell.

Acquisition of data. Kessel, Lippitz, Weinhage, Hinze, Wittkowski, Holzinger, Fall, Grom, Gruen.

Analysis and interpretation of data. Kessel, Lippitz, Weinhage, Hinze, Wittkowski.

REFERENCES

1. Prakken B, Albani S, Martini A. Juvenile idiopathic arthritis. Lancet 2011;377:2138–49.
2. Bruck N, Schnabel A, Hedrich CM. Current understanding of the pathophysiology of systemic juvenile idiopathic arthritis (sJIA) and target-directed therapeutic approaches. Clin Immunol 2015;159:72–83.
3. Calabro JJ, Marchesano JM. Fever associated with juvenile rheumatoid arthritis. N Engl J Med 1967;276:11–8.

4. Kessel C, Holzinger D, Foell D. Phagocyte-derived S100 proteins in autoinflammation: putative role in pathogenesis and usefulness as biomarkers. Clin Immunol 2013;147:229–41.
5. Pascual V, Allantaz F, Arce E, Punaro M, Banchereau J. Role of interleukin-1 (IL-1) in the pathogenesis of systemic onset juvenile idiopathic arthritis and clinical response to IL-1 blockade. J Exp Med 2005;201:1479–86.
6. Nigrovic PA, Mannion M, Prince FH, Zeft A, Rabinovich CE, van Rossum MA, et al. Anakinra as first-line disease-modifying therapy in systemic juvenile idiopathic arthritis: report of forty-six patients from an international multicenter series. Arthritis Rheum 2011;63:545–55.
7. Vastert SJ, de Jager W, Noordman BJ, Holzinger D, Kuis W, Prakken BJ, et al. Effectiveness of first-line treatment with recombinant interleukin-1 receptor antagonist in steroid-naive patients with new-onset systemic juvenile idiopathic arthritis: results of a prospective cohort study. Arthritis Rheumatol 2014; 66:1034–43.
8. Gattorno M, Piccini A, Lasiglie D, Tassi S, Brisca G, Carta S, et al. The pattern of response to anti–interleukin-1 treatment distinguishes two subsets of patients with systemic-onset juvenile idiopathic arthritis. Arthritis Rheum 2008;58:1505–15.
9. Quartier P, Allantaz F, Cimaz R, Pillet P, Messiaen C, Bardin C, et al. A multicentre, randomised, double-blind, placebo-controlled trial with the interleukin-1 receptor antagonist anakinra in patients with systemic-onset juvenile idiopathic arthritis (ANAJIS trial). Ann Rheum Dis 2011;70:747–54.
10. De Benedetti F, Brunner HI, Ruperto N, Kenwright A, Wright S, Calvo I, et al. Randomized trial of tocilizumab in systemic juvenile idiopathic arthritis. N Engl J Med 2012;367:2385–95.
11. Nigrovic PA. Is there a window of opportunity for treatment of systemic juvenile idiopathic arthritis? [review]. Arthritis Rheumatol 2014;66:1405–13.
12. Ombrello MJ, Remmers EF, Tachmazidou I, Grom A, Foell D, Haas JP, et al. HLA-DRB1*11 and variants of the MHC class II locus are strong risk factors for systemic juvenile idiopathic arthritis. Proc Natl Acad Sci U S A 2015;112:15970–5.
13. Omoyinmi E, Hamaoui R, Pesenacker A, Nistala K, Moncrieffe H, Ursu S, et al. Th1 and Th17 cell subpopulations are enriched in the peripheral blood of patients with systemic juvenile idiopathic arthritis. Rheumatology (Oxford) 2012;51:1881–6.
14. Raziuddin S, Bahabri S, Al-Dalaan A, Siraj AK, Al-Sedairy S. A mixed Th1/Th2 cell cytokine response predominates in systemic onset juvenile rheumatoid arthritis: immunoregulatory IL-10 function. Clin Immunol Immunopathol 1998;86:192–8.
15. Hirota K, Hashimoto M, Yoshitomi H, Tanaka S, Nomura T, Yamaguchi T, et al. T cell self-reactivity forms a cytokine milieu for spontaneous development of IL-17+ Th cells that cause autoimmune arthritis. J Exp Med 2007;204:41–7.
16. Yao Z, Painter SL, Fanslow WC, Ulrich D, Macduff BM, Spriggs MK, et al. Human IL-17: a novel cytokine derived from T cells. J Immunol 1995;155:5483–6.
17. Lockhart E, Green AM, Flynn JL. IL-17 production is dominated by γδ T cells rather than CD4 T cells during Mycobacterium tuberculosis infection. J Immunol 2006;177:4662–9.
18. Shin HC, Benbernou N, Esnault S, Guenounou M. Expression of IL-17 in human memory CD45RO+ T lymphocytes and its regulation by protein kinase A pathway. Cytokine 1999;11: 257–66.
19. Michel ML, Keller AC, Paget C, Fujio M, Trottein F, Savage PB, et al. Identification of an IL-17-producing NK1.1(neg) iNKT cell population involved in airway neutrophilia. J Exp Med 2007; 204:995–1001.
20. Avau A, Mitera T, Put S, Put K, Brisse E, Filtjens J, et al. Systemic juvenile idiopathic arthritis–like syndrome in mice following stimulation of the immune system with Freund's complete adjuvant: regulation by interferon-γ. Arthritis Rheumatol 2014; 66:1340–51.
21. De Jager W, Hoppenreijs EP, Wulffraat NM, Wedderburn LR, Kuis W, Prakken BJ. Blood and synovial fluid cytokine signatures in patients with juvenile idiopathic arthritis: a cross-sectional study. Ann Rheum Dis 2007;66:589–98.
22. Macaubas C, Nguyen K, Deshpande C, Phillips C, Peck A, Lee T, et al. Distribution of circulating cells in systemic juvenile idiopathic arthritis across disease activity states. Clin Immunol 2010; 134:206–16.
23. Wallace CA, Giannini EH, Huang B, Itert L, Ruperto N, for the Childhood Arthritis and Rheumatology Research Alliance (CARRA), the Pediatric Rheumatology Collaborative Study Group (PRCSG), and the Paediatric Rheumatology International Trials Organisation (PRINTO). American College of Rheumatology provisional criteria for defining clinical inactive disease in select categories of juvenile idiopathic arthritis. Arthritis Care Res (Hoboken) 2011;63:929–36.
24. Gohar F, Orak B, Kallinich T, Jeske M, Lieber M, von Bernuth H, et al. Correlation of secretory activity of neutrophils with genotype in patients with familial Mediterranean fever. Arthritis Rheumatol 2016;68:3010–22.
25. De Jager W, Prakken BJ, Bijlsma JW, Kuis W, Rijkers GT. Improved multiplex immunoassay performance in human plasma and synovial fluid following removal of interfering heterophilic antibodies. J Immunol Methods 2005;300:124–35.
26. Ringold S, Weiss PF, Beukelman T, DeWitt EM, Ilowite NT, Kimura Y, et al. 2013 update of the 2011 American College of Rheumatology recommendations for the treatment of juvenile idiopathic arthritis: recommendations for the medical therapy of children with systemic juvenile idiopathic arthritis and tuberculosis screening among children receiving biologic medications. Arthritis Rheum 2013;65:2499–512.
27. Berkun Y, Bendersky A, Gerstein M, Goldstein I, Padeh S, Bank I. γδ T cells in juvenile idiopathic arthritis: higher percentages of synovial Vδ1+ and Vγ9+ T cell subsets are associated with milder disease. J Rheumatol 2011;38:1123–9.
28. Foell D, Wittkowski H, Kessel C, Luken A, Weinhage T, Varga G, et al. Proinflammatory S100A12 can activate human monocytes via Toll-like receptor 4. Am J Respir Crit Care Med 2013; 187:1324–34.
29. Reinhardt K, Foell D, Vogl T, Mezger M, Wittkowski H, Fend F, et al. Monocyte-induced development of Th17 cells and the release of S100 proteins are involved in the pathogenesis of graft-versus-host disease. J Immunol 2014;193:3355–65.
30. Frosch M, Ahlmann M, Vogl T, Wittkowski H, Wulffraat N, Foell D, et al. The myeloid-related proteins 8 and 14 complex, a novel ligand of Toll-like receptor 4, and interleukin-1β form a positive feedback mechanism in systemic-onset juvenile idiopathic arthritis. Arthritis Rheum 2009;60:883–91.
31. Bendersky A, Marcu-Malina V, Berkun Y, Gerstein M, Nagar M, Goldstein I, et al. Cellular interactions of synovial fluid γδ T cells in juvenile idiopathic arthritis. J Immunol 2012;188: 4349–59.
32. Black AP, Bhayani H, Ryder CA, Pugh MT, Gardner-Medwin JM, Southwood TR. An association between the acute phase response and patterns of antigen induced T cell proliferation in juvenile idiopathic arthritis. Arthritis Res Ther 2003;5: R277–84.
33. Ramírez-Valle F, Gray EE, Cyster JG. Inflammation induces dermal $V\gamma4^+$ γδT17 memory-like cells that travel to distant skin and accelerate secondary IL-17–driven responses. Proc Natl Acad Sci U S A 2015;112:8046–51.
34. Roark CL, French JD, Taylor MA, Bendele AM, Born WK, O'Brien RL. Exacerbation of collagen-induced arthritis by oligoclonal, IL-17-producing γδ T cells. J Immunol 2007;179:5576–83.
35. Sicard H, Ingoure S, Luciani B, Serraz C, Fournie JJ, Bonneville M, et al. In vivo immunomanipulation of Vγ9Vδ2 T cells with a synthetic phosphoantigen in a preclinical nonhuman primate model. J Immunol 2005;175:5471–80.

36. Vantourout P, Hayday A. Six-of-the-best: unique contributions of γδ T cells to immunology. Nat Rev Immunol 2013;13:88–100.
37. Laggner U, Di Meglio P, Perea GK, Hundhausen C, Lacy KE, Ali N, et al. Identification of a novel proinflammatory human skin-homing Vγ9Vδ2 T cell subset with a potential role in psoriasis. J Immunol 2011;187:2783–93.
38. Wan Q, Kozhaya L, ElHed A, Ramesh R, Carlson TJ, Djuretic IM, et al. Cytokine signals through PI-3 kinase pathway modulate Th17 cytokine production by $CCR6^+$ human memory T cells. J Exp Med 2011;208:1875–87.
39. Wilson NJ, Boniface K, Chan JR, McKenzie BS, Blumenschein WM, Mattson JD, et al. Development, cytokine profile and function of human interleukin 17-producing helper T cells. Nat Immunol 2007;8:950–7.
40. Boniface K, Blom B, Liu YJ, Malefyt RD. From interleukin-23 to T-helper 17 cells: human T-helper cell differentiation revisited. Immunol Rev 2008;226:132–46.
41. Shimizu M, Nakagishi Y, Inoue N, Mizuta M, Ko G, Saikawa Y, et al. Interleukin-18 for predicting the development of macrophage activation syndrome in systemic juvenile idiopathic arthritis. Clin Immunol 2015;160:277–81.
42. Lalor SJ, Dungan LS, Sutton CE, Basdeo SA, Fletcher JM, Mills KH. Caspase-1-processed cytokines IL-1β and IL-18 promote IL-17 production by γδ and CD4 T cells that mediate autoimmunity. J Immunol 2011;186:5738–48.
43. Canna SW, de Jesus AA, Gouni S, Brooks SR, Marrero B, Liu Y, et al. An activating NLRC4 inflammasome mutation causes autoinflammation with recurrent macrophage activation syndrome. Nat Genet 2014;46:1140–6.
44. Companjen AR, van der Velden VH, Vooys A, Debets R, Benner R, Prens EP. Human keratinocytes are major producers of IL-18: predominant expression of the unprocessed form. Eur Cytokine Netw 2000;11:383–90.
45. Horai R, Nakajima A, Habiro K, Kotani M, Nakae S, Matsuki T, et al. TNF-α is crucial for the development of autoimmune arthritis in IL-1 receptor antagonist-deficient mice. J Clin Invest 2004;114:1603–11.
46. Ikeda S, Saijo S, Murayama MA, Shimizu K, Akitsu A, Iwakura Y. Excess IL-1 signaling enhances the development of Th17 cells by downregulating TGF-β-induced Foxp3 expression. J Immunol 2014;192:1449–58.
47. Akitsu A, Ishigame H, Kakuta S, Chung SH, Ikeda S, Shimizu K, et al. IL-1 receptor antagonist-deficient mice develop autoimmune arthritis due to intrinsic activation of IL-17-producing $CCR2^+V\gamma6^+\gamma\delta$ T cells. Nat Commun 2015;6:7464.
48. Acosta-Rodriguez EV, Napolitani G, Lanzavecchia A, Sallusto F. Interleukins 1β and 6 but not transforming growth factor-β are essential for the differentiation of interleukin 17-producing human T helper cells. Nat Immunol 2007;8:942–9.
49. Do JS, Fink PJ, Li L, Spolski R, Robinson J, Leonard WJ, et al. Cutting edge: spontaneous development of IL-17-producing γδ T cells in the thymus occurs via a TGFβ1-dependent mechanism. J Immunol 2010;184:1675–9.
50. Lochner M, Peduto L, Cherrier M, Sawa S, Langa F, Varona R, et al. In vivo equilibrium of proinflammatory $IL\text{-}17^+$ and regulatory $IL\text{-}10^+$ $Foxp3^+$ $ROR\gamma t^+$ T cells. J Exp Med 2008;205:1381–93.
51. Liu LY, Okada S, Kong XF, Kreins AY, Cypowyj S, Abhyankar A, et al. Gain-of-function human STAT1 mutations impair IL-17 immunity and underlie chronic mucocutaneous candidiasis. J Exp Med 2011;208:1635–48.
52. Kagan JC, Su T, Horng T, Chow A, Akira S, Medzhitov R. TRAM couples endocytosis of Toll-like receptor 4 to the induction of interferon-β. Nat Immunol 2008;9:361–8.
53. Sikora KA, Fall N, Thornton S, Grom AA. The limited role of interferon-γ in systemic juvenile idiopathic arthritis cannot be explained by cellular hyporesponsiveness. Arthritis Rheum 2012; 64:3799–808.
54. Canna SW. Interferon-γ: friend or foe in systemic juvenile idiopathic arthritis and adult-onset Still's disease? [editorial]. Arthritis Rheumatol 2014;66:1072–6.
55. De Jager W, Vastert SJ, Beekman JM, Wulffraat NM, Kuis W, Coffer PJ, et al. Defective phosphorylation of interleukin-18 receptor β causes impaired natural killer cell function in systemic-onset juvenile idiopathic arthritis. Arthritis Rheum 2009;60:2782–93.
56. Put K, Vandenhaute J, Avau A, van Nieuwenhuijze A, Brisse E, Dierckx T, et al. Inflammatory gene expression profile and defective interferon-γ and granzyme K in natural killer cells of systemic juvenile idiopathic arthritis patients. Arthritis Rheumatol 2017;69:213–24.

ARTHRITIS & RHEUMATOLOGY
Vol. 69, No. 7, July 2017, pp 1495–1501
DOI 10.1002/art.40122

BRIEF REPORT

Blockade of TANK-Binding Kinase 1/IKKε Inhibits Mutant Stimulator of Interferon Genes (STING)–Mediated Inflammatory Responses in Human Peripheral Blood Mononuclear Cells

Marie-Louise Frémond,[1] Carolina Uggenti,[2] Lien Van Eyck,[2] Isabelle Melki,[3] Vincent Bondet,[4] Naoki Kitabayashi,[2] Christina Hertel,[5] Adrian Hayday,[5] Bénédicte Neven,[6] Yoann Rose,[2] Darragh Duffy,[7] Yanick J. Crow,[8] and Mathieu P. Rodero[2]

Objective. **Gain-of-function mutations in *TMEM173*, encoding the stimulator of interferon (IFN) genes (STING) protein, underlie a novel type I interferonopathy that is minimally responsive to conventional immunosuppressive therapies and associated with high frequency of childhood morbidity and mortality. STING gain-of-function causes constitutive oversecretion of IFN. This study was undertaken to determine the effects of a TANK-binding kinase 1 (TBK-1)/IKKε inhibitor (BX795) on secretion and signaling of IFN in primary peripheral blood mononuclear cells (PBMCs) from patients with mutations in STING.**

Methods. **PBMCs from 4 patients with STING-associated disease were treated with BX795. The effect of BX795 on IFN pathways was assessed by Western blotting and an IFNβ reporter assay, as well as by quantification of IFNα in cell lysates, staining for STAT-1 phosphorylation, and measurement of IFN-stimulated gene (ISG) messenger RNA (mRNA) expression.**

Results. **Treatment of PBMCs with BX795 inhibited the phosphorylation of IFN regulatory factor 3 and IFNβ promoter activity induced in HEK 293T cells by cyclic GMP-AMP or by genetic activation of STING. In vitro exposure to BX795 inhibited IFNα production in PBMCs of patients with STING-associated disease without affecting cell survival. In addition, BX795 decreased STAT-1 phosphorylation and ISG mRNA expression independent of IFNα blockade.**

Conclusion. **These findings demonstrate the effect of BX795 on reducing type I IFN production and IFN signaling in cells from patients with gain-of-function mutations in STING. A combined inhibition of TBK-1 and IKKε therefore holds potential for the treatment of patients carrying STING mutations, and may also be relevant in other type I interferonopathies.**

Dr. Frémond's work was supported by the Institut National de la Santé et de la Recherche Médicale (grant 000427993). Dr. Crow's work was supported by the European Research Council (fellowship GA 309449) and a state subsidy managed by the Agence Nationale de la Recherche (Investments for the Future grant ANR-10-IAHU-01).

[1]Marie-Louise Frémond, MD: Paris Descartes University, Sorbonne-Paris-Cité, Institut Imagine, INSERM UMR 1163, Laboratory of Neurogenetics and Neuroinflammation, and Pediatric Hematology-Immunology and Rheumatology Department, Hôpital Necker-Enfants Malades, AP-HP, Paris, France; [2]Carolina Uggenti, PhD, Lien Van Eyck, PhD, Naoki Kitabayashi, BSc, Yoann Rose, BSc, Mathieu P. Rodero, PhD: Paris Descartes University, Sorbonne-Paris-Cité, Institut Imagine and INSERM UMR 1163, Laboratory of Neurogenetics and Neuroinflammation, Paris, France; [3]Isabelle Melki, MD: Paris Descartes University, Sorbonne-Paris-Cité, Institut Imagine, INSERM UMR 1163, Laboratory of Neurogenetics and Neuroinflammation, Pediatric Hematology-Immunology and Rheumatology Department, Hôpital Necker-Enfants Malades, AP-HP, and General Pediatrics, Infectious Diseases and Internal Medicine Department, Hôpital Robert Debré, AP-HP, Paris, France; [4]Vincent Bondet, BSc: INSERM UMR 1223 and Laboratory of Dendritic Cell Immunobiology, Institut Pasteur, Paris, France; [5]Christina Hertel, PhD, Adrian Hayday, MA, MD, FMedSci: ImmunoQure, Düsseldorf, Germany; [6]Bénédicte Neven, MD, PhD: Paris Descartes University, Sorbonne-Paris-Cité, Institut Imagine, Pediatric Hematology-Immunology and Rheumatology Department, Hôpital Necker-Enfants Malades, AP-HP, and INSERM UMR 1163, Laboratory of Immunogenetics of Pediatric Autoimmune Diseases, Paris, France; [7]Darragh Duffy, PhD: INSERM UMR 1223, and Laboratory of Dendritic Cell Immunobiology, Institut Pasteur, and Center for Translational Research, Institut Pasteur, Paris, France; [8]Yanick J. Crow, MD, PhD: Paris Descartes University, Sorbonne-Paris-Cité, Institut Imagine, INSERM UMR 1163, Laboratory of Neurogenetics and Neuroinflammation, Paris, France, and University of Manchester, Manchester, UK.

Drs. Frémond and Uggenti contributed equally to this work.

Dr. Hertel owns stock or stock options in ImmunoQure. Dr. Hayday has received consulting fees from QureInvest/HS-Lifesciences (more than $10,000), owns stock or stock options in ImmunoQure and Gamma Delta Therapeutics, has a patent application pending related to the expansion and cultivation of human gamma delta T cells, and holds a patent for naturally arising human antibodies that target cytokines.

Address correspondence to Mathieu P. Rodero, PhD, INSERM UMR 1163, Laboratory of Neurogenetics and Neuroinflammation, Imagine Institute, 24 Boulevard de Montparnasse, 75015 Paris, France. E-mail: mathieu.rodero@institutimagine.org.

Submitted for publication January 28, 2017; accepted in revised form April 6, 2017.

The stimulator of interferon (IFN) genes (STING) protein is a major regulator of the innate immune response to viral and bacterial infections. Upon infection, STING promotes the activation of TANK-binding kinase 1 (TBK-1), leading to IFN regulatory factor 3 (IRF-3) translocation into the nucleus and type I IFN transcription. Secretion of IFN induces the expression of IFN-stimulated genes (ISGs) through activation of the ISG factor 3 (ISGF-3) complex, composed of STAT-1, STAT-2, and IRF-9. Gain-of-function mutations in *TMEM173*, encoding STING, have been associated with an autoinflammatory syndrome termed SAVI (STING-associated vasculopathy with onset in infancy) (1–3). STING-associated disease presents a wide phenotypic spectrum that includes systemic inflammation with fever, a severe skin vasculopathy leading, in some cases, to extensive tissue loss, and interstitial lung disease resulting in pulmonary fibrosis and end-stage respiratory failure (1,2,4). Missense mutations in *TMEM173* reported so far have been shown to be associated with constitutive activation of STING, resulting in increased IFNα production (5), phosphorylation of STAT-1 in T and B lymphocytes, and increased transcription of ISGs in peripheral whole blood (1,2). Thus, STING-associated disease can be classified as a type I interferonopathy (3). These observations pave the way for 2 potential therapeutic strategies, one aiming to inhibit the secretion of IFN itself, and the other targeting the IFN receptor signaling cascade.

BX795 has been described as a specific inhibitor of TBK-1, and also an inhibitor of IKKε. BX795 acts through competitive inhibition of ATP binding (6). This bispecificity can be explained by the high homology between TBK-1 and IKKε (7). TBK-1 responds to STING activation by driving type I IFN transcription through the phosphorylation of IRF-3 (3), whereas IKKε inhibits the formation of STAT-1 homodimers favoring the formation of the ISGF-3 complex and ISG transcription (7). Therefore, for the present study, we postulated that IKK inhibitors may reduce the overproduction of IFN in STING-mutated patient cells through inhibition of TBK-1, and may also restrict the transcription of ISGs through IKKε inhibition (as shown in Figure 1A).

PATIENTS AND METHODS

Patients. Four children carrying de novo or inherited gain-of-function mutations in *TMEM173* were recruited. A positive type I IFN signature (8) was observed in all patients. The disease-specific phenotypic details for each of the 4 children are available upon request from the corresponding author. The study received ethics approval from the Comité de Protection des Personnes (ID-RCB/EUDRACT no. 2014-A01017-40).

Cell cultures. Peripheral blood mononuclear cells (PBMCs) were isolated by Ficoll-Paque density gradient (LymphoPrep; Proteogenix) from the blood of patients and healthy donors. Fresh or cryopreserved PBMCs were used for the assays. PBMCs were cultured at 37°C in 5% CO_2 in GlutaMax RPMI 1640 medium (Invitrogen), supplemented with 10% (volume/volume) fetal bovine serum, 100 units/ml penicillin, and 100 μg/ml streptomycin (each from Gibco). The PBMCs were thereafter treated with 2 μM BX795 or DMSO as a control.

Human embryonic kidney cells (HEK 293T cells) were grown in 96-well plates at 37°C in 5% CO_2 in Dulbecco's modified Eagle's medium supplemented with 10% (v/v) fetal bovine serum, 100 units/ml penicillin, and 100 μg/ml streptomycin (each from Gibco). Once the HEK 293T cells had reached 70% confluence, they were cotransfected with 60 ng of a pMSCV-hygro(+) vector, either empty or encoding the *TMEM173* pV.155M variant, 40 ng of IFNβ promoter–driven firefly luciferase reporter plasmid (IFNβ-pGL3), and 1.4 ng of constitutively expressed *Renilla* luciferase reporter plasmid (pRL-TK), using a TransIT-293 transfection reagent (Mirus no. MIR2700; Euromedex). Twenty-four hours later, the cells were stimulated by transfection with 1.3–12 μg/ml 2′3′-cyclic GMP-AMP (cGAMP)–STING ligand (tlrl-nacga23; InvivoGen) using Lipofectamine 2000 (Thermo Fisher Scientific). Subsequently, the cells were treated with 2 μM BX795 or with DMSO as a control.

Twenty-four hours after cGAMP stimulation, the cells were lysed with passive lysis buffer 5X (Promega) containing protease and phosphatase inhibitors. One-third of the lysate for each condition was used for the luciferase assay. The remaining material was used for protein analysis by Western blotting.

IFNβ promoter–driven luciferase (IFN-Luc) reporter assay. An IFNβ-pGL3 plasmid was used to measure IFNβ promoter activity, and a *Renilla* reporter plasmid was used as a control to normalize the transfection efficiency. Luciferase assays were performed using a Dual-Glo Luciferase Assay System (E2940; Promega) in accordance with the manufacturer's protocol. Luminescence was acquired on a FLUOstar OPTIMA microplate reader (BMG Lab Technologies). The values for firefly luciferase activity were normalized against those for *Renilla* luciferase activity.

Western blot analysis. Proteins were extracted from PBMCs and from transfected HEK 293T cells using lysis buffer (radioimmunoprecipitation assay buffer containing 1% protease inhibitor and 1% phosphatase inhibitor). Bolt LDS Sample Buffer (4X) and Bolt Sample Reducing Agent (10X) (both from Novex Life Technologies) were added to the protein lysates, and the samples were resolved on 4–12% Bis-Tris Plus gels (Invitrogen) transferred to nitrocellulose membrane (Invitrogen). When the phosphorylation status of the protein was investigated, membranes were blocked in 5% bovine serum albumin (BSA) in Tris buffered saline (TBS), and primary phospho-antibodies were incubated overnight in blocking solution. Alternatively, membranes were blocked with 5% nonfat milk in TBS, and thereafter primary antibodies were incubated overnight in blocking solution.

Proteins were blotted with mouse anti-STING antibodies, rabbit anti–IRF-3 antibodies, mouse anti–IRF-9 antibodies, mouse anti–pIRF-3 antibodies, rabbit anti–pTBK-1 antibodies, and rabbit anticofilin antibodies (as loading control) (all from Cell Signaling Technology), diluted in 5% BSA–TBS (1X)–0.1% Tween for 1 hour at room temperature. Membranes were incubated with the appropriate anti-mouse or anti-rabbit secondary antibodies for 45 minutes at room temperature (R&D Systems). Signal was detected using an enhanced chemiluminescence and ChemiDoc MP quantification system (Bio-Rad) or using an

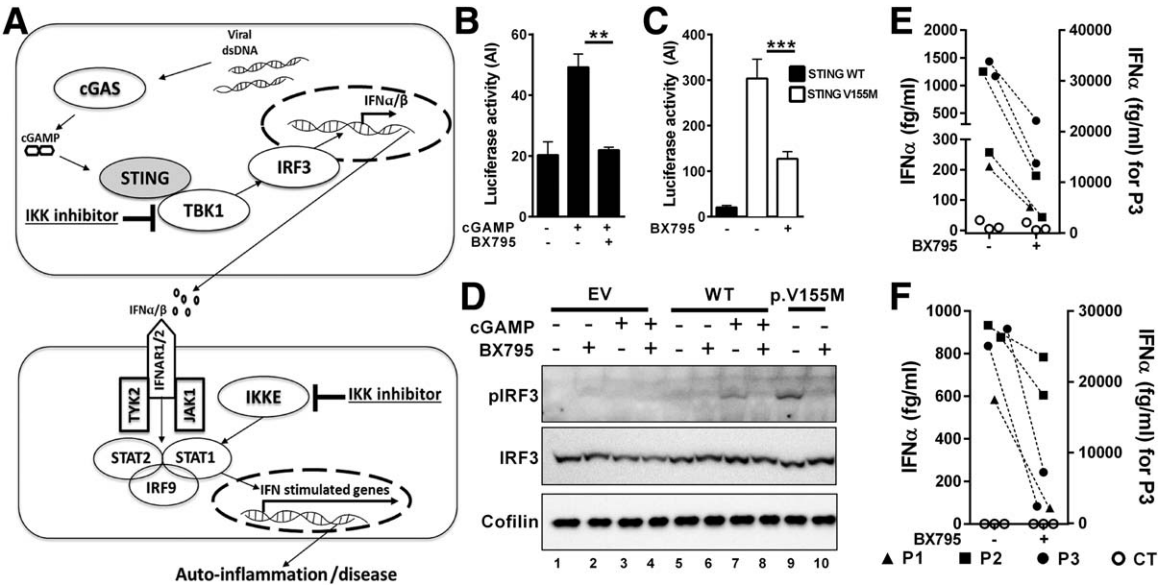

Figure 1. Inhibition of type I interferon (IFN) production by BX795 treatment in HEK 293T cells and peripheral blood mononuclear cells (PBMCs) from patients with *TMEM173* mutations. **A,** Schematic representation of BX795 targets of the type I IFN signaling cascade. **B** and **C,** Effects of BX795 on IFNβ expression, as assessed using a luciferase activity reporter assay in HEK 293T cells transfected with wild-type (WT) stimulator of IFN genes (STING) followed by stimulation with 4 μg/ml cyclic GMP-AMP (cGAMP) or without cGAMP stimulation (**B**) or in HEK 293T cells transfected with WT or mutant (p.V155M plasmid) STING (**C**). Results are the mean ± SD activity index (AI). Representative results from 1 of 3 independent experiments are shown. ** = $P < 0.01$; *** = $P < 0.001$, by Mann-Whitney test. **D,** Effects of BX795 on IFN regulatory factor 3 (IRF-3) phosphorylation, as assessed by Western blotting of HEK 293T cells transfected with WT or p.V155M mutant STING (or empty vector [EV] as a control). Results are representative of 3 independent experiments. **E** and **F,** Effects of BX795 on IFNα concentration (in fg/ml) measured in lysates (**E**) or supernatants (**F**) of PBMCs from 3 patients with mutations in STING (P1–P3) and 3 healthy controls (CT). Samples from patient 2 and patient 3 were collected at 2 different visits. Values from patient 3 are presented on the right axis in **E.** cGAS = cGAMP cyclase; dsDNA = double-stranded DNA; TBK-1 = TANK-binding kinase 1.

Odyssey CLx system (Li-Cor). Comparative signal analyses were performed using Image Lab (Bio-Rad) and Image Studio Lite (Li-Cor).

Quantitative reverse transcription–polymerase chain reaction (qRT-PCR) analysis of gene expression. PBMCs were left untreated or treated with 2 μM BX795 at 37°C for 24 hours. Total RNA was extracted using an RNAqueous-Micro kit (Ambio). RT was performed using a High-Capacity cDNA Reverse Transcription kit (Applied Biosystems). Levels of messenger RNA (mRNA) were quantified by qRT-PCR using a TaqMan gene expression assay (Applied Biosystems), with values normalized to the expression levels of housekeeping gene *HPRT1*. A complete list of the probes used in this study is available upon request from the corresponding author.

Assay for STAT-1 phosphorylation. PBMCs were left untreated or treated with 2 μM BX795 at 37°C for 4 hours (short-term stimulation) or overnight. Cells were fixed using BC PerFix Expose Fixation Buffer (10 minutes at room temperature), and then permeabilized using BC PerFix Expose Permeabilizing Buffer (5 minutes at 37°C). Cells were then protected from light and stained with phycoerythrin (PE)–conjugated anti–STAT1 pY701, PE-conjugated anti-STAT1, and cell surface markers (allophycocyanin-conjugated CD3, BV421-conjugated CD8, and PE–Cy7–conjugated CD19) for 1 hour at room temperature. Flow cytometry analysis was performed on a Gallios Beckman Coulter flow cytometer. Results were analyzed using Kaluza software version 1.3.

Quantification of IFNα in serum and PBMCs by Simoa assay. The Simoa IFNα assay was developed using a Quanterix Homebrew Simoa assay kit in accordance with the manufacturer's instructions, utilizing 2 autoantibodies specific for IFNα isolated and cloned from 2 recently described patients with autoimmune polyendocrinopathy syndrome type 1/autoimmune polyendocrinopathy–candidiasis–ectodermal dystrophy (5,9). The 8H1 antibody clone was used as a capture antibody, after coating on paramagnetic beads (0.3 mg/ml), and the 12H5 antibody was biotinylated (biotin-to-antibody ratio 30: 1) and used as the detector. Recombinant IFNα17/αI (PBL Assay Science) was used to generate a standard curve, after cross-reactivity testing. The limit of detection was calculated as the mean + 3SD value of reactivity from all blank runs, found to be 0.23 fg/ml.

Statistical analysis. Analyses were performed with Prism software (version 6 for Macintosh; GraphPad). Data were tested for normality using the D'Agostino and Pearson test. Data are expressed as the mean ± SD. P values less than 0.05 were considered significant.

RESULTS

Inhibition of type I IFN production by BX795 in HEK 293T cells and PBMCs from patients with STING mutations. Activation of STING by cGAMP is known to promote the activation of IRF-3 and the

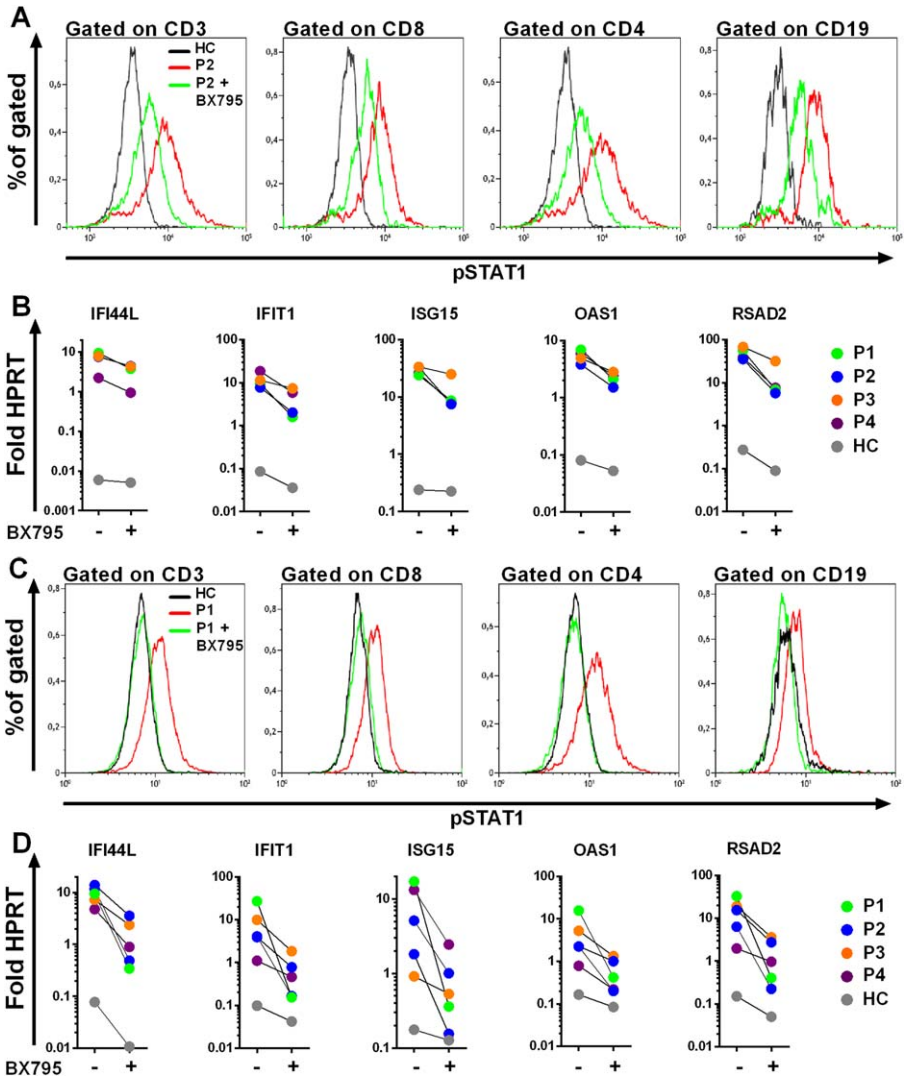

Figure 2. Partial decrease in STAT-1 phosphorylation and inhibition of interferon-stimulated gene (ISG) transcription following short-term and overnight treatment with BX795 in peripheral blood mononuclear cells (PBMCs) from patients with *TMEM173* mutations. **A** and **C,** The effect of 4 hours of BX795 exposure on constitutive phosphorylation of STAT-1 was examined in T and B lymphocytes from patient 2 (P2) (**A**) and patient 1 (P1) (**C**). **B** and **D,** The effects of short-term treatment with BX795 (**B**) and overnight treatment with BX795 (**D**) on ISG expression were examined in PBMCs from all 4 patients. Circles depict the individual fold change in ISG expression levels relative to the expression of *HPRT*. Gray-shaded circles represent the mean values for 4 healthy controls (HC).

subsequent transcription of type I IFN. Using an IFN-Luc reporter assay, we showed that BX795 treatment decreased the cGAMP-dependent overexpression of IFNβ in HEK 293T cells (Figure 1B).

In order to validate the hypothesis that BX795 treatment might prove beneficial in patients carrying gain-of-function mutations in STING, we repeated this experiment using a p.V155M plasmid encoding the $Val^{155}Met$ STING mutation. Treatment of the cells with BX795 significantly decreased the IFNβ promoter activity induced by mutant STING (mean ± SD activity index 303.6 ± 42.70 in untreated cells versus 127 ± 15.85 To in treated cells; $P < 0.001$) (Figure 1C). The reduction in IFNβ promoter activity upon BX795 treatment was mirrored by the total abrogation of IRF-3 phosphorylation, both in cGAMP-stimulated HEK 293T cells expressing wild-type STING and in unstimulated HEK 293T cells expressing gain-of-function mutant STING (Figure 1D). These data suggest that IRF-3 phosphorylation is required for mutant STING–induced type I IFN transcription (10). Thus, our findings validate the hypothesis that IKKε inhibitors might be used to control IFN production in patients with SAVI.

To further test this possibility, we isolated PBMCs from the blood of 3 patients with gain-of-function

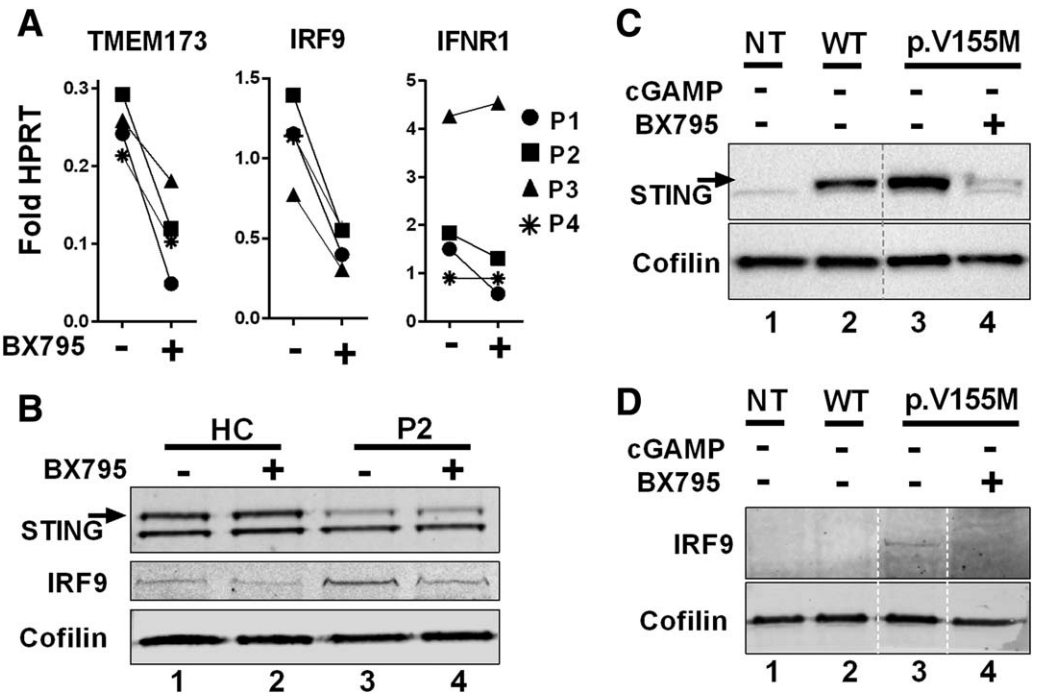

Figure 3. Inhibition of *TMEM173* and interferon (IFN) regulatory factor 9 (IRF-9) transcript and protein expression by BX795. **A,** The effects of overnight treatment with BX795 on the transcript levels of *TMEM173*, *IRF9*, and *IFNR1* were examined in peripheral blood mononuclear cells (PBMCs) from all 4 tested patients (P1–P4). * = $P < 0.05$; ** = $P < 0.005$, by paired *t*-test. **B,** The effects of BX795 treatment on the levels of stimulator of IFN genes (STING) and IRF-9 proteins were assessed by Western blotting of PBMCs from patient 2, as compared with PBMCs from a healthy control (HC). **C** and **D,** The effects of BX795 treatment on the levels of STING protein (**C**) and IRF-9 protein (**D**) were assessed by Western blotting of unstimulated HEK 293T cells transfected with wild-type (WT) or p.V155M mutant STING plasmid. Nontransfected (NT) cells served as a control. Results are representative of 2 independent experiments. cGAMP = cyclic GMP-AMP.

mutations in STING. Using an ultrasensitive digital enzyme-linked immunosorbent assay to quantify IFNα (5), we observed significantly higher levels of both intracellular IFNα and secreted IFNα in patient-derived PBMCs as compared to healthy control PBMCs (for intracellular IFNα, mean ± SD 10,108 ± 13,768 fg/ml versus 15.87 ± 15.17 fg/ml, and for secreted IFNα, mean ± SD 11,330 ± 14,461 fg/ml versus 0.67 ± 0.01 fg/ml; each $P < 0.05$). Furthermore, BX795 treatment decreased the IFNα concentration in total PBMC lysates and supernatants derived from patients with mutations in STING as compared to DMSO-treated control cells (Figures 1E and F). These results were independent of PBMC survival, since BX795 did not affect cell viability at this working concentration (details available upon request from the corresponding author).

Inhibition of STAT-1 phosphorylation and ISG expression by BX795 in cells from patients with STING mutations. As previously reported (1,11), increased levels of STAT-1 phosphorylation were observed in lymphocytes from patients with STING mutations as compared to lymphocytes from healthy controls (Figures 2A and C) (further details available upon request from the corresponding author). In order to evaluate the impact of BX795-induced IKKε inhibition on ISG transcription, as opposed to regulation of ISG transcription through reduction of IFN secretion via inhibition of TBK-1, we examined the STAT-1 phosphorylation status and ISG levels after short-term treatment of PBMCs from 4 patients carrying mutations in STING. After 4 hours of treatment with BX795, we observed a partial reduction of STAT-1 phosphorylation in T and B lymphocytes from 2 patients (Figure 2A). After 6 hours of treatment, the expression of 5 ISGs was decreased in patient cells (Figure 2B), thus indicating an IFN-independent inhibition of ISG transcription by BX795 that likely occurs through inhibition of IKKε.

To assess the overall effect of IKK inhibition on IFN signaling, we evaluated the levels of pSTAT-1 and ISGs in PBMCs from 4 patients after overnight treatment with BX795. This extended time course is sufficient to allow transcription and secretion of IFN, and to observe the subsequent IFN-driven phosphorylation of STAT-1 and transcription of ISGs. In vitro, BX795 treatment resulted in the inhibition of STAT-1 phosphorylation in T and B lymphocytes from all patients with STING mutations (representative results in 1 patient shown in

Figure 2C). Consistently, treatment with BX795 was associated with a decrease in the expression of 5 ISGs in PBMCs from all 4 patients (Figure 2D).

Inhibition of *TMEM173* and IRF-9 expression by BX795 in cells from patients with STING mutations. Consistent with our hypothesis that IFN secretion and ISG transcription could simultaneously be targeted in cells from patients with mutations in STING, we investigated the effect of BX795 treatment on the expression of *TMEM173*/STING itself and on the expression levels of IRF-9 mRNA and protein, since the former drives type I IFN production in patients and the latter is an essential component of the ISGF-3 transcription complex responsible for ISG expression. Following treatment with BX795, we observed a reduction in both *TMEM173* and *IRF9* transcripts in PBMCs from all patients (Figure 3A). This was confirmed at the protein level in both HEK 293T cells and PBMCs from 3 patients, with decreases in protein levels ranging 41–73% for IRF-9 and 20–32% for STING (Figures 3B–D) (further details available upon request from the corresponding author). The reduction in the expression of IRF-9 and STING by BX795 indicates that the treatment simultaneously inhibits not only the signaling cascade responsible for type I IFN and ISG transcription, but also the expression of key molecules in these pathways, thus highlighting a virtuous circle in the context of BX795 treatment of cells from patients carrying mutations in STING.

DISCUSSION

This study is the first to demonstrate the effect of TBK-1/IKKε inhibition in the context of gain-of-function mutations in STING. We assessed the effect of BX795 on the different steps of IFN signaling—from the constitutive overexpression of type I IFN to the increased expression of ISGs via the JAK/STAT pathway. Features of inflammation attributable to STING gain-of-function are associated with a high incidence of childhood morbidity and mortality. To date, conventional immunosuppressive therapies have proven to be minimally effective in this disease. We have previously demonstrated the benefit of JAK-1/2 inhibition in 3 children carrying activating mutations in STING (11). However, this treatment, at the current posology, inhibits the JAK-1/2 pathway only transiently, and does not allow for complete remission of disease features (11). Moreover, we observed a sustained growth defect in treated patients, possibly explained by the role of JAK-2 in growth hormone signaling (12), and hematologic side effects occurred frequently in patients with myelofibrosis who received treatment with JAK-1/2 inhibition (13). Thus, alternative therapeutic strategies are urgently required.

Herein we demonstrate that targeting IKKε is another strategy to inhibit ISG transcription in patient cells. However, inhibition of IKKε or JAK prevents type I IFN signaling but does not abrogate the overproduction of IFN itself (12,14). Targeting STING or its immediate partners, such as TBK-1 or IRF-3, may be relevant to avoid constitutive type I IFN expression in STING-associated vasculopathy, and may therefore represent a valuable therapeutic option.

Interestingly, the lethality of autoinflammation in $Trex1^{-/-}$ mice is significantly rescued when this mouse strain is backcrossed on $Irf3^{+/-}$ mice (15), suggesting that even partial IRF-3 inhibition, with a preserved antiviral response, might be sufficient to provide clinical benefit. In the present study, we demonstrated that TBK-1/IKKε inhibition decreased the production of IFNα by patient PBMCs, and thus this treatment appears to effectively target the first stage of the inflammatory response. This is of particular interest knowing that *TMEM173* and *IRF9* are themselves ISGs (16), most likely acting to further amplify the constitutive activation of type I IFN signaling in patients with STING mutations. Consistently, the levels of *IRF9* and *TMEM173* mRNA and protein were reduced under BX795 treatment, thus highlighting a virtuous circle in the control of disease-associated inflammation in patient cells. Given that STING drives the IFN response in patients with systemic lupus erythematosus (SLE) (17), and that TBK-1 inhibition was recently shown to promote the reduction of the IFN signature in SLE patient–derived leukocytes, we predict that the benefit of combined TBK-1/IKKε inhibition may apply not only to the monogenic interferonopathies, but also to certain complex autoimmune diseases (18).

In conclusion, this report describes, for the first time, the effect of TBK-1/IKKε inhibition treatment on cells from patients with gain-of-function mutations in STING. BX795 treatment reduced both IFNα production and ISG transcription in patient cells. These findings thus support the development of pharmacologic inhibitors of IKK suitable for clinical use in the treatment of STING-associated autoinflammation. Such compounds might also be relevant as a therapeutic option in other monogenic type I interferonopathies and complex autoimmune diseases such as SLE.

ACKNOWLEDGMENTS

We thank Nicolas Manel for providing the wild-type STING, $Val^{155}Met$ mutant STING, and IFNβ-pGL3 plasmids, Gillian Rice for her help with editing of the figures, and Elvira Duchesne for her assistance with logistics.

AUTHOR CONTRIBUTIONS

All authors were involved in drafting the article or revising it critically for important intellectual content, and all authors approved the final version to be published. Dr. Rodero had full access to all of the data in the study and takes responsibility for the integrity of the data and the accuracy of the data analysis.

Study conception and design. Frémond, Uggenti, Hertel, Hayday, Neven, Duffy, Crow, Rodero.

Acquisition of data. Frémond, Uggenti, Van Eyck, Melki, Bondet, Kitabayashi, Rose, Duffy, Crow, Rodero.

Analysis and interpretation of data. Frémond, Uggenti, Rodero.

ADDITIONAL DISCLOSURES

Authors Hertel and Hayday are employees of ImmunoQure.

REFERENCES

1. Liu Y, Jesus AA, Marrero B, Yang D, Ramsey SE, Montealegre Sanchez GA, et al. Activated STING in a vascular and pulmonary syndrome. N Engl J Med 2014;371:507–18.
2. Jeremiah N, Neven B, Gentili M, Callebaut I, Maschalidi S, Stolzenberg MC, et al. Inherited STING-activating mutation underlies a familial inflammatory syndrome with lupus-like manifestations. J Clin Invest 2014;124:5516–20.
3. Crow YJ, Casanova JL. STING-associated vasculopathy with onset in infancy: a new interferonopathy. N Engl J Med 2014; 371:568–71.
4. Picard C, Thouvenin G, Kannengiesser C, Dubus JC, Jeremiah N, Rieux-Laucat F, et al. Severe pulmonary fibrosis as the first manifestation of interferonopathy (TMEM173 mutation). Chest 2016;150:e65–71.
5. Rodero MP, Decalf J, Bondet V, Hunt D, Rice GI, Werneke, et al. Ultra-sensitive detection of interferon α protein by digital ELISA reveals differential levels and cellular sources in distinct human diseases. J Exp Med 2017;214:1547–55.
6. Clark K, Plater L, Peggie M, Cohen P. Use of the pharmacological inhibitor BX795 to study the regulation and physiological roles of TBK1 and IκB kinase ε: a distinct upstream kinase mediates Ser-172 phosphorylation and activation. J Biol Chem 2009;284:14136–46.
7. Tenoever BR, Ng SL, Chua MA, McWhirter SM, García-Sastre A, Maniatis T. Multiple functions of the IKK-related kinase IKKε in interferon-mediated antiviral immunity. Science 2007;315:1274–8.
8. Rice GI, Forte GM, Szynkiewicz M, Chase DS, Aeby A, Abdel-Hamid MS, et al. Assessment of interferon-related biomarkers in Aicardi-Goutières syndrome associated with mutations in TREX1, RNASEH2A, RNASEH2B, RNASEH2C, SAMHD1, and ADAR: a case-control study. Lancet Neurol 2013;12: 1159–69.
9. Meyer S, Woodward M, Hertel C, Vlaicu P, Haque Y, Kärner J, et al. AIRE-deficient patients harbor unique high-affinity disease-ameliorating autoantibodies. Cell 2016;166:582–95.
10. Melki I, Rose Y, Uggenti C, van Eyck L, Frémond ML, Kitabayashi N, et al. Disease-associated mutations identify a novel region in human STING necessary for the control of type I interferon signaling. J Allergy Clin Immunol 2017;139: 1396–9.
11. Frémond ML, Rodero MP, Jeremiah N, Belot A, Jeziorski E, Duffy D, et al. Efficacy of the janus kinase 1/2 inhibitor ruxolitinib in the treatment of vasculopathy associated with TMEM173-activating mutations in 3 children. J Allergy Clin Immunol 2016; 138:1752–5.
12. O'Shea JJ, Holland SM, Staudt LM. JAKs and STATs in immunity, immunodeficiency, and cancer. N Engl J Med 2013;368:161–70.
13. Verstovsek S, Mesa RA, Gotlib J, Levy RS, Gupta V, DiPersio JF, et al. A double-blind, placebo-controlled trial of ruxolitinib for myelofibrosis. N Engl J Med 2012;366:799–807.
14. Vilasco M, Larrea E, Vitour D, Dabo S, Breiman A, Regnault B, et al. The protein kinase IKKε can inhibit HCV expression independently of IFN and its own expression is downregulated in HCV-infected livers. Hepatology 2006;44:1635–47.
15. Stetson DB, Ko JS, Heidmann T, Medzhitov R. Trex1 prevents cell-intrinsic initiation of autoimmunity. Cell 2008;134: 587–98.
16. Ma F, Li B, Yu Y, Iyer SS, Sun M, Cheng G. Positive feedback regulation of type I interferon by the interferon-stimulated gene STING. EMBO Rep 2015;16:202–12.
17. Lood C, Blanco LP, Purmalek MM, Carmona-Rivera C, de Ravin SS, Smith CK, et al. Neutrophil extracellular traps enriched in oxidized mitochondrial DNA are interferogenic and contribute to lupus-like disease. Nat Med 2016;22:146–53.
18. Hasan M, Dobbs N, Khan S, White MA, Wakeland EK, Li QZ, et al. Cutting edge: inhibiting TBK1 by compound II ameliorates autoimmune disease in mice. J Immunol 2015;195:4573–7.

ARTHRITIS & RHEUMATOLOGY
Vol. 69, No. 7, July 2017, pp 1502–1503

CONCISE COMMUNICATION

DOI 10.1002/art.40120

American College of Rheumatology criteria for systemic lupus erythematosus exclude half of all systemic lupus erythematosus patients

For research and administrative reasons, the diagnosis of systemic lupus erythematosus (SLE) describes patients who meet the criteria of either the American College of Rheumatology (ACR) (1) or the Systemic Lupus International Collaborating Clinics (2). To create these criteria, committees solicited scenarios of patients with unequivocal diagnoses of SLE and, for comparison, patients with other well-defined rheumatic illnesses. They then reviewed the scenarios and voted to characterize each as SLE (yes or no). Validations of the criteria have independently studied similarly defined patients (3,4). Criteria and validation studies do not further consider patients submitted to, but rejected by, the committees before adjudication, nor those who received "no" votes for SLE.

In rheumatology clinics, SLE is diagnosed not only in patients who meet the criteria but also in patients with variant forms of SLE. SLE may be an appropriate diagnosis for patients who have typical SLE with no overlapping illness (pure SLE), SLE accompanied by an overlapping second autoimmune illness (overlapping SLE) (5), or an SLE-like illness such as undifferentiated connective tissue disease (UCTD) (6) or mixed connective tissue disease (MCTD) (7).

Whether patients with a variant form of SLE differ from those with pure SLE in clinical and demographic characteristics, and whether mechanistic decision-making and treatment decisions based on results of studies in patients with pure SLE apply equally to those with variant forms of SLE are unknown. Recent editorials (8–13) that acknowledge this concern offer no data to inform discussions of the relative prevalence, clinical differences, or need for different treatments for patients with variant forms of SLE. Contemporary formal studies on clinical manifestations, mechanisms, or treatment of SLE rarely include information regarding whether patients with variant forms of SLE are included or excluded or how an analysis that stratifies patients might alter the results.

To address these concerns, we retrospectively reviewed the charts of all patients in the Barbara Volcker Center electronic chart database (2002 through 2015) in whom SLE was diagnosed. We compared the prevalence, demography, and clinical characteristics of patients with variant SLE with those of patients with pure SLE. After reconfirming the SLE diagnoses, we assigned patients, as of their most recent visits, to 1 of 4 categories. Patients with pure SLE had SLE fulfilling the diagnostic criteria, with no overlapping autoimmune rheumatic illness; patients with overlapping SLE had pure SLE plus an overlapping autoimmune disease, such as rheumatoid arthritis, scleroderma, dermatomyositis, antiphospholipid syndrome (1,14), or Sjögren's syndrome (defined as ophthalmologist-prescribed artificial tear use, punctal plugs, salivary gland hypertrophy, and/or cryoglobulinemia; a biopsy was not required for diagnosis). Patients with MCTD had

Table 1. Characteristics of the patients in the diagnostic groups*

Item	Pure SLE	All variant forms of SLE	Overlapping SLE	MCTD	UCTD
All SLE patients, no. (%)	320 (51)	308 (49)	122 (19)	37 (6)	149 (24)
Age, mean ± SD years	39.8 ± 13.1	42.6 ± 13.5†	43.9 ± 14.1†	44.3 ± 14.9	41.0 ± 12.6
Male	5.9	6.4	9.0	5.4	4.7
Nonwhite	33.4	17.5‡	27.9	18.9	8.7‡
ACR criteria met	81.5	33.4§	46.2§	41.8§	20.0§
No. of patients/cohort	40	117	40	37	40
Symptoms					
Fatigue	50.0	31.6	37.5	21.6†	35.0
Sicca syndrome	22.5	23.1	25.0	18.9	25.0
Mucosal disease	35.0	11.1†	10.0†	10.8‡	12.5‡
Skin rash	67.5	62.4	55.0	75.7	57.5
Raynaud's phenomenon	17.5	38.5	5.0	51.4‡	22.5
Hematologic disease	32.5	17.1	42.5	27.0	15.0
Serosal disease	20.0	17.1	10.0	16.2	10.0
Kidney disease	25.0	15.4	25.0	5.4‡	2.5†
Joint disease	80.0	52.2†	57.5‡	51.4†	47.5†
Nervous system disease	42.5	32.5	30.0	40.5	27.5
Treatment					
Corticosteroid	72.5	56.4	75.0	64.9	35.0§
Hydroxychloroquine	62.5	39.3	60.0	40.5‡	27.5†
Immunosuppressive agent	37.5	29.0	35.0	35.1	17.5

* Except where indicated otherwise, values are the percent. MCTD = mixed connective tissue disease; UCTD = undifferentiated connective tissue disease; ACR = American College of Rheumatology.
† $P < 0.01$ versus pure systemic lupus erythematosus (SLE).
‡ $P < 0.05$ versus pure SLE.
§ $P < 0.001$ versus pure SLE.

the specific syndrome of overlapping SLE, scleroderma, and dermatomyositis, coupled with strong positivity for U1 RNP antibodies (7). Patients with UCTD were positive for antinuclear antibodies and had SLE-like symptoms and findings but had no classic features of SLE, such as rash or nephritis (6).

We calculated age from first visit in the database, not necessarily the first visit to this institution. Laboratory results that confirmed the diagnoses, although often mentioned in the physician's chart notes, were not routinely filed as laboratory reports in the electronic chart until 2007. For tabulation of the ACR criteria for SLE, we reported only those laboratory studies documented by an available laboratory report.

We randomly selected, from each diagnosis subset, cohorts of 20 patients each to test and validate symptoms, physical examination findings, laboratory results, and treatment; we assumed that missing values were normal (the MCTD cohort comprised only 37 patients). Because the test and validation cohorts matched within 20 percentage points in most demographic, symptom, and treatment characteristics, we combined the cohorts (see Table 1). Statistical differences between groups were determined by chi-square test and Student's *t*-test.

In the full database, 628 patients had a diagnosis of SLE (Table 1). Among these patients, 94% (including 2 female-to-male transgender patients) were female, and 26% were nonwhite. As stratified by subgroup, 51% of patients had pure SLE, 19% had overlapping SLE, 6% had MCTD, and 24% had UCTD. Three hundred sixty-five patients met the ACR criteria for SLE; of these, 28% had a variant form of SLE. Thirty-three percent of patients with variant SLE met the ACR criteria for SLE.

Compared with patients with pure SLE, those with variant forms of SLE were older, more often were white, and less often met the ACR criteria. Patients in all 3 variant SLE groups had a lower frequency of mucosal or joint disease; patients with MCTD or UCTD had a lower frequency of kidney disease and less often received hydroxychloroquine; and patients with UCTD less often received corticosteroids. The frequency of sicca symptoms, skin rashes, hematologic disease, nervous system disease, and immunosuppressive drug treatment did not differ between the diagnostic groups. In our clinic, half of all patients with clinically diagnosed SLE and more than one-fourth of patients who fulfill the ACR criteria for SLE have variant SLE. These patients differ from patients with pure SLE, both demographically and clinically. No measured characteristic is unique to any group.

Assuming that our experience is generalizable, guidelines and clinical studies that do not separately identify patients with variant forms of SLE may not apply to half of patients in whom clinicians diagnose and treat SLE. We hypothesize that the differences we observed may lead to biased conclusions in mechanistic, clinical descriptive, and treatment studies, stated to apply to SLE but in fact representing only a proportion of all SLE patients. We cannot test this hypothesis with our retrospective data; prospective studies that stratify patients according to our suggested subgroups will answer this question.

These findings represent a single clinic's experience with SLE as diagnosed by experienced rheumatologists. We cannot exclude referral bias or the possibility that other physicians might diagnose SLE in our patients differently. However, similar concerns apply to studies from other tertiary care clinics and to the patients upon whom SLE criteria are based.

In an era in which treatment protocols, insurers' payment decisions, and other administrative concerns assume that a diagnosis of SLE is unambiguous, we contend that the high prevalence of variant forms of SLE demands more flexible rules. To this end, we offer a vocabulary for future studies.

Supported by the Barbara Volcker Center and Weill Cornell Medical College.

Linjia Jia, BA
Weill Cornell Medical College
Alana B. Levine, MD, MSc
Michael D. Lockshin, MD
Barbara Volcker Center
Hospital for Special Surgery
and Weill Cornell Medical College
New York, NY

AUTHOR CONTRIBUTIONS

All authors were involved in drafting the article or revising it critically for important intellectual content, and all authors approved the final version to be published.

1. American College of Rheumatology. ACR-endorsed criteria for rheumatic diseases. URL: http://www.rheumatology.org/Practice-Quality/Clinical-Support/Criteria/ACR-Endorsed-Criteria.
2. Petri M, Orbai AM, Alarcon GS, Gordon C, Merrill JT, Fortin PR, et al. Derivation and validation of Systemic Lupus International Collaborating Clinics classification criteria for systemic lupus erythematosus. Arthritis Rheum 2012;64:2677–86.
3. Ines L, Silva C, Galindo M, Lopez-Longo FJ, Terroso G, Romão VC, et al. Classification of systemic lupus erythematosus: Systemic Lupus International Collaborating Clinics versus American College of Rheumatology criteria. A comparative study of 2,055 patients from a real-life, international systemic lupus erythematosus cohort. Arthritis Care Res (Hoboken) 2015;67:1180–5.
4. Amezcua-Guerra LM, Higuera-Ortiz V, Arteaga-Garcia U, Gallegos-Nava S, Hubbe-Tena C. Performance of the 2012 Systemic Lupus International Collaborating Clinics and the 1997 American College of Rheumatology classification criteria for systemic lupus erythematosus in a real-life scenario. Arthritis Care Res (Hoboken) 2015;67:437–41.
5. Lockshin MD, Levine AB, Erkan D. Patients with overlap autoimmune disease differ from those with 'pure' disease. Lupus Sci Med 2015;2:e000084.
6. Slight-Webb S, Lu R, Ritterhouse LL, Munroe ME, Maecker HT, Fathman CG, et al. Autoantibody-positive healthy individuals display unique immune profiles that may regulate autoimmunity. Arthritis Rheumatol 2016;68:2492–502.
7. Unprasert P, Crowson CS, Chowdhary VR, Ernste FC, Moder KG, Matteson EL. Epidemiology of mixed connective tissue disease, 1985–2014: a population-based study. Arthritis Care Res (Hoboken) 2016;68:1843–8.
8. Van Vollenhoven RF. Who gets lupus? Clues to a tantalizing syndrome [editorial]. Arthritis Rheumatol 2017;69:483–6.
9. Pisetsky DS, Rovin BH, Lipsky PE. Biomarkers as entry criteria for clinical trials of new therapies for systemic lupus erythematosus: the example of antinuclear antibodies and anti-DNA. Arthritis Rheumatol 2017;69:487–93.
10. Costenbader KH, Schur PH. We need better classification and terminology for "people at high risk of or in the process of developing lupus" [editorial]. Arthritis Care Res (Hoboken) 2015;67:593–6.
11. Ugarte-Gil MF, Alarcon GS. Incomplete systemic lupus erythematosus: early diagnosis or overdiagnosis? [editorial]. Arthritis Care Res (Hoboken) 2016;68:285–7.
12. Behrens-Norman HM, Boackle SA. Subduing lupus: can preclinical autoimmune disease be arrested? [editorial]. Arthritis Rheumatol 2016;68:2357–60.
13. Merrill JT. Connective tissue diseases: is SLE many single-organ diseases or an overlapping spectrum? Nat Rev Rheumatol 2015; 11:385–6.
14. Miyakis S, Lockshin MD, Atsumi T, Branch DW, Brey RL, Cervera R, et al. International consensus statement on an update of the classification criteria for definite antiphospholipid syndrome (APS). J Thromb Haemost 2006;4:295–306.

ARTHRITIS & RHEUMATOLOGY
Vol. 69, No. 7, July 2017, pp 1504–1508

LETTERS

DOI 10.1002/art.40105

Abatacept as adjunctive therapy for the treatment of giant cell arteritis: comment on the article by Langford et al

To the Editor:

Langford and colleagues recently reported results from an interesting multicenter, randomized, double-blind study of treatment of giant cell arteritis (GCA) with abatacept together with glucocorticoids as adjunctive treatment. The authors concluded that the addition of abatacept to a regimen of treatment with prednisone results in a longer duration of relapse-free survival compared with treatment with prednisone alone, and that abatacept possibly has a steroid-sparing effect (1).

Some points deserve to be discussed. First, published studies in GCA usually refer to the dosage of glucocorticoids in mg/kg of body weight, which allows for a more homogeneous comparison of cumulative glucocorticoid dosages between patients. Second, the tapering schedule used in the study by Langford and colleagues is different from that in other trials and current recommendations (2–4). These investigators used a tapering schedule that was very slow during the first 12 weeks (dosage 20 mg/day at week 12, which would correspond to a dose of 0.2 mg/kg and a dose of 0.4 mg/kg [for patients with a body weight of 100 kg and 50 kg, respectively], versus 0.1 mg/kg in other trials [2,3]) and accelerated rapidly during the subsequent 16 weeks. Consequently, as shown in Figure 3 of the Langford article, most relapses in both treatment arms occurred between the fourth and seventh months, which is earlier than in other published cohorts in which relapses occurred after 6 months (2–4). Besides abatacept effect, the fast tapering schedule increases the risk of relapse, especially in the placebo arm, therefore potentially overestimating the effectiveness of abatacept in controlling disease in the experimental arm.

The analysis of adverse events, the number of which typically increases with increasing cumulative glucocorticoid doses, may also be biased by the design of this study, with patients exposed to glucocorticoids for a short period of 28 weeks, but at high doses during the first 3 months. It is not clearly established that cumulative glucocorticoid doses per kg of body weight are lower in this study than in previous studies using classic tapering schedules lasting longer than 28 weeks (which is the actual standard of care). Consequently, this study does not answer the question of whether abatacept acts as a glucocorticoid-sparing agent.

Finally, because of the nonstandard design, especially regarding glucocorticoid management, this study cannot be compared with the standard of care, which is a probable significant bias. Therefore, the place of abatacept as adjunctive treatment to obtain superior effectiveness against relapses or as a glucocorticoid-sparing agent remains to be firmly proven by comparison with standard management.

Hubert de Boysson, MD, MSc
Achille Aouba, MD, PhD
Caen University Hospital
Caen, France

1. Langford CA, Cuthbertson D, Ytterberg SR, Khalidi N, Monach PA, Carette S, et al. A randomized, double-blind trial of abatacept (CTLA4-Ig) for the treatment of giant cell arteritis. Arthritis Rheumatol 2017;69:837–45.
2. Villiger PM, Adler S, Kuchen S, Wermelinger F, Dan D, Fiege V, et al. Tocilizumab for induction and maintenance of remission in giant cell arteritis: a phase 2, randomised, double-blind, placebo-controlled trial. Lancet 2016;387:1921–7.
3. Seror R, Baron G, Hachulla E, Debandt M, Larroche C, Puéchal X, et al. Adalimumab for steroid sparing in patients with giant-cell arteritis: results of a multicentre randomized controlled trial. Ann Rheum Dis 2014;73:2074–81.
4. Proven A, Gabriel SE, Orces C, O'Fallon WM, Hunder GG. Glucocorticoid therapy in giant cell arteritis: duration and adverse outcomes. Arthritis Rheum 2003;49:703–8.

DOI 10.1002/art.40106

Personalized biologic therapy for large vessel vasculitis: comment on the articles by Langford et al

To the Editor:

We read with great interest 2 articles reporting results of the randomized, double-blind trials of abatacept for the treatment of giant cell arteritis (GCA) and Takayasu arteritis (TAK), respectively (1,2). The study of patients with TAK is particularly interesting, because it is the first randomized controlled trial in patients with this very rare condition. Both studies were conducted according to a similar protocol and evaluated the efficacy of maintenance therapy with abatacept as a primary end point.

In our opinion, glucocorticoid tapering could have been slower in patients with TAK. At week 12, treatment with abatacept and prednisone induced remission of GCA and TAK in 83.4% and 76.4% of patients, respectively. However, maintenance therapy with abatacept did not improve relapse-free survival compared with placebo in patients with TAK, while the difference in the rate of sustained remission at 12 months between patients with GCA who received abatacept and those who received placebo was of borderline significance (48% versus 31%; $P = 0.049$). Nevertheless, a longer median duration of remission with abatacept compared with placebo (9.9 versus 3.9 months; $P = 0.023$) along with the relative safety of a biologic agent suggest that it can be an option for a proportion of patients with GCA who do not respond to standard immunosuppressive therapy or require more rapid tapering of glucocorticoids.

The results of the 2 studies by Langford et al add to a discussion regarding whether GCA and TAK are 2 phenotypes of a single disease or 2 different diseases with overlapping phenotypes, and how they should be treated. Over the last decade, the multiple case reports and series and few clinical trials of biologic agents in patients with GCA and TAK shed more light on these issues. The targeted mechanism of action of biologic agents allows exploration of both the similarities and differences between the pathophysiology of these large vessel vasculitides.

Tumor necrosis factor (TNF) seemed to be a promising target for treatment in both patients with GCA and those with TAK, taking into account its role in the development of granulomatous inflammation that is typical of both large

vessel vasculitides. The efficacy of TNF inhibitors (infliximab, adalimumab, etanercept, certolizumab pegol) in relapsing TAK is supported by our own experience treating 16 patients and other observational studies in more than 120 patients (3,4). However, TNF inhibitors have failed to show a significant therapeutic effect or to reduce the glucocorticoid dose in patients with GCA. Therefore, TNF inhibition is not a feasible approach to the treatment of GCA and is not recommended.

Interleukin-6 (IL-6) is another multifunctional cytokine that up-regulates local and systemic inflammatory responses. Expression of IL-6 is increased in the vascular lesions of patients with GCA and those with TAK, while the blood level of IL-6 correlates with disease activity (5,6). The efficacy of tocilizumab (a humanized IL-6 receptor–inhibiting monoclonal antibody) for the induction and maintenance of remission in GCA was shown in a phase II, randomized, double-blind, placebo-controlled trial in 30 patients (7) and is supported by preliminary results of the GiACTA trial in 251 patients (8). Another randomized, placebo-controlled trial (ClinicalTrial.gov identifier: NCT02531633) aims to study sirukumab (a fully human anti–IL-6 IgG1κ) in ~204 patients with a diagnosis of GCA. In patients with TAK, tocilizumab was not tested in the randomized controlled trials. However, its use was reported in several dozen cases in different series. Overall, more than 80% of patients had a clinical and laboratory response by 3 months, and less than 20% experienced a relapse during treatment continuation (9). Notably, IL-6 blockade is associated with reduced hepatic production of C-reactive protein (CRP). Therefore, standard markers of inflammation may be misleading in patients with large vessel vasculitis who are receiving tocilizumab, and silent worsening of arterial stenoses may occur in the setting of normal levels of acute-phase reactants (10).

Conway et al recently reported a significant steroid-sparing effect of ustekinumab (monoclonal antibody to IL-12 and IL-23) in 14 patients with GCA (11), although its efficacy in TAK is currently unknown.

In conclusion, GCA and TAK should be regarded as different diseases. This hypothesis is supported by clinical and genetic data and heterogeneous responses to biologic therapy. Previous data and the results of 2 trials of abatacept confirm that biologic treatment for large vessel vasculitides should be personalized, and that the efficacy of certain biologic agents in GCA cannot be extrapolated to TAK and vice versa. It is noteworthy that even adequately powered randomized clinical trials do not completely rule out a possible therapeutic effect of a biologic agent in selected patients with systemic vasculitis. Therefore, we probably should not give up on abatacept in patients with TAK, particularly those in whom other treatment options failed. Patients with large vessel vasculitis have a relatively favorable prognosis. In our own cohorts of 115 patients with GCA and 128 patients with TAK, 5-year event-free survival reached 89% and 95%, respectively.

Thus, it is hardly possible to expect clinical trials with hard end points, such as cardiovascular outcomes, in these patients. In GCA and TAK clinical trials, the CRP level, the erythrocyte sedimentation rate, and characteristic symptoms have been used as the criteria for remission. However, their reliability is limited, particularly in patients with TAK and those receiving tocilizumab. Imaging modalities, such as ^{18}F-labeled fluorodeoxyglucose positron emission tomography and magnetic resonance angiography, are promising outcomes measures in patients with large vessel vasculitis (12,13). A common argument against their use in clinical trials is incomplete validation as a disease activity tool. Integration of these methods into decision-making may facilitate further clinical trials of biologic agents in patients with large vessel vasculitis.

Sergey Moiseev, MD
Pavel Novikov, MD
Sechenov First Moscow State Medical University
Ilya Smitienko, MD
Medical Center K+31
Moscow, Russia

1. Langford CA, Cuthbertson D, Ytterberg SR, Khalidi N, Monach PA, Carette S, et al. A randomized, double-blind trial of abatacept (CTLA4-Ig) for the treatment of giant cell arteritis. Arthritis Rheumatol 2017;69:837–45.
2. Langford CA, Cuthbertson D, Ytterberg SR, Khalidi N, Monach PA, Carette S, et al. A randomized, double-blind trial of abatacept (CTLA4-Ig) for the treatment of Takayasu arteritis. Arthritis Rheumatol 2017;69:846–53.
3. Novikov PI, Smitienko IO, Moiseev SV. Tumor necrosis factor α inhibitors in patients with Takayasu's arteritis refractory to standard immunosuppressive treatment: cases series and review of the literature. Clin Rheumatol 2013;32:1827–32.
4. Clifford A, Hoffman GS. Recent advances in the medical management of Takayasu arteritis: an update on use of biologic therapies. Curr Opin Rheumatol 2014;26:7–15.
5. Weyand CM, Fulbright JW, Hunder GG, Evans JM, Goronzy JJ. Treatment of giant cell arteritis: interleukin-6 as a biologic marker of disease activity. Arthritis Rheum 2000;43:1041–8.
6. Arnaud L, Haroche J, Mathian A, Gorochov G, Amoura Z. Pathogenesis of Takayasu's arteritis: a 2011 update. Autoimmun Rev 2011;11:61–7.
7. Villiger PM, Adler S, Kuchen S, Wermelinger F, Dan D, Fiege V, et al. Tocilizumab for induction and maintenance of remission in giant cell arteritis: a phase 2, randomised, double-blind, placebo-controlled trial. Lancet 2016;387:1921–7.
8. Stone JH, Tuckwell K, Dimonaco S, Klearman M, Aringer M, Blockmanset D, et al. Efficacy and safety of tocilizumab in patients with giant cell arteritis: primary and secondary outcome from a phase 3, randomized, double-blind, placebo-controlled trial [abstract]. Arthritis Rheumatol 2016;68 Suppl 10. URL: http://acrabstracts.org/abstract/efficacy-and-safety-of-tocilizumab-in-patients-with-giant-cell-arteritis-primary-and-secondary-outcomes-from-a-phase-3-randomized-double-blind-placebo-controlled-trial/.
9. Koster MJ, Matteson EL, Warrington KJ. Recent advances in the clinical management of giant cell arteritis and Takayasu arteritis. Curr Opin Rheumatol 2016;28:211–7.
10. Goel R, Danda D, Kumar S, Joseph G. Rapid control of disease activity by tocilizumab in 10 'difficult-to-treat' cases of Takayasu arteritis. Int J Rheum Dis 2013;16:754–61.
11. Conway R, O'Neill L, O'Flynn E, Gallagher P, McCarthy GM, Murphy CC, et al. Ustekinumab for the treatment of refractory giant cell arteritis. Ann Rheum Dis 2016;75:1578–9.
12. Nakagomi D, Jayne D. Outcome assessment in Takayasu arteritis. Rheumatology (Oxford) 2016;55:1159–71.
13. Moiseev S, Novikov P, Meshkov A, Smitienko I. Biological agents for giant cell arteritis: treat to target. Ann Rheum Dis 2016;75:e58.

DOI 10.1002/art.40107

Reply

To the Editor:

We thank Drs. de Boysson and Aouba and also Dr. Moiseev and colleagues for their interest in our trials and their comments. We readily acknowledge that when designing clinical trials in GCA and TAK, the glucocorticoid dose and tapering

schedule often generate the greatest discussion and differences of opinion. This is in part because there is no firmly established standard of care that optimally balances efficacy and toxicity.

In these 2 trials, all participants initially received prednisone at a dosage of 40–60 mg/day, as selected by their site investigator. This dosage was not calculated based on body weight, but there was latitude within the dosage range to take this factor into account. The prednisone tapering schedule was such that all patients reached a dosage of 20 mg/day at week 12, which was then reduced more slowly until discontinuation at week 28.

Several factors were taken into consideration when designing this prednisone-tapering schedule. The duration of glucocorticoid treatment was similar to that used in previously published multicenter randomized trials in GCA (1,2). Notably, a recent large trial in GCA included a group with a 26-week taper (3).

Another reason for selecting this tapering schedule was recognition of the clinical need for treatment options that provide a means to reduce glucocorticoid exposure. There would likely be limited enthusiasm for use of a biologic therapy from the standpoint of side effects and cost unless the agent were found to have both a statistically significant and clinically meaningful difference when measured against prednisone. Our trial demonstrated that abatacept combined with prednisone reduced the risk of relapse of GCA compared with prednisone alone, through a design that searched for a large difference between treatment arms using a 28-week prednisone taper; this observed difference has clinical relevance and meaning. Because both treatment groups had the same exposure to prednisone, any impact of the tapering schedule on the relapse rate would have affected both arms equally and therefore would not bias the comparison.

The finding that there was no increase in the frequency or severity of adverse events with the addition of abatacept was an important secondary end point in our studies. Although we cannot speculate on whether there would be a difference with a longer course of prednisone, the side effect profile of glucocorticoids and the ability to reduce the amount of glucocorticoid exposure are the main reasons why pursuing novel therapeutic agents remains critical in GCA and TAK.

The letter from Dr. Moiseev and colleagues raises several interesting points regarding disease activity assessment in TAK and the relationship between GCA and TAK. We agree that determining active disease remains one of the greatest challenges in large vessel vasculitis. The definitions used in our trials were determined by the Steering Committee of the Vasculitis Clinical Research Consortium based on clinical and imaging parameters used in practice, outcomes used in prior clinical research in TAK, and experience with GCA. As observed in our study, the vascular and inflammatory manifestations that can prompt a change in treatment are seen during the time span of a trial. It is also of interest that although cardiovascular parameters are perceived as being long-term outcomes, 3 of our 26 randomized TAK patients had evidence by imaging of a new vascular lesion in a new territory during the trial. However, we strongly agree with the enthusiasm to explore promising outcome measures in large vessel vasculitis, including patient-reported outcomes, biomarkers, and novel imaging techniques.

The question as to whether TAK and GCA are unique or part of a single disease spectrum has been of great interest (4,5), with evidence available to support both conclusions. The divergent efficacy of abatacept in our side-by-side randomized trials in GCA and TAK raises intriguing questions about the relationship between these diseases and the need for ongoing clinical and pathophysiologic investigation. While these studies cannot answer the question of whether GCA and TAK are different entities, they demonstrate the value of examining these diseases separately and in parallel when possible.

Both letters raise points about the clinical application of the findings from these trials. We agree that physicians must consider many factors when deciding how these results apply to the care of their patients. In the TAK trial, the addition of abatacept to prednisone did not reduce the risk of relapse. Although we agree that individual patients may respond differently, we cannot advocate for the routine use of a therapy that did not show benefit in an adequately powered randomized trial. The GCA study did demonstrate a statistical difference in the rate of relapse-free survival in patients who received abatacept combined with glucocorticoids. However, the strengths and limitations must continue to be weighed by each physician when choosing how to interpret and utilize these results.

Carol A. Langford, MD, MHS
Cleveland Clinic
Cleveland, OH
Jeffrey P. Krischer, PhD
University of South Florida
Tampa, FL
Peter A. Merkel, MD, MPH
University of Pennsylvania
Philadelphia, PA
on behalf of the Vasculitis Clinical Research Consortium

1. Hoffman GS, Cid MC, Hellmann DB, Guillevin L, Stone JH, Schousboe J, et al. A multicenter, randomized, double-blind, placebo-controlled trial of adjuvant methotrexate treatment for giant cell arteritis. Arthritis Rheum 2002;46:1309–18.
2. Hoffman GS, Cid MC, Rendt-Zagar KE, Merkel PA, Weyand CM, Stone JH, et al. Infliximab for maintenance of glucocorticosteroid-induced remission of giant cell arteritis: a randomized trial. Ann Intern Med 2007;146:621–30.
3. Unizony SH, Dasgupta B, Fisheleva E, Rowell L, Schett G, Spiera R, et al. Design of the tocilizumab in giant cell arteritis trial. Int J Rheumatol 2013:912562.
4. Maksimowicz-McKinnon K, Clark TM, Hoffman GS. Takayasu arteritis and giant cell arteritis: a spectrum within the same disease? Medicine (Baltimore) 2009;88:221–6.
5. Grayson PC, Maksimowicz-McKinnon K, Clark TM, Tomasson G, Cuthbertson D, Carette S, et al. Distribution of arterial lesions in Takayasu's arteritis and giant cell arteritis. Ann Rheum Dis 2012;71:1329–34.

DOI 10.1002/art.40119

Rituximab and Fcγ receptors in granulomatosis with polyangiitis (Wegener's): comment on the article by Cartin-Ceba et al

To the Editor:

We read with interest the article by Cartin-Ceba et al (1) which addressed a very important issue—our knowledge about the mechanism of action of rituximab and the reasons why its partly limited treatment response lags far behind with regard to its broad application in the treatment of systemic inflammatory diseases.

As a rationale for their study, Cartin-Ceba and colleagues hypothesized that responses to rituximab may be affected by Fcγ

receptor (FcγR) single-nucleotide polymorphisms (SNPs). They stated that the anti-CD20 antibody rituximab could mediate B cell killing by inducing antibody-dependent cell-mediated cytotoxicity, in particular via FcγRIIIa expressed on natural killer (NK) cells. Despite the fact that no significant associations between rituximab-induced remission and FcγR SNPs were identified, the findings in their study confirmed a previously described association of FcγR SNPs and clinical disease course in granulomatosis with polyangiitis (Wegener's) (GPA), namely, a favorable course among patients with combined FcγRIIa 519AA and FcγRIIIa 559GG (1,2). This indirectly implicates a pathogenic role of FcγRs in GPA.

We believe that investigating FcγR SNPs alone is not the only way to explore FcγRs as potential biomarkers or to evaluate their potential pathogenic role in GPA. In addition to the binding affinity of FcγRs, which differs depending on the respective SNP, the biologic function of FcγRs is determined by other factors, such as the expression profile of FcγRs on cell surfaces and, essentially, the presence of FcγR-bearing cells such as NK cells. Complementary to the results from the study by Cartin-Ceba et al, we recently found an association between FcγRIIIa-bearing NK cells and GPA disease activity (3), as well as down-regulation of FcγRIIIa on $CD56^{dim}$ NK cells (4). Together with the results described by Cartin-Ceba and colleagues, these findings strengthen the suggestion that FcγRs might be involved, to some degree, in GPA pathogenesis.

We would like to further comment that, despite its being plausible on the basis of the literature on tumor studies, there is very limited evidence confirming that FcγRIIIa on NK cells mediates B cell depletion in patients with rheumatic disease. While rituximab induces the down-regulation of FcγRIIIa and further phenotypic changes of NK cells in peripheral blood mononuclear cells from healthy individuals (5), changes in NK cells from patients with GPA were different from those in cells from healthy individuals (Merkt W, et al: unpublished observations). These changes might impact the immunologic response to rituximab, irrespective of SNPs.

The results described by Cartin-Ceba and colleagues and our data combined suggest that NK cells and FcγRIIIa may play a role in GPA pathogenesis. The assumption that rituximab acts on the same receptor is of great interest and warrants further investigation. Does the interaction between rituximab and FcγRIIIa contribute to its treatment effects or alter the treatment response? Finally, we suggest that NK cells and additional FcγRIIIa characteristics should be investigated in prospective trials to explore their potential use as biomarkers.

Wolfgang Merkt, MD
University Hospital of Heidelberg
Heidelberg, Germany
and Leibniz Research Center for Working Environment and Human Factors at TU Dortmund
Dortmund, Germany
Hanns-Martin Lorenz, MD
University Hospital of Heidelberg
Heidelberg, Germany
Carsten Watzl, PhD
Leibniz Research Center for Working Environment and Human Factors at TU Dortmund
Dortmund, Germany

1. Cartin-Ceba R, Indrakanti D, Specks U, Stone JH, Hoffman GS, Kallenberg CG, et al. The pharmacogenomic association of Fcγ receptors and cytochrome P450 enzymes with response to rituximab or cyclophosphamide treatment in antineutrophil cytoplasmic antibody–associated vasculitis. Arthritis Rheumatol 2017;69:169–175.
2. Dijstelbloem HM, Scheepers RH, Oost WW, Stegeman CA, van der Pol WL, Sluiter WJ, et al. Fcgamma receptor polymorphisms in Wegener's granulomatosis: risk factors for disease relapse. Arthritis Rheum 1999;42:1823–7.
3. Merkt W, Sturm P, Lasitschka F, Tretter T, Watzl, Saure D, et al. Peripheral blood natural killer cell percentages in granulomatosis with polyangiitis correlate with disease inactivity and stage. Arthritis Res Ther 2015;17:337.
4. Merkt W, Claus M, Blank N, Hundemer M, Cerwenka A, Lorenz HM, et al. Active but not inactive granulomatosis with polyangiitis is associated with decreased and phenotypically and functionally altered CD56(dim) natural killer cells. Arthritis Res Ther 2016;18:204.
5. Merkt W, Lorenz HM, Watzl C. Rituximab induces phenotypical and functional changes of NK cells in a non-malignant experimental setting. Arthritis Res Ther 2016;18:206.

DOI 10.1002/art.40121

Reply

To the Editor:

We thank Drs. Merkt, Lorenz, and Watzl for their interest and comments. Their work and ours indeed jointly support the notion that FcγRs have a general role in the pathogenesis of GPA. We also appreciate the important points that they make regarding the biologic function of FCγRs being influenced not only by genetic variation, but also by levels of FcγR-bearing cells and the expression profiles of FcγRs on the surface of these cells, in terms of both absolute and relative amounts.

We would like to point out, however, that the authors' view concerning NK involvement in GPA pathogenesis by way of FcγRIIIa is perhaps stronger than what our study conveys. Our findings of associations between a single FcγR polymorphism and complete disease remission (prediction of, time to) occurred only with FcγRIIa, specifically the FcγRIIa 519AA genotype. The FcγRIIa variant encoded by this genotype exhibits higher binding to IgG2, and as a predictor of complete remission and shorter time to complete remission, appears to implicate IgG2 in GPA pathogenesis. This could be through the clearance of IgG2-containing immune complexes, or through an effect on IgG2 antibody responses. Interestingly, IgG2, the second most common subclass and most common cell surface subclass, predominates in responses to many bacterial polysaccharides, and deficiencies in IgG2 are associated with recurrent sinopulmonary infections. It has been suggested that these infections may trigger GPA flares.

In contrast to FcγRIIa, the FcγRIIIa 559GG genotype was not by itself a predictor of complete remission in our study, but required the presence of the FcγRIIa 519AA genotype. However, even this conclusion requires some skepticism because of the limited sample size of patients with these combined genotypes. If in fact true, this may suggest that cells that express both FcγRIIa and FcγRIIIa are important players in

GPA pathogenesis, or that NK cells may have an added influence on GPA. This latter interpretation certainly complements Merkt and colleagues' work.

Dr. Merkt and colleagues importantly point out that understanding what determines rituximab's efficacy in GPA and other diseases indeed lags far behind its broad application. Unfortunately, our study did not provide any clarification with regard to GPA. Nevertheless, our study and those of Merkt et al suggest that FcγR-mediated pathways have significant influence on GPA onset, flare, and treatment response, and as such warrant further study.

Brad H. Rovin, MD
Dan Birmingham, PhD
Ohio State University Wexner Medical Center
Columbus, OH
Rodrigo Cartin-Ceba, MD, MSc
Ulrich Specks, MD
Mayo Clinic and Foundation
Rochester, MN and Scottsdale, AZ
John H. Stone, MD, MPH
Massachusetts General Hospital
Boston, MA

DOI: 10.1002/art.40103

Clinical Images: Gouty tophus as an unusual cause of talus fracture

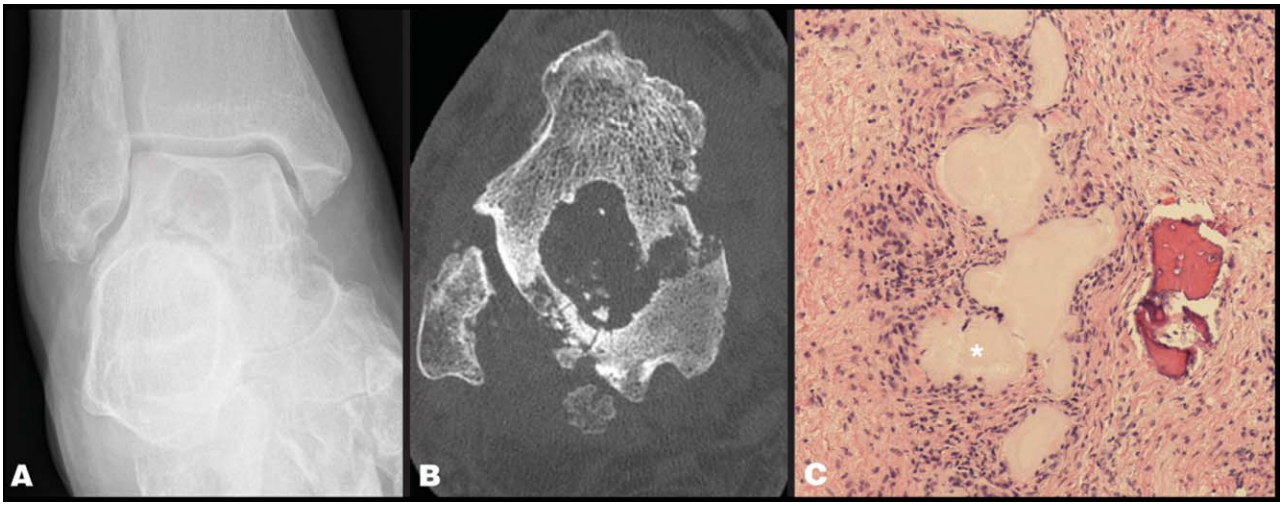

The patient, a 41-year-old man with a 20-year history of untreated gout, presented with atraumatic pain in the right ankle that was dissimilar to prior gout flares. He had been prescribed allopurinol 8 years previously (without prophylaxis), but later experienced a severe polyarticular flare requiring hospitalization and was subsequently lost to follow-up. Radiography of the ankle revealed a central lucency in the dome of the talus of the right ankle (**A**). The differential diagnosis was broad, but concern for neoplastic causes prompted computed tomography (CT) of the ankle. CT revealed a large cystic structure in the talus measuring 3 × 2 × 2 cm, with sclerotic margins extending to the articular surface. A chronic, nonunion fracture of the talus traversed the cyst (**B**). Other ankle bones, including the calcaneus and navicular, had gouty erosions with overhanging edges, as well as smaller intraosseous tophi. The joint was surgically explored, and the contents of the cyst were histopathologically confirmed to be gouty tophus. While the fresh slide demonstrated monosodium urate monohydrate (MSU) crystals, in the hematoxylin and eosin–stained section shown here (**C**) (magnification × 10), the MSU crystals have dissolved, and only amorphous material remains in the tophi locations (**asterisk**). This area of tophus is surrounded by an inflammatory infiltrate. A bone graft was used for fixation and screws for stabilization. Gout is a relatively common disease of MSU deposition in peripheral tissues. It remains a poorly treated condition. Pathologic fractures should be added to the list of potential complications. The differential diagnosis of pathologic fractures is large, and tophi are an underappreciated cause. While there are more than 20 reports of tophaceous fractures in non–weight-bearing bones, this is only the second reported case of tophus causing talus fracture. This may indicate tophaceous compromise of the distal-to-proximal blood supply of the talus leading to cortical destabilization (1,2). This case is not intended to confirm or refute a recent dual-energy CT study of gouty erosions, which found that no urate was deposited in the bone, but only on the surface in cortical defects of erosions (3). We present this unique case simply to raise awareness and cannot draw any pathophysiologic conclusions. Finally, this case highlights the related problems of poor management of acute gout, inadequate flare prophylaxis with urate-lowering therapy, the long-term sequelae of both, and the importance of ongoing follow-up.

1. Yan M, Guo B, Liang D, Shi D, Yang L, Cao J. Gouty arthritis of the ankle masquerading as a talus fracture. J Rheumatol 2012;39:868.
2. Lomax A, Miller RJ, Fogg QA, Madeley NJ, Kumar CS. Quantitative assessment of the subchondral vascularity of the talar dome: a cadaveric study. Foot Ankle Surg 2014;20:57–60.
3. Towiwat P, Doyle AJ, Gamble GD, Tan P, Aati O, Horne A, et al. Urate crystal deposition and bone erosion in gout: "inside-out" or "outside-in"? A dual-energy computed tomography study. Arthritis Res Ther 2016;18:208.

Steven Thomson, MD, MSc
Stefan Urbanski, MD
Paul MacMullan, MD
University of Calgary
Calgary, Alberta, Canada